

**THE ROLE OF THE MLL/AF4 FUSION
ONCOGENE IN ACUTE LYMPHOBLASTIC
LEUKAEMIA MAINTENANCE**

Patricia Garrido Castro

Student no. 079052887



A thesis submitted in part requirement for the degree of

Doctor of Philosophy

**from the Faculty of Medical Sciences at Newcastle University,
Newcastle upon Tyne, UK**

June 2011

Fusion Gene Research Group, Northern Institute for Cancer Research, Paul O' Gorman
Building, Medical School, Framlington Place, Newcastle University, Newcastle upon
Tyne, NE2 4HH, UK.

Declaration

The work reported in this thesis was performed from June 2007 to December 2010 at the Fusion Gene/Leukaemia Stem Cell Research Group , Northern Institute for Cancer Research, Newcastle University; under the supervision of Dr. Olaf Heidenreich and Prof. Josef Vormoor.

Except where specifically indicated and referenced to, this work was carried out by myself, and represents an original piece of work

No part of this thesis has been submitted for the award of any other degree.

Signed: Patricia Garrido Castro (Student no. 07952887)

Abstract

The chromosomal rearrangement t(4;11)(q21;q23) marks an aggressive acute lymphoblastic leukaemia (ALL) subtype particularly prevalent in infants and associated with poor outcome. This cytogenetic abnormality encodes the fusion oncogene *MLL/AF4*, which plays a pivotal role in cell death resistance; however, the underlying molecular processes are not fully understood.

Therefore, to gain further insight, RNAi-mediated ablation of *MLL/AF4* in the t(4;11)-positive ALL cell line SEM was combined with global gene expression profiling and concomitant apoptosis inhibitor studies.

Phenotypically, *MLL/AF4* depletion impaired proliferation, cell cycle progression, clonogenicity and caused a strong apoptosis induction. Global transcriptome analysis found up-regulation of proapoptotic and anti-proliferative genes, while mitogenic signalling mediators and stemness-related markers were down-regulated.

Supplementing *MLL/AF4*-depleted cells with the pan-caspase inhibitor zVAD suppressed apoptosis, but failed to abrogate cell death. Subsequent gene expression profiling showed induction of genes implicated in the necroptotic cell death pathway. Interestingly, addressing this using established necroptosis inhibitors did not rescue the phenotype.

Finally, the cytokine *ANGIOPOIETIN-1* (*ANGPT1*) was identified as a novel *MLL/AF4*-modulated gene; *MLL/AF4* knock-down correlated with a substantial decrease of *ANGPT1* levels. Concordantly, screening an B-precursor ALL patient cohort found *ANGPT1* to be highly overexpressed in t(4;11)-positive ALL. Although no correlation with clinical prognostic factors could be established, *ANGPT1* was found to contribute to the leukaemic phenotype, as RNAi-mediated *ANGPT1* depletion impaired proliferation and viability *in vitro* and impinged on disease development *in vivo*.

Concluding, it was found that t(4;11)-positive ALL cells display a high degree of oncogene addiction towards MLL/AF4, since depletion strongly perturbed the leukaemic phenotype, compromising survival and self-renewal. Furthermore, ANGPT1 was identified as a novel proleukaemic factor cooperating with MLL/AF4 in maintaining the disease.

Acknowledgements

I would like to give my heartfelt thanks to the patients and their parents for supporting this research by giving their consent; we must not ever forget that all science is undertaken with their well-being and health in mind.

The utmost thanks go to my supervisors, Dr. Olaf Heidenreich and Prof. Josef Vormoor, for giving me the opportunity to work at this project and their continuous support and encouragement.

Especially Olaf has been a great mentor to me, he has watched me grow from a little placement student back in Tuebingen into the scientist I am today; and probably taught me all I know; but, what I will treasure most, is that he taught me and encouraged me to think scientifically, critically and, especially, not to be afraid to challenge ideas and dogmas.

I would also like to thank Dr. Johann Greil for his support and his continuous enthusiasm for my work.

A great thank you goes to Dr. Ronald Stam and his group for their significant contribution to the ANGPT1 study, supplying both patient material, data and especially for screening their extensive patient cohort for me. Also, I'm very grateful to him for putting up with such good grace with an absentee Post-Doc while she is finishing up her thesis... Heel vielemalen bedankt!

I am very grateful to Prof. Christine Harrison, Dr. Julie Irving and Dr. Simon Bomken for their kind gifts of patient material, data, healthy controls and cord blood preparations.

Also, a great thanks goes to Dr. Krippner-Heidenreich, for the support in the necroptosis study, and the kind gift of antibodies.

A special thank you goes to Hesta McNeill for her support with the FACS-sort, and for being such a great company in the late night sessions here at the POG.

I would like to thank Mike Batey for his support with the *in vivo* study.

I would like to thank Robert Ernst and Eddy van Roon for introducing me to R and their help with the R scripts.

I definitely need to thank everybody from the Fusion Gene/Leukaemic Stem Cell group, past and present, for their help, support, and for being just awesomely great colleagues!

A PhD is full of up and downs, and I would not have been able to navigate is so successfully if it wasn't for the help of a group of great people, which were not only scientists-in-arms, but are very close friends... Special thanks to Lisa Russell-aka PITB/BB, Marta Radwan, Christine Richter, Vicky Forster, Henrike Knizia, Lars Buechler, Andreas Gessner, Amit Patel, Ghada Malik and Andrea Beyerle... Thank you for rescuing me from myself, for always being there when I needed an ear or more. Without you, these last three and a half years would have been very dreary indeed...

Sobre todo quiero dedicar esta tesis de todo corazón a mis padres, sin los que no hubiera llegado tan lejos. Siempre han estado a mi lado, ayudandome en todo lo que pudiesen, dandome mucho amor y cariño. ¡Un beso muy fuerte!

List of tables

<i>Tab. 1-1: Outcome of infant ALL patients in regards to the MLL-status – historical study groups_</i>	15
<i>Tab. 2-1: qRT-PCR primers (VHBio, Sigma-Aldrich Ltd)</i>	33
<i>Tab. 2-2: RT-PCR primers (Fermentas, Sigma-Aldrich Ltd)</i>	35
<i>Tab. 2-3: siRNA oligonucleotides</i>	35
<i>Tab. 2-4: Immunoblot antibodies</i>	36
<i>Tab. 2-5:FACS antibodies</i>	37
<i>Tab. 2-6: TNF/TNFR antibody –PBAF solution pipetting scheme</i>	56
<i>Tab. 2-7: ANNEXINV-FITC/PI staining pipetting scheme</i>	58
<i>Tab. 2-8: CD marker pipetting scheme</i>	59
<i>Tab. 3-1: RIN values of samples submitted to GEP as determined by Bioanalyzer 2100 RNA 6000 Nano Assay</i>	97
<i>Tab. 3-2: Array Statistics of pre-processed raw data using BeadStudio 3</i>	99
<i>Tab. 3-3: Number of differentially expressed probe sets and genes for the MLL/AF4 signature A at TP1 and TP2</i>	101
<i>Tab. 3-4: Top 50 up-regulated probes in signature A at TP1</i>	102
<i>Tab. 3-5: Top50 down-regulated probes in signature A at TP1</i>	103
<i>Tab. 3-6: Top50 up-regulated probes in signature A at TP2</i>	104
<i>Tab. 3-7: Top50 down-regulated probes in signature A at TP2</i>	105
<i>Tab. 3-8: Top5 networks affected by the MLL/AF4 gene signature at TP1</i>	106
<i>Tab. 3-9: Top 5 significantly enriched functional categories in the MLL/AF4 gene signature at TP1</i>	108
<i>Tab. 3-10: Top5 networks affected by the MLL/AF4 gene signature at TP2</i>	114
<i>Tab. 3-11: Top 5 significantly enriched functional categories in the MLL/AF4 gene signature A at TP2</i>	115
<i>Tab. 3-12: Differentially regulated genes in the MLL/AF4 signature covered by distinct probe sets at both time points</i>	129
<i>Tab. 3-13: MLL/AF4 target genes¹³² present in the MLL/AF4 signature-A at both TP1 and TP2</i>	131
<i>Tab. 3-14: RIN values of samples submitted to GEP as determined by Bioanalyzer2100 RNA 6000 Nano Assay</i>	134

<i>Tab. 3-15: Number of differentially expressed probe sets and genes for the MLL/AF4 signature B at all three time points</i>	135
<i>Tab. 3-16: Top 50 up-regulated genes at TP3</i>	136
<i>Tab. 3-17: Top 50 down-regulated genes at TP3</i>	137
<i>Tab. 3-18: Top 5 networks affected by MLL/AF4 gene signature A at TP3</i>	138
<i>Tab. 3-19: Significantly enriched functional categories in MLL/AF4 gene signature B at TP3</i>	139
<i>Tab. 3-20: MLL/AF4 GEP signature genes associated with stemness and self-renewal</i>	152
<i>Tab. 4-1: RIN values of samples submitted to GEP as determined by Bioanalyzer2100 RNA 6000 Nano Assay</i>	198
<i>Tab. 4-2: Number of differentially expressed probe sets and genes for the zVAD signatures at TP1 and TP2</i>	200
<i>Tab. 4-3: Top 50 up-regulated probes in the zVAD signature at TP1</i>	201
<i>Tab. 4-4: Top 50 down-regulated probes in the zVAD signature at TP1</i>	202
<i>Tab. 4-5: Top 50 up-regulated probes in the zVAD signature at TP2</i>	203
<i>Tab. 4-6: Top 50 down-regulated probes in the zVAD signature at TP2</i>	204
<i>Tab. 4-7: Top 5 networks affected by the zVAD gene signature at TP1</i>	206
<i>Tab. 4-8: Significantly enriched functional categories in the zVAD gene signature at TP1</i>	207
<i>Tab. 4-9: Top 5 significantly enriched networks in the zVAD signature at TP2</i>	211
<i>Tab. 4-10: Significantly enriched functional categories in the zVAD gene signature at TP2</i>	214
<i>Tab. 4-11: MLL/AF4 target genes differentially regulated in both the MLL/AF4 and zVAD signature at all time points</i>	234
<i>Tab. 4-12: Differential expression of necroptosis-associated genes is majorly restricted to the zVAD signature</i>	236
<i>Tab. 5-1: List of signal intensity log₂-ratios and corresponding fold-changes of ANGPT1 probes in siMLL/AF4-treated samples normalised against siCtrl samples</i>	263
<i>Tab. 5-2: Correlation of ANGPT1 expression fold-changes between the different analysis methods</i>	268
<i>Tab. 5-3: MLLr patient cohort characteristics</i>	278
<i>Tab. 5-4 : non-MLLr patient characteristics</i>	279
<i>Tab. 5-5: Statistical analysis on ANGPT1 levels between the different BCP-ALL subtypes using unpaired Student's t-test on log-transformed values</i>	282

<i>Tab. 5-6: Median fold-change ANGPT1 expression between ALL subgroups</i>	283
<i>Tab. 5-7: Patient cohort statistics</i>	286
<i>Tab. 5-8 Statistical Correlation of ANGPT1 and HOXA gene expression</i>	293
<i>Tab. 5-9 Changes in proliferation rates of SEM cells depleted of ANGPT1</i>	307
<i>Tab. 5-10: RIN values of samples submitted to GEP</i>	312
<i>Tab. 5-11: Array Statistics after processing using GenomeStudio</i>	313
<i>Tab. 5-12. Number of differentially expressed probe sets and genes for gene signatures A and B</i>	314
<i>Tab. 5-13: Top-50 Up-regulated Genes in SEM cells depleted of ANGPT1</i>	315
<i>Tab 5-14. Top-50 down-regulated genes in SEM cells depleted of ANGPT1 – Signature A</i>	316
<i>Tab. 5-15 Top-50 down-regulated genes in SEM cells depleted of ANGPT1 – Signature B</i>	317
<i>Tab. 5-16: Significantly enriched functional categories in gene signature A</i>	319
<i>Tab. 5-17: Top 5 significantly enriched networks in gene signature A.</i>	320
<i>Tab. 5-18: Regulation of probes associated with GR signalling in ANGPT1-depleted SEM cells</i>	325
<i>Tab. 5-19. Significantly enriched functional categories in gene signature B.</i>	327
<i>Tab. 5-20: Top 5 significantly enriched networks in gene signature B.</i>	328
<i>Tab. 5-21: Survival and disease burden statistics of both xenograft treatment groups</i>	343

List of Figures

<i>Fig. 1-1: Cluster of Differentiation (CD) marker expression in normal and malignant B-lymphopoiesis⁵⁻⁷</i>	4
<i>Fig. 1-2: Incidence of different ALL subtypes in childhood ALL^{9,13,24}</i>	9
<i>Fig. 2-1: Chemical structure of the pan-caspase inhibitor zVAD</i>	47
<i>Fig. 2-2: Chemical structure of the RIPK1 inhibitor NEC-1</i>	48
<i>Fig. 2-3: Cell cycle histogramme schematic</i>	55
<i>Fig. 2-4: QRT-PCR cycling conditions</i>	64
<i>Fig. 3-1: e9-e4 MLL/AF4 fusion gene breakpoint cDNA sequence</i>	78
<i>Fig. 3-2: Experimental set-up: siRNA electroporation time course for MLL/AF4 knock-down</i>	79
<i>Fig. 3-3: siRNA transfection efficiency</i>	80
<i>Fig. 3-4: MLL/AF4 expression analysis by qRT-PCR</i>	81
<i>Fig. 3-5: Expression analysis of MLL/AF4 by qRT-PCR after siRNA treatment of primary patient blasts.</i>	82
<i>Fig. 3-6: Expression analysis of the MLL/AF4 fusion and the wild-type genes AF4 and MLL in SEM cells 2h post-electroporation</i>	84
<i>Fig. 3-7: AF4 expression analysis in response to MLL/AF4 depletion</i>	85
<i>Fig. 3-8: MLL expression analysis in response to MLL/AF4 depletion</i>	86
<i>Fig. 3-9: MLL/AF4, AF4 and MLL expression analysis in siRNA-treated RS4;11 cells</i>	87
<i>Fig. 3-10: AF4 expression analysis in siRNA-treated Kasumi-1 cells</i>	88
<i>Fig. 3-11: Scheme HOXA gene binding sites within the AF4 promoter</i>	89
<i>Fig. 3-12: Growth curve of siMLL/AF4-treated SEM cells</i>	90
<i>Fig. 3-13: Changes in cell cycle distribution in SEM cells depleted of MLL/AF4</i>	92
<i>Fig. 3-14: Analysis of the sub-G1/G0 population of siRNA-treated SEM cells</i>	93
<i>Fig. 3-15: Clonogenicity assay of MLL/AF4-depleted SEM cells</i>	94
<i>Fig. 3-16: Experimental set-up scheme for GEP samples</i>	95
<i>Fig. 3-17: MLL/AF4 expression analysis of samples allotted for GEP</i>	98
<i>Fig. 3-18: Normalised array intensity values each treatment group at TP1 & TP2</i>	100
<i>Fig. 3-19: MLL/AF4 depletion affects regulatory networks associated with gene expression</i>	109

<i>Fig. 3-20: MLL/AF4 depletion for 2 days (TP1) affects regulatory networks linked to cell death</i>	110
<i>Fig. 3-21: Pathway analysis of the MLL/AF4 gene signature A at TP1</i>	112
<i>Fig. 3-22: MLL/AF4 depletion for 2 days results in down-regulation of several factors of the ephrin and other mitogenic signalling pathways</i>	113
<i>Fig. 3-23: Sustained MLL/AF4 depletion for 4d (TP2) affects factors associated with cellular development and cell cycle regulation</i>	117
<i>Fig. 3-24: Pathway analysis of the MLL/AF4 gene signature A at TP2</i>	119
<i>Fig. 3-25: Sustained MLL/AF4 depletion for 4 d (TP2) results in down-regulation of the BCR signalling machinery involving Ras-ERK1/2- and NFkB-mediated signalling cascades</i>	120
<i>Fig. 3-26: Sustained MLL/AF4 depletion for 4 d (TP2) results in down-regulation of the CD40 signalling machinery involving ERK1/2-, STAT3- and NFkB-mediated signalling cascades</i>	121
<i>Fig. 3-27: Sustained MLL/AF4 depletion for 4 d (TP2) results in down-regulation of IGF1R-mediated signalling</i>	122
<i>Fig. 3-28: Venn diagram of overlapping probes in MLL/AF4 signature A at both time points</i>	123
<i>Fig. 3-29: Heat map of the MLL/AF4 core signature A</i>	124
<i>Fig. 3-30: The MLL/AF4 signature was negatively enriched for SP-1 target genes</i>	126
<i>Fig. 3-31: Venn diagrammes of the MLL/AF4 signature at both time points</i>	127
<i>Fig. 3-32: Venn diagrammes of MLL/AF4 target genes¹³² with MLL/AF4 signature A at both time points</i>	130
<i>Fig. 3-33: Experimental and analysis set-up for MLL/AF4 signature B</i>	133
<i>Fig. 3-34: MLL/AF4 expression analysis for TP3-GEP</i>	134
<i>Fig. 3-35: Sustained MLL/AF4 depletion for 6 days affects regulatory networks associated with development and cellular movement</i>	140
<i>Fig. 3-36: Pathway analysis of the MLL/AF4 gene signature at TP3</i>	142
<i>Fig. 3-37: MLL/AF4 signature-B at TP3 shows down-regulation of PI3K/AKT-, NFkB- as well as Ras- and Rac signalling effectors</i>	143
<i>Fig. 3-38: Venn diagrammes of the MLL/AF4 signature B at all three time points</i>	145
<i>Fig. 3-39: Heat map of a core signature of probes differentially expressed in siMLL/AF4-electroporated SEM cells at all three time points TP1, TP2 and TP3</i>	146
<i>Fig. 3-40: The core signature was significantly enriched for gene sets associated with cellular compromise, immune response and TCF3-target genes</i>	147
<i>Fig. 3-41: Normalised DUSP6 probe signal values in MLL/AF4 signature B</i>	149

<i>Fig. 3-42: DUSP6 expression analysis in t(4;11)-positive ALL cell lines after MLL/AF4 depletion</i>	151
<i>Fig. 3-43: Dependence of HOXA7 and HOXA10 expression in t(4;11)-positive cells on MLL/AF4</i>	154
<i>Fig. 3-44: Dependence of HOXA9 expression in t(4;11)-positive cells on MLL/AF4</i>	155
<i>Fig. 3-45: TERT expression analysis in MLL/AF4 depleted SEM cells</i>	156
<i>Fig. 3-46: MLL/AF4-dependent HMGA2 expression in t(4;11)-positive cells</i>	157
<i>Fig. 3-47: PYGO2 expression in SEM cells depleted of MLL/AF4</i>	159
<i>Fig. 3-48: DNMT3B expression in MLL/AF4-depleted SEM cells</i>	161
<i>Fig. 3-49: Normalised ANXA1 probe signal values in samples depleted of MLL/AF4</i>	162
<i>Fig. 3-50: ANXA1 expression in t(4;11)-positive cells in response to MLL/AF4 depletions</i>	164
<i>Fig. 3-51: Normalised GABARAPL1 probe signal values in samples depleted of MLL/AF4</i>	165
<i>Fig. 3-52: GABARAPL1 expression in MLL/AF4-depleted SEM cells</i>	166
<i>Fig. 3-53: Correlation analysis of the fold-changes of the MLL/AF4 GEP signature and qRT-PCR</i>	167
<i>Fig. 4-1: Experimental set-up</i>	182
<i>Fig. 4-2: Analysis of the sub-G1/G0 population of siRNA-treated SEM cells supplemented with different zVAD concentrations</i>	185
<i>Fig. 4-3: PARP Western blot in zVAD –treated SEM cells</i>	186
<i>Fig. 4-4 : Cell cycle analysis of different zVAD treatment groups</i>	187
<i>Fig. 4-5: MLL/AF4 expression analysis in siRNA treated SEM cells cultured with or without zVAD</i>	188
<i>Fig. 4-6: Analysis of the sub-G1/G0 population of siRNA-treated SEM cells supplemented with or without zVAD</i>	190
<i>Fig. 4-7: Effector caspase activation and action is suppressed in siMLL/AF4-transfected SEM cells by zVAD</i>	191
<i>Fig. 4-8: Apoptosis inhibition in siMLL/AF4-depleted SEM cells causes switch from apoptosis to a necrotic-like PCD.</i>	193
<i>Fig. 4-9: Viability of siMLL/AF4-electroporated SEM cells is compromised despite apoptosis inhibition</i>	195
<i>Fig. 4-10: Confirmation of MLL/AF4 depletion by qRT-PCR in cells treated with or without zVAD prior to GEP analysis</i>	197
<i>Fig. 4-11: Normalised array intensity values of each zVAD treatment group at TP1 & TP2</i>	199
<i>Fig. 4-12: Pathway analysis of the zVAD gene signature at TP1</i>	208

<i>Fig. 4-13: The zVAD signature at TP1 reveals that MLL/AF4 depletion in presence of caspase inhibition results in up-regulation of part of the TNFR2 signalling machinery</i>	209
<i>Fig. 4-14: The zVAD signature at TP1 reveals that MLL/AF4 depletion in presence of caspase inhibition negatively affects PI3K/AKT signalling.</i>	210
<i>Fig. 4-15: Sustained MLL/AF4 depletion for 4 days (TP2) in presence of caspase inhibition affects functions associated with cellular death and gene expression</i>	212
<i>Fig. 4-16: Sustained MLL/AF4 depletion for 4 days (TP2) in presence of caspase inhibition affects functions associated with infectious processes, gene expression and tumour morphology.</i>	213
<i>Fig. 4-17: Pathway analysis of the zVAD gene signature at TP2</i>	215
<i>Fig. 4-18: The zVAD signature at TP2 reveals that MLL/AF4 depletion in presence of caspase inhibition perturbs ERK/MAPK pathways, down-regulating part of the mitogenic signalling machinery.</i>	216
<i>Fig. 4-19: Sustained MLL/AF4 depletion for 4d (TP2) in presence of zVAD up-regulates TNFR1 signalling mediators.</i>	217
<i>Fig. 4-20: Venn diagram of overlapping probes in the zVAD signature at both time points</i>	219
<i>Fig. 4-21: Heat map of the top25 up- and down-regulated genes present at both queried time points of the zVAD signature</i>	220
<i>Fig. 4-22: The zVAD signature was significantly enriched for gene sets associated with TLR, IFN and TNFRSF signalling</i>	221
<i>Fig. 4-23: The zVAD signature was significantly enriched for gene sets associated with cell death, cellular compromise, migration and cytokine signalling.</i>	222
<i>Fig. 4-24: The zVAD signature was significantly enriched for specific transcription factor target genes.</i>	223
<i>Fig. 4-25: Data sets significantly enriched for transcription factor target genes within the zVAD signature.</i>	224
<i>Fig. 4-26: Similarity matrix heat map</i>	225
<i>Fig. 4-27: Hierarchical clustering of the leading edge gene subsets</i>	227
<i>Fig. 4-28: Incidence of the top 10 most frequent leading edge genes</i>	227
<i>Fig. 4-29: Venn diagram depicting shared probe sets between the zVAD and the MLL/AF4 signature at both time points queried.</i>	229
<i>Fig. 4-30: Heat map of a core signature of probes differentially expressed in siMLL/AF4-electroporated SEM cells with or without zVAD at both time points TP1 and TP2</i>	232
<i>Fig. 4-31: Cell surface expression of TNFR1 and TNFR2 in t(4;11)-positive ALL cell lines</i>	237
<i>Fig. 4-32: Expression analysis of necroptotic genes by qRT-PCR</i>	238

<i>Fig. 4-33: Expression analysis of the necroptotic genes BMF,CYLD and PARP2 by qRT-PCR</i>	240
<i>Fig. 4-34: Basal expression levels of necroptotic genes</i>	241
<i>Fig. 4-35: Correlation analysis between array and qRT-PCR results</i>	242
<i>Fig. 4-36: Cell surface expression of TNF receptors TNFR1, TNFR2 and membrane-bound TNF in siRNA-treated SEM cells</i>	243
<i>Fig. 4-37: RIPK1 Immunoblot in siRNA-treated SEM cells with or without zVAD</i>	245
<i>Fig. 4-38: LC3B Immunoblot in siRNA-treated SEM cells with or without zVAD</i>	246
<i>Fig. 4-39: Experimental set-up of necroptosis inhibitor study</i>	247
<i>Fig. 4-40: Necroptosis inhibitors fail to suppress cell death in response to MLL/AF4 depletion</i>	249
<i>Fig. 4-41: Necroptosis inhibitors fail to restore viability in SEMs cells depleted of MLL/AF4</i>	250
<i>Fig.5-1: Normalised ANGPT1 probe signal values in samples depleted of MLL/AF4</i>	263
<i>Fig. 5-2: ANGPT1 levels in MLL/AF4-depleted cells determined by qRT-PCR</i>	265
<i>Fig. 5-3: ANGPT1 protein secretion in MLL/AF4-depleted SEM cells as determined by ELISA</i>	266
<i>Fig. 5-4 Scheme comparing fold-change of ANGPT1 RNA and protein expression in MLL/AF4-depleted SEM cells as determined by different analysis methods.</i>	267
<i>Fig. 5-5: Expression analysis of ANGPT1 by qRT-PCR after siRNA treatment of primary patient blasts.</i>	270
<i>Fig. 5-6: ANGPT1 expression analysis in purified and fractioned CB cell populations</i>	272
<i>Fig. 5-7: ANGPT1 expression analysis in peripheral blood (PB) cell subpopulations</i>	273
<i>Fig. 5-8: ANGPT1 expression analysis in an acute leukaemia cell line cohort</i>	275
<i>Fig. 5-9: ANGPT1 expression analysis in MLLr acute leukaemia cell lines</i>	276
<i>Fig. 5-10: ANGPT1 expression in BCP-ALL patients according to MLL-status</i>	280
<i>Fig. 5-11: ANGPT1 expression in BCP-ALL patients sorted according to cytogenetic subtype</i>	281
<i>Fig. 5-12: ANGPT1 expression in BCP-ALL patients according to age and immunophenotype</i>	284
<i>Fig. 5-13: ANGPT1 level in infant MLLr patients according age-risk stratification</i>	287
<i>Fig. 5-14: Correlation between ANGPT1 expression levels and WBC in ALL</i>	288
<i>Fig. 5-15: Scheme HOXA gene binding sites within the ANGPT1 promoter</i>	291
<i>Fig. 5-16: Correlation between ANGPT1 and HOXA gene expression levels</i>	291
<i>Fig. 5-17: HOXA7 and ANGPT1 expression in siHOXA7 treated SEM cells</i>	293

<i>Fig. 5-18: ANGPT1 secretion determined in the supernatant of cultured t(4;11)+ patient blasts</i>	295
<i>Fig. 5-19 TIE2 expression analysis in leukaemic cell lines and patients</i>	298
<i>Fig. 5-20:TIE1 expression analyses in an acute leukaemia cell line panel</i>	299
<i>Fig. 5-21: Expression analysis of non-canonical ANGPT1 receptors</i>	300
<i>Fig. 5-22: Scheme of the ANGPT1 exon structure including position of siRNAs and qRT-PCR primers</i>	301
<i>Fig. 5-23: Determination of silencing efficiency of ANGPT1 siRNAs</i>	302
<i>Fig. 5-24: siRNA electroporation time course for ANGPT1 knock-down</i>	303
<i>Fig. 5-25: ANGPT1 levels in SEM cells treated with siANGPT1</i>	304
<i>Fig. 5-26 :ANGPT1 secretion levels in SEM cells treated with siANGPT1</i>	305
<i>Fig. 5-27: Growth curve of ANGPT1-depleted SEM cells</i>	306
<i>Fig. 5-28: Changes in cell cycle distribution in SEM cells depleted of ANGPT1</i>	308
<i>Fig. 5-29: SEM cell viability and survival are compromised upon sustained ANGPT1 depletion analysis</i>	309
<i>Fig. 5-30: ANGPT1 background level in standard and serum-free growth medium</i>	311
<i>Fig. 5-31: ANGPT1 expression analysis of siRNA-treated SEM cells in serum-free medium</i>	312
<i>Fig. 5-32. ANGPT1 depletion affects functions associated with cellular growth, proliferation and development</i>	321
<i>Fig. 5-33: ANGPT1 depletion results in down-regulation of the functions associated with cell-to-cell signalling and interactions, cellular motility and haematological disease.</i>	322
<i>Fig. 5-34: Pathway analysis of gene signature A</i>	324
<i>Fig. 5-35: GR signalling pathway machinery is up-regulated in response to ANGPT1 depletion</i>	326
<i>Fig. 5-36: ANGPT1 depletion results in down-regulation of the functions associated with proliferation and haematological processes.</i>	329
<i>Fig. 5-37: Pathway analysis of gene signature B</i>	330
<i>Fig. 5-38: GPCR/cAMP/PKA signalling is down-regulated in response to ANGPT1 depletion.</i>	331
<i>Fig. 5-39: Pathways associated with stemness signalling are down-regulated in response to ANGPT1 depletion.</i>	332
<i>Fig.5-40: Dexamethasone response curve of siRNA-treated SEM cells.</i>	335
<i>Fig. 5-41: Scheme depicting the workflow for lentiviral particle production and subsequent infection of the target cell line SEM-SLIEW</i>	337

<i>Fig. 5-42: Flow cytometric analysis of shRNA induction</i> _____	338
<i>Fig. 5-43: qRT-PCR analysis of ANGPT1 in SEM-SLIEW cells expressing shRNA</i> _____	339
<i>Fig. 5-44: Scheme - Purification of the GFP-expressing shRNA-SEM-SLIEW fraction by fluorescence-activated cell sorting (FACS) and subsequent IF injection into NSG mice</i> _____	340
<i>Fig. 5-45: Bioassay to determine doxycycline plasma levels</i> _____	343
<i>Fig. 5-46: Kaplan-Meyer plot depicting survival of the two treatment groups</i> _____	344
<i>Fig. 5-47 : Engraftment of human ALL cells in the BM and splenic infiltration</i> _____	345
<i>Fig. 5-48: Spleen characteristics in transplanted NSG mice</i> _____	346
<i>Fig. 5-49: Bioluminescence in vivo imaging of leukaemic disease spread in NSG mice</i> _____	347
<i>Fig. 5-50: Tumour characteristics of SEM-SLIEW shANGPT1-transplanted mice.</i> _____	348
<i>Fig. 5-51: Terminal body weight loss in xenograft treatment groups</i> _____	349
<i>Fig. 5-52: Expression Analysis of ANGIOPOIETIN family members in ALL cell lines</i> _____	350
<i>Fig. 5-53: Normalised ANGPTL2 probe signal values in samples depleted of MLL/AF4</i> _____	351
<i>Fig. 5-54: ANGPTL2 expression analysis by qRT-PCR in MLL/AF4 depleted SEM cells</i> _____	352
<i>Fig. 5-55: ANGPTL2 expression analysis by qRT-PCR in MLL/AF4 depleted primary patient blasts.</i> _____	353
<i>Fig. 5-56: ANGPTL2 expression analysis in purified and fractioned CB cell populations</i> _____	354
<i>Fig. 5-57: ANGPT2 expression analysis by qRT-PCR in MLL/AF4 depleted SEM cells</i> _____	355
<i>Fig. 5-58: ANGPT2 expression analysis by qRT-PCR in MLL/AF4 depleted primary patient blasts.</i> _____	356
<i>Fig. 5-59: ANGPT2 expression analysis in purified and fractioned CB cell populations</i> _____	357
<i>Fig. 9-1: Vector map of the lentiviral pCMVdeltaR8.91 packaging plasmid</i> <i>(http://tronolab.epfl.ch/)</i> _____	421
<i>Fig. 9-2: Vector map of the lentiviral envelope plasmid pMD2.G</i> (http://tronolab.epfl.ch/) _____	422
<i>Fig. 9-3: Vector map of the lentiviral expression vector pTRIPZ-shRNA</i> (www.openbiosystems.com) _____	423

List of Abbreviations

%	Percent
µg	Microgram
µl	Microlitre
µM	Micromolar
aa	Amino acid
APC	Allophycocyanin
APS	Ammonium persulfate
CD	Cluster of differentiation
Cy5	Cyanin5
DNA	Deoxyribonucleic acid
EDTA	Ethylenediaminetetraacetic acid
ELISA	Enzyme-linked immunosorbent assay
FACS	Fluorescence-activated cell sorting
FCS	Foetal calf serum
FITC	Fluorescein isothiocyanate
h	Hour
HRP	Horseradish peroxidase
IgG	Immunoglobulin G
M	Molar
mg	Milligram
ml	Millilitre
MLL	Mixed lineage leukaemia
MLLr	Mixed lineage leukaemia-rearranged
mM	Millimolar
nm	Nanometre
nM	Nanomolar
OD	Optical density
PAGE	Polyacrylamide gel electrophoresis
PBS	Phosphate buffered saline

PCR	Polymerase chain reaction
Pe-Cy7	Phycoerythrin-Cyanin7
PerCP-Cy5.5	Peridinin Chlorophyll Protein Complex -Cyanin 5.5
PI	Propidium iodide
PVDF	Poly-1,1-difluoroethene
qRT-PCR	Real-time reverse transcription polymerase chain reaction
RNA	Ribonucleic acid
RT-PCR	Reverse transcription polymerase chain reaction
SDS	Sodium dodecyl sulphate
siRNA	Small interfering RNA
TAE	Tris(hydroxymethyl)aminomethane-acetate-ethvlenediaminetetraacetic acid
TBE	Tris(hydroxymethyl)aminomethane-borate-ethvlenediaminetetraacetic acid
TEMED	N,N,N',N'-tetramethyl-ethane-1,2-diamine
Tris	Tris(hydroxymethyl)aminomethane
v/v	volume per volume
w/v	weight per volume

Table of contents

1. Introduction	1
1.1 Acute Lymphoblastic Leukaemia – a Short Introduction	2
1.1.1 ALL - one disease with diverse classifications	3
1.2 Childhood BCP-ALL – Cytogenetics and Clinical Aspects	6
1.2.1 Cytogenetic subgroups, incidence and clinical outcome	6
1.2.2 Disease aetiology	10
1.2.3 Childhood ALL - Clinical Aspects and Treatment	11
1.2.3.1 Brief outline of course of chemotherapy	12
1.2.4 Infant ALL –a distinct ALL category	14
1.2.5 Intensive chemotherapy can cause late adverse effects	16
1.3 t(4;11)-positive ALL – an Epigenetically Driven Malignancy?	17
1.3.1 MLL – a histone methyltransferase disrupted in leukaemia: structure-function relationship	18
1.3.2 MLL – a Master Regulator of Haematopoiesis and HSC Homeostasis	21
1.3.3 MLL regulates cell cycle progression and is implicated in DNA damage response	22
1.3.4 AF4 – a Transcription Elongation Factor and Epigenetic Mediator	23
1.3.5 T(4;11)-positive ALL: a Complex Pathobiology	24
1.3.5.1 MLL/AF4 vs. AF4/MLL vs. MLL/AF4 & AF4/MLL- who’s the bad guy?	24
1.3.5.2 T(4;11)-ALL shows major deregulation of epigenetic pathways	26
1.3.5.3 T(4;11)-positive ALL is associated with glucocorticoid-resistance	28
1.3.5.4 Specific gene expression signatures contribute to the immortalisation of t(4;11)-positive ALL	28
1.3.5.5 MLL/AF4 perturbs cell cycle regulation	29
1.4 Aims of the thesis	30
2. Material & Methods	32
2.1 General Materials	33
2.1.1 General Chemicals	33
2.1.2 Oligonucleotides	33
2.1.3 Antibodies	36
2.1.4 General equipment	38
2.1.4.1 Centrifuges	38
2.1.4.2 Thermocycler	38
2.1.4.3 Flow cytometer	38
2.1.4.4 Spectrophotometer	38
2.1.4.5 Electroporator	38

2.2	Tissue culture techniques	39
2.2.1	Freezing and thawing of viable cell lines	39
2.2.2	Freezing and thawing of viable patient material	39
2.2.3	Culture of cell lines	40
2.2.3.1	SEM (DSMZ No. ACC 546)	40
2.2.3.2	RS4;11 (DSMZ No. ACC 508)	40
2.2.3.3	MV4;11 (DSMZ No. ACC 102)	40
2.2.3.4	NALM6 (DSMZ No. ACC 128)	41
2.2.3.5	PreB-697 (DSMZ No. ACC 42)	41
2.2.3.6	REH (DSMZ No. ACC 22)	41
2.2.3.7	Kasumi-1 (DSMZ No. ACC 220)	42
2.2.3.8	K562 (DSMZ No. ACC 10)	42
2.2.3.9	TK-6 (ATCC No. CRL-8015)	42
2.2.3.10	MUTZ5 (DSMZ No. ACC 490)	42
2.2.3.11	MHH-CALL4 (DSMZ No. ACC 337)	43
2.2.3.12	SK-HEP (ACC 141)	43
2.2.3.13	293T (ACC 635)	43
2.2.4	Cell number determination using the Trypan Blue exclusion assay	44
2.2.5	Preparation of duplexed siRNA solutions	46
2.2.6	Electroporation of leukaemic cell lines with siRNA	46
2.2.7	Drug and Inhibitor Treatment	47
2.2.7.1	zVAD-FMK	47
2.2.7.2	Necrostatin-1 (NEC-1)	47
2.2.7.3	α -TNF (Infliximab)	48
2.2.7.4	Dexamethasone	48
2.2.7.5	recombinant human ANGPT1	49
2.2.8	Determination of cell viability by the MTT assay	49
2.2.9	Determination of cell viability by the CellTiter-Glo® assay	50
2.2.10	Caspase-Glo® Caspase-3/-7 Activity Assay	51
2.2.11	Lentivirus particle production in the packaging cell line 293T using the CaPO ₄ transfection method	52
2.2.12	Harvest and concentration of lentiviral particles	53
2.2.13	Lentiviral transduction of acute leukaemia cell lines by spinoculation	53
2.2.14	Selection of stably transduced cells using puromycin	54
2.2.15	Induction of shRNA expression with Doxycycline	54
2.3	Flow cytometry techniques	54
2.3.1	Cell cycle analysis	54
2.3.2	Measurement of cells with endogenous fluorescence	55

2.3.3	Expression analysis of membrane-bound TNF and its cognate receptors TNFR1 and TNFR2 by flow cytometry	56
2.3.4	Multi-colour flow cytometry	57
2.3.4.1	Cell death determination via ANNEXIN V-FITC/PI-staining	57
2.3.4.2	Five-colour flow cytometry analysis	58
2.4	Molecular Biology Techniques	60
2.4.1	RNA purification and Concomitant Protein Isolation Using the QIAGEN RNeasy Mini Kit	60
2.4.2	RNA Concentration Determination	61
2.4.3	RNA Integrity Measurement	61
2.4.4	cDNA Synthesis	61
2.4.5	Real-time RT-PCR (qRT-PCR) using SyBr-Green	62
2.4.5.1	$\Delta\Delta\text{Ct}$ Method	64
2.4.5.2	ΔCt -Method	65
2.4.6	RT-PCR	65
2.4.7	DNA-Polyacrylamid gel electrophoresis (DNA-PAGE)	66
2.4.8	Agarose gel electrophoresis	67
2.4.9	Isolation of endotoxin-free plasmids for mammalian transfection	67
2.5	Proteomic Methods	68
2.5.1	Protein Isolation	68
2.5.2	SDS-PAGE	68
2.5.3	Immunoblotting	69
2.5.3.1	Luminol-based detection using Immobilon™ Western Chemiluminiscent HRP Substrate	70
2.5.3.2	Luminol-based detection using SuperSignal West Dura Chemiluminiscent Substrate	70
2.5.4	Enzyme-linked immunosorbent assay (ELISA) for ANGPT1 detection in cell culture supernatant	71
2.6	In vivo Techniques	71
2.6.1	Xenotransplantation of leukaemic cell lines by intrafemoral injection (performed by Mr. M. Batey)	71
2.6.2	<i>In vivo</i> bioluminescence imaging (performed by Mr. M. Batey)	72
2.6.3	Necropsy and harvest of material	72
2.7	Bioinformatic Methods	73
2.7.1	Array Analysis	73
2.7.2	Pre-processing of raw data using BeadStudio/GenomeStudio Software packages (Illumina Inc.)	73

2.7.3	Normalisation and differential gene expression analysis using GeneSpring GX 11 software (Agilent Technologies UK Ltd)	73
2.7.4	Comparison analysis using R	74
2.7.5	Ingenuity Pathway Analysis	74
2.7.6	Gene Set Enrichment Analysis (GSEA)	75
2.7.7	Heat map generation using GenePattern	75
2.8	Statistical Analysis	75
3.	<i>The role of MLL/AF4 in leukaemic maintenance</i>	76
3.1	RNAi-mediated Depletion of MLL/AF4 Affects Cell Proliferation and Viability	77
3.1.1	siRNA-mediated ablation of <i>MLL/AF4</i> in t(4;11)-positive ALL cells	77
3.1.2	Effects of siMLL/AF4 on the MLL and AF4 wild-type genes	83
3.1.3	MLL/AF4 depletion is associated with a phenotype	90
3.2	Gene Expression Profiling of SEM cells depleted of MLL/AF4	95
3.2.1	Biological QC analysis of array samples	97
3.2.2	Array analysis	99
3.2.3	Functional analysis of the MLL/AF4 gene signature	106
3.2.3.1	IPA analysis of the MLL/AF4 signature at TP1	106
3.2.3.2	IPA analysis of the MLL/AF4 signature A at TP2	114
3.2.4	Gene Set Enrichment Analysis of a MLL/AF4 Core Signature	123
3.2.5	Comparison Analysis with Published <i>MLL/AF4</i> Target Gene Data Sets	127
3.3	GEP of MLL/AF4-Depleted SEM CELLS at Time Point TP3	132
3.3.1.1	Analysis of MLL/AF4 signature at TP3 using Ingenuity Pathway Analysis	138
3.3.2	Comparison Analyses	144
3.4	Validation of Biologically Interesting MLL/AF4 Signature Genes in Vitro	148
3.4.1	<i>MLL/AF4</i> depletion and mitogenic signalling	148
3.4.2	MLL/AF4 depletion down-regulates factors associated with stemness and self-renewal	152
3.4.2.1	MLL/AF4 depletion results in HOXA gene down-regulation	153
3.4.2.2	MLL/AF4 depletion results in decreased TERT expression	156
3.4.2.3	MLL/AF4 depletion results in down-regulation of the chromatin remodelling factor HMGA2, but not PYGO2 and DNMT3B	157
3.4.3	<i>MLL/AF4</i> depletion induces genes associated with autophagy and cell death	162
3.4.4	Correlation of Array and Q-RT-PCR Results	167
3.5	Conclusions	169

3.6	Discussion	170
3.6.1	MLL/AF4 signature shows differential regulation of factors linked to apoptosis and proliferation	171
3.6.1.1	A putative role of NOXA and oxidative stress in MLL/AF4-depletion mediated apoptosis	171
3.6.1.2	The proapoptotic gene ANXA1 is induced in response to MLL/AF4	172
3.6.1.3	The autophagy-related gene GABARAPL1 is induced in response to MLL/AF4-depletion	174
3.6.2	MLL/AF4 depletion perturbs mitogenic signalling	174
3.6.3	MLL/AF4 depletion results in decreased expression of stemness-associated genes	176
3.6.4	MLL/AF4 signature has only a limited overlap across the time point and with published data	179
4.	<i>t(4;11)-positive Cells Display Oncogenic Addiction to MLL/AF4</i>	181
4.1	Combined Treatment of SEM Cells with siMLL/AF4 and the pan-Caspase Inhibitor zVAD-FMK	182
4.1.1	zVAD dosage titration	184
4.1.2	zVAD inhibits caspase-dependent apoptosis activation, but does not abrogate cell-death	188
4.2	Gene Expression Profiling of SEM cells depleted of MLL/AF4 and Cultured with zVAD	196
4.2.1	Biological QC analysis of array samples	196
4.2.2	Functional analysis of the zVAD gene signature	205
4.2.2.1	Analysis of the zVAD signature using Ingenuity Pathway Analysis	205
4.2.2.2	Gene Set Enrichment Analysis	218
4.2.3	Comparison of the zVAD signature with the MLL/AF4 signature	228
4.3	The zVAD Signature Comprises Key Factors of the Novel Programmed Cell Pathway Necroptosis	235
4.4	Necroptosis Inhibitor Studies	247
4.5	Conclusion	251
4.6	Discussion	252
4.6.1	Suppression of necroptosis key processes fail to rescue the cell death phenotype	256
4.6.2	Intersection analysis of the zVAD and MLL/AF4 signature reveals a core gene set comprising cell death and stemness-associated factors	258
5.	<i>ANGIOPOIETIN-1, a novel factor implicated in t(4;11)-positive ALL</i>	261

5.1	ANGPT1 expression is dependent on the MLL/AF4 status of the t(4;11)-positive ALL cell	262
5.1.1	Analysis of MLL/AF4-dependent ANGPT1 expression regulation in the t(4;11)-positive ALL cell line SEM	262
5.1.2	Analysis of MLL/AF4-dependent ANGPT1 expression regulation in t(4;11)-positive ALL patient blasts	269
5.2	ANGPT1 is overexpressed in MLL-rearranged ALL	271
5.2.1	ANGPT1 expression levels in normal blood cells from healthy donors	271
5.2.2	ANGPT1 expression in acute leukaemia cell lines	274
5.2.3	ANGPT1 expression in ALL patients	277
5.3	Correlating ANGPT1 expression with prognostic factors	285
5.3.1	ANGPT1 expression correlates with clinical parameters	285
5.3.2	Correlation analysis of ANGPT1 expression with biological prognostic factors	290
5.3.3	ANGPT1 secretion in t(4;11)-positive ALL patients	295
5.4	Functional Analysis of ANGPT1 in t(4;11)-positive ALL in Vitro	296
5.4.1	Expression Analyses of ANGPT1 Receptors in t(4;11)-positive ALL	296
5.4.2	ANGPT1 Depletion in the t(4;11)-positive Cell Line SEM Impinges on Proliferation and Reduces Cell Viability	301
5.5	Whole Genome Expression Profiling of SEM cells depleted of ANGPT1	311
5.5.1	Functional categorisation of gene expression profiling data using Ingenuity Pathway Analysis	318
5.5.1.1	Functional analysis of gene signature A	318
5.5.1.2	Functional analysis of gene signature B	327
5.5.2	ANGPT1 Depletion Does Not Sensitise the t(4;11)-positive Cell Line SEM Towards the Glucocorticoid Dexamethasone	333
5.6	ANGPT1 Depletion Affects Leukaemogenesis In Vivo	336
5.6.1	Establishing an inducible shRNA expression system in SEM-SLIEW cells	336
5.6.2	Effects of RNAi-mediated ANGPT1 knock-down in vivo	340
5.7	Expression Analysis of Other ANGIOPOIETIN Gene Family Members and Angiogenic Factors in t(4;11)-positive ALL and their regulation by MLL/AF4	350
5.8	Conclusions	358
5.9	Discussion – ANGPT1 is overexpressed in MLLr-ALL and regulated in a fusion gene-dependent manner	359
6.	Concluding Remarks	369

6.1.1	MLL/AF4 depletion perturbs leukaemic cell survival	369
6.1.2	MLL/AF4 depletion results in down-regulation of stemness-associated markers	371
7.	<i>Future work</i>	373
8.	<i>Bibliography</i>	375
9.	<i>Appendix I</i>	420
9.1	Supplementary Data	421
9.1.1	Vector maps	421
9.2	R-scripts	424
9.2.1	*Venn*-Script for intersection analysis of data sets	424
9.2.2	*Extraction* Script in order to extract expression data of a specific entity set from a parental file	425
9.2.3	DVD with array metrics and IPA results	425
10.	<i>Appendix II</i>	426
10.1	Curriculum Vitae	427
10.2	Publications	429

1. Introduction

1.1 ACUTE LYMPHOBLASTIC LEUKAEMIA – A SHORT INTRODUCTION

Acute lymphoblastic leukaemia (ALL) refers to a malignancy of the haematologic tissue, involving cells of lymphopoietic lineage. It is a clinically and biologically heterogeneous disease with a common cellular aetiology; haematopoietic progenitors acquire single or multiple genetic lesions, which subsequently confer archetypical oncogenic properties onto them, resulting in their transformation into malignant cancer cells. Common features of leukaemic cells are an increased resistance to cell death and growth inhibitory signals, augmented proliferative capacity and self-renewal capability¹⁻². Normal lymphopoietic differentiation is disrupted in these cells, resulting in the generation of immature and non-functional lymphocytes, referred to as leukaemic blasts. Uncontrolled clonal expansion of these transformed cells in the bone marrow (BM) perturbs normal haematopoiesis, hindering production of functional blood cells and resulting in BM failure. Furthermore, this is accompanied by egress of the leukaemic blasts from the BM into the peripheral blood (PB), frequently resulting in a potentially life-threatening high white blood cell count (WBC). Concomitantly, these blasts can also infiltrate extramedullary tissues such as, e.g., liver, spleen, lymph nodes and the central nervous system (CNS). In ALL, this disease pattern emerges quickly; at first, patients suffering from ALL display diffuse symptoms of general unwellness, decreased fitness, bruising, anaemia, fever and high susceptibility to infections, which all can be directly linked to the disrupted blood cell generation in the BM. In addition, infiltration and accumulation of the blasts in extramedullary organs results in painful enlargement which may compromise normal organ function; hepato- and splenomegaly are often present at diagnosis¹.

1.1.1 ALL - one disease with diverse classifications

ALL is an umbrella term that encompasses a disease of highly heterogeneous presentation; as a result, ALL is subdivided according to several criteria, and these subgroups describe distinct clinical and biological entities:

Age at diagnosis: The first and foremost category is age at presentation, which defines the disease as infant (<12 months), paediatric (1- 18 years) and adult ALL (>18 years). There is an ambiguous stage concerning late adolescent and young adult ALL patients (15-25 years), where classification and treatment often occurs according to the patient referral to either a paediatric or an adult oncologist; indeed some clinical studies define childhood ALL and concomitant eligibility for a trial until the age of 25²⁻⁴.

Immunophenotype: The main biologic categorisation occurs in relation to the haematopoietic cell lineage of the blasts, identified by expression analysis of the cluster of differentiation (CD) immunophenotype. The two main categories are T-cell-precursor (TCP) and B-cell precursor (BCP) ALL; characterised by T-lineage (CD3) and B-lineage CD markers (CD19, CyCD79), respectively⁵. Much rarer is a biphenotypic acute leukaemia (BAL), where lymphoid and myeloid or B- and T- cell markers are coexpressed.

Further immunophenotyping allows subclassification of the ALL subtypes according to the combinatorial expression of specific CD markers, referred to as leukaemia-associated immunophenotype (LAIP). The LAIP reflects the differentiation status of the blasts, *i.e.*, at which stage the of normal haematopoiesis the maturation arrest occurred (see fig. 1-1)⁵.

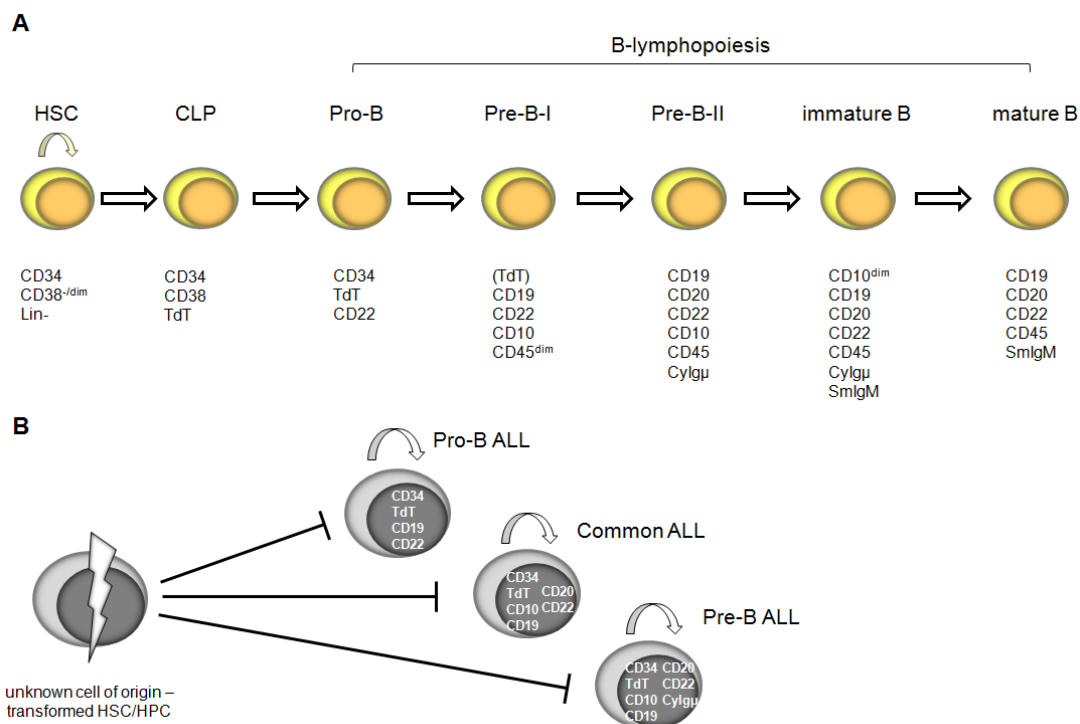


Fig. 1-1: Cluster of Differentiation (CD) marker expression in normal and malignant B-lymphopoiesis⁵⁻⁷

Normal haematopoiesis in the BM is a hierarchical and linear event; uncommitted, lineage marker-negative (lin-), multipotent haematopoietic stem cells (HSCs) give rise to haematopoietic progenitors (HPC). In normal lymphopoiesis, HSCs differentiate into committed lymphoid progenitors (CLP), losing their self-renewal ability. This CLP then mature into functional B-cells in a sequential differentiation process, which comprises 5 main steps: pro-B, pre-B-I, pre-B-II, immature B- and, eventually, mature B-cells. Each differentiation stage is characterised by the differential expression of specific CD markers, Terminal Deoxynucleotidyl Transferase (TdT), as well as cytoplasmic (Cy) or surface membrane (Sm) immunoglobulins (Ig) (A). In malignant B-lymphopoiesis, the genetic lesion occurs in the HSC/HPC compartment, and results in differentiation arrest at different stages. In addition, the leukaemic cells retain an aberrant self-renewal capability, also referred to as “stemness”. According to the expression of LAIPs by the blasts, BCP-ALL is classified as pro-B, common or pre-B ALL.

Karyotype/cytogenetic subtype: A hallmark of leukaemia in general is the recurrent incidence of specific cytogenetic lesions, which can be numerical or structural in nature. In ALL, numerical aberrancies of a normal karyotype can be focal copy number alterations (CNA), such as intrachromosomal amplification, internal tandem duplications (ITD), as well as mono- or biallelic deletions of specific gene *loci*. Other CNA affect cellular ploidy, resulting in gain or loss of one or more chromosomes.

Structural abnormalities are recurring inter- and intra chromosomal rearrangements between specific loci, resulting in derivative (der) chromosomes, frequently coding for fusion oncogenes. Other structural lesions apart from rearrangements can be partial loss of specific chromosomes, for instance deletion of the p or q arm [del(p)/del(q)].

Both numerical and structural genetic lesions represent the cytogenetic subtype of the disease and define clinical entities with specific underlying pathobiologies; some are predictors of outcome, and as such, the cytogenetic phenotype is used for therapy stratification of ALL patients⁸⁻¹⁰.

Morphology: Historically, ALL blasts have been categorised according to morphologic parameters using the French-American-British (FAB) - classification system. Cell size, nucleus to cytoplasm (N/C) ratio, appearance of nucleoli and the shape of the nuclear membrane are assessed and assigned a specific value; the final sum determining the cytomorphological classification of the blasts¹.

- L1-ALL: small, uniform blasts with high N/C ratio, undefined nucleolus and smooth nuclear membrane
- L2-ALL: large varied blasts with varying N/C ratio, distinct multiple nucleoli and irregular nuclear shape
- L3-ALL: large varied blasts with low N/C ratio, vacuolated cytoplasm as well as distinct nucleoli.

However, morphological classification has been superseded in favour of the other categories¹¹.

1.2 CHILDHOOD BCP-ALL – CYTOGENETICS AND CLINICAL ASPECTS

Acute lymphoblastic leukaemia is the most common childhood cancer, accounting for approximately one quarter of the malignant diagnoses between the ages of 1 and 18 years, with a median age at diagnosis of 4-5 years⁴. Nearly nine tenths of these ALL cases involve the B-cell lineage⁹ (fig. 1-2). Like all leukaemia subtypes, childhood BCP-ALL is characterised by recurring cytogenetic aberrations inherent of the malignant cell. These acquired somatic mutations define a distinct pathobiology which can vastly differ between the different genotypes. As such, the cytogenetic phenotypes carry important prognostic power and contribute to the stratification of patients in regards to risk of treatment failure, facilitating identification of both patients requiring more intensive chemotherapy and those who might be eligible for a reduced treatment.

From this section on, if not stated differently, ALL refers exclusively to BCP-ALL.

1.2.1 Cytogenetic subgroups, incidence and clinical outcome

There are several dozen recurring cytogenetic abnormalities in childhood ALL¹², but only a few have a sufficiently high incidence – or particularly unfavourable outcome- to be of clinical relevance. The most common cytogenetic subgroups in ALL are patients with high hyperdiploidy (HeH), with an leukaemic karyotype of >50 chromosomes, occurring in nearly 40% of the cases, and patients carrying the translocation $t(12;21)(p12;q22)$, coding for the *TEL/AML1* fusion gene, with an incidence of 25%. Both of these subgroups is associated with a highly favourable prognosis of >92% survival¹³. Another major cytogenetic subgroup is marked by rearrangements involving the gene locus 11q23, which encodes the *MLL (Mixed Lineage Leukaemia)* gene¹⁴, occurring in

approximately 2-8% of the cases^{8-9,13}. MLL-rearranged (MLLr) ALL is characterised by its promiscuity of translocation partners; to date, over 60 different gene loci have been described in literature¹⁵. However, by far the most common one involves the *AF4* (*ALL-1 fused to chromosome 4*) gene on locus 4q21. This results in t(4;11)(q21;23), which codes for the *MLL/AF4* fusion oncogene, and represents about 30-50% of the MLLr BCP-ALL cases¹⁵. MLLr BCP-ALL *per se* is associated with a poor outcome and is considered a cytogenetic subgroup at high risk of treatment failure^{3,13}. A more detailed review of the associated pathobiology, particularly of t(4;11)-positive ALL, will be discussed in section 1.3.5.

Another important chromosomal aberration in BCP-ALL is the translocation event t(1;17)(q23;p13), which generates the *E2A/PBX1* fusion gene¹⁶. The incidence is approximately 4%, it is considered intermediate risk associated with an average prognosis¹³.

One of the most difficult to treat ALL subgroups is Ph⁺ ALL, carrying the translocation t(9;22)(q34;q11). The resulting derived chromosome is historically referred to as Philadelphia (Ph) chromosome, and encodes the chimaerical oncogene *BCR/ABL1*¹⁷. Although very rare, with an incidence of approximately 2%, it is of high clinical relevance, describing a patient cohort at very high-risk of relapse¹³.

In the last five years, new major cytogenetic ALL subcategories associated with outcome have been discovered, ALL with intrachromosomal amplification of chromosome 21 (iAMP21)¹⁸⁻¹⁹, and ALL with up-regulation of the gene *CRLF2* (*CRLF2-d*)²⁰⁻²¹.

In iAMP21-positive ALL, the amplified region on chromosome 21 involves *RUNX1*, as well as gene *loci* within the Down-Syndrome associated region²². Prior to classification, the iAMP21 subgroup was previously linked to poor prognosis. Identification of this abnormality and its inherent prognostic value resulted in administration of an intensive chemotherapy regimen to this patient cohort, as well as consideration of haematopoietic stem cell transplantation^{3,23};

current data analysis is still outstanding, the new treatment regimen appears to have improved outcome (personal communication with Prof. C. Harrison).

In the cytogenetic subgroup characterised by *CRLF2* overexpression, this deregulation has two distinct cytogenetic lesions as underlying mechanisms, a translocation of the *CRLF2* gene with the *IGH@* locus, or a focal deletion upstream of *CRLF2*. Both mechanisms result in juxtaposition of the *CRLF2* gene to powerful promoters or transcriptional enhancers, which subsequently drive the gene overexpression²⁰⁻²¹. *CRLF2* deregulation occurs in approximately 6% of childhood ALL; in regards to its prognostic significance, there is still controversy, as it is associated with increased risk of relapse, but intermediate-to high-risk according to overall survival²⁴⁻²⁵.

Another novel subgroup, termed BCR/ABL-like ALL, was determined according to gene expression profile (GEP) classifiers. The GEP of this subgroup showed great similarity to the ones from Ph+ ALL patients, and BCR/ABL-like ALL patients had a comparably poor response to treatment. Analysis of this previously unclassified patient group revealed that in contrast to most other ALL cases, BCR/ABL-like ALL is not characterised by a single major chromosomal abnormality, but by the acquisition of one or more focal deletions in a particular subset of genes associated with haematopoiesis, such as *PAX5*, *IKZF1*, *VPREB1*, *E2A* and *EBF1*, amongst others. These genetic lesions were also present to a certain extent in BCR/ABL-positive ALL patients, which might indicate an inherent driver mutation-like quality causative and supportive of malignant transformation²⁶⁻²⁷.

One of the rarest cytogenetic subgroup but nevertheless with a major clinical implication is t(17;19)(q22;p13), which codes for the *E2A/HLF* fusion gene. It occurs at a frequency of 0.1%; however, overall survival is 0%. Consequently, presence of *E2A/HLF* is one of the high-risk cytogenetic features employed for treatment stratification³.

The scheme in fig. 1-2 illustrates the frequency of the differing BCP-ALL subtypes in children.

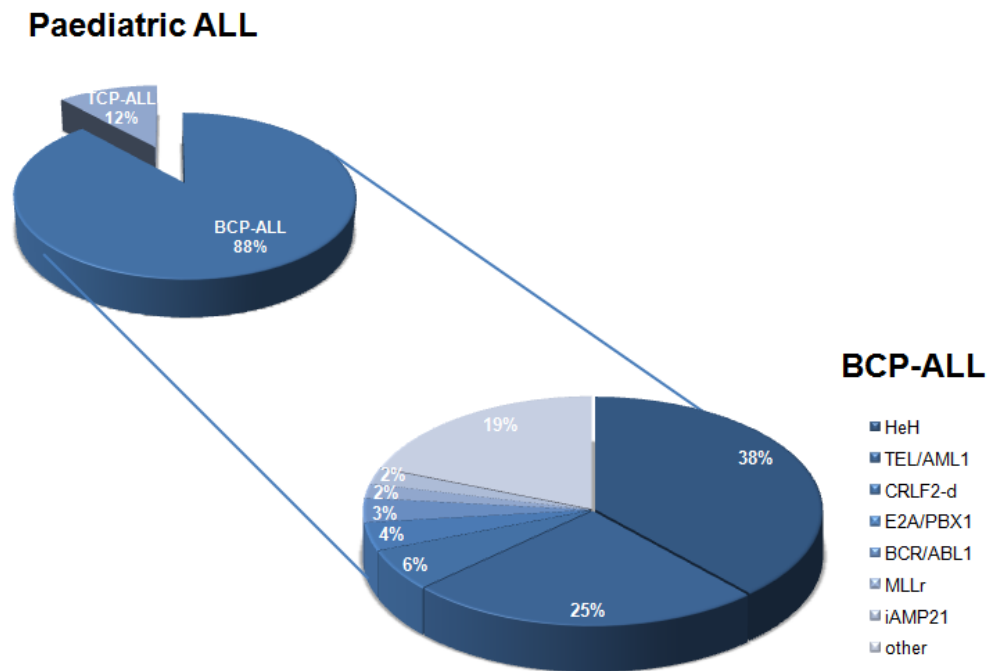


Fig. 1-2: Incidence of different ALL subtypes in childhood ALL^{9,13,24}

The vast majority of ALL cases in children is BCP-ALL, comprising nearly 90%. These subgroup can be further subdivided according to the cytogenetic phenotype; the most frequent ones are high hyperdiploidy (HeH), TEL/*AML1*-positive ALL, ALL with *CRLF2* overexpression (CRLF2-d); MLL-rearranged ALL (MLLr), Ph+ ALL (BCR/ABL), as well as ALL with the t(1;19) rearrangement (E2A/PBX1) and intrachromosomal amplification of chromosome 21 (iAMP21).

1.2.2 Disease aetiology

ALL disease aetiology is unknown, bar rare cases where there is genetic predisposition, *i.e.*, children with Down-syndrome²⁸⁻³⁰, the acquisition of the genetic mutations and development of the disease is idiopathic. Studies in monozygotic twins with leukaemia as well as analyses of Guthrie cards (neonatal blood spots) revealed evidence of a pre-natal origin of childhood ALL, with the leukaemia-specific genetic lesions arising *in utero* during foetal haematopoiesis³¹⁻³⁶. Interestingly, most of these initial cytogenetic abnormalities are not sufficient to cause overt leukaemia, and require secondary genetic hits for full transformation^{34,37,38}. These primary lesions result in non-malignant preleukaemic clones, which predispose the cell to the acquisition of further mutations. A current hypothesis indicates that de-regulated response of these preleukaemic cells to immunity-mediated modulation of haematopoiesis in the BM, *i.e.* due to infections, results in transformation and overt leukaemia in a small subset of the population. The vast majority of the populace with pre-leukaemic clones however never develops the disease, and the prevalence of pre-leukaemic clones is lost with age.

Over the years, a few pre-natal and peri-natal exogenous factors have been correlated with leukaemogenesis in children, such as a high birth weight³⁰ and maternal alcohol and elevated coffee consumption during pregnancy³⁹. Interestingly, a maternal diet rich in isoflavonoids, which are natural topoisomerase-II inhibitors and induce DNA cleavage as well as MLL rearrangements *in vitro*⁴⁰⁻⁴¹, were found to be positively associated with infant AML, but not ALL⁴².

1.2.3 Childhood ALL - Clinical Aspects and Treatment

Once a “certain death” diagnosis, the overall survival in children with ALL has improved in leaps and bounds over the last decades, reaching now a cure rate of over 85%⁴³⁻⁴⁶. Apart from the use of aggressive chemotherapy, this progress can be largely attributed to improved risk stratification; clinical features at diagnosis such as age, WBC as well as the karyotype/cytogenetic phenotype are strong prognostic factors and used to adjust treatment intensity. However, although survival is very high, this varies vastly within to the cytogenetic subgroups; patients with HeH ALL or carrying the t(12;21) rearrangement have a favourable prognosis of over 90% overall survival, in contrast, children with either Ph+ ALL, positive for *MLL/AF4* or *E2A/HLF* have a poorer outcome, with survival ranging from 0-60%¹³.

Currently, three major risk categories are established in ALL: low-/ standard-risk ALL (SR), intermediate risk (IR) and high-risk (HR) ALL. Factors associated with favourable outcome are age at presentation between 1 and 10 years and a low WBC (<50x10⁹ cell/L). In contrast, adverse clinical characteristics in paediatric ALL are considered anyone of the following: age at presentation over 10 years, a WBC >50x10⁹ cells/L, CNS involvement, slow early response to induction therapy, as well as presence of an unfavourable karyotype. For instance, the Ph+ chromosome, rearrangements of the *MLL* gene locus, t(17;19)(q22;p13), iAMP21 or hypodiploidy (n<44 chromosomes) are considered unfavourable cytogenetic subgroups linked to increased risk of treatment failure, and thus defined as HR-ALL. IR-ALL patients are characterised by being either older than 10 years at diagnosis, or having a high WBC. Other essential stratification parameters are determined during early treatment, such as delayed or refractory response to chemotherapy and the presence of minimal residual disease (MRD)³. MRD refers to the persistence of very low numbers of leukaemic cells in the BM after induction treatment. Analysis for leukaemia cell-specific genetic markers such as fusion genes, characteristic rearrangements of the *Ig* (*immunoglobulin*) or the *TCR* (*T-cell receptor*) locus occur on a molecular level using PCR-based methods⁴⁷. In addition, patient BM cells are immunophenotyped and characterised for a LAIP

by multi-colour flow cytometry. These techniques allow detection of as little as 1 leukaemic blast in 10,000 -100,000 cells. A blast frequency of $>10^{-4}$ at specific time points during treatment denotes presence of therapy-resistant blasts, enabling identification of patients at high risk of relapse; even if at diagnosis there were no other apparent risk factors present. MRD is a measure of *in vivo* response a strong outcome predictor, thus initial risk stratification and treatment regimen is corrected appropriately in concordance with the MRD scores. Moreover, MRD negativity strongly predicts event-free survival. Interestingly, patients with HR-ALL cytogenetics and/or poor response to induction therapy sometimes present with low MRD scores, and this is associated with increased survival; in these cases, the MRD diagnosis supersedes the initial risk stratification, and has proven to be a more powerful predictive measurement for outcome⁴⁸. However, whether the HR-ALL subgroups with favourable MRD would be permissive for a reduction of treatment intensity remains as of yet unclear.

1.2.3.1 Brief outline of course of chemotherapy

Current treatment strategy for ALL remains intensive cytotoxic chemotherapy spanning several years. The course of treatment is subdivided into different stages, each involving intense multi-drug regimens with different combinations of chemotherapeutic agents. The treatment protocol of the ongoing paediatric ALL trial UKALL-2003 is briefly outlined as follows³, this treatment is highly comparable to other international treatment strategies⁴⁹.

The first chemotherapy phase is induction of complete remission (CR), defined by a blast burden of less than 5% in the BM. Treatment in this phase aims at clearing blasts from the blood circulation, the BM, and other affected tissue. This is achieved by the combinatorial use of glucocorticoids such as prednisolone and/or dexamethasone, along with the anti-metabolite drugs methotrexate, L-asparaginase, 6-mercaptopurine and the mitotic inhibitor vincristine. For IR-

and HR-ALL, current protocols include the use of genotoxic anthracyclines such as daunorubicine.

Induction is immediately followed by the consolidation phase, which targets the remaining leukaemic cells within the body. This course of treatment is risk-adapted according to both clinical prognostic factors at presentation and initial response, in particular the MRD scores. The consolidation of remission phase consists of several rounds of intensification and CNS-directed therapy, which comprise the chemotherapeutic drugs received during induction, as well as treatment with genotoxic agents such as the DNA alkylating drug cyclophosphamide, the anthracycline doxorubicine and the nucleoside analogue cytarabine. Dosages and administration frequencies vary in respect to the risk stratification of the patient.

Although infiltration of the CNS does not frequently occur in childhood ALL, the CNS remains a potential reservoir of leukaemic cells as well as a site of relapse, due to the difficulty of chemotherapeutic agent to cross the blood-brain barrier. In order to deplete leukaemic blasts present in the CNS and to prevent relapse in this site, CNS prophylaxis therapy is given during the consolidation phase, consisting of intrathecal administration of high-dose methotrexate. In cases of persistent CNS disease, patients also undergo cranial irradiation.

At the end of the consolidation phase, MRD scores are assessed; disease-free patients go on to the maintenance phase, lasting up to two years for girls and three years for boys. This phase consists of low dose drug treatment with the antimetabolite 6-mercaptopurine and methotrexate, combined with monthly pulses cycles of low dose of glucocorticoids and vincristine, as well as ongoing CNS prophylaxis with intrathecal methotrexate every three months. In contrast, patients with refractory disease at the end of the consolidation phase, experiencing relapse or with unfavourable cytogenetics at very high-risk of relapse, may be eligible for a haematopoietic stem cell transplant⁵⁰.

In addition to conventional chemotherapy, contemporary treatment strategies include novel targeted approaches based on subtype-specific pathobiology, i.e.,

the use of the tyrosine kinase inhibitors imatinib or its close homologue dasatinib in *BCR/ABL*-positive ALL⁵¹, or FLT3 inhibitors for MLL-rearranged ALL⁵². In adult ALL, the use of immunotherapy is being investigated in clinical trials; antibodies targeting leukaemia-specific epitopes are employed, such as Rituximab, which recognises CD20, a cell surface marker expressed on over half of the adult ALL patients⁵³. This rationale can be potentially extended to paediatric ALL.

1.2.4 Infant ALL –a distinct ALL category

Infant acute lymphoblastic leukaemia (ALL) is a disease biologically and clinically distinct from childhood ALL and can be cytogenetically categorised into two relevant subgroups: infant ALL carrying chromosomal rearrangements in the *MLL* gene on locus 11q23, and infant ALL with a germline *MLL* configuration. While MLLr ALL also occurs in children and adults, the incidence is very low, ranging from 2-8%^{9,13}. This is stark contrast with the recurrence of *MLL* rearrangement in infants, where they represent up to 80% of the overall cases⁵⁴⁻⁵⁶. Comparable to MLLr childhood BCP-ALL, by far the most frequent MLL abnormality in infants is the reciprocal translocation between *MLL* and the gene *AF4* on locus 4q21, resulting in t(4;11)(q21;q23). This aberrancy represents about 50% of the MLLr ALL cases. Other recurring MLL translocations involve the genes *ENL* on 19p13.3, and *AF9* on 9p22, generating t(11;19)(q23;p13.3) and t(9;11)(p22;q23) with an incidence of approximately 20% and 10%, respectively. Rearrangements involving *MLL* and other gene loci occur at a much lower frequency. Another discerning feature of infant ALL is the overrepresentation of ALL blasts with a very immature pro-B immunophenotype, corresponding to approximately 60% of the cases⁵⁴.

Despite many groundbreaking advances in the treatment of paediatric ALL, where an overall cure rate of over >85% has been achieved, MLL-rearranged infant ALL remains associated with poor treatment response and dismal prognosis, with an event-free survival (EFS) of 34-37%⁵⁴⁻⁵⁶. MLL rearrangements are an independent adverse prognostic factor, and characterise

an infant ALL with an aggressive clinical presentation, linked to extreme hyperleukocytosis, CNS involvement and slow response to therapy. Although at the end of the induction therapy complete morphological remission (CR) is achieved in 95% of the cases, initial morphological clearance is slow, and complete molecular response to treatment is not achieved in the majority of the cases. Consequently, infant ALL patients with MLL-rearrangements present with MRD scores in the BM. Relapse on treatment, mainly localised in the BM, remains the primary cause of treatment failure.^{54,57}

In contrast, infant ALL with germline MLL has an outcome comparable to paediatric ALL cases without MLL rearrangement, with an EFS ranging from 60-92%⁵⁴⁻⁵⁶.

Tab. 1-1: Outcome of infant ALL patients in regards to the MLL-status - historical study groups

Clinical trial	Trial period	Patients (n)	MLL status		4-year-EFS	
			MLLr	germline	MLLr	germline
MLL96 ⁵⁶	1995- 1998	55	76%	24%	34%	92%
CCG 1953 ⁵⁵	1996- 2000	115	69%	31%	34%	60%
Interfant-99 ⁵⁴	1999- 2004	482	79%	21%	37%	74%

Although appraising the same clinical features, the parameters applied for risk stratification in infants differ from childhood ALL. Apart from the *MLL* status, age and WBC have been shown to be the most powerful predictors of outcome; children presenting at an age younger than 6 months or with a WBC of $>300 \times 10^9/L$ are considered high-risk patients. Furthermore, CNS involvement and an immature pro-B-like LAIP of the blasts represent adverse prognostic factors⁵⁴. As with paediatric ALL, *in vivo* response during treatment plays an important role in therapy stratification; and infant ALL patients are categorised as high-risk or standard-risk⁵⁷ according to response to induction and blast burden at the end of the induction phase.

Infant ALL chemotherapy is a hybrid protocol based on the childhood ALL treatment regimen, with the addition of reinduction phases after consolidation, derived from AML treatment protocols. Moreover, the nucleoside analogue cytarabine is administered at high doses during all treatment phases together with the conventional multi-drug therapy. CNS prophylactic treatment excludes cranial irradiation. The benefit of allogeneic haematopoietic stem cell transplantation is currently being investigated in the Interfant-06 trial, previous studies showed improvement in outcome of a defined subset of patients⁵⁸.

1.2.5 Intensive chemotherapy can cause late adverse effects

Risk-stratification and the concomitant intensification of treatment protocols has resulted in a substantially improved outcome in paediatric and infant ALL patients. However, this comes at a cost, as the toxicity of the therapies not only results in an increased overall survival, but is also associated with treatment-derived morbidities and other adverse sequelae in long-term survivors. High-dose cytotoxic drug treatment, especially combined with irradiation therapies, cannot only cause secondary neoplasms, but are also linked to endocrinopathies, cardiac damage, obesity and compromised fertility⁵⁹⁻⁶⁰. Particularly in infants and young children, the use of cranial irradiation has shown to be correlated with decreased growth, and more importantly, impaired neurocognitive functions⁶¹; as such, contemporary multi-centre trial protocols in infant ALL do not include irradiation in their treatment strategies anymore⁵⁴.

Thus, the remaining challenges in paediatric and infant ALL therapy are not only increasing overall survival of high-risk subgroups, but the development of improved stratification strategies, aiming towards a more tailored and personalised treatment. This includes, amongst others, recognition of subgroup-specific therapeutic targets as well as single nuclear polymorphism (SNP)-linked pharmacodynamic and -kinetic criteria. Alternative therapies in order to diminish toxicity, as, for instance, immunotherapy or cell-specific delivery of small molecular weight drugs, including therapeutic siRNAs⁶², are being intensively investigated.

1.3 t(4;11)-POSITIVE ALL – AN EPIGENETICALLY DRIVEN MALIGNANCY?

The prevalence of MLL rearrangements in ALL displays a prominent age-related bias; while it is the hallmark of infant ALL, where this subgroup constitutes 70-80% of all cases, the incidence declines sharply in childhood and adult ALL, with a frequency of 2-8% and 5-10%, respectively. MLL rearrangements also belong to the predominant cytogenetic subgroup in therapy-related acute leukaemia (t-AL), particularly if the primary cancer had been treated with topoisomerase-II poisons, such as the epipodophyllotoxins etoposide, teniposide and similar⁶³. Here, the overall frequency was 37% for therapy-related ALL⁶⁴ and 3% (Chicago series) for therapy-related AML. Regardless of age and aetiology, MLLr ALL is associated with an unfavourable outcome, and is considered a high-risk cytogenetic subgroup.

Rearrangements of the MLL locus on 11q23 are recurring cytogenetic lesions in both AML and ALL; a particular feature of MLLr acute leukaemia is the heterogeneity of the translocation partners. To date, reciprocal translocations of the *MLL* gene locus on 11q23 with over 60 different gene loci have been reported¹⁵. The majority of these rearrangements occurs at a low frequency or are single-case reports. However, in MLLr-ALL, three genes constitute up to 80% of the translocations: *AF4* on locus 4q21, resulting in t(4;11)(q21;q23)⁶⁵, *ENL* on 19p13.3, and *AF9* on 9p22, generating t(11;19)(q23;p13.3) and t(9;11)(p22;q23)⁶⁶. By far the most frequent is t(4;11)-positive MLLr ALL, comprising approximately 50% of the MLL rearrangements. It results in two chromosomes derivatives, der11 and der4. The disruptions of the involved gene *loci* occur in intronic regions, fusing the 5'- and 3'- portions of the separate translocation partner genes in frame. Consequently, the rearrangement generates two proteinogenic fusion genes, *MLL/AF4* on der11 and *AF4/MLL* on der4. While the penetrance of *MLL/AF4* is 100%, in approximately 20% of the ALL cases the reciprocal fusion gene *AF4/MLL* is lost⁶⁷; analyses on genomic level have here revealed further complex rearrangements of *AF4/MLL* with other gene loci, resulting in novel fusions⁶⁸.

The fusion genes derived from the t(4;11) rearrangement have altered properties compared to their wild-type counterparts, representing chimaeric oncogenes capable of leukaemic transformation and maintenance of the disease. In the following sections, both wild-type genes will be discussed in detail, and how their disruption and the resulting fusions contribute to the pathobiology of t(4;11)-positive ALL.

1.3.1 MLL - a histone methyltransferase disrupted in leukaemia: structure-function relationship

MLL is encoded on 11q23, comprising a genomic region of approximately 90 kb; it consists of 36 exons, which generate a protein of 3969 amino acids length and a molecular weight of 430 kDa. A characteristic of the *MLL* gene locus is the 8.3 kb long breakpoint cluster region spanning exon number 8 to 13, which is a preferred site for chromosomal disruption, referred to as breakpoint cluster region (BCR)⁶⁹. This genomic region contains topoisomerase II consensus and DNase I hypersensitivity sites, both features that are implicated in recombination events⁷⁰⁻⁷². Furthermore, a recent publication reported a transcriptionally active gene-internal promoter prior to exon 12, resulting in a N-terminally truncated MLL protein of unknown function⁷³, indicating a less densely packed and more accessible chromatin structure.

The MLL protein has a highly complex organisation, comprising several different domains that confer a unique multifunctionality. At the N-terminus, MLL contains three AT-hook motifs, enabling DNA binding⁷¹; this is followed by a SAG and an NTC (N-terminally conserved) domain, which are required for oncogenic transformation by MLL fusion genes. Further on, MLL has a two nuclear localisation signals, SNL-1 and SNL-2, which confer a distinct subnuclear localisation pattern⁷⁴⁻⁷⁵. Adjacent to this is a DNMT (DNA methyltransferase) homology domain, which contains a CXXC zinc finger motif consisting two repeats RG1 and RG2, and a third conserved cysteine-rich sequence. This motif recognises unmethylated CpG dinucleotides, and mediates target recognition of MLL. This domain is retained in MLL fusions and vital for

malignant transformation; moreover, it has been shown that binding of MLL or its oncogenic derivatives prevents epigenetic silencing of both MLL wild-type and fusion target genes⁷⁶⁻⁷⁹. In continuation lies the PHD (plant homology domain) cassette. This regulatory motif mediates divergent MLL functions; on the one hand, the PHD fingers recognises chromatin marked by the activating modification of lysine residue 4-trimethylation (K4me3) on histone H3, and binding to this histone mark is required for MLL transcriptional activation⁸⁰. On the other hand, the PHD domain has been shown to recruit the corepressor Cyp33, resulting in down-regulation of MLL target genes. This PHD-Cyp33 interaction functions as a molecular switch to modulate MLL transcriptional activity⁸¹⁻⁸³. Interestingly, incorporation of the PHD domain in MLL fusions abrogates their oncogenic potential⁸⁴⁻⁸⁵.

Adjoining to the PHD cassette are other structural motifs, such as a transactivation domain and the dimerisation motifs FYRN and FYRC. The carboxy-terminus contains a SET-domain which confers MLL histone methyltransferase (HMT) activity specific for histone H3 lysine(4)-methylation (H3K4)⁸⁶. MLL is post-translationally cleaved by a specific threonine aspartase, *taspase1*, at two conserved cleavage sites, CS1 and CS2, yielding a N-terminal fragment of 300 kDa size, MLL^N, and a 180 kDa MLL^C fragment. Both subunits dimerise over association of the FYRN and FYRC domain, respectively⁸⁷⁻⁸⁹. Each subunit possesses opposed transcriptional activities, MLL^N has repressor properties, associating with core repressors, such as HDACs and the MLL antagonist BMI-1, a member of the polycomb group of proteins (PcG) which antagonise the function of Trx group of genes, of which the MLL gene is considered the founder member (TrxG)⁹⁰. In contrast, the C-terminal subunit MLL^C possesses activating characteristics⁸⁹; MLL interacts via its C-terminal SET domain with multiprotein supercomplexes associated with nucleosome remodelling (NuRD, Sin3a, SWI/SNF), but also comprising factors involved RNA processing and transcriptional activation. Moreover, core components of the SET1-like HMT complex (WDR5, RBBP5, ASH2L), also termed COMPASS, have been shown to be associated with MLL, as well as the histone acetyltransferase MOF, which possesses specificity for lysine residue 16 on histone H3. Other important MLL interaction partners are MENIN (*MEN1*, *multiple endocrine*

neoplasia type 1), and LEDGF (*lens epithelium-derived growth factor*), which both bind the immediate N-terminus of MLL within the first 150bp⁹¹, forming a ternary complex required for MLL-mediated target gene regulation. These factors and the other components of these multimeric complexes colocalise with MLL on *HOX* gene promoters *in vivo* promote transcription^{88,92-94,86,95}.

The protein domain structure of MLL is severely disrupted by the leukaemogenic rearrangement of the *MLL* gene locus, and normal function abrogated. However, despite its vast array of fusion partners, there is one striking common characteristic: the first 1400 aa upstream of the BCR are absolute conserved in all MLL fusion genes. Therefore, the MLL fusion proteins retain the AT hook motifs, the CxxC domain, the SAG domain, essential for target recognition and DNA binding, as well as the nuclear localisation signals, but lose the transactivation and the SET domain, and concomitantly, its HMT activity. Although MLL fusions conserve the interaction with MENIN and LEDGF, their corresponding binding sites located at the beginning of the MLL N-terminus⁸⁸, association with the other components of the SET-like multiprotein complexes is lost, as well as their transactivation capacity. Indeed, the translocation partner moiety contributes importantly towards the oncogenic function of the MLL fusion proteins⁹⁶.

1.3.2 MLL - a Master Regulator of Haematopoiesis and HSC Homoestasis

MLL is the mammalian orthologue of the *Drosophila trithorax (trx)* gene¹⁵, an important regulator of homoeotic gene expression during development^{14,97-98}. This function is conserved in mammals, where MLL plays an essential role for the maintenance of the *HOX* gene clusters, the mammalian counterparts of the *trx*-regulated homoeotic genes. Consequently, MLL plays an important part in establishing correct segment identity, and is required for skeletal, neuronal and craniofacial development. *Mll*-deficiency results in embryonic lethality^{94,99-100}. Furthermore, MLL has been implicated in endothelial cell sprouting¹⁰¹ and post-natal neuronal differentiation¹⁰².

However, MLL is best characterised as a master regulator of early and definitive haematopoiesis as well as HSC homoestasis: yolk sac cells from *Mll*^{-/-} and *Mll*^{+/-} mice showed a block in haematopoietic differentiation, impaired proliferation and clonogenicity¹⁰³. Furthermore, loss of *Mll* abrogated inherent HSC-activity in both early haematogenic and fetal liver cells, and *Mll*-null HSCs failed to reconstitute haematopoietic stem cell function in lethally irradiated recipient mice. In addition, loss of *Mll* also impaired normal lymphopoiesis in adult mice¹⁰⁴⁻¹⁰⁶. In post-natal haematopoiesis, conditional knock-out of *Mll* resulted in lethal BM failure due to abrogation of haematopoietic stem-cell quiescence as well as proliferation defects in committed progenitors¹⁰⁷. Part of the effects of *Mll* ablation are due to concomitant reduction of specific *Hox* gene levels; ectopic reexpression of only one gene of the *Hox* family could rescue the *Mll*^{-/-} phenotype *in vitro*¹⁰⁸.

1.3.3 MLL regulates cell cycle progression and is implicated in DNA damage response

In addition to its role as modulator of HSC quiescence, MLL exerts other important regulatory functions during cell cycle; it is an important modulator of S-phase entry and G2/M transition, and loss of MLL attenuates cycling. This is reflected in the MLL protein levels, which fluctuate during cell cycle, showing a biphasic expression pattern; with peaks at G1/ early S and G2/early M phase, and reduction during S- and late M-phase. This cell cycle –dependent expression is mediated through the cell cycle ubiquitin proteasome system (UPS), specifically the SCF^{Skp2} and APC^{Cdc20} E3 ubiquitin ligase complexes. Aberrant stabilisation of MLL impinges on replication, resulting in a stalled DNA replication¹⁰⁹. This effect is also observed as part of the cellular DNA damage response, where activated ATR kinase targets MLL, disrupting the interaction with the SCF^{Skp2} complex. As a result, MLL accumulates on chromatin and trimethylates H3K4 residues, impairing replication initiation¹¹⁰, thus exerting a key role during the S-phase checkpoint. Although the ubiquitination site is retained in the MLL fusions, interactions with both cell cycle E3 ligase complexes is diminished, both abrogating the cell cycle-dependent expression and stabilising the fusion oncogenes¹⁰⁹. Moreover, the MLL fusions block interaction of wild-type MLL with ATR, consequently abolishing the S-phase checkpoint, deregulating an important DNA damage response mechanism¹¹⁰. In addition, low expression of MLL in T-ALL was associated with increased resistance to genotoxic agents¹¹¹. During M-phase, MLL is retained on specific gene loci, promoting rapid transcriptional reactivation after cytokinesis and expression at high levels¹¹².

Interestingly, the MLL complex components have been shown to interact with the cell cycle regulator E2F1, recruiting MLL to E2F1 target genes promoters and implicating it in E2F-dependent transactivation¹¹³. Moreover, MLL itself has been reported to bind and regulate expression of cell cycle regulating genes such as the cyclin-dependent kinase (CDK) inhibitors p27^{KIP} (*CDKN1B*), p16^{INK4} (*CDKN2A*) and p18^{INK4} (*CDKN2C*)¹¹⁴⁻¹¹⁵.

To date, the *HOX* gene cluster and several cell cycle regulators are the best established MLL target genes, however MLL has been found to localise to >5000 genomic loci¹¹⁶, indicating a global role in transcription regulation. Conceivably, disruption of this epigenetic master regulator by oncogenic rearrangement should result in a myriad of deregulated processes.

1.3.4 AF4 - a Transcription Elongation Factor and Epigenetic Mediator

The MLL translocation partner AF4 (*ALL-1 fused on chromosome 4*) is part of the ALF protein family, whose other members AF5q31, AF10 and LAF4 have been identified as MLL translocation partners in leukaemia¹¹⁷⁻¹¹⁸, with the exception of FMR2. AF4 plays a role in lymphocyte development¹¹⁹ and has been implicated in neurodegenerative diseases, where accumulation of mutant AF4 results in post-natal loss of purkinje cells and ataxia in mice. This phenotype, referred to as “robotic mouse”, also shows growth retardation and a defect in T-cell development¹²⁰⁻¹²².

The nuclear protein AF4 directly interacts with AF9¹²³ and ENL, both recurring MLL translocation partners. Incidentally, both AF9 and ENL form the part of the DOT1L histone methyltransferase complex, which mediates methylation of the lysine79 residue on histone H3 (H3K79), an epigenetic marker for transcriptional activity and essential for normal haematopoietic development¹²⁴⁻¹²⁸. A seminal paper by Bitoun *et al.* found AF4 to be part of this complex, moreover, it reported that AF4 directly stimulates the P-TEFb kinase (CDK9) to phosphorylate the C-terminal domain of RNA Polymerase II (Pol II), thus linking transcription elongation with chromatin remodelling¹²⁹. Recently, Lin *et al.* reported AF4 to be part of another multimeric complex implicated in elongation, termed the super-elongation complex (SEC), which comprises several MLL fusion translocation partners, notably the AF4 family member AF5q31 (AFF4), and was exempt of DOT1L histone methyltransferases activity¹³⁰. The interaction moieties of AF4 for both complexes are retained in the MLL fusion genes^{123,130}, and fusion gene-dependent mistargeting of these

complexes has been widely proposed as fundamental oncogenic mechanism of the bulk of MLLr acute leukaemias^{129,131-134}.

Nothing is known about AF4 expression regulation, however, it has shown to be regulated on a post-translational level; AF4 has a short half-life; and degradation is mediated by SIAH E3 ubiquitin ligases¹²¹. Anomalous stabilisation against degradation has also been implicated in t(4;11)-ALL pathobiology, as the mature reciprocal fusion protein AF4/MLL interacts with SIAH proteins, but cannot be targeted for degradation¹³⁵.

1.3.5 T(4;11)-positive ALL: a Complex Pathobiology

Acute lymphoblastic leukaemia with the t(4;11) rearrangement is a high-risk ALL subtype marked by poor outcome. It is characterised by a very immature pro-B immunophenotype¹³⁶⁻¹³⁹, and the blasts are highly resistant to chemotherapy. The disruption of the wild-type gene involved in this translocation has pronounced effect on biochemical level, and recent studies have tried to shed light onto the molecular mechanisms promoting this disease.

1.3.5.1 MLL/AF4 vs. AF4/MLL vs. MLL/AF4 & AF4/MLL- who's the bad guy?

The contribution of the reciprocal t(4;11)-fusion proteins MLL/AF4 and AF4/MLL to the leukaemogenic process is being controversially discussed in the field. Most MLL rearrangements only require der11 for transformation and leukaemogenesis in *in vitro* and *in vivo* models¹⁴⁰⁻¹⁴⁴; however, ectopic expression of MLL/AF4 does not transform *in vitro*¹⁴⁵⁻¹⁴⁶. Conversely, introducing ectopic MLL/AF4 and AF4/MLL alone or in combination revealed the transforming potential of AF4/MLL; MLL/AF4 alone showed no effect, but was required to maintain viability of the der4-transformed cells¹⁴⁶. In contrast, RNAi-mediated depletion of AF4/MLL in t(4;11)-positive cell lines was not associated with a marked phenotype, and RNAi studies in these cell lines performed by us and others revealed MLL/AF4 to be essential for maintaining the inherent leukaemogenic potential¹⁴⁷⁻¹⁴⁸. These divergent findings are also

reflected in the *in vivo* setting, as there is no *bona fide* animal model able to satisfactorily recapitulate the disease. Currently, there are four transgenic mouse models investigating the expression of MLL/AF4 in murine haematopoietic progenitors; two developed B-cell lymphomas and myeloid malignancies after a long latency^{149,150}, while another model resulted in overt leukaemia after 5-6 months of latency. However, the resulting malignancy showed a mixed lineage or myeloid phenotype, and only a fraction of the mice developed pre-B ALL¹³³. This differs vastly from the human setting, where 95% of the MLL/AF4-positive acute leukaemia cases are ALL, predominantly with a pro-B immunophenotype. Furthermore, since MLL/AF4-positive leukaemia is associated with a high incidence of RAS mutations¹⁵¹, a transgenic mouse model co-expressing MLL/AF4 and constitutively activated KRAS was developed, in order to explore whether this was a cooperating mutation that would confer MLL/AF4 the required and correct transforming capacity. However, also in this model the mice did not develop ALL, but lymphomas, albeit with as drastically reduced latency when compared to the previous knock-in models¹⁵². Concordantly, a xenograft mouse model with MLL/AF4-transduced human CD34-positive cord blood cells failed to generate a malignant phenotype¹⁵³. In contrast to MLL/AF4, there is only one mouse model exploring the role of AF4/MLL in t(4;11)-positive ALL. Remarkably, transgenic mice expressing the AF4/MLL fusion oncogene developed overt pro-B, biphenotypic or mixed-lineage ALL, albeit with a low penetrance of approximately 40%¹⁵⁴.

These observations challenge the current perception that all MLLr acute leukaemias arise from a single oncogenic mutation, referred to as “one-hit model”, where the der11 fusion gene product acts as the main transforming oncogene. Although no comprehensive model has been suggested yet, evidence indicates that, at least in t(4;11)-positive ALL, two mutations, as in both fusion genes, are required for initial transformation. This is then subsequently superseded by MLL/AF4, which is required for the survival of the transformed cells. In this model, AF4/MLL acts as a “hit-and-run” oncogene.

1.3.5.2 *T(4;11)-ALL shows major deregulation of epigenetic pathways*

The t(4;11)-translocation results in disruption of two epigenetic modulators, MLL and AF4, generating two fusion oncogenes with acquired novel functions: MLL/AF4 retains the DNA binding and target recognition domains from MLL, however loses the corresponding HMT activity for H3K4. Instead, this is replaced by the truncated AF4 moiety, and the associated DOT1L HMT activity. Indeed, aberrant H3K79 methylation of specific gene loci is one of the hallmarks of MLL/AF4-positive ALL¹³²⁻¹³³, and DOT1L expression has been shown to be essential for MLL fusion gene-dependent leukaemogenesis and disease maintenance^{124,133,155-156}. Interestingly, disruption of the interaction of AF4 and AF9, which is retained in MLL/AF4, and putatively links this fusion with the DOT1L complex, results in cell death in t(4;11)-positive leukaemia cells¹⁵⁷⁻¹⁵⁹.

The aberrant H3K79 methylation pattern found in MLLr acute leukaemia cells is accompanied by abnormally extended H3K4 methylation marks¹³³. There is an increasing body of evidence for MLL fusion protein interactions with wild-type MLL, which results in recruitment of aberrant H3K4 HMT activity to the DOT1L complex. This MLL fusion- MLL wild-type interaction is required for malignant transformation, and suppression of MLL results in diminished target gene transactivation, proliferation and viability of leukaemic cells *in vitro*, as well as inhibiting leukaemogenesis *in vivo*. Moreover, knock-down of MLL wild-type reduces both H3K4 and H3K79 methylation marks on MLL fusion target gene promoters. The interaction appears to be mediated by the MLL-binding protein MENIN, which interacts with the immediate N-terminus of both wild-type MLL and the oncogenic fusions¹⁶⁰.

In contrast, the reciprocal fusion protein AF4/MLL gains the SET domain from the MLL moiety, which confers putative H3K4-HMT activity and enables interaction with the multimeric COMPASS-like complex. Indeed, Benedikt *et al.* recently showed AF4/MLL to copurify with key components of the COMPASS complex, such as ASH2L, WDR5 and RBBP5. Other factors of this AF4/MLL complex comprise NFkB1 and NPM1, and, unexpectedly, RNA Pol II and the pTEFb-kinase. Moreover, AF4/MLL showed inherent HMT activity and associated with histone methyltransferases of different histone modification

specificities, amongst which also was the DOT1L complex¹⁶¹. AF4/MLL has also acquired the conserved TASPASE1 cleavage site and the dimerisation domains FYRN and FYRC of the MLL moiety. Indeed, AF4/MLL is cleaved by TASPASE1, and the MLL^C domain associates with the remnant MLL^N moiety found in AF4/MLL. This heterodimerisation results in aberrant protein stabilisation¹³⁵, and disruption of this association with small peptides results in degradation of the fusion protein, suppressing formation of the AF4/MLL-COMPASS complex¹⁶².

In addition to the aberrant histone modification signatures, there is also deregulation of another major epigenetic pathway in MLLr ALL cells: t(4;11)- and t(11;19)-ALL cells possess a specific DNA methylation pattern distinct from other ALL subtypes. This results in aberrant silencing of several hundreds of genes, including tumour suppressors, such as FHIT, and miRNA gene loci. Concomitantly, this signature also revealed hypomethylation and aberrant expression of protooncogenes. DNA methyltransferase inhibitor treatment could partially reverse this aberrant signature, and, notably, exerted a selective cytotoxic effect against MLLr ALL cells, a finding with major clinical implications, as DNA methyltransferases inhibitors are part of the chemotherapy regimen of other haematologic malignancies. Furthermore, reexpression of hypermethylated miRNAs resulted in reactivation of an important regulatory mechanism for the post-transcriptional modulation of *DNMT1* (*DNA methyl transferase 1*), a key mediator of DNA methylation, as well as MLL, and, hypothetically, AF4/MLL. These observations have interesting implications in the context of the aforementioned functional cooperation of wild-type MLL with the MLL fusions, and highlight an intrinsic deregulation of the DNA methylation pathway¹⁶³⁻¹⁶⁵.

Remarkably, the two major epigenetic pathways, histone modifications and DNA methylation, are deregulated in MLL/AF4-positive ALL, exerting a concerted malignant effect.

1.3.5.3 *T(4;11)-positive ALL is associated with glucocorticoid-resistance*

In addition to the altered intrinsic epigenetic functions of MLL/AF4 and AF4/MLL, there are also other molecular changes which contribute to the pathobiology of t(4;11)-positive ALL. One of the major clinical aspects of MLLr ALL is the poor and delayed response to glucocorticoid treatment during induction. This has been recently attributed to the overexpression of the Bcl-2 family members BCL-2¹⁶⁶ and MCL-1¹⁶⁷, which have been previously described as contributory factors of glucocorticoid resistance in ALL. Concordantly, a resensitisation of MLL/AF4-positive ALL cells towards prednisolone was achieved by down-regulation of MCL-1¹⁶⁷, and BCL-2 inhibition synergised with other chemotherapeutic drugs, suppressing t(4;11)-positive ALL cell survival¹⁶⁶.

1.3.5.4 *Specific gene expression signatures contribute to the immortalisation of t(4;11)-positive ALL*

High-throughput profiling of MLL/AF4 binding sites in the t(4;11)-positive ALL cell line SEM showed MLL/AF4 occupancy on promoters of genes linked to self-renewal, such as *MEIS1*, *FLT3*, *PROM1* and the *HOXA* gene cluster, indicating that MLL/AF4 might regulate the transcription of a haematopoietic stem cell-like signature¹³². In concordance with the altered epigenetic functions of MLL/AF4, these promoter loci were associated with a distinct H3K79 methylation profile¹³²⁻¹³³. Gene expression profiling of t(4;11)-patient cohorts showed a concordant up-regulation of the aforementioned genes¹⁶⁸⁻¹⁶⁹, and further studies revealed also expression of embryonic stem cell markers such as NANOG and OCT-4¹⁴⁶. Concordantly, our group observed that MLL/AF4 depletion in the SEM cell line results in down-regulation of *PROM1* and its encoded surface marker protein CD133¹⁴⁸, and we have now reported an important link between MLL/AF4 and the expression regulation of TERT, a critical component of the telomerase enzyme, which is a major mediator of self-renewal¹⁷⁰.

In other BCP-ALL subtypes the self-renewal capability is supported by the acquisition of a variety of secondary mutations next to the main cytogenetic

abnormality, often negative copy number alterations (CNA) of transcription factors regulating B-cell development¹⁷¹. Notably, t(4;11)-positive ALL cells typically do not carry CNA¹⁷²⁻¹⁷³; however MLL/AF4-positive ALL has a high incidence of KRAS and NRAS mutations¹⁵¹, as well as loss of function of the transcription factor Ikaros, important for B-cell development, due to aberrant alternative splicing¹⁷⁴. The high degree of genomic integrity in t(4;11), as indicated by the lack of secondary CNA, suggests that the bulk of the malignant changes occurs from the transcriptional level onwards.

1.3.5.5 MLL/AF4 perturbs cell cycle regulation

MLL is an important regulator of cell cycle progression and implicated in cell cycle checkpoint response. As mentioned before, these functions are mediated by the cell cycle E3 ligase complexes as well as the DNA damage-activated kinase ATR, and this regulatory mechanism is abolished in MLL/AF4-positive ALL, resulting in aberrant stabilisation of the fusion gene and compromising MLL wild-type functions¹⁰⁹⁻¹¹⁰. Consequentially, t(4;11)-positive ALL cells have an inherent cell cycle regulation defect, and are resistant to chemical and mitogenic stimuli which would normally activate the different cell cycle checkpoints¹⁰⁹. In good accordance, forced expression of MLL/AF4 in *Drosophila* resulted in a deranged cell cycle progression and pupal lethality¹⁷⁵, and the CDK inhibitor p27^{Kip} (CDKN1B) was found to be a direct target gene of MLL/AF4 in lymphoid progenitor cells as well as t(4;11)-positive cell lines¹⁷⁶.

1.4 AIMS OF THE THESIS

The chromosomal rearrangement t(4;11) and its resulting fusion genes disrupt the epigenetic machinery, generating aberrant histone modification marks and deregulating the DNA methylation pathway. Consequently, an abnormal gene expression programme is induced, immortalising the cell. Concomitantly, abolishment of cell cycle checkpoints, impaired DNA damage response and high expression of pro-survival factors contribute to therapy-resistance.

Therefore, MLL/AF4 is pivotal for leukaemic propagation by

- interfering with the cell cycle machinery
- inhibiting apoptotic cell death, and by
- supporting malignant self-renewal.

The scope of this thesis was to gain insight into the transcriptional programmes underlying this phenotype, in order to identify processes and key mediators regulating the MLL/AF4-dependent survival machinery, novel MLL/AF4-regulated genes, and to subsequently characterise them regarding their contribution to the leukaemic phenotype.

In order to do so

- I performed loss-of-function studies in the t(4;11)-ALL positive cell line model SEM, combining a RNAi-mediated *MLL/AF4* ablation time course approach with subsequent high-throughput gene expression profiling. Genes differentially expressed in response to *MLL/AF4* depletion were analysed for functional signatures using bioinformatic methods.
- Concomitantly, the dependency of the leukaemic cell on MLL/AF4 for survival was investigated, combining MLL/AF4 ablation with apoptosis-inhibitor studies and global gene expression profiling. The resulting differentially expressed gene set was analysed for functional signatures using bioinformatic methods, as well as compared for unique and

common signatures with the expression data set generated without inhibitors.

- Identified candidate genes and pathways were validated, and interesting targets functionally characterised, exploring their role in leukaemic cell survival and proliferation *in vitro*, as well as their relevance for *in vivo* disease development.

2. Material & Methods

2.1 GENERAL MATERIALS

2.1.1 General Chemicals

All chemicals, if not stated specifically, were purchased at analytical grade from Sigma-Aldrich Company Ltd, Fisher Scientific, Life Science Technologies or VWR International, LLC.

2.1.2 Oligonucleotides

Tab. 2-1: qRT-PCR primers (VHBio, Sigma-Aldrich Ltd)

Name	Sequence 5'→3'
ACTB_1	fw:GGTCATCACCATTGGCAATG rev: CTCCATGCCAGGAAGGAA
ACTB_2	rev: AGGACTCCATGCCAGGAA
AF4 sense	fw: CAGAAGCCCACGGCTTATGT
ANGPT1_1	fw: TCTCTTCCCAGAACTTCAACATCT rev: TCATGTTTTCCACAATGTAATTCTCA
ANGPT2_001	fw: AGGGACAAACCTGTTGAACCA rev: TTAATACTTGGGCTTCCACATCAG
ANGPT4	fw: GCAAGTGTGCCCAAGTGATG rev: ACGCCGTTGAGGTTTGACA
ANGPTL2	fw: CGCCTGGATGGCTCTGTAA rev: CCAGTATTCGCCGTCATGTT
ANGPTL4	fw: GGACAAGAACTGCGCCAAGA rev: CGGAAGTACTGGCCGTTGA
ANXA1_all	fw: TCAAAGCAGCATATCTCCAGGAA rev: CCTCCTCAAGGTGACCTGTAAGG
BMF2;3	fw: CCCAGCGACTCTTTTATGC rev: CAAAGCAAGGTTGTGCAGGAA
BMF3;4	fw: CCGGCCTAGGAGAGATGGA rev: CCCCATCCTCTGGTTGGAA
CYLD_1;2	fw: CGTCGGAGTTTCCCCCTTT rev: GGGCGCACCTTTCAACTAAG
DNMT3B	fw: GCCACCTCTGACTACTGCCC rev: CCTCGGTCTTTGCCGTTGT
DUSP6	fw: AGCTCAAGGACGAGGGCTG rev: GGAGAACTCGGCTTGGAAGTT
GABARAPL1_all	fw: CGGAAAAAGGAAGGAGAAAAGAT rev: CTTTTGGAGCCTTCTCTACAATCAC
GAPDH	fw: TGG CAT GGC CTT CCG T rev: TCT CCA GGC GGC ACGT T

HMGA2	fw: CCCAAAGGCAGCAAAAACAA rev: GCCTCTTGGCCGTTTTTCTC
HOXA6	fw: CGGTTTACCCTTGGATGCA rev: GCCCATGGCTCCCATACAC
HOXA7	fw: GAGGCAATTTCCGCATCTA rev: GCGGTTGAAGTGGAACCTCTT
HOXA9	fw: CCACCATCCCCGACA rev: TTTCCAAGGCAAACCCTGTT
HOXA10.2	fw: CAGGCCACCTCGTGCTCTT rev: TTTGTCCGCCGAGTCGTAG
JUN	fw: TGGGAGGACCGGAGACAAG rev: TCTTTACCGCCGTGGAGAAG
LC3B	fw: TGCCGTCGGAGAAGACCTT rev: TCGAATAAGTCGGACATCTTCTACTC
MLL antisense	rev: GCAAACCACCCTGGGTGTTA
MLL/AF4	fw: ACAGAAAAAAGTGGCTCCCCG rev: TATTGCTGTCAAAGGAGGCGG
PARP2	fw: GCCCCTTGACCATGAAAGT rev: TCGCTGTGTGTTGGGAGCAT
PYGO2_all	fw: TCTGCAAATGAAGAGTCCAGAAAA rev: GTGCAAACCTCCGTCAGATGTGA
RIPK1	fw: CAACTGCATTGAGCACAACGA rev: CACCACCCGGCTGTGTCT
TBP	fw: CCTAAAGACCATTGCACTTCGT rev: GTTCGTGGCTCTCTTATCCTCA
TERT	fw: GGA GAA CAA GCT GTT TGC GG rev: AGG TTT TCG CGT GGG TGA G
TIE1	fw: ACCTGTGCCGAGCTCTATGAA rev: TGACGCATCAGCTCGTACACT
TNF	fw: ATCTTCTCGAACCCCGAGTGA rev: AGCTGCCCTCAGCTTGAG
TNF_2	fw: TGGCCCAGGCAGTCAGA rev: GGTGCTACAACATGGGCTACA

Tab. 2-2: RT-PCR primers (Fermentas, Sigma-Aldrich Ltd)

Name	Sequence 5'→3'	T _M [°C]
GAPDH (Fermentas)	fw: CAAGGTCATCCATGACAACCTTTG rev: GTCCACCACCCTGTTGCTGTAG	56°
ITGA4	fw: GCAATGGAAACAAACCTCGT rev: TCTTGGTGAGACTCTGCCT	56°
ITGA5	fw: CAGATCCTGTCTGCCACTCA rev: CAGAGCCAAAGAAGTCTGGG	56°
ITGAV	fw: GTTCCAAGAGCAGCAAGGAC rev: TGCTCCCTTTTGCTTGAGTT	56°
ITGB1-a	fw: AATGAAGGGCGTGTGGTAG rev: CTGCCAGTGTAGTTGGGGTT	56°
ITGB3	fw: GCAATGGGACCTTTGAGTGT rev: AACGGTTGCAGGTATTTTCG	56°
ITGB5	fw: GTGCTCCAAAGAGGACTTCG rev: GAAGTTGCTGGTGAGCTTCC	56°
TEKa	fw: GCATGGACTCTTTAGCCAGC rev: CTGAGCATGAGGCAGGTGTA	56°

Tab. 2-3: siRNA oligonucleotides

Name	(Target) Sequence 5'→3'	Company
siMLL/AF4	s 5'- AAGAAAAGCAGACCUACUCCA -3' as 5'- UGGAGUAGGUCUGCUUUUCUUUU -3'	Purimex
siAML1/MTG8	s 5'-CCUCGAAAUCGUACUGAGAAG-3' as 5'-UCUCAGUACGAUUUCGAGGUU-3'	Purimex
siANGPT1_1 (siGENOME D-007802-01)	CCAGAAAGCUGACAGAUGU	Dharmacon
siANGPT1_2 (siGENOME D-007802-02)	not available	Dharmacon
siANGPT1_3 (siGENOME D-007802-03)	GAACCAGCCUCCUCUCUCA	Dharmacon
siANGPT1_5 (siGENOME D-007802-05)	not available	Dharmacon
Hs_HOXA7_6 FlexiTube siRNA	not available	QIAGEN
Hs_HOXA7_8 FlexiTube siRNA	GCCUGAUGUUUCCUAUAATT-	QIAGEN
siRNA-Cy5	not available	QIAGEN

Lentiviral shRNA Expression plasmids

Name	clone	Target sequence	Company
pTRIPZ-shANGTP1	V2THS_94475	CCTTGTC AATCTTTGCACTAA	Open Biosystems
pTRIPZ-shNTC	RHS4743	Not available	Open Biosystems

2.1.3 Antibodies

Tab. 2-4: Immunoblot antibodies

epitope	dilution	Company
rabbit α -cleaved CASPASE-3	1:1000	Cell Signalling Technology, Inc
rabbit α -cleaved CASPASE-7	1:1000	Cell Signalling Technology, Inc
rabbit α -DUSP6	1:800	kind gift from DR. P.
mouse α -GAPDH,	1:50000	HyTest, Turku, Finland
rabbit α -LC3B	1:1000	Cell Signalling Technology, Inc
rabbit α -PARP1	1:1000	Cell Signalling Technology, Inc
α -RIPK1	1:1000	Kind gift from Dr. Krippner-Heidenreich
mouse- α -TUBULIN (Ab-2 DMIA)	1:3000	Neomarker (Labvision)
α -mouse IgG-HRP	1:5000- 1:10000	Amersham
α -rabbit IgG-HRP	1:1000	Cell Signalling Technology, Inc
α -rabbit IgG-HRP	1:1000	DAKO UK Ltd

Tab. 2-5:FACS antibodies

epitope	clone	Company
α -hCD19-APC	SJ25C1	BD Biosciences
α -hCD34-PerCP-Cy5.5	8G12	BD Biosciences
α -murine Cd45-PE-Cy7	30-F11	BD Biosciences
α -murine Ter119-PE-Cy7	Ter119	BD Biosciences
α -hTNFR1	H398	kind gift from Dr. Krippner-Heidenreich
α -hTNFR2	MR2-1	Hbt HyCult (Netherlands)
α -hTNF	T1	kind gift from Dr. Krippner-Heidenreich
α -mouse IgG-FITC	not applicable	Jackson ImmunoResearch Laboratories Inc. (USA)

2.1.4 General equipment

2.1.4.1 Centrifuges

Allegra X-12R centrifuge (Beckman Coulter, Buckinghamshire, UK)

Allegra X-22R centrifuge (Beckman Coulter, Buckinghamshire, UK)

5415 R microfuge (Eppendorf, Cambridgeshire, UK)

L870M Ultracentrifuge (Beckman, High Wycombe, UK)

2.1.4.2 Thermocycler

GeneAmp PCR System 2700 (applied Biosystems)

2.1.4.3 Flow cytometer

FACSCalibur (Beckton Dickinson, Oxford, UK)

FACScan (Beckton Dickinson, Oxford, UK)

FACS Canto II (Beckton Dickinson, Oxford, UK)

2.1.4.4 Spectrophotometer

Spectramax 250 Multiwell plate reader (Molecular Devices, Crawley, UK)

ND-1000 spectrophotometer (Nanodrop Technologies Ltd., USA)

2.1.4.5 Electroporator

Elektroporations-Impulsgenerator EPI 2500, Dr. L Fischer, Heidelberg

2.2 TISSUE CULTURE TECHNIQUES

2.2.1 Freezing and thawing of viable cell lines

Cells were harvested by centrifugation at 335 g for 5 min at room temperature, and the pellet resuspended in pre-chilled freeze-mix medium (90% FCS, 10% DMSO, v/v %) to a concentration of 5×10^6 - 1×10^7 cells/ml. The cell suspension was immediately transferred into cryovials and frozen down at -80C. Subsequently, the vials were transferred to liquid nitrogen (-192C) for long-term storage.

Frozen viable cells were thawed quickly at 37C, diluted 1:10 in pre-warmed corresponding growth medium and the DMSO contained in the medium removed by centrifugation at approximately 335 g for 5 min at room temperature. The cells were resuspended in growth medium and seeded put at a concentration of 1×10^6 cells/ml.

2.2.2 Freezing and thawing of viable patient material

Pre-purified patient lymphoblasts obtained by Ficoll-density centrifugation were harvested by centrifugation at approximately 335 g for 10-15 min at room temperature, and the pellet resuspended in pre-chilled freeze-mix medium (90% FCS, 10% DMSO, v/v %) to a concentration of 5×10^6 - 1×10^7 cells/ml. The cell suspension was immediately transferred into cryovials and frozen down at -80C. Subsequently, the vials were transferred to liquid nitrogen (-192C) for long-term storage.

Frozen cells were thawed quickly at 37C, diluted 1:10 in pre-warmed appropriate growth medium and the DMSO contained in the medium removed by centrifugation at approximately 300 g for 10-15 min at room temperature. The cells were resuspended in growth medium and seeded out at a concentration of $1-2 \times 10^6$ cells/ml.

2.2.3 Culture of cell lines

2.2.3.1 SEM (DSMZ No. ACC 546)

Human B-cell precursor acute lymphoblastic leukaemia cell line derived from the peripheral blood of a 5-year-old female patient in relapse, positive for t(4;11)(q21;q23) rearrangement, expresses MLL/AF4 and AF4/MLL fusion genes. Cells growing in suspension were maintained in culture in RPM1-1640 growth medium, HEPES-modified, supplemented with 2 mM L-Gln and 10% FCS. Cell concentrations were kept between 0.5×10^6 - 3×10^6 cells/ml by splitting the cultures 1:5 to 1:10 every 2-3 days by removing and adding medium.

2.2.3.2 RS4;11 (DSMZ No. ACC 508)

Human B-cell precursor acute lymphoblastic leukaemia cell line derived from the bone marrow of a 32-year-old female patient in relapse, positive for t(4;11)(q21;q23) rearrangement, expresses MLL/AF4 and AF4/MLL fusion genes. Cells growing in suspension were maintained in culture in RPM1-1640 growth medium, HEPES-modified, supplemented with 2 mM L-Gln and 10% FCS. Cell concentrations were kept between 0.5×10^6 - 2×10^6 cells/ml by splitting the cultures 1:4 every 2-3 days by removing and adding medium.

2.2.3.3 MV4;11 (DSMZ No. ACC 102)

Human acute monocytic leukaemia cell line (AML FAB M5) derived from a 10-year-old male patient at diagnosis, positive for t(4;11)(q21;q23) rearrangement, expresses MLL/AF4 and AF4/MLL fusion genes. Cells growing in suspension were maintained in culture in RPM1-1640 growth medium, HEPES-modified, supplemented with 2 mM L-Gln and 10% FCS. Cell concentrations were kept between 0.5×10^6 - 2×10^6 cells/ml by splitting the cultures 1:5 every 2-3 days by removing and adding medium.

2.2.3.4 NALM6 (DSMZ No. ACC 128)

Human B-cell precursor acute lymphoblastic leukaemia cell line derived from the peripheral blood of a 19-year-old male patient in relapse, positive for t(5;21) rearrangement, expresses TEL/PDGFRB fusion gene. Cells growing in suspension were maintained in culture in RPM1-1640 growth medium, HEPES-modified, supplemented with 2 mM L-Gln and 10% FCS. Cell concentrations were kept between 0.5×10^6 - 2×10^6 cells/ml by splitting the cultures 1:5 every 2-3 days by removing and adding medium.

2.2.3.5 PreB-697 (DSMZ No. ACC 42)

Human B-cell precursor acute lymphoblastic leukaemia cell line derived from the bone marrow of a 12-year-old male patient in relapse, positive for t(1;19)(q23;p13), rearrangement, expresses E2A/PBX1 fusion gene. Cells growing in suspension were maintained in culture in RPM1-1640 growth medium, HEPES-modified, supplemented with 2 mM L-Gln and 10% FCS. Cell concentrations were kept between 0.5×10^6 - 2×10^6 cells/ml by splitting the cultures 1:5 every 2-3 days by removing and adding medium.

2.2.3.6 REH (DSMZ No. ACC 22)

Human B-cell precursor acute lymphoblastic leukaemia cell line derived from the peripheral blood of a 15-year-old female patient in relapse, positive for t(12;21) rearrangement, expresses TEL/AML1 fusion gene. Cells growing in suspension were maintained in culture in RPM1-1640 growth medium, HEPES-modified, supplemented with 2 mM L-Gln and 10% FCS. Cell concentrations were kept between 0.5×10^6 - 2×10^6 cells/ml by splitting the cultures 1:5 every 2-3 days by removing and adding medium.

2.2.3.7 *Kasumi-1 (DSMZ No. ACC 220)*

Human acute myeloid leukaemia cell line (AML FAB M2) derived from the peripheral blood of a 7-year-old male patient in 2nd relapse after bone marrow transplantation, positive for t(8;21)(q22;q22) rearrangement, expresses AML1/MTG8. Cells growing in suspension were maintained in culture in RPM1-1640 growth medium, HEPES-modified, supplemented with 2 mM L-Gln and 10% FCS. Cell concentrations were kept between 0.5×10^6 - 2×10^6 cells/ml by splitting the cultures 1:3 every 2-3 days by removing and adding medium.

2.2.3.8 *K562 (DSMZ No. ACC 10)*

Human chronic myeloid leukaemia cell line derived from pleural effusions of a 53-year-old female patient in blast crisis, positive for t(9;22) rearrangement, expresses BCR-ABL b3-a2 fusion gene. Cells growing in suspension were maintained in culture in RPM1-1640 growth medium, HEPES-modified, supplemented with 2 mM L-Gln and 10% FCS. Cell concentrations were kept between 0.5×10^6 - 3×10^6 cells/ml by splitting the cultures 1:5 to 1:10 every 2-3 days by removing and adding medium.

2.2.3.9 *TK-6 (ATCC No. CRL-8015)*

Human lymphoblastic cell line derived from the spleen of a 5-year-old male non-leukaemic patient. Cells growing in suspension were maintained in culture in RPM1-1640 growth medium, HEPES-modified, supplemented with 2 mM L-Gln and 10% FCS. Cell concentrations were kept between 0.5×10^6 - 1.5×10^6 cells/ml by splitting the cultures 1:10 every 2-3 days by removing and adding medium.

2.2.3.10 *MUTZ5 (DSMZ No. ACC 490)*

Human B-cell precursor acute lymphoblastic leukaemia cell line derived from the peripheral blood of a 26-year-old male patient in relapse. Cells growing in suspension were maintained in culture in RPM1-1640 growth medium, HEPES-

modified, supplemented with 2 mM L-Gln and 20% FCS. Cell concentrations were kept between 1×10^6 - 2×10^6 cells/ml by splitting the cultures 1:2 every 7 days by removing and adding medium.

2.2.3.11 MHH-CALL4 (DSMZ No. ACC 337)

Human B-cell precursor acute lymphoblastic leukaemia cell line derived from the peripheral blood of a 10-year-old male patient at diagnosis. Cells growing in suspension were maintained in culture in RPM1-1640 growth medium, HEPES-modified, supplemented with 2 mM L-Gln and 20% FCS. Cell concentrations were kept between 1×10^6 - 2×10^6 cells/ml by splitting the cultures 1:2 every 7 days by removing and adding medium.

2.2.3.12 SK-HEP (ACC 141)

Human liver adenocarcinoma cell line derived from ascites of a 52-year-old male patient. Adherent cells growing in a monolayer were maintained in culture in RPM1-1640 growth medium, HEPES-modified, supplemented with 2 mM L-Gln and 20% FCS. In order to maintain the cells in a logarithmic growth phase, cells were passaged after achieving a confluence of approximately 90%. The cell monolayer was washed once with warmed PBS and subsequently detached via enzymatic digestion from the tissue culture flask by adding 0.5-1 ml of 1x trypsin/EDTA-solution (0.05% trypsin, 0.02% EDTA, Sigma-Aldrich Company Ltd) onto the monolayer and incubating it shortly at 37C. Detachment was stopped by adding 9 volumes growth medium; 1/4th of this single cell suspension was transferred into a new flask containing 14 ml of pre-warmed growth medium.

2.2.3.13 293T (ACC 635)

Human embryonic kidney cell line transduced to carry a plasmid containing a mutant of SV-40 large T-antigen. Adherent cells growing in a monolayer were

maintained in culture in DMEM (Sigma-Aldrich Company Ltd) growth medium, HEPES-modified, supplemented with 2 mM L-Glutamine and 10% FCS. In order to maintain the cells in a logarithmic growth phase, cells were passaged after achieving a confluence of approximately 90%. The cell monolayer was washed once with warmed PBS and subsequently detached from the tissue culture flask via enzymatic digestion with 0.5-1 ml 1x trypsin/EDTA-solution (0.05% trypsin, 0.02% EDTA, Sigma-Aldrich Company Ltd) onto the monolayer and incubating it shortly at 37C. Detachment was stopped by adding 9 volumes growth medium; 1/4th to 1/5th of this single cell suspension was transferred into a new flask containing pre-warmed growth medium.

2.2.4 Cell number determination using the Trypan Blue exclusion assay

In order to determine the number and concentration of cells in culture, a single cell suspension is required; obtained either by careful mixing, in case of suspension cell lines, or by tryptic digest of adherent cell monolayers, stopped by subsequent addition of 9 volumes growth medium, as described in section 2.2.3. Approximately 10-20 µl of the cell suspension were mixed with 1x volume of trypan blue solution (0.4%, w/v, Sigma-Aldrich Company Ltd), a vital dye taken up by non-viable cells, staining them blue, while being excluded from viable cells. Approximately 10 µl of this mixture are applied onto an assembled haemocytometer and counted under a light microscope, using 20x magnification.

A haemocytometer, also called Neubauer counting chamber, consists of four counting square units composed of 16 smaller squares aligned 4x4 (see figurexxxx). Only shining, unstained cells in all four counting square units were counted; the sum of cells averaged and the cell concentration determined using following equation:

$$\text{conc}_{\text{cells}} = n_{\text{cells}} \times F \times D = \text{cells/ml}$$

$\text{conc}_{\text{cells}}$ = concentration of cells in solution

n_{cells} = sum of counted cells

$$F = \text{chamber factor} = \frac{V_d}{V_{\text{sq}}} = 10,000$$

$$\begin{aligned} V_{\text{sq}} &= \text{counting square unit volume} \\ &= \text{surface area} \times \text{chamber depth} \\ &= 1\text{mm}^2 \times 0.1\text{mm} \\ &= 0.1\text{mm}^3 = 0.0001\text{ml} \end{aligned}$$

$$V_d = \text{desired final volume} = 1\text{ml}$$

D = dilution factor

The dilution factor D corresponds to the fold dilution of the applied cell suspension with the trypan blue dye solution, in this case 2.

2.2.5 Preparation of duplexed siRNA solutions

Lyophilised siRNA oligonucleotides were present as either separate oligonucleotide sense or antisense strands, or in already duplexed form. In the case of separate sense and antisense strands, each strand was reconstituted with siRNA hybridisation buffer (25mM Tris, 100 mM NaCl, pH 7.51) to a final concentration of 100 μ M. Equimolar amounts of both oligonucleotides strand stock solutions were mixed and diluted in siRNA hybridisation buffer to a final working concentration of 20 μ M. Hybridisation occurred by heat-denaturing the solution at 95C for 30s, in order to remove secondary structures which might possible impinge on the process, and subsequent annealing of both complimentary strands by slowly cooling down the solution to room temperature.. In the case of lyophilised siRNA oligonucleotides in duplexed form, the siRNA was reconstituted with siRNA hybridisation buffer to a final concentration of 100 μ M, using a thermo shaker at maximal shaking speed (1200 rpm) for 15 min. A 20 μ M siRNA working solution was prepared by dilution with siRNA hybridisation buffer. SiRNA working solutions were stored at -20C, and siRNA stock solutions at -80C.

2.2.6 Electroporation of leukaemic cell lines with siRNA

Cell concentration was determined as described in section 2.2.4, and cells harvested by centrifugation at 335g for 5min at room temperature. Subsequently, the cells were adjusted to a density of 10^7 cells/ml, and between 100 μ l and 800 μ l of this suspension were pipetted into the electroporation cuvette. A 20 μ M siRNA stock solution was diluted into this reaction mixture yielding a final cuvette concentration of 500 nM, if not stated differently. Immediately after the cell suspension was electroporated using a single pulse of 10ms at 350V (SEM cell line), 330V (Kasumi-1 cell line) or 370V (RS4;11 cell line). The cells were incubated for 15-30 min at room temperature before being diluted 20-fold in pre-warmed growth medium, resulting in a density of 5×10^5 cells/ml. Cells were cultured under standard conditions. If required, serial electroporations were performed every other day in the case of the SEM cell

line, or at three-day intervals for the Kasumi-1 cell line following the same procedure.

2.2.7 Drug and Inhibitor Treatment

2.2.7.1 zVAD-FMK

The pancaspase inhibitor carboxybenzoxy-valyl-alanyl-aspartyl-[O-methyl]-fluoromethylketone (zVAD-FMK, Enzo Life Sciences, Inc.) is a cell permeable drug that acts as an irreversible caspase inhibitor. For treatment, the substance was reconstituted with DMSO following manufacturer's protocol, resulting in a 20 mM stock solution. Since high DMSO concentrations have a cytotoxic effect on cells, the zVAD stock solution was prediluted 10-fold in medium, yielding a 2 mM working solution. Immediately before seeding out electroporated cells, zVAD was added to growth culture medium to the desired final concentration; cells were then co-cultured in the zVAD-supplemented medium for two days. This procedure was repeated for subsequent electroporations.

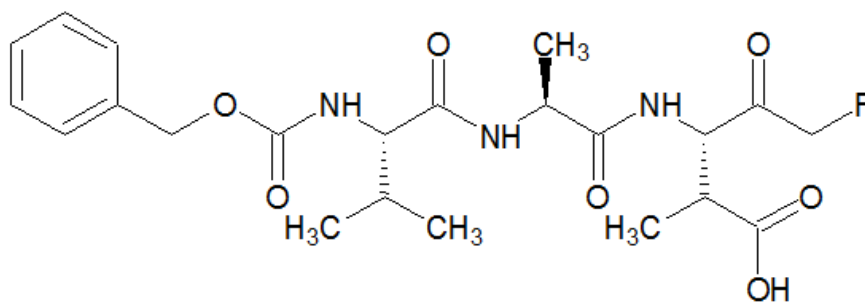


Fig. 2-1: Chemical structure of the pan-caspase inhibitor zVAD

2.2.7.2 Necrostatin-1 (NEC-1)

Necrostatin-1 (5-(1H-Indol-3-ylmethyl)-3-methyl-2-thioxo-4-imidazolidinone), also referred to as NEC-1, is a kinase inhibitor specific for RIPK1, a key regulator of the necroptotic cell death pathway. Consequently, NEC-1 blocks necroptosis.

For treatment, Necrostatin-1 (Sigma-Aldrich Company Ltd) was reconstituted with DMSO to a 100 mM stock solution. SEM cells serially electroporated with siRNA and treated with or without zVAD were supplemented immediately after the second electroporation with NEC-1 to a final concentration of 100 μ M, and cultured for two days at standard conditions.

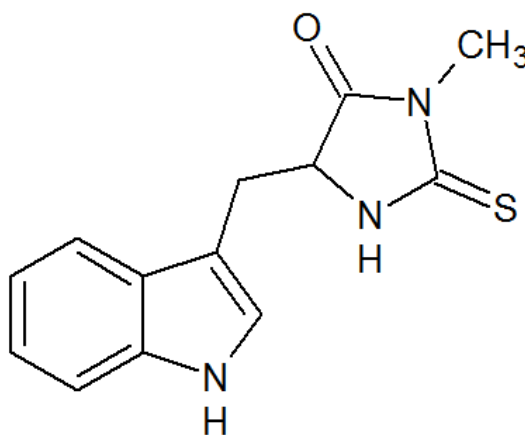


Fig. 2-2: Chemical structure of the RIPK1 inhibitor NEC-1

2.2.7.3 α -TNF (Infliximab)

The monoclonal antibody Infliximab is specific for the cytokine TNF (Tumour Necrosis Factor); binding blocks the interaction of TNF with its cognate receptors.

Briefly, SEM cells serially electroporated with siRNA and treated with or without zVAD were supplemented immediately after the second electroporation with Infliximab to a final concentration of 100 μ M, and cultured for two-days at standard conditions.

2.2.7.4 Dexamethasone

The glucocorticoid dexamethasone (Sigma-Aldrich Company Ltd) is a cytotoxic drug administered in ALL chemotherapy. For treatment, the substance was

reconstituted in 100% ethanol to a 20 mM stock solution. Singly electroporated SEM cells were seeded out into 96-well plates at a concentration of 0.5 mio cells/ml, and equilibrated for 6h in a standard cell culture incubator. Subsequently, the cells were supplemented with dexamethasone at a dose range (0.001-100 μ M) and cultured for four days under standard conditions. Viability was determined using an MTT assay as described in 2.2.8.

2.2.7.5 recombinant human ANGPT1

SEM cells were electroporated as described in 2.2.6, growth medium was supplemented with 2 μ g/ml recombinant human ANGPT1 (ENZO Life Sciences Inc.) and cells cultured for 96h.

2.2.8 Determination of cell viability by the MTT assay

This assay functions on the principle that only viable cells possess intact mitochondria with active mitochondrial dehydrogenases. Addition of the membrane permeable MTT dye (Thiazolyl Blue Tetrazolium Bromide, Sigma-Aldrich Company Ltd) to the cell culture results in its metabolism to insoluble violet formazan crystals by the aforementioned dehydrogenases. Solubilisation of the crystal precipitates results in a violet solution, whose optical absorbance (OD) correlates directly to the number of viable cells. Briefly, 100 μ l of a cell suspension are seeded out in a flat-bottomed 96-well plate and treated according to the specific experimental set-up. In parallel, culture medium alone or containing the drug vehicle is also added to separate wells for blanking. At the experimental endpoint, the amount of viable cells is determined by adding 1/10 volume of MTT solution (5 mg/ml in PBS) and incubation of the plate for 4h-5h at standard cell culture conditions (37C, 5% CO₂, 100% humidity). The formed crystals are dissolved by addition of 100 μ l MTT solubilisation solution (0.1 N HCl, 10% Triton-X in isopropanol) and repeated pipet-mixing. The OD of the solution is measured with a plate reader at 570 nm wavelength with reference wavelength of 650 nm. For viability calculation, the

OD values of each blank control was averaged and subtracted from the mean of the corresponding treated sample wells. Afterwards, the OD values of the treated cells were normalised against the control sample.

2.2.9 Determination of cell viability by the CellTiter-Glo® assay

The principle of the CellTiter-Glo® assay (Promega) is based on the measurement of cellular ATP as a surrogate marker for viability. In brief, the CellTiter-Glo® reagent contains both luciferase and its substrate luciferin; after cell lysis, luciferin is metabolised into oxyluciferin by the luciferase enzyme, hydrolysing the released cellular ATP into AMP and pyrophosphate; this reaction generates a light signal detected and recorded by a luminometer, and converted into arbitrary light units (ALU). There is a linear correlation between light intensity and the amount of ATP, which corresponds to the number of viable cells.

The experimental set-up was as follows: CellTiter-Glo® reagent was generated by reconstituting lyophilized CellTiter-Glo® substrate with CellTiter-Glo® buffer according to manufacturer's instructions. 50 µl of treated cell culture suspension was transferred to white-walled 96-well plates, and lysed with an equal volume of CellTiter-Glo® reagent for 2 min on an orbital shaker at 600-800 rpm, followed by incubation for 10 minutes at room temperature. Each sample was performed in duplicates; additionally, blank controls with either zVAD-, NEC-1 or DMSO-supplemented growth medium were pipetted in duplicates as well and treated accordingly. Luminescence was recorded within 1h of lysis. For the calculation of the activity fold-change between the different treatments, the ALU of the blank controls were averaged and subtracted from the mean of the corresponding treated sample wells. Afterwards, the ALU of the siRNA-treated SEM cells were normalised against the controls sample (MOCK).

2.2.10 Caspase-Glo® Caspase-3/-7 Activity Assay

The Caspase-Glo® Caspase-3/-7 Activity Assay (Promega) is a luciferase-based assay that measures the proteolytic activity of the effector caspases caspase-3 (CASP3) and caspase-7 (CASP7). The Caspase-Glo® reagent contains both the tetrapeptide DEVD conjugated to a luciferin-derivate (aminoluciferin) as well as the luciferase enzyme. Activated caspases-3/-7 recognise DEVD as a proteolytic substrate, cleaving off the aminoluciferin, which is subsequently metabolised by luciferase into oxyluciferin, generating a light signal. This signal is detected and recorded by a luminometer, and converted into arbitrary light units (ALU).

The experimental set-up was as follows: Caspase-3/-7-Glo® reagent was generated by reconstituting lyophilized Caspase-Glo® substrate with Caspase-Glo® buffer according to manufacturer's instructions. The density of treated cells was determined using a trypan blue exclusion assay, as indicated in 2.2.4. For each sample, 10^5 viable cells were harvested and washed once with PBS and subsequently resuspended in normal growth medium to a concentration of 10^5 cells/ml. 50-75 μ l of this suspension were transferred into white-walled 96-well flat bottom plates and supplemented with equal volume of Caspase-3/-7-Glo® reagent, resulting in a cell number of $5-7.5 \times 10^4$ cells per well. Each sample was performed in duplicates. In addition, two blank controls with either zVAD- or DMSO-supplemented growth medium were pipetted in duplicates as well and treated accordingly. After cell lysis and incubation for 1-2h, the resulting luminescence was recorded by a luminometer, and converted into arbitrary light units (ALU). For the calculation of the activity fold-change between the different treatments, the ALU of the blank controls were averaged and subtracted from the mean of the corresponding treated sample wells. Afterwards, the ALU of the siRNA-treated SEM cells were normalised against the controls sample (siAML1/MTG8).

2.2.11 Lentivirus particle production in the packaging cell line 293T using the CaPO₄ transfection method

Virus particles containing shRNA expression cassettes were produced in the packaging cell line 293T by transient cotransfection of lentiviral envelop, packaging and expression plasmids using the CaPO₄ transfection method. In order to prepare the 293T cells for the transfection the cells were harvested by tryptic digestion of the adherent monolayer as described in 2.2.3; digestion was stopped by addition of 9 volumes growth medium. After cell concentration determination by trypan blue exclusion assay, 2-2.5x10⁶ cells were seeded out in a 90mm² tissue culture disk containing 10 ml of growth medium. The cells were cultured overnight under standard conditions. The following day, if the cells had reached 30-50% confluency, cotransfection was carried out under sterile conditions. All required solutions were warmed to room temperature. At first, 5 µg pMD2.G envelope plasmid, 15 µg pCMVdR8.91 packaging plasmid and 20 µg lentiviral transfer vector containing the expression cassette (pTRIPZ-shRNA), were mixed in a reaction tube, and the volume of the mixture adjusted to 250 µl using special water solution (2.5 mM HEPES, pH 7.3). Addition of 250 µl 0.5 M CaCl₂ solution resulted in complexation of the plasmid DNA with Ca²⁺. This mixture was added drop-wise to 500 µl of 2x HeBS solution (0.28M NaCl, 0.05M HEPES, 1.5 mM Na₂HPO₄, pH 7.00), under continuous air-bubbling, followed by incubation for 30 min at room temperature, in order to facilitate DNA-CaPO₄ complex precipitate formation in the solution. Subsequently, the mixture was added drop-wise onto the 293T cells prepared the day before, and the cells cultured overnight under standard conditions. The following day, the growth medium was removed and the precipitates washed off the cells with pre-warmed PBS, fresh growth medium added and the cells cultured under standard conditions for 3 days before harvesting the produced viral particles as described in section (2.2.12), plasmid cards are listed in the appendix.

2.2.12 Harvest and concentration of lentiviral particles

On day 4 post co-transfection of the 293T cells with the lentiviral plasmids, produced lentiviral particles were harvested. The supernatant of the transfected 293T cells was collected and cell debris removed by centrifugation at 3000 rpm for 15 min at room temperature. The cells and the cell debris pellet were discarded, and the supernatant filtered using a sterile PVDF membrane filter with 0.45 μM pore size. The supernatant was adjusted to a volume of 25-30 ml with filtered growth medium, and the particles harvested by ultracentrifugation at 120,000 g in a swinging bucket rotor (Beckman Instruments Inc.) for 2h at 4C. Subsequently, the supernatant was discarded by careful decantation and the virus pellet resuspended in 3 ml of target cell line growth medium. Concentrated lentiviral particles were aliquoted and kept at 4C if used the same day, or transferred to -80C for long-term storage.

2.2.13 Lentiviral transduction of acute leukaemia cell lines by spinoculation

Infection and transduction of leukaemia cell lines with lentiviral particles occurred by spinoculation. Approximately 2×10^6 leukaemic cells were harvested by centrifugation at 335g, for 5 min at room temperature; the pellet resuspended in 2 ml of pre-warmed growth medium, and seeded out per well of a six-well tissue culture plate. Approximately 700 μl - 1ml of concentrated lentiviral particles were added to the cells, and the suspension supplemented with polybrene solution (8 mg/ml) to a final concentration of 8 $\mu\text{g/ml}$. Subsequently, the cells were spinoculated by centrifugation at 1500g for 2h at 32C, followed by incubation overnight under standard conditions. On the following day, the polybrene-containing medium was removed from the cells by centrifugation at 335g for 5 min at room temperature. Subsequently, the cell pellet was resuspended of with 4 ml of pre-warmed growth medium. The transduced cells were cultured under standard conditions for at least 3 days before applying selection procedures.

2.2.14 Selection of stably transduced cells using puromycin

In order to enrich lentivirally transduced cells to a desired purity of >80%, cells were treated with puromycin. Selection was started not earlier than 72h post-infection by supplementing normal cell growth medium with puromycin (Sigma-Aldrich Company Ltd) to a final concentration of 0.5 µg/ml. In subsequent culturing steps, this concentration was incremented until reaching a 2 µg/ml puromycin dose in the culture medium. Selection pressure was maintained by culturing the cells at this or higher doxycycline concentrations up to 4 µg/ml. For experiments, cells were taken off selection medium by brief centrifugation at 335g for 5 min at room temperature and resuspended in standard growth medium.

2.2.15 Induction of shRNA expression with Doxycycline

SEM and SEM-SLIEW cells transduced with an doxycycline-inducible expression vector were grown in normal growth medium supplemented with 1 µg/ml Doxycycline (Sigma-Aldrich Company Ltd), unless otherwise stated. Full induction was attained after at least 72h doxycycline exposure, but induction could be observed already after 24h.

2.3 FLOW CYTOMETRY TECHNIQUES

2.3.1 Cell cycle analysis

Analysis of the cell cycle distribution of a cell population by flow cytometry is based on measurements of the cellular DNA content. Cells undergoing different cell cycle stages have varying DNA content, from a normal diploid (=2n) DNA content during G1/G0-phase, up to a tetraploid (=4n) chromosome set during the late S-, G2- and early M-Phase. Cellular DNA content can be quantitated with fluorescent DNA-intercalating dyes. The corresponding fluorescent signal shows

a characteristic histogramm (fig. 2-3); the fluorescence intensity correlating with the cellular DNA content and concomitantly the cell cycle distribution of a cell population.

In order to stain cells of interest, 100-300 μl of cell suspension (approximately 0.5 to 5×10^5 cells) were pipetted into a polystyrene round bottom FACS tube, the volume adjusted to 4 ml with PBS, and the cells harvested by centrifugation at 335g for 5 min at room temperature. After carefully discarding the supernatant, the cells were stained using hypotonic lysis: the cell pellet was resuspended in 100 μl citrate buffer before adding 400 μl of DNA staining and lysis buffer and 1-3 μl of DNase-free RNase A (100 mg/ml, Qiagen). The samples were kept at 4C in the dark before carrying out cell cycle analysis on the flow cytometer. Analysis of the results was performed with ModFit LT software (Verity Software House).

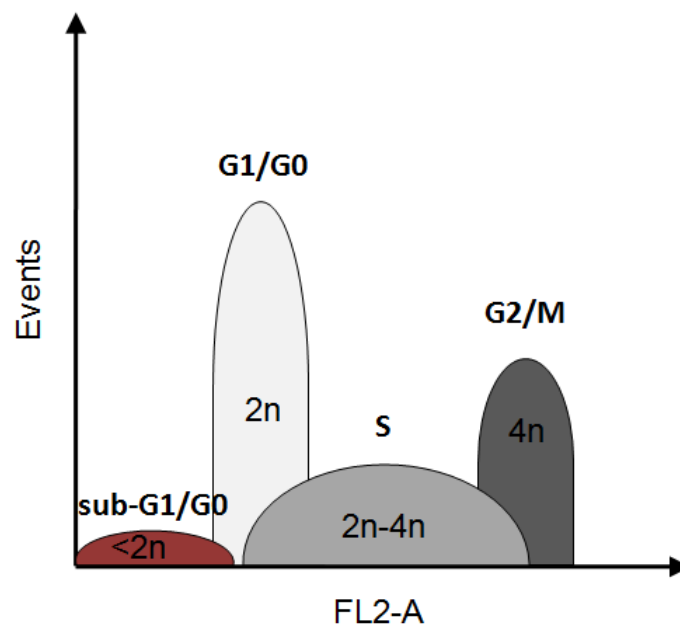


Fig. 2-3: Cell cycle histogramme schematic

2.3.2 Measurement of cells with endogenous fluorescence

Approximately 0.5 to 1 ml of cells of interest were harvested by centrifugation at 335g for 5 min at RT. The cell pellet was washed once with PBS and

resuspended with 0.5 ml of PBS. Fluorescent cells were measured by flow cytometry using the appropriate fluorescence channels.

2.3.3 Expression analysis of membrane-bound TNF and its cognate receptors TNFR1 and TNFR2 by flow cytometry

Approximately 2×10^6 cells per sample were harvested by centrifugation for 5 minutes at 400g and 4°C. All the subsequent incubation and centrifugation steps were performed on ice or at 4°C, respectively. The pellet was resuspended in 600 μ l PBAF buffer (0.02% NaN₃; 0.025% BSA, 1% FCS) and the suspension pipetted in 100 μ l aliquots into a FACS tube or the well of a v-shaped 96-well plate. Subsequently, the cells were washed by centrifugation for 5 min at 400g, followed by resuspension of the cell pellets in 100 μ l of the appropriate primary antibody-PBAF solution, according to tab. 2-6. The cells were stained in the dark for 1h, followed by wash steps with PBAF buffer for 5 min at 400g. Each cell pellet was subsequently resuspended with 100 μ l of the corresponding secondary antibody-PBAF solution (tab. 2-6) and stained for approximately 1h in the dark. After two-wash steps, the cells resuspended in 400 μ l PBAF buffer and analysed on the flow cytometer.

Tab. 2-6: TNF/TNFR antibody -PBAF solution pipetting scheme

Sample	1° antibody	dilution	2° antibody	dilution
unstained control	PBAF	PBAF	anti-mouse IgG-FITC	0.75 μ g/ml
TNFR1	TNFR1(H398)	2 μ g/ml	anti-mouse IgG-FITC	0.75 μ g/ml
TNFR2	TNFR2(MR2-1)	5 μ g/ml	anti-mouse IgG-FITC	0.75 μ g/ml
membraneTNF	TNF-T1	3 μ g/ml	anti-mouse IgG-FITC	0.75 μ g/ml

2.3.4 Multi-colour flow cytometry

Multi-colour flow cytometry is performed if more than one fluorophor is analysed in parallel. This is possible because different fluorescent dyes possess specific excitation and emission spectra, which allow excitation and subsequent recording of emitted signals in separate channels. However, in case where the emission spectra of two or more fluorophors overlap, “spill-over” of one fluorophor signal into the signal channel from another one occurs, falsifying the measurement. This has to be corrected for by a process termed compensation. In order to apply compensation, a single stain control tube has to be acquired individually for each fluorophor, including an unstained control. Using software-specific compensation controls (automated compensation controls for FACSDiva, manual compensation controls for CellQuestPro) and the underlying algorithms, a compensation matrix is generated which deconvolutes the overlapping emission spectra, allocating each signal assigned to the correct channel. This compensation matrix is the applied on the actual acquisition of the samples of interest.

2.3.4.1 Cell death determination via ANNEXINV-FITC/PI-staining

Under normal conditions, the phospholipid phosphatidylserine is usually located on the inner membrane leaflet; however, at the onset of apoptosis, this phospholipid becomes exposed on the cell surface. ANNEXINV specifically recognises and binds phosphatidylserine. Consequently, staining of the cells with ANNEXINV conjugates allows detection of cells undergoing apoptosis.

Approximately 2.5×10^5 cells per sample were harvested by centrifugation at 335g for 5 min, and washed twice with 2-3 ml PBS. The pellets were resuspended in 250 μ l 1x binding buffer (2.5 mM HEPES, 35 mM NaCl, 62.5 μ M CaCl₂, pH 7.5), supplemented with recombinant hANNEXINV-FITC (Sigma-Aldrich Company Ltd), as indicated in the tab. 2-7, resulting in a cell concentration of approximately 10^6 cells/ml. Subsequently, 5 μ l of propidium iodide solution (20 μ g/ml) was added to all samples bar the unstained and

FITC-single stain control, and incubated for 15 min in the dark at room temperature before measuring the fluorescence on the flow cytometer.

Tab. 2-7: ANNEXINV-FITC/PI staining pipetting scheme

sample	ANNEXINV-FITC	Propidium iodide
unstained control	1x binding buffer only	0
PI single stain control	1x binding buffer only	5 µl
FITC single stain control	1:750 in 1x binding buffer	0
sample of interest	1:750 in 1x binding buffer	5 µl

2.3.4.2 Five-colour flow cytometry analysis

Five-colour flow cytometry was employed in order to determine the extent of human chimerism of mouse xenografts. Tissue was derived and processes as described in 2.6.3. Single cell suspensions were centrifuged at 3355 g for 5 min, room temperature, and cell number determined using trypan blue exclusion counting. If possible, at least 500,000 cells were harvested and resuspended in 100 µl PBS. Cells were stained with antibodies against human or mouse-specific CD markers all added together at one, as seen in (tab. 2-8); the cells analysed were endogenously positive for GFP (green fluorescent protein) and RFP (red fluorescent protein). Cells were stained for approximately half an hour in the dark and subsequently acquired on the FACS Canto II flow cytometer (Becton Dickinson, UK) and analysed using FACSDiva v6.1.2 software (BD Biosciences). Gating strategy was on PE-Cy7^{dim}/ APC^{high}, in order to differentiate between human and mouse tissue.

Tab. 2-8: CD marker pipetting scheme

clone		
α -hCD19-APC	SJ25C1	2.5 μ l
α -hCD34-PerCP-Cy5.5	8G12	10 μ l
α -murine Cd45-PE-Cy7	30-F11	2.5 μ l
α -murine Ter119-PE-Cy7	Ter119	2.5 μ l

2.4 MOLECULAR BIOLOGY TECHNIQUES

2.4.1 RNA purification and Concomitant Protein Isolation Using the QIAGEN RNeasy Mini Kit

RNA was isolated from patient material and cell lines using the RNeasy Mini Kit (Qiagen, Crawley, UK), according to manufacturer's protocol. All steps were carried out at room temperature unless otherwise indicated. Briefly, 1×10^6 to 5×10^6 cells were centrifuged at 335g for 5 min, the medium removed and the pellet washed once with PBS. Lysis of the cells was performed by pipetting 350 μ l RLT buffer containing 0.1% β -mercaptoethanol (v/v) and thorough mixing. If not immediately used afterwards, the lysate was stored at -80°C , otherwise it was applied onto a QIAshredder column (Qiagen, Crawley, UK) and homogenised by centrifuging it at full speed for 2 min. The flow-through was mixed with 350 μ l 70% ethanol and transferred to a RNeasy spin column. The RNA was bound to the column membrane by a quick centrifugation step of 30s at full speed. The resulting flow-through was stored on ice in order to isolate proteins.

The RNeasy spin column was transferred into a new 2 ml collection tube provided by the manufacturer, and washed once with 750 μ l RW1 buffer and twice with 500 μ l RPE buffer. In each instance, the flow-through was discarded. In the last washing step with RPE buffer the column was centrifuged 2 min at full speed, to remove any residual liquid. As an additional step, the column was transferred to a new collection tube and the membrane by an additional centrifugation step at full speed for 1 min, before eluting the RNA with 30-50 μ l of RNase-free water and centrifugation for 1 min at full speed into RNase-free 1.5 ml reaction tubes provided by the manufacturer. In the case that the RNA was utilised for subsequent reactions on the same day, the samples were stored on ice or at 4°C , otherwise the storage conditions were $-80^\circ\text{C}/-20^\circ\text{C}$, to minimise degradation.

In order to isolate proteins for subsequent immunoblotting analyses, the flow-through of the first washing step of the RNEasy column was kept on ice. Proteins were precipitated by adding 2-3 volumes of acetone and incubation on

ice for 2h or overnight at -20°C. The proteins were harvested by centrifugation at full speed for 15min and at 4°C. The supernatant was completely removed and the pellet air-dried on ice. Finally, the proteins were resuspended in 30-50 µl urea buffer (9M urea, 4% DTT, 1% CHAPS) and stored at -20°C.

2.4.2 RNA Concentration Determination

The concentration of an RNA preparation was determined by measuring the absorbance at 260 nm using a ND1000 spectrophotometer (Nanodrop, USA).

2.4.3 RNA Integrity Measurement

The quality of a RNA preparation was analysed by lab-on-chip technology. Samples were prepared using an RNA 6000 Nano Kit (Agilent Technologies UK Ltd.) according to manufacturer's instruction; the analysis was performed on a 2100 BioAnalyzer (Agilent Technologies UK Ltd.), and the RNA integrity number (RIN) determined using the Agilent 2100 Expert Software (Agilent Technologies UK Ltd.), using the default analysis settings.

2.4.4 cDNA Synthesis

RNA was reverse transcribed into copyDNA (cDNA) using RevertAid H Minus First-Strand cDNA synthesis kit (Fermentas). The manufacturer's protocol was slightly adapted: 200ng-1 µg of RNA was mixed with random hexamer (dN6) primers (0.2 µg/µl) and deionised water (ddH₂O) to a volume of 12µl (see pipetting scheme A). Secondary structures present in the template RNA were heat-denatured at 70°C for 5 min, followed by cooling the reaction to 4°C, allowing free annealing of the dN6 primers. A reaction mastermix was prepared (see pipetting scheme B) and added to the sample mix (A). After incubation for 10 min at 25°C, reverse transcription was carried out for 60 min at 42°C and the reaction stopped by inactivation of the reverse transcriptase at 70°C for 10 min.

The cDNA sample was diluted 1.5-fold by addition of 30 μ l of deionised water and stored at -20C until further use.

Pipetting scheme A

Sample mix (A)	recipe 1x	
RNA (200ng-1 μ g)	x	μ l
dN6 primers (0.2 μ g/ μ l)	1	μ l
ddH ₂ O	ad 12	μ l
	$\Sigma=12 \mu$ l	

Pipetting scheme (B)

Reaction mastermix (B)	recipe 1x	
MMLV RT H- reaction buffer (5x)	4	μ l
dNTPs (10 mM)	2	μ l
RNaseLock Inhibitor (20U/ μ l)	1	μ l
Mu-MLV RT H- (200U/ μ l)	1	μ l
	$\Sigma=8 \mu$ l	

2.4.5 Real-time RT-PCR (qRT-PCR) using SyBr-Green

Real-time RT-PCR (qRT-PCR) is a semi-quantitative PCR-based method to determine the amounts of specific transcript in RNA preparations, cDNA is used as template. In this variant, the qRT-PCR reaction buffer (Platinum® SYBR® Green qPCR SuperMix-UDG with ROX, 2x, Invitrogen) contains SyBr-Green as reporter dye, which intercalates double-stranded DNA, emitting a fluorescent signal of a specific wavelength, thus allowing to monitor the accumulation of amplification product. The intensity of this emitted SyBR Green signal can be assumed as being proportional to the amount of amplified DNA.

Briefly, a reaction mastermix for each individual primer was prepared as indicated by the pipetting scheme (see below), 8 μ l were added per well of a

384-well plate (MicroAmp® Optical 384-Well Reaction Plate, Applied Biosystems), followed by 2 µl cDNA solution. Each sample was pipetted at least in duplicates, typically in triplicates. Eventually, the plate was sealed (MicroAmp® Optical Adhesive Film, Applied Biosystems), briefly centrifuged, and placed in a 7900 HT Real Time PCR System thermal cycler (Applied Biosystems). Cycling conditions are indicated in fig. 2–4; the data was acquired with the ABI SDS 2.2 System software (Applied Biosystems) and subsequently analysed by applying manual baseline and threshold adjustments. The resulting C_T-values were utilised for quantification analyses as specified in 2.4.5.1 and 2.4.5.2.

Pipetting scheme-general primers

<u>Reaction mix:</u>	<u>recipe 1x</u>		<u>final con</u>
Primer (10 uM fw+rev mix)	0.3	µl	300 nM
SyBr-Green master mix (2x)	5	µl	1x
H ₂ O	2.7	µl	
cDNA	2	µl	20%
	Σ = 10	µl	

Pipetting scheme-MLL/AF4 primers

<u>Reaction mix:</u>	<u>recipe 1x</u>		<u>final con</u>
Primer (5 uM fw+rev mix)	0.1	ul	50 nM
SyBr-Green master mix (2x)	5	ul	1x
H ₂ O	2.9	ul	
cDNA	2	ul	20%
	Σ = 10	ul	

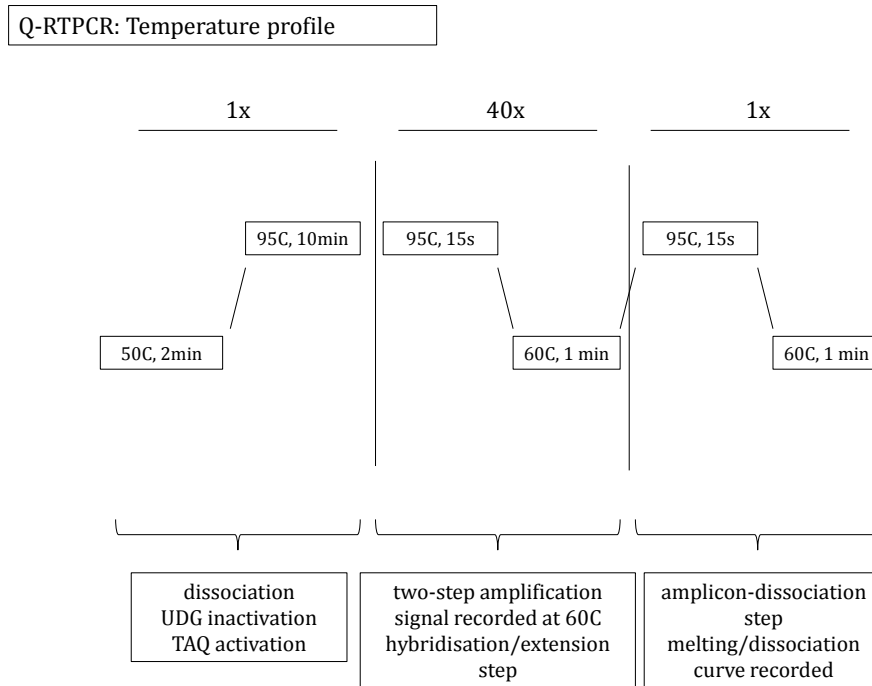


Fig. 2-4: QRT-PCR cycling conditions

2.4.5.1 $\Delta\Delta Ct$ Method

This analysis method compares the expression of a gene of interest (GOI) against the expression of a housekeeping gene (HKG) of a sample, yielding $-\Delta Ct$ - values, and subsequently normalises this $-\Delta Ct$ -value against the $-\Delta Ct$ -value of a reference sample, resulting in normalised relative expression values. Following mathematical equation is used:

$$(1) \quad -\Delta Ct_{sample} = Ct_{GOI} - Ct_{HKG}$$

$$(2) \quad -\Delta Ct_{reference} = Ct_{GOI} - Ct_{HKG}$$

$$(3) \quad -\Delta\Delta Ct_{sample} = \Delta Ct_{sample} - \Delta Ct_{reference}$$

Since each Ct value corresponds to a log₂-fold change the $\Delta\Delta Ct$ -values have to be linearised by using antilog to the base of 2:

$$(4) \quad 2^{-\Delta\Delta Ct} = rel. RNA \text{ expression}$$

2.4.5.2 ΔCt -Method

This analysis method compares the expression of a gene of interest (GOI) against the expression of a housekeeping gene (HKG), without normalising it against a control sample, reflecting absolute expression levels of the gene of interest for each individual sample. Expression is stated as %HKG. Following equation is used:

$$(1) \quad -\Delta Ct = Ct_{GOI} - Ct_{HKG}$$

Since each Ct value corresponds to a log₂-fold change, the ΔCt -values have to be linearised by using antilog to the base of 2:

$$(2) \quad \% HKG = (2^{-\Delta Ct}) \times 100$$

2.4.6 RT-PCR

RT-PCR allows qualitative detection of transcripts. RNA is first reverse transcribed into cDNA, which is the subsequently used for the PCR reaction. cDNA was mixed with 50% (v/v), which already contains the appropriate amounts of MgCl₂, dNTPs and Taq-polymerase, and supplemented with 300 nM forward and reverse primer (see sceme below). PCR was performed in the GeneAmp PCR System 2700 (Applied Biosystems), using following standard conditions: after an initial heat-denaturation step at 95C for 5 min, the cycling reaction was started; the reaction was cooled down for 30s to 56C, in order to allow annealing of the primers to the template, followed by increasing the temperature to 72C, which is the optimum temperature for *Taq* polymerase-mediated extension. After 30s, the temperature was increased again to 95C for 30s, resulting in denaturation of the newly synthesised DNA. This process was repeated for 35 cycles, after the final one, the temperature was held for 10 min at 72C in order to allow full extension of the synthesised DNA.

The PCR products were subsequently detected by agarose gel electrophoresis.

Pipetting scheme-general

<u>Reaction mix:</u>	<u>recipe 1x</u>	<u>final conc</u>
Primer (10 μ M fw+rev mix)	0.625 μ l	300 nM
PCR 2x	5 μ l	1x
H ₂ O	2.7 μ l	
cDNA	1 μ l	20%
	$\Sigma = 25$ μ l	

2.4.7 DNA-Polyacrylamid gel electrophoresis (DNA-PAGE)

DNA-polyacrylamide gel electrophoresis was performed to analyse PCR products smaller than 300 bp. In brief, a vertical immunoblotting casting chamber was assembled, consisting of two glass plates separated by spacers and fastened on a casting stand by holders (Mini-Protean II, BIORAD). An 8% polyacrylamide gel was poured using 1x TBE buffer (0.09 M Tris, pH 8, 0.09 M H₃BO₄, 2 mM EDTA) as denoted in the recipe below). Immediately afterwards, a comb was set into the liquid gel in order to generate wells via the comb teeth. After polymerisation, the cassette was transferred to the electrophoresis tank for vertical gel electrophoresis. The DNA samples of interest were mixed with the appropriate amount of 6x DNA-loading buffer (25% glycerine; 0.05% bromphenol blue) and loaded into the wells. Electrophoresis buffer was 1x TBE (0.09 M Tris, pH 8, 0.09 M H₃BO₄, 2 mM EDTA); the gel was run at 50-70V. Subsequently, the DNA was visualised by counterstaining the gel in an EtBr solution (3-5 μ g/ml) and detected using Quantity One software.

<u>DNA-polyacrylamide gel recipe</u>	<u>1x</u>
5x TBE	2 ml
Acrylamide/bisacrylamide (19:10), 40%	2 ml
APS (10%)	0.5%
TEMED	0.1%
H ₂ O	6 ml
	$\Sigma = 10$ ml

2.4.8 Agarose gel electrophoresis

Agarose gel electrophoresis was performed to visualise DNA fragments. A gel was prepared by mixing agarose with 1x TAE buffer (0.04 M Tris, pH 8, 0.114% acetic acid, 1 mM EDTA) or 1x TBE buffer (0.09 M Tris, pH 8, 0.09 M H₃BO₄, 2 mM EDTA) to a final concentration that ranged from 0.8 to 2.5% according to the size of the DNA to detect. This suspension was heated until the agarose was fully melted, and this gel was poured into a horizontal gel tray. In order to generate wells, a comb was introduced before the gel had an opportunity to set. After polymerisation, the gel was transferred into a horizontal electrophoresis tank and this unit filled up with electrophoresis buffer (1x TAE or 1X TBE). DNA premixed with 6x DNA loading dye (Fermentas) was applied into the wells, as well as a DNA size marker, in order to determine fragment size, and the electrophoresis was performed at 80-120V.

Subsequently, the DNA was visualised by counterstaining the gel in an EtBr solution (3-5 µg/ml) and detected using Quantity One software.

2.4.9 Isolation of endotoxin-free plasmids for mammalian transfection

Plasmids employed for transfection into a mammalian cell line were purified using the EndoFree Plasmid MAXI Kit (Qiagen, Crawley, UK) according to manufacturer's protocol.

2.5 PROTEOMIC METHODS

2.5.1 Protein Isolation

Protein isolation was performed as described in section 2.4.1.

2.5.2 SDS-PAGE

This electrophoresis method separates proteins in a polyacrylamide gel based upon their size, as migration through the gel is proportional to \log_{10} of the molecular weight. The discontinuous Laemmli-buffer system was utilised to generate a SDS-polyacrylamide gel: First, a casting chamber was assembled, consisting of two glass plates separated by spacers and fastened on a casting stand by holders (Mini-Protean II, BIORAD). A resolving gel of a specific acrylamide-concentration (0.35 M Tris, pH 8.8; 5% - 15% acrylamide/bisacrylamide solution, 19:1; 0.1% SDS, 0.05% APS, 0.1% TEMED) was poured into three quarters (approximately 3ml) of the chamber, and overlaid with 1 ml isopropanol, in order to protect the gel border from setting unevenly due to air currents. After polymerisation, the isopropanol was poured off and a stacking gel (0.125M Tris, pH 6.8; 3.9% acrylamide/bisacrylamide solution, 19:1; 0.1% SDS, 0.05% APS, 0.1% TEMED) was cast on top of the resolving gel. Immediately afterwards, a comb was set into the liquid stacking gel in order to generate wells in the stacking gel via the comb teeth. After polymerisation, the cassette was transferred to the electrophoresis tank for vertical gel electrophoresis. The protein samples of interest were mixed with the appropriate amount of 2x SDS-loading buffer (100 mM Tris, pH 6.8; 2.5 mM EDTA, pH 8.0; 25% glycerine; 0.05% bromphenol blue; 100 mM DTT) and loaded into the wells. Electrophoresis buffer (25 mM Tris; 190 mM glycine; 0.1% SDS) was added the electrophoresis tank, and the run started by applying current: 80V for the migration of the proteins through the stacking gel, 130V for the remainder of the run.

2.5.3 Immunoblotting

This technique encompasses transfer of proteins from a SDS-PAGE gel onto a membrane and subsequent detection with specific antibodies against the protein of interest.

After the SDS-PAGE run, the holder cassette for the protein transfer was assembled as follows: first a sponge pad and a sheet of absorbent filter paper, then the gel, the membrane (Immobilon-P PVDF, Millipore), a sheet of absorbent filter paper and finally another sponge pad. All components were pre-soaked in transfer buffer (25 mM Tris; 190 mM glycine; 10% methanol) and the cassette assembled submerged in transfer buffer in order to prevent trapping air bubbles between gel and membrane. The PVDF membrane was first pre-wet for 30s-1 min in 100% methanol, before soaking it in transfer buffer. The cassette was placed into the electrode assembly membrane facing the anode and the transfer tank filled with transfer buffer. Transfer conditions were 1h to 1h 30 min at 100V. After the transfer and disassembling of the cassette, the membrane was briefly rinsed in water and the transfer verified by staining for 5 min in Ponceau S-solution. Eventually, the membrane was rinsed in TST buffer (10 mM Tris, pH 7.5; 100 mM NaCl; 1 mM EDTA, pH 8.0; 0.1% Tween-20) and blocked for 30 min with 5% milk/TST solution (w/v) before transferring it into a universal containing 3 ml of antibody-milk/TST-solution (see tab. 2-4) and incubated overnight at 4°C on a rotating platform. The next day, the membrane was washed with TST buffer 3x for 5 min on a rotating platform, in order to remove unbound antibody. The membrane was probed with a secondary antibody against the primary antibody in 3 ml of antibody-milk/TST-solution for 1h-2h at room temperature on a rotating platform. Excess unbound antibody was washed off 3x in TST buffer for 5 min. Detection was carried out using a luminol-based detection system.

2.5.3.1 Luminol-based detection using Immobilon™ Western Chemiluminiscent HRP Substrate

The secondary antibodies used were conjugated to the enzyme horseradish peroxidase (HRP). This enzyme is able to metabolise the luminol contained in the detection reagent into a luminescent compound which can be visualized by exposing an X-ray film (KODAK); the region of the protein-antibody complex appears on the X-ray film as a band. First, the membrane was incubated with the detection solution made up with 1 volume HRP substrate peroxide solution and 1 volume HRP luminol reagent (Immobilon™ Western Chemiluminiscent HRP Substrate, Millipore) was applied on the PVDF membrane and incubated for 5 min (1 min if GAPDH or Tubulin were detected) at room temperature. Next, excess detection reagent was drained off, the membrane wrapped in cling film and placed into a film cassette. Then, under exclusion of light, an X-ray film (KODAK) was laid on top of the membrane and exposed for varying time periods (1 sec to 10 min), and subsequently developed.

2.5.3.2 Luminol-based detection using SuperSignal West Dura Chemiluminiscent Substrate

The secondary antibodies used were conjugated to the enzyme horseradish peroxidase (HRP). This enzyme is able to metabolise the luminol contained in the detection reagent into a luminescent compound which can be visualized by exposing an X-ray film (KODAK); the region of the protein-antibody complex appears on the X-ray film as a band. First, the membrane was incubated with the detection solution made up with 1 volume Stable Peroxide Buffer and 1 volume Luminol/Enhancer reagent (SuperSignal West Dura Chemiluminescent Substrate, Pierce, Thermo Scientific Inc.) was applied on the PVDF membrane and incubated for 5 min at room temperature. Next, excess detection reagent was drained off, the membrane wrapped in cling film and placed into a film cassette. Then, under exclusion of light, an X-ray film (KODAK) was laid on top of the membrane and exposed for varying time periods (1 sec to 10 min), and subsequently developed.

2.5.4 Enzyme-linked immunosorbent assay (ELISA) for ANGPT1 detection in cell culture supernatant

Cells growing in culture were pelleted by centrifugation for 5 min at 335g, room temperature, and the supernatant harvested for ANGPT1 protein level determination, and stored at -20C until the time of analysis. ANGPT1 concentration in the cell culture supernatant of cells was determined using the Quantikine® ANGPT1 ELISA Kit (Quantikine® Colorometric Sandwich ELISA, R&D Sustems, Inc.) exactly according to manufaturer's instructions.

2.6 IN VIVO TECHNIQUES

2.6.1 Xenotransplantation of leukaemic cell lines by intrafemural injection (performed by Mr. M. Batey)

6-month-old NOD.Cg-*Prkdc^{scid} Il2rgtm1^{Wjl/Szj}* (NSG) mice were anaesthetised using isoflurane (IsoFlo, Abbott laboratories, Maidenhead, UK) as an oxygen/isoflurane gas mix (4-5%) in an induction chamber, at approximately 1500cc/min oxygen until the animal lost consciousness. To test whether the required depth of anaesthesia had been attained, unconsciousness was verified by testing righting and pinching reflex. Subsequently, the mice were transferred to a face mask supplying an oxygen/isoflurane gas mix of 3-4% in order to maintain unconsciousness throughout the surgical procedure. An analgesic, Carprofen (Rimadyl, Pfizer, Kent, UK), was injected subcutaneously, using a dose of 5 mg/kg body weight. Subsequently, mice were laid in a supine position, the fur from the right hind limb shaved off, and the skin disinfected with a Chlorhexidine spray (Hydrex Pink, Ecolab, Yorkshire, UK). The right leg of the mouse was flexed and this position tightly maintained throughout the procedure. The bottom of the femur was punctured from the direction of the knee using an insulin syringe. The needle was subsequently withdrawn, while keeping the leg tightly in position, and a new insulin needle, containing the cells to be transplanted, was introduced into the pre-drilled hole. Approximately 10

μl of the cell suspension were injected, which corresponded to a cell number of $\sim 50,000$ cells. After the surgery, the mice were returned to their cage and monitored for satisfactory recovery from anaesthesia.

2.6.2 *In vivo* bioluminescence imaging (performed by Mr. M. Batey)

Anaesthesia was induced as described in 2.6.1.; mice were injected intraperitoneally with approximately 150mg/kg body weight D-luciferin (Xenolight RediJect D-luciferin, Caliper Life Science), and placed into the imaging chamber of the IVIS® Spectrum Imaging System (Xenogen Corporation), anaesthesia was maintained with an oxygen/isoflurane mixture supplied via a coupled XGI-8 Gas Anaesthesia System (Xenogen Corporation). Pictures were acquired under a firefly luciferase filter and analysed using the IVIS Spectrum Living Image® 4.0 software (Caliper Life Science).

2.6.3 Necropsy and harvest of material

Mice presenting clinically unwell were sacrificed using cervical dislocation. Typically, the femora and tibiae from the hind limbs were harvested, and the bone marrow flushed from these bones using a syringe with PBS. The spleen, and, when present, tumour tissue, were harvested, weighed and measured, and then processed using a BD™ Medimachine System (BD BioSciences), to obtain single cell suspension. Briefly, the tissue was cut into small pieces with a scalpel and placed into the Medicon shredder cartridges (BD BioSciences), which were filled with approximately 1 ml of PBS. The cartridges were introduced into the BD™ Medimachine System and the tissues processed until completely shredded; the cartridge was refilled with PBS repeatedly.

2.7 BIOINFORMATIC METHODS

2.7.1 Array Analysis

RNA samples were processed for Illumina HT12-v3 BeadChip (Illumina Inc.) and Illumina HT12-v4 BeadChip (Illumina Inc.) arrays according to manufacturer's protocol at a service provider facility (Gen-Probe Inc., formerly Tepnel Life Sciences).

2.7.2 Pre-processing of raw data using BeadStudio/GenomeStudio Software packages (Illumina Inc.)

Raw data files were pre-processed using BeadStudio V3 or GenomeStudio V1 software packages (Illumina Inc.) in separate experimental groupings, each comprising control-treated and siMLL/AF4-treated samples for one time point and one inhibitor condition. Background subtraction was applied, and the data of each experimental group exported as SampleProbeProfile format specific for the GeneSpring GX 11 software package (Agilent Technologies UK Ltd).

2.7.3 Normalisation and differential gene expression analysis using GeneSpring GX 11 software (Agilent Technologies UK Ltd)

SampleProbeProfile files generated by BeadStudio or the Genomestudio software suites were imported and analysed using the advanced settings option as follows:

Samples were assigned the parameter "siRNA", and grouped according to conditions:

- siMLL/AF4 = siMLL/AF4-treated samples
- Ctrl = corresponds to MOCK and siAML1/MTG8

This was followed by normalization of the samples using a quantile normalisation algorithm. Furthermore, each sample was baseline-transformed

over the median intensity values of the control samples (MOCK, siAML1/MTG8). Next, samples were filtered according to flag “calls”, three out of three samples had to call P(resent) for each probe. Flags were assigned using GeneSpring GX 11 default settings as follows:

- P(resent): Illumina Flag-values of 1.0-0.8
- M(arginal): Illumina Flag-values of 0.79-0.6
- A(bsent): Illumina Flag-values <0.59

Differential expression of siMLL/AF4 vs. Ctrl was performed by applying a 2.0-fold change; signal intensities of multiple samples in one condition (i.e., MOCK and siAML1/MTG8 are both designated “Ctrl”) were averaged.

Thus derived entity lists were subsequently exported as text files for further analyses.

2.7.4 Comparison analysis using R

The overlap of entities between two datasets was analysed using the Limma package (Bioconductor) in the R x64 2.12.2 software, using script *Venn*; subsets of expression data were extracted from the paternal expression data sets using script *Extraction* (see appendix). Both scripts were kind gifts from Mr. R. Ernst and Mr. E. van Roon.

2.7.5 Ingenuity Pathway Analysis

A text file comprising Probe IDs and the corresponding fold-changes was generated from the GeneSpring output text-file. This signature was loaded into the Ingenuity Pathway Analysis Software (Ingenuity Inc.). A core analysis was performed according to the software documentation, which resulted in an output of networks, pathways and biological and molecular functions, which were enriched for the loaded signature.

2.7.6 Gene Set Enrichment Analysis (GSEA)

Core signatures were generated by intersecting data sets according to 2.7.4. Consequently, text files in the appropriate format were generated, as well as phenotype label files, as specified, and loaded into GSEA (Gene Set Enrichment Analysis) software (<http://www.broadinstitute.org/gsea/index.jsp>). The ranking metrics applied were Diff_of_Classes, gene sets of a size between 10 and 1000 were included. The analysis algorithm performed 1000 permutations. A gene set was assumed to be significantly enriched if the adjusted *p*-Value was <0.25. Leading edge analysis was performed with significantly positive enriched datasets that fit these criteria.

2.7.7 Heat map generation using GenePattern

Core signatures were generated by intersecting data sets according to 2.7.4. Consequently, text files were generated in the appropriate format for the HeatMapImage module of the GenePattern genomic analysis software (<http://www.broadinstitute.org/cancer/software/genepattern/>).

2.8 STATISTICAL ANALYSIS

Statistical differences between parametric samples were assessed by Student's *t*-test using GraphPad Prism 5 software (GraphPad Software, Inc.; La Jolla, USA) or Excel 2007 (Microsoft Inc.). Non-parametric cohorts were tested using Mann-Whitney U test. When testing larger sample cohorts, normal distribution was confirmed using a Shapiro-Wilk test; if non-normally distributed, the values were log-transformed, allowing subsequent analysis for statistical significance using parametric Student's *t*-tests (if two groups were compared), or one-way ANOVA analyses (if several cohorts were analysed at once). Multiple testing correction was applied when required. Here, the GraphPad Prism 5 software was used in all instances. Significance levels were indicated as * = $p < 0.05$; ** <math>p < 0.01</math> and *** = $p < 0.001$.

3. The role of MLL/AF4 in leukaemic maintenance

3.1 RNAI-MEDIATED DEPLETION OF MLL/AF4 AFFECTS CELL PROLIFERATION AND VIABILITY

3.1.1 siRNA-mediated ablation of *MLL/AF4* in t(4;11)-positive ALL cells

Acute lymphoblastic leukaemia harbouring an MLL aberration carries in >50% of the cases the t(4;11)(q21;23) rearrangement, regardless of age at presentation. This balanced translocation results in two reciprocal proteinogenic fusion genes, *MLL/AF4* (der11) and *AF4/MLL* (der4). While der11 is present in 100% of the cases, der4 is lost in at least 20% due to further genetic lesions. The breakpoint region in the t(4;11) rearrangement spans exon 8-13 in the *MLL*, and exon 2-7 in the *AF4* locus, and therefore offers multiple fusion combinations with unique breakpoints. In current study the t(4;11)-positive cell line SEM was employed as model cell line for investigating how loss of endogenous MLL/AF4 affected cells on a molecular level. The SEM cell line harbours the MLL/AF4 (e9-e4) gene, where the breakpoint in the wild-type genes occurred in the intronic region between exon 9 (e9) and exon 10 (e10) of MLL/AF4, and in intron 4 of *AF4*. The resulting fusion transcript results in a chimaera constituting of a truncated *MLL* including e9, and the *AF4* gene from exon 4 (e4) downstream.

Previously, our group designed a siRNA directed against this fusion sequence (siMLL/AF4), and suitable qRT-PCR primers for detection. Fig. 3-1 depicts schematically the target sequence of the siMLL/AF4 siRNA and the position of suitable qRT-PCR primers for detection within the fusion transcript. For analysis of the *MLL* or *AF4*, the reverse or the forward primers were exchanged for ones binding in the wild-type gene sequence, respectively (not shown). The MLL/AF4 qRT-PCR primers were also capable to detect the fusion transcript of other two t(4;11)-positive cell lines acute leukaemia cell line, RS4;11 (e10-e4) and MV4;11 (e9-e5) (not shown).

MLL_(ENSE00001799616)/**AF4**_(ENSE00001196741) • ENSE00001196741

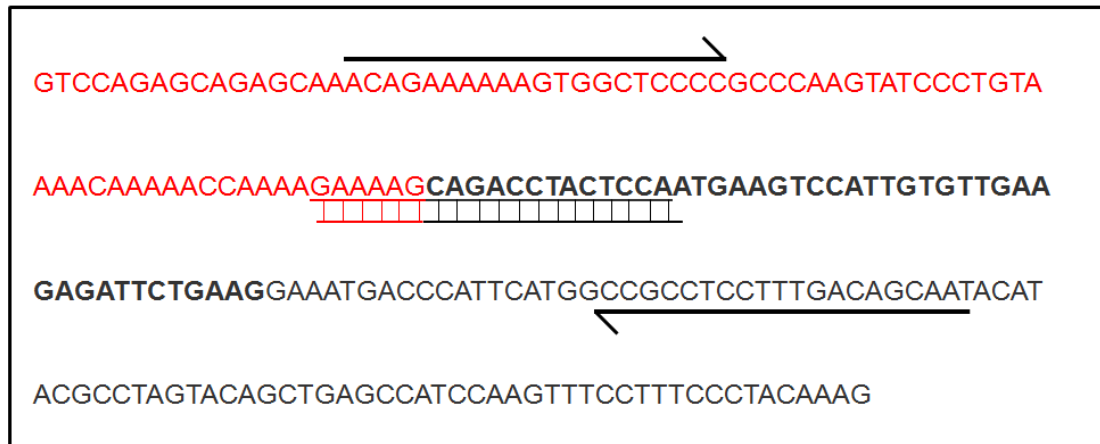


Fig. 3-1: e9-e4 MLL/AF4 fusion gene breakpoint cDNA sequence

The *MLL/AF4* fusion gene inherent of the SEM cell line results from the in-frame fusion of the N-terminal *MLL* until exon 9 (red, ENSEMBL_ID ENSE00001799616) to the *AF4* moiety from exon 4 onwards (bold black font, ENSEMBL_ID ENSE00001196741). The siRNA against *MLL/AF4* (si*MLL/AF4*) spans the fusion sequence, the corresponding qRT-PCR primers lie in the *MLL* exon 9 and *AF4* exon 5 (black font, ENSEMBL_ID ENSE00001196741).

In order to study the role of *MLL/AF4* in t(4;11)-positive leukaemic maintenance, the following experimental set-up was chosen: the t(4;11)-positive ALL cell line SEM was serially electroporated at two day intervals with either siRNA against *MLL/AF4* (si*MLL/AF4*) or an active control siRNA (si*AML1/MTG8*), which targets the *AML1/MTG8* fusion gene harboured by t(8;21)-positive AML cells and absent in this cell line. In addition, a pulse-control was performed as well, where cells were electroporated without siRNA oligonucleotides (MOCK). This transfection was carried out up to three times, and cells were harvested prior to the subsequent electroporations at day 2

(TP1) and 4 (TP2), and at the final time point TP3, corresponding to day 6 (fig. 3-2).

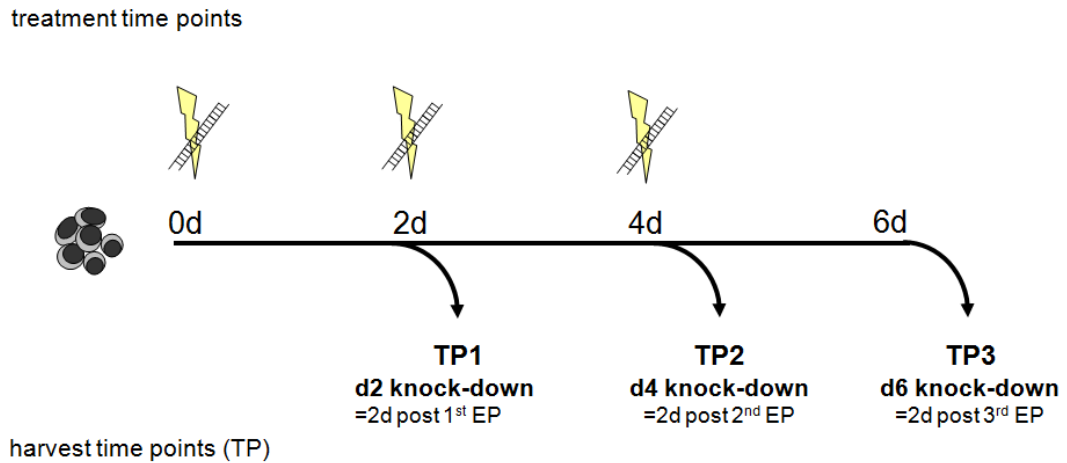


Fig. 3-2: Experimental set-up: siRNA electroporation time course for MLL/AF4 knock-down

The SEM cell line was sequentially transfected with either siRNAs against MLL/AF4 (siMLL/AF4), control siRNA (siAML1/MTG8), or mock-electroporated (MOCK) at two day intervals for up to 3 times, representing a sustained depletion period of 6 days (6d). Material was harvested for analyses immediately prior to the subsequent electroporation (TP1, TP2), and at the final time point, two days after the 3rd electroporation (TP3/6d).

In order to ascertain that the employed electroporation settings did indeed result in uptake of siRNA, SEM cells were electroporated with a fluorochrome-conjugated siRNA and subsequently analysed by flow cytometry at 2h, 4h and 25h post-transfection. Electroporation of SEM cells at 350V for a 10 ms pulse resulted in siRNA uptake in 80% of the cells; this dropped to 67% 4h post-transfection. On the following day, fluorescent siRNA could still be detected in 20% of the cells (fig. 3-3).

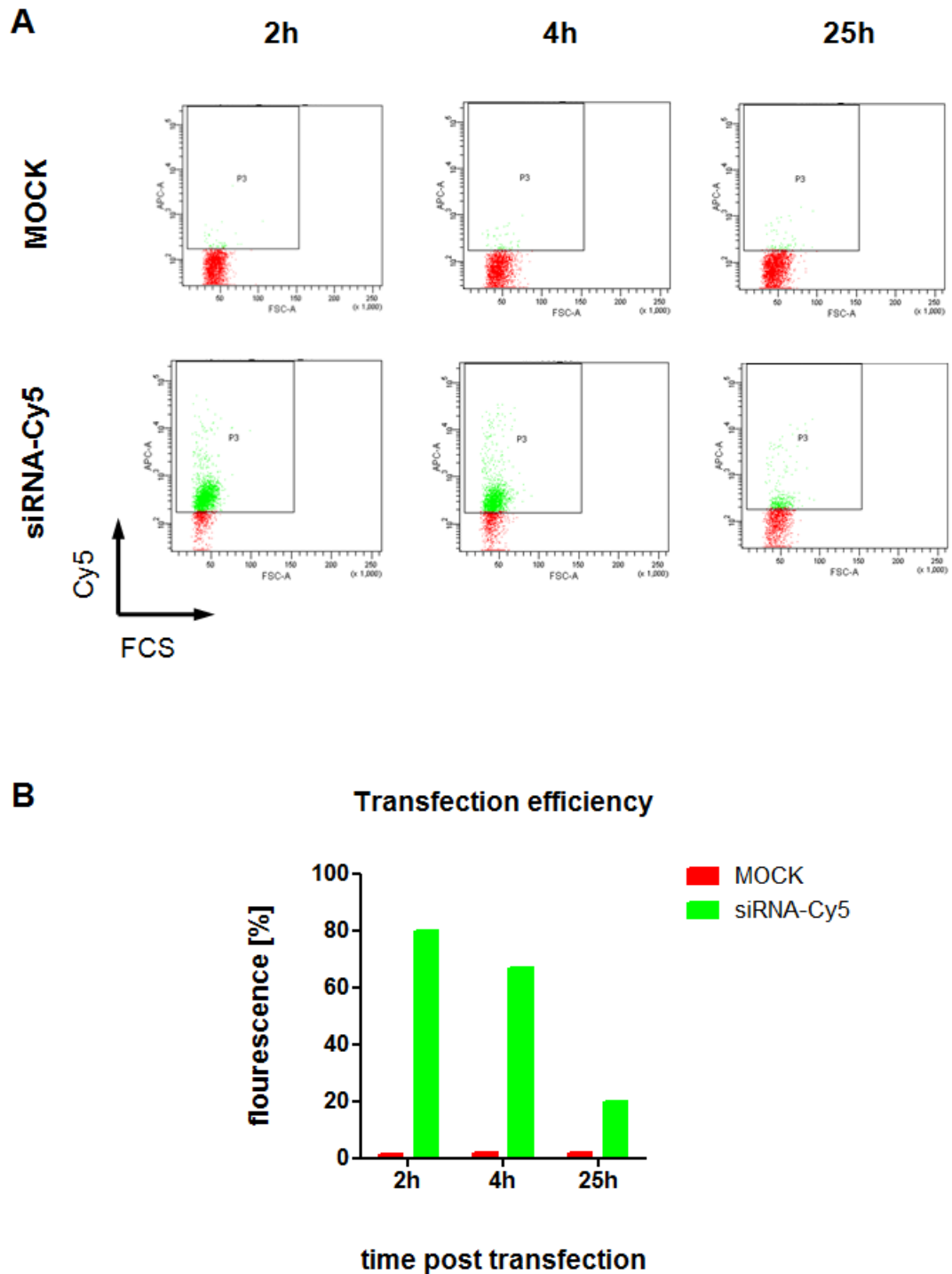


Fig. 3-3: siRNA transfection efficiency

SEM cells were electroporated once with a fluorescently-labelled siRNA (siRNA-Cy5) using a rectangular electronic pulse of 350V and 10ms. The corresponding pulse controls was electroporated with the same settings, but without siRNA (MOCK). Transfection efficiency was determined at different time points post-electroporation (2h, 4h and 25h) using flow cytometry (A), quantifying the percentage of the Cy5-positive SEM subpopulation (B).

Depletion mediated by siMLL/AF4 was confirmed by qRT-PCR; MLL/AF4 levels showed a sustained decrease by 70-80% over all three time points compared to controls (fig. 3-4).

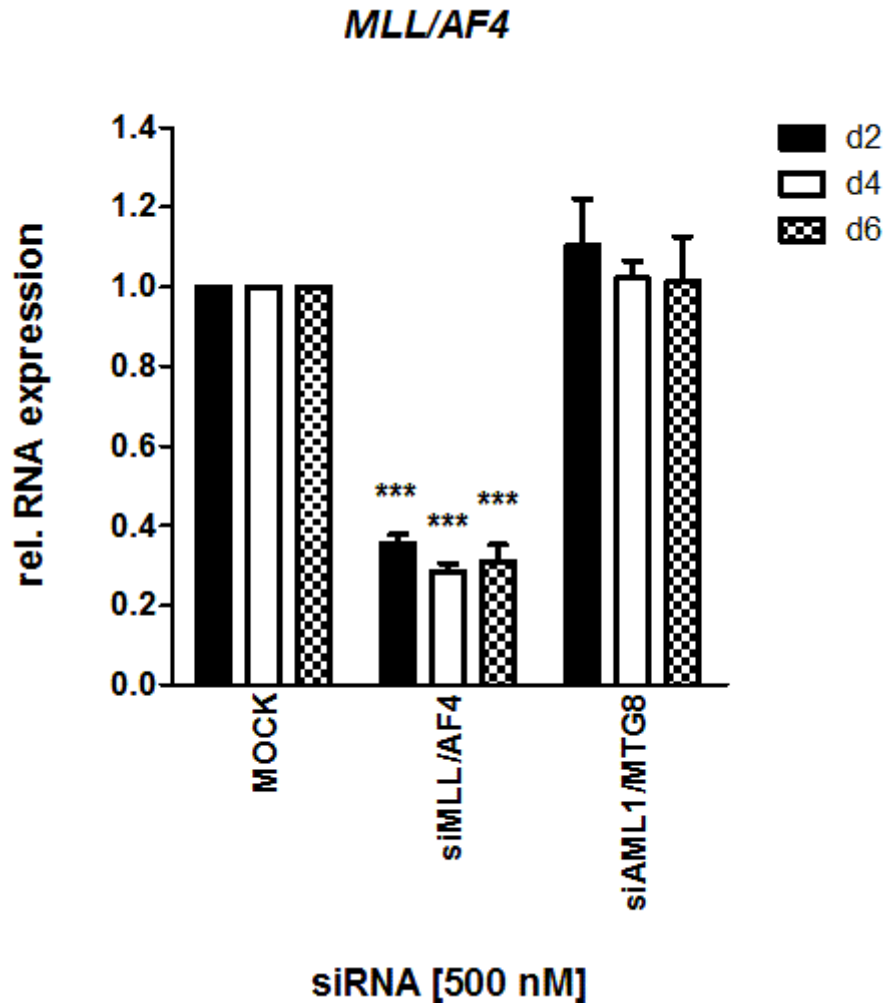


Fig. 3-4: MLL/AF4 expression analysis by qRT-PCR

SEM cells were serially electroporated three times at two-day intervals with either siMLL/AF4, control siRNA (siAML1/MTG8) or no siRNA (MOCK). Treatment with siMLL/AF4 resulted in MLL/AF4 down-regulation by 65-72%, which was sustained for up to 6 days. The graph represents the mean of n=5 independent experiments, error bars indicate standard error of the mean (S.E.M.). Statistic analysis was carried out using an unpaired Student's t-test (***) = $p < 0.001$).

The siRNA against *MLL/AF4* did not only work efficiently in the SEM cell line, but also in primary patient cells. Viable leukaemic blasts from a patient with t(4;11)-positive ALL, carrying the same *MLL/AF4* breakpoint fusion site as the cell line SEM (courtesy of Dr. Ronald Stam), were singly electroporated with either siMLL/AF4, control siRNA (siAML1/MTG8), or without siRNA (MOCK). RNA was harvested at 24h, 48h and 72h post electroporation, and *MLL/AF4* expression assessed by qRT-PCR. A knockdown of *MLL/AF4* transcript levels comparable to the one in the SEM cells was achieved, with a sustained reduction by 54-64% over the course of three days.

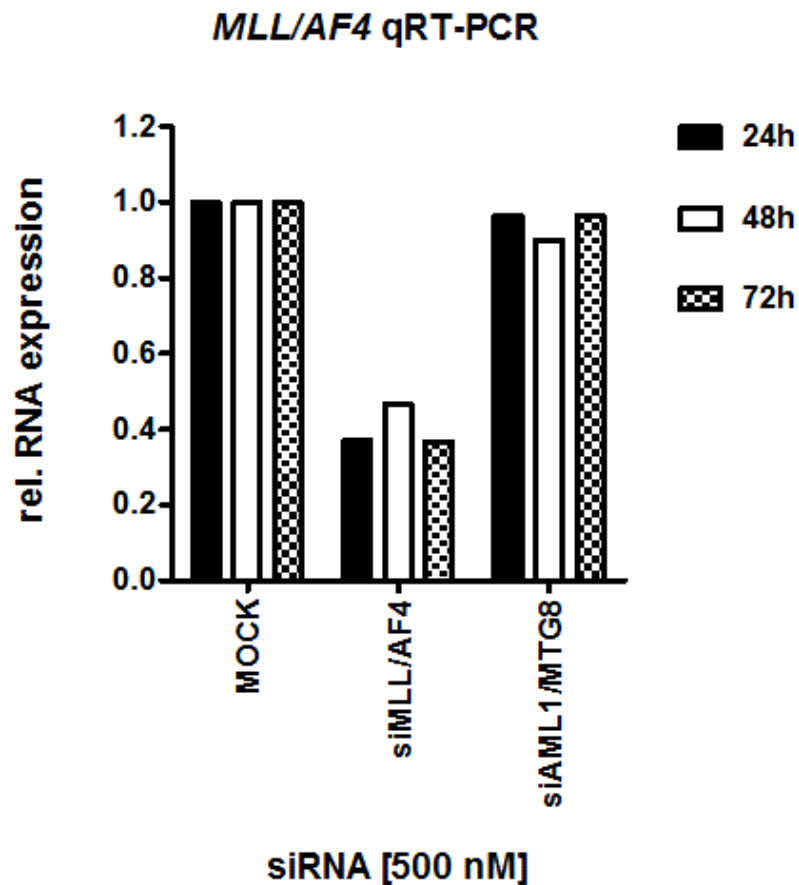


Fig. 3-5: Expression analysis of MLL/AF4 by qRT-PCR after siRNA treatment of primary patient blasts.

Primary patient blasts were electroporated once with siMLL/AF4, control siRNA (siAML1/MTG8) or without oligonucleotides (MOCK). *MLL/AF4* depletion was verified by qRT-PCR for the time points 24h, 48h and 72h post siRNA treatment. The graph represents the mean of one single experiments; each reaction was performed in triplicate.

3.1.2 Effects of siMLL/AF4 on the MLL and AF4 wild-type genes

The siRNA against *MLL/AF4* targeted the breakpoint (e9-e4) of the fusion transcript inherent of the SEM cell line and did not directly affect the expression of the wild-type genes *MLL* and *AF4*. This was confirmed when analysing the *MLL/AF4*, *MLL* and *AF4* transcript levels 2h after the siRNA electroporation; while *MLL/AF4* was already depleted by ~50%, no changes could be observed in *MLL* and *AF4* expression (fig. 3-6).

However, when *MLL* and *AF4* were monitored over a sustained siRNA treatment period of up to 6 days; *AF4* showed a time-dependent decrease (fig. 3-7), while *MLL* levels remained unchanged (fig. 3-8). Although the delayed response of *AF4* already indicated towards a mechanism downstream of *MLL/AF4* knock-down, it was essential to rule out possible off-target effects. One efficient way to do so was to transfect another cell line with siMLL/AF4 which either expressed a *MLL/AF4* fusion transcript with a differing breakpoint, or did not carry the translocation. Electroporation of RS4;11, a t(4;11)-positive BCP-ALL cell line harbouring the *MLL/AF4* translocation with e10-e4 breakpoint showed no down-regulation of *MLL/AF4*, *MLL* and *AF4* (fig. 3-9).

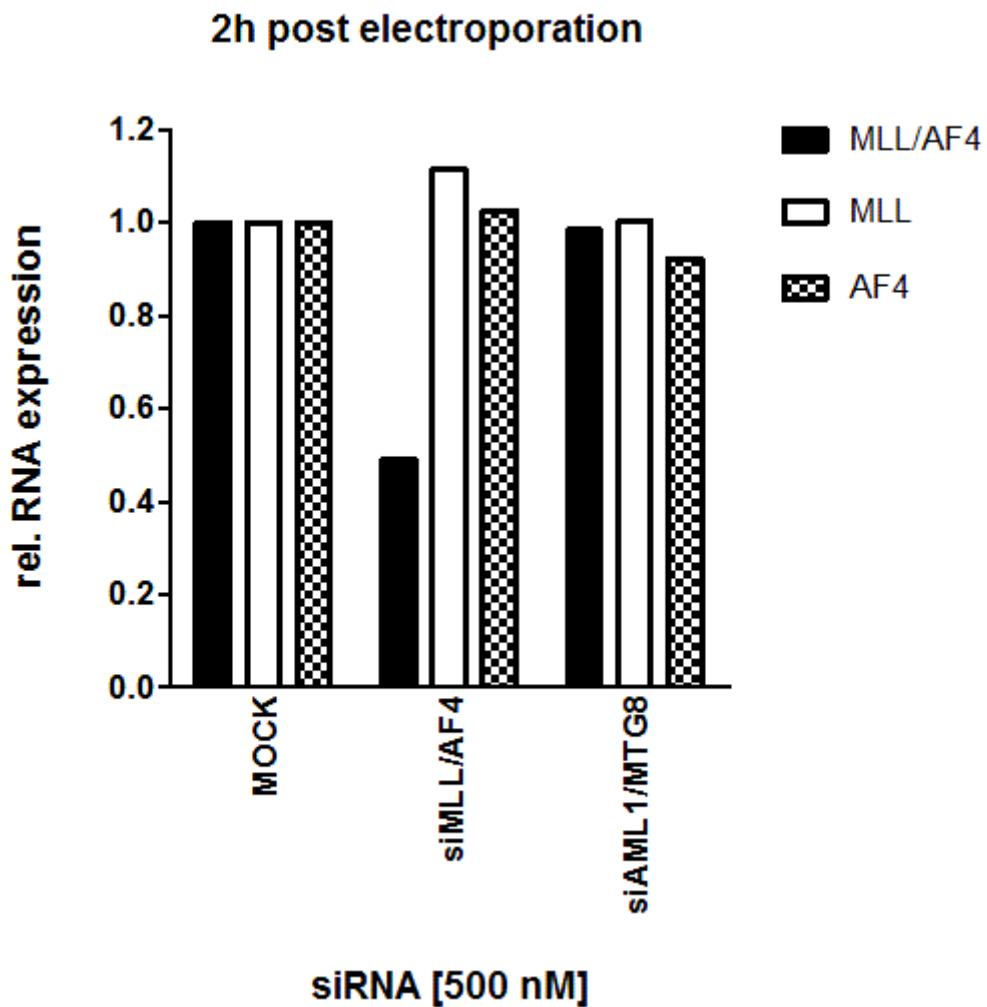


Fig. 3-6: Expression analysis of the *MLL/AF4* fusion and the wild-type genes *AF4* and *MLL* in SEM cells 2h post-electroporation

SEM cells were once electroporated with either siMLL/AF4, control siRNA (siAML1/MTG8) or no siRNA (MOCK). RNA was harvested 2h after transfection; SEM cells treated with siMLL/AF4 resulted in a 50% reduction in *MLL/AF4*, while expression of the wild-type gene *MLL* and *AF4* were not affected. The graph represents one single experiment; each sample was performed in triplicates.

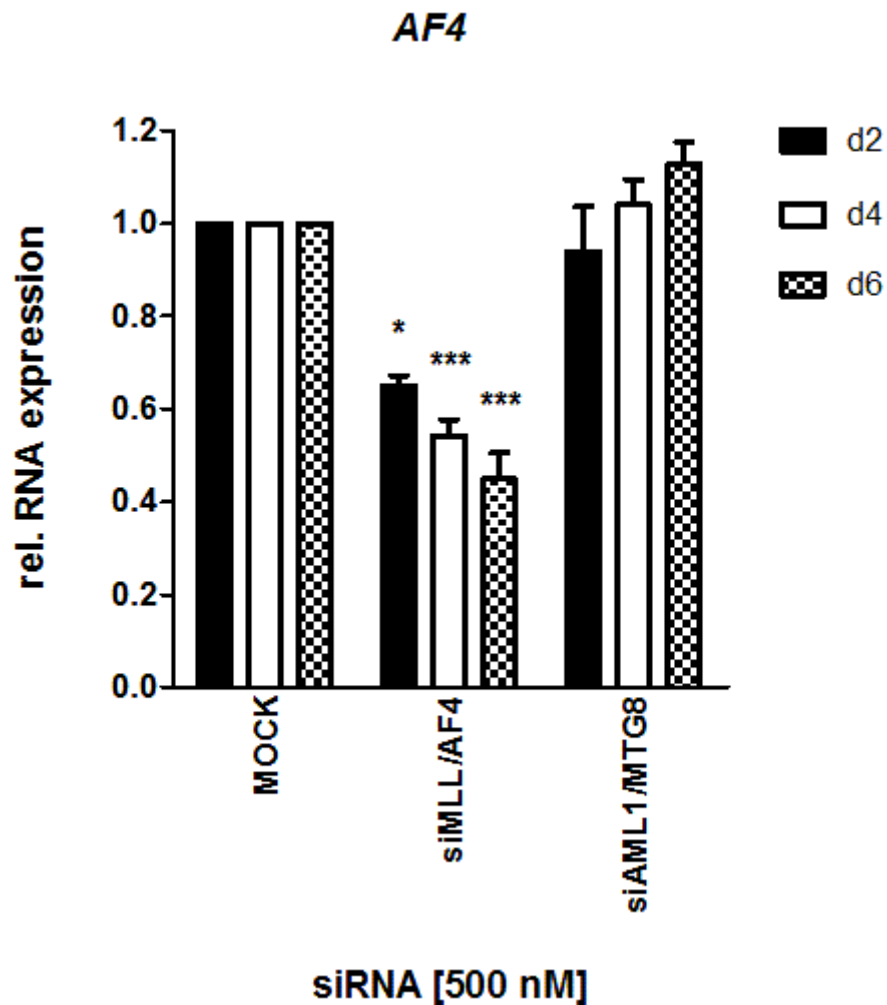


Fig. 3-7: *AF4* expression analysis in response to MLL/AF4 depletion

SEM cells were serially electroporated three times at two-day intervals with either siMLL/AF4, control siRNA (siAML1/MTG8) or no siRNA (MOCK). RNA was harvested prior to the subsequent electroporation and expression analysed by qRT-PCR. SEM cells transfected with siMLL/AF4 showed a time-dependent reduction on *AF4* transcript levels when compared to controls. The graph represents the mean of at least $n=3$ independent experiments, error bars indicate standard error of the mean (S.E.M.). Statistic analysis was carried out using an unpaired Student's t-test (* = $p < 0.05$; *** = $p < 0.001$).

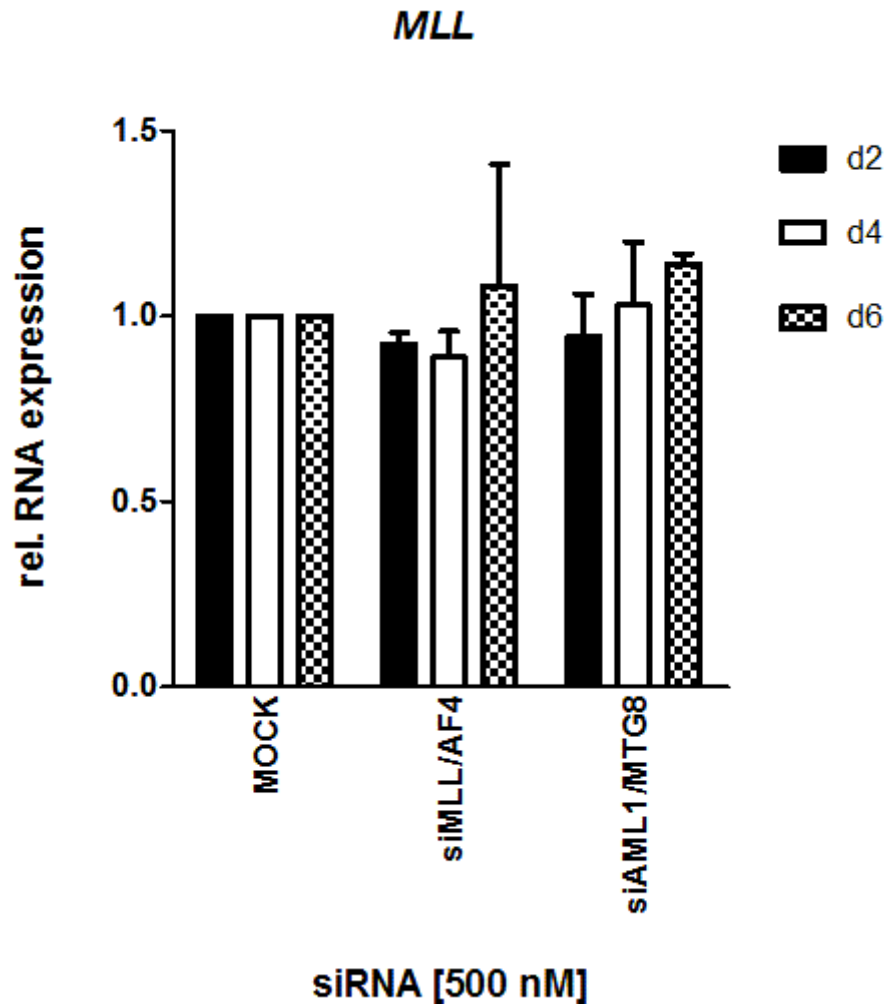


Fig. 3-8: MLL expression analysis in response to MLL/AF4 depletion

SEM cells were serially electroporated three times at two-day intervals with either siMLL/AF4, control siRNA (siAML1/MTG8) or no siRNA (MOCK). Treatment with siMLL/AF4 had no effect *MLL* transcript levels when compared to controls as determined by qRT-PCR. The graph represents the mean of n=3 independent experiments, error bars indicate standard error of the mean (S.E.M.). Statistic analysis was carried out using an unpaired Student's t-test (***) = $p < 0.001$).

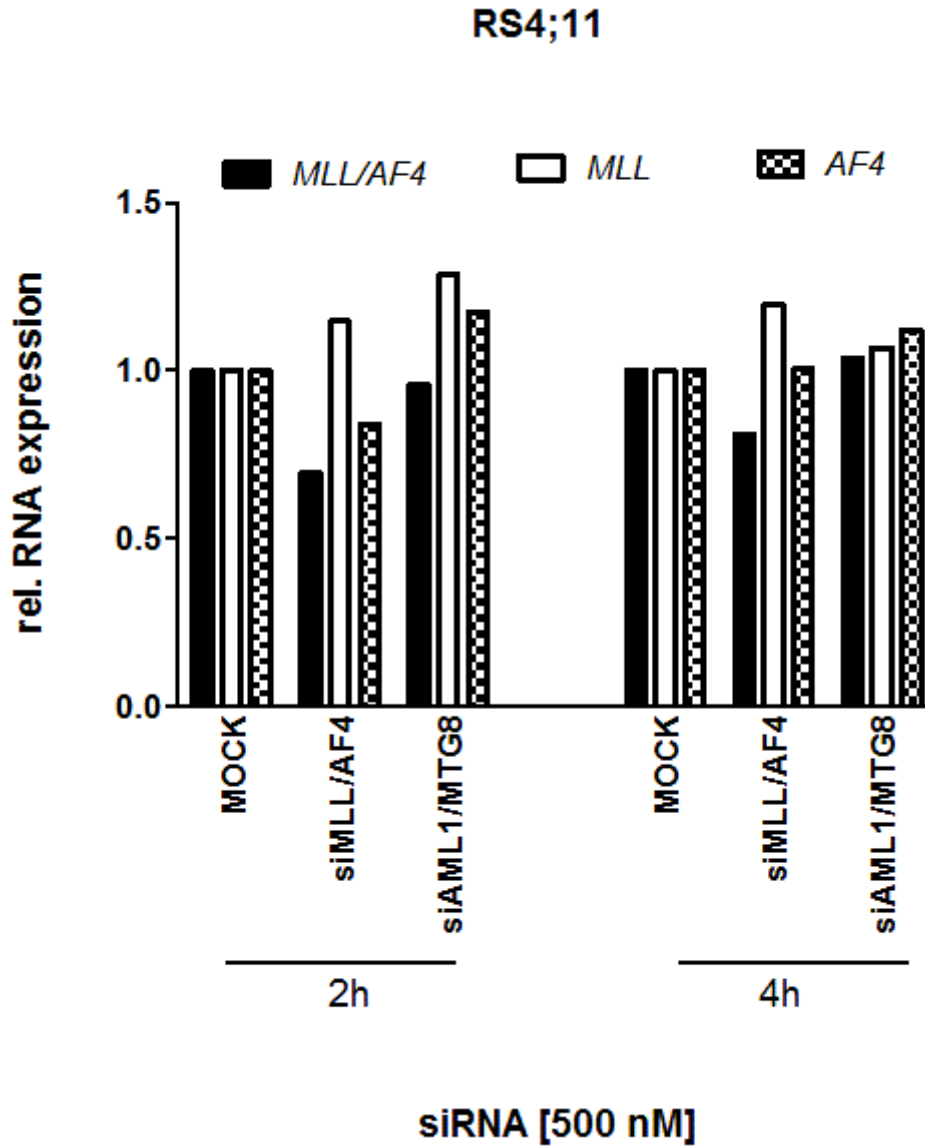


Fig. 3-9: MLL/AF4, AF4 and MLL expression analysis in siRNA-treated RS4;11 cells

The t(4;11)-positive cell line RS4;11 was electroporated once with either siMLL/AF4, control siRNA (siAML1/MTG8) or no siRNA (MOCK) and RNA was harvested 2h and 4h after transfection and gene expression determined by qRT-PCR. Treatment with siMLL/AF4 did not result in down-regulation of either the e10-e4 MLL/AF4 fusion transcript, wild-type MLL and AF4. The graph represents one single experiment; each sample was performed in triplicates.

Concomitantly, long-term siMLL/AF4 treatment of the t(8;21)-positive AML cell line Kasumi-1, which lacks MLL/AF4 but codes for the fusion gene AML1/MTG8, did not result in a *AF4* expression level reduction. Of note was that electroporation of the Kasumi-1 cells with siAML1/MTG8, which targets the AML1/MTG8 transcript inherent of this cell line, subtly induced *AF4* expression. This effect was not observed in the context of the SEM cell line, where siAML1/MTG8 was employed as an active control siRNA.

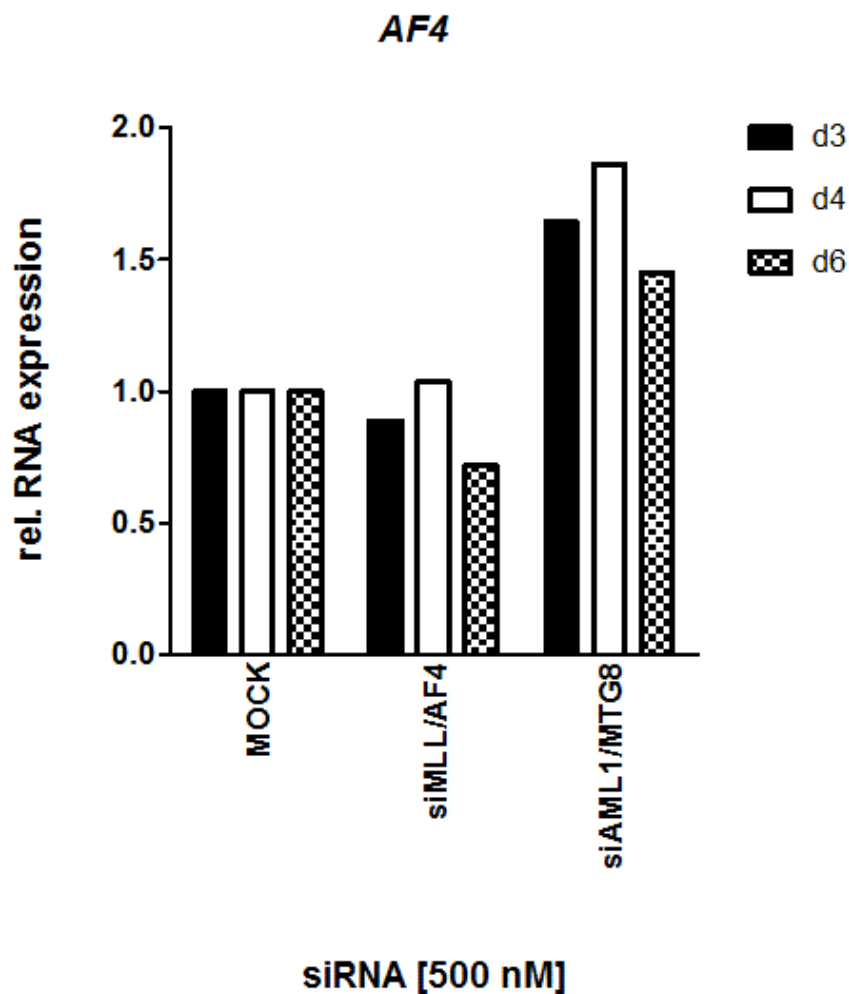


Fig. 3-10: *AF4* expression analysis in siRNA-treated Kasumi-1 cells

The t(4;11)-negative AML cell line Kasumi-1 was serially electroporated twice with either siMLL/AF4, siAML1/MTG8 or no siRNA (MOCK). RNA was harvested after 3, 4 and 6 days. Treatment with siMLL/AF4 did not result in changes *AF4* expression. The graph represents the combination of two independent experiments of which each time point was performed once; every sample was performed in triplicates.

Since transfection of siMLL/AF4 did not down-regulate *AF4* expression *per se*, this observation was suggestive of an effect mediated down-stream of MLL/AF4. Recently, it has been reported that wild-type MLL is required in MLLr leukaemia for transformation and disease maintenance; thus it might also be possible that the fusion genes regulate their wild-type counterparts. *In silico* analysis of the *AF4* promoter revealed several HOXA gene and TALE - protein binding sites; further studies are required to elucidate a potential MLL/AF4-HOXA-AF4 axis (fig. 3-11:).

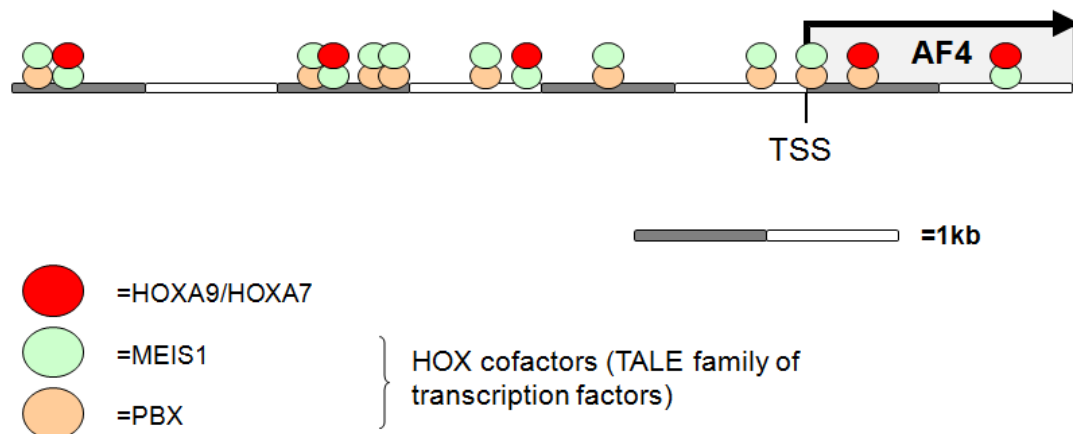


Fig. 3-11: Scheme HOXA gene binding sites within the AF4 promoter

Bioinformatic analysis of transcription factor binding sites within the *AF4* promoter region encompassing 3000bp upstream and 1000bp downstream of the transcription site (TSS) using MatInspector module of the Genomatix software suite (Genomatix Software GmbH).

3.1.3 MLL/AF4 depletion is associated with a phenotype

Cells carrying the MLL/AF4 fusion gene are reportedly highly resistant against genotoxic stress and mitogen-deprivation mediated cell death. Remarkably, RNAi-mediated ablation of MLL/AF4 severely impaired viability and proliferation, as illustrated by the negative growth curve in fig. 3-12.

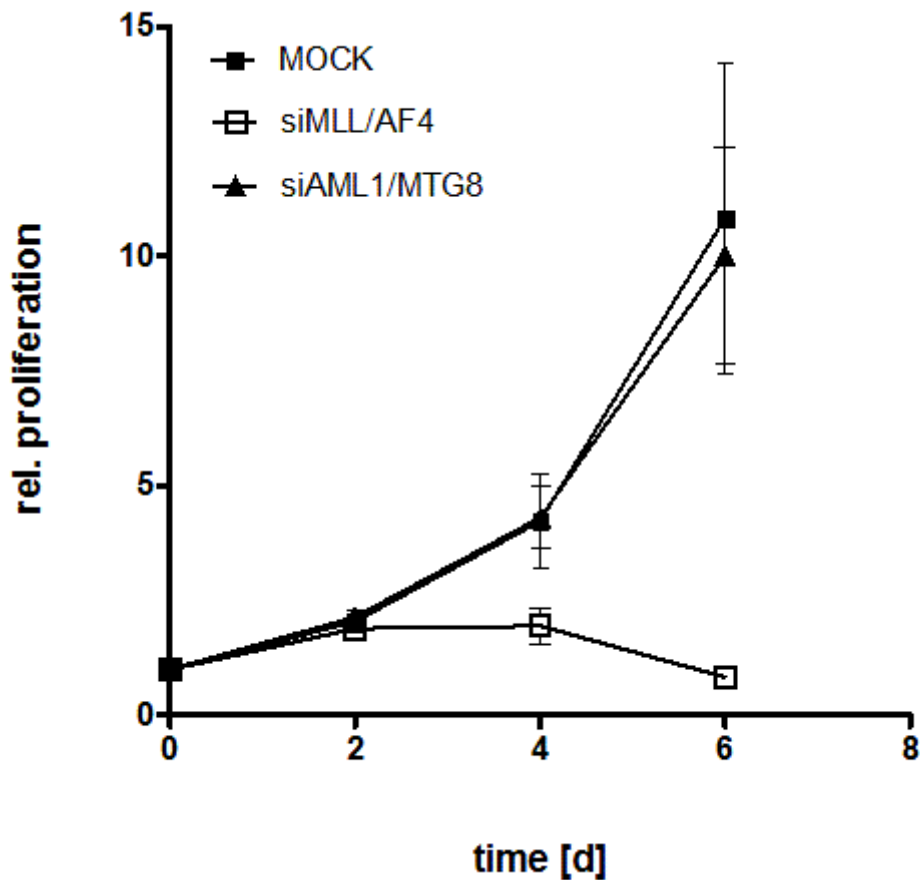


Fig. 3-12: Growth curve of siMLL/AF4-treated SEM cells

Sustained knock-down of *MLL/AF4* over a period of 6 days was achieved by serial transfection of the SEM cell line with siMLL/AF4 at two day-intervals; controls were electroporated with either a control siRNA (siAML1/MTG8) or no siRNA (MOCK). SEM cells depleted of *MLL/AF4* showed substantially reduced proliferation and viability compared to controls. Cell numbers were determined immediately prior to the siRNA-transfection time points using a haematocytometer; viability was assessed by trypan blue exclusion. The graph represents the mean of at least n=3 (n=4 for d2 & d4; n=3 for d6) independent experiments, the error bars indicate standard error (S.E.M.).

This was accompanied by changes in cell cycle distribution; prolonged *MLL/AF4* knock-down resulted in an increase in SEM cells accumulating both in the G1/G0- and the G2/M-phase as well as a concomitant depletion in the S-phase (fig. 3-13).

Furthermore, prolonged reduction of MLL/AF4 levels resulted in a marked induction of apoptosis as indicated by the increase of the sub-G1/G0 population in fig. 3-14; siMLL/AF4 treated cells show a 6.5-fold increase in cell death when compared to controls (MOCK = 5.9%; siAML1/MTG8 = 6.4%; siMLL/AF4 = 38.4).

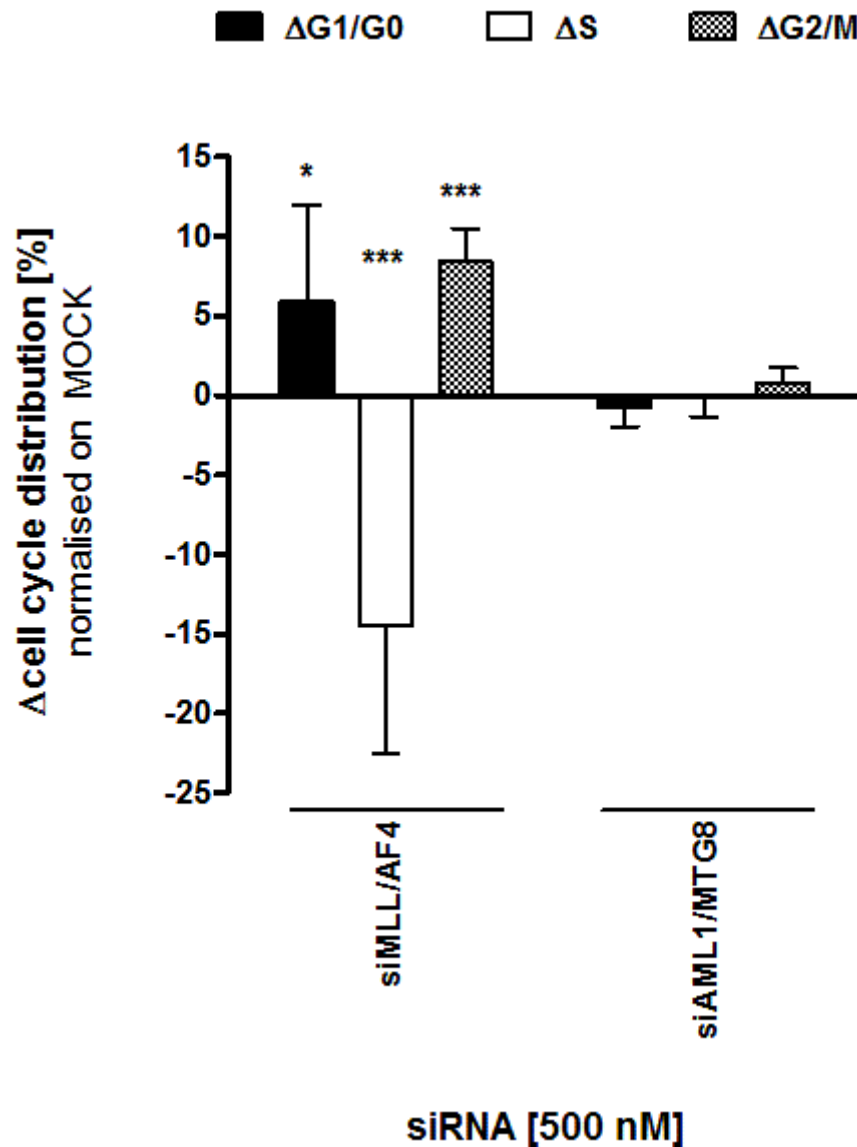


Fig. 3-13: Changes in cell cycle distribution in SEM cells depleted of MLL/AF4

Cell cycle analysis by flow cytometry showed that, compared to controls (MOCK, siAML1/MTG8), siMLL/AF4-treatment for 4 days led to an increased proportion of SEM cells in G1/G0- and G2/M-phase, while the subpopulation in the S-phase was reduced. Cell cycle distribution was determined using the ModFit LT analysis programme (Verity Software House), and the changes in siRNA-treated cells calculated by normalising on the cell cycle distribution of MOCK-transfected cells. The mean of n=5 independent experiments are shown; error bars represent S.E.M. Statistical analysis was performed using an unpaired Student's t-test (* = $p < 0.05$; *** = $p < 0.001$)

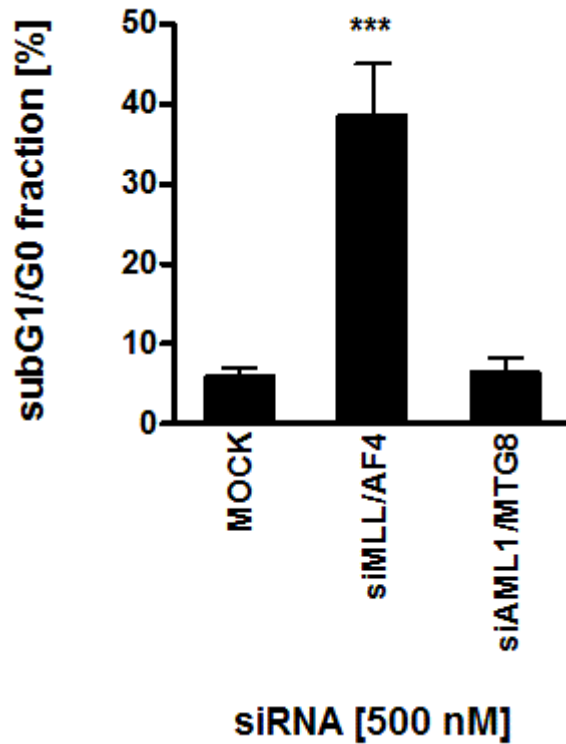


Fig. 3-14: Analysis of the sub-G1/G0 population of siRNA-treated SEM cells

SEM cells were serially electroporated with siMLL/AF4 or control-transfected (siAML1/MTG8, MOCK). At TP2, corresponding to four days of sustained *MLL/AF4* depletion, the cell cycle distribution of the electroporated cells was analysed by flow cytometry. Apoptosis was determined by measuring the proportion of SEM cells in the sub-G0/G1 population using the ModFit LT analysis software (Verity Software House). The graph represents the mean of n=5 independent experiments, statistical significance was determined by Student's t-test (***) = $p < 0.001$)

In addition to the effects on proliferation and viability, clonogenicity was reduced in MLL/AF4-depleted SEM cells by 4.4 fold when compared to control siRNA (fig. 3-15).

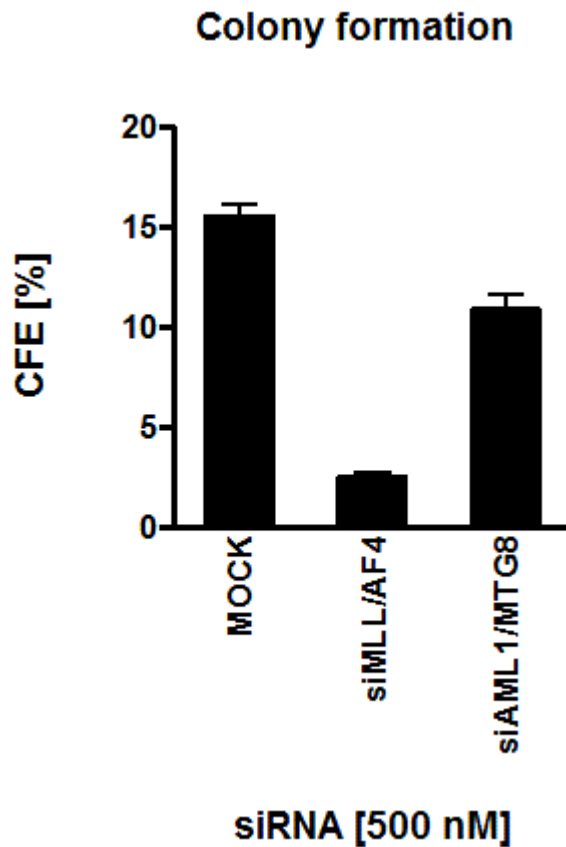


Fig. 3-15: Clonogenicity assay of MLL/AF4-depleted SEM cells

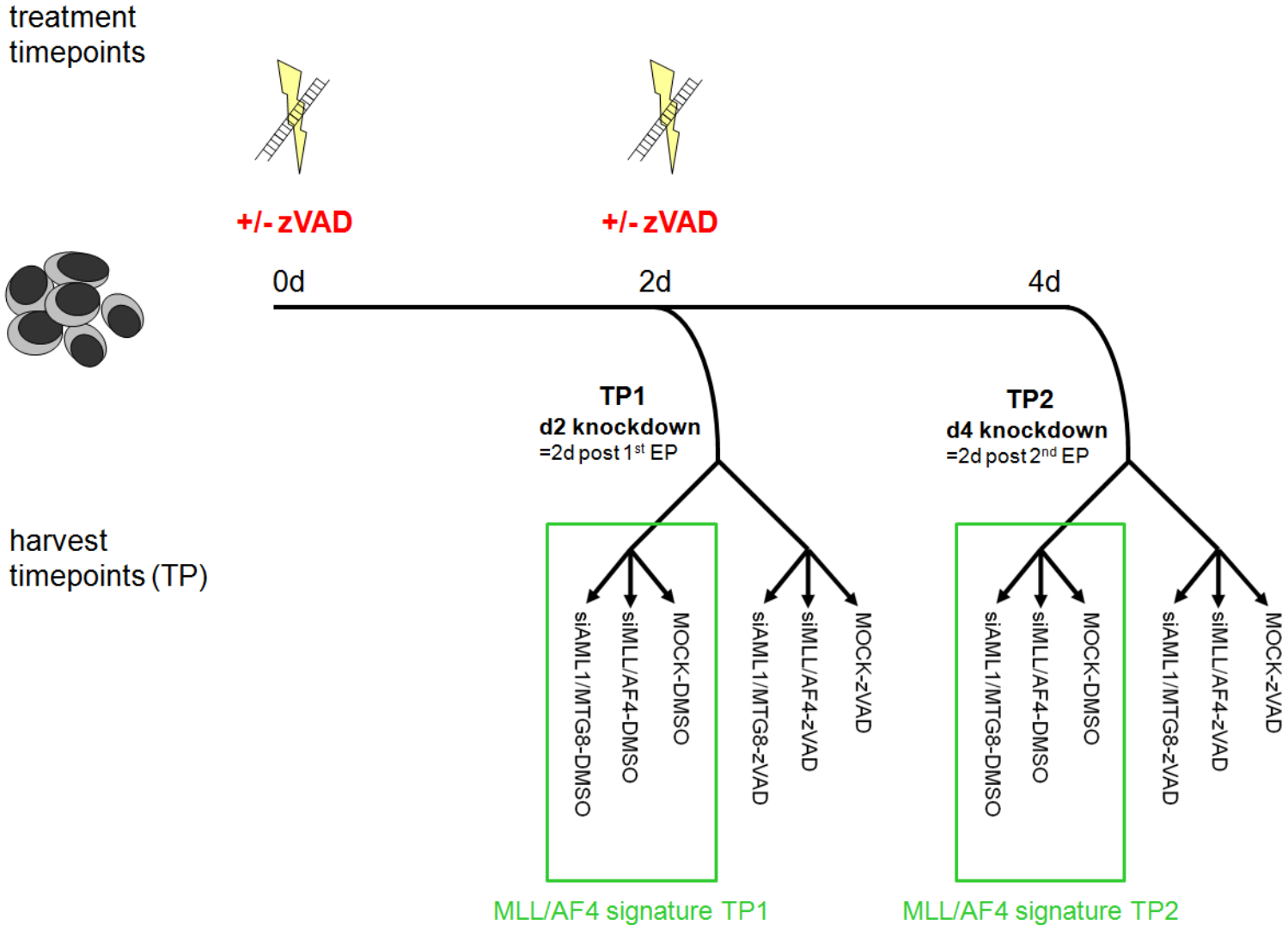
SEM cells were seeded out in triplicates for colony formation in sloppy agar 24h after a single electroporation with either siMLL/AF4 or controls (MOCK, siAML1/MTG8). Colony number was determined approximately after one-week incubation and normalised against the starting number of cells.

3.2 GENE EXPRESSION PROFILING OF SEM CELLS DEPLETED OF MLL/AF4

Prolonged depletion of *MLL/AF4* in the context of the t(4;11)-positive cell line SEM displayed a remarkable phenotype, with a clear adverse effect on cell proliferation, clonogenicity and overall viability. Since in clinics t(4;11)-positive ALL is commonly refractory to treatment, resulting in a high relapse rate and poor overall survival, it was of outstanding interest to investigate the underlying molecular mechanisms exerted by MLL/AF4, and particularly which pathways or factors were affected by knock-down of the fusion transcript. Thus, a siRNA time course experiment was carried out and whole genome expression profiling (GEP) performed on the Illumina HT-12 Bead Array platform. Additionally, in order to investigate the aspect of apoptosis induction, the siRNA time course was subdivided into two experimental subgroups: one group was supplemented with the caspase-inhibitor zVAD-FMK in order to block apoptosis, while the other was the vehicle control group, which was cultured in presence of 0.25% DMSO. The analysis of the zVAD-treatment group and the surrounding investigations are reported in the following section 4, in current section only the results from the control groups are shown. The experimental set up scheme is illustrated in fig. 3-16

Fig. 3-16: Experimental set-up scheme for GEP samples

SEM cells were serially electroporated at two-day intervals with siRNA against *MLL/AF4* (siMLL/AF4), control siRNA (siAML1/MTG8) or without oligonucleotides (MOCK) and subsequently subdivided into two treatment groups; one group was supplemented with the pancaspase inhibitor zVAD, the other with the equal amount of vehicle solvent (DMSO). Cells were harvested for analyses at TP1 (2 days post the 1st electroporation), corresponding to a 2-day MLL/AF4 knockdown, and at TP2 (2 days post the 2nd electroporation), which represents a sustained down-regulation of *MLL/AF4* for 4 days. Gene expression profiling (GEP) was performed on RNA derived from DMSO-treated cells at TP1 and TP2, and the following results were termed MLL/AF4 signature at TP1 or TP2. The results from the GEP from the electroporated cells treated with zVAD will be discussed in the following chapter.



3.2.1 Biological QC analysis of array samples

SEM cells were electroporated twice according to the scheme in (fig. 3-16), and TP1 and TP2 harvested for RNA. Before the RNA was labelled, hybridised and scanned off-site at a service provider core facility, the siRNA-treated samples underwent quality control (QC) measures: successful *MLL/AF4* knockdown was confirmed by qRT-PCR (fig. 3-17), and RNA integrity determined using lab-on-chip technology with a Bioanalyzer 2100 assay. A RNA integrity number (RIN) above 7 characterises RNA of good enough quality for GEP (tab. 3-1).

Tab. 3-1: RIN values of samples submitted to GEP as determined by Bioanalyzer 2100 RNA 6000 Nano Assay

sample	RIN
TP1	
<i>MOCK</i>	8.9
<i>siMLL/AF4</i>	8.4
<i>siAML1/MTG8</i>	8.4
TP2	
<i>MOCK</i>	7.1
<i>siMLL/AF4</i>	8.2
<i>siAML1/MTG8</i>	8.9

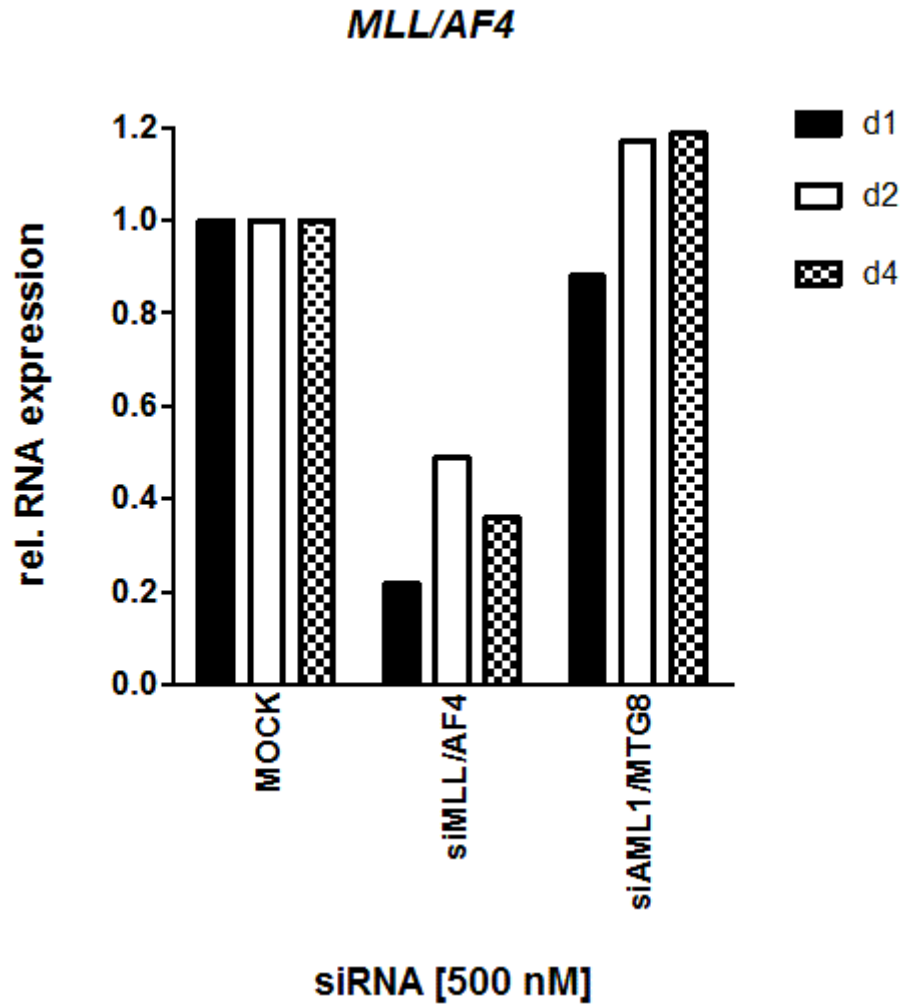


Fig. 3-17: MLL/AF4 expression analysis of samples allotted for GEP

SEM cells were serially electroporated twice at two-day intervals with either siMLL/AF4, control siRNA (siAML1/MTG8) or no siRNA (MOCK). MLL/AF4 expression was determined by qRT-PCR day one (d1), two (d2) and day 4 (d4) of siRNA treatment. Compared to controls, siMLL/AF4-transfected cells showed a *MLL/AF4* down-regulation by 55-80%. The graph represents one single experiment; each sample was performed in triplicates.

3.2.2 Array analysis

The samples were processed off-site at a service provider facility according to manufacturer's protocols, and assayed using an Illumina HT-12 V.3 Bead Array (Illumina Inc.). The obtained raw data was then preprocessed by me using BeadStudio 3 software (Illumina Inc), applying background subtraction. Missing probe values were not imputed (for arrays statistics see tab. 3-2).

Tab. 3-2: Array Statistics of pre-processed raw data using BeadStudio 3

	No. Detected probes <i>(P-value <0.05)</i>	No. Detected probes <i>(P-value <0.01)</i>
MOCK (TP1)	11135	8835
siMLL/AF4 (TP1)	12162	9737
siAML1/MTG8 (TP1)	11707	9077
MOCK (TP2)	11166	9194
siMLL/AF4 (TP2)	11968	9130
siAML1/MTG8 (TP2)	11894	9137

Subsequently, the differential gene expression analysis of the arrays was performed using GeneSpring GX11 software (Agilent Technologies, Inc). Each time point was analysed as an individual treatment group consisting of siMLL/AF4, MOCK and siAML1/MTG8-transfected cells. The arrays were normalised using a quantile normalisation algorithm, and for each array the baseline was transformed over the median baseline of the control samples (fig. 3-18). Probe signal values associated with siAML1/MTG8 & MOCK were averaged, resulting in a control group termed Ctrl, against which the differential expression analysis for siMLL/AF4 was performed (siMLL/AF4 vs. Ctrl).

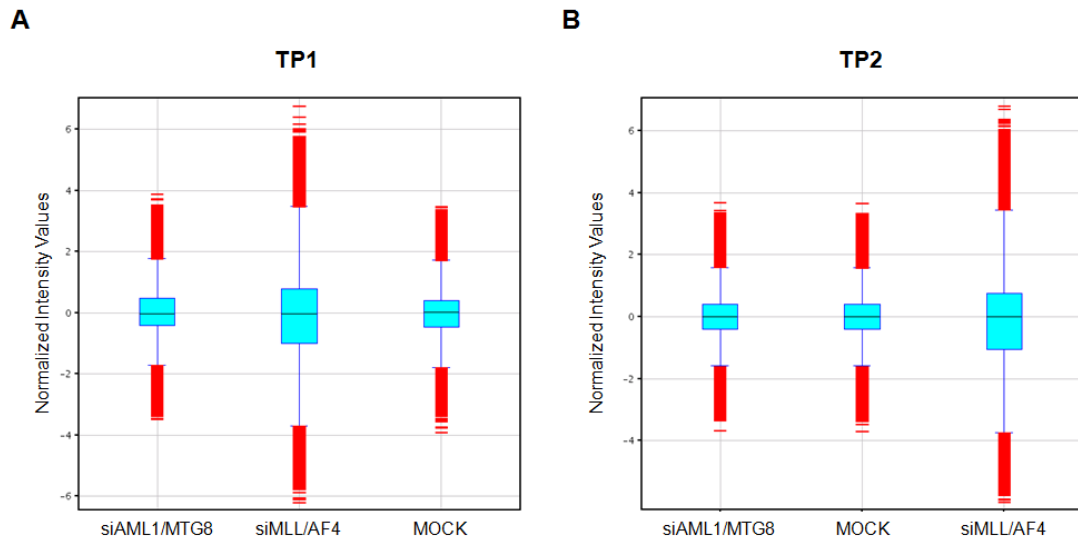


Fig. 3-18: Normalised array intensity values each treatment group at TP1 & TP2

The siRNA treatment time course were grouped according to time point, each treatment group consisting of control- (MOCK, siAML1/MTG8) and siMLL/AF4-transfected samples. Each of these treatment groups was normalised independently using the quantile normalisation algorithm and transforming the baseline of each sample over the median baseline of the control samples. The box and whisker plots indicate the spread of the probe signal values of the treatment group at TP1 (A) and TP2 (B).

The results were filtered according to the array signal calls or “flags” according to the GeneSpring GX software default settings: Present calls (P) were attributed to flags with an Illumina p -value of $p > 0.8-1$, marginal calls (M) had flag p -values of $p > 0.6-0.8$; a flag with $p < 0.6$ was tagged as absent (A). Array probes were filtered on “present” calls only for all samples; differentially expressed probes were determined by calculating the signal intensity in the siMLL/AF4 array vs. the signal intensity values in the Ctrl samples. A linear fold-change expression value cut-off of 2.0 applied; this generated dataset was termed MLL/AF4 gene signature A.: at TP1, there were 599 up- and 1060 down-regulated probe sets, which could be collapsed into 577 and 945 genes which were induced or down-regulated, respectively. At TP2, 1373 probes were differentially expressed, of

which 689 were up- and 684 down-regulated, representing 654 and 663 genes, respectively (tab. 3-3). The top50 up- and down-regulated probes for each time point of MLL/AF4 signature are listed in tab. 3-4 to tab. 3-7.

Tab. 3-3: Number of differentially expressed probe sets and genes for the MLL/AF4 signature A at TP1 and TP2

siMLL/AF4 vs. Ctrl	TP1-A	TP2-A
No. of differentially expressed probes	1615	1373
<i>up-regulated probes</i>	599	688
<i>down-regulated probes</i>	1016	684
No. of differentially expressed genes	1523	1271
<i>up-regulated genes</i>	577	654
<i>down-regulated genes</i>	945	663

Tab. 3-4: Top 50 up-regulated probes in signature A at TP1

ILMN_Gene	Fold-change [siMLL/AF4] vs [Ctrl]	Accession	Probe_Id
IFI44	9.61	NM_006417.3	ILMN_1760062
FCRLA	8.69	NM_032738.3	ILMN_1691071
COL8A1	7.33	NM_020351.2	ILMN_1685433
ARRDC4	6.25	NM_183376.1	ILMN_1660544
GABARAPL1	5.90	NM_031412.2	ILMN_2151281
NLGN4X	5.18	NM_020742.2	ILMN_2341067
REEP3	5.12	NM_001001330.1	ILMN_1722642
IFRD1	4.64	NM_001007245.1	ILMN_1687390
ZNF572	4.58	NM_152412.1	ILMN_1802974
ENPP2	4.54	NM_001040092.1	ILMN_2373791
TLR10	4.50	NM_001017388.1	ILMN_1719905
LOC653125	4.47	XM_931236.1	ILMN_1732291
EEPDI	4.34	NM_030636.2	ILMN_1811616
ARRDC2	4.30	NM_015683.1	ILMN_1655612
PLEKHH3	4.26	NM_024927.3	ILMN_1804652
ELMO1	4.24	NM_014800.9	ILMN_1784320
TARSL2	4.16	NM_152334.2	ILMN_1720267
ANXA1	4.12	NM_000700.1	ILMN_2184184
PIR	4.07	NM_001018109.1	ILMN_2383383
DLX1	4.02	NM_001038493.1	ILMN_2388445
HS.581580	4.00	AA383422	ILMN_1880761
SORBS2	4.00	NM_003603.4	ILMN_2407879
GNPDA1	3.94	NM_005471.3	ILMN_1784709
TLR10	3.93	NM_030956.2	ILMN_2414762
ZNF397	3.90	NM_032347.1	ILMN_1685467
RGS1	3.85	NM_002922.3	ILMN_1656011
PROS1	3.84	NM_000313.1	ILMN_1671928
PER3	3.83	NM_016831.1	ILMN_1660986
LRSAM1	3.80	NM_138361.3	ILMN_1811102
ZNF228	3.79	NM_001083335.1	ILMN_1815885
ASB7	3.78	NM_024708.2	ILMN_1680419
HS.581234	3.70	BU928253	ILMN_1880340
PGBD4	3.68	NM_152595.3	ILMN_1651690
RGMA	3.67	NM_020211.1	ILMN_1717636
CYP2E1	3.66	NM_000773.3	ILMN_1665437
KIAA1804	3.66	NM_032435.1	ILMN_1719876
LOC728014	3.64	XM_001127981.1	ILMN_1812721
ABLIM1	3.63	NM_001003407.1	ILMN_2396672
SLC43A2	3.62	NM_152346.1	ILMN_1787127
ELL2	3.59	NM_012081.4	ILMN_1655930
C17ORF87	3.55	NM_207103.1	ILMN_1682761
KPNA5	3.54	NM_002269.2	ILMN_1669700
RPL32P3	3.49	NR_003111.1	ILMN_2175020
NAV2	3.47	NM_145117.3	ILMN_2399300
NLGN4X	3.47	NM_020742.2	ILMN_1728011
UNKL	3.42	NM_023076.3	ILMN_1692826
HS.556255	3.42	AY726563	ILMN_1886515
TOP1P1	3.39	NR_002719.1	ILMN_2086952
CRIM1	3.38	NM_016441.1	ILMN_2146418
GBP2	3.37	NM_004120.3	ILMN_1774077

Tab. 3-5: Top50 down-regulated probes in signature A at TP1

ILMN_Gene	Fold-change [siMLL/AF4] vs [Ctrl]	Accession	Probe_ID
HIST1H4H	-31.36	NM_003543.3	ILMN_1751120
HIST2H3C	-16.63	NM_021059.2	ILMN_1666179
HIST1H3C	-14.84	NM_003531.2	ILMN_1712184
KIAA1666	-11.82	XM_942124.2	ILMN_1732988
HIST1H4E	-11.44	NM_003545.3	ILMN_1681542
LOC644739	-10.31	XM_933679.1	ILMN_1660320
LOC653604	-10.25	XM_497711.2	ILMN_1664706
RN7SK	-9.40	NR_001445.1	ILMN_1739423
HIST1H1B	-8.64	NM_005322.2	ILMN_1653251
SNORD13	-8.05	NR_003041.1	ILMN_1892403
PCDHGA5	-7.66	NM_018918.2	ILMN_2251961
RN7SK	-7.00	NR_001445.1	ILMN_2074860
CD74	-6.66	NM_001025159.1	ILMN_1761464
CD1A	-6.47	NM_001763.2	ILMN_1723520
C20ORF149	-6.30	NM_024299.2	ILMN_1720430
RNF41	-6.24	NM_194358.1	ILMN_1700345
POLR2J4	-6.14	NR_003655.1	ILMN_1699383
GNG5	-5.88	NM_005274.1	ILMN_1701854
C19ORF47	-5.82	NM_178830.2	ILMN_1735608
FUT6	-5.79	NM_000150.2	ILMN_2312228
DGKD	-5.71	NM_152879.2	ILMN_1735301
LOC641972	-5.68	XM_935742.1	ILMN_1803968
HIST1H4K	-5.36	NM_003541.2	ILMN_1662359
LOC440731	-5.33	XM_933693.2	ILMN_1683250
LOC654085	-5.29	XM_942123.1	ILMN_1741105
HOXA10	-5.23	NM_018951.3	ILMN_1682110
LOC644338	-5.23	XM_938091.2	ILMN_1721895
TNFAIP8L1	-5.21	NM_152362.1	ILMN_1684346
ATP8B2	-5.20	NM_001005855.1	ILMN_2301193
EFNB1	-5.08	NM_004429.3	ILMN_1654563
C21ORF58	-4.93	NM_199071.2	ILMN_1769471
LOC347376	-4.93	XM_937928.1	ILMN_1704385
HS.573102	-4.91	AA725539	ILMN_1887973
SNORD36A	-4.67	NR_002448.1	ILMN_2135175
HIST1H2BD	-4.66	NM_138720.1	ILMN_1758623
AIF1	-4.64	NM_032955.1	ILMN_1792473
HIST2H2AA3	-4.59	NM_003516.2	ILMN_1659047
MTL5	-4.57	NM_001039656.1	ILMN_2389528
ARSD	-4.54	NM_001669.2	ILMN_1684956
CHI3L2	-4.54	NM_001025199.1	ILMN_1685045
HMHB1	-4.50	NM_021182.1	ILMN_1709173
IFITM3	-4.49	NM_021034.2	ILMN_1805750
LOC654069	-4.44	XM_942086.1	ILMN_1805726
LOC440917	-4.43	XM_937554.2	ILMN_1657421
OR6M1	-4.34	NM_001005325.1	ILMN_1815093
PYCARD	-4.28	NM_145182.1	ILMN_2398274
HS.562219	-4.24	BP873537	ILMN_1901419
MTRF1	-4.23	NM_004294.2	ILMN_2181992
MGC33556	-4.22	NM_001004307.1	ILMN_1663068
STRN4	-4.21	NM_013403.2	ILMN_2394102

Tab. 3-6: Top50 up-regulated probes in signature A at TP2

ILMN_Gene	Fold-change [siMLL/AF4] vs [Ctrl]	Accession	Probe_ID
RN7SK	104.09	NR_001445.1	ILMN_1739423
SSX4	14.69	XM_942793.1	ILMN_1791645
JMJD1C	13.65	NM_032776.1	ILMN_1677589
FCRLA	11.49	NM_032738.3	ILMN_1691071
RN7SK	11.34	NR_001445.1	ILMN_2074860
REEP3	10.49	NM_001001330.1	ILMN_1722642
SNORD46	9.02	NR_000024.2	ILMN_1682402
SLC12A8	8.95	NM_024628.4	ILMN_1762529
IFI44	8.63	NM_006417.3	ILMN_1760062
HS.545589	8.24	U62823	ILMN_1908824
NLGN4X	7.45	NM_020742.2	ILMN_1728011
LOC100008589	7.41	NR_003287.1	ILMN_1733559
KLF2	7.35	NM_016270.2	ILMN_1735930
ANXA1	6.46	NM_000700.1	ILMN_2184184
LOC541471	6.20	XR_001013.1	ILMN_1696846
NLGN4X	6.16	NM_020742.2	ILMN_2341067
FGFBP2	6.05	NM_031950.2	ILMN_1761945
KIAA1666	6.04	XM_942124.2	ILMN_1732988
ST6GAL1	5.73	NM_003032.2	ILMN_1653120
AGPAT9	5.56	NM_032717.3	ILMN_1794875
GABARAPL1	5.45	NM_031412.2	ILMN_2151281
TMEM158	5.42	NM_015444.2	ILMN_1792455
LOC646358	5.42	XM_929287.1	ILMN_1693404
NR4A2	5.25	NM_006186.2	ILMN_1782305
LOC285033	5.19	NM_001037228.1	ILMN_2115453
LOC400120	5.15	NM_203451.1	ILMN_1797526
TLR10	5.15	NM_001017388.1	ILMN_1719905
IGLL3	4.95	NM_001013618.1	ILMN_2083066
NQO2	4.93	NM_000904.2	ILMN_1712918
CMTM8	4.75	NM_178868.3	ILMN_1710124
PIR	4.68	NM_001018109.1	ILMN_2383383
SEPT1	4.63	XM_944593.1	ILMN_1671854
TLR10	4.59	NM_030956.2	ILMN_2414762
CALCOCO1	4.55	NM_020898.1	ILMN_1774427
VNN2	4.52	NM_004665.2	ILMN_1758864
IL9R	4.51	NM_176786.1	ILMN_1794686
ZNF322B	4.45	NM_199005.1	ILMN_2224290
SORBS2	4.36	NM_003603.4	ILMN_2407879
ALDOA	4.34	NM_184043.1	ILMN_2251253
SORBS1	4.30	NM_001034954.1	ILMN_1663446
PRPF39	4.25	NM_017922.2	ILMN_1692779
PIR	4.24	NM_001018109.1	ILMN_1761247
SNORD15B	4.18	NR_000025.1	ILMN_1713832
DYNLRB2	4.13	NM_130897.1	ILMN_1697317
COL7A1	4.12	NM_000094.2	ILMN_1751161
LSP1	4.11	NM_001013255.1	ILMN_2355225
CYFIP1	4.09	NM_014608.2	ILMN_1715815
SMPDL3A	4.06	NM_006714.2	ILMN_1796349
ASB7	3.99	NM_198243.1	ILMN_1753040
IDS	3.99	NM_006123.2	ILMN_1798448

Tab. 3-7: Top50 down-regulated probes in signature A at TP2

ILMN_Gene	Fold-change [siMLL/AF4] vs [Ctrl]	Accession	Probe_ID
HOXA10	-12.55	NM_018951.3	ILMN_1682110
ARHGEF10	-12.04	NM_014629.2	ILMN_2132809
PMP22	-8.26	NM_153321.1	ILMN_1785646
LOC401093	-7.58	XM_379228.2	ILMN_1813055
ZNF717	-7.15	XM_936239.1	ILMN_1717644
PPARD	-6.89	NM_006238.2	ILMN_1674282
PAIP1	-6.53	NM_182789.2	ILMN_2312386
SIRPA	-6.47	NM_080792.2	ILMN_2372974
PI16	-6.23	NM_153370.2	ILMN_1766264
IGFBP4	-6.12	NM_001552.2	ILMN_1665865
FLJ39653	-6.00	NM_152684.1	ILMN_1666633
MAP2K3	-5.86	NM_145109.2	ILMN_1680777
H6PD	-5.83	NM_004285.3	ILMN_1721136
MVK	-5.74	NM_000431.1	ILMN_1786310
STARD13	-5.59	NM_178006.1	ILMN_2341254
CD1A	-5.49	NM_001763.2	ILMN_1723520
HIST1H2AG	-5.47	NM_021064.3	ILMN_1686478
PCBP4	-5.27	NM_020418.2	ILMN_1728498
OAZ3	-5.26	NM_016178.1	ILMN_1681892
LOC650037	-5.12	XM_939126.1	ILMN_1696999
ADAM15	-5.06	NM_207195.1	ILMN_1751500
HLA-DPA1	-4.79	NM_033554.2	ILMN_1772218
GPR84	-4.78	NM_020370.1	ILMN_1785345
PPP1R3E	-4.72	XM_927029.2	ILMN_1735064
PCDHGA5	-4.61	NM_018918.2	ILMN_2251961
LOC401002	-4.54	XR_018284.1	ILMN_1686852
PHF11	-4.53	NM_001040443.1	ILMN_2284706
DOK4	-4.49	NM_018110.2	ILMN_1774261
MAZ	-4.49	NM_001042539.1	ILMN_2295620
EFNB1	-4.45	NM_004429.3	ILMN_1654563
RALGPS1	-4.43	NM_014636.1	ILMN_1674135
LOC649754	-4.41	XM_941963.1	ILMN_1729421
TMEM120B	-4.38	NM_001080825.1	ILMN_2108493
LOC91461	-4.29	NM_138370.1	ILMN_1734445
RAP1A	-4.28	NM_001010935.1	ILMN_1766176
LOC645128	-4.26	XM_928159.1	ILMN_1751814
FMNL3	-4.22	NM_198900.2	ILMN_2395214
LOC642236	-4.17	XM_943005.1	ILMN_1685125
ZNF493	-4.17	NM_001076678.1	ILMN_2278653
PCTK3	-4.10	NM_212503.1	ILMN_1784110
SPRY4	-4.09	NM_030964.2	ILMN_2086105
SCAF1	-4.02	NM_021228.1	ILMN_1694194
KRTAP10-11	-3.99	NM_198692.2	ILMN_1776412
SYTL1	-3.97	NM_032872.1	ILMN_1750785
LOC646561	-3.92	XM_937933.2	ILMN_1739570
PARP3	-3.87	NM_001003931.1	ILMN_1796682
PLAGL1	-3.85	NM_001080951.1	ILMN_1815121
ENAH	-3.84	NM_018212.4	ILMN_1716552
XPA	-3.79	NM_000380.2	ILMN_1787591
DUSP6	-3.78	NM_022652.2	ILMN_2396020

3.2.3 Functional analysis of the MLL/AF4 gene signature

The Ingenuity Pathway Analysis (IPA) software (Ingenuity Systems Inc.) is a powerful tool for the identification of pathways, biological networks and physiological processes overrepresented in gene expression signatures, enabling a functional characterisation of the GEP dataset. The MLL/AF4 signature at TP1 and TP2 were both analysed independently.

3.2.3.1 IPA analysis of the MLL/AF4 signature at TP1

The MLL/AF4 signature at TP1 contained differentially expressed genes that belonged to networks regulating cell death, gene expression, cell cycle, growth and proliferation, as well as molecular transport (tab. 3-8). Moreover, these network categories were also the top molecular functions attributed to the MLL/AF4 signature. In concordance with the t(4;11)-pathobiology, the MLL/AF4 signature contained probes involved in haematopoiesis and haematological system development and function, as well as probes associated with tumourigenesis and haematological disease (tab. 3-9).

Tab. 3-8: Top5 networks affected by the MLL/AF4 gene signature at TP1

Name	Score
Gene Expression, Cancer, Reproductive System Disease	30
Cell Death, Cellular Growth and Proliferation, Cell Cycle	26
Cancer, Cell Death, Molecular Transport	25
Gene Expression, Cancer, Renal and Urological Disease	20
Cell Death, Cell Morphology, Psychological Disorders	16

Several of the top5 networks represented by the MLL/AF4 signature at TP1 were involved in the gene expression machinery (tab. 3-8). A closer look at the composition of one of these networks (fig. 3-19) showed down-regulation of

several epigenetic modulators, such as the histone deacetylase *HDAC5* and the polycomb group genes (PcG) *CBX3* and *CBX5*, also known as HP-1 proteins, important mediators of cross-talk between the DNA methylation and histone modification pathways. Additionally, several core histone subunits were also down-regulated (*HIST1H2AB*, *HIST1H4C*, *HIST2H3C*, *H3*). Conversely, the histone methyltransferases *MLL3* and *G9a* (*EHMT2*), as well as the transcription elongation factor *ELL2*, were up-regulated. Interestingly, several metallothionein genes showed reduced expression (*MT1H*, *MT1X*, *MT2H*), while other enzymes involved in metal metabolism, such as ferredoxin (*FDX1*) and ferredoxin reductase (*FDXR*) were induced. The latter two have been recently implicated in promoting cell death, and are thus in good concordance with the phenotype associated with *MLL/AF4* depletion¹⁷⁷⁻¹⁷⁸. Lastly, the small GTPases *RAB27A*, shown to promote tumour cell proliferation and metastasis¹⁷⁹, and *RAB33A*, involved in autophagy¹⁸⁰⁻¹⁸¹, were down- and up-regulated, respectively, also agreeing with the phenotype.

Apart from gene expression, three out of the top5 networks associated with the *MLL/AF4* signature at TP1 were involved in regulating cell death (tab. 3-8). As illustrated in the representative network in (fig. 3-20), there was down-regulation of the pro-survival BH3-family member *BCL-XL* (*BCL2L1*). Counter intuitively, the pro-apoptotic BH3-family member *BAX* also showed reduced expression. Nevertheless, genes associated with cell survival, such as *TNFSF14* and *TERT*¹⁸²⁻¹⁸³, were down-regulated, as well as the superoxide dismutase *SOD2* and the glutathione peroxidase *GPX4*, two key regulators for maintaining low cellular reactive oxygen species (ROS) levels, thus protecting the cell from ROS-induced cell death¹⁸⁴⁻¹⁸⁶.

Tab. 3-9: Top 5 significantly enriched functional categories in the *MLL/AF4* gene signature at TP1

Top Biofunctions	<i>P</i>-value
Diseases and Disorders	
<i>Cancer</i>	8.50E-05 - 3.90E-02
<i>Reproductive System Disease</i>	8.50E-05 - 3.32E-02
<i>Gastrointestinal Disease</i>	1.94E-04 - 2.41E-02
<i>Haematological Disease</i>	5.72E-04 - 5.72E-02
<i>Immunological Disease</i>	5.72E-04 - 3.45E-02
Molecular and Cellular Functions	
<i>Cell Death</i>	4.16E-04 - 4.95E-02
<i>DNA Replication, Recombination and Repair</i>	4.21E-04 - 3.84E-02
<i>Cellular Development</i>	7.14E-04 - 4.19E-02
<i>Cellular Growth and Proliferation</i>	7.14E-04 - 4.95E-02
<i>Molecular Transport</i>	1.04E-03 - 3.99E-02
Physiological System Development and Function	
<i>Connective Tissue Development & Function</i>	1.08E-03 - 2.41E-02
<i>Nervous System Development & Function</i>	4.40E-03 - 1.26E-02
<i>Reproductive System Development & Function</i>	1.26E-02 - 3.84E-02
<i>Haematological System Development & Function</i>	2.41E-02 - 4.95E-02
<i>Haematopoiesis</i>	2.41E-02 - 3.84E-02

P-Value range describes the *p*-values of associated subcategories as determined by Fisher's exact test.

Gene Expression, Cancer, Reproductive System Disease

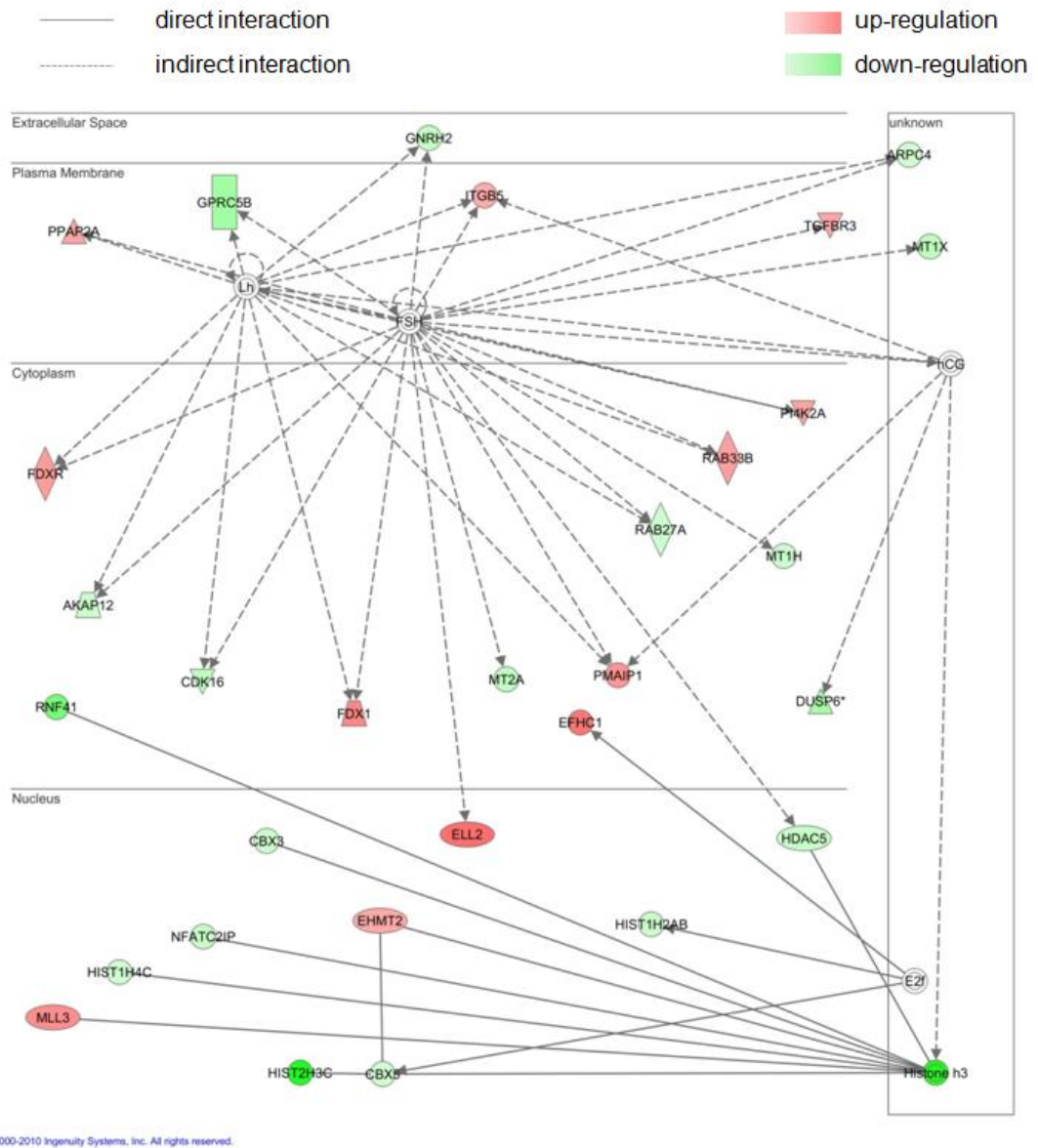


Fig. 3-19: MLL/AF4 depletion affects regulatory networks associated with gene expression

Cancer, Cell Death, Molecular Transport

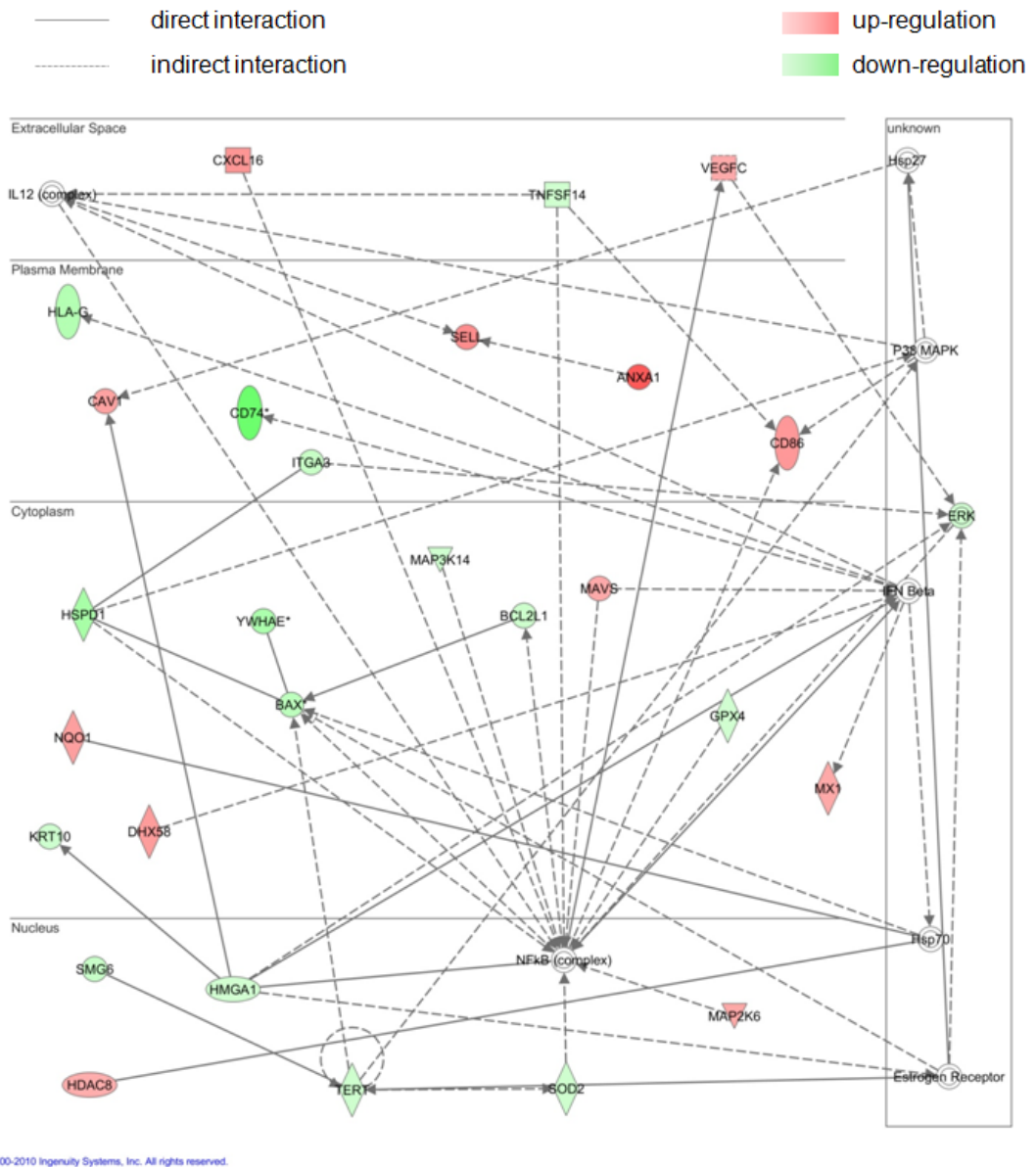


Fig. 3-20: MLL/AF4 depletion for 2 days (TP1) affects regulatory networks linked to cell death

Pathway analyses revealed 32 significantly enriched canonical pathways in the MLL/AF4 signature at TP1. The top20 pathways are depicted in (fig. 3-21) and could be attributed to 7 functional categories: mitogenic signalling, immune response, apoptosis-related signalling, metabolism, cytoskeleton-associated and GPCR-mediated signalling, as well as signalling linked to cancer.

One of the top5 significantly enriched pathways (tab. 3-9) is the ephrin pathway, which is involved in cytoskeleton-associated signalling, and linked to oncogenesis. Of particular interest is that ephrins and their receptors have shown to be regulated in a MLL/AF4-dependent manner¹⁸⁷. The ephrin pathway has strong crosstalk between the P13K/AKT cascade and also GPCR-mediated signalling. Several key factors of these genes, such as *AKT* and the ephrin ligand *EFNB1* (as well as *EFNA4*, see appendix) are down-regulated in the MLL/AF4 signature at both TP1 and TP2; this indicates a disturbance of these important mitogenic pathways in response of MLL/AF4 depletion (fig. 3-22).

Overall, several key mediators of mitogenic signalling which promotes proliferation and survival, are compromised in the MLL/AF4 signature at TP1, suggesting a challenge of the cellular survival machinery in response to MLL/AF4 depletion, very much in accordance with the consequences of sustained MLL/AF4 depletion in SEM cells.

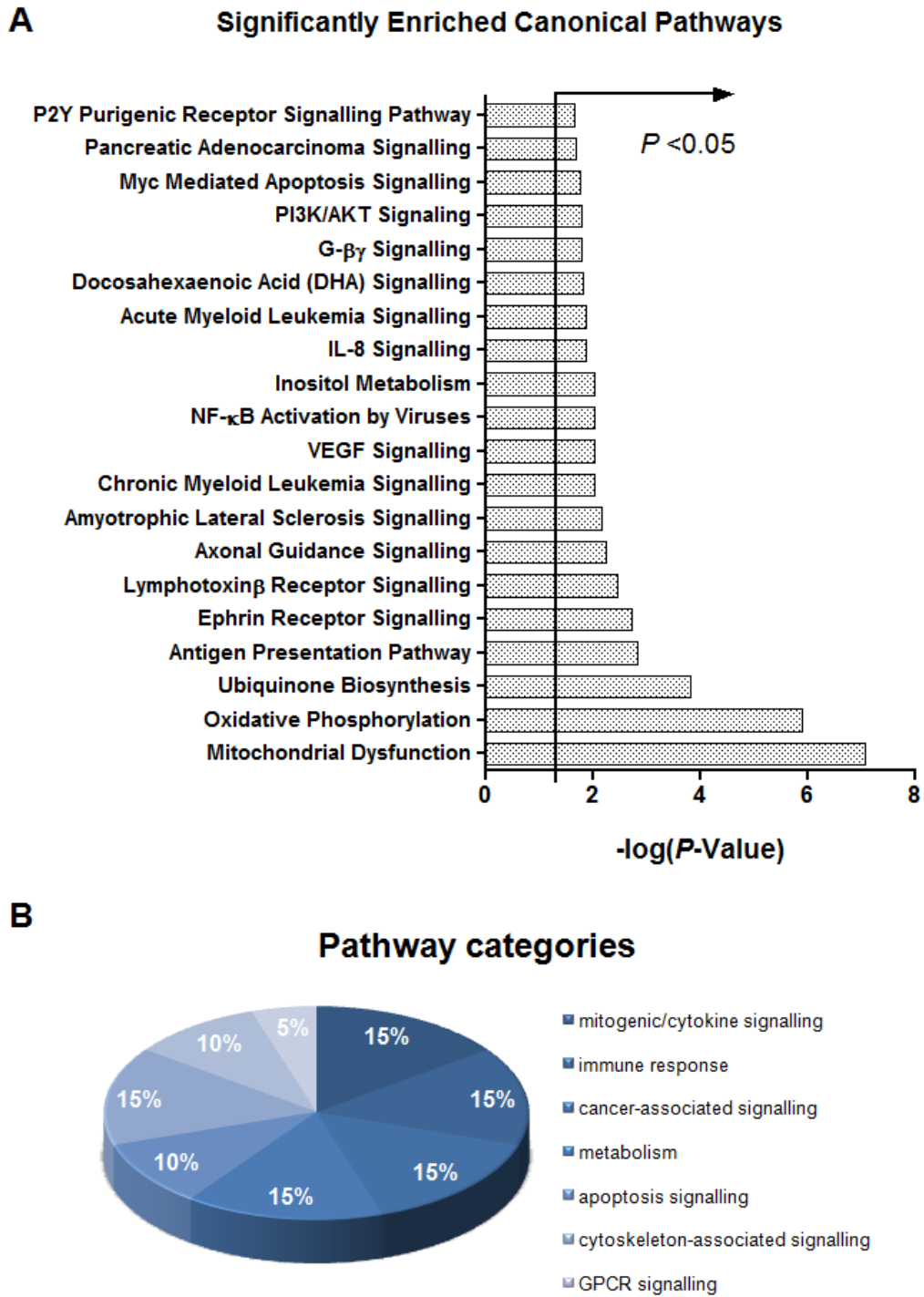


Fig. 3-21: Pathway analysis of the MLL/AF4 gene signature A at TP1

Pathway analysis was performed using IPA Software (Ingenuity Inc.). At TP1, the top20 significantly enriched canonical pathways (A) could be attributed to 8 functional categories (B). Statistical significance was determined by Fisher's Exact test.

3.2.3.2 IPA analysis of the MLL/AF4 signature A at TP2

Characterisation of the MLL/AF4 signature at TP2 using the IPA software yielded very similar results as the signature at TP1; the probes contained in this signature were ascribed to networks involved in cell death, cell cycle, cellular proliferation, movement and development. In addition, this signature also had an enrichment of genes associated with lipid metabolism and inflammatory responses. These networks were to some extent mirrored in the molecular function categories found to be overrepresented in this signature, such as gene expression, cellular development and morphology, as well as lipid metabolism, small molecule biochemistry and, most significantly, processes associated with cancer. Unsurprisingly, the physiological and pathological functions linked to the signature were cancer and tumour morphology, haematopoiesis and haematological function and development as well as disease (tab. 3-10, tab. 3–11).

Tab. 3-10: Top5 networks affected by the MLL/AF4 gene signature at TP2

Name	Score
Cell Death, Cardiac Necrosis/Cell Death, Developmental Disorder	33
Cellular Development, Dermatological Diseases and Conditions, Cell Cycle	29
Inflammatory Response, Cellular Development, Haematological System Development and Function	22
Cell-To-Cell Signalling and Interaction, Cellular Growth and Proliferation, Lipid Metabolism	13
Cellular Development, Cellular Movement, Connective Tissue Disorders	11

Tab. 3-11: Top 5 significantly enriched functional categories in the *MLL/AF4* gene signature A at TP2

Top Biofunctions	P-value
Diseases and Disorders	
<i>Cancer</i>	1.04E-03 - 4.78E-02
<i>Reproductive System Disease</i>	2.94E-03 - 4.43E-02
<i>Genetic Disorder</i>	3.76E-03 - 4.91E-02
<i>Haematological Disease</i>	3.76E-03 - 4.78E-02
<i>Neurological Disease</i>	3.76E-03 - 4.91E-02
Molecular and Cellular Functions	
<i>Cell Morphology</i>	5.97E-05 - 4.56E-02
<i>Cellular Development</i>	1.28E-04 - 4.91E-02
<i>Gene Expression</i>	2.57E-04 - 3.32E-02
<i>Lipid Metabolism</i>	3.20E-04 - 4.78E-02
<i>Small Molecule Biochemistry</i>	3.20E-04 - 4.78E-02
Physiological System Development and Function	
<i>Haematological System Development and Function</i>	1.28E-04 - 4.91E-02
<i>Haematopoiesis</i>	2.29E-03 - 4.91E-02
<i>Tumour Morphology</i>	3.76E-03 - 2.22E-02
<i>Connective Tissue Development and Function</i>	1.08E-02 - 2.60E-02
<i>Nervous System Development and Function</i>	1.08E-02 - 4.78E-02

P-Value range describes the *p*-values of associated subcategories as determined by Fisher's exact test.

Indeed, as illustrated in (fig. 3-23), several genes associated with both a haematopoietic stem cell (HSC)-like signature and leukaemogenesis are down-regulated in response to *MLL/AF4* depletion, such as the HOXA genes *HOXA5* and *HOXA9*, the transcription factor *RUNX1 (AML1)* and the catalytic telomerase subunit *TERT*. This correlates well with reported data by us¹⁷⁰ and others¹⁶⁸. Furthermore, *ID1*, a negative transcription regulator expressed in haematopoietic progenitors and shown to promote tumourigenesis, is down-regulated as well¹⁸⁸⁻¹⁸⁹. Of note is the dysregulation of several factors associated with post-transcriptional RNA processing, such as the RNA helicases *DDX20* and the small nuclear ribonucleoprotein *SNRPD2*, both involved in splicing, as well as the helicase *DHX9* and the RNA binding protein *CUGBP1 (CELF1)*, linked to mRNA decay regulation and post-transcriptional expression inhibition. Furthermore, factors associated with DNA damage response (*XPA*, *H2AFX*, *MGMT*) and cell cycle progression (*CDKN2B*, *CDKN1A*, *TSPYL2*) show MLL/AF4-dependent expression as well.

Cellular Development, Dermatological Diseases and Conditions, Cell Cycle

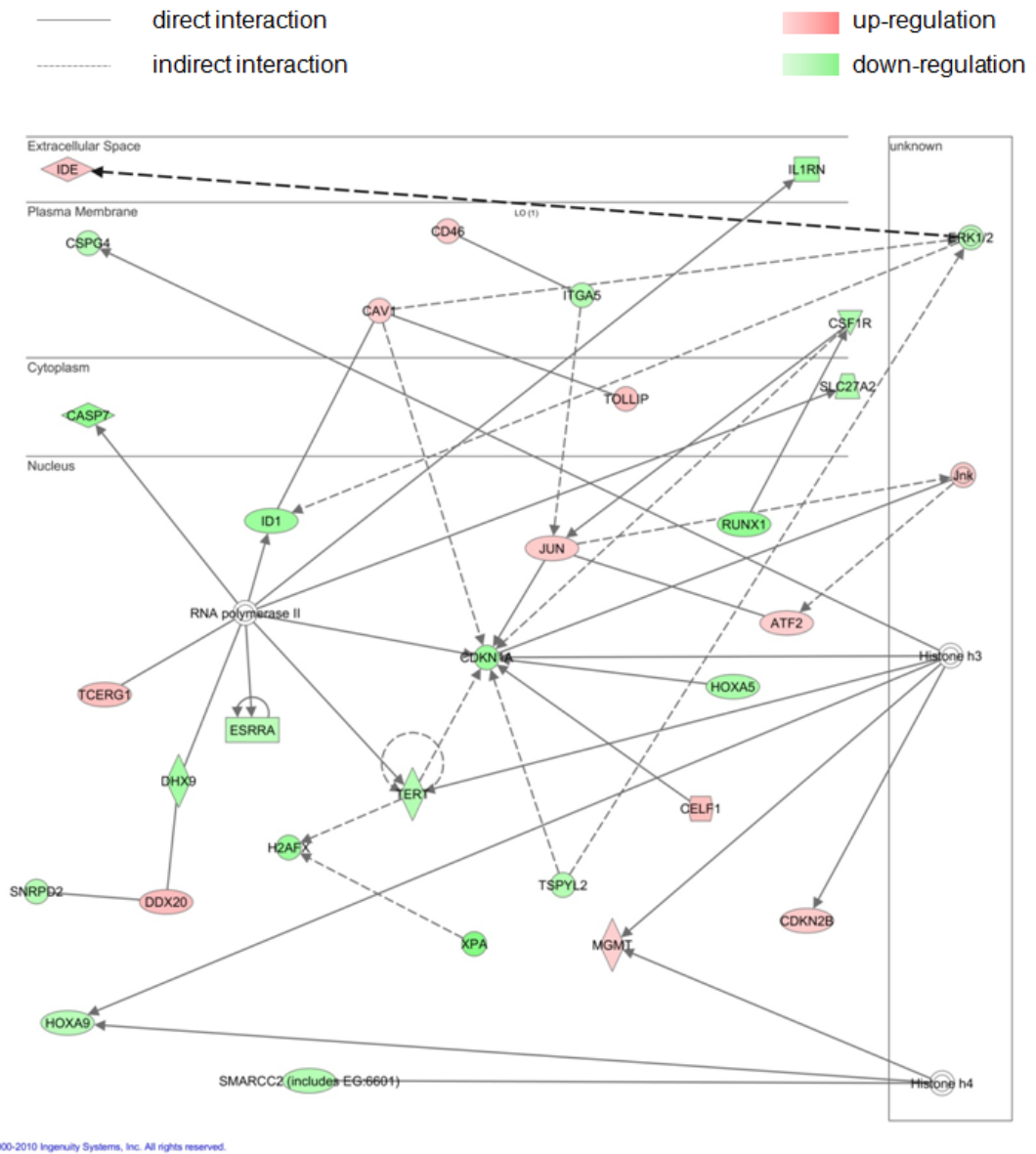


Fig. 3-23: Sustained *MLL/AF4* depletion for 4d (TP2) affects factors associated with cellular development and cell cycle regulation

Pathway analysis reveals >80 significantly enriched canonical pathways. The top20 of the signalling networks fit into five functional categories; interestingly, the vast majority belong to the mitogenic/cytokine signalling cascades, followed by pathways involved in immunity, particularly mediating inflammatory response. The remaining categories are, like at TP1, metabolism, cell death and GPCR signalling (fig. 3-24). As illustrated in the pathway schemes depicting B-cell receptor and CD40 signalling (fig. 3-25), which have extensive cross-talk between different mitogenic signalling pathways, there was down-regulation of their major mediators, *ERK1* and *ERK2* as well as factors of the PI3K-pathway. Confusingly, the cell death-promoting MAPK p38 (*MAPK14*) is indicated to be down-regulated, while its upstream mediator is up-regulated. This, however, is erroneous, and occurred due to an IPA software-inherent misannotation, in which *MAPK1* (*ERK2*) is also annotated as *p38* (see appendix).

Furthermore, there was down-regulation of *STAT3* signalling (Fig. 3-26), another important pathway associated in leukaemic cell survival. Concomitantly, there was up-regulation of stress-related MAPK pathways, such as the JNK pathway; both *JNK* and several down-stream factors, as *JUN* (*c-JUN/AP-1*) and *ATF-2* were up-regulated (fig. 3-26). MLL/AF4 depletion also affects NFkB-signalling, ostensibly shutting it down (fig. 3-25, fig. 3-26). Several reports have associated IGF1R signalling and aberrant RAS activation with MLL/AF4-mediated oncogenesis^{152,190}. Notably, *MLL/AF4* depletion results in decrease expression levels of both the receptor kinase *IGF1R* and *RAS* (fig. 3-27). These results are in good concordance with the observations both for the TP1 signature and the phenotype associated with *MLL/AF4* knock-down.

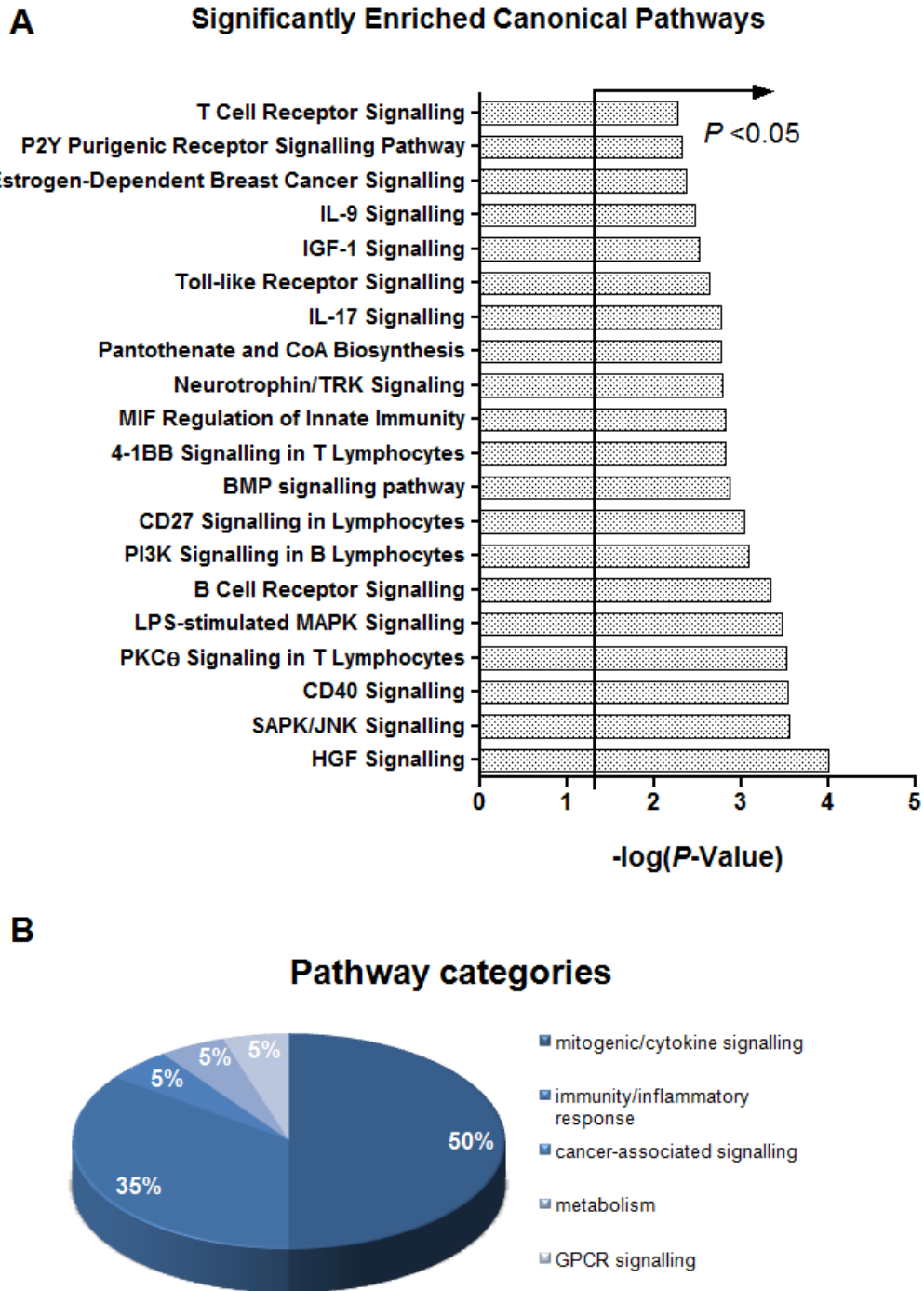
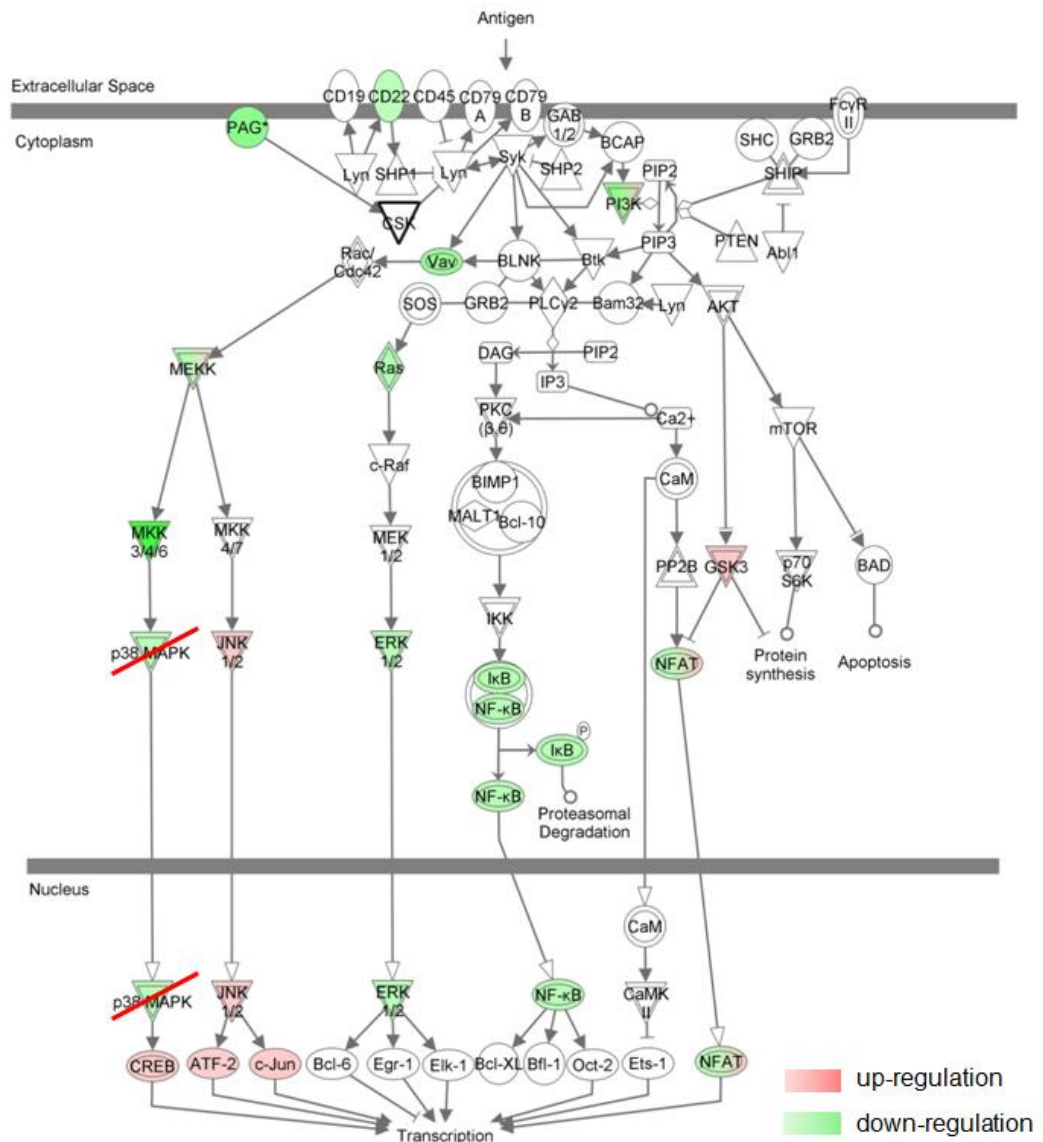


Fig. 3-24: Pathway analysis of the MLL/AF4 gene signature A at TP2

Pathway analysis was performed using IPA Software (Ingenuity Inc.). At TP2, the top20 significantly enriched canonical pathways (A) could be attributed to 5 functional categories (B). Statistical significance was determined by Fisher's Exact test.

B Cell Receptor Signaling

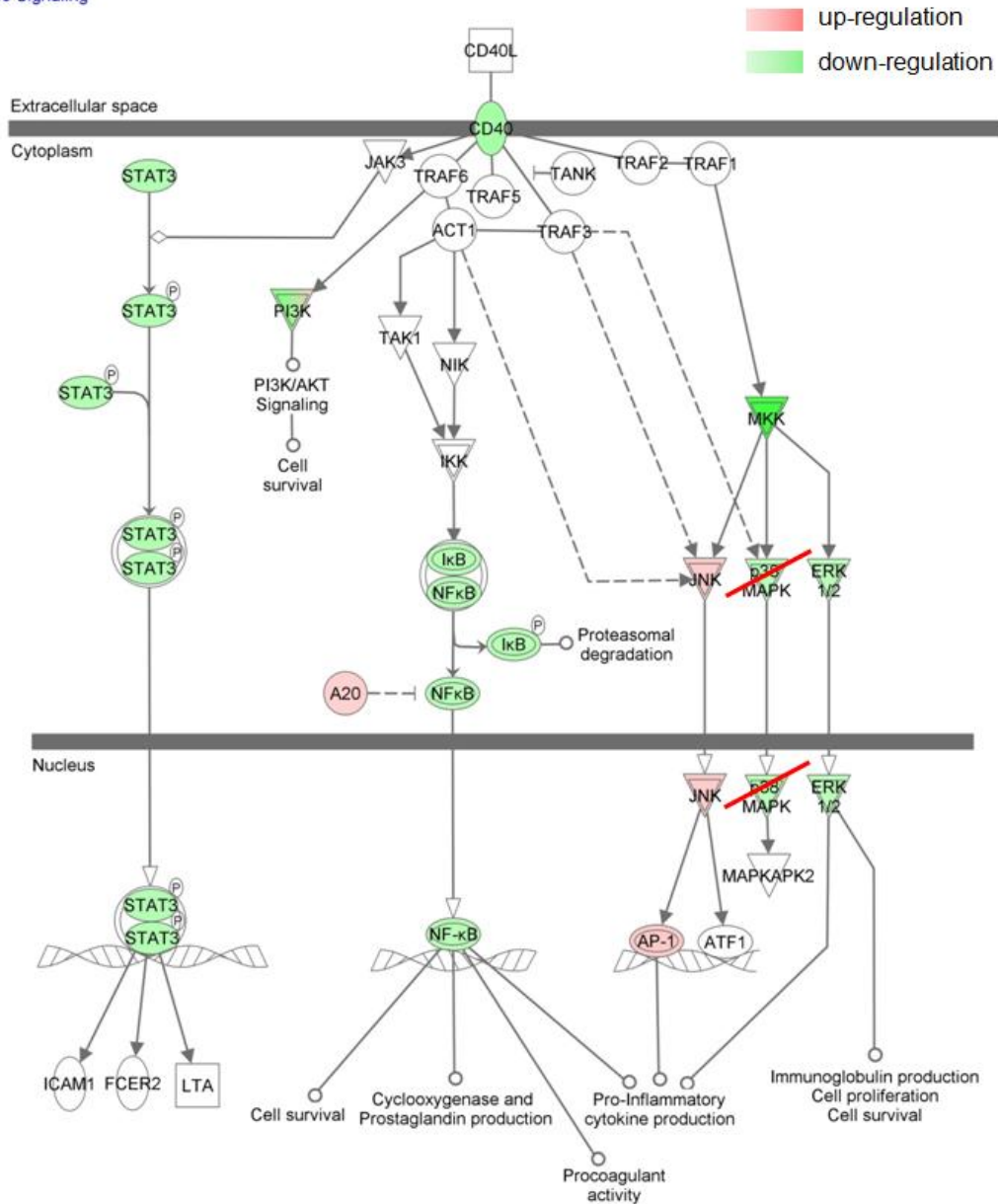


© 2000-2010 Ingenuity Systems, Inc. All rights reserved.

Fig. 3-25: Sustained *MLL/AF4* depletion for 4 d (TP2) results in down-regulation of the BCR signalling machinery involving Ras-ERK1/2- and NFκB-mediated signalling cascades

Entities crossed out in red are due to erroneous annotation by the Ingenuity Pathway Analysis software (Ingenuity Inc.).

CD40 Signaling



© 2000-2010 Ingenuity Systems, Inc. All rights reserved.

Fig. 3-26: Sustained *MLL/AF4* depletion for 4 d (TP2) results in down-regulation of the CD40 signalling machinery involving ERK1/2-, STAT3- and NFκB-mediated signalling cascades

Entities crossed out in red are due to erroneous annotation by the Ingenuity Pathway Analysis software (Ingenuity Inc.).

3.2.4 Gene Set Enrichment Analysis of a MLL/AF4 Core Signature

In order to define a signature of common differentially regulated genes between the two time points, comparison analysis of the MLL/AF4 signatures was performed. An overlap 246 probes between TP1 and TP2 represented 18% of dataset with the lowest probe numbers (TP2). Filtering the probes according to their regulation, TP and TP2 shared 98 up-regulated probes, an overlap of 16%, while having down-regulated 90 probe sets in common, corresponding to 13% of identifiers at TP2 (fig. 3-28).

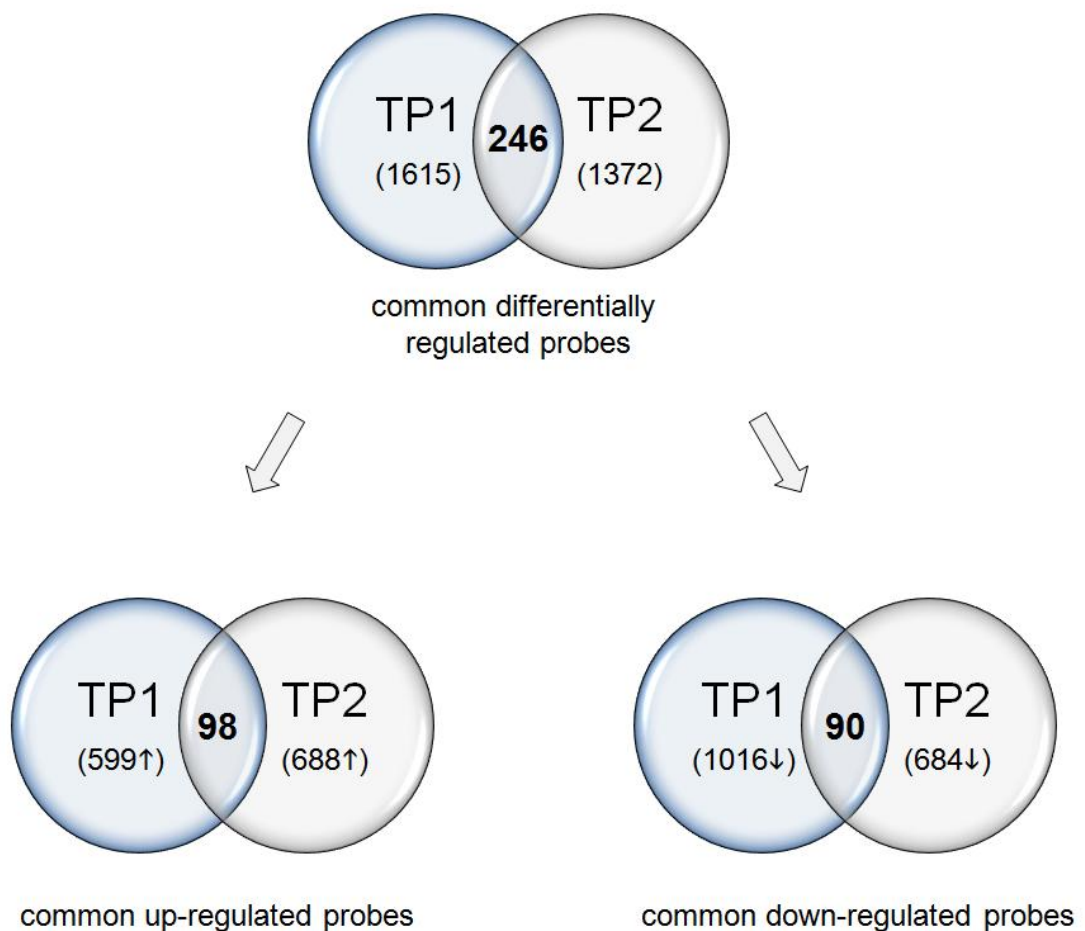


Fig. 3-28: Venn diagram of overlapping probes in MLL/AF4 signature A at both time points

Comparison analysis of the zVAD signatures at TP1 and TP2 share 246 probes, which represents an overlap of 18% of the probe set at TP1. Correcting for an equal regulation, the MLL/AF4 signatures share 98 up- and 90 down-regulated probe sets, which corresponds to 16% and 13% of entities at TP1, respectively. Numbers in parentheses correspond to total numbers.

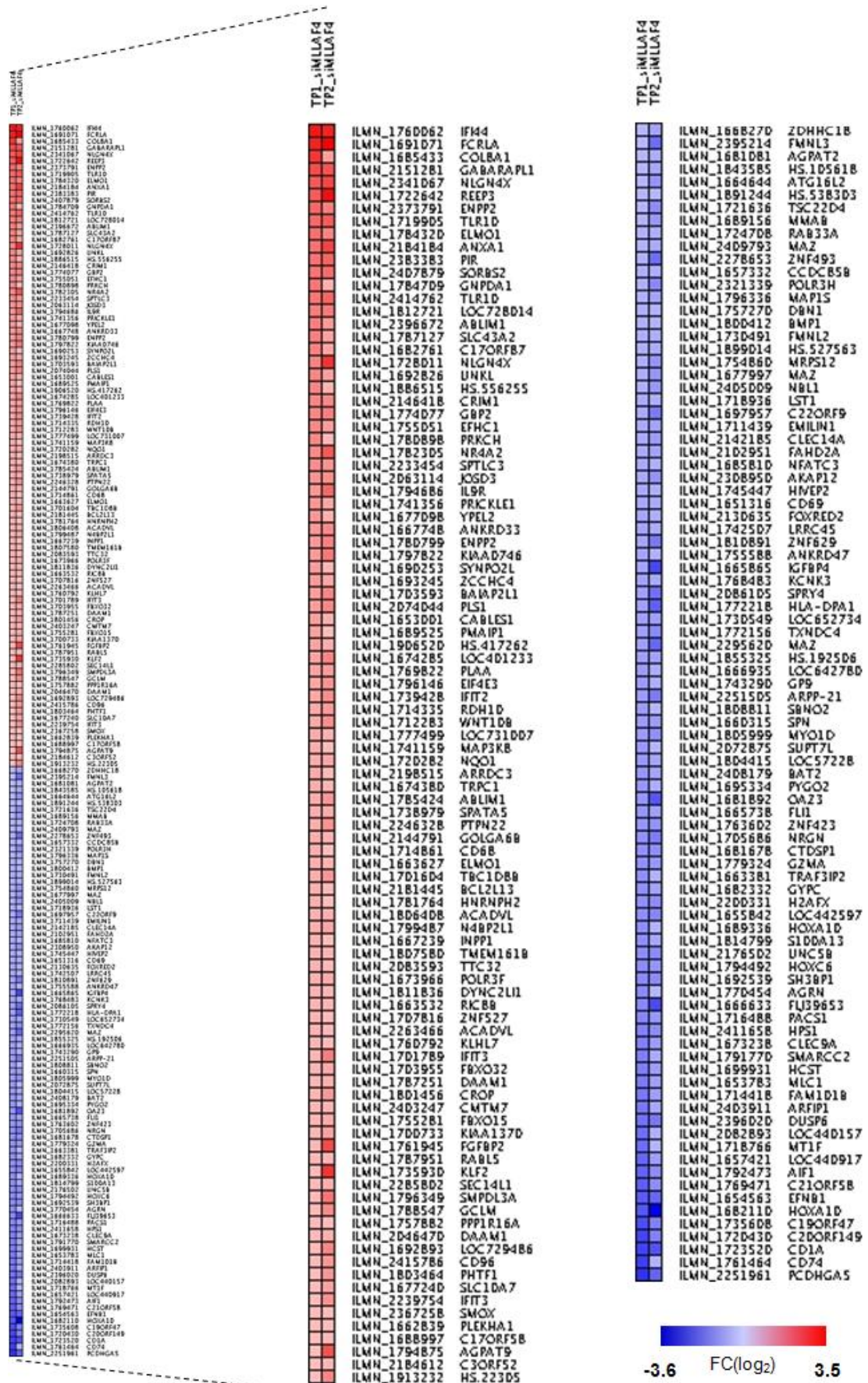
The discrepancy of 58 probes is due to the fact of differing regulation: a probe with induction at TP1 being down-regulated at TP2, and *vice versa, e.g.*, probe ILMN_1739423 for RNS7K, one of the top 50 down-regulated at TP1, while at the same time being one of the top 50 up-regulated probes at TP2 (tab. 3-5 and tab. 3-6, respectively).

A curated core signature data set was derived from the 188 overlapping probes; these entities are illustrated in the heat map in (fig. 3-29). For subsequent analysis, the normalised expression values of siMLL/AF4 and Ctrl at TP1 and TP2 were used.

GSEA analysis was performed on this curated data set, as described in section 2.7.6; three data sets were found to be significantly enriched when adjusting to a false-discovery rate (FDR) cut-off of 25%. These three sets were motif gene sets, consisting of genes containing conserved cis-regulatory motifs such as transcription factor binding sites or miRNA seed sequences. Out of these three data sets, only one corresponded to a known transcription factor, namely SP1. In this analysis, the MLL/AF4 signature was negatively enriched for SP1 target genes at both time points (fig. 3-30A). A closer study of the MLL/AF4 signature genes present in the SP1 motif data set revealed overrepresentation of factors linked with cytoskeleton-associated functions and signalling; particularly the RHO and RAC pathways; e.g., the RHOA-GTPase activating protein (Rho-GAP) *SH3BP1*¹⁹¹, the RAC and ARF binding protein *ARFIP1*¹⁹², as well as the receptors *UNC5B* and *CD74*, both important mediators in cellular migration, adhesion and, interestingly, angiogenesis¹⁹³⁻¹⁹⁷.

Fig. 3-29: Heat map of the MLL/AF4 core signature A

Overlap analyses of the MLL/AF4 expression arrays at TP1 and TP2 revealed a core signature consisting of 188 shared probes with the same regulation and a linear fold change (FC) of ≥ 2.0 . The FC scale represented in this heat map is \log_2 -transformed; a FC of 1 represents a linear FC of 2. The graph was generated using the HeatmapImage module of the Genepattern software.



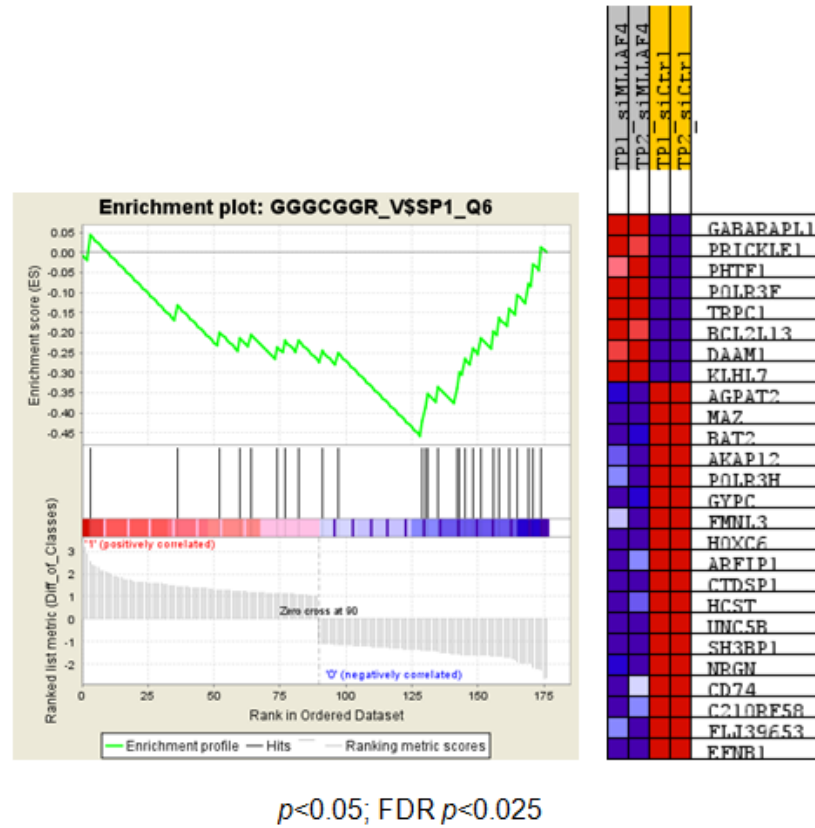


Fig. 3-30: The MLL/AF4 signature was negatively enriched for SP-1 target genes

The combined MLL/AF4 signature showed as statistically significant negative correlation with a gene set corresponding to SP-1 target genes.

3.2.5 Comparison Analysis with Published *MLL/AF4* Target Gene Data Sets

When comparing the differentially expressed genes between the two time-points, there were 107 up-regulated and 106 down-regulated entities shared (fig. 3-31). This numerical discrepancy can be attributed to the fact that some genes are covered by multiple probes, and different probes for the same genes are differentially expressed at both time points. This indicates towards a trend in regards to the regulation of these genes in response to *MLL/AF4* depletion. The relevant entities are listed in (tab. 3-12).

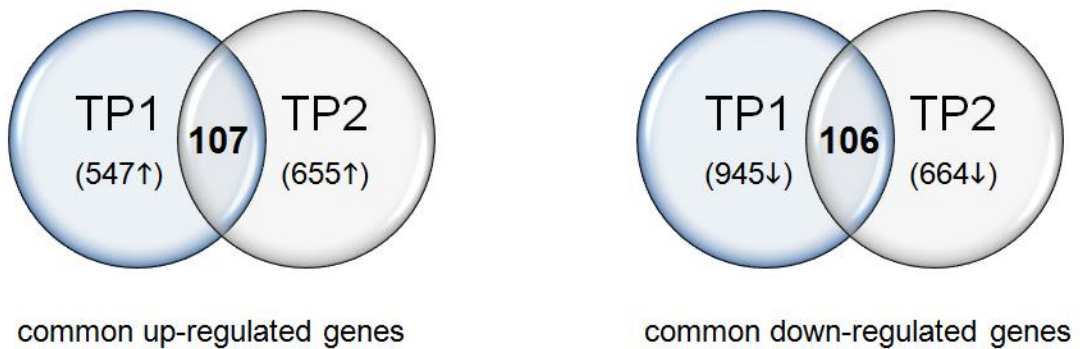


Fig. 3-31: Venn diagrammes of the *MLL/AF4* signature at both time points

Comparison of differentially expressed genes at both time points TP1 and TP2 revealed an overlap of 20% and 16 % of the up-regulated and down-regulated genes, respectively. Numbers in parenthesis indicate the total number of differentially expressed genes in each data set.

Among those genes covered by different probes at the TP1 and TP2 is *TERT*, coding for the catalytic telomerase subunit, as well as the PcG protein *SCMH1*, both linked to self-renewal in normal and malignant stem cells¹⁹⁸. Other genes of interest are *GRP177 (EVI/WLS)*, a GPCR involved in WNT signalling during development¹⁹⁹⁻²⁰², the cell cycle regulator *CDKN2D (p19^{INK4})*, the calpain inhibitor *calpastatin (CAST)* as well as *MSH5*, a major DNA repair factor, all of which are down-regulated in response to *MLL/AF4* depletion. In contrast, *IL7R*, a receptor involved in lymphopoiesis and cellular proliferation²⁰³, and the apoptosis inducer *RIPK5*²⁰⁴ are up-regulated, as well as the gene coding for the glycoprotein GP-180 (*VNN2*), linked to myeloid differentiation²⁰⁵. Of note is *DICER1*, one of the major regulators of miRNA biosynthesis. Lately, there is an increasing body of evidence associating monoallelic loss and/or reduced expression of functional DICER-1 with solid and haematologic malignancies²⁰⁶⁻²⁰⁹. The deregulation of these genes is in keeping with the results of the functional characterisation of the MLL/AF4 signature at both TP1 and TP2 (3.2.3).

Recently, Guenther and colleagues identified potential MLL/AF4 target genes using the ChIP-Seq technology in the SEM cell line¹³². Clearly, these genes were likely candidates to be differentially regulated in response to *MLL/AF4* knock-down. Therefore, the MLL/AF4 gene signature at both time points was analysed for presence of these genes. Since the platform employed differed from the one used in current study, the entity lists provided by Guenther *et al.* was transformed to a gene symbol list using the DAVID Gene ID Conversion tool²¹⁰⁻²¹². Comparison analysis revealed very little overlap between the MLL/AF4 signature at both time points and the putative MLL/AF4 target genes; at TP1 there were 7 common up- and 22 common down-regulated genes; a number that falls below a 5% FDR. A similar observation was made for TP2, where there were 9 shared up-regulated genes and 16 that showed decreased expression in response to *MLL/AF4* depletion. Indeed, only 2 of the up-regulated and 7 of the down-regulated genes are shared between both time points (fig. 3-32). The shared genes are listed in tab. 3-13.

Tab. 3-12: Differentially regulated genes in the MLL/AF4 signature covered by distinct probe sets at both time points

Gene_Symbol	TP1		TP2	
	linear FC	Probe_ID	linear FC	Probe_ID
AGXT2L2	-2.85	ILMN_1686370	-2.32	ILMN_1673529
ALAS1	2.16	ILMN_1700047	2.67	ILMN_2385647
ALDH4A1	-3.31	ILMN_2244841	-2.09	ILMN_1656368
ASB7	3.78	ILMN_1680419	3.99	ILMN_1753040
ATE1	2.06	ILMN_1791400	2.12	ILMN_1812479
C14ORF37	2.14	ILMN_2138745	3.17	ILMN_1796377
CAST	2.58	ILMN_1672947	3.20	ILMN_2322806
CAV1	2.31	ILMN_2149226	2.12	ILMN_1687583
CDKN2D	-2.08	ILMN_1748883	-2.02	ILMN_1740597
CLIC4	-2.60	ILMN_1671250	-2.67	ILMN_2063584
CMTM1	-2.55	ILMN_2287911		
			-2.07	ILMN_1693494
			-2.17	ILMN_2328363
DICER1	2.07	ILMN_1772692	2.94	ILMN_2349831
GPR177	-2.48	ILMN_1660549	-3.15	ILMN_2399769
HDLBP	-3.06	ILMN_1678252	-2.22	ILMN_1756426
IL7R	2.12	ILMN_1691341	2.73	ILMN_2342579
LOC650339	-2.53	ILMN_1735832	-2.61	ILMN_1729791
LOC653604	2.38	ILMN_1793461	2.08	ILMN_1664706
LOC728417	3.11	ILMN_1776483	2.05	ILMN_1665540
LPGAT1	2.73	ILMN_2151277	2.05	ILMN_1687998
MSH5	-2.17	ILMN_1675708	-2.83	ILMN_1651787
OPA3	-2.37	ILMN_2284591	-2.16	ILMN_1652819
PCDHGC3	-2.61	ILMN_1656955	-3.12	ILMN_1675428
PDLIM7	-2.69	ILMN_2396639	-2.67	ILMN_1814985
RIPK5	3.02	ILMN_1779600	2.06	ILMN_2352023
SCMH1	-2.28	ILMN_2276504	-2.07	ILMN_2375557
SLA	2.17	ILMN_1667371	2.84	ILMN_2345898
STRN4	-4.21	ILMN_2394102	-2.13	ILMN_1696190
SYNGR1	-2.64	ILMN_1810875	-2.02	ILMN_1721712
TERT	-2.18	ILMN_1796005	-2.27	ILMN_2373119
TNRC6A	-2.04	ILMN_1714622	-2.49	ILMN_1739573
VNN2	2.44	ILMN_1678939	4.52	ILMN_1758864
ZFP1	2.42	ILMN_1695902	3.13	ILMN_2133936

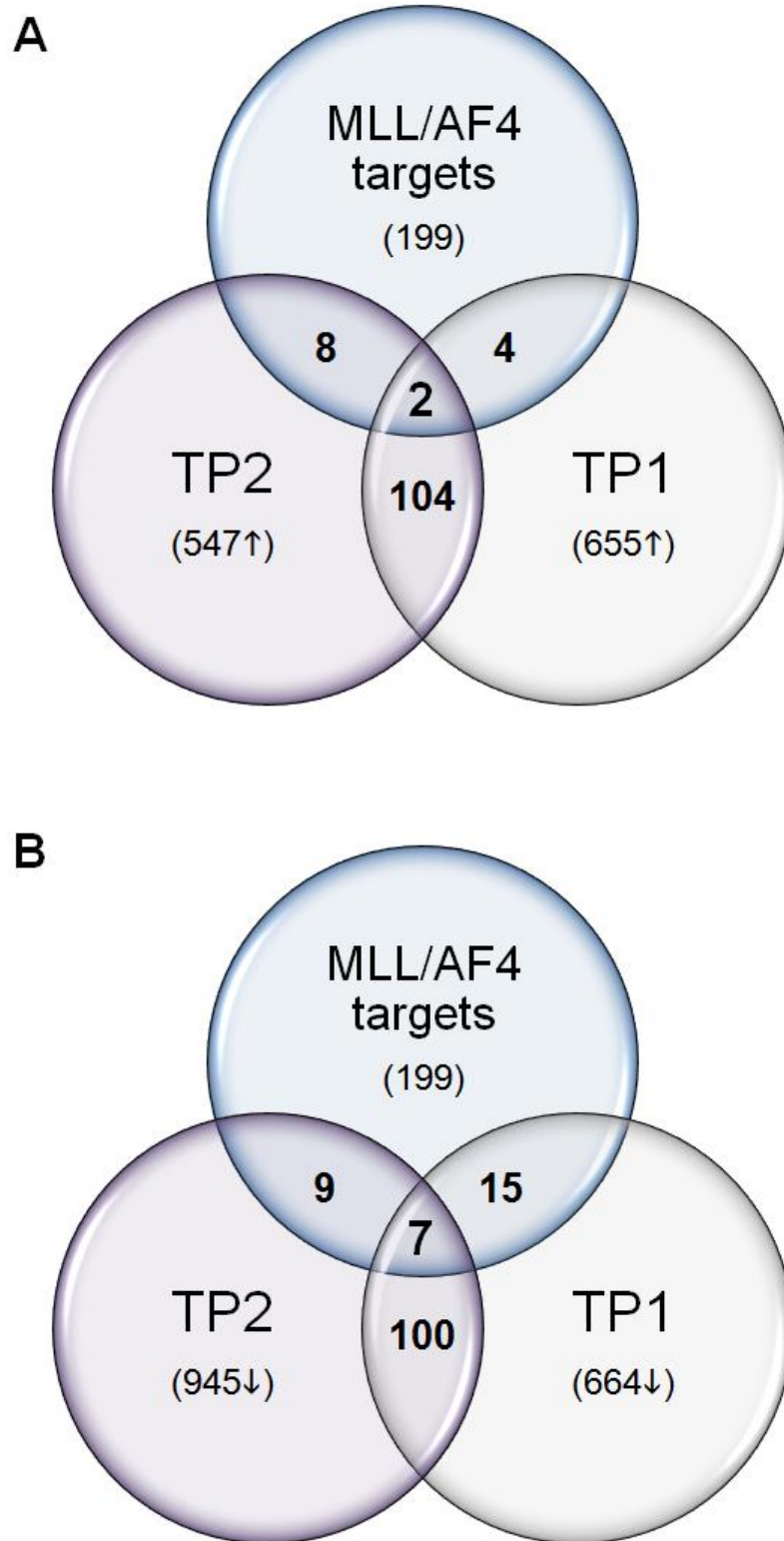


Fig. 3-32: Venn diagrammes of MLL/AF4 target genes¹³² with MLL/AF4 signature A at both time points

Comparison analysis of the induced (A) and down-regulated (B) genes of the MLL/AF4 signature with published MLL/AF4 target genes shows very little overlap.

Tab. 3-13: MLL/AF4 target genes¹³² present in the MLL/AF4 signature-A at both TP1 and TP2

Gene_Symbol	Probe_ID	Fold-change		Accession
		TP1-A	TP2-A	
REEP3	ILMN_1722642	5.12	10.49	NM_001001330
CD96	ILMN_1711573	1.47	2.32	NM_198196.2
	ILMN_2415786	2.05	2.85	NM_005816.4
PCDHGC3	ILMN_1656955	-2.61	-1.73	NM_032403.1
	ILMN_1675428	1.38	-3.12	NM_032403.1
CLEC9A	ILMN_1673238	-3.46	-2.64	NM_207345.2
FMNL2	ILMN_1730491	-2.16	-2.20	NM_052905.3
SPN	ILMN_1801040	-2.81		NM_001030288.1
	ILMN_1658017	-2.11		NM_001030288.1
	ILMN_1660315	-2.62	-2.62	NM_003123.3
HOXA10	ILMN_1689336	-2.99	-2.08	NM_018951.3
	ILMN_1682110	-5.23	-12.55	NM_018951.3
HIVEP2	ILMN_1745447	-2.31	-2.16	NM_006734.3
DUSP6	ILMN_1677466	-2.70	<u>P->M</u>	NM_001946.2
	ILMN_2396020	-3.98	-3.78	NM_022652.2

Bold font represents up-regulated genes, italics indicate that the fold-change (FC) falls below the cut-off-value of $FC \geq 2.00$ but is above 1.3.

P->M denotes such a strong down-regulation, that the probe flags in these siMLL/AF4-treated cells go from present (P) to marginal (M).

3.3 GEP OF MLL/AF4-DEPLETED SEM CELLS AT TIME POINT TP3

In the previous sections, gene expression profiles of SEM cells depleted of MLL/AF4 at TP1 and TP2 were analysed, corresponding to an early and intermediate molecular response of the cells towards the ablation of *MLL/AF4*. Conversely, TP3 represents a late time point of six days sustained MLL/AF4 depletion. In order to analyse these late molecular events, gene expression profiling of SEM cells electroporated for three times with siRNA was performed. Due to technical reasons, a MOCK control was excluded. For more accurate comparison of the gene signature at TP3 with the previously analysed MLL/AF4 signature at TP1 and TP2, the expression sets at these two earlier time points were reanalysed, excluding the MOCK control.

The scheme in fig. 3-33 depicts the experimental set-up for the analysis; in brief, SEM cells were serially electroporated every other day for three times, at day 0, day 2 and day 4. For confirmation of sustained MLL/AF4 depletion, RNA was harvested at TP1, TP2 and TP3, which corresponds to a knock-down period of 2, 4 and 6 days, analysed for MLL/AF4 expression by qRT-PCR. SEM cells electroporated with siMLL/AF4 showed a reduction of *MLL/AF4* transcript levels of 63-72% over all three time points when compared so control-treated cells (fig. 3-34). Prior to GEP, TP3 RNA was assessed for integrity using lab-on-chip technology (tab. 3-14); a RIN>7 was determined for both samples, indicating acceptable RNA quality for GEP experiments.

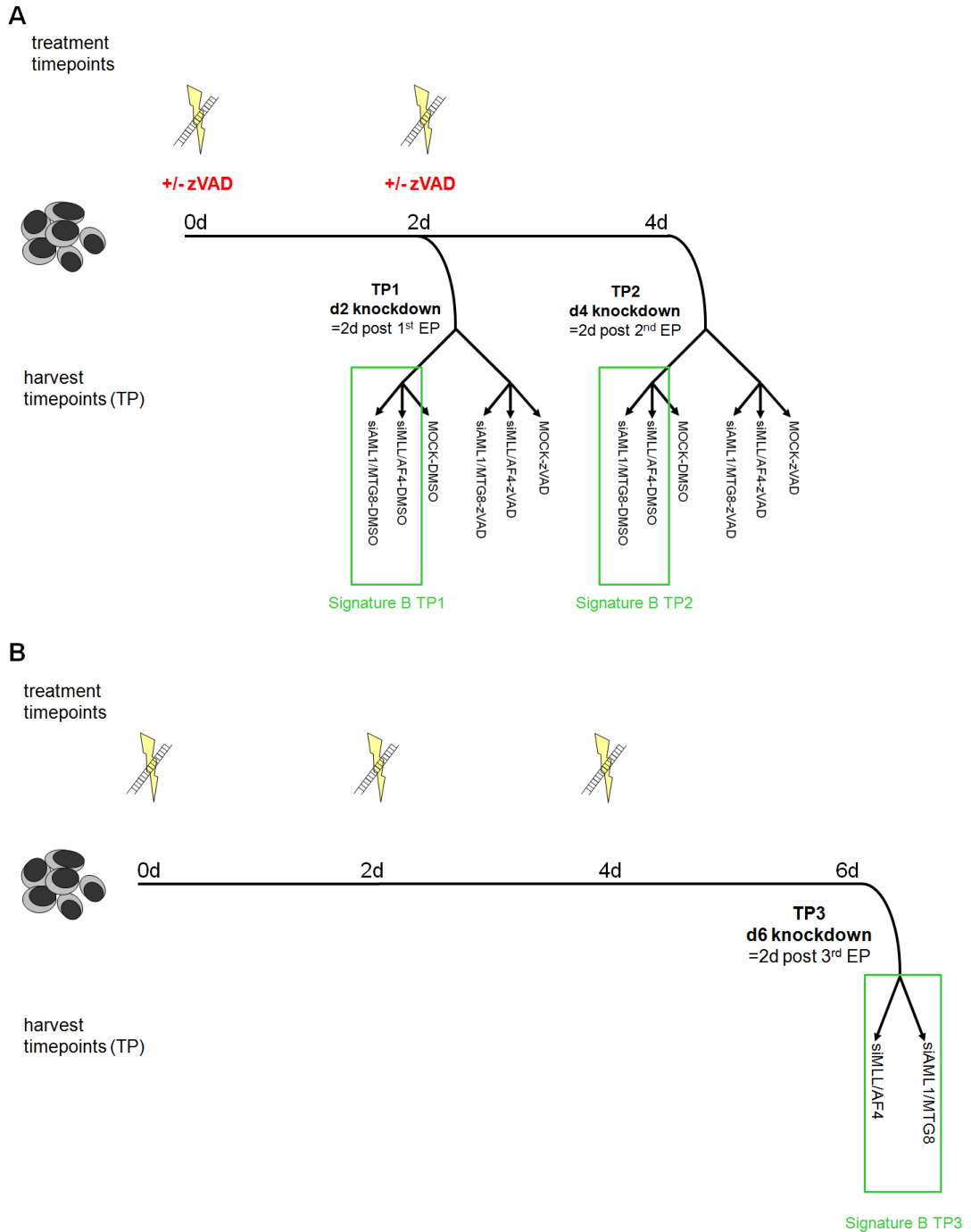


Fig. 3-33: Experimental and analysis set-up for MLL/AF4 signature B

Samples for TP1 and TP2 were derived from signature A, excluding the MOCK control. For a better understanding, the original experimental set-up is depicted in panel (A). TP3 is derived from SEM cells serially electroporated with siMLL/AF4 and control siRNA (siAML1/MTG8) at two-day intervals; RNA for GEP was harvested at TP3, corresponding to six days sustained MLL/AF4 knock-down (B).

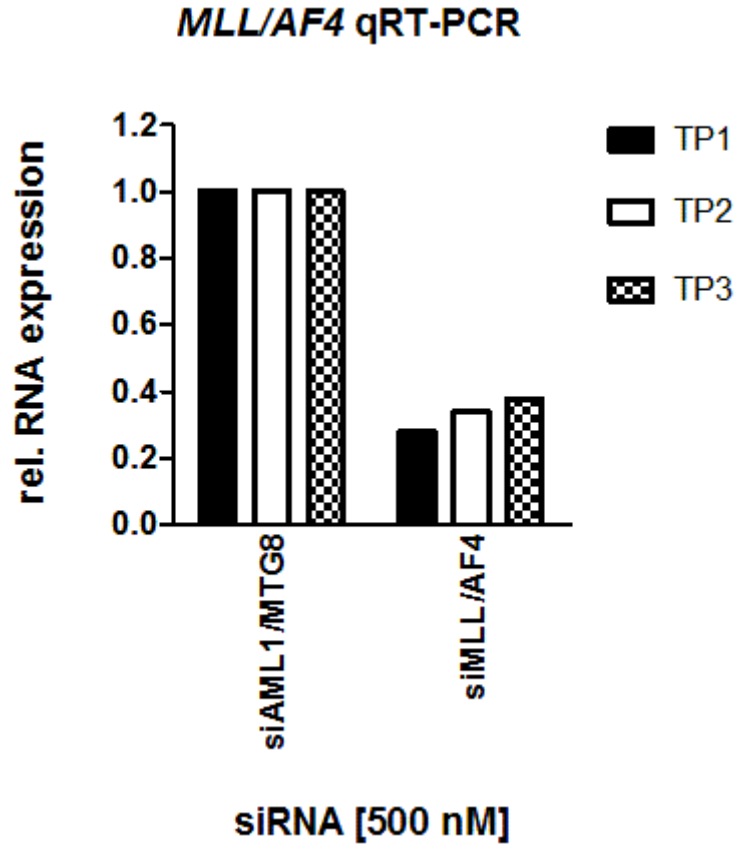


Fig. 3-34: MLL/AF4 expression analysis for TP3-GEP

SEM were serially electroporated with siMLL/AF4 or control siRNA (siAML1/MTG8) at two-day intervals for three times. RNA was harvested at TP1, TP2 and TP3, representing a sustained knockdown period of two, four and six days, respectively. *MLL/AF4* expression was assessed by qRT-PCR. The graph represents one single continuous experiment, each sample was assayed in triplicates.

Tab. 3-14: RIN values of samples submitted to GEP as determined by Bioanalyzer2100 RNA 6000 Nano Assay

sample	RIN
TP3	
<i>siAML1/MTG8</i>	9.3
<i>siMLL/AF4</i>	7.0

The raw data files were preprocessed in the Genome Studio gene expression module (Illumina Inc.), subtracting background, and further analysed using GeneSpring GX 11 software as described earlier. The number of differentially probes and genes associated with MLL/AF4 signature B is listed in tab. 3-15: there were 2708 differentially expressed probes at TP1, which corresponded to 2616 genes, of which 1483 were up- and 1133 down-regulated. At TP2 there were 2150 differentially regulated probes, which could be collapsed into 1973 genes, of which 992 were induced, and 981 genes showed reduced expression. 2505 probes showed differential expression at TP3, consisting of 1449 up-regulated and 1056 down-regulated probes.

The top50 up- and down-regulated probes for TP3 are listed in tab. 3-16 and tab. 3-17, respectively. Of note is the overrepresentation of probes covering provisional RefSeq, EST and unannotated loci, representing 20 out of the top50 probes.

Tab. 3-15: Number of differentially expressed probe sets and genes for the MLL/AF4 signature B at all three time points

siMLL/AF4 vs. siCtrl	TP1(B)	TP2(B)	TP3
No. of differentially expressed probes	2708	2150	2505
<i>up-regulated probes</i>	1177	1034	1449
<i>down-regulated probes</i>	1516	1016	1056
No. of differentially expressed genes	2616	1973	2386
<i>up-regulated genes</i>	1483	992	1388
<i>down-regulated genes</i>	1133	981	1007

Tab. 3-16: Top 50 up-regulated genes at TP3

ILMN_Gene	Fold-change [siMLL/AF4] vs [Ctrl]	Accession	Probe_ID
LOC100008589	92.87	NR_003287.1	ILMN_3251587
LOC100008589	42.61	NR_003287.1	ILMN_1733559
LOC100132394	21.27	XM_001713809.1	ILMN_3249578
FCRLA	20.53	NM_032738.3	ILMN_1691071
RN5S9	18.13	NR_023371.1	ILMN_3234762
IFIT1	17.83	NM_001548.3	ILMN_1707695
OAS2	16.74	NM_016817.2	ILMN_1674063
RN7SK	16.17	NR_001445.1	ILMN_1739423
IFI44	14.22	NM_006417.3	ILMN_1760062
IFIT2	13.64	NM_001547.4	ILMN_1739428
LOC100128274	13.24	XM_001725558.1	ILMN_3253787
ZNF626	12.71	NM_001076675.1	ILMN_2290732
SAMD9L	11.66	NM_152703.2	ILMN_1799467
GABARAPL1	11.22	NM_031412.2	ILMN_2151281
IFIT3	10.75	NM_001031683.1	ILMN_1701789
LOC728678	10.72	XR_039547.1	ILMN_3305628
RNU4-2	10.29	NR_003137.2	ILMN_3308138
LOC100133950	9.49	XM_001721634.1	ILMN_3239388
SLC25A20	9.48	XM_001133926.1	ILMN_1783060
LOC440157	9.41	NM_001013701.1	ILMN_2082893
RN7SK	9.10	NR_001445.1	ILMN_2074860
LOC728755	9.07	XM_001128377.2	ILMN_3226214
PATE2	9.05	NM_212555.1	ILMN_2133784
ANKRD44	8.49	NM_153697.1	ILMN_2059844
KIAA1666	7.88	XM_942124.2	ILMN_1732988
LOC100130764	7.63	XM_001723713.1	ILMN_3256926
C14ORF82	7.26	XM_944991.1	ILMN_1690443
ZNF93	7.20	NM_001004126.1	ILMN_1679083
LOC727962	7.14	XM_001718648.1	ILMN_3275275
MX2	7.06	NM_002463.1	ILMN_2231928
GSDMB	7.05	NM_018530.2	ILMN_2260756
LOC644852	6.93	XM_934218.1	ILMN_1727165
ENPP2	6.92	NM_001040092.1	ILMN_1780799
LOC649456	6.84	XM_938534.1	ILMN_1705759
LOC644591	6.81	XM_927706.2	ILMN_1710362
LOC646897	6.75	XM_929859.1	ILMN_1693225
LOC654350	6.69	XM_940587.3	ILMN_3281651
GCLM	6.68	NM_002061.2	ILMN_2225974
RNF213	6.53	NM_020954.2	ILMN_1731203
TFIP11	6.52	NM_001008697.1	ILMN_1695000
ISG15	6.40	NM_005101.1	ILMN_2054019
RAB3IP	6.31	NM_001024647.2	ILMN_2291619
HS.579631	6.30	BU536065	ILMN_1881909
KCNK6	6.25	NM_004823.1	ILMN_2074773
IRF9	6.24	NM_006084.4	ILMN_1745471
LOC728779	6.23	XM_001128458.2	ILMN_3305508
LOC647295	6.20	XM_930360.1	ILMN_1800055
HS.125087	6.20	BQ437417	ILMN_1835092
PRO1853	6.14	NM_144736.3	ILMN_2394132
HS.580797	6.13	BF996074	ILMN_1900734

Tab. 3-17: Top 50 down-regulated genes at TP3

ILMN_Gene	Fold-change [siMLL/AF4] vs [siCtrl]	Accession	Probe_ID
VPS24	-9.58	NM_001005753.1	ILMN_2406043
LOC442597	-7.95	XM_944534.1	ILMN_1655842
HCST	-7.67	NM_001007469.1	ILMN_1699931
SCAND1	-7.07	NM_016558.2	ILMN_1795317
MTP18	-7.01	NM_001003704.1	ILMN_2372040
KLHL23	-6.42	NM_144711.3	ILMN_1732550
MACROD1	-6.40	NM_014067.2	ILMN_1740960
ALG1	-6.29	NM_019109.3	ILMN_1718093
RAB43	-5.99	NM_198490.1	ILMN_2155480
PI16	-5.66	NM_153370.2	ILMN_1766264
KCNMB1	-5.61	NM_004137.2	ILMN_1652065
PRPF40A	-5.51	NM_017892.3	ILMN_1666648
FAM43A	-5.50	NM_153690.4	ILMN_1706015
ELMO1	-5.40	NM_130442.2	ILMN_1740231
A2M	-5.34	NM_000014.4	ILMN_1745607
ANGPT1	-5.33	NM_001146.3	ILMN_1677723
ANGPT1	-5.30	NM_001146.3	ILMN_2086890
MYBBP1A	-5.26	NM_014520.2	ILMN_1806757
LOC641518	-5.04	XR_017788.1	ILMN_1707904
CLEC14A	-5.02	NM_175060.1	ILMN_2142185
SPAST	-5.01	NM_199436.1	ILMN_2373556
HLA-DPA1	-4.94	NM_033554.2	ILMN_1772218
POLR3H	-4.92	NM_001018052.1	ILMN_1786024
CD93	-4.89	NM_012072.3	ILMN_1704730
FAM108A3	-4.88	NM_001080422.1	ILMN_2307978
PPP1R12B	-4.86	NM_032103.1	ILMN_1756289
LOC732360	-4.86	XR_016089.2	ILMN_3305871
MDK	-4.85	NM_001012334.1	ILMN_2261876
OS9	-4.76	NM_006812.2	ILMN_2361807
SERPINB8	-4.73	NM_002640.3	ILMN_2397028
EFNA4	-4.65	NM_182689.1	ILMN_1755710
LOC100132060	-4.62	XM_001720144.1	ILMN_3244611
HCP5	-4.58	NM_006674.2	ILMN_1803945
SLC22A18AS	-4.58	NM_007105.1	ILMN_1691048
HIVEP2	-4.57	NM_006734.3	ILMN_1745447
MGC3196	-4.57	XM_938324.1	ILMN_1722674
ASGR2	-4.54	NM_080914.1	ILMN_2342638
TMEM185A	-4.44	NM_032508.1	ILMN_2140389
FAM129B	-4.42	NM_022833.2	ILMN_1661755
CHST14	-4.41	NM_130468.2	ILMN_1743340
HOXA10	-4.41	NM_018951.3	ILMN_1689336
PRKAR2A	-4.41	NM_004157.2	ILMN_1681888
PRR7	-4.39	NM_030567.3	ILMN_1677509
LIN7C	-4.35	NM_018362.2	ILMN_2184708
LAIR1	-4.35	NM_021706.2	ILMN_1768598
XKR8	-4.34	NM_018053.2	ILMN_2087303
IL1RN	-4.32	NM_173843.1	ILMN_1774874
LST1	-4.29	NM_205839.1	ILMN_1688373
MAZ	-4.29	NM_001042539.1	ILMN_2295620
RYK	-4.27	NM_001005861.1	ILMN_1769671

3.3.1.1 Analysis of MLL/AF4 signature at TP3 using Ingenuity Pathway Analysis

Analysing the MLL/AF4 signature at TP3 using the IPA software showed enrichment of genes in networks involved in cytoskeleton-associated processes such as cellular movement, assembly and organisation, morphology and cell-to-cell signalling. Furthermore, networks linked to cellular growth and proliferation, cellular development, cell cycle as well as DNA repair were affected (tab. 3-18). These networks are mirrored also in the molecular functions attributed to the signature, with the addition of cell death. As with previous TPs, amongst the top5 physiological functions and associated disorders are haematologic development, cancer and haematologic disease. There is also an bias towards immunological functions, such as infection mechanism and immune cell trafficking (tab. 3-19), which indicates, as observed at TP1 and TP2 in the MLL/AF4 signature, an enrichment of proinflammatory pathways and genes.

Tab. 3-18: Top 5 networks affected by MLL/AF4 gene signature A at TP3

Name	Score
Nervous System Development and Function, Tissue Morphology, Cellular Movement	26
Cell-To-Cell Signalling and Interaction, Tissue Development, Haematological System Development and Function	24
DNA Replication, Recombination, and Repair, Cell Cycle, Cellular Assembly and Organization	24
Cellular Development, Cellular Growth and Proliferation, Haematological System Development and Function	23
Organismal Injury and Abnormalities, Reproductive System Disease, Genetic Disorder	18

Tab. 3-19: Significantly enriched functional categories in MLL/AF4 gene signature B at TP3

Top Biofunctions	P-value
Diseases and Disorders	
<i>Organismal Injury and Abnormalities</i>	9.20E-08 - 4.45E-02
<i>Cancer</i>	4.56E-05 - 4.95E-02
<i>Neurological Disease</i>	4.56E-05 - 4.03E-02
<i>Infection Mechanism</i>	5.88E-04 - 4.45E-02
<i>Haematological Disease</i>	2.11E-03 - 4.95E-02
Molecular and Cellular Functions	
<i>Cellular Growth and Proliferation</i>	5.37E-06 - 4.59E-02
<i>Cell Death</i>	5.23E-05 - 4.69E-02
<i>Cell Cycle</i>	8.94E-05 - 4.95E-02
<i>DNA Replication, Recombination, and Repair</i>	8.94E-05 - 4.07E-02
<i>Cellular Development</i>	3.07E-04 - 4.95E-02
Physiological System Development and Function	
<i>Haematological System Development and Function</i>	3.92E-03 - 4.31E-02
<i>Endocrine System Development and Function</i>	5.74E-03 - 4.03E-02
<i>Nervous System Development and Function</i>	5.74E-03 - 2.64E-02
<i>Reproductive System Development and Function</i>	5.74E-03 - 4.03E-02
<i>Immune Cell Trafficking</i>	7.56E-03 - 4.80E-02

P-Value range describes the *p*-values of associated subcategories as determined by Fisher's exact test.

Nervous System Development and Function, Tissue Morphology, Cellular Movement

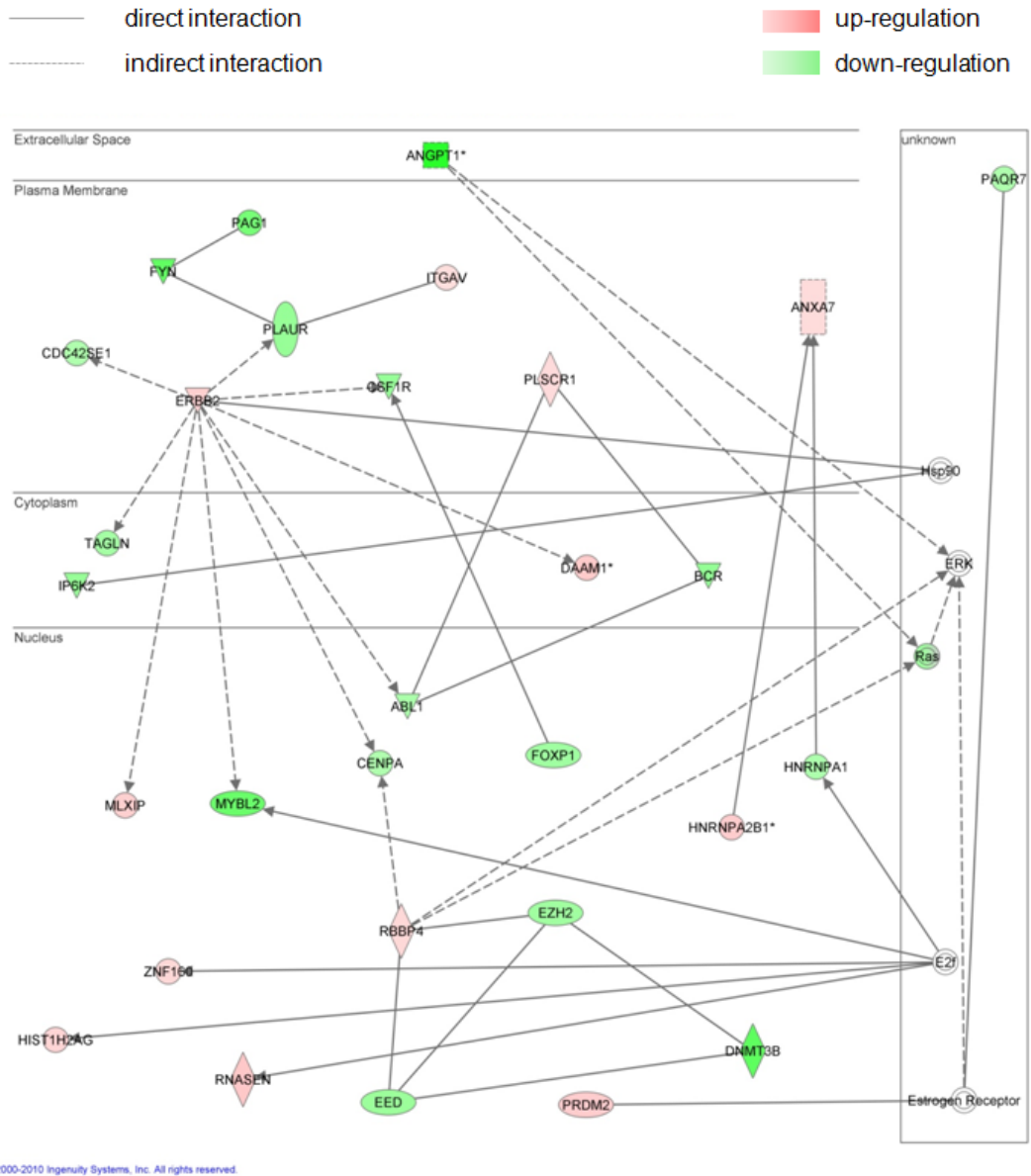


Fig. 3-35: Sustained *MLL/AF4* depletion for 6 days affects regulatory networks associated with development and cellular movement

A closer look into the regulatory networks affected by prolonged MLL/AF4 depletion revealed down-regulation of several genes linked to cytoskeleton-mediated processes and signalling, such as *PLAUR*, *CDC42SE* and *TAGLN*. Furthermore, genes associated with early cellular development, *e.g.*, the PcG genes *EED* and *EZH2*, as well as the DNA methyltransferases *DNMT3B*, also showed decreased expression. Several protooncogenes were affected by sustained MLL/AF4 depletion, the transcription factor *MYBL2*, the Src family kinase *FYN* and the oncogenic tyrosine kinases *ABL* and *HER2*, linked to breast cancer²¹³, however, are induced. Conversely, the WNT signalling modulator *DAAM1* is up-regulated (fig. 3-35).

Characterisation of the top20 canonical pathways significantly enriched MLL/AF4 signature at TP3 showed that they could be assigned to six major functional categories; as already seen at the other time points of the MLL/AF4 signature, there is a high incidence of pathways involved in immune response and inflammatory processes. The other pathway categories are mitogenic as well as GPCR-/cytokine signalling. Interestingly, the second major groups relates to metabolism, particularly mediating amino acid catabolism, beta-oxidation and respiration (fig. 3-36).

As seen in the MLL/AF4 signature at TP1 and TP2, there is down-regulation of several mitogenic mediators, such as the protein kinase *AKT* and the phospholipase *PLC*, tyrosine kinases (*ABL*, *FYN*, and *SYK*) and the small GTPases *RAC* and *RAS*. Similarly, both transcription factors of the NFkB family as well as NFkB activators such as *PKC β* and *BCL10* are negatively regulated on transcriptional level, indicating a MLL/AF4-dependent shut-down of NFkB signalling (fig. 3-37).

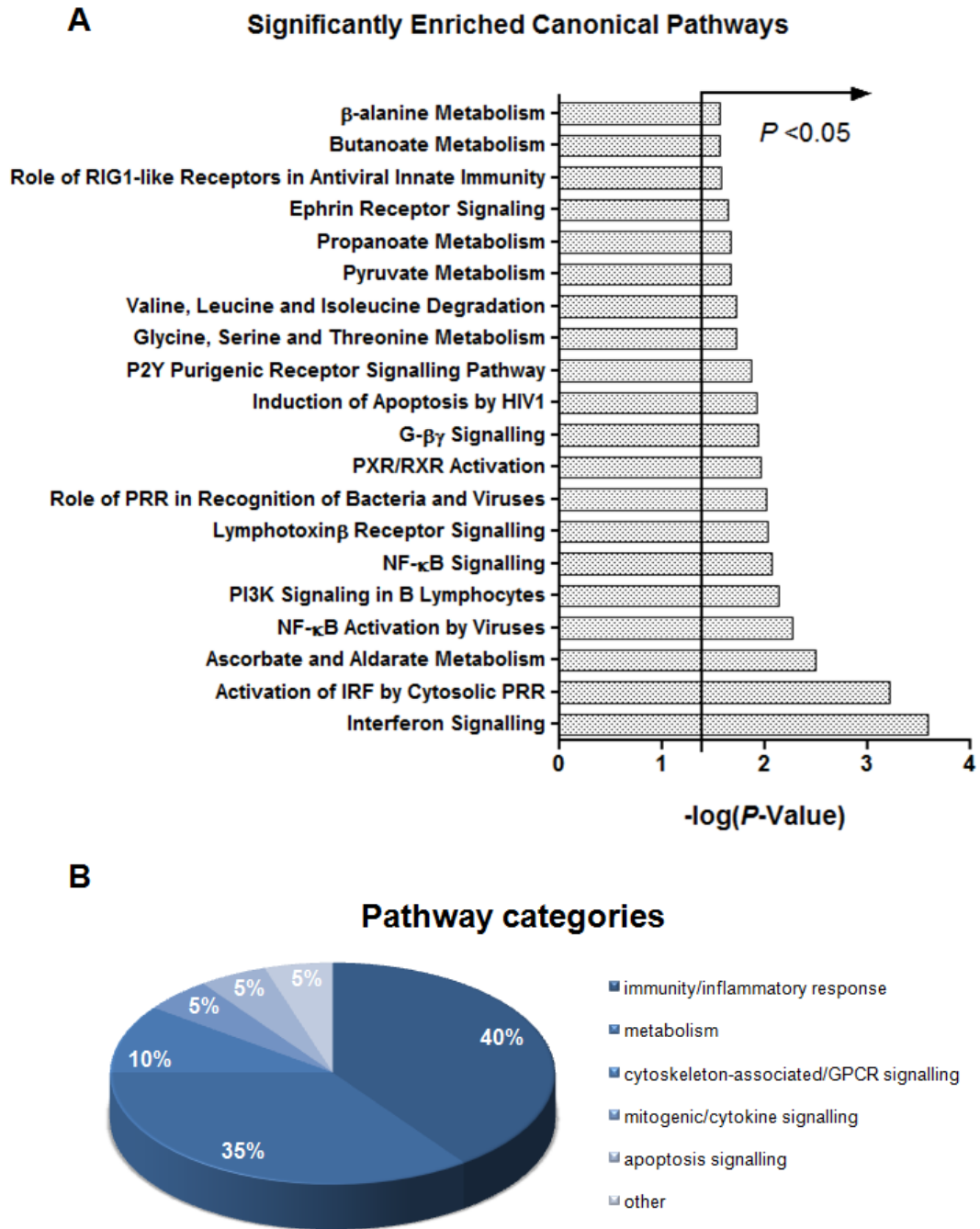


Fig. 3-36: Pathway analysis of the MLL/AF4 gene signature at TP3

Pathway analysis was performed using IPA Software (Ingenuity Inc.). At TP3, the top20 significantly enriched canonical pathways (A) could be attributed to 6 functional categories mainly involving a proinflammatory response and metabolism (B). Statistical significance was determined by Fisher's Exact test.

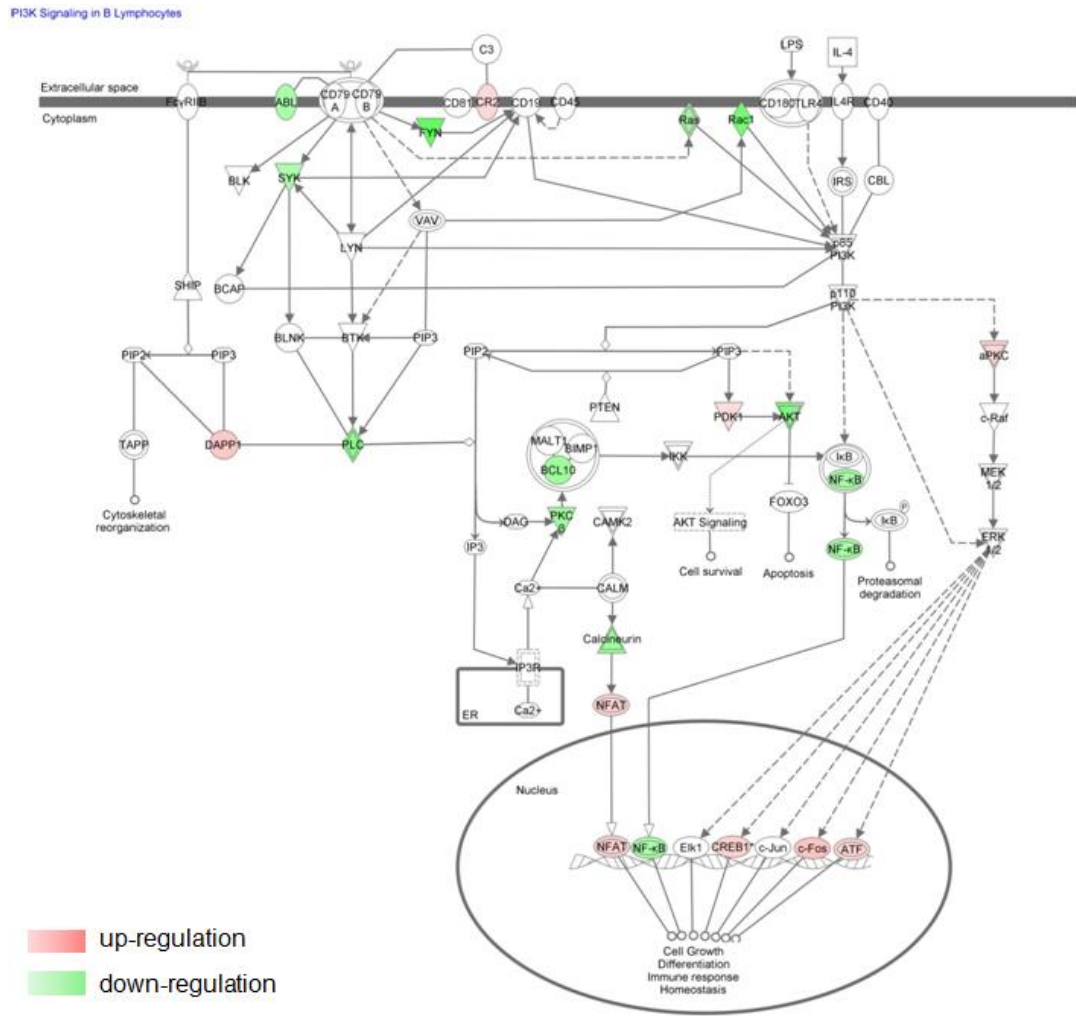


Fig. 3-37: MLL/AF4 signature-B at TP3 shows down-regulation of PI3K/AKT-, NFκB- as well as Ras- and Rac signalling effectors

3.3.2 Comparison Analyses

In order to identify a core signature and underlying functional motifs, all three time points of the MLL/AF4 signature B were compared with each other. Very little overlap was identified; all three TP of gene signature B shared only 43 up-regulated and 20 down-regulated probes, which represents less than 1% overlap (fig. 3-38). This core signature B is listed in the heatmap (fig. 3-39). Interestingly, *ANGPT1*, a gene not present in the core signature A is contained in the core signature B, covered by two probes at all time points.

This core signature consisting 63 probes was used to create a curated data set for GSEA analysis, in order to identify further biological and functional motifs. Only two gene sets were statistically significantly enriched, with a FDR of ≤ 0.25 . This signature was positively enriched for genes annotated with GO-terms corresponding to stress, immune response and signalling (fig. 3-40A). Conversely, the signature was negatively correlated with TCF3 (E2A) target genes (fig. 3-40B), potentially indicating an influence in beta-catenin signalling.

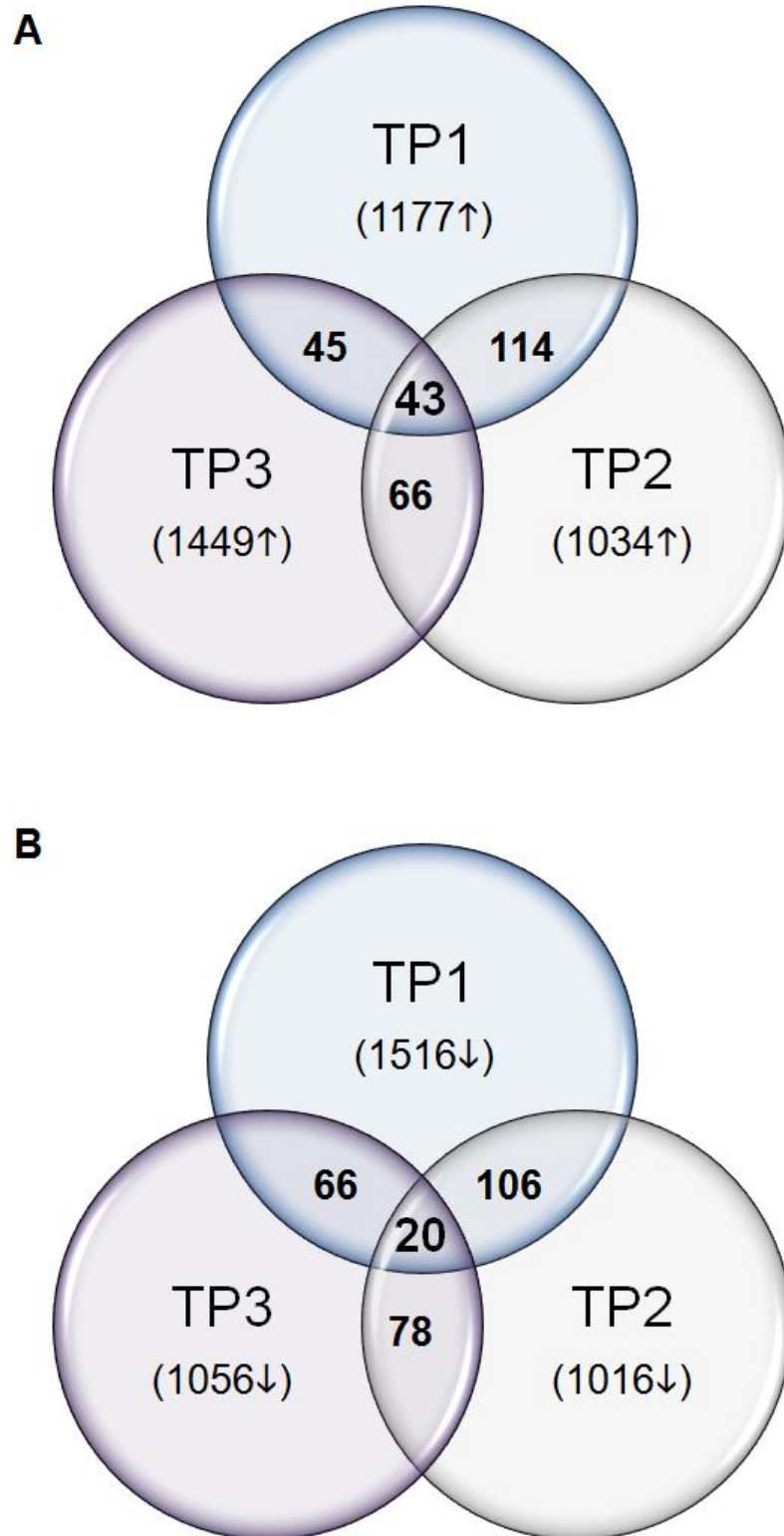


Fig. 3-38: Venn diagrammes of the MLL/AF4 signature B at all three time points

Comparison analysis of induced (A) and down-regulated (B) genes of the MLL/AF4 B signature at all three time points. Numbers in parentheses denote total numbers of differentially expressed genes in that data set.

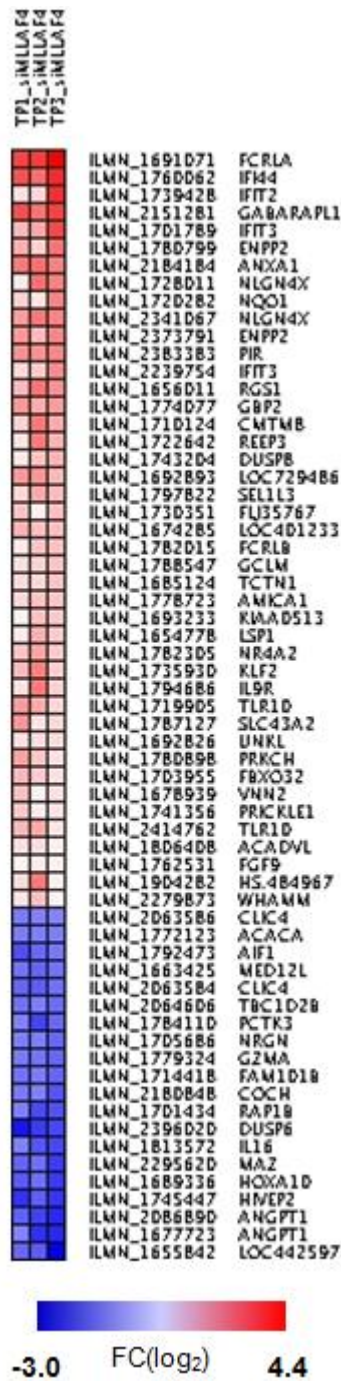


Fig. 3-39: Heat map of a core signature of probes differentially expressed in siMLL/AF4-electroporated SEM cells at all three time points TP1, TP2 and TP3

Overlap analyses of the MLL/AF4 signature B at all three time points revealed a core signature consisting of 63 shared probes showing the same regulation at all time points queried. The core probe set consisted of 43 up- and 20 down-regulated probes with a linear fold change (FC) cut-off of 2.0. The FC scale represented in this heat map is log₂-transformed; a FC of 1 represents a linear FC of 2. The graph was generated using the HeatmapImage module of the Genepattern software.

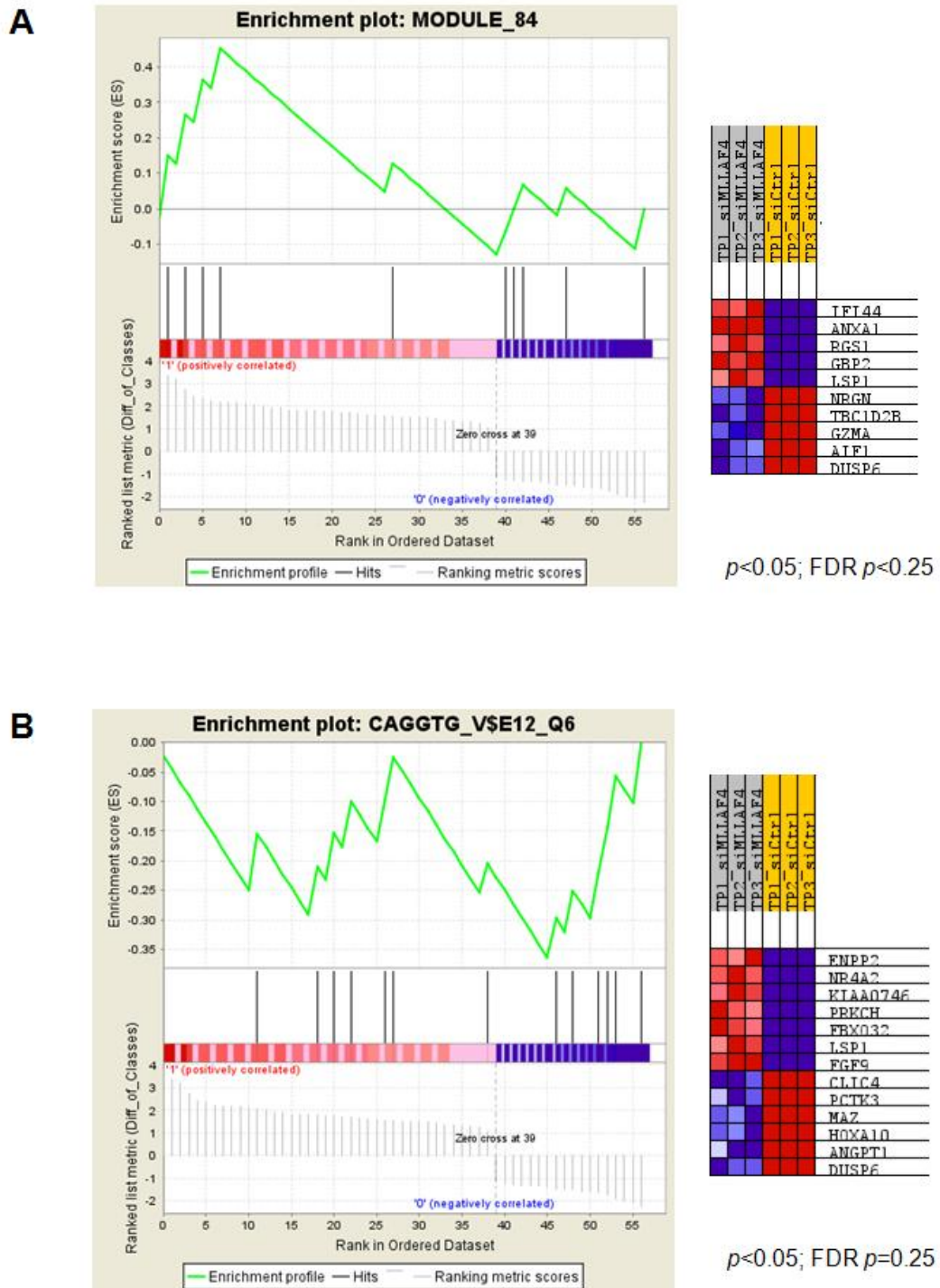


Fig. 3-40: The core signature was significantly enriched for gene sets associated with cellular compromise, immune response and TCF3-target genes

The MLL/AF4 core signature showed positive correlation with one gene set enriched for GO terms associated with stress, immune response and cell signalling (A); there was negative correlation with genes containing TCF3 binding sites (B).

3.4 VALIDATION OF BIOLOGICALLY INTERESTING MLL/AF4 SIGNATURE GENES IN VITRO

Gene expression profiling revealed that *MLL/AF4* depletion results in deregulation of mitogenic signalling, down-regulation of stem-cell associated factors and induction of inflammatory mediators as well as genes linked with cell death. In order to confirm these observations, the results were validated on RNA and protein level. The rationale for the selection of genes to be validated was based on a potential functional relevance as well as novelty.

3.4.1 *MLL/AF4* depletion and mitogenic signalling

A well-established mechanism in oncogenesis is constitutive activation of mitogenic signalling, such as, *e.g.*, the PI3K/AKT pathway or the RAS cascade. Several distinct mechanisms underlie this process, including gain-of function mutations of activators and/or genetic lesions or aberrant epigenetic silencing of negative regulators of these pathways. One important negative regulator is the dual-specificity phosphatase *DUSP6* which targets the MAPKs ERK1 and ERK2; loss of this gene has been implicated in carcinogenesis, and until recently, *DUSP6* was thought to act as a tumour suppressor. Interestingly, *DUSP6* has now been identified as a direct target gene of *MLL/AF4*¹³²; moreover, *DUSP6* overexpression has been linked to increased chemotherapy-resistance in glioblastomas²¹⁴. In this study, probes covering the *DUSP6* transcripts were part of the MLL/AF4 core signature at all three time points, showing consistent down-regulation in response to *MLL/AF4* depletion (fig. 3-41).

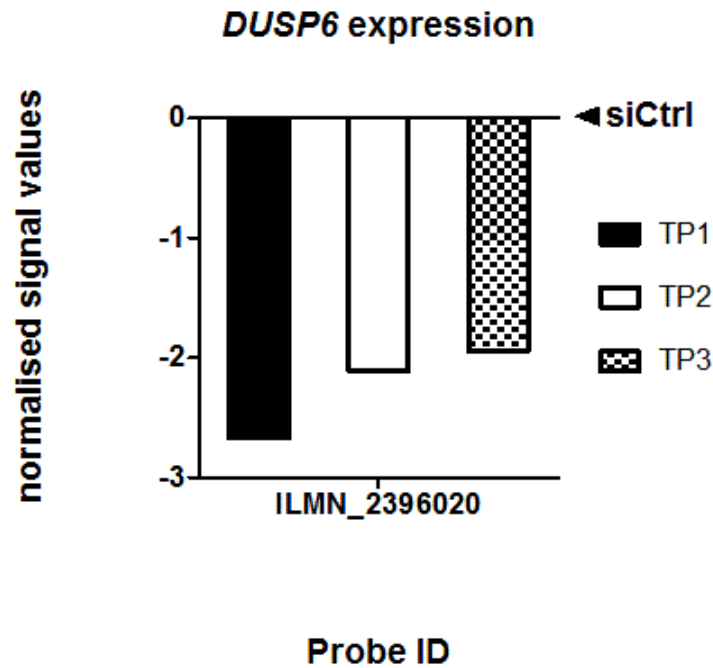


Fig. 3-41: Normalised *DUSP6* probe signal values in MLL/AF4 signature B

SEM cells had been depleted of MLL/AF4 for 2, 4, 6 days (TP1, TP2, TP3) using siMLL/AF4, or cells were transfected with control siRNA (siAML1/MTG8, here termed siCtrl). Signal intensity values of the Illumina HT12 bead array probe for *DUSP6* of the siMLL/AF4 samples at each time point were normalised against the corresponding controls, and the signal value fold-change \log_2 -transformed.

This observation could be confirmed on both RNA and protein level; qRT-PCR analysis showed a substantial decrease of *DUSP6* expression in SEM cells depleted of MLL/AF4 at TP1, TP2 and TP3, ranging from 51% to 72% knock-down (fig. 3-42A). In concordance, immunoblotting of SEM cells treated with siMLL/AF4 for four days confirmed a marked reduction of the two *DUSP6* isoforms when compared to controls (fig. 3-42B). However, knock-down of MLL/AF4 in primary patient material carrying the same MLL/AF4 fusion transcript as the SEM cells did not result in a substantial reduction of *DUSP6* levels (fig. 3-42C). *DUSP6* is a phosphatase specific for ERK1/2; unfortunately it had not been possible to successfully probe for alterations of the phosphosignal of these kinases.

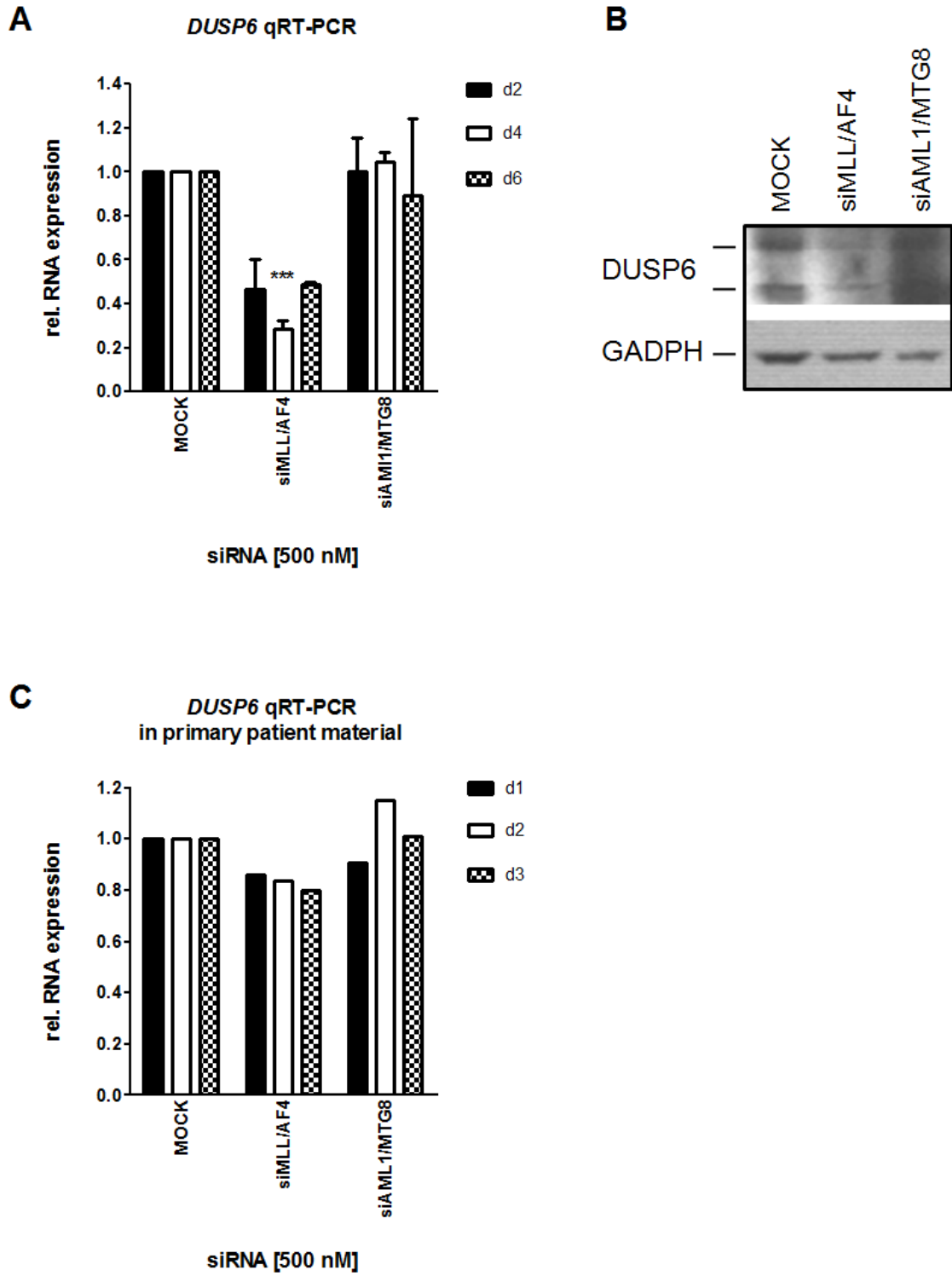


Fig. 3-42: DUSP6 expression analysis in t(4;11)-positive ALL cell lines after MLL/AF4 depletion

The SEM cell line was serially electroporated three times with siMLL/AF4, control siRNA (siAML1/MTG8) or without siRNA (MOCK); RNA was harvested at each time point prior to the subsequent transfection, corresponding to material derived from cells treated with siRNA for 2, 4 and 6d. SEM cells depleted of MLL/AF4 show a substantial reduction of DUSP6 at all three time points (A). This was confirmed by immunoblotting on protein level; SEM cells treated with siMLL/AF4 for 4 days expressed markedly less of both DUSP6 isoforms (B). Interestingly, a single electroporation of primary t(4;11)-positive patient material with either siMLL/AF4 or corresponding controls did not show a substantial effect on *DUSP6* expression as determined by qRT-PCR expression analysis at day one, two and three post-transfection. Figure (A) represents the mean of n=3 independent experiments at d2 & d4, and n=2 experiments at d6. Error bars indicate S.E.M. *DUSP6* expression analysis by immunoblotting was performed once (B); the qRT-PCR of the primary patient material (C) represents one single experiment, each sample performed in triplicates.

3.4.2 MLL/AF4 depletion down-regulates factors associated with stemness and self-renewal

Acute lymphoblastic leukaemia is associated with a differentiation block, and the blasts are arrested at an early stage in haematopoiesis, retaining self-renewal capability. MLLr-ALL in general, and MLL/AF4-positive ALL in particular is characterised with a very immature pro-B immunophenotype; furthermore, recent studies have described the aberrant expression of a gene signature associated with stemness and self-renewal¹³². In this study, GEP showed down-regulation of several of these genes in response to MLL/AF4 depletion, a selection of these genes were investigated on transcript level (tab. 3-20).

Tab. 3-20: MLL/AF4 GEP signature genes associated with stemness and self-renewal

Gene_Symbol	Probe_Id	Fold-change		Accession
		TP1-A	TP2-A	
HMGA1	ILMN_2311537	-2.06	-1.87	NM_207345.2
HMGA2	ILMN_2344662	-1.29	-37.3 (P->A)	NM_003483.4
TERT	ILMN_1796005	-2.18	1.46	NM_003219.1
	ILMN_2373119	1.18	-2.27	NM_198253.2
DNMT3B	ILMN_2328972	-1.68	-1.44	NM_006892.3
	ILMN_1794692	-1.56	-2.20	NM_006892.3
PYGO2	ILMN_1695334	-2.75	-2.31	NM_138300.3
HOXA4	ILMN_1677018	-50.86	-3.73	NM_002141.4
HOXA5	ILMN_1753613	-1.132	-2.58	NM_019102.2
HOXA6	ILMN_1815570	-1.22	-50.06	NM_024014.2
HOXA7	ILMN_1706478	-1.54	-26.04	NM_006896.3
HOXA9	ILMN_1702479	-1.13	-2.15	NM_152739.3
HOXA10	ILMN_1689336	-2.99	-2.08	NM_018951.3
	ILMN_1682110	-5.23	-12.55	NM_018951.3

3.4.2.1 *MLL/AF4 depletion results in HOXA gene down-regulation*

One of the hallmarks of MLLr acute leukaemia is *HOXA* gene up-regulation. Indeed, several probes covering the *HOXA* genes showed persistent down-regulation in the MLL/AF4 signature. For some of these probes the down-regulation was so strong that the signal in the MLL/AF4 depleted cells did not pass the the P-call threshold, but were flagged as “absent” and “marginal” (Tab. 3-20).

These results were validated by qRT-PCR; expression of *HOXA7*, *HOXA9* and particularly *HOXA10*, one of the MLL/AF4 core signature genes, was strongly reduced in MLL/AF4 depleted cells (fig. 3-43A, C; fig. 3-44A). Although the complete 5'-cluster is known to up-regulated by MLL-fusion genes, the study performed by Guenther *et al.* only described *HOXA7*, *HOXA9* and *HOXA10* as immediate *MLL/AF4* target genes¹³². However, on the grounds of the genomic organisation of this gene cluster, it seems unlikely that only these three genes are regulated by *MLL/AF4*, and not also the immediate neighbours *HOXA6* and *HOXA5*. Interestingly, when assessing *MLL/AF4*-dependent expression of *HOXA7*, *HOXA9* and *HOXA10* in primary t(4;11)-positive patient material, only *HOXA10* showed a marked down-regulation in response to siMLL/AF4 treatment, with 20% reduction 24h post electroporation, up to 52% at day 3 (fig. 3-43D). The decrease in *HOXA7* was less substantial, 30-40% reduced transcript levels in siMLL/AF4 blasts (fig. 3-43B). However, there was no effect on *HOXA9* expression in blasts at any time point queried (fig. 3-44B).

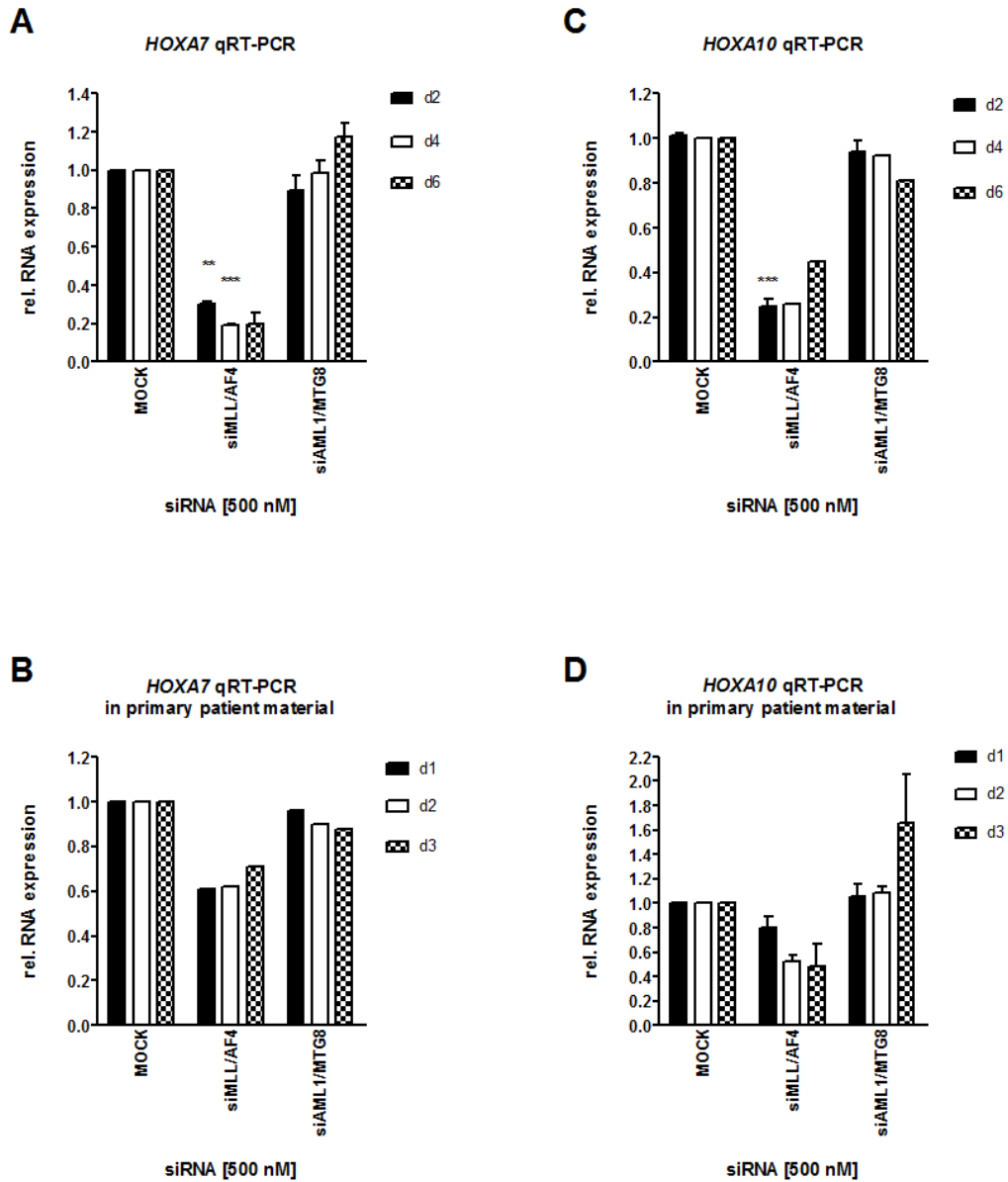


Fig. 3-43: Dependence of *HOXA7* and *HOXA10* expression in t(4;11)-positive cells on *MLL/AF4*

SEM cells were serially electroporated three times with siMLL/AF4, control siRNA (siAML1/MTG8) or without siRNA (MOCK). RNA was harvested at TP1, TP2 and TP3, corresponding to material derived from cells treated with siRNA for two, four and six days. Expression levels of *HOXA7* and *HOXA10* were assessed by qRT-PCR. SEM cells depleted of *MLL/AF4* show a substantial reduction of *HOXA7* and *HOXA10* at all three time points (A, C). These results were confirmed in primary t(4;11)-positive patient blasts; a single electroporation with either siMLL/AF4 resulted in a decrease of *HOXA7* and *HOXA10* levels when compared to controls, as determined by qRT-PCR at day one, two and three post-transfection (B, D). The graphs represents the mean of n=3 independent experiments at TP1 for both genes, n=5 for TP2 and n=2 for *HOXA7*. TP2 and TP3 for *HOXA10* were performed once. The graphs (B) and (D) represent one single experiment; a technical replicate was performed for *HOXA10* (D). Error bars indicate S.E.M. Statistical analysis was performed using an unpaired Student's t-test (** = $p < 0.01$, *** = $p < 0.001$).

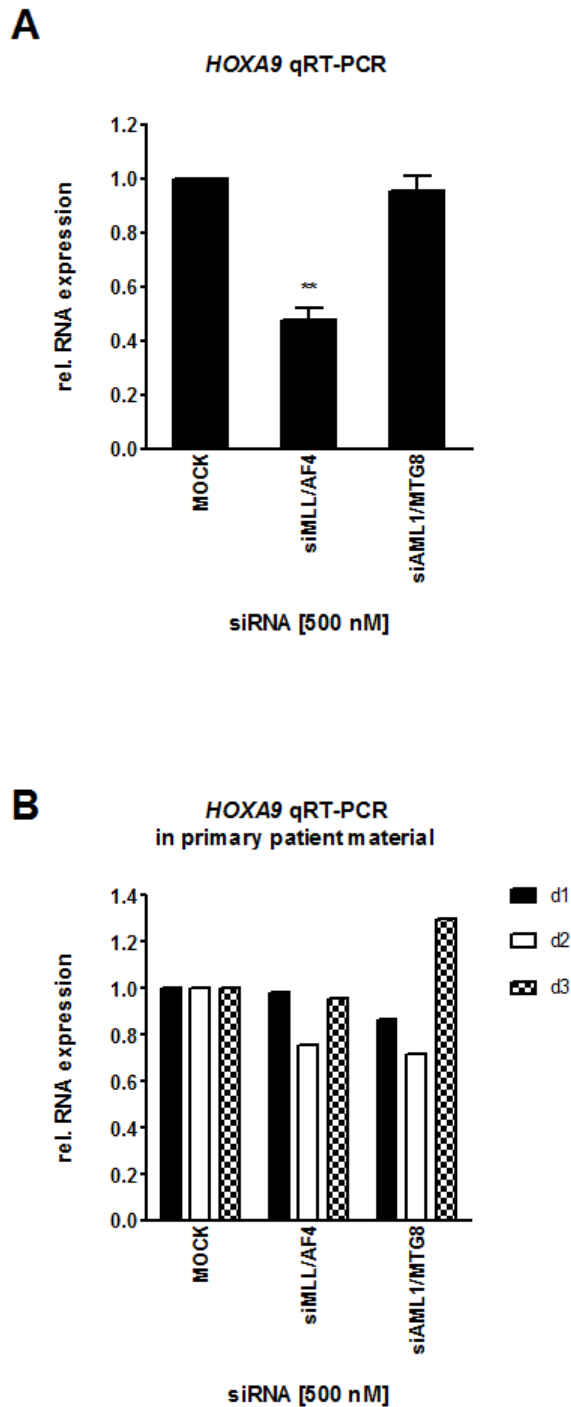


Fig. 3-44: Dependence of *HOXA9* expression in t(4;11)-positive cells on *MLL/AF4*

SEM cells were serially electroporated twice with siMLL/AF4, control siRNA or without siRNA. RNA was harvested at TP2, corresponding to material derived from cells treated with siRNA for four days and *HOXA9* expression assessed by qRT-PCR. SEM cells depleted of *MLL/AF4* show a substantial reduction of *HOXA9* (A). Conversely, electroporation of primary t(4;11)-positive patient blasts with siRNA did not affect *HOXA9* levels. Graph (A) represents the mean of n=3 independent experiments; (B) represents one single experiment. Error bars indicate S.E.M. Statistical analysis was performed using an unpaired Student's t-test (**= $p < 0.01$).

3.4.2.2 *MLL/AF4* depletion results in decreased *TERT* expression

Another stemness-associated gene differentially expressed in response to MLL/AF4 depletion was *TERT*. This gene codes for the catalytic subunit of the ribozyme telomerase, one of the key regulators of self-renewal and heavily implicated in malignant transformation. As listed in tab. 3-12, *TERT* expression showed down-regulation at TP1 and TP2. This result was confirmed by qRT-PCR, showing a depletion of 33-40% (fig. 3-45).

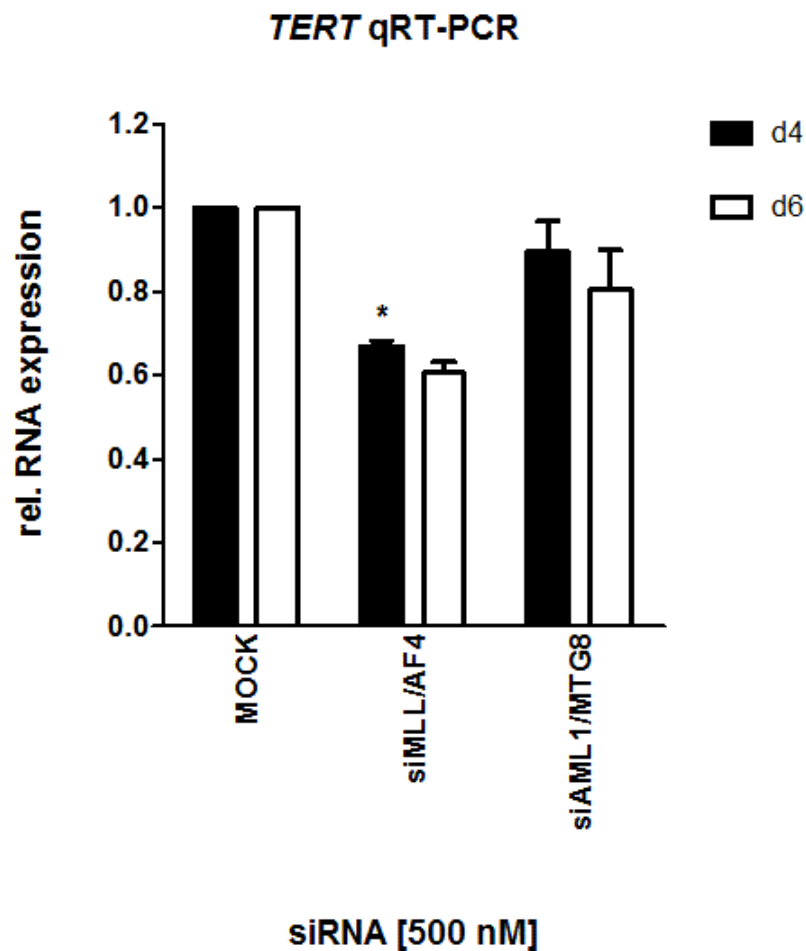


Fig. 3-45: *TERT* expression analysis in *MLL/AF4* depleted SEM cells

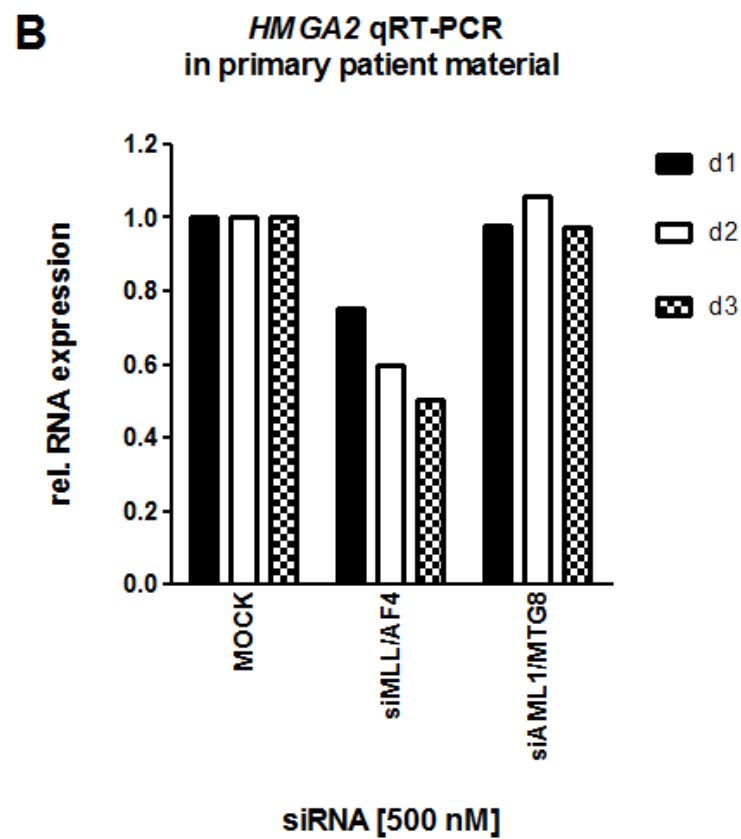
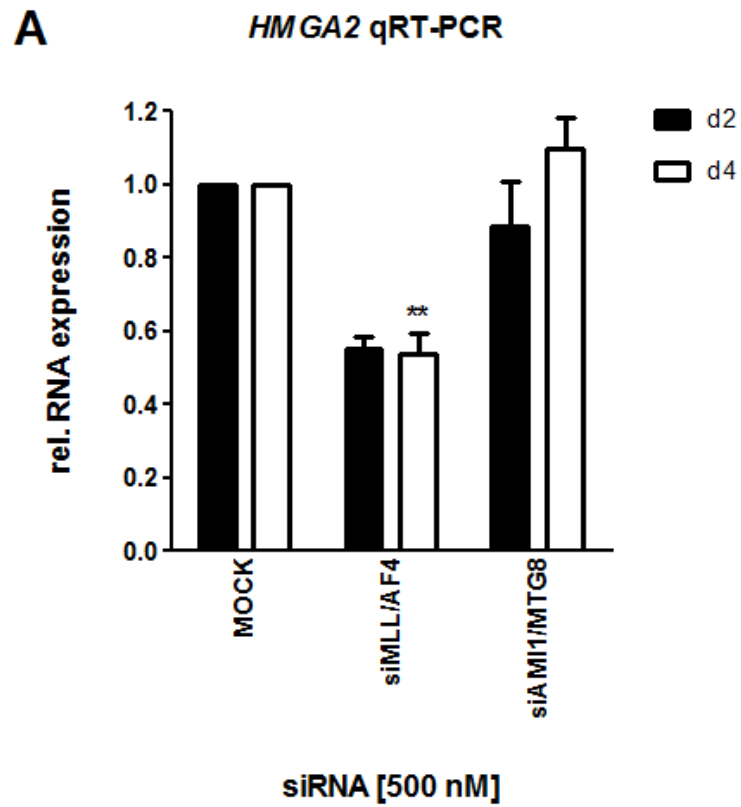
SEM cells were serially electroporated with siMLL/AF4, control siRNA (siAML1/MTG8) or no siRNA; expression was assessed by qRT-PCR at TP2 and TP3, corresponding to four and six days *MLL/AF4* depletion. The graph shows the mean of n=5 and n=2 experiments for d4 and d6, respectively. Error bars indicate S.E.M., statistical significance determined using an unpaired Student's t-test (* = $p < 0.05$).

3.4.2.3 *MLL/AF4* depletion results in down-regulation of the chromatin remodelling factor *HMGA2*, but not *PYGO2* and *DNMT3B*

The high-mobility group A proteins are a family of chromatin modifying transcription regulators which play an important role in development and maintenance of adult stem cells, and are strongly implicated in tumourigenesis and therapy-resistance. One of these proteins, *HMGA2*, has been identified as a direct MLL/AF4 target gene¹³². In this array, *HMGA1*, a close homologue, was found to be down-regulated. On further analysis, *HMGA2* also showed decreased expression levels, however, the signal level in the siMLL/AF4 treated sample fell so low that it called “absent” (tab. 3-20). Expression analysis of *HMGA2* showed a marked decrease in transcript levels by in both siMLL/AF4-treated SEM cells and primary patient blasts by ~45% and 25-50%, respectively (fig. 3-46 A, B)

Fig. 3-46: *MLL/AF4*-dependent *HMGA2* expression in t(4;11)-positive cells

The SEM cell line was serially electroporated three times with siMLL/AF4, control siRNA (siAML1/MTG8) or without siRNA (MOCK); RNA was harvested at each time point prior to the subsequent transfection, corresponding to material derived from cells treated with siRNA for two and four days, and assessed for *HMGA2* expression by qRT-PCR. SEM cells depleted of *MLL/AF4* show a substantial reduction of *HMGA2* at all three time points. Graph represents the mean of n=3 independent experiments, error bars indicate S.E.M. Statistical analysis was performed using an unpaired Student’s t-test (* = $p < 0.05$) (A). This results was further validated in primary t(4;11)-positive patient blasts; a single electroporation with either siMLL/AF4 resulted in a time-dependent decrease of *HMGA2* when compared to controls, as determined by qRT-PCR expression analysis at day one, two and three post-transfection(B). The graph shows the results of one single experiment, each sample was performed in triplicates.



Another chromatin remodelling factor implicated in both normal and malignant development is *PYGO2*, which forms part of the β -catenin/TCF/LEF transcription factor complex. *PYGO2* recognises and binds lysine residue-4 histone H3 (H3K4) di- and trimethylation marks on euchromatin and subsequently recruits β -catenin via its adaptor protein BCL9, mediating transactivation of WNT target genes. Additionally, in a WNT-independent role, *PYGO2* also recruits other H3K4 histone methyltransferases to dimethylated H3K4, promoting chromatin-activating trimethylation²¹⁵⁻²¹⁸. *PYGO2* expression is important for development of different tissue, regulating progenitor expansion and self-renewal capability^{215,219-220}. Concomitantly, *PYGO2* activity has been implicated in diverse solid tumours²²¹⁻²²².

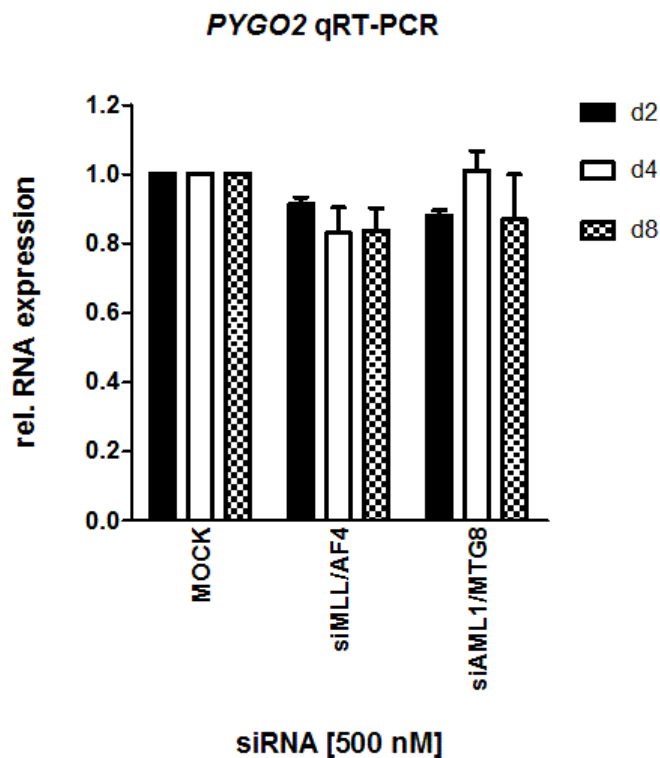


Fig. 3-47: *PYGO2* expression in SEM cells depleted of MLL/AF4

SEM cells were serially electroporated three times, and RNA harvested at TP1, TP2 and TP3, corresponding to a sustained MLL/AF4 depletion of two, four and six days. *PYGO2* expression was determined by qRT-PCR; no changes in response to MLL/AF4 knock-down were detected. Graph represents the mean of n=2 experiments, error bars represent data range.

In this study, PYGO2 was part of the down-regulated MLL/AF4 signature at all time points (tab. 3-19), however, this could not be validated *in vitro*, as sustained depletion of MLL/AF4 in SEM cells did not result in altered PYGO2 expression levels (fig. 3-47).

DNMT3B belongs to the family of DNA methyl transferases, and mediates in concert with its homologue DNMT3A *de novo* cytidine methylation of CpG dinucleotides. These *de novo* DNA methyltransferases are highly expressed in embryonic stem cells and down-regulated in differentiation. Concomitantly, aberrant DNMT3B activity promotes tumourigenesis in a variety of cancers. DNMT3B showed down-regulation over at TP2 and TP3, which was less pronounced at TP1 (tab. 3-20). Assaying DNMT3B expression in siMLL/AF4 treated SEM cells could not completely validate these results, as although the regulatory trend was confirmed, there was only a subtle decrease in transcript levels (fig. 3-48).

Two other genes associated with stem-cell functions, ANGPT1 and ANGPTL2, were also present in the MLL/AF4 signature; they were validated in section 5.

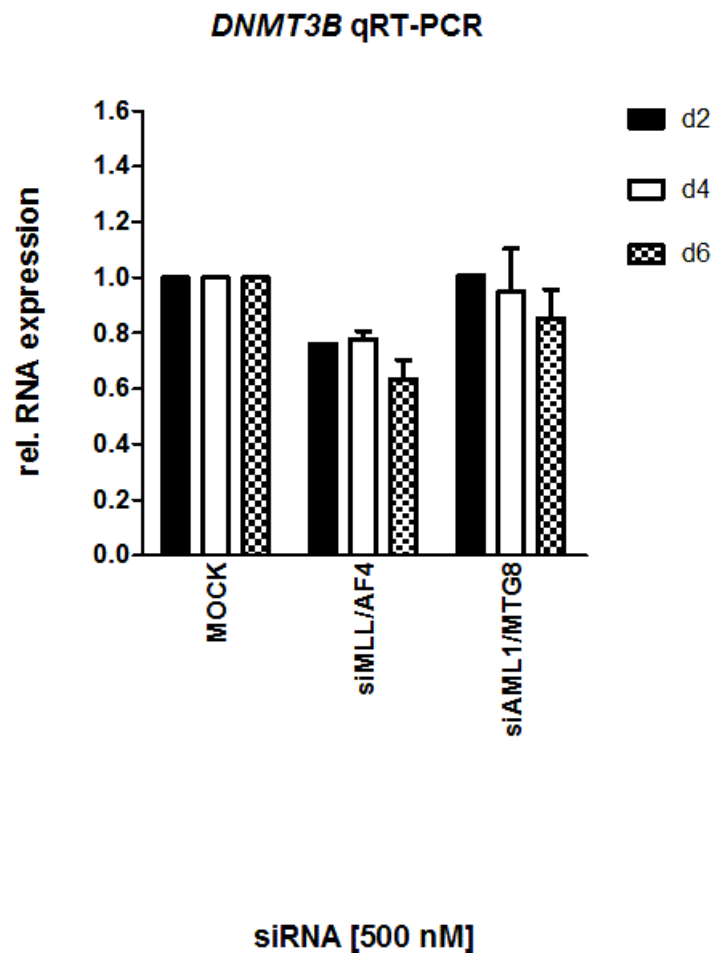


Fig. 3-48: DNMT3B expression in MLL/AF4-depleted SEM cells

The SEM cell line was serially electroporated for three times with siMLL/AF4, control siRNA (siAML1/MTG8) or without siRNA (MOCK); RNA was harvested at each time point prior to the subsequent transfection, corresponding to material derived from cells treated with siRNA for 2, 4 and 6 days (TP1, TP2, TP3). *DNMT3B* expression was assessed qRT-PCR. SEM cells depleted of *MLL/AF4* show only a subtle decrease in *DNMT3B* levels. The graph represents the mean of n=2 independent experiments for TP2 and TP3, n=1 at TP1. Error bars indicate data range.

3.4.3 *MLL/AF4* depletion induces genes associated with autophagy and cell death

ANNEXINA1 (*ANXA1*) belongs to the annexin family of phospholipid binding proteins. It acts as a negative regulator of inflammation, but has been shown to promote cell death and suppress tumour cell proliferation in a context-dependent manner. In this GEP study, the probes for *ANXA1* were up-regulated in SEM cells depleted of MLL/AF4 at all three time points (fig. 3-49). This was validated *in vitro* by qRT-PCR, MLL/AF4 knock-down resulted in a marked and significant induction of *ANXA1* levels (fig. 3-50A). However, *MLL/AF4* depletion in primary patient material did not show a substantial increase in expression (fig. 3-50B).

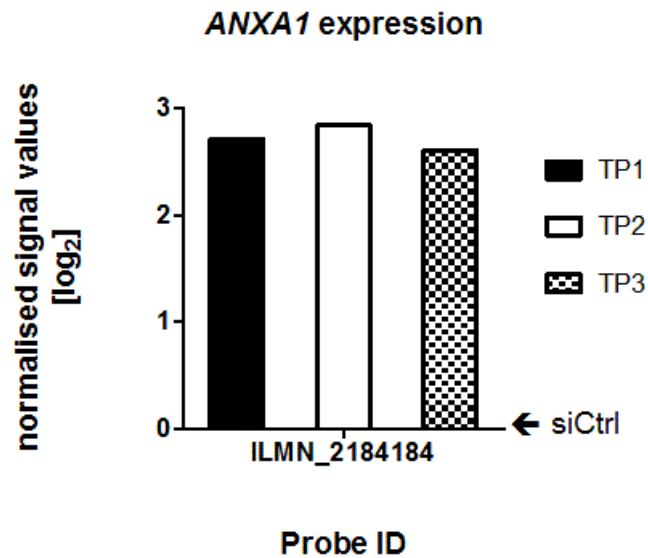


Fig. 3-49: Normalised *ANXA1* probe signal values in samples depleted of MLL/AF4

SEM cells had been treated for 2, 4 and 6 days (TP1, TP2, TP3) with either siMLL/AF4 or control siRNA (siAML1/MTG8, here termed siCtrl). Signal intensity values of the Illumina HT12 bead array probes for *ANXA1* of the siMLL/AF4 samples at each time point were normalised against corresponding controls, and the signal value fold-change log₂-transformed.

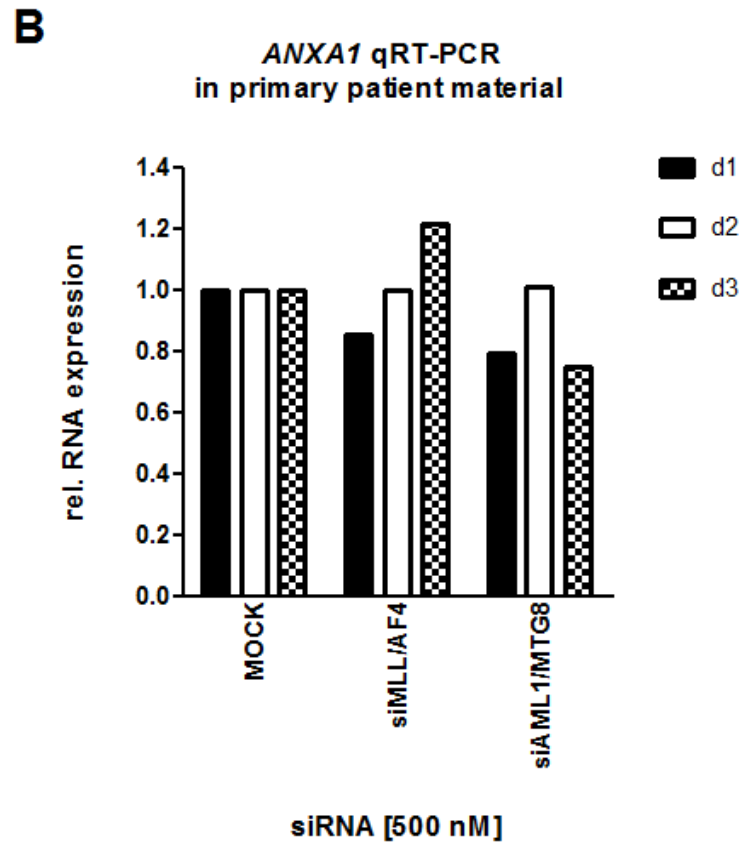
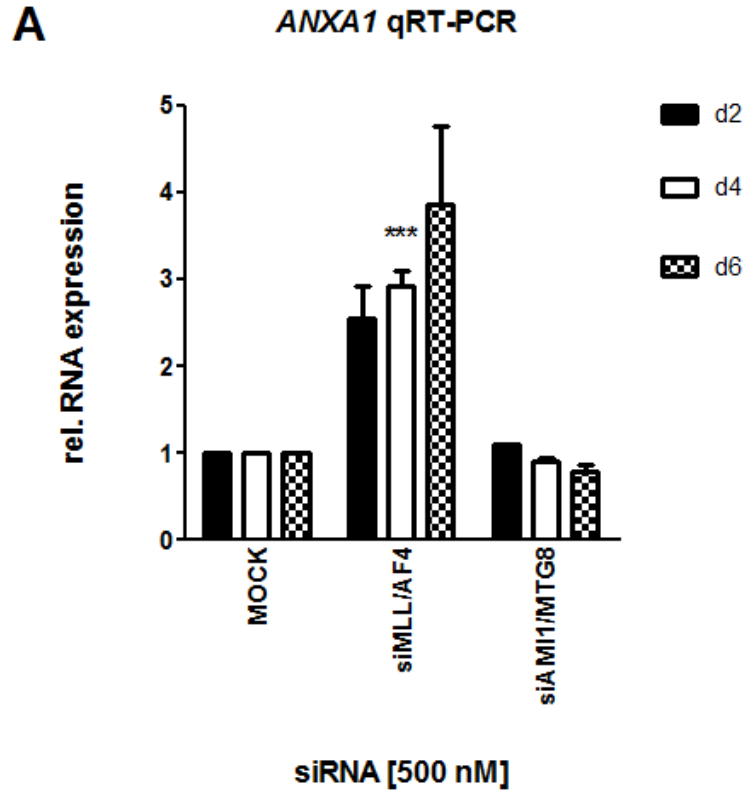


Fig. 3-50: *ANXA1* expression in t(4;11)-positive cells in response to *MLL/AF4* depletions

The SEM cell line was serially electroporated for three times with siMLL/AF4, control siRNA (siAML1/MTG8) or without siRNA (MOCK); RNA was harvested at each time point prior to the subsequent transfection, corresponding to material derived from cells treated with siRNA for 2, 4 and 6 days (TP1, TP2 & TP3), and assessed for *ANXA1* expression by qRT-PCR. SEM cells depleted of *MLL/AF4* show a substantial induction of *ANXA1* at all three time points. Graph represents the mean of n=3 independent experiments, error bars indicate S.E.M. Statistical analysis was performed using an unpaired Student's t-test (***) = $p < 0.001$) (A). A single electroporation of primary t(4;11)-positive patient ALL blasts with either siMLL/AF4 or controls did not affect *ANXA1* levels, as determined by qRT-PCR (B). The graph shows the results of one single experiment, each sample was performed in triplicates.

Like ANXA1, the autophagy-associated gene *GABARAPL1* is one of the genes constituting the MLL/AF4 core signature, showing induction at all three time points (fig. 3-51). This was confirmed *in vitro* by qRT-PCR, siMLL/AF4 treated SEM cells showed up-regulation in a time-dependent manner, expressing 3-, 8- and- 13-fold more *GABARAPL1* than corresponding controls. (fig. 3-52).

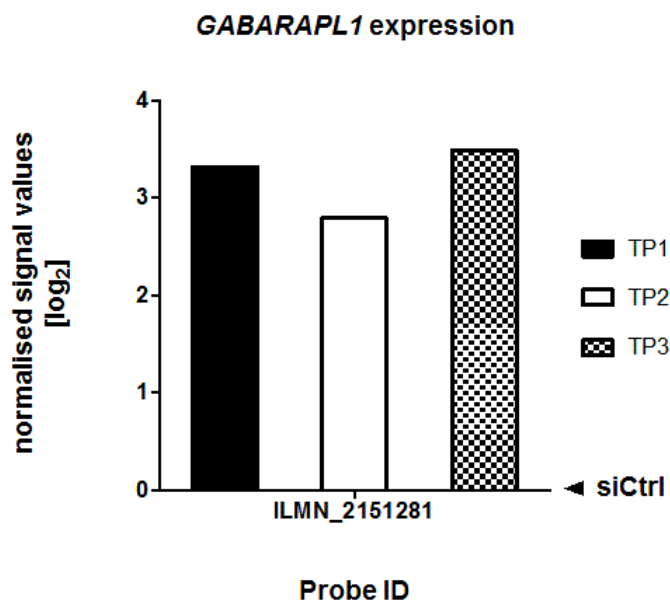


Fig. 3-51: Normalised *GABARAPL1* probe signal values in samples depleted of MLL/AF4

SEM cells had been treated for 2, 4 and 6 days (TP1, TP2, TP3) with either siMLL/AF4 or control siRNA (siAML1/MTG8, here termed siCtrl). Signal intensity values of the Illumina HT12 bead array probes for *GABARAPL1* of the siMLL/AF4 samples at each time point were normalised against corresponding controls, and the signal value fold-change log₂-transformed.

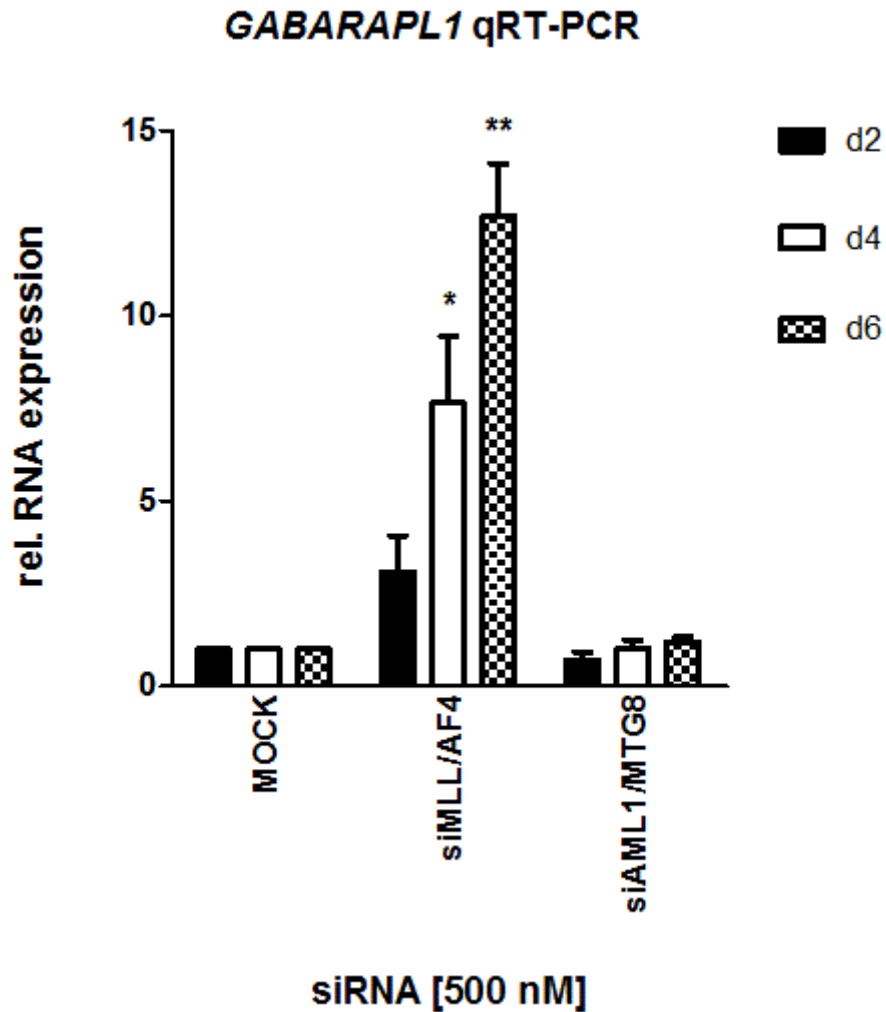


Fig. 3-52: *GABARAPL1* expression in MLL/AF4-depleted SEM cells

The SEM cell line was serially electroporated for three times with siMLL/AF4, control siRNA (siAML1/MTG8) or without siRNA (MOCK); RNA was harvested at each time point prior to the subsequent transfection, corresponding to material derived from cells treated with siRNA for 2, 4 and 6 days (TP1, TP2, TP3). *GABARAPL1* expression was assessed qRT-PCR. SEM cells depleted of *MLL/AF4* show a substantial induction of *GABARAPL1* at all three time points. The Graph represents the mean of n=3 independent experiments, error bars indicate S.E.M. Statistical analysis was performed using an unpaired Student's t-test (* = $p < 0.05$; ** = $p < 0.01$).

3.4.4 Correlation of Array and Q-RT-PCR Results

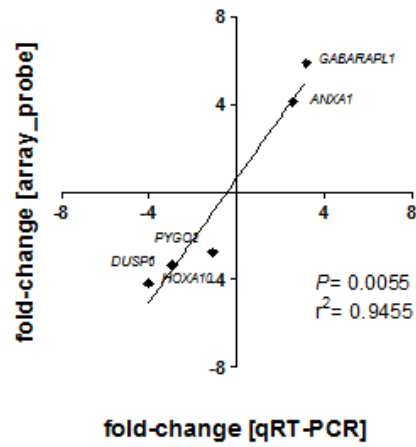
A selection of biologically interesting genes of the MLL/AF4 signatures A and B were validated both on RNA and protein level. 14 genes were analysed *in vitro*, *DUSP6*, *HOXA7*, *HOXA9*, *HOXA10*, *HMGA2*, *PYGO2*, *TERT*, *ANXA1*, *GABARAPL1*, *DNMT3B*, as well as *ANGPT1* & *ANGPTL2* (s. Section 5); out of these 14 genes 12 could be confirmed; one showed no effect (*PYGO2*) and the remaining one (*DNMT3B*) was only subtly regulated in response to *MLL/AF4* depletion.

Correlation analysis of the linear fold-changes determined by qRT-PCR with the linear fold-changes of the normalised signal values of the corresponding GEP probes, showed good concordance at all three time points (fig. 3-53) as well as a statistically significant correlation, as determined by Pearson statistics.

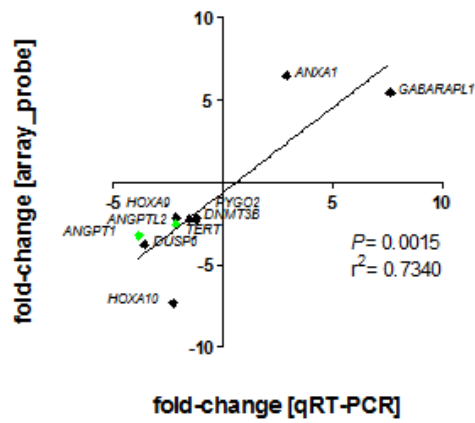
Fig. 3-53: Correlation analysis of the fold-changes of the MLL/AF4 GEP signature and qRT-PCR

Pearson correlation analysis shows a good concordance between the fold-changes of genes in MLL/AF4 depleted genes obtained by GEP and qRT-PCR at TP1 (A) and TP3 (B). The correlation at TP2 (B) was less high, but still statistically significant. The GEP fold-changes are derived from the differentially regulated probes of the MLL/AF4 signature A at TP1 and TP2, while TP3 corresponded to MLL/AF4 signature B. If several probes had a linear fold-change of above 2.0, the mean was applied. These values were correlated to the fold changes determined by qRT-PCR analysis of siMLL/AF4-treated SEM cells at the corresponding time points. Values highlighted green correspond to the genes *ANGPT1* and *ANGPTL2*, validated in section 5.

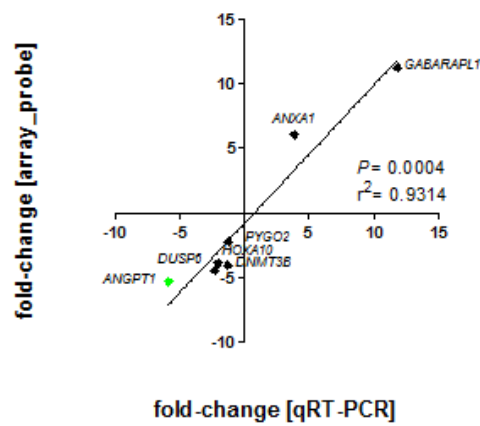
A MLL/AF4 signature at TP1



B MLL/AF4 signature TP2



C MLL/AF4 signature at TP3



3.5 CONCLUSIONS

MLL/AF4 depletion impinges on the leukaemic phenotype:

- Loss of MLL/AF4 induces cell death, and this accompanied by induction of pro-apoptotic and anti-proliferative genes, as well as a concerted down-regulation of mitogenic signalling cascades.
- Loss of MLL/AF4 impinges on self-renewal, as illustrated by the compromised clonogenicity. Concomitantly, MLL/AF4 ablation correlates with decreased expression of self-renewal-associated genes.
- Loss of MLL/AF4 blocks proliferation and cell cycle progression.

3.6 DISCUSSION

In order to elucidate the pathobiology of t(4;11)-positive ALL on a molecular level, RNAi-mediated knock-down of the MLL/AF4 fusion gene was combined with a gene expression profiling time course, analysing the changes in gene expression levels corresponding to a MLL/AF4 depletion period of two, four and six days. The siRNA used, siMLL/AF4, was specific for the break-point of the MLL/AF4 fusion transcript found in the SEM cell line, and did not affect wild-type MLL and AF4 expression levels at an early time point (2h), while it already resulted in substantial decrease of *MLL/AF4* levels (fig. 3-6). This remained true for MLL (fig. 3-8), however, siMLL/AF4 treatment led to a delayed down-regulation of AF4, which was potentiated in a time-dependent manner (fig. 3-7). An off-target effect could be ruled out, as transfection of siMLL/AF4 in other cell lines that did not express the same MLL/AF4 fusion gene (RS4;11, fig. 3-9), or only MLL in its wild-type configuration (Kasumi-1, fig. 3-10), did not decrease AF4 expression levels, even after being treated for up to six days with siMLL/AF4 (fig. 3-10). This observation suggests a possible fusion gene-dependent regulation of *AF4*, indeed, *in silico* screening of the *AF4* promoter found several putative binding sites for *HOXA* genes and members of the TALE (Three Amino acid Loop Extension) homeodomain transcription factor family (fig. 3-xxx), which comprises the established HOX gene cofactors PBX1-PBX3 and MEIS1-MEIS3²²³⁻²²⁴. Since *MLL/AF4* depletion resulted in a down-regulation of several HOXA family members (fig. 3-43, fig. 3-44, tab. 3-20), there might be a potential modulation of *AF4* expression via an MLL/AF4-HOXA-TALE axis. Further work is required in order to test this hypothesis, as this observation might have important implications in MLLr acute leukaemias in general and MLL/AF4-positive ALL in particular, *AF4* and *AF4/MLL* possessing the same genomic promoter sequence.

3.6.1 MLL/AF4 signature shows differential regulation of factors linked to apoptosis and proliferation

Phenotypically, sustained siRNA-mediated ablation of the MLL/AF4 fusion transcript inherent of the t(4;11)-positive ALL cell line SEM resulted in a striking phenotype: *MLL/AF4* down-regulation impaired proliferation, cell cycle progression, clonogenicity and viability (fig. 3-12 to fig. 3-15). These findings show that MLL/AF4 depletion reverts the pathobiology previously described for t(4;11)-ALL, particularly the aspect of cell death evasion; MLL/AF4-positive cells have been shown to be highly resistant to stress- and death ligand-induced apoptosis²²⁵⁻²²⁶, and gain-of-function studies found that ectopic expression of MLL/AF4 conferred an increased apoptosis-resistance¹⁴⁶. Furthermore, the phenotype observed due to sustained MLL/AF4 down-regulation is in agreement with previous loss-of-function studies, which reported a comparable growth inhibition and apoptosis induction¹⁴⁷⁻¹⁴⁸.

Concordantly, on a molecular level, gene expression profiling and subsequent functional analysis of the MLL/AF4 gene signature for the different depletion time periods showed an enrichment for networks and cellular functions linked to cell death (tab. 3-8 to tab. 3-10) as well as apoptosis signalling (fig. 3-24, fig. 3-36). A closer investigation highlighted a few interesting candidate genes that might be key for apoptosis mediation, for instance *PMAIP1* (*NOXA*) and *ANXA1* for which the corresponding probes show a consistent up-regulation in both core signatures A and B (fig. 3-29, fig. 3-39).

3.6.1.1 A putative role of NOXA and oxidative stress in MLL/AF4-depletion mediated apoptosis

PMAIP1 encodes the proapoptotic BH3-only protein NOXA, which mediates apoptosis in response to oxidative and metabolic stress signals, as well as part of the DNA damage response in a p53-dependent and independent manner. Moreover, NOXA targets the anti-apoptotic Bcl2-family member MCL-1 for proteasomal degradation²²⁷⁻²²⁸, which is a particularly point of interest in this cellular context, as aberrant MCL-1 overexpression has recently been implicated

in glucocorticoid resistance in MLLr infant ALL¹⁶⁷. Consequently, NOXA-induction in response to MLL/AF4 depletion might be able to revert or mitigate the prednisolone-resistance. Concordantly, NOXA induction has been implicated in mediating cell death in response to chemotherapeutic drug treatment in both haematologic and solid cancers²²⁹⁻²³¹.

NOXA can be induced by various factors, for instance, in response to elevated cellular reactive oxygen species (ROS); this is mediated by the stress-related MAP kinases such as JNK and p38²²⁸. In good concordance, both JNK and its down-stream mediators, particularly *JUN* and *ATF-2*, are up-regulated on transcriptional level in the MLL/AF4 signature at TP2 (fig. 3-25). Concomitantly, there are several indicators within the MLL/AF4 signature suggesting that *MLL/AF4* depletion results in a disturbance of the cellular ROS level balance in favour of oxidative stress: the key antioxidant enzymes manganese superoxid dismutase (*SOD2*) and glutathione peroxidase (*GPX4*) were down-regulated at TP1 (fig. 3-19). Moreover, there is also reduced expression of several metallothioneins (fig. 3-19), which can act as ROS scavengers, protecting DNA from oxidative damage²³². One of these genes, metallothionein-1F (*MTF1*), forms part of the core MLL/AF4 signature A, showing consistent down-regulation at both time points (fig. 3-29). Interestingly, both markers of a redox metabolism disruption and the induction of NOXA occur at TP1, preceding the onset of apoptosis.

3.6.1.2 The proapoptotic gene ANXA1 is induced in response to MLL/AF4

Another major proapoptotic gene of interest in the MLL/AF4 signature is ANNEXIN-1 (ANXA1), which represents a core gene of the MLL/AF4 signature A and B, the corresponding probe set indicating increased expression levels in response to MLL/AF4 depletion at all three time points (fig. 3-49). ANXA1 is of particular interest, as has been shown to act as a potent tumour suppressor in a context-dependent manner. ANXA1 expression is lost in a variety of solid tumours, such as cervix²³³, lymphoma²³⁴ and breast carcinomas, and this correlated adversely with prognosis²³⁵⁻²³⁷. Consequently, ectopic expression of

ANXA1 in breast cancer cells suppressed proliferation²³⁸, and ablated metastases²³⁵. In haematologic malignancies, low ANXA1 expression was implicated in drug resistance in a chronic myeloid leukaemia model²³⁹, furthermore, a recent report found ANXA1 to be crucial for mediating apoptosis in response to therapeutic histone acetylase inhibitors in t(8;21)-positive AML cells²⁴⁰.

The exact mechanism by which ANXA1 regulates apoptosis induction are not fully understood. Physiologically, ANXA1 is a Ca²⁺- and lipid binding protein, and acts as a potent anti-inflammatory mediator, i.e., by binding to NFκB, and suppressing its activity; this NFκB modulation has been linked to ANXA1-mediated cell death in response to drug treatment²⁴¹. Interestingly, pathway analysis of the MLL/AF4 signature did indeed show a reduced expression of NFκB signalling mediators (fig. 3-25, fig. 3-26, fig. 3-37). Thus, ANXA1 could potentially contribute to the down-regulation of NFκB-signalling; however, to date, the status and the role of NFκB in MLL-rearranged leukaemia has not been investigated.

The ANXA1 induction observed in the array could be validated *in vitro* by qRT-PCR analysis in the SEM cell line, showing an time-dependent induction by 2.6- to 3.8-fold in siMLL/AF4-treated cells compared to controls (fig. 3-50A). However, this could not be confirmed in t(4;11)-positive patient blasts treated with siMLL/AF4 (fig. 3-50B). In recent years, there is an increasing perception about an inherent pathophysiological heterogeneity of t(4;11)-positive ALL, based on whether the leukaemic cells express high or low *HOXA* gene levels, whether they express the reciprocal fusion *AF4/MLL* transcript, as well as whether the disease occurs in infants or children^{146,168-169}. The SEM cell line is derived from a paediatric ALL patient, and expresses *AF4/MLL* (data not shown), while the patient cells originated from an infant ALL patient of unknown *AF4/MLL* status. Therefore, a possible explanation for the differential response of *ANXA1* to MLL/AF4 could be based on these particular subcategorisations. Also, it cannot be excluded that the observed *ANXA1* up-regulation might represent a cell-line specific response; RNAi-mediated

depletion of *MLL/AF4* in different cell line models as well as patients could clarify this.

3.6.1.3 The autophagy-related gene *GABARAPL1* is induced in response to *MLL/AF4*-depletion

An interesting candidate gene present in the MLL/AF4 core signatures is *GABARAPL1*; the corresponding probe indicates up-regulation in response to MLL/AF4 depletion at all three time points (fig. 3-51). Electroporation of the SEM cell line with siMLL/AF4 resulted in a strong induction of *GABARAPL1* (fig. 3-52), validating the array result, however, as with *ANXA1*, this effect could not be observed in t(4;11)-positive patients (data not shown). Possible explanations could be found in the aforementioned intrinsic differences between the SEM cell line and the leukaemic material derived from an infant ALL patient.

GABARAPL1, also termed *GEC-1* or *ATG8L*, is an orthologue of the yeast Atg8 protein family, which also includes *GABARAP*, *GABARAPL2*, *LC-3A*, *LC3-B* and *LC3-C*²⁴². To date, the function of this gene remains poorly understood. *GABARAPL1* is involved in protein trafficking of specific receptors to the cell surface, such as GAB(A) and the kappa opioid receptors, both involved in neurosignalling, and is implicated in microtubule-reorganisation²⁴³⁻²⁴⁵. Furthermore, *GABARAPL1* plays a role in autophagy²⁴⁶⁻²⁴⁸. Recently, low expression of *GABARAPL1* has been reported in high-grade breast cancer; and reexpression impinged on tumour cell proliferation²⁴⁹. Therefore, MLL/AF4-dependent *GABARAPL1* induction could indicate a disturbance of the autophagy pathway, but also impact on leukaemic cell proliferation and cycling.

3.6.2 MLL/AF4 depletion perturbs mitogenic signalling

Aberrant mitogenic signalling activity plays a predominant role in malignancies, uncoupling the cells from exogenous growth signals²⁵⁰⁻²⁵¹. This aspect has been previously reported for MLL/AF4-positive cells, where growth and viability was not grossly affected by starvation²²⁵, a finding corroborated by observations

made in present study (data not shown). Screening the MLL/AF4 signatures for enrichment of canonical pathways revealed concerted down-regulation of key mediators of canonical mitogenic signalling, such as the MAP kinases *ERK1* and *ERK2* and *STAT3* (Fig. 3-25, Fig. 3-26), which are important regulators of proliferation and survival. Both ERK1/2-mediated MAPK signalling^{187,252} and the JAK/STAT3 pathway²⁵³ have recently been shown to be constitutively activated in MLLr ALL cells, and chemical inhibition of their key mediators compromised ALL cell viability; MLL/AF4-ablation dependent suppression of these signalling events might contribute to the lethal phenotype observed. Interestingly, DUSP6 (dual-specificity phosphatase 6), a negative regulator of ERK1/2 signalling, is part of the down-regulated MLL/AF4 core signatures A and B; the corresponding probes show decreased signal-intensity at all three time points (fig. 3-41). At first sight, this appears contradictory, as DUSP6 has been widely perceived as a tumour suppressor lost in cancer. However, *DUSP6* overexpression has been linked to increased chemotherapy-resistance in glioblastomas²¹⁴, and might be a biomarker for constitutive ERK activity. Additionally, MLL/AF4 has been found to directly bind the DUSP6 promoter¹³². In accordance with the array results, a decrease in DUSP6 expression on both RNA and protein levels were confirmed in siMLL/AF4-treated SEM cells (fig. 3-42). Interestingly, this effect could not be observed in siMLL/AF4-transfected primary patient material, a counterintuitive observation in the context of *DUSP6* being a direct MLL/AF4 target. A possible explanation could be that DUSP6 down-regulation might require a certain level of MLL/AF4 depletion not attained in the primary material, as the extent of siRNA-mediated knock-down in the SEM cell line was higher than in the patient cells. Furthermore, the MLL/AF4 promoter binding studies were performed in the SEM cell line, therefore this could indicate a cell-specific effect, possibly also based on the aforementioned intrinsic differences between the t(4;11)-ALL cell line and the t(4;11)-positive infant ALL patient cells.

In addition to the ERK and STAT3 signalling, the MLL/AF4 signature also indicated perturbation of the ephrinB pathway, which links cytoskeleton-associated and mitogenic signalling. Here, the Ephrin receptor ligands *EFNB1* and *EFNA4* show a decreased expression in the MLL/AF4 signature (fig. 3-22).

This is in good concordance with previously published data, reporting a MLL/AF4-dependent expression of the ephrinA family members as well as their cognate receptors¹⁸⁷. Similarly, MLL/AF4 ablation also impaired the IGFR1 signalling pathway, which has been previously implicated in t(4;11)-positive ALL¹⁹⁰. Pathway analysis showed a decreased *IGFR1* expression (fig. 3-27). Previously, IGFR1 expression in the t(4;11)-ALL cell line RS4;11 was found to be dependent on *HOXA9*¹⁹⁰; this regulatory axis was corroborated by present results, as both *IGFR1* and *HOXA9* expression regulation correlated in *siMLL/AF4* depleted SEM cells, suggesting a MLL/AF4-HOXA9-IGFR1 axis. Since inhibition of IGFR1 signalling repressed malignant growth and survival of the leukaemic cells¹⁹⁰, loss of IGFR1 might contribute together with the MLL/AF4-dependent down-regulation of the ERK, ephrinB and JAK/STAT pathways to a switch-off of prosurvival signalling in t(4;11)-positive ALL cells, therefore mediating the loss in viability in response to MLL/AF4 knock-down.

Concordantly, GSEA analysis found a negative correlation in the MLL/AF4 signature A with putative target genes of the SP-1 transcription factor (fig. 3-30), which has been reported to be one of the down-stream effectors of IGFR1²⁵⁴, and ERK1/2²⁵⁵ signalling. Interestingly, amongst these genes were several genes involved in cytoskeleton-mediated signalling, such as the RHOA-GTPase activating protein (Rho-GAP) *SH3BP1*¹⁹¹, the RAC and ARF binding protein *ARFIP1*¹⁹², as well as the receptors *UNC5B* and *CD74*, both important mediators in cellular migration, adhesion and, interestingly, angiogenesis¹⁹³⁻¹⁹⁷.

3.6.3 MLL/AF4 depletion results in decreased expression of stemness-associated genes

Recently, MLL/AF4-positive ALL has been associated with a HSC-like gene expression signature¹³². Concordantly, our group has previously shown that *MLL/AF4* knock-down compromised *in vivo* engraftment of the t(4;11)-positive cell line SEM in NOD/SCID mice¹⁴⁸, which represents an important read-out for leukaemic self-renewal^{7,256-257}. Here, in this current study, a single electroporation with *siMLL/AF4* compromised clonogenicity of the SEM cell line

in soft agar cultures (fig. 3-15), which serves as an *in vitro* model for self-renewal ability. In addition, gene expression profiling revealed several genes associated with haematopoietic stem and progenitor cells to be dependent on MLL/AF4 expression, i.e., *SPN*, the *HOXA* gene cluster and *TERT* amongst others.

SPN, also termed Leukosialin (CD43), showed reduced expression levels at TP1 and TP2 in the MLL/AF4 signature A. CD43 is one of the earliest haematopoietic markers, expressed in HSCs and immature progenitors, and down-regulated during B-cell differentiation²⁵⁸⁻²⁶⁰; incidentally, *SPN* is a direct MLL/AF4 target gene¹³². The same applies for *HOXA10*, which is down-regulated in response to MLL/AF4 depletion at all time points. *HOXA10* constitutes together with *HOXA7* and *HOXA9* the most consistently up-regulated genes in MLLr acute leukaemias, and is a direct MLL/AF4 target¹³². In a MLLr leukaemia-independent context, *HOXA10* overexpression also marks MLL germline AML and T-ALL with poor prognosis²⁶¹⁻²⁶⁵. Furthermore, similar to the other *HOXA* genes, *HOXA10* is a haematopoietic master regulator, implicated in HSC self-renewal, proliferation and involved in differentiation of the myeloid lineage²⁶⁵⁻²⁶⁶.

The gene expression profiling results for the *HOXA* members were validated *in vitro* in both SEM cells and viable blast cells from a t(4;11)-positive infant ALL patient, which were transfected with siMLL/AF4; expression analysis by qRT-PCR showed a substantial reduction in transcript levels. Although not part of the MLL/AF4 core signature, other *HOXA* family members, (*HOXA4*, *HOXA5*, *HOXA6*, *HOXA7*, *HOXA9*) were also differentially expressed in the GEP analyses. However, their response was delayed, as the corresponding probe sets did not show a two-fold change in expression compared to Ctrl at TP1 (*HOXA4*-*HOXA9*), or the expression down-regulation at TP2 was so strong (*HOXA6*, *HOXA7*) that the corresponding probe sets flagged up as absent or marginal (tab. 3-20). This indicates a comprehensive regulation of the *HOXA* gene cluster by MLL/AF4, which is in keeping with current literature. *HOXA7* and *HOXA9* down-regulation in response to MLL/AF4 depletion was also validated in the SEM cell line; however, remarkably, MLL/AF4 ablation in t(4;11)-positive patient blasts did not substantially decrease *HOXA7* levels, and *HOXA9* was not affected at all, a result which is highly counterintuitive. A plausible cause could be a threshold

effect; not all HOXA genes are expressed at the same level within the same cells (fig. 5-16), although there is wide-spread MLL and MLL/AF4 occupancy across the 5'-end of the cluster^{116,132}. *HOXA10* is expressed at lower levels than *HOXA7* and *HOXA9*, which might suggest a higher dependency on MLL/AF4 for the expression. Consequentially, *HOXA9*, which has the highest transcript levels, might require a more pronounced *MLL/AF4* depletion than the 50% achieved in the patient cells. Concordantly, *HOXA9* down-regulation in response to *MLL/AF4* depletion in the SEM cell line (fig. 3-44) occurred to a lesser extent than the effects observed for *HOXA7* and *HOXA10* (fig. 3-43). MLL/AF4-mediated HOXA gene expression and its subsequent loss in siMLL/AF4-treated cells do not only reflect a possible loss of stemness, but also have implications for the MLL/AF4-dependent survival, as *HOXA9* expression has been shown to be required for survival of MLLr ALL cells *in vitro* and *in vivo*²⁶⁷.

Another stemness-related gene present in the functional networks associated with the MLL/AF4 signature A was *TERT*, which encodes the catalytic subunit of the Telomerase ribozyme, a key regulator of self-renewal in normal and malignant cells²⁶⁸. *TERT* expression was decreased in response to *MLL/AF4* depletion for both time points (fig. 3-45), which was corroborated by qRT-PCR in siMLL/AF4-treated SEM cells. Recently, we have shown that this is regulated in a HOXA7-dependent manner¹⁷⁰, linking MLL/AF4 with the expression of one of the most prominent regulators of stem cell self-renewal.

Another factor shown to play a role in early development is for instance the chromatin modifying factor HMGA2 (high mobility group protein A2). HMGA2 is a direct MLL/AF4 target¹³², and showed such a strong down-regulation in response to MLL/AF4 that the probe flagged as absent in the array (tab. 3-20). In good concordance, MLL/AF4-dependent down-regulation could be validated *in vitro* by qRT-PCR in both SEM cells and t(4;11)-patient blasts transfected with siMLL/AF4 (fig. 3-46).

This body of data suggests that MLL/AF4 is required to maintain a stem cell-like character of the leukaemic cell, as it mediates the expression of genes linked to self-renewal.

3.6.4 MLL/AF4 signature has only a limited overlap across the time point and with published data

The MLL/AF4 signatures were compared across the experimental time points, which correspond to different periods of depletion. The overlap between each time point was surprisingly small, below 20%. Some of it could be potentially attributed to the stringent filtering settings applied for the analysis, as the probes had to both have assigned a present flag and to show at least a two-fold change in signal intensity. This could result in loss of genes which respond very strongly to MLL/AF4, as the sustained down-regulation might result in a very low expression of the particular gene, causing the probe flag to change from present to marginal or even absent (tab. 3-13). Additionally, genes having delayed response to MLL/AF4, perhaps requiring a more sustained depletion, will pass the fold-change threshold at TP2 and TP3, but not TP1, i.e. *PROM1*. Thus, applying such stringent analysis settings might filter out potentially interesting genes that actually do show a differential regulation in response to MLL/AF4 depletion. However, one of the overall weaknesses of this GEP study is the lack of replicate analyses; each time point corresponds to a single array for siMLL/AF4-treated SEM cells, and two arrays for the corresponding controls. This lacks statistical power, and opens the door for potential artefacts, which cannot be reproduced from one experimental time point to the other. Interestingly, removing the MOCK control from the analyses for MLL/AF4 signature B strongly increased the numbers of differentially regulated probes between siMLL/AF4 and siCtrl-treated samples; however, the overlap between the different time points remained as small, or even decreased. To date, the extent of these artefacts in the MLL/AF4 signatures cannot be estimated, but seems to be substantial.

In addition, there is a special caveat for the analysis of TP3, as the PM/MM2 ratio (perfect match probe to mismatch probe ratio) is approximately 2.5, while for TP1 and TP2 it is 8. A lower PM/MM2 ratio could indicate problems with specificity (see appendix). Moreover, the array format was slightly changed, as it was a HT-12 V4 BeadChip for TP3, and a HT-12 V3 BeadChip for TP1 and TP2; this BeadChip arrays differ in probe coverage as well as in probe numbers.

In order to address these and the aforementioned issues, a different analysis strategy should be applied, which could not be done anymore within the period of this PhD degree:

- COMBAT analysis to remove potential batch effects due to differences in array chip version²⁶⁹
- Significance testing for differential gene expression analyses across the three time points, i.e., using Student's t-test-based methods and multiple testing correction algorithms.

Nevertheless, 12 out of 14 genes identified in the GEP study could be validated *in vitro* using qRT-PCR, and, for DUSP6 and ANGPT1 (section 5), the differential expression was also verified on protein level, and the fold-changes derived from the array analysis and the qRT-PCR experiments showed a good correlation.

The MLL/AF4 signatures were also compared with a published data set comprising MLL/AF4 target genes. Again, the overlap was exceedingly low, corresponding to approximately 10% or less. However, a similar observation was just published recently; using ChIP-on-chip technology, Wang *et al.* identified approximately 223 genomic binding sites of the MLL/ENL fusion protein, corresponding to putative target genes. However, subsequent overexpression studies showed only changes in transcript expression in 12 of these genes in response to MLL/ENL expression²⁷⁰. This extent of overlap corresponds to the changes in expression levels of putative MLL/AF4 target genes observed in this study. This interesting finding highlights that occupancy of a transcription factor does not necessarily translate in transactivation or transcription regulation. Indeed, some of the MLL/AF4 target genes are up-regulated in this study, such as REEP3 and CD96 (tab. 3-13), although these genes showed high expression and correlation with transcriptional active chromatin¹³².

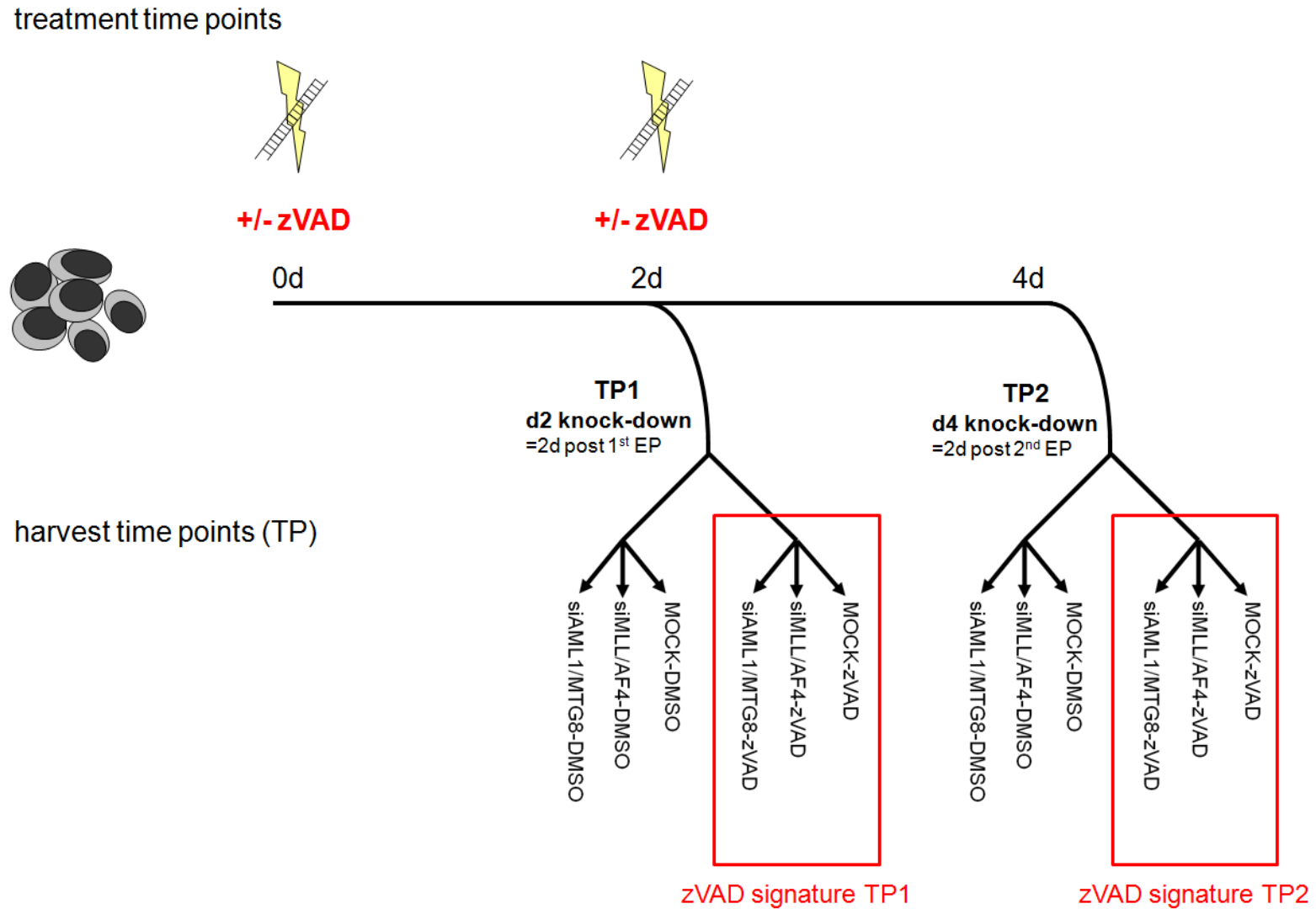
4. t(4;11)-positive Cells Display Oncogenic Addiction to MLL/AF4

4.1 COMBINED TREATMENT OF SEM CELLS WITH siMLL/AF4 AND THE PAN-CASPASE INHIBITOR zVAD-FMK

MLL/AF4 confers increased viability and resistance to apoptosis both when expressed as an endogenous factor or when ectopically introduced into different cellular contexts. Concurrently, siRNA-mediated MLL/AF4 down-regulation results in induction of cell death in the t(4;11)-positive cell line SEM. In order to understand this on a molecular level, we performed whole genome expression profiling of MLL/AF4-depleted SEM cells at time points where cell death was not yet elevated (TP1) and when cells were already undergoing apoptosis TP2 (section 3). Additionally, in an attempt to gain further insight into the molecular hierarchy involved in MLL/AF4-dependent apoptosis, siRNA-electroporated SEM cells were treated simultaneously with the pancaspase inhibitor carbobenzoxy-valyl-alanyl-aspartyl-[O-methyl]-fluoromethylketon (zVAD-FMK, in future referred to as zVAD) and subsequently analysed by whole-genome gene expression profiling (GEP). For the experimental set-up please refer to the scheme in (fig. 4-1)

Fig. 4-1: Experimental set-up

SEM cells were serially electroporated at two-day intervals with siRNA against MLL/AF4 (siMLL/AF4), control siRNA (siAML1/MTG8) or without oligonucleotides (MOCK). Subsequently, cells were subdivided into two treatment groups; one group was supplemented with the pancaspase inhibitor zVAD, the other with the equal amount of solvent (DMSO). Cells were harvested for analyses at TP1 (2 days post 1st electroporation), corresponding to a 2-day MLL/AF4 knockdown, and at TP2 (2 days post 2nd electroporation), which represents a sustained down-regulation of MLL/AF4 for 4 days. Gene expression profiling (GEP) was performed on the RNA derived from zVAD-treated cells at TP1 and TP2, and the following results were termed zVAD signature at TP1 or TP2. The GEP results from the electroporated cells treated with DMSO have already been described in the previous chapter.



4.1.1 zVAD dosage titration

Prior to the actual GEP experiment, it was necessary to optimise the zVAD treatment. In parallel to the siRNA electroporations with siMLL/AF4 or siAML1/MTG8, three different inhibitor treatment conditions were applied:

- (a) a daily dose of 50 μ M zVAD
- (b) a dose of 50 μ M zVAD at the time point of the electroporation, corresponding to a 2-day interval of inhibitor treatment, or
- (c) a daily dose of 25 μ M zVAD.

For each treatment group controls were supplemented with the corresponding vehicle control (DMSO) concentration.

All three zVAD treatment conditions proved to be equally effective in blocking apoptosis, as illustrated by flow cytometry analyses: the proportion of cells present in sub-G1/G0 population, which corresponds to the apoptotic cell fraction, was reduced to near basal levels in siMLL/AF4-transfected cells cocultured with zVAD (fig. 4-2).

Furthermore, cleavage of PARP1 (PARP), an indicator of caspase activity and a well-established apoptosis characteristic, was markedly decreased in the siMLL/AF4-zVAD samples (fig. 4-3). In contrast, siMLL/AF4-mediated fusion gene depletion resulted in both apoptosis (fig. 4-2) and PARP cleavage (fig. 4-3) induction in the DMSO control groups.

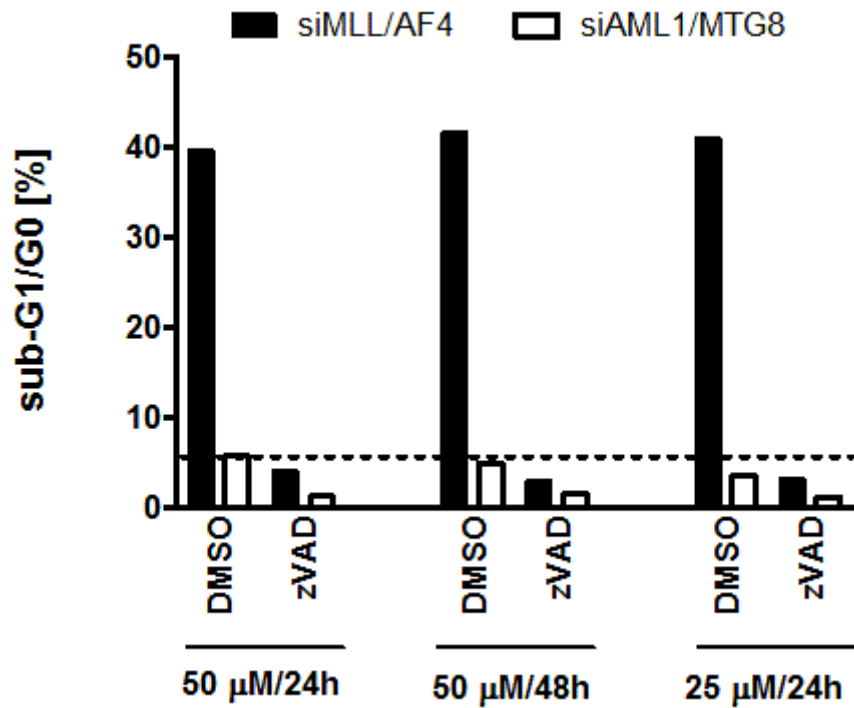


Fig. 4-2: Analysis of the sub-G1/G0 population of siRNA-treated SEM cells supplemented with different zVAD concentrations

SEM cells serially electroporated with siMLL/AF4 or control siRNA were subjected to three different zVAD culture conditions. Cell cycle was analysed by flow cytometry after a four day depletion period. Apoptosis was determined by measuring the proportion of SEM cells in the sub-G0/G1 population using the ModFit LT software (Verity Software House). The dotted line across the graph represents approximate basal apoptosis levels as indicated by the control samples of each treatment group.

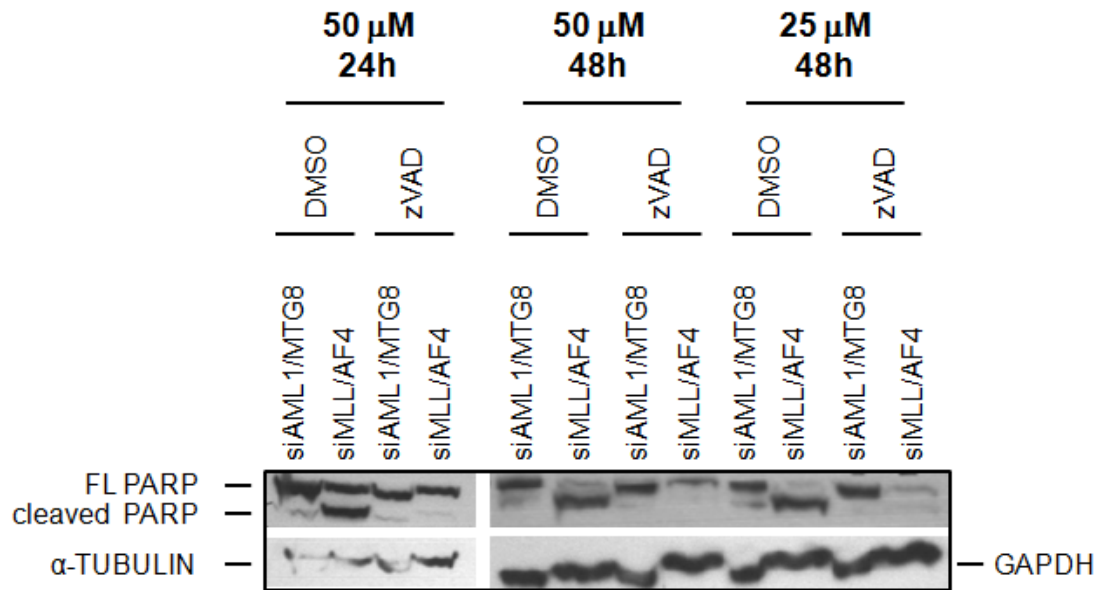


Fig. 4-3: PARP Western blot in zVAD –treated SEM cells

SEM cells serially electroporated with siMLL/AF4 or siAML1/MTG8 were subjected to three different zVAD culture conditions and analysed 2 days after the 2nd electroporation for PARP cleavage, a surrogate marker for caspase activation (TP2, d4).

While the efficiency of the different zVAD concentration was dose-independent, there was evidence that zVAD treatment *per se* affected SEM cell cycle progression. When comparing control-siRNA-transfected cells (siAML1/MTG8) with and without zVAD, cell cycle analysis showed an increased accumulation of cells in the G1-phase, accompanied by depletion in the S- and G2/M-phase. This effect was subtle in the instance of treatments (b) and (c), but condition (a) showed a marked effect, increasing the G1/G0 fraction by 22%, while cells in the replicative S-phase were reduced by 19% (fig. 4-4). Thus, this condition was discarded for further studies, and out of the two remaining options treatment regimen (b) – 50 μ M zVAD at two-day intervals, subsequent to the electroporation – was eventually chosen, as it was deemed compatible with the siRNA treatment set-up.

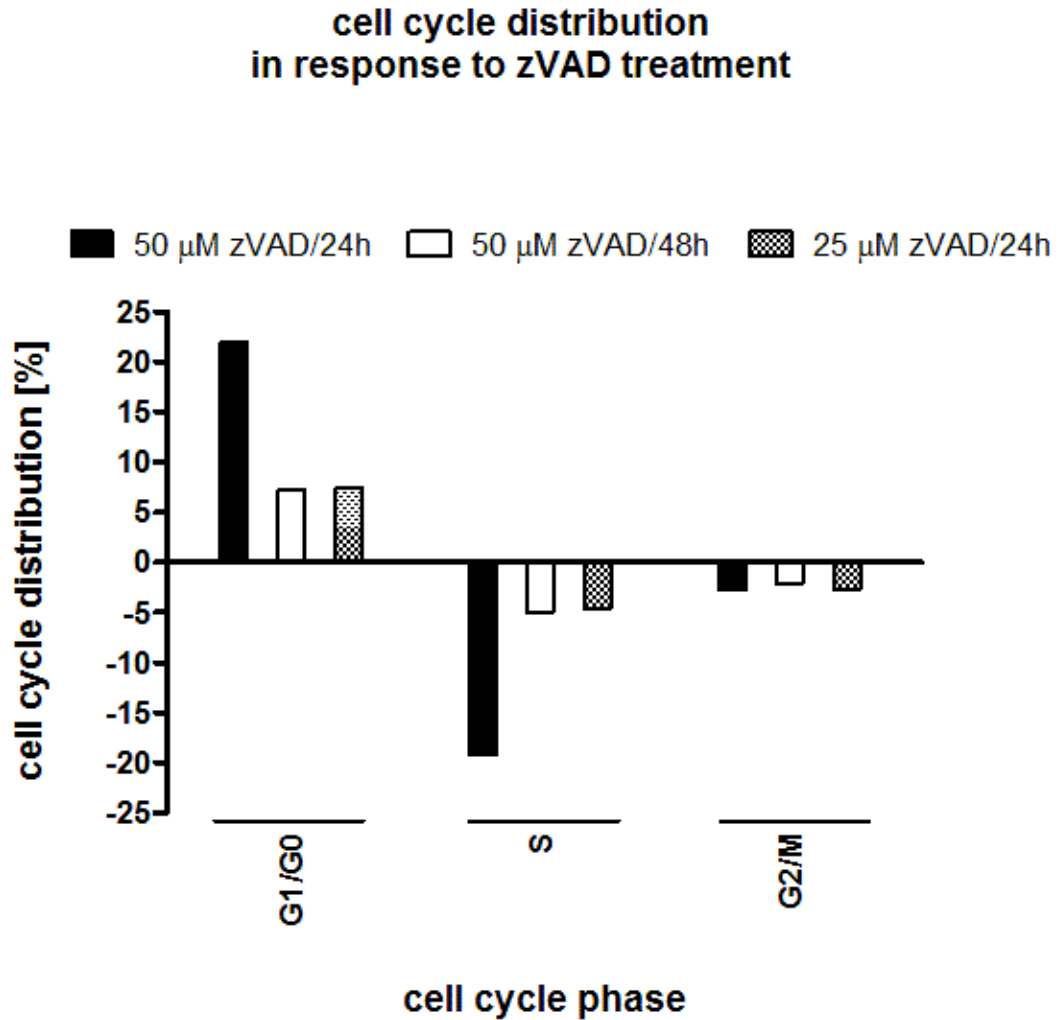


Fig. 4-4 : Cell cycle analysis of different zVAD treatment groups

SEM cells serially electroporated with siAML1/MTG8 were subjected to three different zVAD culture conditions and analysed at TP2 (2 days after the 2nd electroporation), for changes in cell cycle distribution attributable to the effect of zVAD.

4.1.2 zVAD inhibits caspase-dependent apoptosis activation, but does not abrogate cell-death

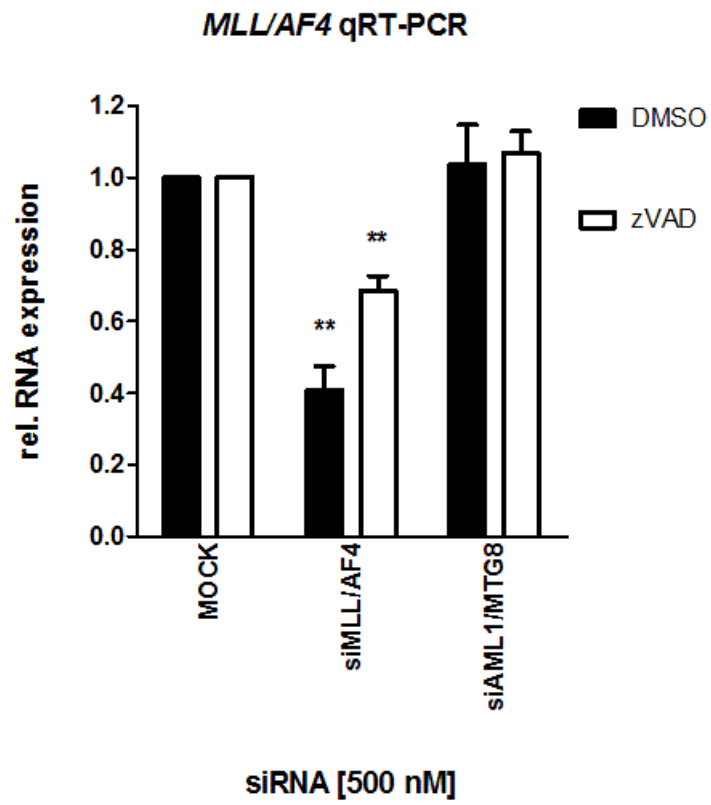
SEM cells were electroporated according to the conventional experimental set-up (fig. 4-1); transfection of siMLL/AF4 in SEM cells treated with zVAD resulted in a slightly less pronounced *MLL/AF4* depletion at TP1 and TP2 as the corresponding vehicle control group (fig. 4-5). This effect was due to a quicker recovery of *MLL/AF4* transcript levels, as analysis 24h after the initial electroporation showed no significant difference in MLL/AF4 expression (fig. 4-10).

As observed in the titration experiments, treatment of zVAD resulted in a decrease of the apoptotic sub-G1/G0 population to basal levels; furthermore, it nearly completely suppressed the sub-G1/G0 fraction in the controls samples of the zVAD group (fig. 4-6). *MLL/AF4* depletion in the DMSO control group resulted in proteolytic activation of the effector caspases CASP3 and CASP7, as well as subsequent PARP processing, as indicated by the presence of the resulting cleavage products by immunoblotting. In contrast, the active form of both effector caspases was absent in SEM cells electroporated with siMLL/AF4 and cultured with zVAD, and PARP cleavage was severely diminished (fig. 4-7A). Inhibition of caspase activity by zVAD was further confirmed through a luciferase-based CASPASE-3/-7 activity assay, in which the activity was more than 90% reduced in cells cultured with zVAD regardless of siRNA treatment, and up to 10-fold induced in SEM cells in the siMLL/AF4-DMSO sample (fig. 4-7B).

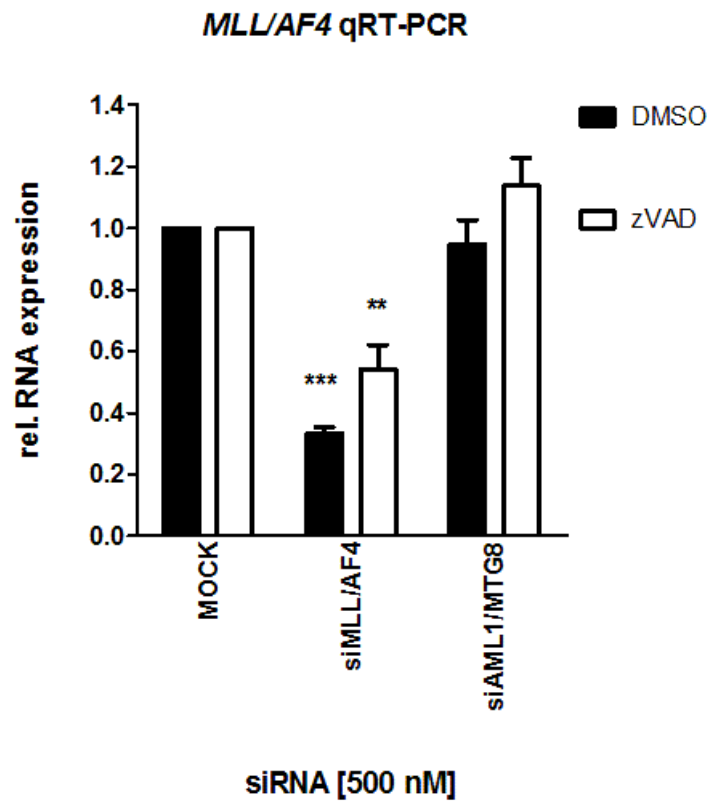
Fig. 4-5: MLL/AF4 expression analysis in siRNA treated SEM cells cultured with or without zVAD

SEM cells electroporated with siMLL/AF4 and treated with or without zVAD show reduced *MLL/AF4* levels at TP1 (A) and TP2 (B) when compared to controls. The figure shows the mean of n=3 (d2)/ n=4 (d4) individual experiments, error bars indicate standard error of the mean (S.E.M.). Statistic analysis was carried out using an unpaired Student's t-test (** = $p < 0.01$; *** = $p < 0.001$).

A



B



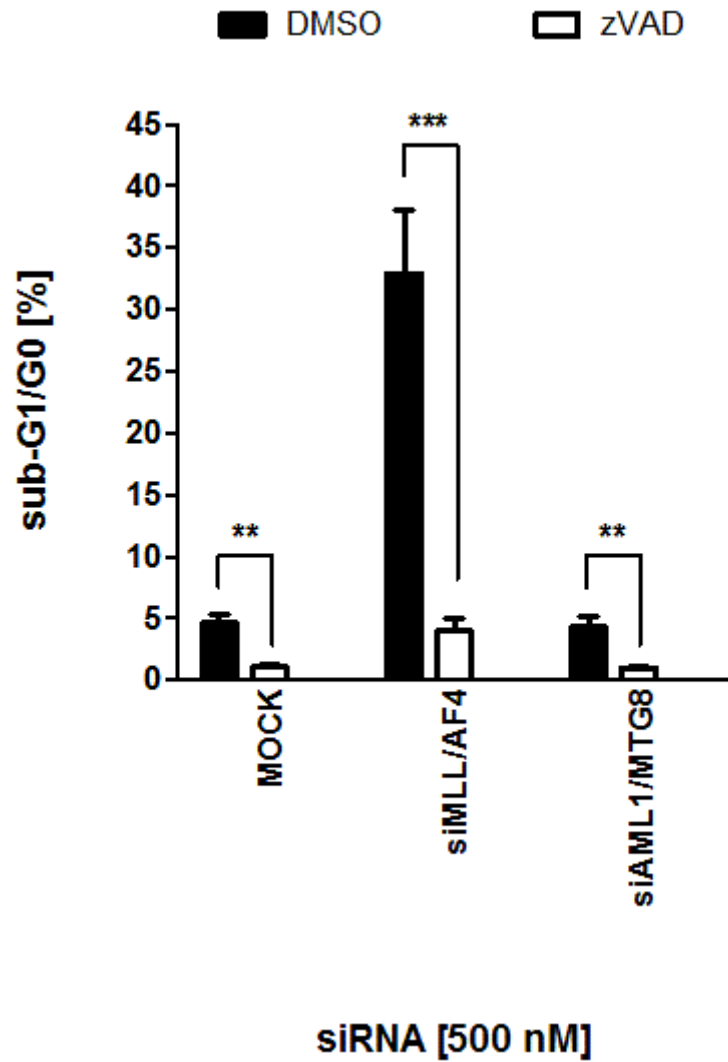


Fig. 4-6: Analysis of the sub-G1/G0 population of siRNA-treated SEM cells supplemented with or without zVAD

SEM cells serially electroporated with siMLL/AF4 or control-transfected (siAML1/MTG8, MOCK) and supplemented with zVAD or corresponding vehicle (DMSO). After four days of sustained MLL/AF4 depletion, the cell cycle distribution was analysed by flow cytometry. Apoptosis was determined by measuring the proportion of SEM cells in the sub-G0/G1 population using the ModFit LT software (Verity Software House). The graph represents the mean of $n=5$ independent experiments, statistical significance was determined by Student's *t*-test (** = $p < 0.01$; *** = $p < 0.001$).

Although these results clearly showed that zVAD was able to abrogate apoptosis induction in response to MLL/AF4-depletion in the SEM cell line, a very striking observation was made by another highly discriminatory flow cytometric cell death assay: binding of fluorescently-tagged ANNEXIN V in conjunction with uptake of the DNA-intercalating dye propidium iodide (PI), an approach which allows to differentiate between caspase-dependent and -independent programmed cell death (PCD) pathways (fig. 4-8). As expected, SEM cells electroporated with siMLL/AF4 in the DMSO group showed a distinctly apoptotic pattern, defined by binding of rhANNEXIN V on the cell surface while excluding PI, and a late apoptotic/secondary necrotic stage, where the cell membrane integrity had been compromised and PI taken up, resulting in a double positive population. Remarkably, while the apoptotic ANNEXIN V-single positive stage was at basal levels in siMLL/AF4-zVAD co-cultured cells, massive induction of cell death could be still be observed, as indicated by the presence of double-positive population. These results suggested that a caspase-independent programmed cell death pathway had been activated in the siMLL/AF4-zVAD-treated cells. This loss of viability was further confirmed by an MTT assay, where the loss of number of uncompromised SEM cells was comparable between the siMLL/AF4-DMSO and siMLL/AF4-zVAD electroporated samples (fig. 4-9).

Fig. 4-7: Effector caspase activation and action is suppressed in siMLL/AF4-transfected SEM cells by zVAD

SEM cells serially electroporated with siMLL/AF4 or controls (MOCK, siAML1/MTG8) were assayed for effector caspase activity at TP2. Immunoblotting showed a lack of activation of the procaspases CASP3 and CASP7 in zVAD treated cells, as denoted by the absence of the cleavage products. In contrast, active CASP3 and CASP7 forms could be detected in the siMLL/AF4-DMSO cells (A). Moreover, suppression of the proteolytic activity could be confirmed by immunoblotting for PARP cleavage, a surrogate marker for caspase activity; the characteristic PARP fragments were only present in siMLL/AF4-DMSO cells, but not in siMLL/AF4-zVAD treated cells or controls. The full-length (FL) form could also be detected in samples (A). Concordantly, the caspase activity assay showed complete suppression of proteolytic activity in zVAD treated cells regardless of the siRNA treatment, while siMLL/AF4-DMSO cells had a 10-fold increase when compared to the corresponding control (siAML1/MTG8-DMSO) (B). The immunoblot panel (A) is representative of n=3 comparable experiments, graph (B) show the mean of n=3 experiments. Statistical significance was determined using one-way ANOVA.

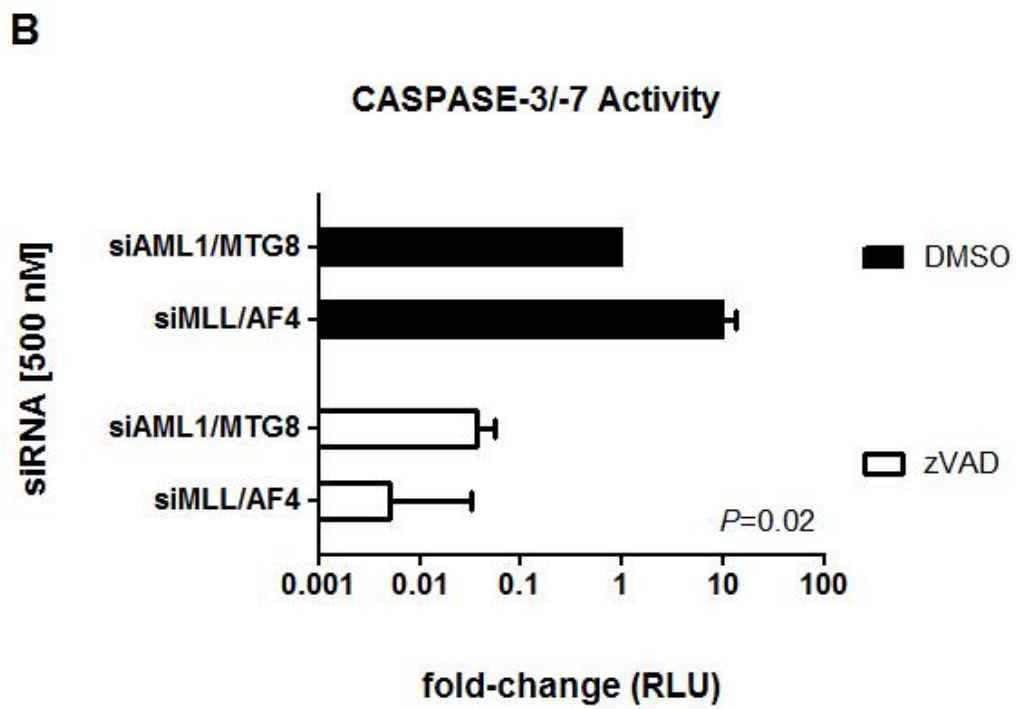
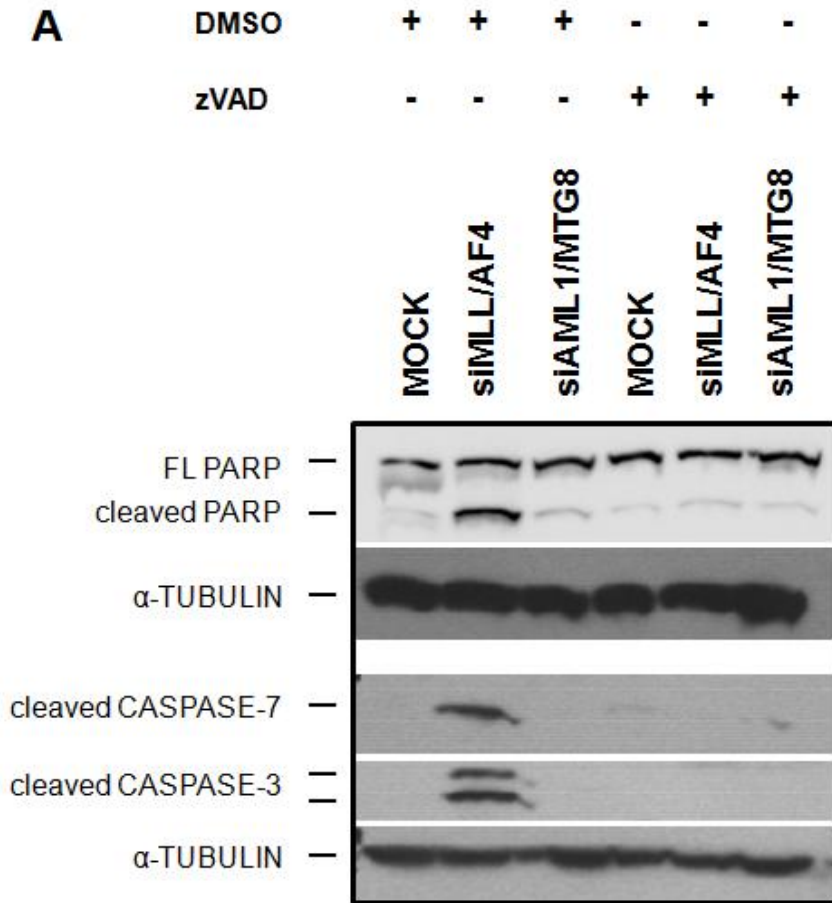
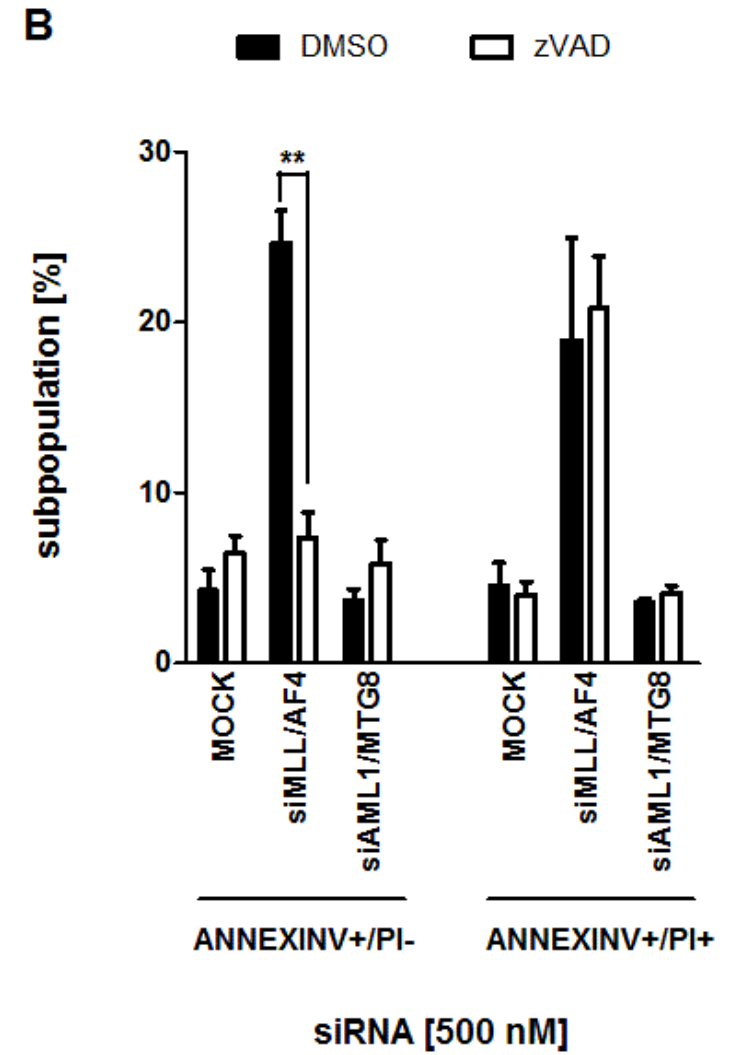
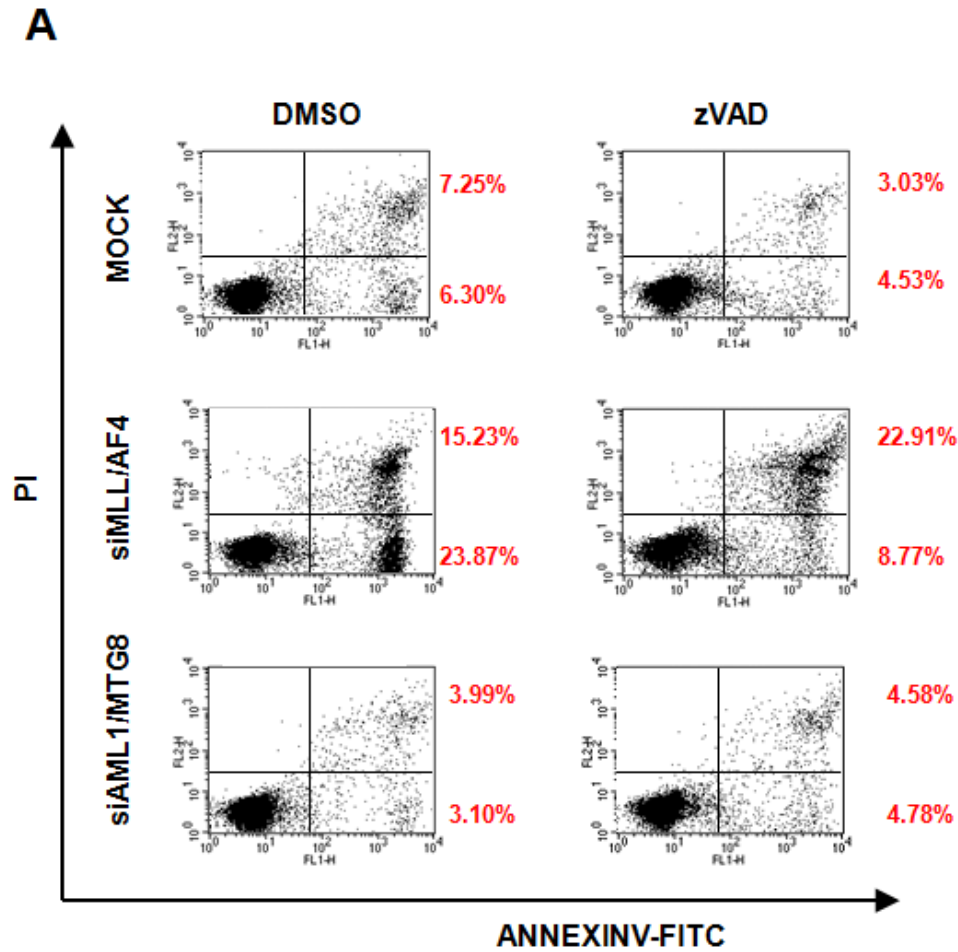


Fig. 4-8: Apoptosis inhibition in siMLL/AF4-depleted SEM cells causes switch from apoptosis to a necrotic-like PCD.

SEM cells were serially electroporated with siMLL/AF4 or controls (siAML1/MTG8, MOCK) and treated with and without zVAD, followed by assessment of cell death by flow cytometry at TP2. SEM cells treated with siMLL/AF4-DMSO show the characteristic apoptotic pattern, with an increased ANNEXIN V-single positive population, but also the presence of a secondary necrotic population which was ANNEXIN V/PI-double positive. In concordance with previous results, zVAD treatment suppresses the apoptotic single positive population to near basal levels, however induction of a double positive necrotic population is still present (A, B). The reduction of the apoptotic single positive population was highly significant, as determined by Student's t-test (***) = $p < 0.001$). Graph (A) shows one representative flow cytometry dot plot panel, graph (B) represents the mean of $n=5$ independent experiments; error bars indicate S.E.M



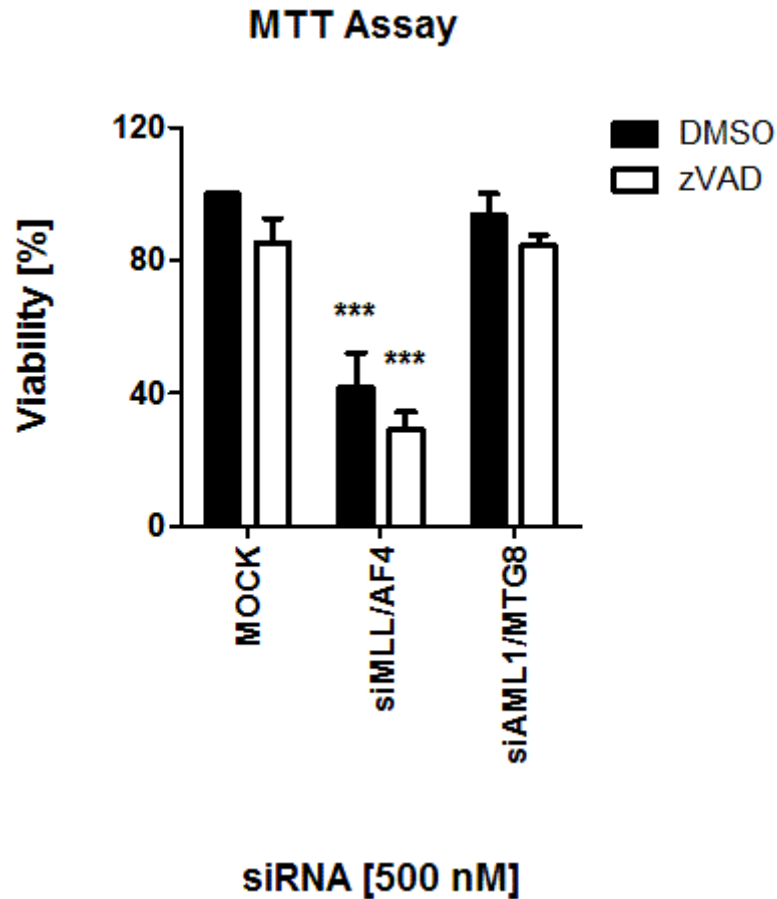


Fig. 4-9: Viability of siMLL/AF4-electroporated SEM cells is compromised despite apoptosis inhibition

SEM cells were serially electroporated with siMLL/AF4 or controls (siAML1/MTG8, MOCK) and treated with and without zVAD. Viability was measured by MTT at TP2. Both siMLL/AF4-treated cells showed a strong reduction in viable cells, regardless of the inhibitor treatment. The graph represents the mean of n=4 independent experiments, error bars indicate S.E.M. Statistical significance was determined by Student's t-test (***) = $p < 0.001$.

4.2 GENE EXPRESSION PROFILING OF SEM CELLS DEPLETED OF MLL/AF4 AND CULTURED WITH zVAD

Apoptosis inhibition in MLL/AF4-depleted SEM cells revealed an interesting aspect of oncogene addiction, as presence of the caspase inhibitor zVAD could not block the induction of cell death, but seemingly altered the cell death type. This finding was investigated further on a molecular level; SEM cells electroporated with siMLL/AF4, control siRNA (siAML1/MTG8) or no siRNA (MOCK) and cultured with zVAD were harvested at TP1 and TP2, and subsequently analysed gene expression profiling (GEP), using the Illumina HT-12 Bead Array platform.

4.2.1 Biological QC analysis of array samples

SEM cells were serially electroporated twice according to the scheme in fig. 4-1 , and TP1 and TP2 harvested for RNA. Before the RNA was processed as described by the manufacturer at a service provider core facility, the siRNA-treated samples underwent quality control measures.

Efficient *MLL/AF4* knock-down was confirmed by qRT-PCR (fig. 4-10); in both the zVAD treated and the DMSO control group more than 70% *MLL/AF4* depletion was attained. RNA quality was assessed by lab-on-chip technology using a Bioanalyzer 2100 RNA Nano assay (tab. 4-1). A RNA integrity number (RIN) above 7 characterises RNA of good enough quality for GEP; the RIN of two samples was not calculable due to a migration shift of the gel, however, the corresponding histograms and gel pictures showed the RNA to be of good quality, allowing the samples to be processed for array analysis (see appendix).

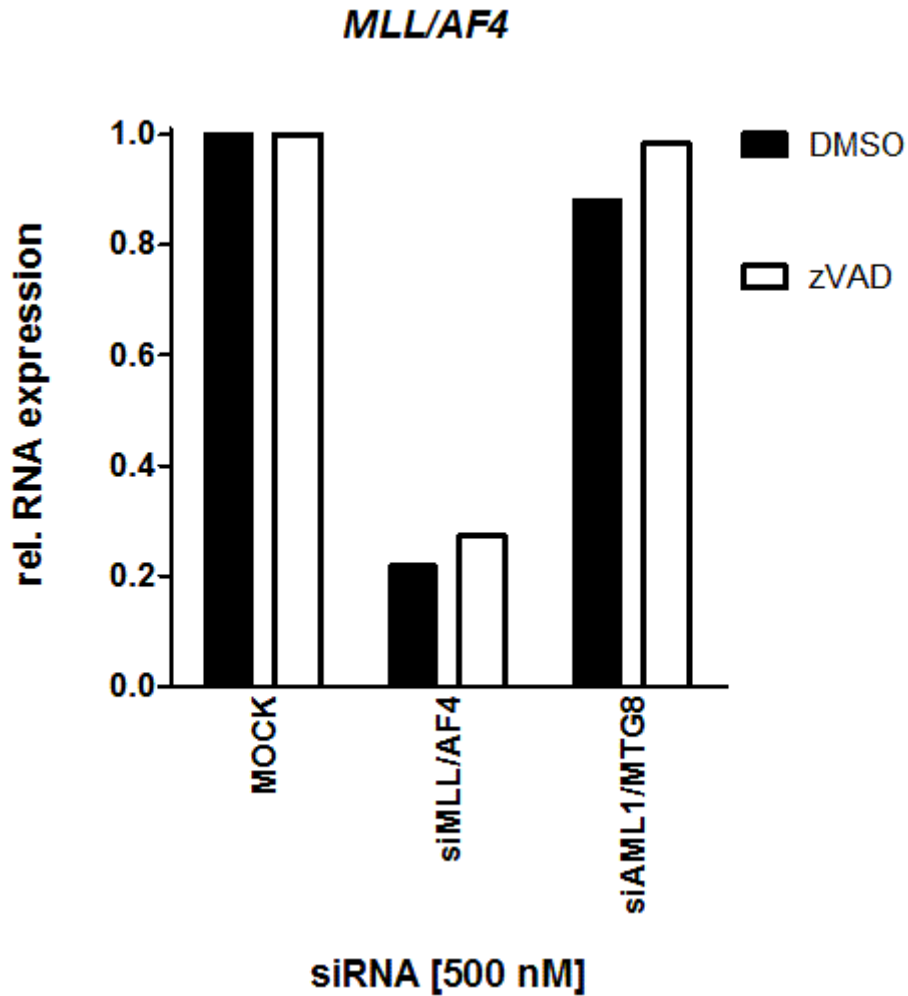


Fig. 4-10: Confirmation of *MLL/AF4* depletion by qRT-PCR in cells treated with or without zVAD prior to GEP analysis

SEM cells were serially electroporated twice at two-day intervals with either siMLL/AF4, control siRNA (siAML1/MTG8) or no siRNA (MOCK). *MLL/AF4* expression was determined by qRT-PCR day one (d1) of siRNA treatment. Compared to controls, siMLL/AF4-transfected cells showed a *MLL/AF4* down-regulation of >70% in both the zVAD and DMSO treatment group. The graph represents one single experiment; each sample was examined in triplicates.

Tab. 4-1: RIN values of samples submitted to GEP as determined by Bioanalyzer2100 RNA 6000 Nano Assay

Sample	RIN
TP1 (+zVAD)	
<i>MOCK</i>	7.5
<i>siMLL/AF4</i>	7.7
<i>siAML1/MTG8</i>	9.2
TP2 (+zVAD)	
<i>MOCK</i>	N/A
<i>siMLL/AF4</i>	N/A
<i>siAML1/MTG8</i>	8.9

The samples were processed off-site at a service provider facility according to manufacturer's protocols, and assayed using an Illumina HT-12 V.3 Bead Array (Illumina Inc.). The obtained raw data was preprocessed by me using BeadStudio 3 software (Illumina Inc.). Missing probe values were not imputed.

Differentially expressed genes were determined using GeneSpring GX11 software (Agilent Technologies, Inc); each time point was analysed as an individual treatment group consisting of siMLL/AF4, MOCK and siAML1/MTG8-transfected cells; a quantile normalisation algorithm was applied, and the baseline of each array transformed over the median baseline of the control samples siAML1/MTG8 & MOCK. Probe signal values associated with the controls were averaged, resulting in a control group termed Ctrl, against which the differential expression analysis for siMLL/AF4 was performed (siMLL/AF4 vs. Ctrl).

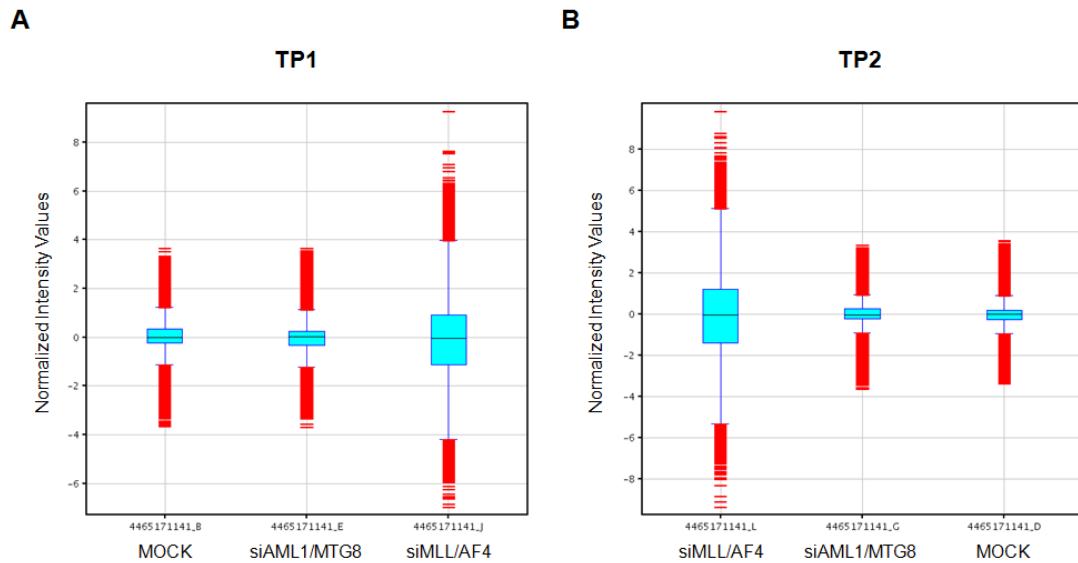


Fig. 4-11: Normalised array intensity values of each zVAD treatment group at TP1 & TP2

The siRNA treatment time course were grouped according to time point, each treatment group consisting of control- (MOCK, siAML1/MTG8) and siMLL/AF4-transfected samples. Each of these treatment groups was normalised independently using the quantile normalisation algorithm and transforming the baseline of each sample over the median baseline of the control samples. The box and whisker plots indicate the spread of the probe signal values of the treatment group at TP1 (A) and TP2 (B).

The results were filtered according to the array signal calls or “flags” as described in section 3, only performing a stringent analysis, were all flags in all samples had to have a present call. Differentially expressed probes were determined by calculating the signal intensity in the siMLL/AF4 array vs. the signal intensity values in the Ctrl samples. A linear fold-change expression value cut-off of 2.0 was applied; this generated dataset was termed gene signature zVAD.

As summarised in tab. 4-2, at TP1 there were 3239 differentially expressed probes, which could be collapsed into 2939 genes, of which 1484 were up- and 1475 down-regulated. At TP2 there were 6479 differentially regulated probes, corresponding to 5541 genes, of which 2635 were induced and 2965 genes showed reduced expression.

The mathematical discrepancy between up- and down-regulated genes and the overall differentially expressed genes resulted from different probes covering the same gene but associated with opposing regulation.

Tab. 4-2: Number of differentially expressed probe sets and genes for the zVAD signatures at TP1 and TP2

siMLL/AF4 vs. siCtrl	TP1 (+zVAD)	TP2 (+zVAD)
No. of differentially expressed probes	3239	6479
<i>up-regulated probes</i>	1616	3007
<i>down-regulated probes</i>	1623	3472
No. of differentially expressed genes	2939	5541
<i>up-regulated genes</i>	1484	2635
<i>down-regulated genes</i>	1475	2965

The top 50 up- and down-regulated probes for each time point of signature zVAD are listed in tab. 4-3 to tab. 4-6, respectively. There is a notable overrepresentation of chemo- and cytokines and their receptors in the up-regulated probe sets at both time points, which include *MIP1- α* (*CCL3*), *IL8*, *CXCL10*, *RANTES* (*CCL5*), *CCR7*, as well as members of the tumour necrosis factor super family (TNFSF) and their receptors (TNFRSF), such as *TNF*, *LTA* and *LIGHTR* (*TNFRSF14*). Conversely, amongst the down-regulated probes there were genes associated with early haematopoietic differentiation (*IGFBP2*, *HOXA10*, *VPREB1*, *IGLL1*, *IGLL3*). Of particular interest in this group is the gene *OPRS1*, also termed *sigma non-opioid intracellular receptor-1* (*SIGMAR1*), a neuroprotective receptor implicated in Alzheimer, frontal lobe dementia and motor neuron disease²⁷¹⁻²⁷³, but to date not reported in haematopoietic cells.

Tab. 4-3: Top 50 up-regulated probes in the zVAD signature at TP1

ILMN_Gene	Fold-change [siMLL/AF4] vs. [siCtrl]	Accession	Probe_ID
CCL3	77.22	NM_002983.1	ILMN_1671509
CCR7	58.31	NM_001838.2	ILMN_1715131
CCL3L1	54.97	NM_021006.4	ILMN_1747355
CXCL10	53.32	NM_001565.2	ILMN_1791759
CCL3L3	49.35	NM_001001437.3	ILMN_2105573
CCL3L1	47.49	NM_021006.4	ILMN_2218856
CCL4L2	38.94	NM_207007.2	ILMN_1716276
KLF4	37.02	NM_004235.3	ILMN_2137789
IL8	36.63	NM_000584.2	ILMN_2184373
IL8	33.07	NM_000584.2	ILMN_1666733
CCL5	29.97	NM_002985.2	ILMN_2098126
CXCL11	28.24	NM_005409.3	ILMN_2067890
LINCRC	27.58	NM_001080535.1	ILMN_2235851
CEACAM1	24.23	NM_001024912.1	ILMN_1716815
ANXA1	21.81	NM_000700.1	ILMN_2184184
CCL5	20.91	NM_002985.2	ILMN_1773352
BHLHB2	20.80	NM_003670.1	ILMN_1768534
JUN	19.57	NM_002228.3	ILMN_1806023
TRAF1	18.93	NM_005658.3	ILMN_1698218
TNFRSF14	18.52	NM_003820.2	ILMN_1697409
BIRC3	18.34	NM_001165.3	ILMN_1776181
ZMIZ2	17.59	NM_031449.3	ILMN_1760718
IFIT2	17.37	NM_001547.4	ILMN_1739428
IFIT1	16.74	NM_001548.2	ILMN_1699331
EBI2	16.05	NM_004951.3	ILMN_1798706
FOSB	15.78	NM_006732.1	ILMN_1751607
MX1	15.00	NM_002462.2	ILMN_1662358
PLA2G4C	14.96	NM_003706.1	ILMN_1810191
LTA	14.72	NM_000595.2	ILMN_1795464
TNF	14.72	NM_000594.2	ILMN_1728106
PTGS2	13.94	NM_000963.1	ILMN_2054297
RANBP3L	13.43	NM_145000.2	ILMN_2094856
PMAIP1	13.30	NM_021127.1	ILMN_2098446
IFI27	12.82	NM_005532.3	ILMN_2058782
OASL	12.73	NM_003733.2	ILMN_1681721
OASL	12.70	NM_198213.1	ILMN_1674811
RSAD2	12.63	NM_080657.4	ILMN_1657871
NR4A2	12.59	NM_006186.2	ILMN_1782305
IL4I1	12.52	NM_172374.1	ILMN_1659960
ATF3	11.23	NM_001040619.1	ILMN_2374865
TNFSF10	11.23	NM_003810.2	ILMN_1801307
PPP1R15A	10.48	NM_014330.2	ILMN_1659936
PLA2G2D	10.38	NM_012400.2	ILMN_2233050
PRRG4	10.07	NM_024081.4	ILMN_1661809
FZD4	9.94	NM_012193.2	ILMN_1743367
GEM	9.77	NM_181702.1	ILMN_2367883
GEM	9.61	NM_181702.1	ILMN_1677092
TNFRSF9	9.33	NM_001561.4	ILMN_1813379
RAGE	9.28	NM_014226.1	ILMN_1745282
FOS	9.25	NM_005252.2	ILMN_1669523

Tab. 4-4: Top 50 down-regulated probes in the zVAD signature at TP1

ILMN_Gene	Fold-change [siMLL/AF4] vs. [siCtrl]	Accession	Probe_ID
NRGN	-16.84	NM_006176.1	ILMN_1705686
VPREB1	-13.26	NM_007128.2	ILMN_1738549
MACROD1	-10.52	NM_014067.2	ILMN_1740960
HS.538303	-10.28	BX091728	ILMN_1891244
IPLL1	-10.15	NM_020070.2	ILMN_2393765
RPL37A	-10.12	NM_000998.3	ILMN_1808757
FLJ12355	-9.44	XR_000645.1	ILMN_1697115
UNC5B	-8.18	NM_170744.2	ILMN_2176502
DDN	-7.64	NM_015086.1	ILMN_1673450
CHN2	-7.58	NM_004067.2	ILMN_2292187
HS.572064	-7.36	BM930393	ILMN_1880256
FADS2	-7.30	NM_004265.2	ILMN_2075065
IPLL3	-7.26	NM_001013618.1	ILMN_2083066
MAP2K6	-7.20	NM_002758.3	ILMN_1697729
ZDHHC9	-7.16	NM_016032.2	ILMN_1748803
METTL9	-6.78	NM_016025.3	ILMN_1726421
IGFBP2	-6.72	NM_000597.2	ILMN_1725193
LOC91461	-6.65	NM_138370.1	ILMN_1734445
PCDHGB6	-6.65	NM_018926.2	ILMN_2274355
NTN1	-6.60	NM_004822.2	ILMN_1873621
LOC127099	-6.57	XM_060328.1	ILMN_1784634
OPRS1	-6.47	NM_147157.1	ILMN_1717925
PRSSL1	-6.47	NM_214710.2	ILMN_1673605
KIF18B	-6.38	NM_001080443.1	ILMN_2327655
CD3EAP	-6.36	NM_012099.1	ILMN_1747870
ENAH	-6.17	NM_018212.4	ILMN_1716552
ERP27	-6.15	NM_152321.1	ILMN_1655261
SEPT6	-6.10	NM_145799.2	ILMN_1661342
RBM15B	-6.09	NM_013286.3	ILMN_1673024
LAT2	-6.09	NM_022040.2	ILMN_1803560
LPHN3	-6.08	NM_015236.3	ILMN_1692623
LOC645128	-6.06	XM_928159.1	ILMN_1751814
CUX1	-5.98	NM_001913.2	ILMN_2330213
ARRB2	-5.83	NM_199004.1	ILMN_2395711
LOC642773	-5.82	XM_926195.1	ILMN_1765640
OCA2	-5.80	NM_000275.1	ILMN_1746116
MLC1	-5.78	NM_015166.3	ILMN_1751471
SS18	-5.75	NM_005637.2	ILMN_2359096
SYNGR1	-5.74	NM_004711.3	ILMN_1810875
ABCB8	-5.74	NM_007188.2	ILMN_2102422
ABLIM1	-5.66	NM_001003407.1	ILMN_2396672
ATPBD4	-5.63	NM_080650.2	ILMN_2140207
ANGPT1	-5.62	NM_001146.3	ILMN_2086890
ZHX3	-5.61	NM_015035.3	ILMN_1774387
CEBPA	-5.52	NM_004364.2	ILMN_1715715
NUDT6	-5.42	NM_007083.3	ILMN_1780659
HS.512096	-5.41	BF375676	ILMN_1871233
DUSP7	-5.40	NM_001947.2	ILMN_1782581
KIAA1545	-5.37	XM_495939.3	ILMN_1760305
LOC401002	-5.36	XR_018284.1	ILMN_1686852

Tab. 4-5: Top 50 up-regulated probes in the zVAD signature at TP2

ILMN_Gene	Fold-change [siMLL/AF4] vs. [siCtrl]	Accession	Probe_ID
KLF4	83.55	NM_004235.3	ILMN_2137789
CCR7	72.55	NM_001838.2	ILMN_1715131
SPINK1	66.01	NM_003122.2	ILMN_1787266
CCL3L1	58.69	NM_021006.4	ILMN_1773245
TNFRSF14	55.66	NM_003820.2	ILMN_1697409
RANBP3L	51.15	NM_145000.2	ILMN_2094856
ATF3	49.22	NM_001030287.2	ILMN_1661109
PLA2G4C	41.83	NM_003706.1	ILMN_1810191
NR4A2	41.37	NM_006186.2	ILMN_1782305
BHLHB2	41.04	NM_003670.1	ILMN_1768534
ABCB1	40.76	NM_000927.3	ILMN_1812070
PTGS2	38.31	NM_000963.1	ILMN_2054297
HSPA6	31.96	NM_002155.3	ILMN_1806165
CCL3L1	31.48	NM_021006.4	ILMN_2218856
FAM46C	31.00	NM_017709.3	ILMN_1713266
CCL3L3	28.86	NM_001001437.3	ILMN_2105573
CEACAM1	28.11	NM_001024912.1	ILMN_1716815
RND3	26.81	NM_005168.3	ILMN_1759513
PTPRO	24.59	NM_030671.1	ILMN_2316878
TRAF1	24.30	NM_005658.3	ILMN_1698218
LTA	24.29	NM_000595.2	ILMN_1795464
CSAG3A	24.28	NM_203311.1	ILMN_2043126
FZD4	23.58	NM_012193.2	ILMN_1743367
RGS1	23.54	NM_002922.3	ILMN_1656011
CCL3L1	23.16	NM_021006.4	ILMN_1747355
EBI2	22.70	NM_004951.3	ILMN_2168217
ATF3	22.68	NM_001040619.1	ILMN_2374865
BAMBI	21.95	NM_012342.2	ILMN_1691410
ZMIZ2	21.70	NM_031449.3	ILMN_1760718
IL8	21.48	NM_000584.2	ILMN_1666733
GEM	21.37	NM_181702.1	ILMN_1677092
GEM	21.37	NM_181702.1	ILMN_2367883
CCL3	21.04	NM_002983.1	ILMN_1671509
ARRDC3	20.34	NM_020801.1	ILMN_2198515
CPEB4	20.27	NM_030627.1	ILMN_1722025
PSD2	20.24	NM_032289.2	ILMN_1662963
ADM	20.17	NM_001124.1	ILMN_1708934
KIAA0423	19.67	NM_015091.2	ILMN_1778876
CXCL11	19.62	NM_005409.3	ILMN_2067890
DUSP10	19.41	NM_144729.1	ILMN_2401878
BIRC3	19.37	NM_001165.3	ILMN_1776181
JUN	19.26	NM_002228.3	ILMN_1806023
GADD45A	18.16	NM_001924.2	ILMN_2052208
PMAIP1	17.65	NM_021127.1	ILMN_2098446
IFNB1	17.45	NM_002176.2	ILMN_1682245
KIAA1370	16.92	NM_019600.1	ILMN_2102960
CDKN2B	16.79	NM_078487.2	ILMN_2376723
IL8	16.79	NM_000584.2	ILMN_2184373
EBI2	16.48	NM_004951.3	ILMN_1798706
PPP1R15A	15.63	NM_014330.2	ILMN_1659936

Tab. 4-6: Top 50 down-regulated probes in the zVAD signature at TP2

ILMN_Gene	Fold-change [siMLL/AF4] vs. [siCtrl]	Accession	Probe_ID
VPREB1	-87.60	NM_007128.2	ILMN_1738549
HOXA10	-54.26	NM_018951.3	ILMN_1682110
SLC29A1	-52.22	NM_001078174.1	ILMN_1723971
HS.508682	-43.15	AV762101	ILMN_1821517
FAM64A	-37.05	NM_019013.1	ILMN_1728972
BRI3BP	-33.68	XM_941876.1	ILMN_1693410
RPS15	-32.33	NM_001018.3	ILMN_2219131
LOC57228	-30.87	NM_001031628.1	ILMN_2380243
AIF1	-28.28	NM_032955.1	ILMN_1792473
CENPM	-27.67	NM_001002876.1	ILMN_2368721
UGT3A2	-27.21	NM_174914.2	ILMN_1655565
SLC29A1	-26.94	NM_001078174.1	ILMN_2338963
BDH1	-26.67	NM_203314.2	ILMN_1799280
PI16	-26.11	NM_153370.2	ILMN_1766264
ACY1	-25.57	NM_000666.1	ILMN_1683883
KIAA0101	-25.50	NM_001029989.1	ILMN_1732150
OPRS1	-25.36	NM_147157.1	ILMN_1717925
PTPRCAP	-25.25	NM_005608.2	ILMN_1672417
HOPX	-22.98	NM_139212.2	ILMN_2316236
ZNF423	-22.19	NM_015069.2	ILMN_2154950
FADS2	-22.06	NM_004265.2	ILMN_2075065
PXMP2	-21.51	NM_018663.1	ILMN_1799015
UCP2	-21.05	NM_003355.2	ILMN_1685625
CTDSP1	-20.81	NM_021198.1	ILMN_1681678
CHST14	-20.41	NM_130468.2	ILMN_1743340
ELF3	-20.35	NM_004433.3	ILMN_1769201
BRI3BP	-19.28	NM_080626.5	ILMN_1797693
TSPO	-19.01	NM_000714.4	ILMN_2260991
FAM101B	-18.89	NM_182705.2	ILMN_1714418
CENPM	-18.74	NM_024053.3	ILMN_1668814
NFIB	-18.45	NM_005596.2	ILMN_1778991
LOC255620	-18.37	XM_173132.4	ILMN_1807114
FAM81A	-18.24	NM_152450.2	ILMN_1699623
SPC25	-18.10	NM_020675.3	ILMN_1814281
IGFBP2	-17.96	NM_000597.2	ILMN_1725193
NME2	-17.54	NM_001018138.1	ILMN_2234873
GCDH	-17.17	NM_013976.2	ILMN_1797482
PRSSL1	-17.04	NM_214710.2	ILMN_1673605
LOC643997	-17.04	XM_292963.6	ILMN_1679280
C21ORF58	-16.59	NM_199071.2	ILMN_2310296
HSPB7	-16.59	NM_014424.3	ILMN_2200836
PKMYT1	-16.30	NM_182687.1	ILMN_2401436
ADA	-16.28	NM_000022.2	ILMN_1803686
CDK5	-16.24	NM_004935.2	ILMN_1781987
CLEC11A	-16.22	NM_002975.2	ILMN_1807359
NT5DC2	-16.11	NM_022908.1	ILMN_1708743
MLC1	-15.74	NM_015166.3	ILMN_1751471
C14ORF149	-15.58	NM_144581.1	ILMN_2053281
LOC647074	-15.45	XM_930080.1	ILMN_1709891
EEF1B2	-15.31	NM_021121.3	ILMN_1675541

4.2.2 Functional analysis of the zVAD gene signature

The gene signature derived from MLL/AF4 depletion in combination with zVAD was investigated for functional aspects using the Ingenuity Pathway Analysis (IPA) software (Ingenuity Systems Inc.) as well as the GSEA software (<http://www.broadinstitute.org/gsea/index.jsp>); these analyses facilitated identification of potential pathways and biological networks disturbed in response to MLL/AF4 down-regulation in the presence of apoptosis inhibition.

4.2.2.1 Analysis of the zVAD signature using Ingenuity Pathway Analysis

For each time point the complete data set of differentially expressed probes was analysed independently.

At time point TP1, constituting of 1616 up-regulated and 1623 down-regulated probe sets, the affected networks involved cellular structure, gene expression, cell cycle, DNA repair and metabolic dysfunctions (tab. 4-7). In keeping with this, the most significantly associated molecular functions encompassed cell death, proliferation and development, as well as gene expression and lipid metabolism. Physiological functions linked with the signature were haematologic system development and haematopoiesis, as well as embryonic development and endocrine system function. Furthermore, disease-associated categories that correlated with the dataset included haematological diseases and cancer (tab. 4-8).

Tab. 4-7: Top 5 networks affected by the zVAD gene signature at TP1

Name	Score
Cellular Assembly and Organization, Cancer, Genetic Disorder	28
Gene Expression, RNA Trafficking, Cellular Assembly and Organization	25
Genetic Disorder, Metabolic Disease, Cardiovascular System Development and Function	22
DNA Replication, Recombination, and Repair, Gene Expression, Infection Mechanism	22
Cancer, Cell Cycle, Cellular Development	20

Due to data set size of over 3000 genes, pathway analysis revealed significant enrichment of >100 canonical pathways. Hence, only the top 20 signalling pathways were probed. These pathways could be summed up in 7 functional categories (fig. 4-12); the majority were associated with immunity/and or inflammatory response, particularly involving the tumour necrosis factor receptor superfamily (TNFRSF), and showed a net up-regulation. Conversely, mitogenic signalling, particularly involving the PI3K/AKT pathway, was down-regulated.

Tab. 4-8: Significantly enriched functional categories in the zVAD gene signature at TP1

Top 5 Biofunctions	P-value
Diseases and Disorders	
<i>Cancer</i>	4.06E-09 - 1.92E-02
<i>Haematological Disease</i>	5.26E-06 - 1.87E-02
<i>Gastrointestinal Disease</i>	7.02E-06 - 7.18E-03
<i>Genetic Disorder</i>	7.02E-06 - 1.92E-02
<i>Connective Tissue Disorders</i>	2.39E-05 - 1.10E-02
Molecular and Cellular Functions	
<i>Cell Death</i>	5.19E-11 - 1.99E-02
<i>Gene Expression</i>	1.25E-09 - 1.85E-02
<i>Cellular Growth and Proliferation</i>	7.07E-07 - 2.04E-02
<i>Cellular Development</i>	2.44E-06 - 2.03E-02
<i>Lipid Metabolism</i>	1.53E-05 - 1.45E-02
Physiological System Development and Function	
<i>Endocrine System Development and Function</i>	5.28E-05 - 5.28E-05
<i>Embryonic Development</i>	1.57E-04 - 1.10E-02
<i>Cardiovascular System Development and Function</i>	2.40E-04 - 1.99E-02
<i>Haematological System Development and Function</i>	2.55E-04 - 1.92E-02
<i>Haematopoiesis</i>	2.88E-04 - 1.92E-02

P-Value range describes the *p*-values of associated subcategories as determined by Fisher's exact test.

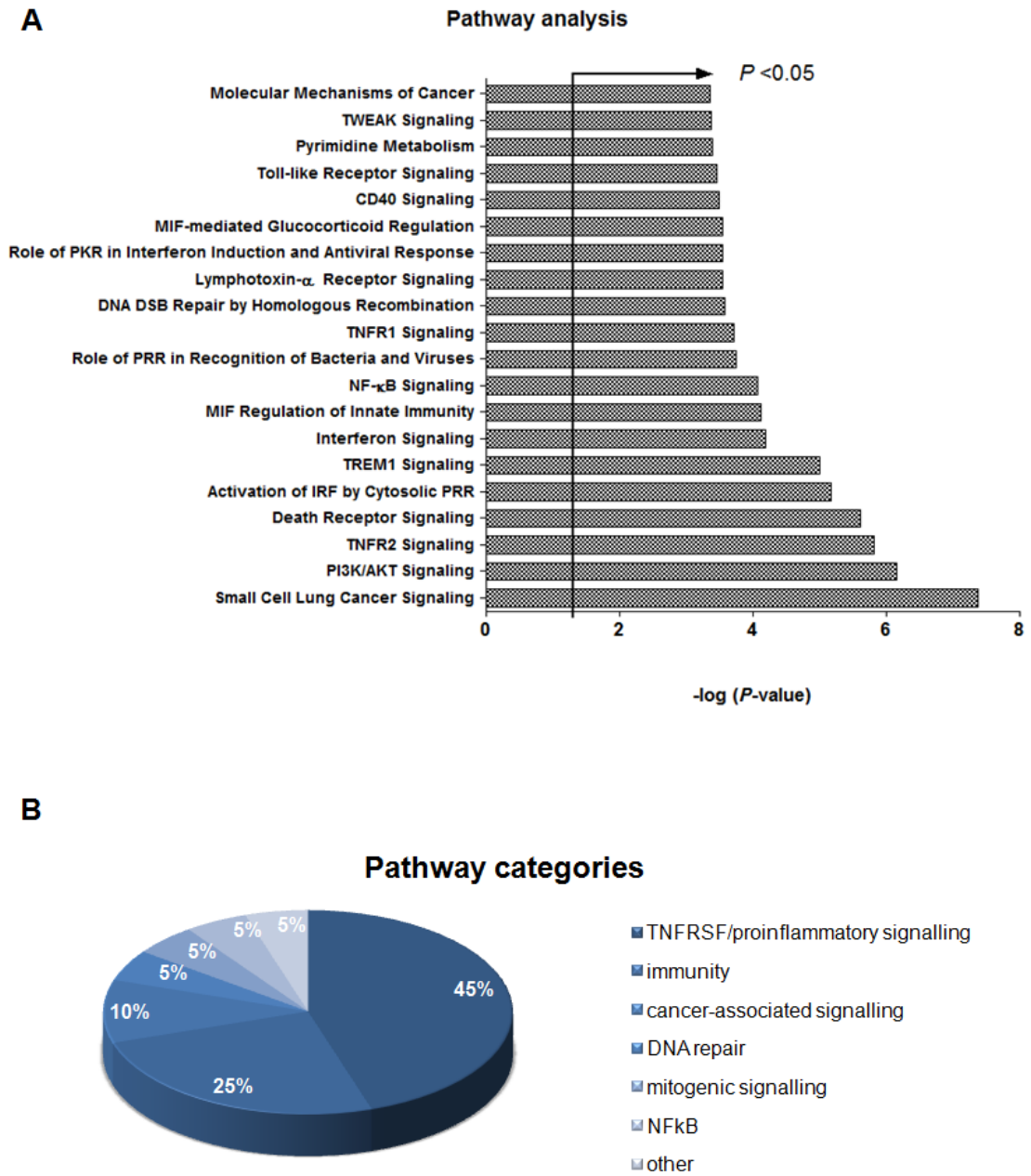


Fig. 4-12: Pathway analysis of the zVAD gene signature at TP1

Pathway analysis was performed using IPA Software (Ingenuity Inc.). At TP1, the top 20 significantly enriched canonical pathways (A) could be attributed to 7 functional categories mainly involving a proinflammatory response and related signalling cascades (B). Statistical significance was determined by Fisher's Exact test.

TNFR2 Signaling

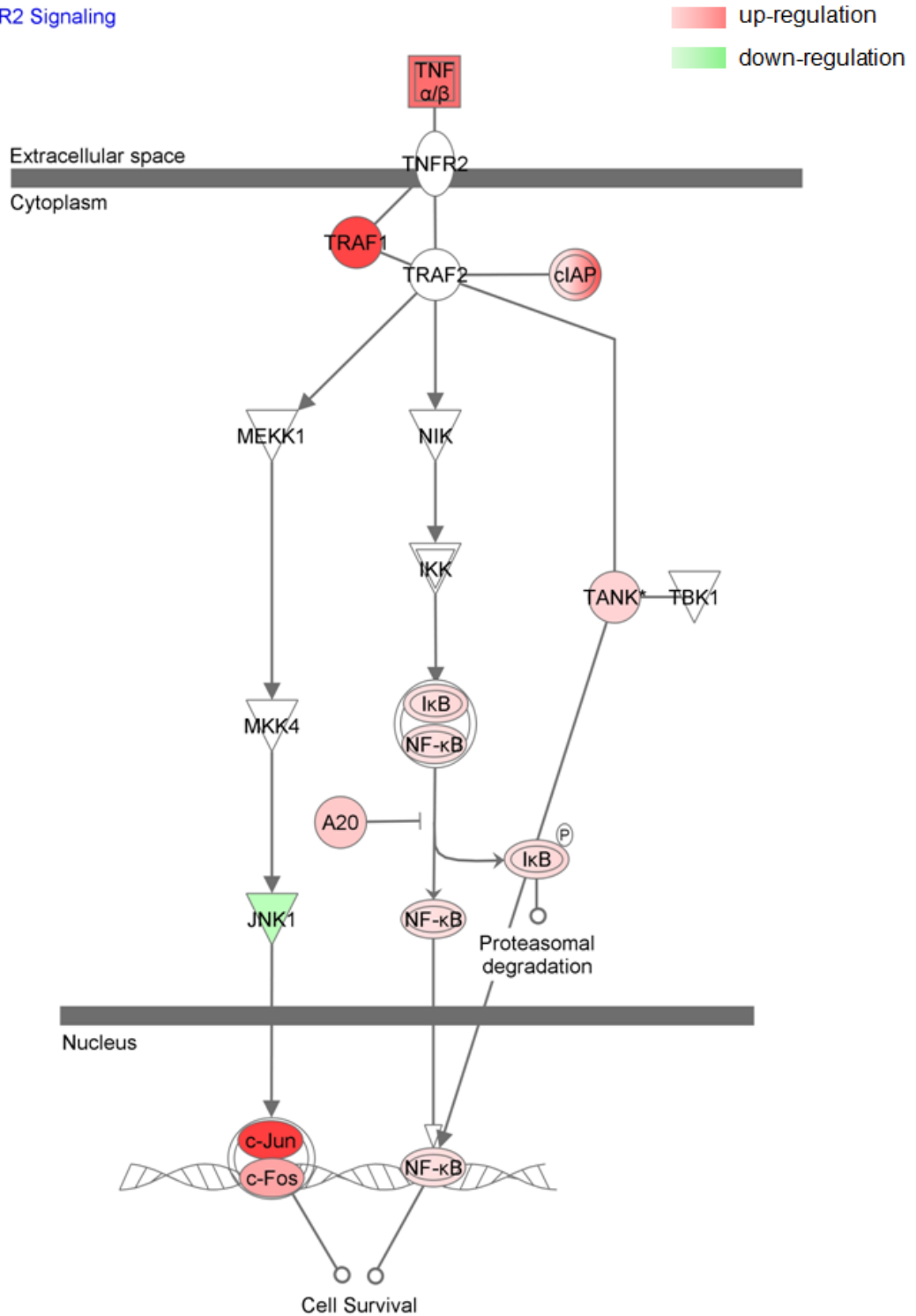


Fig. 4-13: The zVAD signature at TP1 reveals that MLL/AF4 depletion in presence of caspase inhibition results in up-regulation of part of the TNFR2 signalling machinery

Performing the same analysis for the zVAD signature at TP2 showed similar results as TP1; the most affected networks were associated with cell death, gene expression, cell cycle and DNA repair. In addition, differentially expressed genes at TP2 were part of the post-translational modification machinery (tab. 4-9). Concordantly, the zVAD signature was linked to the corresponding molecular functions, including cellular proliferation. Moreover, as seen at TP1, the main physiological functions connected with the zVAD signature at TP2 were haematologic system development and haematopoiesis, as well as embryonic development and endocrine system function, and the disease-associated categories included haematological diseases and cancer (tab. 4-10).

Tab. 4-9: Top 5 significantly enriched networks in the zVAD signature at TP2

Name	Score
Cell Death, Embryonic Development, Gene Expression	18
Gene Expression, Infection Mechanism, Tumour Morphology	18
Post-Translational Modification, Protein Folding, Lipid Metabolism	18
Cell Cycle, Cellular Compromise, Cancer	18
Cancer, DNA Replication, Recombination, and Repair, Cell Cycle	16

Cell Death, Embryonic Development, Gene Expression

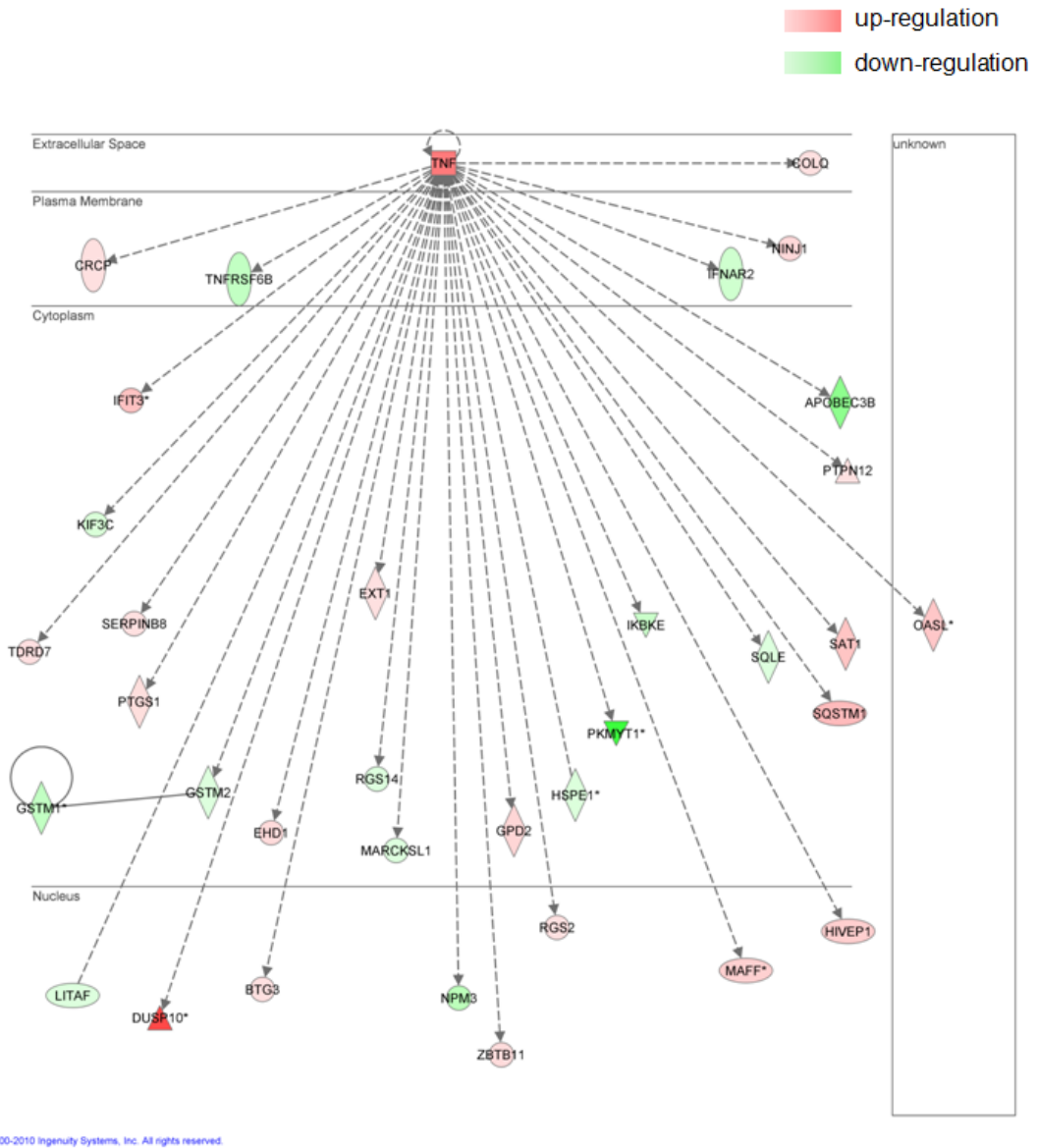


Fig. 4-15: Sustained MLL/AF4 depletion for 4 days (TP2) in presence of caspase inhibition affects functions associated with cellular death and gene expression

Gene Expression, Infection Mechanism, Tumour Morphology

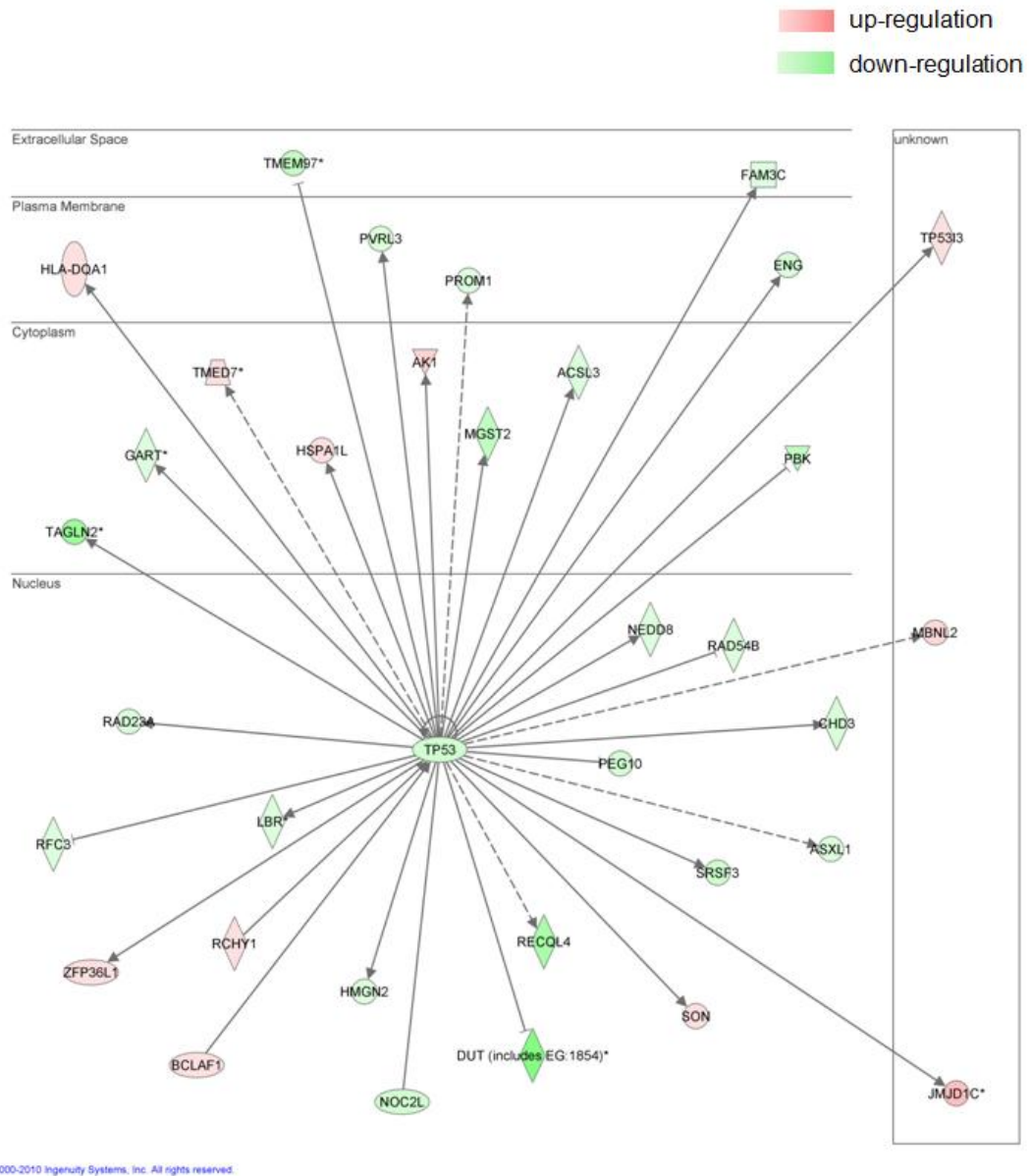


Fig. 4-16: Sustained MLL/AF4 depletion for 4 days (TP2) in presence of caspase inhibition affects functions associated with infectious processes, gene expression and tumour morphology.

Tab. 4-10: Significantly enriched functional categories in the zVAD gene signature at TP2

Top 5 Biofunctions	P-value
Diseases and Disorders	
<i>Cancer</i>	4.18E-11 - 1.81E-02
<i>Gastrointestinal Disease</i>	4.18E-11 - 1.54E-02
<i>Genetic Disorder</i>	4.18E-11 - 1.33E-02
<i>Haematological Disease</i>	1.01E-08 - 1.62E-02
<i>Immunological Disease</i>	1.01E-08 - 1.23E-02
Molecular and Cellular Functions	
<i>Cell Cycle</i>	2.42E-15 - 1.87E-02
<i>Cell Death</i>	4.26E-15 - 1.87E-02
<i>Gene Expression</i>	3.56E-13 - 1.87E-02
<i>Cellular Growth and Proliferation</i>	2.72E-08 - 1.63E-02
<i>DNA Replication, Recombination, and Repair</i>	2.12E-07 - 1.85E-02
Physiological System Development and Function	
<i>Haematological System Development and Function</i>	6.31E-04 - 1.66E-02
<i>Endocrine System Development and Function</i>	1.19E-03 - 1.19E-03
<i>Embryonic Development</i>	1.50E-03 - 1.33E-02
<i>Haematopoiesis</i>	2.10E-03 - 1.66E-02
<i>Tissue Morphology</i>	2.16E-03 - 3.23E-03

Similarly to TP1, pathway analysis for the differentially expressed probes at TP2 found >100 significantly affected pathways, which could be classified into comparable functional categories as for the earlier time point. Most of the pathways belonged to TNFRSF signalling cascades or mediated pro-inflammatory responses; in addition, the zVAD signature was associated with immunity-related pathways. All these three aspects showed considerable overlap in the molecules affected and cross-talk between the signalling pathways. The net effect indicated up-regulation of these pathways. Mitogenic

signalling involving the MAPK and PI3K/AKT pathway was perturbed as well, indicating a down-regulation.

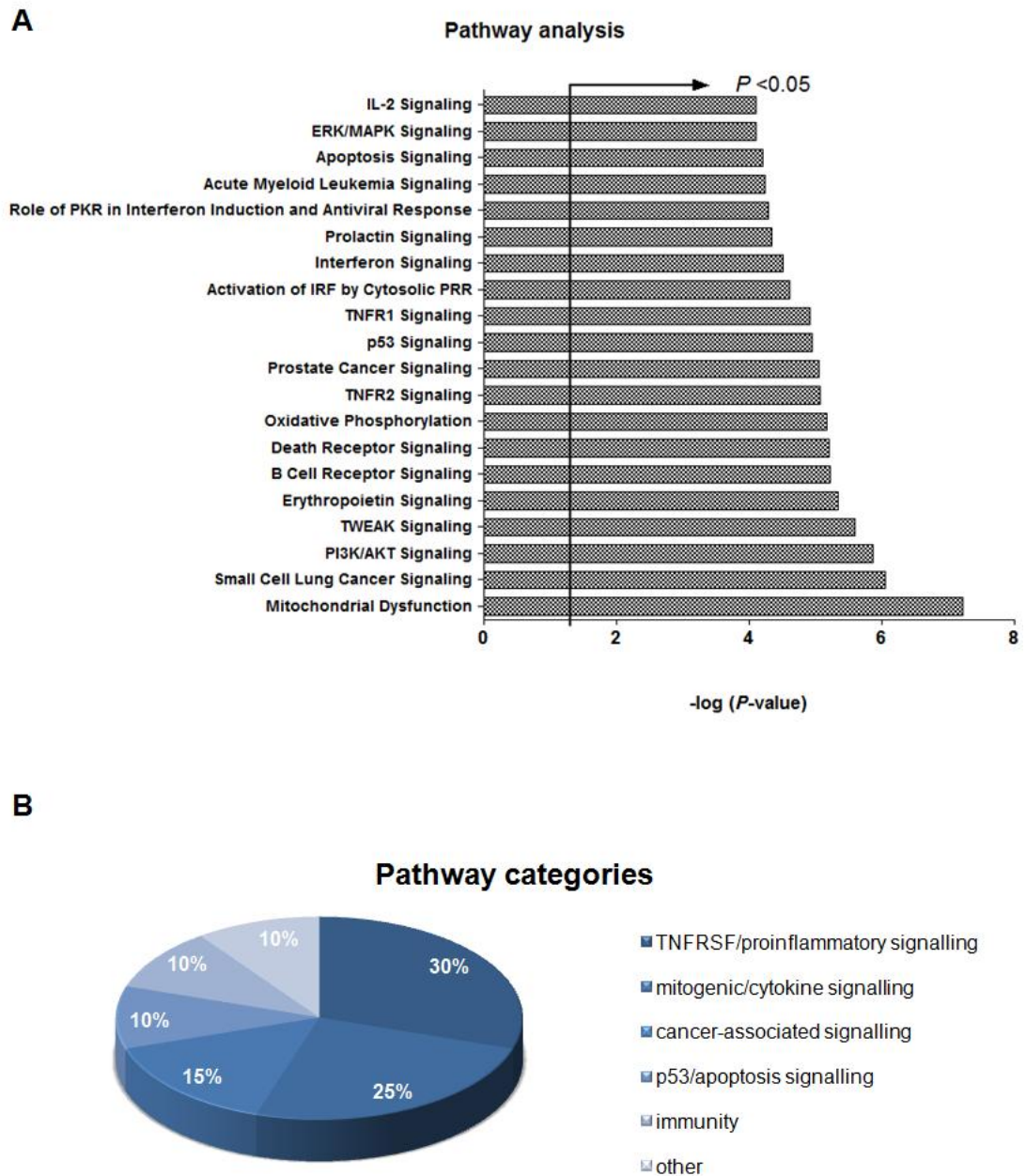


Fig. 4-17: Pathway analysis of the zVAD gene signature at TP2

Pathway analysis was performed using IPA Software (Ingenuity Inc.). At TP2, the top20 significantly enriched canonical pathways (A) could be attributed to 6 functional categories. As observed at TP1, there was an over-representation of pathways involved in inflammation and related signalling cascades (B). Statistical significance was determined by Fisher's Exact test.

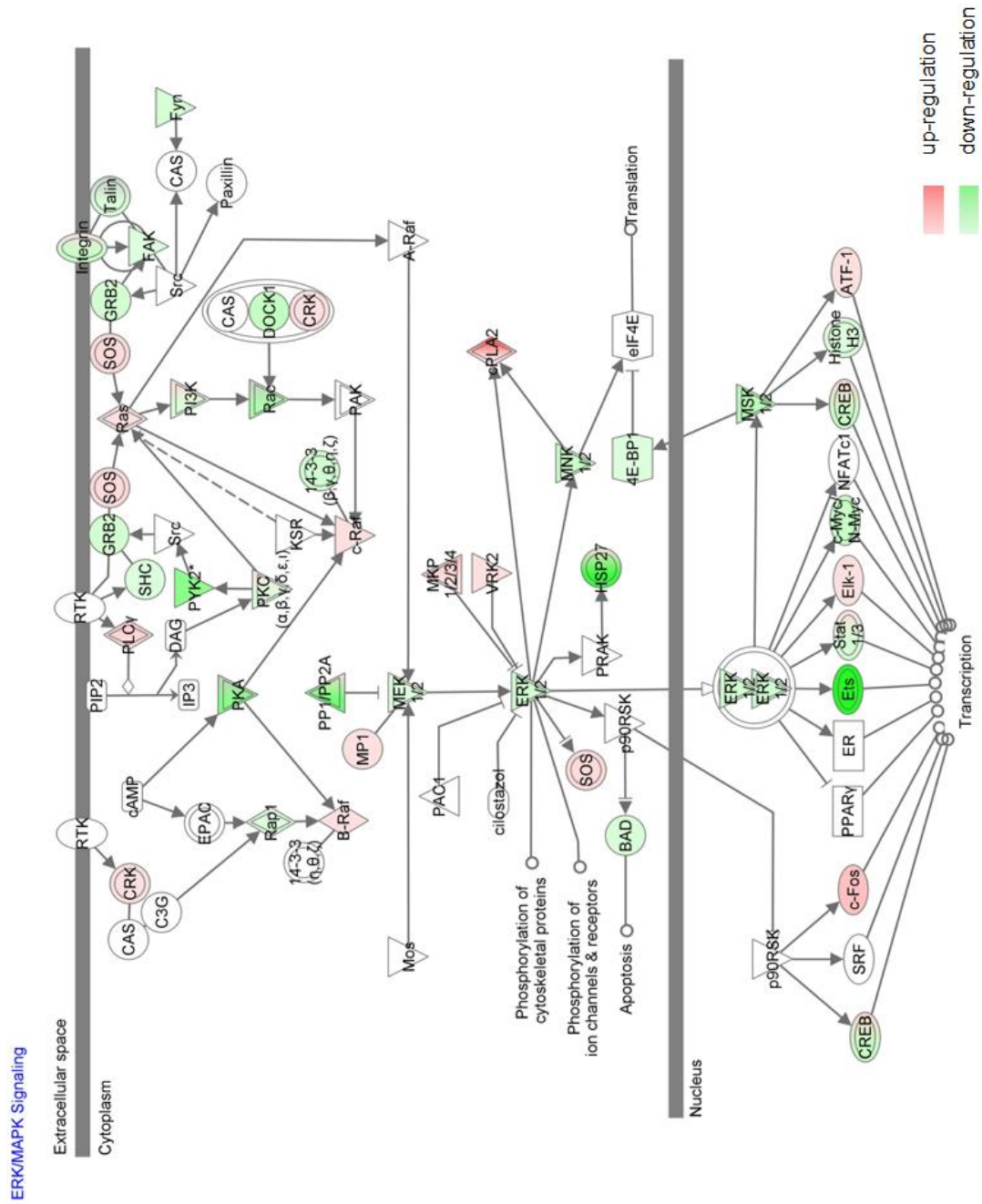


Fig. 4-18: The zVAD signature at TP2 reveals that MLL/AF4 depletion in presence of caspase inhibition perturbs ERK/MAPK pathways, down-regulating part of the mitogenic signalling machinery.

TNFR1 Signaling

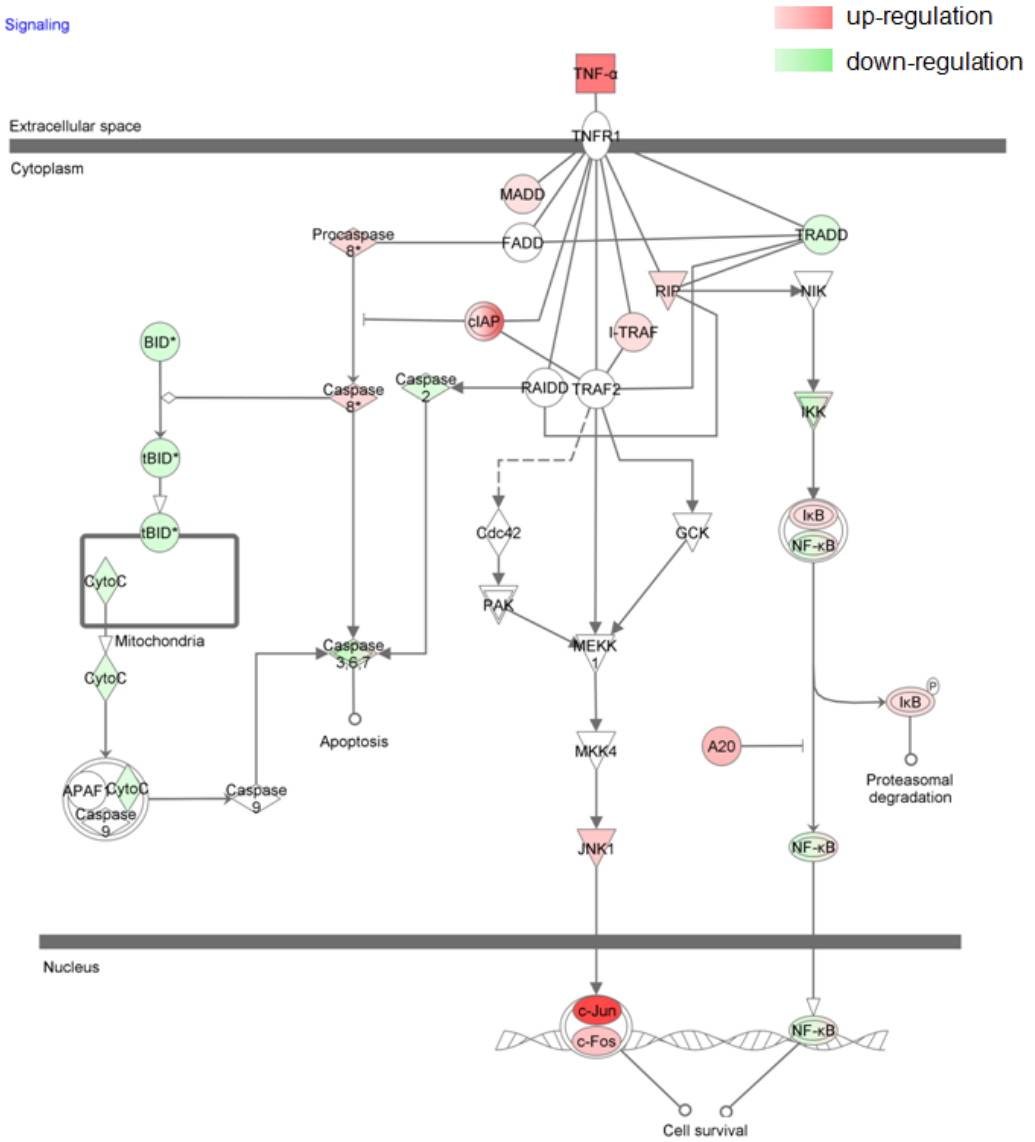


Fig. 4-19: Sustained MLL/AF4 depletion for 4d (TP2) in presence of zVAD up-regulates TNFR1 signalling mediators.

4.2.2.2 Gene Set Enrichment Analysis

The common motif of the zVAD signature at both time points indicated an activation of the TNFRSF signalling cascades, which are involved in mediating caspase-dependent and -independent cell death, a finding very much in line with the observed phenotype. In order to investigate this further, GSEA analysis on a curated expression data set, constituting of combined common up- and down-regulated genes at TP1 and TP2, was performed.

In order to identify the shared probe sets, comparison analysis of the zVAD signature at both time points was performed. There was an overlap of 2191 common differentially expressed probes at TP1 and TP2, however, when subdividing the probe set according to regulation, the overlap was smaller: 1111 induced and 1032 down-regulated probes were found to be present at both TP1 and TP2 (fig. 4-20). This difference of 79 probes resulted from ones with opposing regulation at both time points, i.e. up-regulated at TP1 while down-regulated at TP2, and vice versa. Using these 2143 overlapping probes, a curated data set was created, consisting of the normalised expression values of siMLL/AF4 and siCtrl at TP1 and TP2. GSEA analysis was performed according to section 2.7.6; 93 data sets were found to be significantly enriched when applying a false-discovery rate (FDR) cut-off of 25%, as proposed. The corresponding heat map of the top 50 differentially expressed genes at both time points (fig. 4-21) showed a high prevalence of pro-inflammatory genes, similar to the results described for tab. 4-3 to 4-5. Furthermore, in good concordance with the results obtained using IPA analysis, the zVAD signature showed positive correlation with gene sets linked to inflammation (fig. 4-22B) and immunity (fig. 4-22C), particularly involving TNFRSF signalling (fig. 4-22A, D), as well as cell death (fig. 4-23D), cellular stress response (fig. 4-23A), migration (fig. 4-23B) and cytokine signalling (fig. 4-23C). Moreover, the zVAD signature was enriched for target genes of the STAT5, CEBP/ β , CREB (fig. 4-24A-D), as well as the FOXO2, NF κ B and IRF transcription factors (fig. 4.-25)

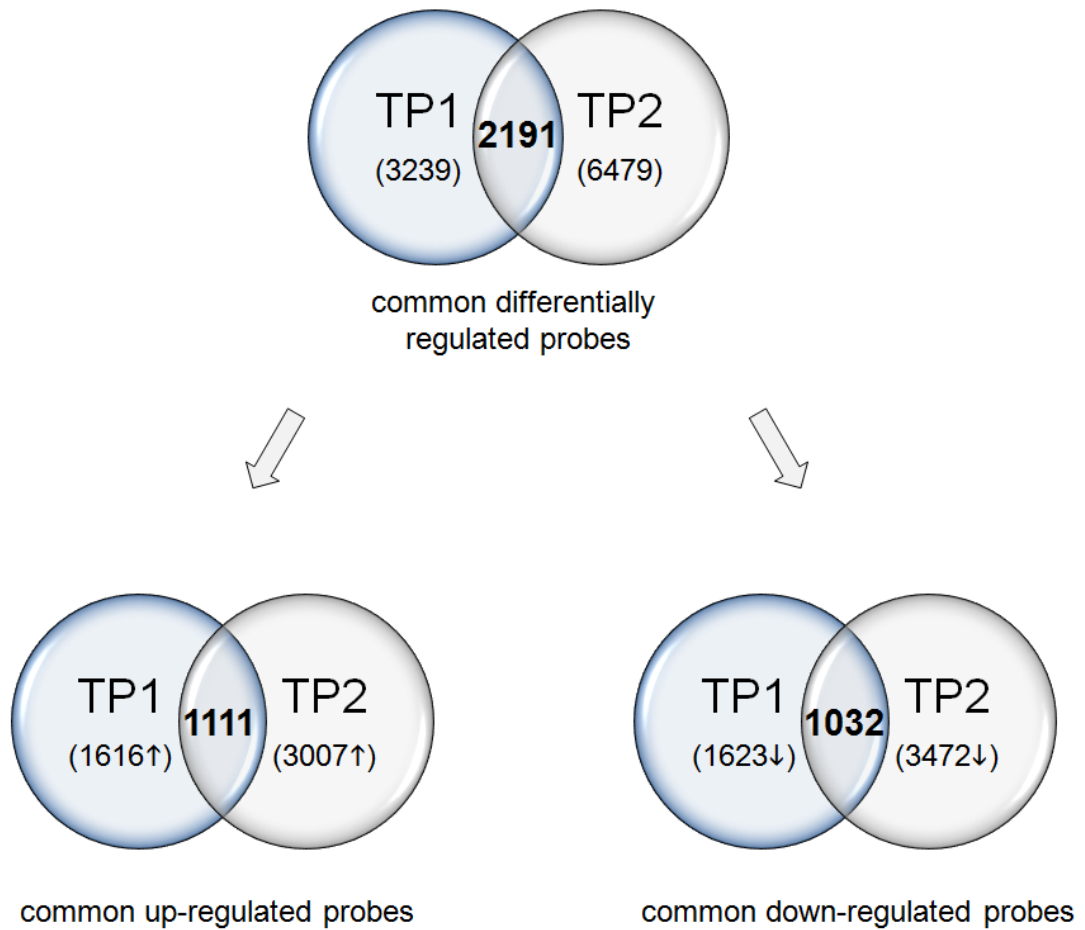


Fig. 4-20: Venn diagram of overlapping probes in the zVAD signature at both time points

Comparison analysis of the zVAD signatures at TP1 and TP2 share 2191 probes, which represents an overlap of 68% of the probe set at TP1. Correcting for an equal regulation, the zVAD signatures share 1111 up- and 1032 down-regulated probe sets, which corresponds to 69% and 64% of entities at TP1, respectively. Parentheses denote total numbers.

T(4;11)-positive Cells Display Oncogenic Addiction to MLL/AF4

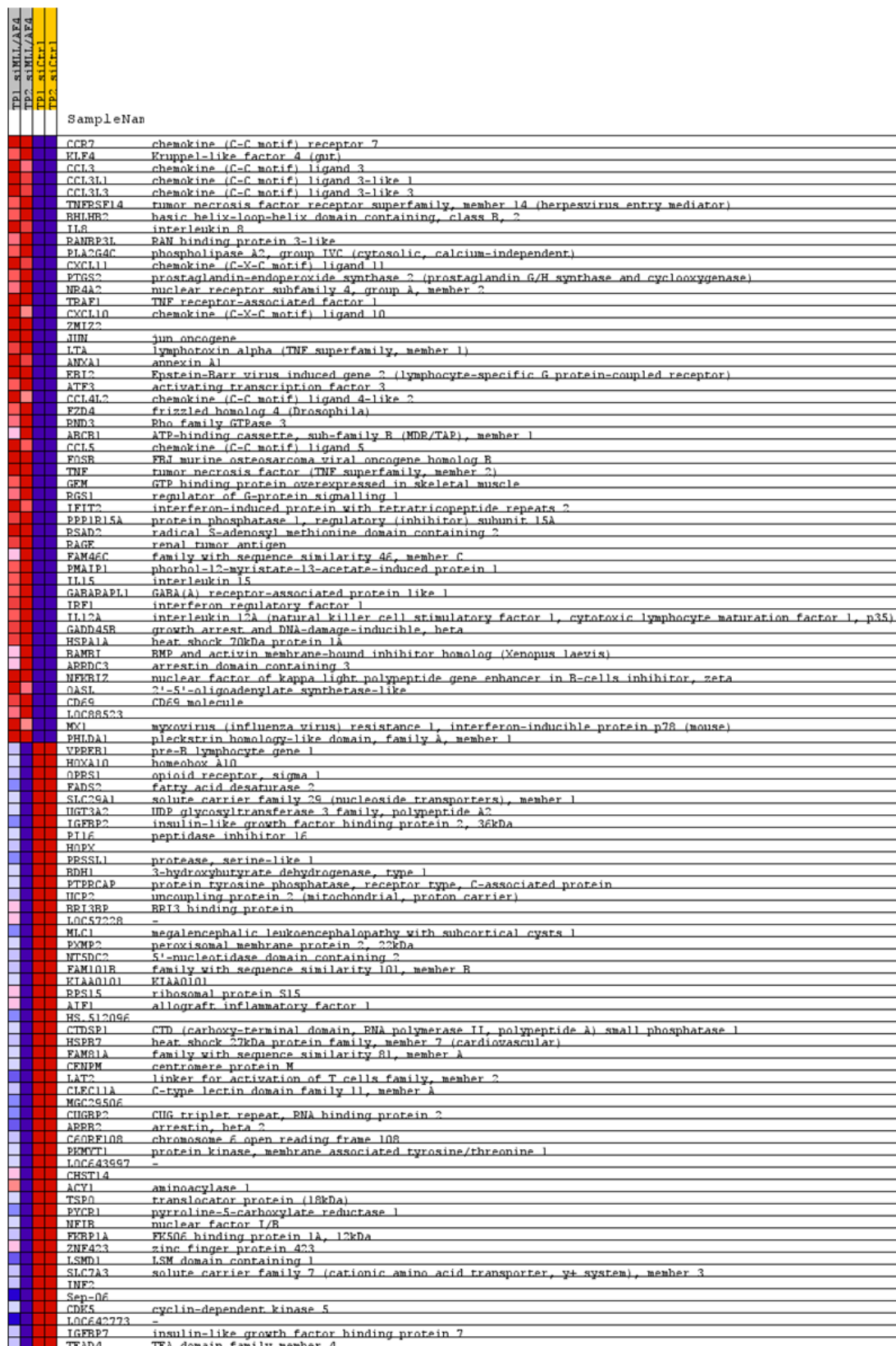


Fig. 4-21: Heat map of the top25 up- and down-regulated genes present at both queried time points of the zVAD signature

Heat map of a manually curated expression dataset consisting of common differentially-regulated genes at TP1 and TP2 was generated by the GSEA software.

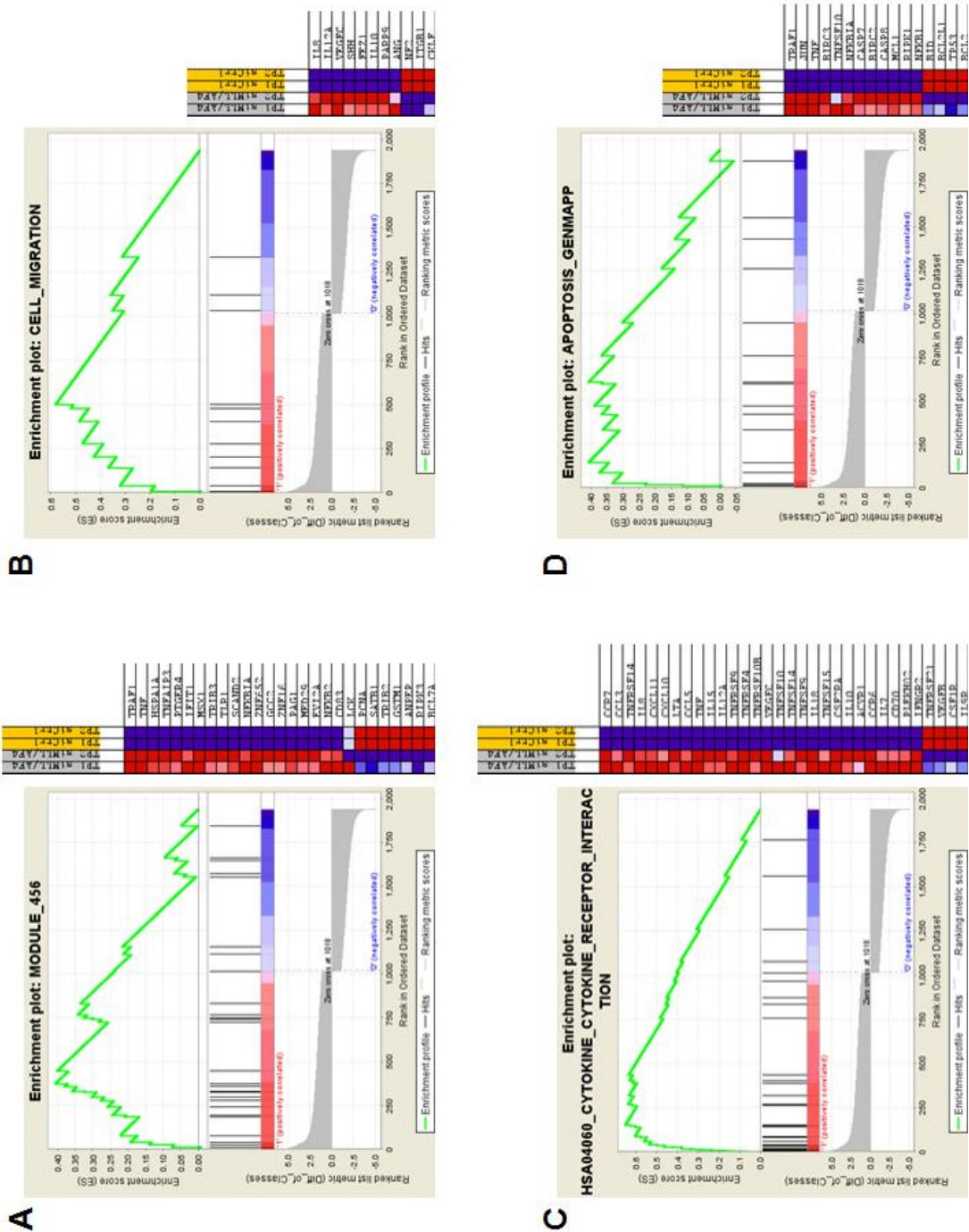


Fig. 4-23: The zVAD signature was significantly enriched for gene sets associated with cell death, cellular compromise, migration and cytokine signalling.

The combined zVAD signature showed positive correlation with data sets describing genes enriched for the GO terms describing cellular stress (A) and cell migration (B), as well as showing overlap with genes associated with the canonical apoptosis pathway (D). In addition, the zVAD signature was enriched for cytokines and their receptors (C) All data sets had a nominal p -value of $p < 0.05$, and an adjusted p -value of $p < 0.25$.

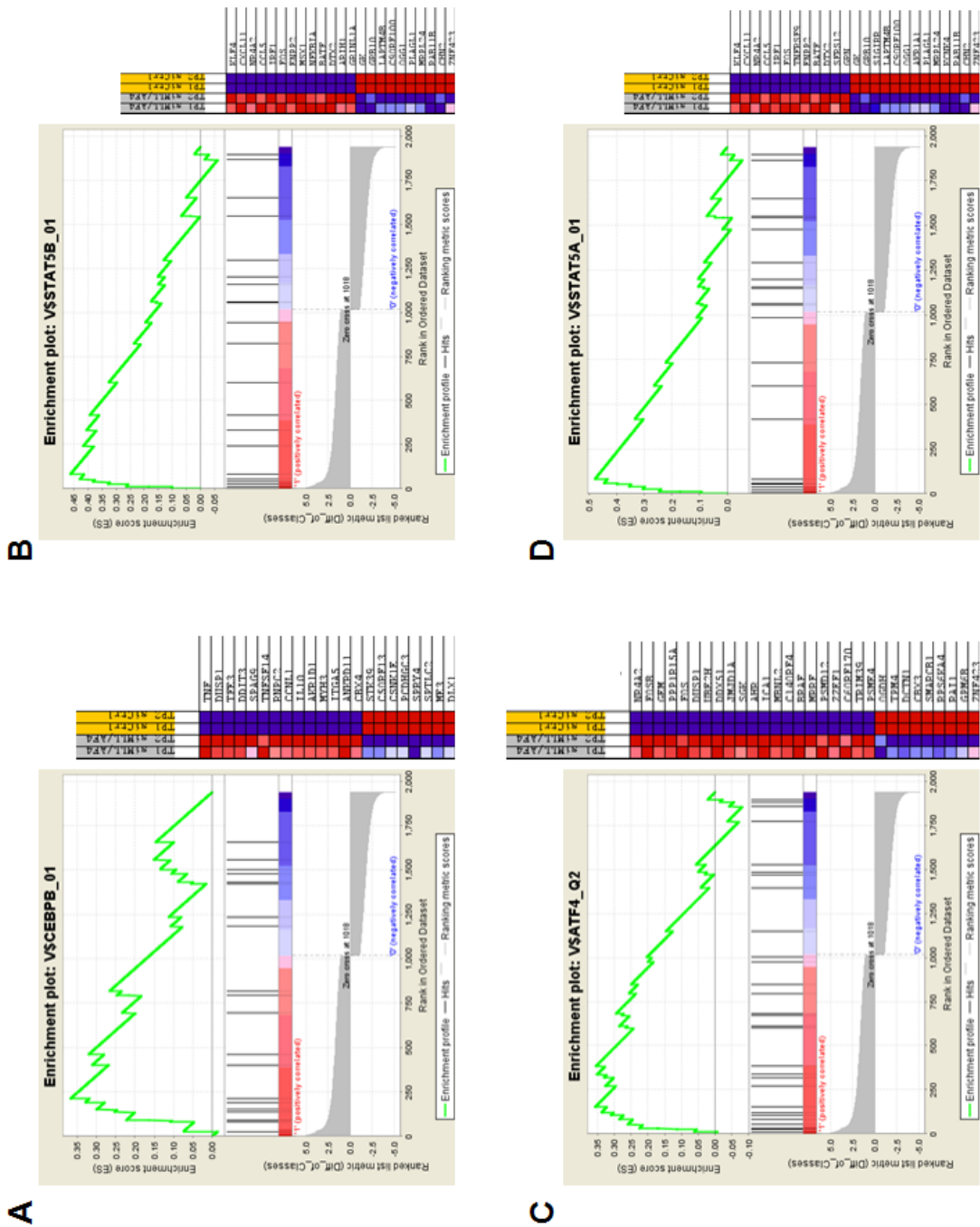
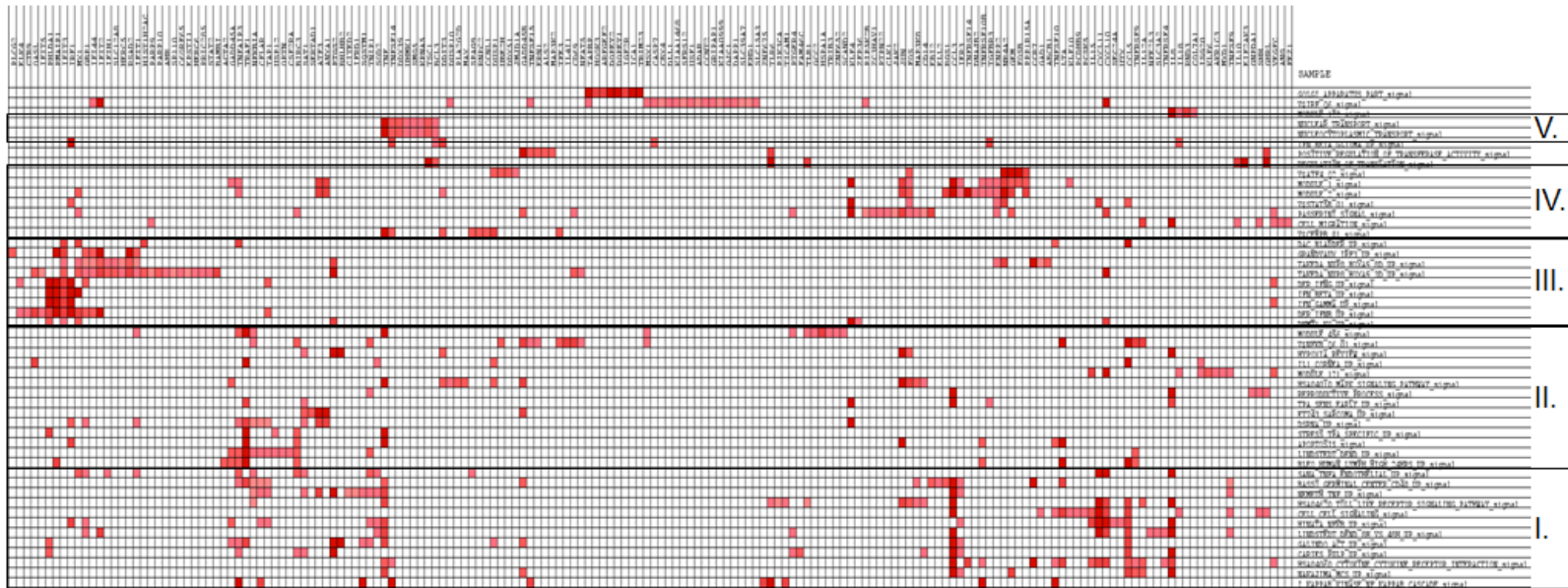


Fig. 4-24: The zVAD signature was significantly enriched for specific transcription factor target genes.

The zVAD signature comprised several with the promoter regions containing motifs annotated for C/EBP β (A), CREB-2 (C) and the STAT5 α/β transcription factors (B, D). All data sets had a nominal p -value of $p < 0.05$, and an adjusted p -value of $p < 0.25$.



SANA_TNEA_ENDOTHELIAL_UP_signal
 BASSO_GERMINAL_CENTER_CD40_UP_signal
 NEMETH_TNF_UP_signal
 HSA04650_TOLL_LIKE_RECEPTOR_SIGNALING_PATHWAY_signal
 CELL_CELL_SIGNALING_signal
 HINATA_NFEB_UP_signal
 IINDSTEDT_DEND_2H_VS_48H_UP_signal
 GALINDO_ACT_UP_signal
 CABIES_EHLF_UP_signal
 HSA04070_CYTOKINE_CYTOKINE_RECEPTOR_INTERACTION_signal
 NAKAJIMA_MCS_UP_signal
 I_KAPPA_KINASE_NF_KAPPA_CASCADE_signal

I.

MODULF_45E_signal
 V6NEFR_06_B1_signal
 HYPOXIA_REVIEW_signal
 ILL_CORNEA_UP_signal
 MODULF_12J_signal
 HSA04010_MAPK_SIGNALING_PATHWAY_signal
 REPRODUCTIVE_PROCESS_signal
 TEA_SENS_EARLY_UP_signal
 FT243_SARCOMA_UP_signal
 DSENA_UP_signal
 STRESS_TEA_SPECIFIC_UP_signal
 APOPTOSIS_signal
 IINDSTEDT_DEND_UP_signal
 BLEO_HUMAN_LYMPH_HIGH_24HRS_UP_signal

II.

V6NEFR_06_B1_signal
 DAC_BLADEE_UP_signal
 GRANDVAUX_IEF3_UP_signal
 TAKEEDA_MUPB_HOXA9_3D_UP_signal
 TAKEEDA_MUPB_HOXA9_3D_UP_signal
 DER_IENG_UP_signal
 IEF1_BETA_UP_signal
 IEF1_GAMMA_UP_signal
 DER_IENG_UP_signal

III.

REPRODUCTIVE_PROCESS_signal
 V6ATP4_Q2_signal
 MODULF_1_signal
 MODULF_2_signal
 V6STAT5B_01_signal
 PASSEFINI_SIGNAL_signal
 CELL_MIGRATION_signal

VI.

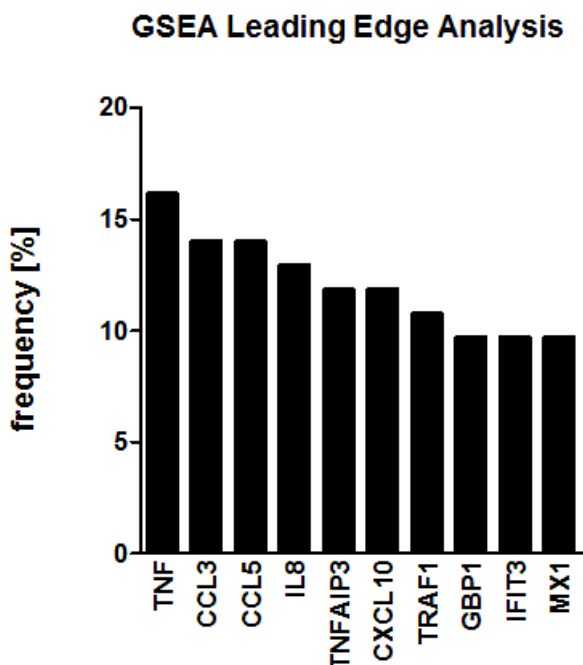
NUCLEAR_TRANSPORT_signal
 NUCLEOCYTOPLASMIC_TRANSPORT_signal

V.

Fig. 4-27: Hierarchical clustering of the leading edge gene subsets

Hierarchical clustering of the leading edge genes with the gene sets showed formation of five signatures where particular entities had an increased incidence. These clusters represented gene sets associated with inflammatory mechanisms, such as TNFRSF-, NF κ B- and TLR signalling (I.), cell death, cellular stress and DNA damage response (II.) and interferon response (III.). Furthermore, one cluster included genes associated with cell adhesion and extracellular matrix components, as well as the CREB pathway (IV.), and another cluster was linked to nuclear transport (V.)

Since most of the enriched gene sets were in one way or the other associated with inflammatory response, it was unsurprising that examination of the incidence of individual factors across all gene sets revealed inflammatory mediators to be over-represented in the top 10 most frequent genes (fig. 4-28), with TNF being the most frequent one, being part of 17% of the analysed datasets.

**Fig. 4-28: Incidence of the top 10 most frequent leading edge genes**

Leading edge analysis of the core subset of the 93 significantly enriched gene sets showed an over-representation of pro-inflammatory cytokines.

4.2.3 Comparison of the zVAD signature with the MLL/AF4 signature

The zVAD signature showed a high incidence of genes involved in immune response and inflammation, as well as genes implicated in haematopoietic development. In order to remove bystander effects resulting from zVAD treatment, the zVAD dataset was compared to the MLL/AF4 signature, which represents the corresponding vehicle control. At TP1, there was a 23% overlap of up-regulated probes between both expression sets; similarly, 24% of the down-regulated probes coincided (A). At TP2, the intersection of both signatures showed 37% up- and 33% down-regulated probes shared in common (B). This could be further distilled into a core signature of 64 probes representing 61 genes, which were differentially expressed in all signatures and time points (fig. 4-29).

Interestingly, this core signature showed a similar enrichment for pro-inflammatory and haematopoietic development mediators. Amongst the induced probes, there were several factors associated with inflammation, such as the interferon-induced genes *IFIT2*, *IFIT3* and *IFI44*, as well as the nucleotide pyrophosphatase *ENPP2* and the MAP kinase kinase *TPL2* (*MAP3K8*) which plays an important role in TNF-, TLR- and NFkB-mediated ERK signalling²⁷⁴⁻²⁷⁸. Of note is the induction of *ANXA1*, which, as previously described in section 3., acts both pro-apoptotic and as a potent modulator of inflammation and the NFkB pathways. Furthermore, both the pro-apoptotic BH3-family member *NOXA* (*PMAIP1*) which is up-regulated in response to intracellular reactive oxygen species (ROS), and the glutamate-cysteine ligase *GCLM*, a key enzyme in glutathione synthesis²⁷⁹, were induced, suggesting the activation of the cellular oxidative stress response. The up-regulation of the transcription factors *KLF2* and *NURR1* (*NR4A2*), which regulate pleiotropic functions in differentiation²⁸⁰⁻²⁸¹, inflammation²⁸²⁻²⁸³, cell death²⁸⁴⁻²⁸⁵ and tumourigenesis²⁸⁶⁻²⁸⁸ in a cell-type-dependent manner is in good concordance with the phenotype observed and might indicate a potential regulatory network.

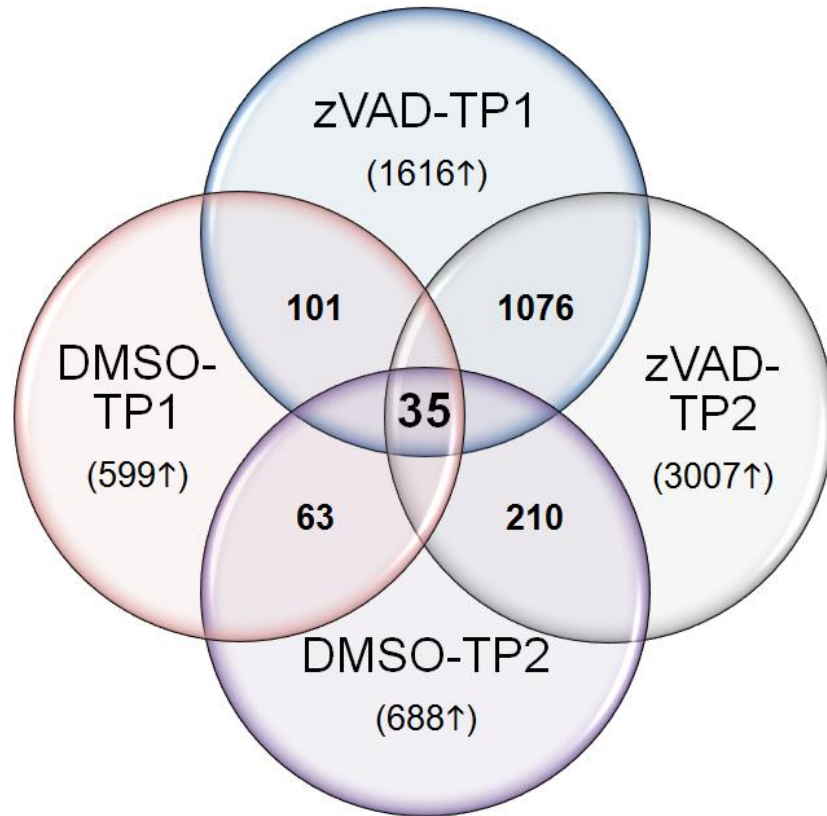
Additionally, the signature also included the autophagy marker *GABARAPL1* and several factors of the ubiquitin-proteasome system, such as the E3 ligases

FBXO32 and *FBXO15*, and showed induction of several haematopoietic maturation markers (*CD68*, *FCRLA*). In contrast, the down-regulated core signature comprised several haematopoietic stem/progenitor cell markers (HSPCs), such as *HOXA10* and *SPN1* (*CD43*). Other genes showing reduced expression were the epigenetic cofactors *SMARCC2*, a component of the SWI/SNF complex⁸⁶, and *PYGO2*, which has also been implicated as part of the WNT transcription factor machinery²²⁰. One transcription factor was part of this signature, *MAZ*, which has recently been linked to tumour progression and metastases in breast cancer, as well as modulator of *K-RAS* expression²⁸⁹.

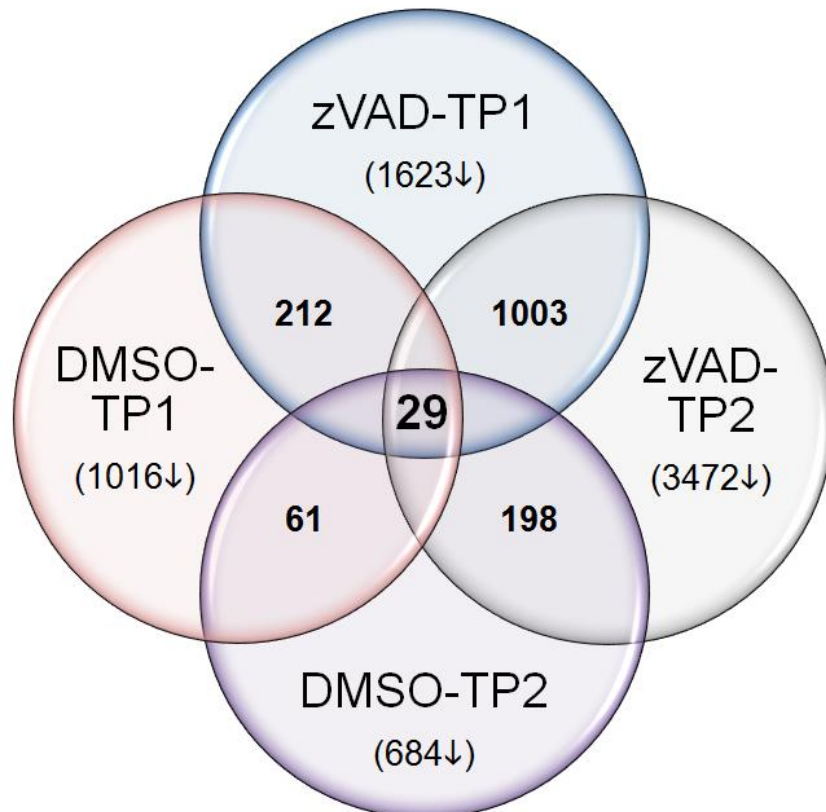
Fig. 4-29: Venn diagram depicting shared probe sets between the zVAD and the MLL/AF4 signature at both time points queried.

Comparison analysis showed that the zVAD and MLL/AF4 signatures had 134 up-regulated probe sets in common at TP1, and 245 at TP2. At all time points and conditions, there were 35 probes that showed induction in siMLL/AF4 treated SEM cells compared to Ctrl, corresponding to an overlap of 23, 36 and 6 % (A). When comparing the down-regulated probes, it was found that both signatures share 241 probes at TP1 and 237 probes at TP2, which represents an overlap of 35%. Comparing all time points and conditions, 29 down-regulated entities were shared, representing an overlap of 4% (B). Parentheses denote total numbers.

A



B



T(4;11)-positive Cells Display Oncogenic Addiction to MLL/AF4

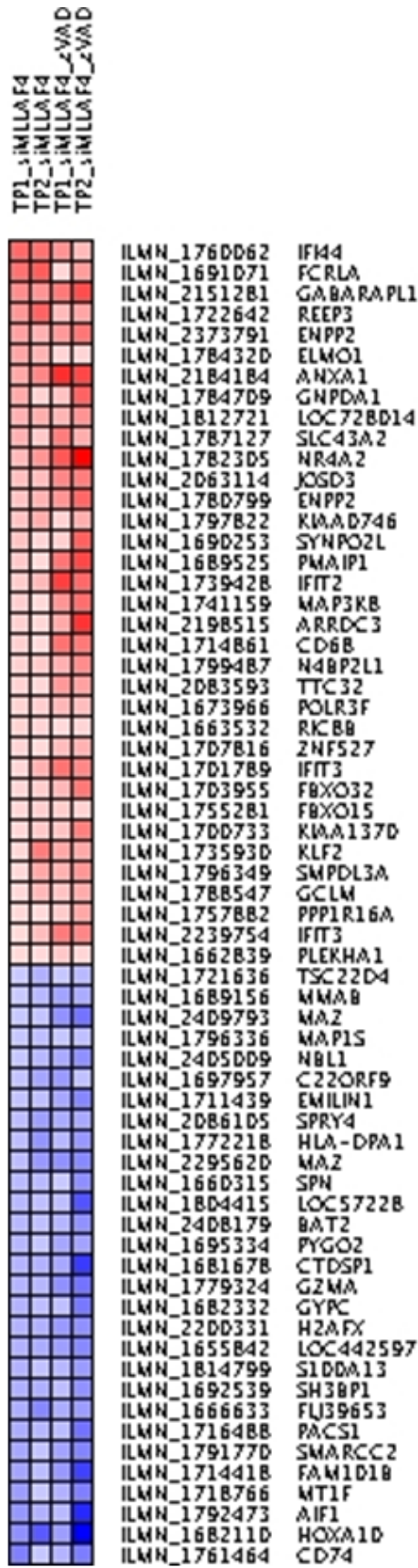


Fig. 4-30: Heat map of a core signature of probes differentially expressed in siMLL/AF4-electroporated SEM cells with or without zVAD at both time points TP1 and TP2

Overlap analyses of the MLL/AF4 and zVAD expression arrays at TP1 and TP2 revealed a core signature consisting of 63 shared probes showing the same regulation at all time points queried. The core probe set consisted of 35 up- and 29 down-regulated probes with a linear fold change (FC) cut-off of 2.0. The FC scale represented in this heat map is \log_2 -transformed; a FC of 1 represents a linear FC of 2. The graph was generated using the HeatmapImage module of the Genepattern software.

Interestingly, only 3 of these 61 genes were found to be direct MLL/AF4 target genes when compared to the Guenther data set (*HOXA10*, *SPN*, *REEP3*), corresponding to an overlap of 5%. Analysing the probe sets shared at TP1 by both the MLL/AF4 and the zVAD signature showed the presence of 7 MLL/AF4 target genes mapped by 9 probes, which falls below a potential FDR of 5%, as well. At TP2, there are 11 probes overlapping. Combining these two data sets of overlapping probes resulted in a shared signature of 14 genes. Analysis of the expression arrays showed that in all conditions and at both time points these genes showed the same regulation, albeit often at TP1 to a reduced extent, so that it did not pass the differential expression fold-change cut-off of 2.0. Conversely, in some cases, at TP2 the down-regulation of these genes was so potent that the associated probes flagged up as marginally expressed or had absent calls (tab. 4-11).

Most of the MLL/AF4 target genes are down-regulated in response to siMLL/AF4 treatment, with the exception of *REEP3* (*receptor accessory protein 3*), *PTGER4* (*prostaglandin receptor E 4*) and *JMJ1DC*, which are consistently up-regulated in MLL/AF4 depleted SEM cells (tab. 4-11). *REEP3* represents together with five other REEP proteins (*REEP1-6*) the human orthologues of the yeast gene *Yop1p*, a putative regulator of vesicle trafficking also implicated in cell growth and viability, as it has been shown to induce cell death upon overexpression²⁹⁰, a function very much in agreement with the accompanying cellular phenotype. *PTGER4* action seems to be cell context dependent, as it has been linked to tumour cell proliferation and metastases in a variety of solid cancers, but reportedly acts as a tumour suppressor in B-cell lymphoma. The induction of the histone demethylase *JMJD1C* is counterintuitive, as it is expressed in HSCs, embryonic stem cells and in a variety of tumours, as well as being up-regulated in t(4;11)-positive patient cells.

Tab. 4-11: MLL/AF4 target genes differentially regulated in both the MLL/AF4 and zVAD signature at all time points

MLL/AF4 target genes	Probe_ID	Fold-change				Accession
		TP1	TP2	TP1(+zVAD)	TP2(+zVAD)	
CLEC9A	ILMN_1673238	-3.46	-2.64		-2.04	NM_207345.2
FMNL2	ILMN_1730491	-2.16	-2.20		-2.71	NM_052905.3
HOXA10	ILMN_1682110	-5.23	-12.55	-4.16	-54.26	NM_018951.3
	ILMN_1689336	-2.99	-2.08	-1.77	-3.50	NM_018951.3
IGF1R	ILMN_1675048	-1.36	-2.77	-1.41	-2.98	NM_000875.2
JMJD1C	ILMN_1677589		13.65		6.74	NM_032776.1
PROM1	ILMN_1786720		-2.88	-1.99	-2.07	NM_006017.1
PRSS12	ILMN_1672720		-2.07	-1.87	-2.47	NM_003619.2
PTGER4	ILMN_1795930	1.38	2.04	3.25	6.42	NM_000958.2
REEP3	ILMN_1722642	5.12	10.49	3.17	4.18	NM_001001330.1
SPN	ILMN_1801040	-2.81		-2.05	-4.47	NM_001030288.1
	ILMN_1658017	-2.11		-2.30	-2.66	NM_001030288.1
	ILMN_1660315	-2.62	-2.62	-2.02	-5.19	NM_003123.3
DUSP6	ILMN_1677466	-2.70	<u>P->M</u>	-2.34		NM_001946.2
	ILMN_2396020	-3.98	-3.78			NM_022652.2
CLECL1	ILMN_1782729	-2.18		-2.17	-2.35	NM_172004.2
CACNB4	ILMN_2257652	-2.48	<u>P->A</u>	-3.60	-4.00	NM_001005746.1
BCL7A	ILMN_1706886	-2.23		-2.26	-2.36	NM_001024808.1
	ILMN_2378081	-2.92	-1.64	-3.31	-9.96	NM_001024808.1

Bold font represents up-regulated genes, italics indicate that the fold-change (FC) falls below the cut-off of 2.00 but is above 1.3

P->M and P->A denote such a strong down-regulation, that the probes in these siMLL/AF4-treated cells go from present (P) to marginal (M) or absent (A)

4.3 THE zVAD SIGNATURE COMPRISES KEY FACTORS OF THE NOVEL PROGRAMMED CELL PATHWAY NECROPTOSIS

The results from the pathway analyses performed with the IPA and GSEA software suggest a major role for TNFRSF and TLR signalling in mediating the observed phenotype in siMLL/AF4-zVAD treated SEM cells. Indeed, TNF has long been firmly established as a regulator of both apoptotic and necrotic/caspase-independent cell death. Recently, an increasing body of evidence have uncovered a novel programmed cell death pathway, termed necroptosis, which integrates aspects of TNF and TLR signalling, autophagy and a unique downstream mediator machinery involving CYLD, BMF, PARP2 and JUN, amongst others²⁹¹.

Analysing the siMLL/AF4 arrays at TP1 and TP2 with and without zVAD showed that specifically within the zVAD signature key genes implicated with the necroptotic machinery were affected, while on the other hand these genes showed no or less differential expression in the corresponding DMSO groups (tab. 4-12).

Taking these finding into account, it seemed probable that the underlying mechanism for the caspase-independent cell death induction in siMLL/AF4-zVAD SEM cells was linked to the necroptotic signalling pathway. In order to test this hypothesis, the array results were validated both on expression level, as well as investigated functionally.

Tab. 4-12: Differential expression of necroptosis-associated genes is majorly restricted to the zVAD signature

Gene Symbol	Probe_ID	TP1	Fold-change		
			TP2	TP1(+zVAD)	TP2(+zVAD)
ATP6V1G2	ILMN_1654541	-	-	-	2.23
CD40	ILMN_1779257	-	-2.74	3.32	-
COMMD4	ILMN_33223	-	-	-	-3.17
CYLD	ILMN_1775508	-	3.03	2.96	2.91
GRB2	ILMN_1742521	-	-	-2.44	-3.72
JPH3	ILMN_26563	-	-	2.38	-
JUN	ILMN_1806023	-	2.29	19.57	19.26
LC3B	ILMN_1703244	-	-	2.00	4.32
PARP2	ILMN_1757995	-	-	-	3.25
RIPK1	ILMN_2119535	-	-	2.00	3.62
RIPK3	ILMN_1763763	-	-	-4.09	-4.13
RIPK5	ILMN_2352023	-	2.06	2.15	2.77
RIPK5	ILMN_1779600	3.02	-	-	2.12
SPATA2	ILMN_1681135	-	-	-	2.90
TMEM57	ILMN_1718831	-	-	2.09	-
TNF	ILMN_1728106	-	-	14.72	14.04
TNFAIPL8L1	ILMN_1684346	-5.20	-	3.73	-

First, it was ascertained whether the t(4;11)-positive ALL cell lines SEM and RS4;11 possessed the intrinsic machinery to mediate necroptotic signalling. With TNFR1 being one the key receptors implicated, the expression of both TNFR1 and its close homologue TNFR2, another important mediator of TNF signalling, was confirmed by flow cytometry on the cell surface of both cell lines analysed. Interestingly, TNFR2 was expressed at a higher level than TNFR1 in the SEM cell line, while both receptors showed a comparable copy number on the surface of the RS4;11 cell line (fig. 4-31).

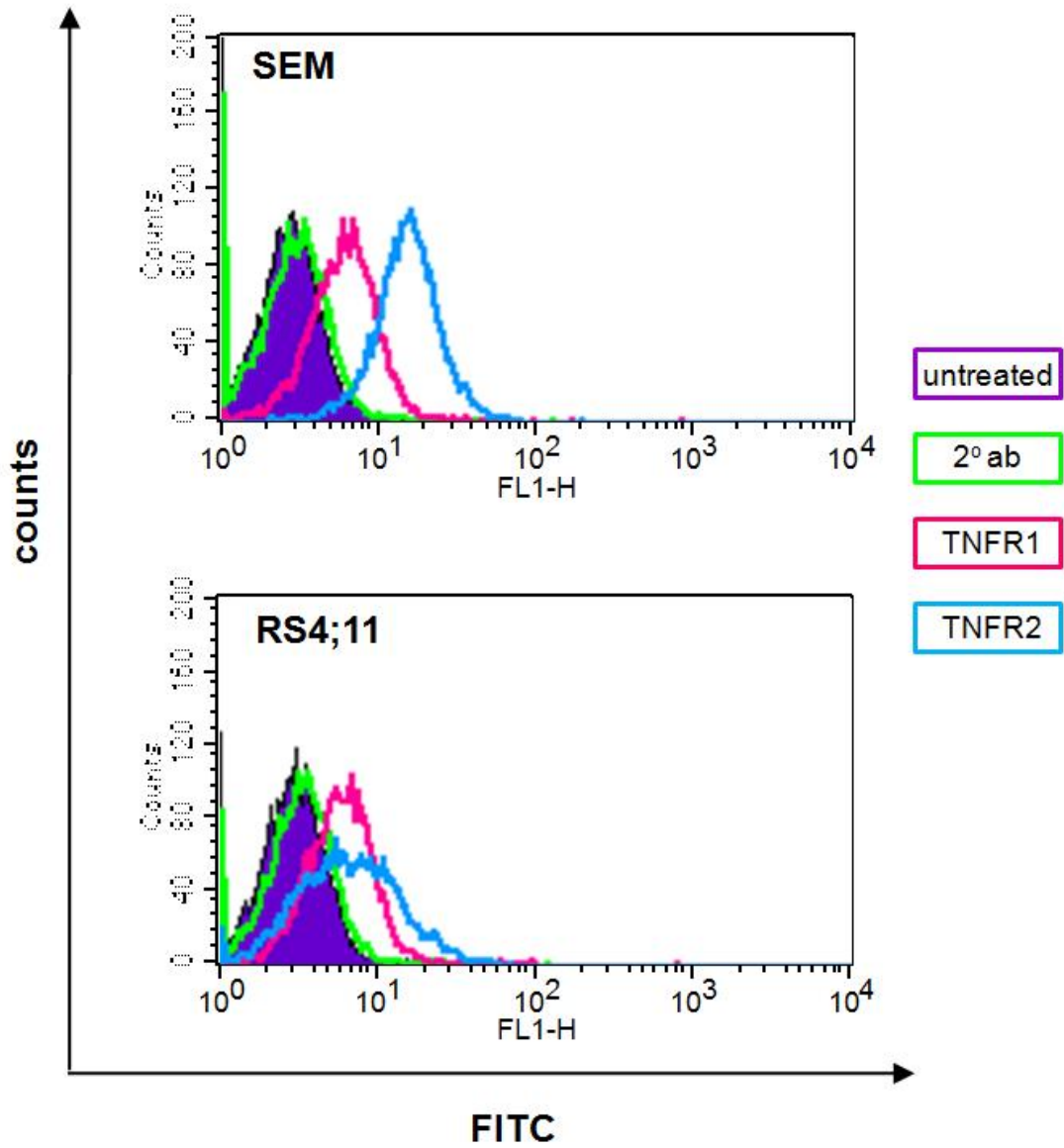


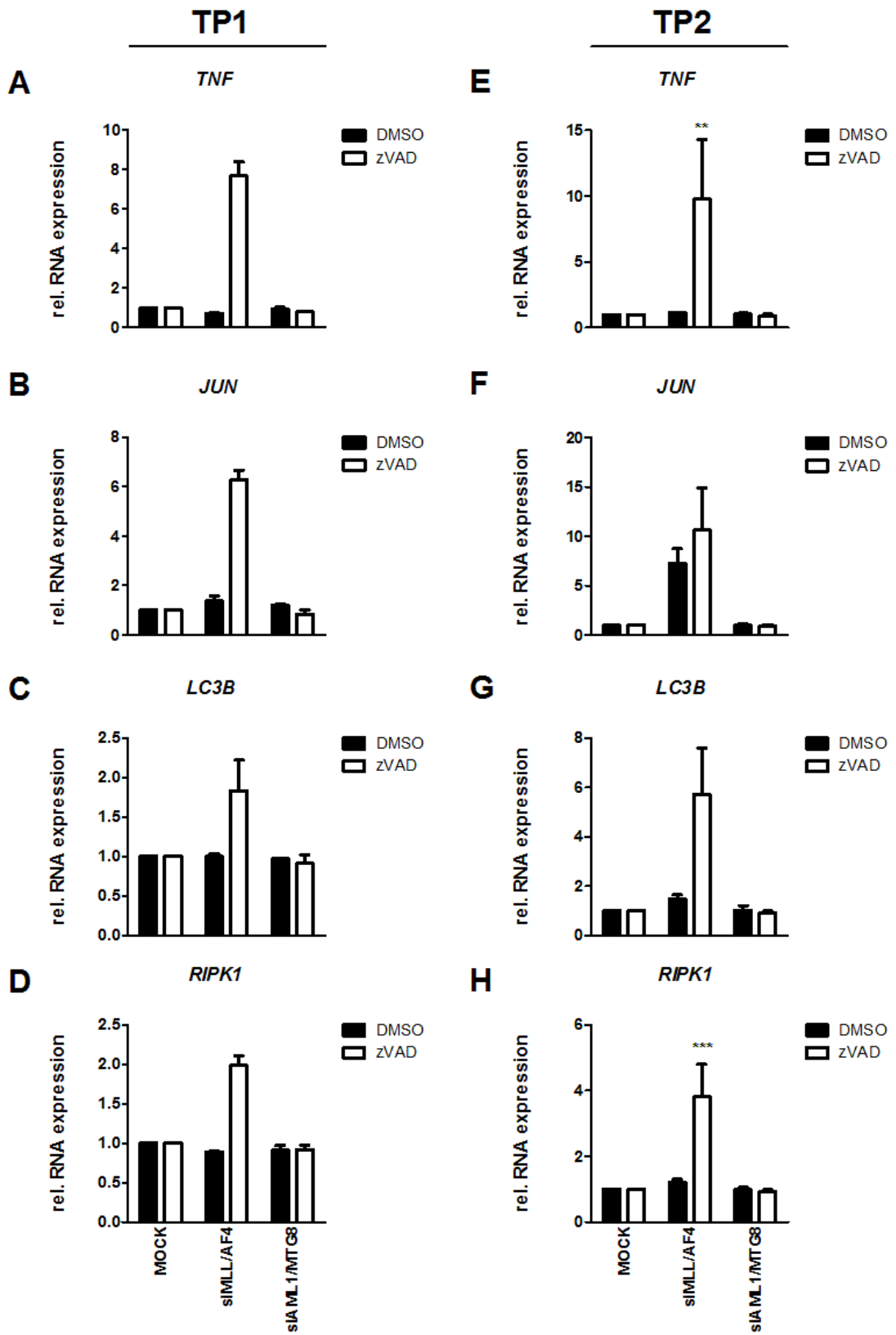
Fig. 4-31: Cell surface expression of TNFR1 and TNFR2 in t(4;11)-positive ALL cell lines

The two t(4;11)-positive ALL cell lines SEM and RS4;11 expressed both TNFR1 and TNFR2 on the cell surface, as determined by flow cytometry. The graph shows one representative overlay of n=3 comparable experiments.

Having confirmed the presence of TNF receptors on the SEM cell line, the array results were validated by qRT-PCR. Six genes were analysed, *RIPK1*, *TNF*, *JUN*, *PARP2*, *CYLD* and *LC3B*, and 6/6 showed the same results as observed in the array: *TNF* was 7.7- to 9.8-fold up-regulated in the siMLL/AF4-zVAD cells at both TP1 (fig. 4-32A) and TP2 (fig. 4-32E), respectively, when compared to MOCK-zVAD, but showed no differential expression in the corresponding DMSO group. The same trend could be observed for the autophagy marker *LC3B*, with an 1.8-fold induction at TP1 (fig. 4-32C) and a 5.7-fold up-regulation at TP2 (fig. 4-32G), as well as the kinase *RIPK1*, which induced 2- and 2.9-fold respectively, when compared to the corresponding MOCK control (fig. 4-32B, F). The transcript levels of those genes were not affected in siMLL/AF4-DMSO treated SEM cells. The notable exception was *JUN*; this gene showed a marked up-regulation in both siMLL/AF4-DMSO and siMLL/AF4-zVAD cells at TP2 (fig. 4-32F). However, at TP1, *JUN* gene expression was only increased in siMLL/AF4-zVAD cells when normalised on MOCK-zVAD (fig. 4-32B). Both the DNA damage response gene *PARP2* (fig. 4-33B) and the deubiquitinase *CYLD* (fig. 4-33A) were analysed only at TP2, transcript levels were elevated 4.7- and 3.2-fold, respectively. In addition, another key player involved in necroptosis, but which did not show up as differentially regulated in the arrays, was the proapoptotic BH3-family member *BMF*. Expression analysis by qRT-PCR found this gene to be induced in siMLL/AF4-treated SEM cells in both the zVAD and the DMSO group, albeit the up-regulation was slightly higher in the siMLL/AF4-zVAD cells (fig. 4-33C, D).

Fig. 4-32: Expression analysis of necroptotic genes by qRT-PCR

SEM cells were serially electroporated with either siMLL/AF4, control siRNA (siAML1/MTG8) or without siRNA (MOCK) and cultured with zVAD or the corresponding vehicle control DMSO. SEM cells treated with siMLL/AF4 and zVAD showed up-regulation of the necroptosis key regulators *TNF*, *RIPK1*, *LC3B* and *JUN* at both TP1 (2d post 1st electroporation) and TP2 (2d post 2nd electroporation) when compared to both corresponding controls and siMLL/AF4-treated-DMSO cells. Graphs represent the mean of at least n=2 (A-D) or n=3 (E-H) independent experiments; error bars indicate S.E.M. Statistical significance was determined using Student's t-test (** = $p < 0.01$; *** = $p < 0.001$).



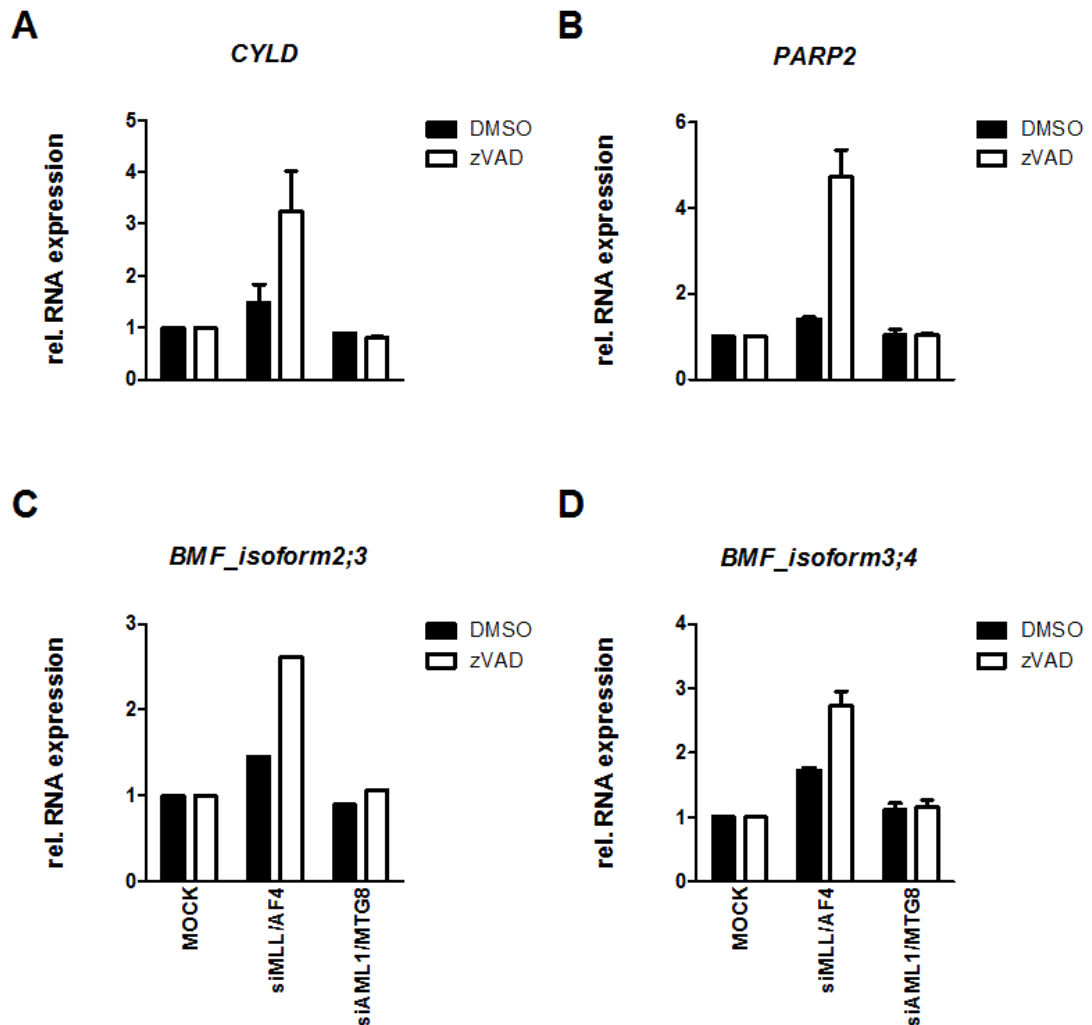


Fig. 4-33: Expression analysis of the necroptotic genes *BMF*, *CYLD* and *PARP2* by qRT-PCR

SEM cells were serially electroporated with either siMLL/AF4, control siRNA (siAML1/MTG8) or without siRNA (MOCK) and cultured with zVAD or the corresponding vehicle control DMSO. SEM cells treated with siMLL/AF4 and zVAD showed up-regulation of the necroptotic key players *CYLD* (A) and *PARP2* (B) at TP2 when compared to both corresponding controls and siMLL/AF4-DMSO cells. The BH3-family member *BMF* was induced in both siMLL/AF4-DMSO and siMLL/AF4-zVAD cells at TP2 (C, D). Graphs represent the mean of n=2 independent experiments (n=1 for C); error bars indicate data range.

Although, the inductions observed were specific for siMLL/AF4-transfected cells treated with zVAD, assessment of the basal expression of these genes showed that zVAD treatment alone elevated *TNF* and *JUN* levels in the controls. Thus, the actual induction of the gene expression in siMLL/AF4-zVAD SEM cells was even stronger, as the actual fold-changed were reduced by 5- to 8-fold due the $\Delta\Delta\text{Ct}$ normalisation process (fig. 4-34).

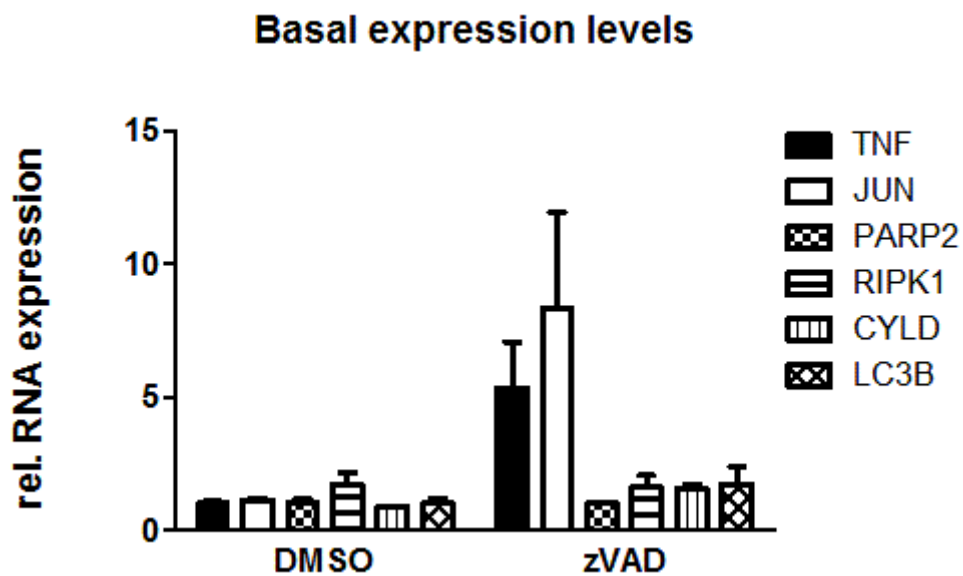


Fig. 4-34: Basal expression levels of necroptotic genes

RNA transcription of key genes of the necroptotic machinery in siAML1/MTG8-transfected SEM cells treated with or without zVAD was analysed by qRT-PCR at TP2 (d4) by the $\Delta\Delta\text{Ct}$ -method, normalising against the MOCK-DMSO control sample. Culturing siRNA-electroporated SEM cells with zVAD did not affect the basal levels of *PARP2*, *RIPK1*, *CYLD* and *LC3B*, but there was a substantial induction of *TNF* and *JUN* expression. The graph shows the mean of at least n=2 independent experiment, error bars indicate S.E.M. (standard error of the mean).

Comparison of gene expression fold-changes derived from the different analysis methods for *TNF*, *PARP2*, *CYLD*, *LC3B*, *RIPK1* and *JUN* at TP2 showed a highly significant correlation between both the array and the qRT-PCR results (fig. 4-35).

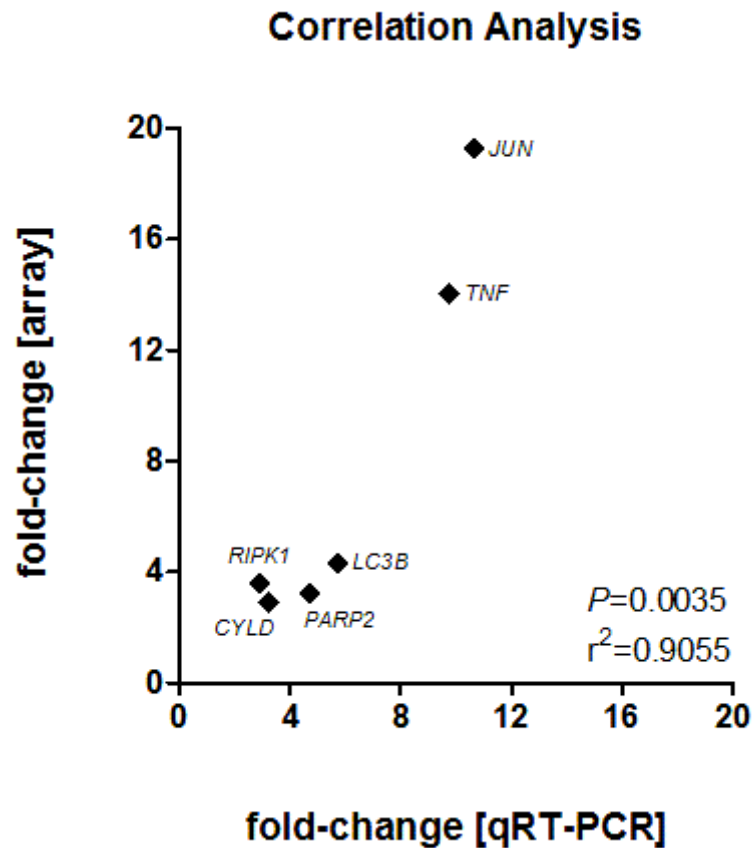


Fig. 4-35: Correlation analysis between array and qRT-PCR results

The linear fold-changes of the genes derived from the array probes in the zVAD signature at TP2 and the corresponding qRT-PCR expression analysis results show a highly significant correlation, as determined by Pearson's correlation analysis.

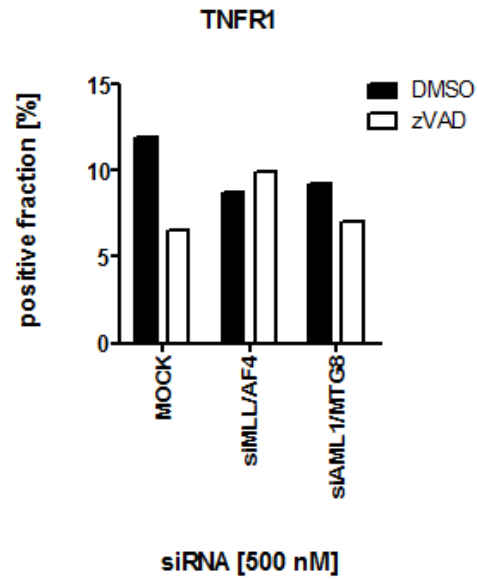
The PCD pathway necroptosis implicates both TNF receptor signalling and the autophagy machinery. Some of those markers require post-translational processing to be active, therefore in addition to the RNA expression analyses, some genes were also investigated at the protein level.

TNF and TNFR signalling playing such a prominent role in caspase-independent cell death. Expression of TNF receptors on the surface of siRNA-electroporated SEM cell treated with or without zVAD revealed down-regulation of TNFR2 (fig. 4-36B), while TNFR1 levels remained largely unaffected, only subtly increased in MLL/AF4-zVAD-treated cells (fig. 4-36A). Since TNFR2 is internalised upon ligand binding²⁹², this observation could indicate active TNF signalling. In contrast to TNFR1, TNFR2 has increased specificity of membrane bound TNF; and indeed, siMLL/AF4-zVAD treated SEM cells expressed at least three-fold more TNF on the cell surface than the corresponding controls (fig. 4-36C). This induction was not to the same extent as the up-regulation observed by qRT-PCR; but it has to be taken into account that membrane-bound TNF is only a fraction of the TNF produced, with the bulk being shed and secreted.

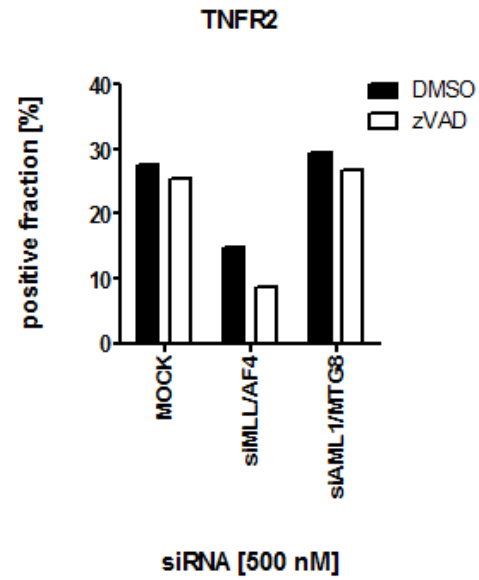
Fig. 4-36: Cell surface expression of TNF receptors TNFR1, TNFR2 and membrane-bound TNF in siRNA-treated SEM cells

SEM cells were serially electroporated with siRNA and treated with or without zVAD. TNF and TNFR surface expression was determined at TP2 by flow cytometry. Graph represents one single experiment.

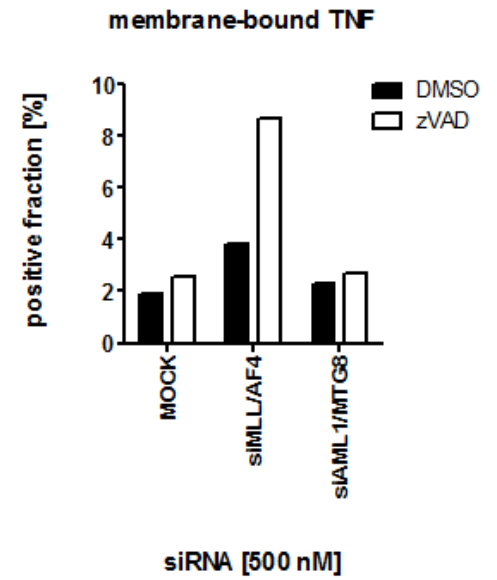
A



B



C



A central player in necroptosis is the kinase RIPK1; incidentally, RIPK1 is a cellular target of the effector caspase CASP8, and failure to process RIPK1 has been associated with a switch from apoptosis to caspase-independent cell death pathways²⁹³. When assessing protein expression of RIPK1, the characteristic cleavage product could be detected in siMLL/AF4-DMSO cells, suggesting a role of CASP8 in mediating MLL/AF4 depletion-dependent apoptosis. In contrast, only the full-length form of RIPK1 was visible in siMLL/AF4-zVAD-treated cells. However, although RIPK1 levels were increased compared to the MOCK-zVAD sample, when compared to both the siAML1/MTG8-zVAD and the DMSO treatment group, no induction was observed (fig. 4-37).

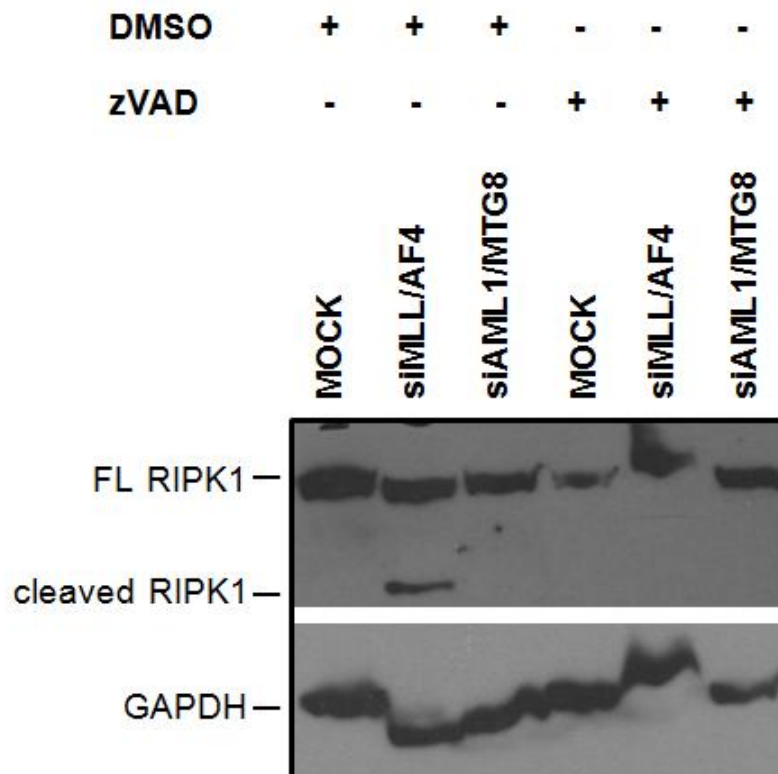


Fig. 4-37: RIPK1 Immunoblot in siRNA-treated SEM cells with or without zVAD

SEM cells were serially electroporated with siRNA and treated with or without zVAD. RIPK1 expression was determined at TP2. The graph represents one single experiment.

The autophagy marker LC3B is cleaved posttranslationally into the LC3B-I form, and lipidated into the LC3B-II form when it is incorporated into mature autophagosomes ²⁹⁴. Immunoblotting (fig. 4-38) showed increase of LC3B-II to be present in siMLL/AF4-zVAD SEM cells, but not in the corresponding DMSO cells. Also, in good concordance with the qRT-PCR, more LC3B-I could be detected in siMLL/AF4-zVAD cells when compared to the zVAD controls (MOCK-zVAD, siAML1/MTG8 zVAD). Incidentally, the zVAD control samples also show an increase in the LC3B-I form compared to DMSO controls, indicating increased background levels of the autophagy marker resulting from zVAD treatment alone, corroborating the qRT-PCR results illustrated in fig. 4-34.

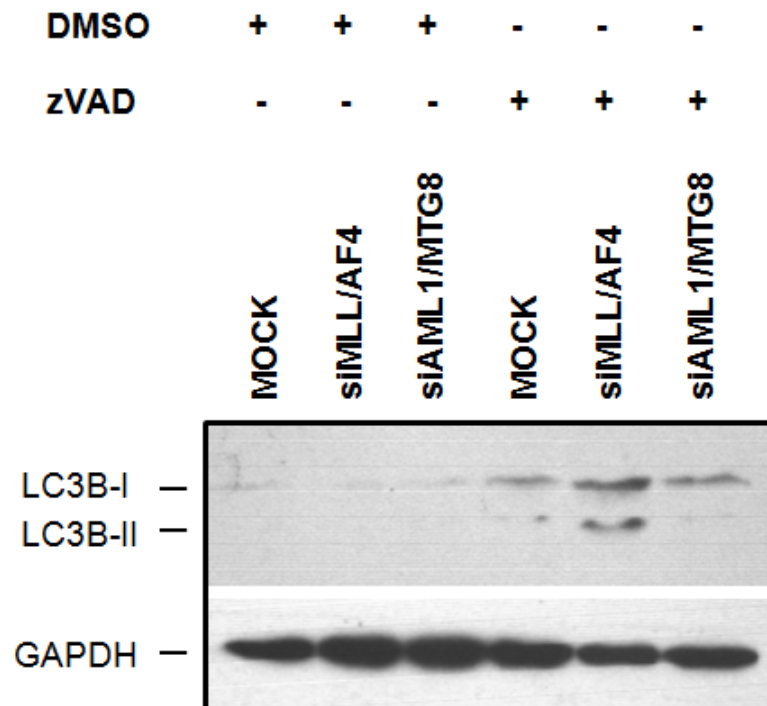


Fig. 4-38: LC3B Immunoblot in siRNA-treated SEM cells with or without zVAD

SEM cells were serially electroporated with siRNA and treated with or without zVAD. LC3B expression was determined at TP2. The graph represents one single experiment.

4.4 NECROPTOSIS INHIBITOR STUDIES

Several research groups have identified RIPK1 as one of the master regulators of necroptosis, and have shown that supplementing cells with the RIPK1 inhibitor Necrostatin-1 (NEC-1) completely blocked this cell death pathway, restoring viability. Also, suppression of TNF signalling using inhibitory TNF antibodies has been associated with inhibition of death.

Therefore, to elucidate the mechanisms of the caspase-independent cell death observed in siMLL/AF4-zVAD SEM cells, inhibitor studies were performed co-culturing siRNA-transfected SEM cell with either NEC-1 or the TNF-antibody Infliximab (α -TNF). The experimental set-up was similar to the standard procedure, and is depicted in scheme 4—39 .

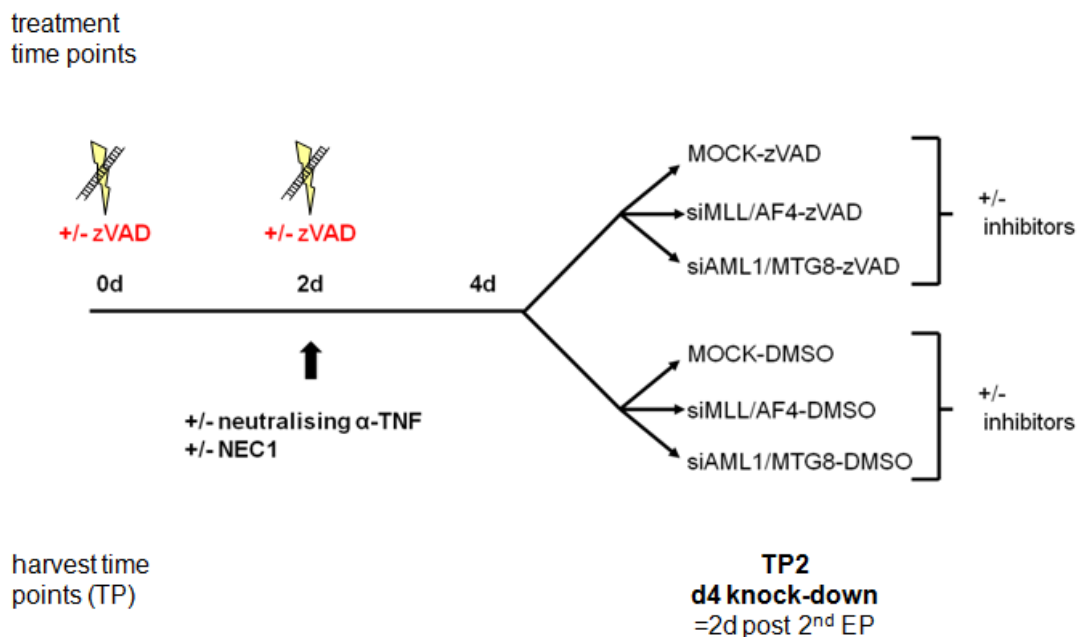


Fig. 4-39: Experimental set-up of necroptosis inhibitor study

SEM cells were serially electroporated with siRNA and treated with or without zVAD according to the standard set-up. In addition, after the 2nd electroporation the samples were further subdivided and supplemented with or without the RIPK1-inhibitor NEC-1 or a neutralising TNF-antibody.

Remarkably, neither of the inhibitors were able to suppress the cell death induction in either siMLL/AF4-zVAD or siMLL/AF4-DMSO cells. Analysing the cell death by flow cytometry, using the ANNEXIN V/PI assay showed that there was no difference in neither the ANNEXIN V single positive nor the ANNEXIN V/PI double positive subpopulations in siMLL/AF4 depleted cells treated with either inhibitor. Rather, NEC-1 increased the double-positive fractions in the siMLL/AF4-DMSO cells and also elevated it in the the zVAD control samples (fig. 4-40).

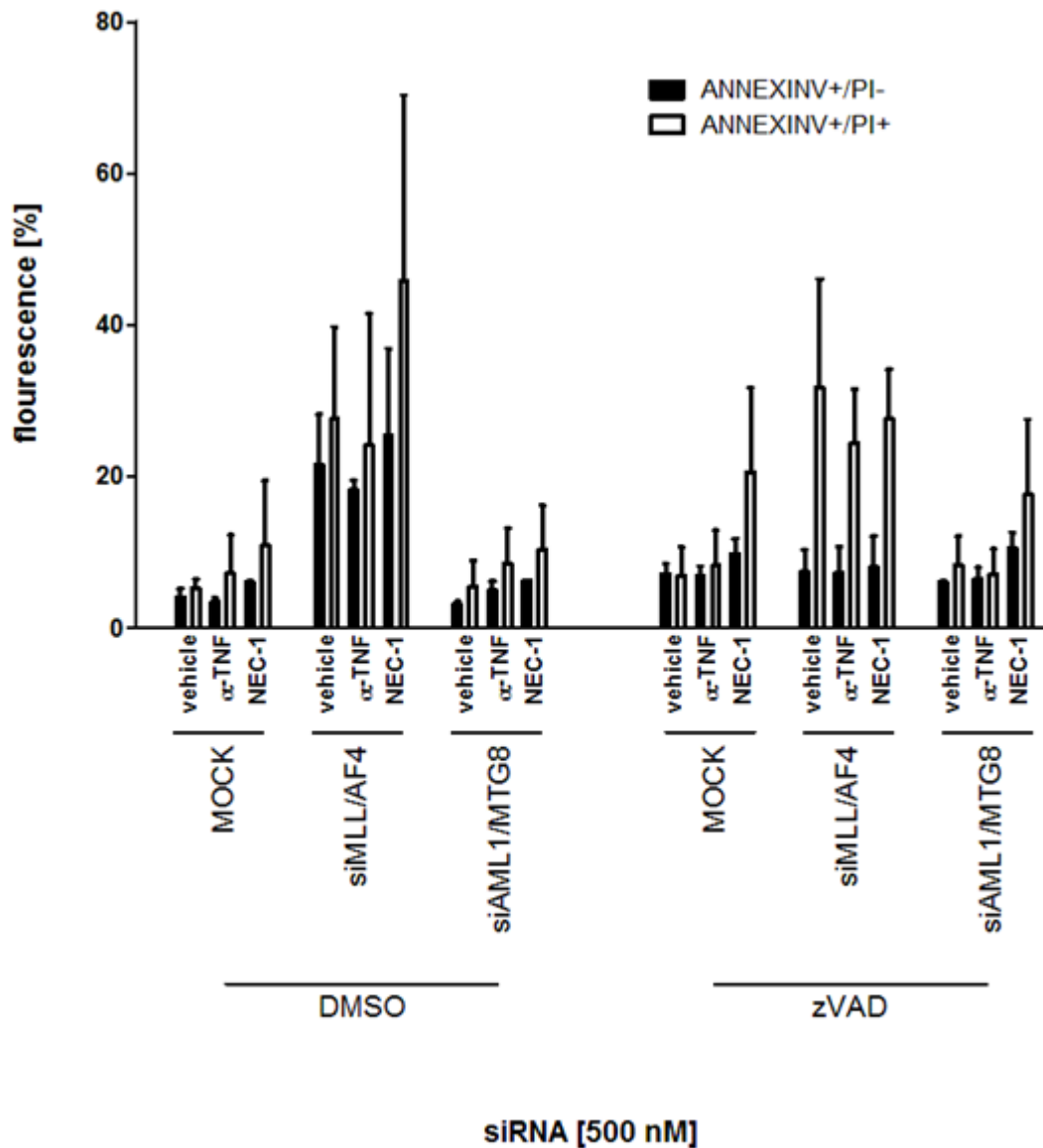


Fig. 4-40: Necroptosis inhibitors fail to suppress cell death in response to *MLL/AF4* depletion

SEM cells were serially electroporated with siRNA and cultured with or without zVAD. In addition, at TP1, the siRNA-treated SEM cells were further supplemented with either 100 μ M of the RIPK1-inhibitor NEC-1, or 10 μ M of TNF-neutralising antibody (-TNF). Flow cytometric analysis at TP2 showed that neither apoptotic nor necroptotic cell death could be prevented by addition of these inhibitors, as determined by ANNEXIN V/PI staining. Graph represents the mean of n= 2 independent experiments, error bars indicate data range.

The flow cytometry results were corroborated by viability analyses by both MTT and a luciferase-based viability assay. NEC-1 treatment strongly reduced viability of zVAD treated cells, regardless of siRNA-treatment, and increased cell death of siMLL/AF4-DMSO cells (fig. 4-41B). Viability measured by the MTT assay indicated that there was a slightly lower cell number in zVAD-treated control cells cultured with or without inhibitors (fig. 4-41A). However, this could be explained by a slower proliferation as both the ANNEXIN V/PI flow cytometry analysis and the luminescent cell viability assay showed that there was not an increase in cell death due to zVAD treatment alone (fig. 4-40, fig. 4-41B). Moreover, cycle progression was affected by zVAD, with a slight increase in G1/G0- and G2/M-phase accompanied by S-phase reduction (fig. 4-4).

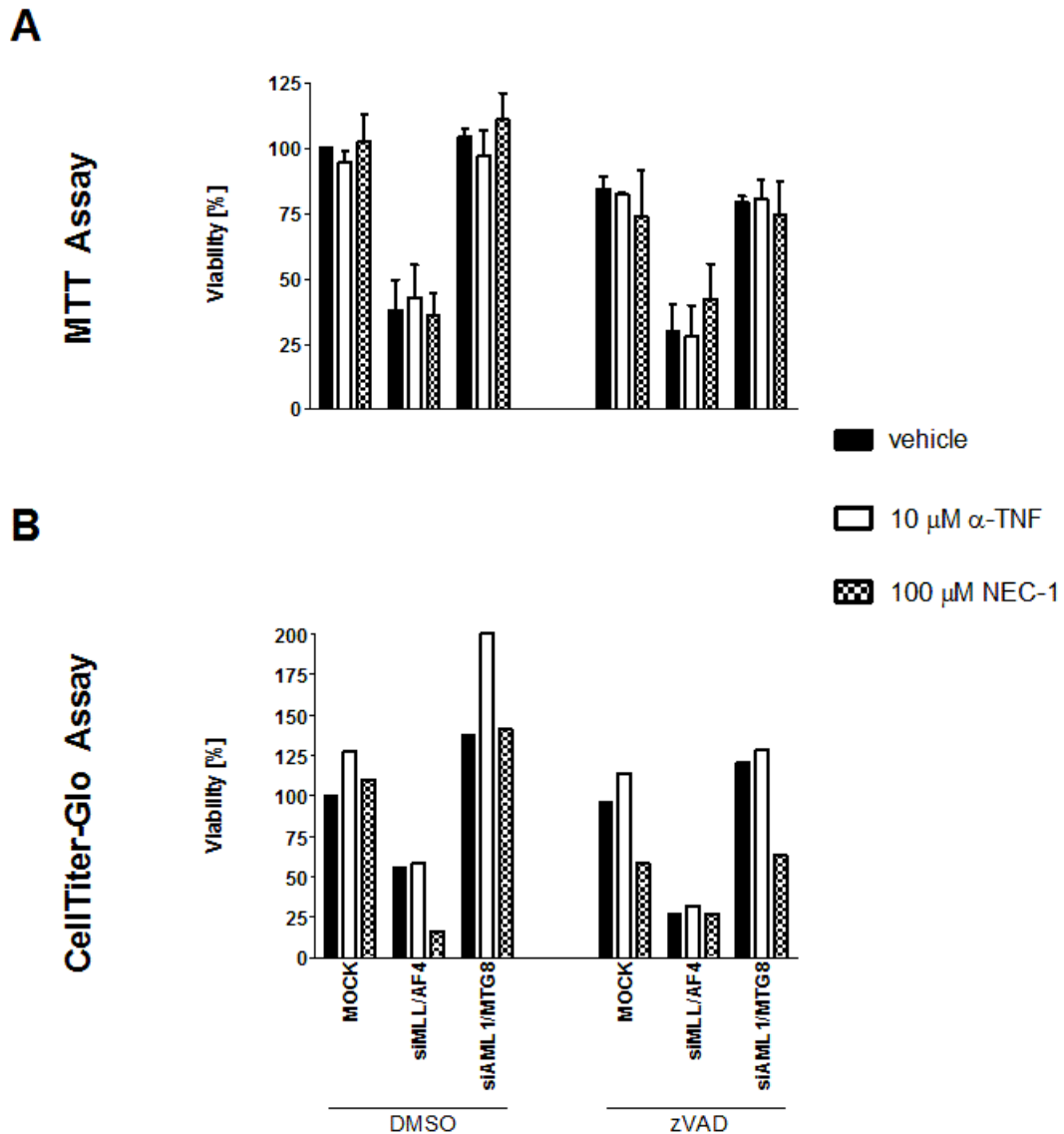


Fig. 4-41: Necroptosis inhibitors fail to restore viability in SEMs cells depleted of *MLL/AF4*

SEM cells were serially electroporated with siRNA and cultured with or without zVAD. In addition, at TP1, the siRNA-treated SEM cells were further supplemented with either 100 μ M of the RIPK1-inhibitor NEC-1, or 10 μ M of TNF-neutralising antibody (-TNF). Viability was assessed by MTT (A) or a luciferase-based ATP assay (B) at TP2. Neither apoptotic nor necroptotic cell death could be prevented by addition of these inhibitors. Graph (A) represents the mean of $n=2$ independent experiments, graph (B) shows one single experiment; each sample was performed in duplicates. Error bars indicate data range.

4.5 CONCLUSION

The results from this chapter suggest that there is an oncogenic addiction of t(4;11)-positive ALL cells towards MLL/AF4.

- Ablation of the fusion oncogene results in caspase-dependent apoptosis; suppression of this process with the pancaspase inhibitor zVAD switches the cells towards a more necroptotic-like cell death pathway
- Concomitantly, MLL/AF4-depletion in a caspase-deficient environment results in specific induction of several key mediators of the necroptotic machinery.
- Yet, inhibition of the main players of this alternative death pathway could not block cell death and restore viability.

Further studies are required to elucidate this phenotype, e. g., by blocking autophagy, as well as to identify the molecular mechanism by which cell survival is irretrievably compromised.

4.6 DISCUSSION

The results from the previous chapter established MLL/AF4 as a key mediator of leukaemic cell survival; MLL/AF4 knock-down resulted in apoptosis induction, accompanied by a concerted down-regulation of pro-survival signalling cascades. In an attempt to elucidate the hierarchy and the key steps of this process, RNAi-mediated MLL/AF4 depletion was combined with apoptosis inhibitor treatment, followed by global transcriptome analysis.

Caspase inhibition in MLL/AF4-depleted cells causes a switch from apoptosis to a necroptosis-like cell death type; co-culture of siRNA-transfected SEM cells with the pan-caspase inhibitor zVAD-FMK suppressed apoptotic markers, blocking effector caspase processing, consequently abrogating their proteolytic activity (fig. 4-7A, B). This was also corroborated by the absence of cleavage of the caspase target protein PARP1 (fig. 4-7) and diminished nuclear fragmentation (fig. 4-6), which represents an important morphologic marker of apoptosis²⁹⁵. However, intriguingly, apoptosis inhibition did not restore viability (fig. 4-9), and flow cytometry analysis indicated a phenotypic switch to a more necrotic-like cell death: siMLL/AF4-zVAD treated cells showed early loss of plasma membrane integrity, evidenced by PI uptake, while the corresponding siMLL/AF4-DMSO cells predominantly displayed loss of membrane lipid asymmetry, but not integrity (fig. 4-8). Gene expression profiling of SEM cells treated in combination with siMLL/AF4 and zVAD showed an over-representation of proinflammatory cytokines and chemokines in the top50-upregulated genes, such as *MIP-1 α* (*CCL3*, chemokine C-C motif ligand 3), *IL8* (interleukin 8), *RANTES* (*CCL5*), *CXCL10* (chemokine C-X-C motif ligand 10), *TNF* (tumour necrosis factor) and *LTA* (lymphotoxin alpha). In addition, there was up-regulation of immediate early/adaptive response genes, such as the transcription factors *JUN* (jun proto-oncogene), *FOS* (FBJ murine osteosarcoma viral oncogene homolog) and *ATF3* (activated transcription factor 3), implicated in stress-response and immunity²⁹⁶ (tab. 4-3, tab. 4-5). These results are in concordance with previous observations that death stimuli in combination with chemical caspase inhibition induce proinflammatory cytokines, such as TNF, interferon-gamma (IFNG) and IL8²⁹⁷⁻²⁹⁸. Interestingly, pathway analysis of the zVAD signature at each time point using the

IPA software showed a high enrichment for signalling mediated by the Tumour necrosis factor receptor superfamily (TNFRSF) as well as immune response pathways mediated by pattern recognition receptors, including Toll-like receptor (TLR) signalling (fig. 4-12). A similar observation was made for the zVAD core signature, which was derived from comparing analyses between both time points, comprising common differentially expressed genes. Functional analysis using GSEA yielded 93 gene sets with a significant enrichment for the zVAD core signature; in concordance with the IPA results, there was overrepresentation of gene sets associated with inflammatory processes resulting from cytokine stimulation, such as TNF, IFNG, but also gene sets linked to activation of TNFRSF signalling, *i.e.*, CD40 (TNFRSF5) (fig. 4-22). Genes involved in immune response, including canonical TLR signalling, were also enriched (fig. 4-22). Moreover, the zVAD core signature contained target genes of immediate early/adaptive response transcription factors, *i.e.*, ATF4, modulator of cellular stress response mechanisms and involved in cell death signalling²⁹⁹⁻³⁰¹, and CEBPB (*CCAAT/enhancer binding protein, beta*), a pleiotropic transcription factor which has been shown to regulate the expression of interferons, TNF and other cytokines³⁰². These results correlate well with the top50 induced gene lists of the zVAD signatures, as well as with the other enriched GSEA gene sets (fig. 4-26). Concordantly, other gene sets linked to the zVAD core signature comprise apoptosis signalling (fig. 4-23), cytokines and their cognate receptors (fig. 4-23), stress response (fig. 4-23), and the transcription factor IRF-1 (interferon regulatory factor-1), involved in cytokine-, toll-like receptor³⁰³ and apoptosis signalling³⁰⁴ (fig. 4-24). Furthermore, leading edge analysis of the 93 GSEA sets showed clustering of the core genes into distinct motifs describing TNFRSF and TLR signalling, IFN signalling, cell death and stress response (fig. 4-27); and TNF was the most prevalent gene in all 93 significantly enriched gene set (fig. 4-28), Particularly TNF has been well-characterised in its dual ability to promote inflammation, but also cell death in a caspase-dependent and -independent manner.

These observations suggested that the switch in the type of cell death observed could be towards necroptosis, a novel programmed cell death pathway mediated by the TNF receptor - and Toll-like receptor (TLR)-signalling machinery, and

involving autophagy²⁹¹. Therefore, the zVAD signature was screened for published mediators. Interestingly, the expression of a subset of these genes was induced, including the key factors *RIPK1*, *CYLD*, *TNF*, and *JUN*, as well as the autophagy marker *LC3B* and the poly-(ADP-ribose) polymerase family member *PARP2*²⁹¹. Comparison with the MLL/AF4 signature showed that this induction was restricted to siMLL/AF4-zVAD treated cells (tab. 4-12), supporting the necroptosis hypothesis. This observation was validated by qRT-PCR expression analysis; only SEM cells electroporated with siMLL/AF4 in combination with zVAD showed up-regulation of *RIPK1*, *CYLD*, *LC3B*, *PARP2* and *TNF*, while the expression levels in the corresponding vehicle-treated cells remained unaltered (fig. 4-34). *JUN* was highly up-regulated as well, but this induction was not restricted to siMLL/AF4-zVAD treated cells (fig. 4-32). Surprisingly, the basal levels of *TNF* and *JUN* were already elevated in zVAD-treated controls when compared to vehicle-treated controls (fig. 4-34); a recent report indicated that this might occur in a PKC (protein kinase C)-dependent manner, due to an as of yet unknown effect mediated by zVAD³⁰⁵.

Necroptosis is characterised by presence of hyperautophagic signalling; in good concordance, LC3B is up-regulated in siMLL/AF4-zVAD cells, and LC3B is present in its lipidated form (LC3B-II, fig. 4-38), indicating increased presence of mature autophagosomes. However, the role of autophagy induction in necroptosis is not fully understood, as inhibition of autophagy has shown to increase cell death³⁰⁶; conversely, knock-down of key regulators of autophagy, such as ATG7 and Beclin-1 rescued cells undergoing autophagic cell death³⁰⁷.

Since TNFR1 signalling seems to be the predominant pathway involved in necroptosis, expression of TNFR1 and TNFR2, which has been shown to promote TNFR1-mediated cell death signalling was confirmed by flow cytometry on the t(4;11)-positive cell lines SEM and RS4;11 (fig. 4-31). Interestingly, while TNFR1 levels on the cell surface of MLL/AF4-depleted SEM cells remained largely unaltered (fig. 4-36A), there was an approximately 1.6-fold decrease of TNFR2 in MLL/AF4-ablated SEM cells, which was even more exacerbated in the corresponding MLL/AF4-zVAD samples, where there was 3.2-fold less TNFR2 on

the surface (fig. 4-36B). This correlated with a 1.7-fold induction and a 3.2-fold induction of membrane-bound TNF, respectively. Since TNFR2 has a high affinity for membrane-bound TNF, and is internalised upon ligand binding²⁹², this observation could indicate active TNF signalling. In contrast to its high induction on RNA level, the increase in membrane-bound TNF protein is more modest (fig. 4-36C); but it has to be taken into account that the TNF can be present in both membrane-bound and soluble form.

The interplay of TNF, the deubiquitinase CYLD and the kinase RIPK1 have been shown to be essential in necroptosis signalling: under non-cytotoxic conditions, TNF engages TNFR1 and promotes the assembly of a multimeric complex containing RIPK1 and E3 ligases such as cIAP (cellular inhibitors of apoptosis) and TRAF2 (TNF receptor associated factor 2), which catalyse lysine63-linked polyubiquitylation of RIPK1³⁰⁸. This modification is recognised and bound by NEMO, a moiety of the IKK (inhibitor of NFκB kinase kinase) kinase complex, resulting in its activation, subsequently promoting NFκB signalling³⁰⁹. Under cytotoxic conditions, deubiquitinases such as CYLD are recruited to the TNFR1-RIPK1 complex; removal of the polyubiquitin chain results in disassociation of RIPK1 and its phosphorylation, promoting its kinase activity³¹⁰. In a caspase-proficient context, RIPK1 is targeted by caspase-8 and inactivated, resulting in apoptosis induction³¹¹. Conversely, in a caspase-deficient context, RIPK1 remains active and mediates necroptotic signalling, i.e., by promoting the production of ROS and perturbing of metabolic processes³¹⁰.

Concordantly, immunoblotting of RIPK1 showed the characteristic caspase-mediated cleavage pattern in siMLL/AF4-vehicle treated cells, but only full-length RIPK1 in the siMLL/AF4-zVAD sample, with a slightly higher migration size than the other bands, a possible indication for phosphorylation (fig. 4-37). Whether there was a concomitant increase of RIPK1 protein levels remained unclear, however, the induction of RIPK1 on RNA was subtle, 2- to 3-fold (fig. 4-32), and Western blotting might not have had the sufficient sensitivity to detect these changes. Intriguingly, the characteristic proteolysis of RIPK1 implicates that MLL/AF4 ablation not only initiated the intrinsic caspase cascade as previously

reported by us¹⁴⁸, but that apoptosis induction also occurs via the extrinsic pathway, involving caspase-8.

In agreement with the differential regulation of NFkB pathway by RIPK1, there was up-regulation of NFkB signalling at TP1 of the zVAD signature, indicating an inflammatory response. Conversely, at TP2, at the time point where the cell death programme was already underway, the NFkB transcription factors, and consequently, NFkB signalling was down-regulated (fig. 4–19). Recently, Wu *et al.* showed that RNAi-mediated depletion of the NFkB transcription factors RELA and RELB, as well as components of the IKK complex greatly sensitised cells towards zVAD-mediated necroptosis³⁰⁵; in this context, the observed down-regulation of NFkB at TP2 might contribute towards the cell death signalling process.

4.6.1 Suppression of necroptosis key processes fails to rescue the cell death phenotype

Both TNF signalling and RIPK1 activity have been heavily implicated in promoting necroptosis. In order to further mechanistic insight into the underlying processes of siMLL/AF4-mediated cell death in a caspase-deficient context, both aspects were functionally addressed. Interestingly, co-culturing of SEM treated siRNA-zVAD in the presence of the TNF-neutralising antibody Infliximab did not suppress cell death (fig. 4-40). Possibly, treatment with Infliximab missed the therapeutic window, as it was only supplemented after the second electroporation, and as the zVAD signature at TP1 indicates up-regulation of the necroptotic machinery already at this time point (fig. 4-32, fig. 4-33, tab. 4-12), which might have primed the cells to the point of no return, uncoupling it from TNF signalling.

Similarly, since RIPK1 activity has been reported to be indispensable for necroptotic cell death, SEM cells treated with siMLL/AF4 and zVAD were supplemented with the RIPK1-inhibitor NEC-1. Surprisingly, viability of the cells could not be restored; moreover, NEC-1 seemed to have a cytotoxic effect on zVAD-treated SEM cells *per se* (fig. 4-40, fig. 4-41). Lower concentrations of NEC-1 were also not able to rescue the necroptotic phenotype (data not shown). This

surprising finding is in disagreement with current literature, where RIPK1 inhibition by NEC-1 has been reported to completely block or at least attenuate cell death in a variety of cell types^{291,312}. While a technical issue, such as a non-working inhibitor, cannot be ruled out due to lack of a positive control, the unresponsiveness of the cells towards NEC-1 could also be due to a biological reason inherent of the SEM cell line, *i.e.*, a mutation in RIPK1, which would interfere with binding of the inhibitor to the enzyme. Structure analysis of RIPK1 found the activating region to be homologous to the T-loop domain of the B-RAF kinase, which is often targeted by oncogenic mutations. Concomitant mutation studies identified the S161E mutation in RIPK1 to be structurally equivalent to described activating mutations in B-RAF; this particular mutation conferred full activity to RIPK1, but abrogated inhibitor actions³¹³. Although there are no reports of naturally occurring RIPK1 mutations in literature, this does not exclude the possibility, and either mutation screening of this region or the use of alternative RIPK1 inhibitors which are unaffected by this mutation, *i.e.* NEC-5, might be able to elucidate this aspect.

Another possible explanation for the failed cell death suppression by NEC-1 might be that the cell death programme occurs in a RIPK1-independent manner. This could be due to a degree of redundancy within the RIP kinase family; although both RIPK1 and RIPK3 have been shown to be essential for necroptosis³¹⁴, and even to act in concert in promoting cell death³¹⁵, not much is known about RIPK5. This family member is induced in MLL/AF4-depleted cells regardless of zVAD treatment (tab. 4-12), and it had been reported to mediate cell death in a caspase-dependent and -independent manner²⁰⁴. Consequently, RIPK5 might play a role in the caspase-independent cell death observed.

In addition, there are reports in regards to a TNF-dependent, RIP kinase- and caspase-independent cell death pathway³¹⁶ (also alluded to in Wu *et al.*, as data not shown³⁰⁵). Moreover, NEC-7, a necrostatin derivative, has been able to inhibit TNF-induced necrotic cell death in a RIPK1-independent manner, suggesting a differing molecular mechanism, which has not been elucidated to date³¹⁷. Concordantly, a caspase-independent autophagy-like cell death pathway has just been recently described, which was shown to be mediated by the death-associated protein

kinase (DAPK)³¹⁸. Since the presence of the mature autophagy marker LC3B-II is shared between necroptosis, autophagy-like cell death and this novel DAPK-mediated programme, further studies are required to elucidate the mechanism by which t(4;11)-cells die in response to MLL/AF4 ablation in a caspase-deficient environment. Ultimately, these results illustrate the high degree of oncogene addiction of the SEM cells towards MLL/AF4, as fusion gene ablation invariably dooms the cell to die. A similar observation has been made for BCR/ABL, where imatinib treatment in combination with zVAD resulted in a switch from caspase-dependent to a more necrotic-like cell death³¹⁹, and these results highlight the importance of these single oncogenic mutations for the maintenance of the disease phenotype.

4.6.2 Intersection analysis of the zVAD and MLL/AF4 signature reveals a core gene set comprising cell death and stemness-associated factors

Despite the technical limitations of this gene expression profiling study discussed in chapter 3, there was a high degree of overlap between time point TP1 and TP2 in the zVAD signature (fig. 4-20), indicating that the combined treatment of MLL/AF4 depletion and caspase inhibition exerted a concerted regulatory pressure. Comparing the zVAD signature with the MLL/AF4 target genes described by Guenther *et al.*¹³² showed, as observed with the MLL/AF4 signature (tab. 3–13), that only a small subset responded to MLL/AF4 ablation (tab. 4-11). Probing both the MLL/AF4 and the zVAD signature beyond the fold-change threshold revealed a trend towards to a differential expression of these genes, suggesting that the observed differential expression is indeed a MLL/AF4-regulated effect.

Intersection analysis of the MLL/AF4 signature A with the zVAD signature showed a core set of 61 genes with the same differential regulation in response to MLL/AF4 depletion (fig. 4-30); performing the analysis in this manner, the time points, regardless of inhibitor treatment, served as replicates, revealing genes that are highly dependent on MLL/AF4. In good concordance with the results from the previous chapter, this core signature contains several genes associated with cell

death, such as *ANXA1* and *PMAIP1*, autophagy (*GABARAPL1*), as well as revealing down-regulation of haematopoietic stem/progenitor cell markers, (*HOXA10*, *SPN1/CD43*) and the ERK-specific phosphatase *DUSP6*, which were already discussed in section 3.6.2. In addition, this core signature showed induction of genes associated with inflammatory and stress-related processes, such as Toll-like receptor 10 (TLR10), recently shown to be induced in response to immunity-independent cellular stress³²⁰, *IFIT2* (interferon-induced protein with tetratricopeptide repeats 2), which promotes interferon-independent cell death³²¹, *IFIT3* (interferon-induced protein with tetratricopeptide repeats 3) and *IFI44* (interferon-induced protein 44), an inhibitor of proliferation in interferon-resistant cancer cells³²². Moreover, there is induction of the nucleotide pyrophosphatase *ENPP2* (ectonucleotide pyrophosphatase/phosphodiesterase 2/ autaxin), which plays a dual role as tumour promoter and tumour suppressor in a cell-type dependent manner³²³, and the MAP kinase kinase *TPL2* (MAP3K8) which plays an important role in TNF-, TLR- and NFκB-mediated ERK signalling²⁷⁴⁻²⁷⁸.

Another member of this core signature, *REEP3*, is of particular interest, as it is one of the few MLL/AF4 targets which are up-regulated in response to fusion gene ablation (tab. 3-13, tab. 4-11). *REEP3* represents together with five other *REEP* proteins (*REEP1-6*) the human orthologues of the yeast gene *Yop1p*, a putative regulator of vesicle trafficking, but also implicated in proliferation and viability, as it has been shown to induce cell death upon overexpression³²⁴. Furthermore MLL/AF4-depletion also affects members of the ubiquitin-proteasome system, showing up-regulation of the putative tumour suppressor *FBXO32*, an E3 ligase lost in a variety of cancers and implicated in p21 degradation³²⁵⁻³²⁶.

The core signature also shows down-regulation of the epigenetic cofactor *SMARCC2* (SWI/SNF related, matrix associated, actin dependent regulator of chromatin, subfamily c, member 2), a component of the SWI/SNF chromatin-remodelling complex and part of the multimeric protein complex associated with MLL⁸⁶. Loss of *SMARCC2* might perturb MLL (and putatively AF4/MLL via its SET domain)-linked chromatin modifying functions. Interestingly, *SMARCC2* has recently been reported to be significantly up-regulated in infant ALL²⁵³. Furthermore, the core signature contained one transcription factor, *MAZ* (c-MYB

associated zinc finger), which was down-regulated in response to *MLL/AF4* depletion. MAZ has been implicated in transactivation of the proto-oncogene K-RAS²⁸⁹ and might thus promote high K-RAS expression in t(4;11)-positive ALL, consequently contributing to the MLL/AF4 pathobiology, since aberrant K-RAS activity has shown to be prevalent in infant MLLr ALL patients¹⁵¹, and K-RAS mutations accelerate MLL/AF4-mediated transformation in a mouse model¹⁵².

Taking these results together, MLL/AF4 ablation results in the differential induction of cell death-associated and anti-proliferative genes, while suppressing factors promoting stemness and proliferation. These findings are in good concordance with the phenotype observed in response to *MLL/AF4* depletion.

5. ANGIOPOIETIN-1, a novel factor implicated in t(4;11)-positive ALL

5.1 ANGPT1 EXPRESSION IS DEPENDENT ON THE MLL/AF4 STATUS OF THE T(4;11)-POSITIVE ALL CELL

5.1.1 Analysis of MLL/AF4-dependent ANGPT1 expression regulation in the t(4;11)-positive ALL cell line SEM

Whole-genome expression profiling of the t(4;11)-positive cell line SEM depleted of MLL/AF4 for a period of 2, 4 and 6 days (d2, d4 & d6, respectively) revealed a core signature of 63 genes whose expression was shown to be regulated in a MLL/AF4-dependent manner (fig. 3-39). Interestingly, one of the most prominently affected transcripts of this MLL/AF4-regulated gene signature was the angiogenic growth factor *ANGPT1*. The Illumina HT-12 bead array contained two specific oligonucleotides probes for *ANGPT1* (ILMN_2086890; ILMN_1677723), and both displayed consistently, at all three interrogated time points, normalised signal intensities which were at least twofold lower in MLL/AF4 depleted samples (siMLL/AF4) compared to the corresponding control samples (siCtrl) (fig.5-1). The decrease of the *ANGPT1* transcript was time-dependent, as the extent of the probe signal intensity reductions increased with the time of the MLL/AF4 depletion. At the time point d2, representing 2 days of MLL/AF4 knockdown, the *ANGPT1* probe signal intensities showed a decrease by 2.9-fold (ILMN_2086890) and 2.0-fold (ILMN_1677723) when compared to the corresponding probe intensities of the control cells (siCtrl). In cells depleted of MLL/AF4 for 4 days, the probe intensities were reduced by 4-fold (ILMN_2086890) and 4.8-fold (ILMN_1677723), and at the final time point queried, 6 days of MLL/AF4 depletion, the intensities of both probes showed a decrease by 5.3-fold when normalized against siCtrl-treated cells (tab. 5-1).

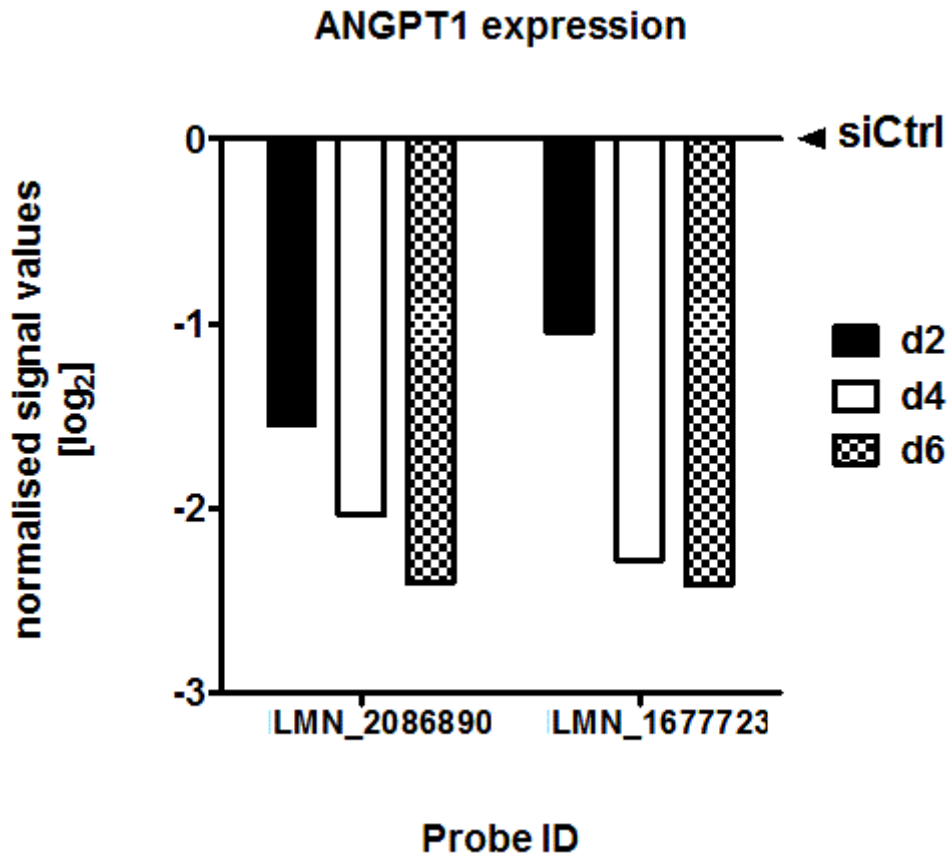


Fig.5-1: Normalised *ANGPT1* probe signal values in samples depleted of MLL/AF4

SEM cells were treated for 2, 4, 6 days (d2, d4, d6) with either siMLL/AF4 or with control siRNA (siCtrl). Signal intensity values of the Illumina HT12 BeadChip array probes for *ANGPT1* of the siMLL/AF4 samples at each time point were normalised against corresponding controls samples, and the signal value fold-change \log_2 -transformed.

Tab. 5-1: List of signal intensity \log_2 -ratios and corresponding fold-changes of *ANGPT1* probes in siMLL/AF4-treated samples normalised against siCtrl samples

	ILMN_2086890		ILMN_1677723	
	signal intensity (norm. against siCtrl)	fold-change	signal intensity (norm. against siCtrl)	fold-change
TP1	-1.55	-2.93	-1.04	-2.06
TP2	-2.04	-4.10	-2.28	-4.86
TP2	-2.41	-5.30	-2.41	-5.33

These observations implied a dependency of *ANGPT1* on MLL/AF4; in order to elucidate the role of MLL/AF4 in *ANGPT1* expression regulation, these results were validated *in vitro*. The t(4;11)-positive SEM cells were serially electroporated at two day intervals with either siRNA against MLL/AF4 (siMLL/AF4), an active control siRNA (siAML1/MTG8) or without siRNA oligonucleotides (MOCK). Cells and cell culture supernatant were harvested at day 2 (d2) and 4 (d4), prior to the subsequent electroporation, and at the final time point, corresponding to day 6 (d6). *MLL/AF4* depletion was confirmed by qRT-PCR; MLL/AF4 levels in siMLL/AF4 treated cells showed a sustained decrease by 70-80% over all three time points compared to controls (fig. 3-4).

ANGPT1 expression was analysed on RNA level by qRT-PCR (fig. 5-2), and the amount of secreted ANGPT1 protein in the cell culture supernatant measured using enzyme-linked immunosorbent assays (ELISAs) (fig. 5-3). As observed in the array, siRNA-mediated depletion of *MLL/AF4* correlated with reduced expression of *ANGPT1* levels when compared to siAML1/MTG8-transfected and MOCK-treated cells. Moreover, the reduction showed the same time-dependent trend; *MLL/AF4* depletion for 2 days revealed 45% decrease of *ANGPT1*; SEM cells in which *MLL/AF4* had been knocked-down for 4 and 6 days showed a decline of *ANGPT1* transcript levels by 74% and 83%, respectively. These results were statistically significant, as determined by an unpaired Student's t-test (fig. 5-2).

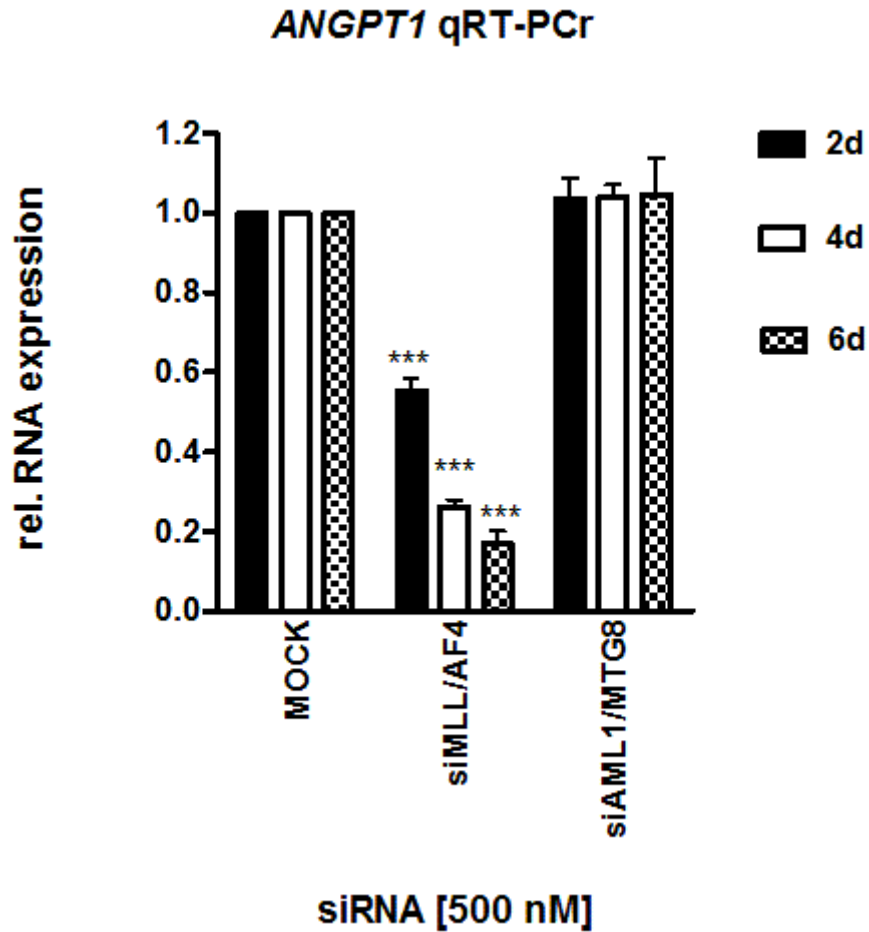


Fig. 5-2: *ANGPT1* levels in MLL/AF4-depleted cells determined by qRT-PCR

SEM cells electroporated with siMLL/AF4 show *ANGPT1* down-regulation in a time-dependent manner when compared to controls. The figure shows the mean of n=8 (d2), n=10 (d4) and n=5 (d6) individual experiments, error bars indicate standard error of the mean (S.E.M.). Statistic analysis was carried out using an unpaired Student's t-test (***) = $p < 0.0001$.

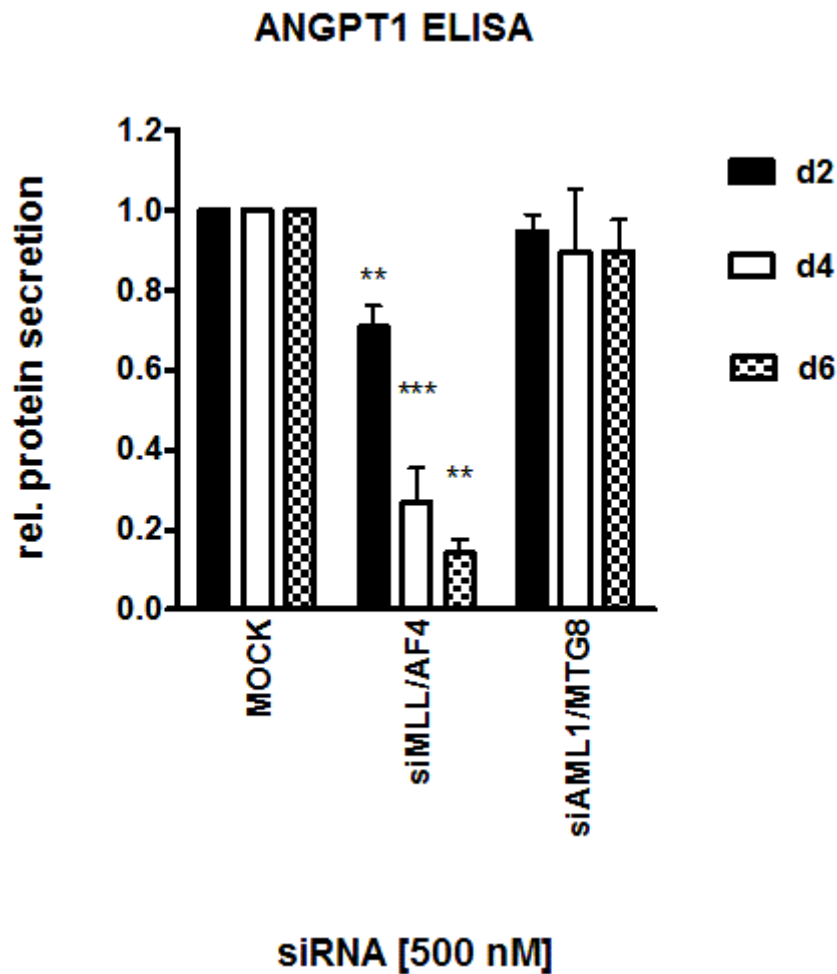


Fig. 5-3: ANGPT1 protein secretion in MLL/AF4-depleted SEM cells as determined by ELISA

Cell culture supernatant of SEM cells electroporated with either siRNA against MLL/AF4, control siRNA (siAML1/MTG8) or pulsed without siRNAs (MOCK) was harvested over a time course of 2, 4 and 6 days and soluble ANGPT1 protein levels quantified using an enzyme-linked immunosorbent assay (ELISA). SEM cells depleted of MLL/AF4 showed a significantly decreased ANGPT1 secretion in a time-dependent manner. Error bars indicate standard error of the mean (S.E.M.) of at least n=3 independent experiments. Statistical analysis was performed using an unpaired parametric Student's t-test (*= $p < 0.05$; ** = $p < 0.01$; *** = $p < 0.001$)

The reduction of *ANGPT1* expression was also reflected on protein levels: normalised on the controls, the relative secretion of ANGPT1 in the cell culture supernatant of *MLL/AF4*-depleted cells was decreased by 30%, 74% and 90% at day 2, 4 and 6, displaying the same time-dependency already observed for the RNA expression (fig. 5-3).

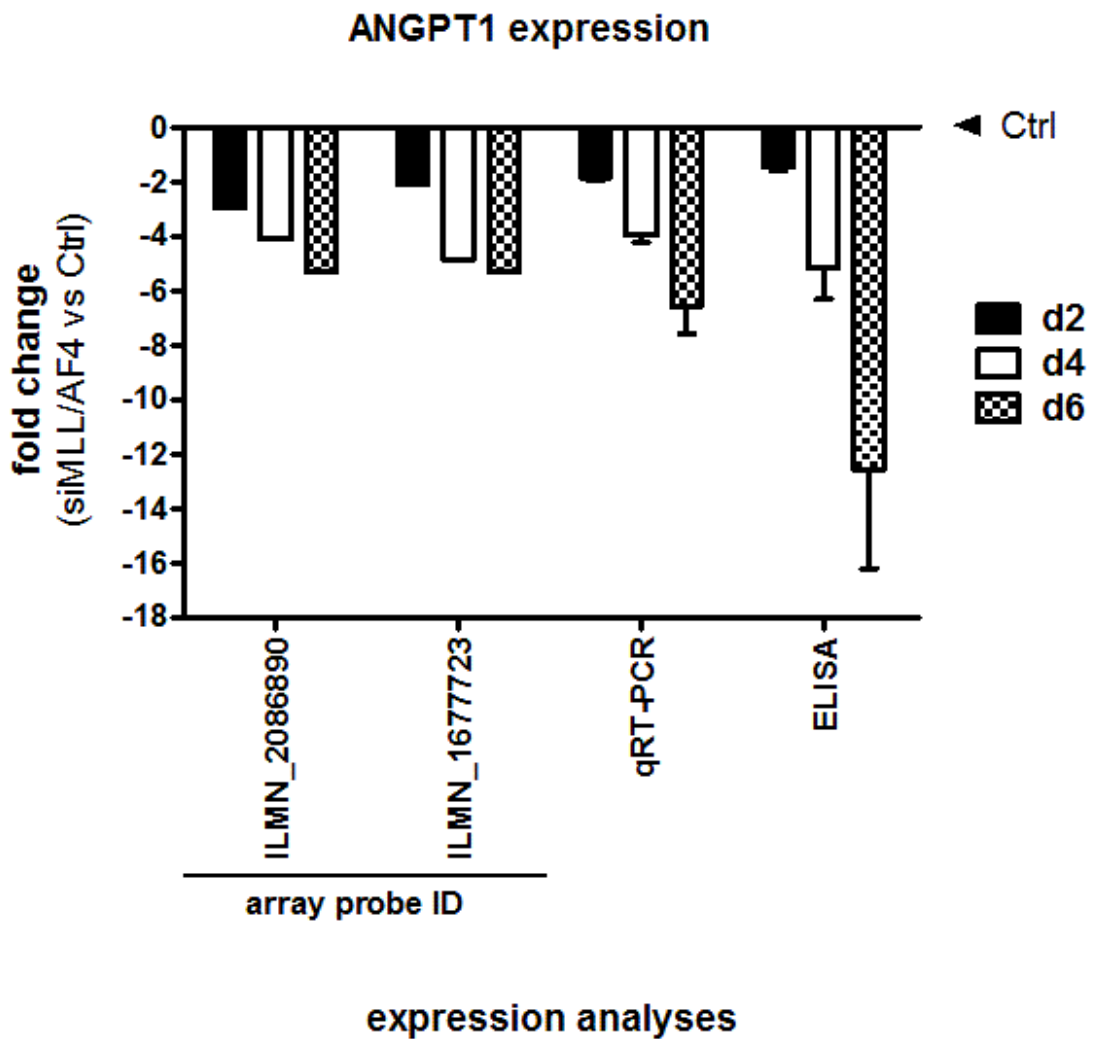


Fig. 5-4 Scheme comparing fold-change of *ANGPT1* RNA and protein expression in *MLL/AF4*-depleted SEM cells as determined by different analysis methods.

ANGPT1 expression in SEM was analysed over a time course of 2, 4 and 6 days of sustained *MLL/AF4* knock-down using gene expression profiling, qRT-PCR and ELISA, showing a concordant time-dependent decrease of *ANGPT1* levels compared to controls.

The differential expression of *ANGPT1* in response to MLL/AF4 knock-down observed in the arrays could be validated *in vitro* in SEM cell on both RNA and protein levels, showing a good concordance, as seen in the fig. 5-4, where the fold-changes in *ANGPT1* expression determined by all three analysis methods are summarised. Linear regression analysis showed a good correlation between the *ANGPT1* array probes, the qRT-PCR and the ELISA results. The corresponding correlation coefficients are listed in tab. 5-2.

Tab. 5-2: Correlation of ANGPT1 expression fold-changes between the different analysis methods

	ILMN_2086890	qRT-PCR	ELISA
ILMN_1677723	$r^2 = 0.8461$	$r^2 = 0.8489$	$r^2 = 0.6999$
ELISA	$r^2 = 0.9692$	$r^2 = 0.9678$	
qRT-PCR	$r^2 = 1.0000$		$r^2 = 0.9678$

5.1.2 Analysis of MLL/AF4-dependent ANGPT1 expression regulation in t(4;11)-positive ALL patient blasts

ANGPT1 expression is differentially regulated by MLL/AF4 in the model cell line SEM; in order to rule out an cell line artefact and to prove that this dependency is also present in t(4;11)-positive leukaemia, this correlation between MLL/AF4 and *ANGPT1* expression levels was investigated in patient blasts. Viable leukaemic blasts from a patient with t(4;11)-positive ALL, carrying the same MLL/AF4 breakpoint fusion site as the cell line SEM (courtesy of Dr. Ronald Stam), were singly electroporated with either siMLL/AF4, control siRNA (siAML1/MTG8), or mock-electroporated (MOCK). Cells were harvested at 24h, 48h and 72h post electroporation, and MLL/AF4 and *ANGPT1* expression determined by qRT-PCR. A knockdown of MLL/AF4 transcript levels comparable to the one in the SEM cells was achieved, with a sustained reduction by 54-64% over the course of three days (fig. 3-5). This MLL/AF4 decrease was accompanied with a time-dependent reduction of *ANGPT1* expression, 22% at 24h, 47% at 48h and 60% at the final time point (fig. 5-5B); thus confirming the link between MLL/AF4 and *ANGPT1* expression in t(4;11)-positive ALL.

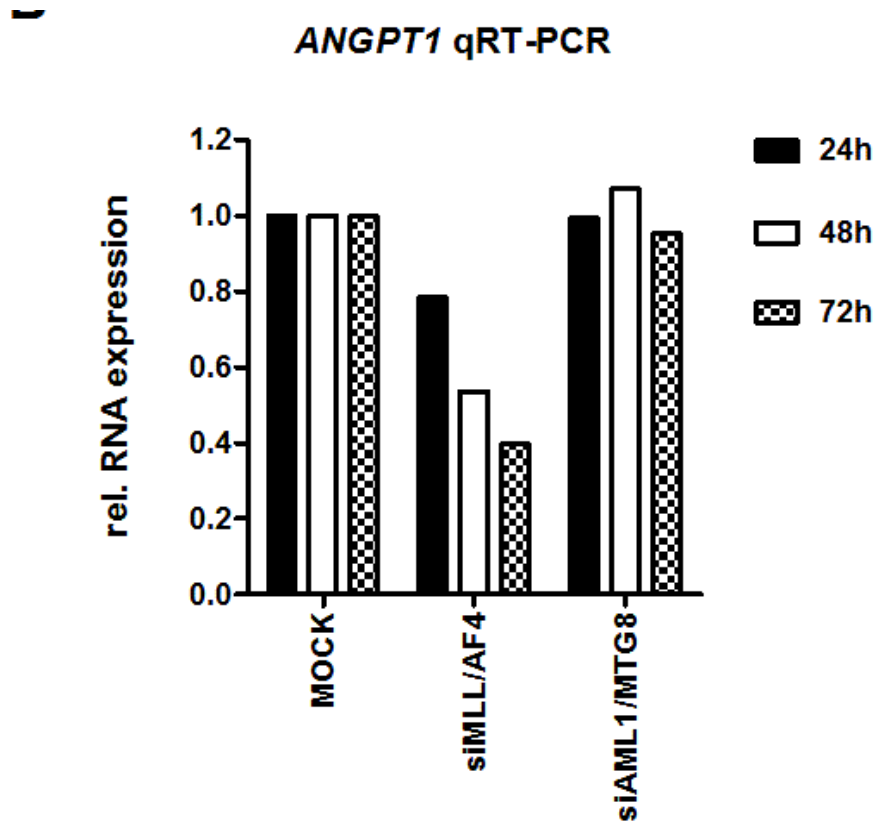


Fig. 5-5: Expression analysis of *ANGPT1* by qRT-PCR after siRNA treatment of primary patient blasts.

Primary patient blasts were electroporated once with siMLL/AF4, control siRNA (siAML1/MTG8) or without oligonucleotides (MOCK). *ANGPT1* expression analysis shows a time-dependent down-regulation of transcript levels in response to *MLL/AF4* knockdown from 22% at 24h to 60% at 72h. The graph represents the mean of one single experiments; each reaction was performed in triplicate.

5.2 ANGPT1 IS OVEREXPRESSED IN MLL-REARRANGED ALL

5.2.1 ANGPT1 expression levels in normal blood cells from healthy donors

Having shown that ANGPT1 levels in t(4;11)-positive cells correlate with their MLL/AF4 status, the next question to investigate was the overall *ANGPT1* expression in both normal blood cells and B-cell precursor ALLs (BCP-ALLs) in order to elucidate how the *ANGPT1* levels in t(4;11)-positive ALLs compare to other MLL-rearranged and MLL wild type (non-MLL) BCP-ALL and how the levels in the leukaemic cells related to the expression in healthy controls.

First, *ANGPT1* expression in healthy controls was assessed in order to gain insight in the normal *status quo*. Fractionated and purified peripheral blood (PB) subpopulations and umbilical cord blood (CB) cells derived from healthy donors were assayed for *ANGPT1* by qRT-PCR. The PB fractions consisted of purified T- (CD3+) and B-lymphocytes (CD19+), monocytes (CD14+) and neutrophils (CD15+), while hematopoietic stem and progenitors cells (HSPC) were enriched from the bulk CB population using the surface protein CD34 as selection marker. Fractionation of the cell subpopulations was carried out by Dr. Simon Bomken, who kindly gifted the corresponding RNA utilised for the qRT-PCR analyses.

Consistent with current findings implicating *ANGPT1* with HSC quiescence³²⁷, CD34+ CB cells showed a strong *ANGPT1* up-regulation when related to the bulk CB population (fig. 5-6). The mean *ANGPT1* expression in CD34-positive CB cells was 26.4-fold higher than in the bulk population.

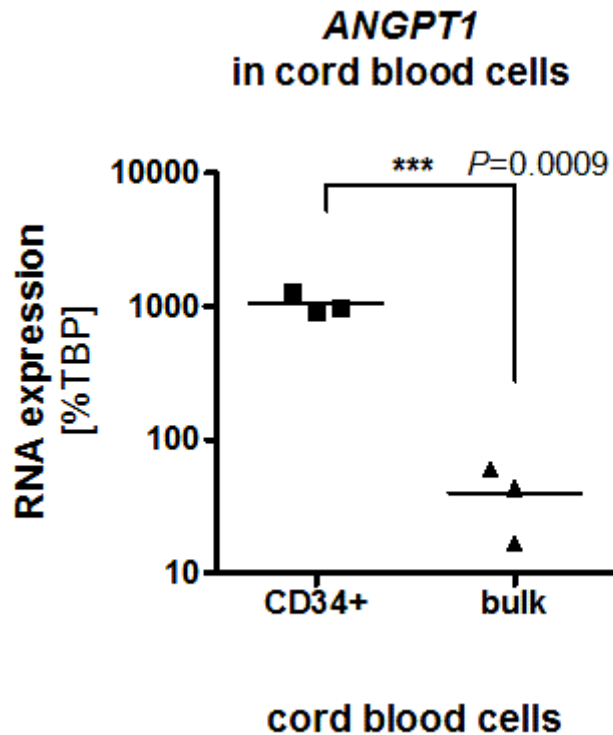


Fig. 5-6: *ANGPT1* expression analysis in purified and fractioned CB cell populations

Mononuclear CB cells were fractionated using MACS on the cell surface marker CD34. The bulk population was simultaneously purified by negative selection. *ANGPT1* levels were determined by qRT-PCR. The graph represents n=3 individual CB. Statistical analysis was performed using an unpaired Student's t-test.

In contrast, analysis of the PB cells showed *ANGPT1* to be expressed the lowest in the lymphoid lineage, both B- & T-cells having comparable quantities. Myeloid cells displayed higher *ANGPT1* levels with monocytes expressing *ANGPT1* approximately 15 times more than in the lymphocytes, and the neutrophils/granulocytes showing the highest expression with approximately 300 times the *ANGPT1* amount found in B-cells (fig. 5-7). This last result is in good concordance with published observations, in which *ANGPT1* secretion by neutrophils was shown to play a role in mediation of inflammatory processes.

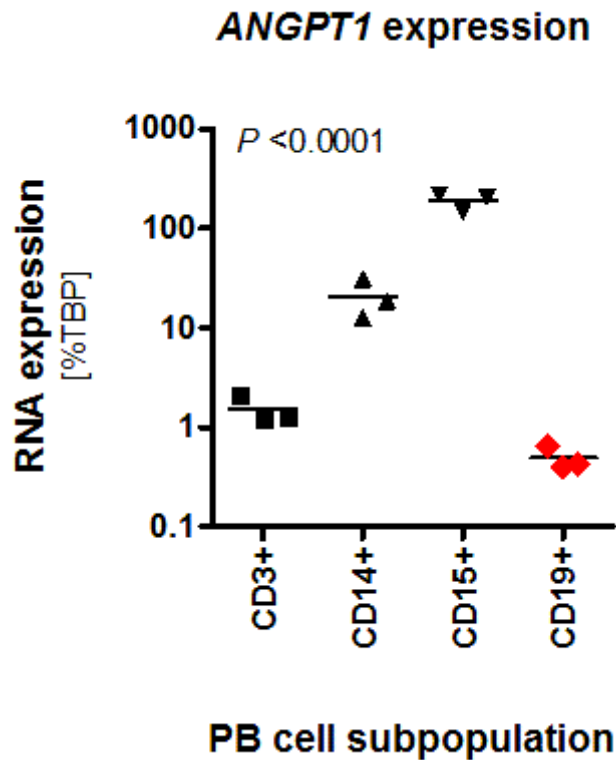


Fig. 5-7: *ANGPT1* expression analysis in peripheral blood (PB) cell subpopulations

Peripheral blood (PB) from 3 healthy donors was fractionated using magnetic activated cell sorting (MACS) on subtype-specific cell-surface markers: T-cells were isolated using CD3-antibodies, monocytes via CD14-, neutrophils purified on CD15- and B-cells were separated with CD19-antibody-conjugated beads. *ANGPT1* expression in the PB subpopulations was assessed by qRT-PCR and quantified using the Δ Ct-method, with *TBP* expression as endogenous control. Statistical analysis was performed using a parametric one-way ANOVA test.

5.2.2 ANGPT1 expression in acute leukaemia cell lines

Subsequent to establishing the *ANGPT1* expression patterns in healthy blood cells, *ANGPT1* levels were determined in leukaemic cell lines and patient blasts. An analysis cohort comprising 8 BCP-ALL cell lines was screened for *ANGPT1* expression by qRT-PCR. Strikingly, *ANGPT1* was restricted to the t(4;11)-positive cell lines, and no transcripts could be detected in the other cell lines (Fig. 5-8, upper panel). Comparing the two t(4;11)-positive ALL cell lines SEM and RS4;11, they showed a difference of approximately 10-fold in *ANGPT1* expression, SEM being the high expressing cell line. Additionally of note was the finding that the t(4;11)-positive ALL cell lines had approximately 1,000-fold to 10,000-fold higher *ANGPT1* levels than the t(4;11)-positive AML cell line MV4;11 (fig. 5-8, lower panel).

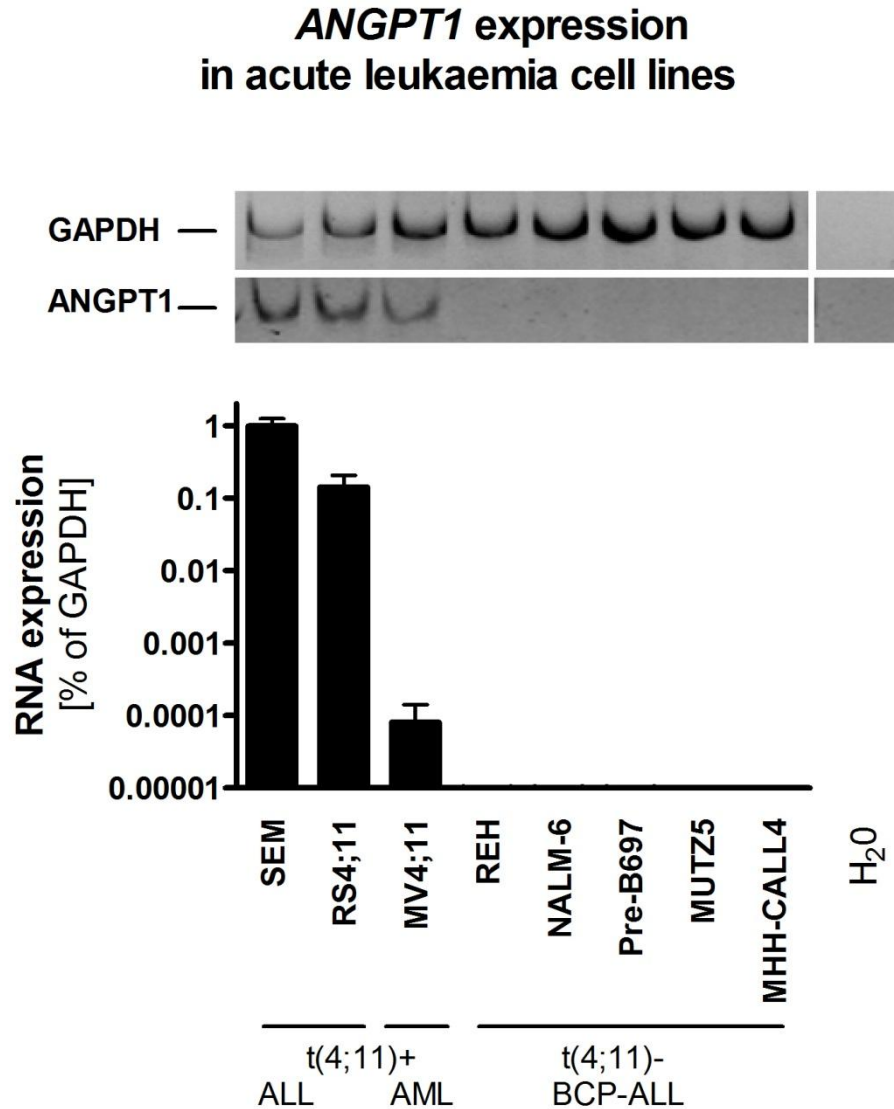


Fig. 5-8: *ANGPT1* expression analysis in an acute leukaemia cell line cohort

ANGPT1 levels in a leukaemia cell line panel were determined by qRT-PCR using the Δ CT-method with *GAPDH* expression as endogenous reference (lower panel). PCR products were visualised by DNA-polyacrylamide gel electrophoresis (upper panel). *ANGPT1* expression is restricted to the t(4;11)-positive leukaemic subtype, and showed massive up-regulation in the t(4;11)-positive ALL cell lines SEM and RS4;11 when compared to the t(4;11)+ AML cell line MV4;11. Graph represents mean of two individual experiments, error bars show data range.

Analysing *ANGPT1* expression in a small MLL-rearranged acute leukaemia cell line cohort which included the t(9;11)-positive AML cell line THP-1, this observation was corroborated, as the t(4;11)-positive ALL cell lines SEM and RS4;11 had a 10,000-1,000 fold higher expression than either of the MLL-rearranged AML cell lines (fig. 5-9).

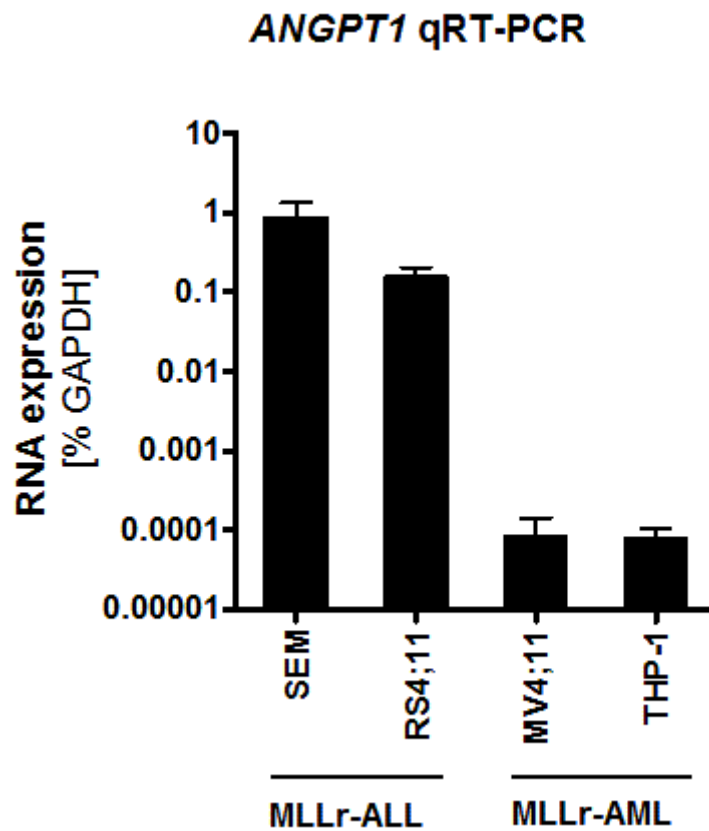


Fig. 5-9: *ANGPT1* expression analysis in MLLr acute leukaemia cell lines

ANGPT1 levels in a MLLr - acute leukaemia cell line panel were determined by qRT-PCR using the Δ CT-method with *GAPDH* expression as endogenous control. The t(4;11)+ ALL cell lines SEM and RS4;11 showed a 1,000-10,000-fold higher *ANGPT1* levels when compared to the MLLr AML cell lines MV4;11 and THP-1. The graph shows the mean of two individual experiments, error bars indicate the value range.

5.2.3 ANGPT1 expression in ALL patients

The results from the leukaemia cell line screen implied *ANGPT1* expression to be exquisitely restricted to the t(4;11)-positive ALL compartment. In order to validate this finding, *ANGPT1* levels were analysed in a BCP-ALL cohort of 43 patients, containing both MLL-rearranged (MLLr, n=31) and MLL wild type BCP-ALL (non-MLLr, n=12) cases. The cohort composition approximated incidence rates regarding cytogenetics, median age and gender ratio as observed in the clinical setting.

For instance, the MLLr panel comprised the three most common 11q23 abnormalities in ALL, t(4;11)-, t(9;11)- and t(11;19)-positive ALL. Moreover, the cytogenetic subgroups showed a similar distribution frequency to the one observed at clinical presentation: the cohort was composed of 55% t(4;11)-positive patients (n=17), 29% t(11;19)-positive ALL (n=9) and 16% BCP-ALL patients (n=5) with the t(9;11) abnormality. Additionally, 30 out of the 31 MLL-rearranged patients screened were infants (97%), the median age of presentation within the group being 5.18 months. The one exception was a paediatric BCP-ALL patient aged 14.7 years.

Concomitantly, the non-MLL rearranged group consisted of 4 infant and 8 paediatric BCP-ALLs, containing patients with both standard-risk cytogenetics such as hyperdiploidy (HeH, n=2) and t(12;21)-positive ALL (n=2), and intermediate to high risk cytogenetics such t(17;19) (n=1), t(1;17) (n=1) or dic(9;20) (n=1). No BCR/ABL-positive patients were included, but one of the infant patients was a down-syndrome-ALL (DS-ALL) patient (+21c). The median age at presentation of paediatric non-MLL cohort was 4.3 years, ranging from 1.4 to 14.2 years. Further patient details, such as white blood cell count (WBC) at presentation, immunophenotype and gender, were listed in table 5-3 for MLLr-ALL and table 5-4 for non-MLLr patients

Tab. 5-3: MLLr patient cohort characteristics

Patient ID	Cytogenetic phenotype	Immunophenotype	WBC [10⁹cells/L]	age at presentatio	gender
L826	MLLr t(4;11)	no data	346	7.5 months	male
L876	MLLr t(4;11)	no data	334	4.5 months	female
636	MLLr t(4;11)	pro-B	571.2	2.83 months	male
929	MLLr t(4;11)	pro-B	230	3.58 months	male
1587	MLLr t(4;11)	pro-B	234	0.62 months	female
3230	MLLr t(4;11)	pro-B	556.7	5.91 months	female
LR6073	MLLr t(4;11)	pro-B	28.1	4.00 months	female
LR11037	MLLr t(4;11)	no data	263.5	14.7 yrs	male
v9815	MLLr t(4;11)	pro-B	740	3.22 months	male
178	MLLr t(4;11)	pro-B	677	5.59 months	male
788	MLLr t(4;11)	pro-B	757	9.43 months	female
1174	MLLr t(4;11)	no data	25	no data	no data
1227	MLLr t(4;11)	pro-B	555	10.28 months	female
1488	MLLr t(4;11)	pro-B	326	4.21 months	female
1966	MLLr t(4;11)	pro-B	263	1.91 months	female
1977	MLLr t(4;11)	pro-B	291	6.41 months	female
1990	MLLr t(4;11)	pro-B	204	6.44 months	male
L880	MLLr t(9;11)	no data	171	2.3 months	female
119	MLLr t(9;11)	no data	132	7.28 months	male
148	MLLr t(9;11)	B-lineage not specified	88.2	0.36 months	female
620	MLLr t(9;11)	pre-B	57.5	9.82 months	female
656	MLLr t(9;11)	pre-B	55.8	4.21 months	male
39	MLLr t(11;19)	pro-B	574	7.72 months	male
474	MLLr t(11;19)	B-lineage not specified	no data	0.00 months	male
743	MLLr t(11;19)	pre-B	410.5	7.79 months	male
888	MLLr t(11;19)	pro-B	226.8	5.32 months	female
1037	MLLr t(11;19)	Common	226	8.77 months	female
1060	MLLr t(11;19)	pre-B	194	5.72 months	female
1191	MLLr t(11;19)	pre-B	741.3	9.10 months	male
1225	MLLr t(11;19)	Common	916	3.65 months	female
2009	MLLr t(11;19)	pro-B	416	0.00 months	female

Tab. 5-4 : non-MLLr patient characteristics

Patient ID	Age group	Cytogenetics	Immuno-phenotype	WBC [10 ⁹ cells/L]	age at presentation	gender
v9932	infant	+21c	pro-B	167.2	0.0 months	male
382	infant	t(1;19)	no data	no data	no data	no data
824	infant	complex karyotype	pro-B	178	9.07 months	male
945	infant	no known aberration	no data	324.1	no data	no data
L554	paediatric	t(3;17)	no data	78.5	7.0 yrs	male
L578	paediatric	HeH	no data	4.1	3.7 yrs	female
L625	paediatric	t(17;19)	no data	3.5	14.0 yrs	male
L679	paediatric	dic(9;20)	no data	3.1	4.9 yrs	male
L682	paediatric	G-Band. failed	no data	279	1.4 yrs	male
L749	paediatric	t(12;21)	no data	37.7	6.1 yrs	female
L848	paediatric	t(12;21)	no data	13.7	2.5 yrs	male
L855	paediatric	HeH	no data	9.5	3.3 yrs	female

ANGPT1 levels in the patient cohort were determined by qRT-PCR using the Δ CT-method as described. *TBP* served as endogenous reference gene, and the resulting Δ CT-values were given as percentage of TBP expression. The patient material source was either PB or BM, in cases where both sources had been assessed in the same patient, the resulting *ANGPT1* expression was averaged. The patient screen was a collaborative effort between my person at the Northern Institute for Cancer Research, Newcastle University, UK, and the laboratory of Dr. R. W. Stam, at the Erasmus MC in Rotterdam, the Netherlands. The BCP-ALL patient and part of the MLLr patient cohort was screened here, and the non-MLL infant and part of the MLLr cohort had been analysed by my collaborators. The subsequent expression data shown in the following figures are the summarised results from both centres.

First, in order to relate *ANGPT1* levels to known biological and clinical parameters associated with disease progression and survival, the patient cohort was grouped according to its major cytogenetic subdivisions, MLLr and non-MLLr BCP-ALL, regardless of age at presentation, since clinically, MLLr ALL patients have an overall worse outcome. As illustrated in fig. 5-10, there is strong up-regulation of

ANGPT1 expression in MLLr patients, with a median of 33-fold higher *ANGPT1* levels when compared to MLL-wild type cells. This result was statistically significant, as determined by an unpaired Student's t-test ($p= 0.027$).

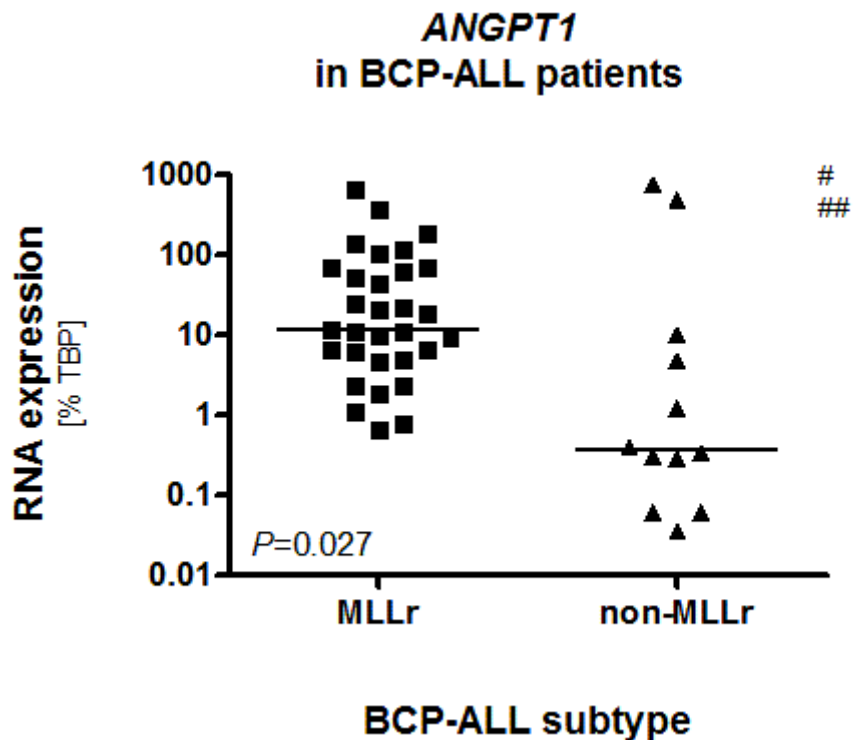


Fig. 5-10: *ANGPT1* expression in BCP-ALL patients according to MLL-status

Patients were grouped according to the cytogenetic MLL-status. *ANGPT1* RNA levels in ALL blasts were determined by qRT-PCR using the ΔC_t -method with *TBP* expression as endogenous control. Patients with MLL-rearranged (MLLr) ALL (n= 31) showed a significantly higher *ANGPT1* expression than patients with non-MLLr (n=12). Samples highlighted by # and ## are infant nonMLLr patients either pre-treated with Allopurinol (#) or a DS-ALL patient with congenital ALL (##). Statistical analysis was performed using an unpaired Student's t-test on log-transformed values.

These cohorts were subdivided further according to cytogenetic and age-related categories; the MLLr group was separated into t(4;11)+, t(9;11)+ and t(11;19)+ ALL, and the non-MLL ALL cohort sorted into infant and non-infant non-MLL ALL. As a point of comparison with healthy levels, the Δ CT of values of CD19+ cells derived from the PB of healthy donors were also included (fig. 5-11).

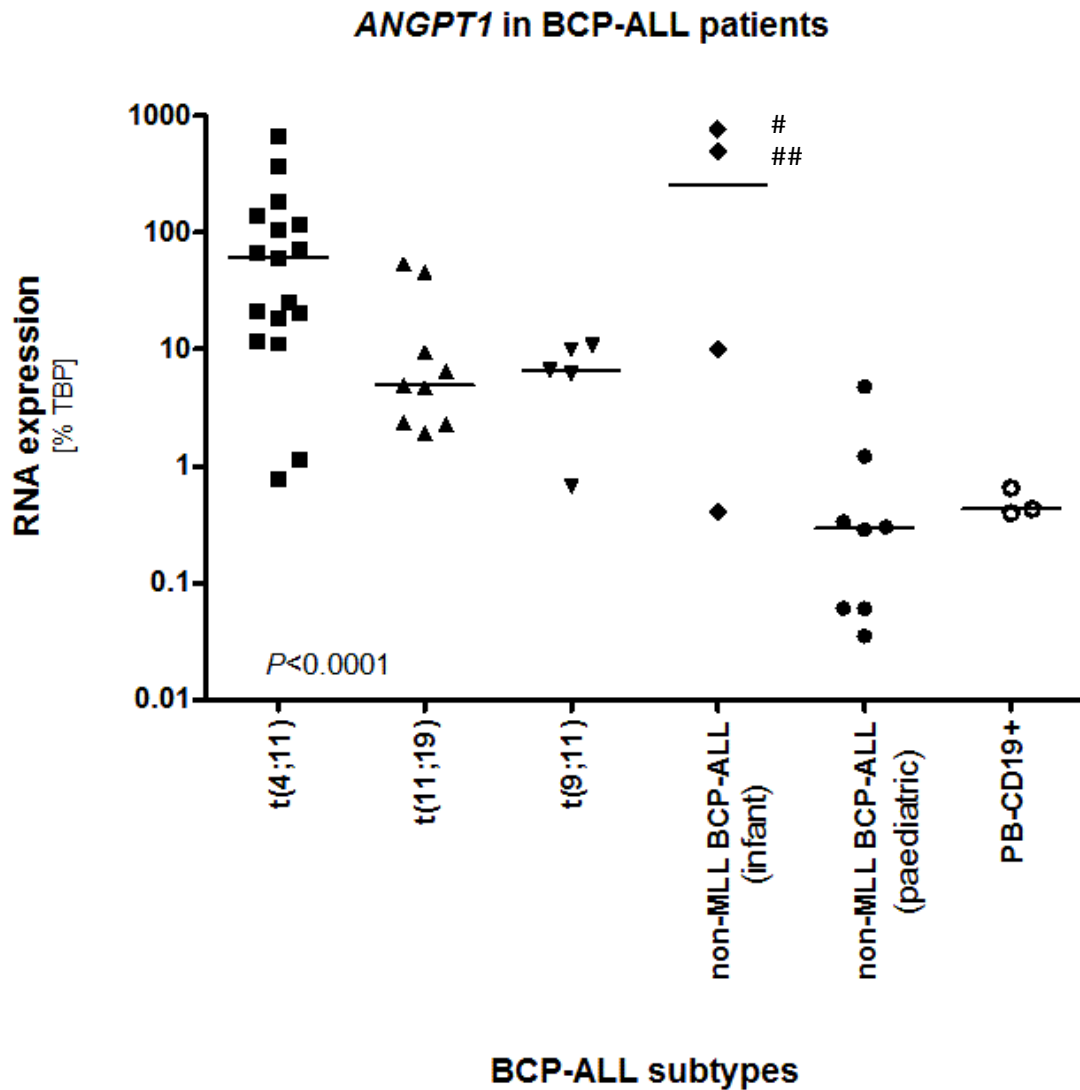


Fig. 5-11: ANGPT1 expression in BCP-ALL patients sorted according to cytogenetic subtype

The patient panel was subdivided according to cytogenetic and biological subtype; ANGPT1 levels determined by qRT-PCR using the Δ Ct-method with TBP expression as endogenous control. Statistical analysis was performed using ANOVA on log-transformed values. (## = DS-ALL, # = patient pre-treated with Allopurinol)

Tab. 5-5: Statistical analysis on *ANGPT1* levels between the different BCP-ALL subtypes using unpaired Student's t-test on log-transformed values

Analyses	P-Value
t(4;11) vs. non-MLL paediatric BCP-ALL	<0.0001
t(11;19) vs. non-MLL paediatric BCP-ALL	0.0003
t(9;11) vs. non-MLL paediatric BCP-ALL	0.0054
non-MLL infant vs. non-MLL paediatric BCP-ALL	0.0074
t(4;11) vs. t(11;19)	0.0190
t(4;11) vs. t(9;11)	0.0287
t(11;19) vs. t(9;11)	0.6271
t(4;11) vs. non-MLLr infant BCP-ALL	0.9517
t(11;19) vs. non-MLLr infant BCP-ALL	0.2311
t(9;11) vs. non-MLLr infant BCP-ALL	0.2777

The t(4;11) positive cohort significantly expressed the highest *ANGPT1* levels, with a median up-regulation of 143-fold compared to normal B-cells, followed by the t(9;11) cohort, expressing 11-fold more *ANGPT1*, and the t(11;19)-positive groups, with 15.4-fold increased median *ANGPT1* levels when comparing to healthy control cells. In contrast, the paediatric non-MLL patients did not show up-regulation of *ANGPT1*, but slightly reduced levels, with a median expression of 0.7-fold compared to healthy B-cells. Normalising the MLLr subcategories against the non-MLLr cases showed that *ANGPT1* was 208-times higher expressed in t(4;11)-positive cases, while t(11;19)- and t(9;11)-positive patients had a 17- and 22-fold up-regulation. The notable exception was the non-MLL infant ALL group, with n=4 patients also the smallest cohort. Here, the trend of the *ANGPT1* expression was not as clearly defined as with the other subgroups, as two patients massively up-regulated *ANGPT1*, while the remainder expressed *ANGPT1* to much lower extent. Clearly, with this extent of inter-patient variance, the patient number was too small to draw definitive conclusions. Of interest was that the two high expressing patients deviated from the overall patient cohort, one being an infant DOWN-

Syndrome ALL (DS-ALL) patient, and the other having been treated with Allopurinol prior to sampling, a drug administered to prevent tumour lysis and thus affecting leukemic blasts directly. Hence, both patients, although included in the analyses, have to be interpreted with caution.

The median expression differences between the BCP-ALL subcategories are summarised in tab. 5-6.

Tab. 5-6: Median fold-change ANGPT1 expression between ALL subgroups

	median Fold-change (vs. BCP-ALL)	median Fold-change (vs. PB)
t(4;11)	207.92	142.59
t(11;19)	16.62	11.40
t(9;11)	22.40	15.36
MLL germline	856.76	587.55
BCP-ALL	/	0.69

Summarising these results, the overall *ANGPT1* expression levels were significantly different between the cytogenetic groups, as determined using one-way ANOVA test ($p < 0.0001$, fig. 5-5). Patients with MLLr ALL, particularly carrying the t(4;11) abnormality, significantly overexpressed *ANGPT1* compared to patients with other MLL wild-type BCP-ALL subtypes. Additionally, there seemed to be a clear tendency towards up-regulation of *ANGPT1* in infant ALL compared to paediatric ALL. Hence, taking into account that *ANGPT1* is expressed the highest in CD34+ cord blood cells in healthy controls, and that infant ALL patients have a higher incidence of more immature pro-B ALL, the infant MLLr ALL patients were sorted according to the blast maturity into pro-B and pre-B ALL patients. Indeed, infant patients with pro-B ALL significantly over-expressed *ANGPT1* compared to pre-B-ALL patients ($p = 0.0031$, unpaired Student's t-test), with a median expression of 117-fold versus 5-fold, respectively (fig. 5-12).

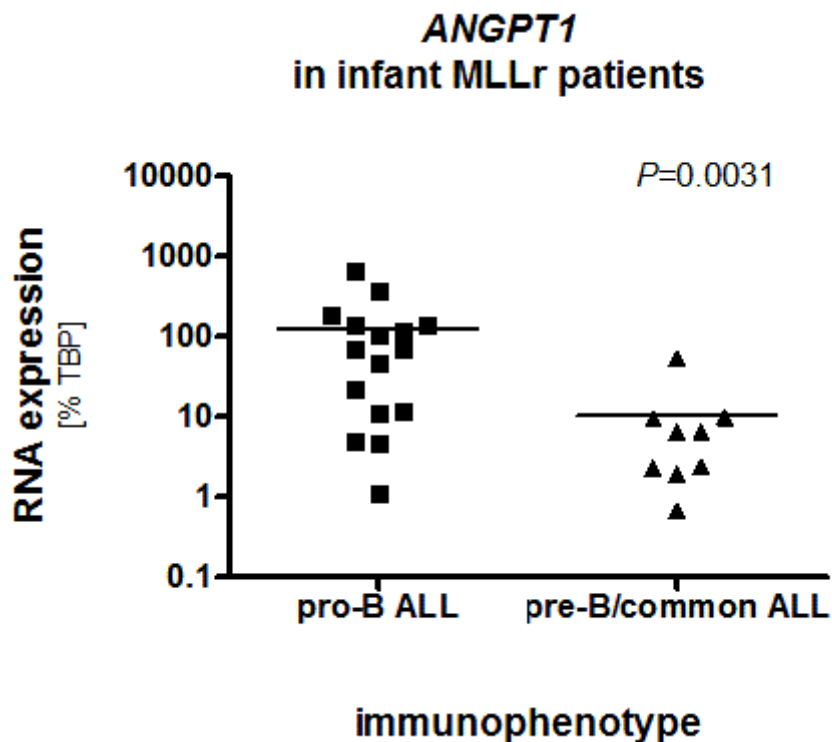


Fig. 5-12: ANGPT1 expression in BCP-ALL patients according to age and immunophenotype

Infant MLLr patients with known leukaemia-associated immunophenotype (LAIP) (n= 25 , age at diagnosis < 12 months) were sorted according to CD10-status (pro-B: CD10-ve, pre-B/common ALL: CD10+ve) at presentation, as this has been linked to prognosis. *ANGPT1* was determined by qRT-PCR using the Δ Ct-method with *TBP* levels as endogenous control. Patient blasts with a pro-B LAIP (n=16 cases) expressed 10.85 times more *ANGPT1* than blasts from patients with a more mature LAIP (n=9). Statistical analysis was performed using an unpaired Student's t-test on of-transformed values.

5.3 CORRELATING ANGPT1 EXPRESSION WITH PROGNOSTIC FACTORS

5.3.1 ANGPT1 expression correlates with clinical parameters

ANGPT1 is overexpressed in MLL-rearranged ALL, especially in the t(4;11)-positive subtype. These cytogenetic categories are both adverse prognostic factors, specifically t(4;11)-positive ALL is associated with poor outcome across infant, paediatric and adult ALL. In order to elucidate the role of *ANGPT1* in MLLr-ALL in general and t(4;11)-positive ALL in particular, *ANGPT1* expression levels in patients were correlated with clinical parameters employed to risk-stratify patients. The parameters available were age at presentation and white blood cell count (WBC); however, these parameters differ between infant and paediatric BCP-ALL. In infants, independent adverse prognostic factors are an age at presentation below 6 months and a WBC > 300x10⁹/L. In contrast, patients presenting at an age above 10 years or a WBC > 50x10⁹/L are associated with poor outcome in paediatric BCP-ALL .

Surveying the patient cohort statistics listed in tab. 5-7, there seems to be a trend between high *ANGPT1* levels and the association with adverse prognostic factors: the highest median *ANGPT1* expression could be found associated with the highest median WBC, and vice versa. However, in order to be able to give definitive correlations and associations, statistical analyses were performed.

Tab. 5-7: Patient cohort statistics

	age range	median age at presentation	median WBC [10⁹/L]	geometric mean <i>ANGPT1</i> [%TBP]
MLLr	0.00 months to 14.7 yrs	5.18 months	277.25	33.83
<i>t(4;11)</i>	0.62 months to 14.7 yrs	5.05 months	326.00	37.93
<i>t(9;11)</i>	0.38 - 9.82 months	3.26 months	88.20	6.92
<i>t(11;19)</i>	0.00 - 9.82 months	5.72 months	413.25	4.95
non-MLL	0.01 months-14.0 yrs		27.77	2.75
<i>infant</i>	0.01months-9 months	No data	178	35.21
<i>paediatric</i>	1.4-14 yrs	4.3 yrs	11.6	0.26

First, *ANGPT1* expression was correlated with age at presentation. Since the paediatric BCP-ALL group only contained n=2 patients in the age-risk category, no analysis was performed, as the cohort was too small to yield statistically significant results. The infant MLLr-ALL panel however had an appropriate age distribution. Information on age at presentation of n=30 patients was available; the patients were grouped into the two risk categories of age at presentation <6 and >6 months at presentation. As depicted in fig. 5-13, there is no significant difference in *ANGPT1* expression between the two groups ($p=0.8566$).

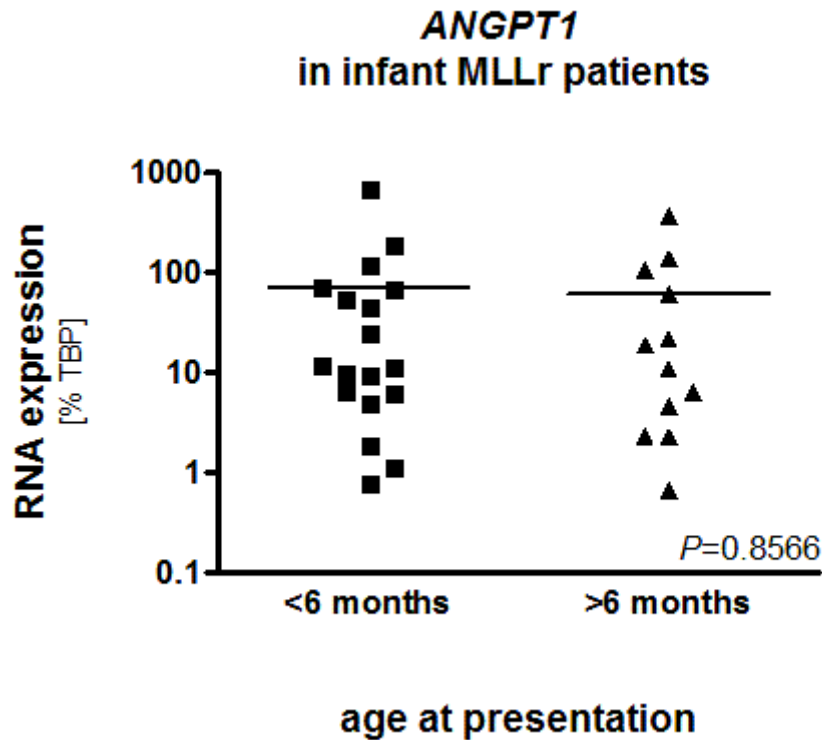


Fig. 5-13: *ANGPT1* level in infant MLLr patients according age-risk stratification

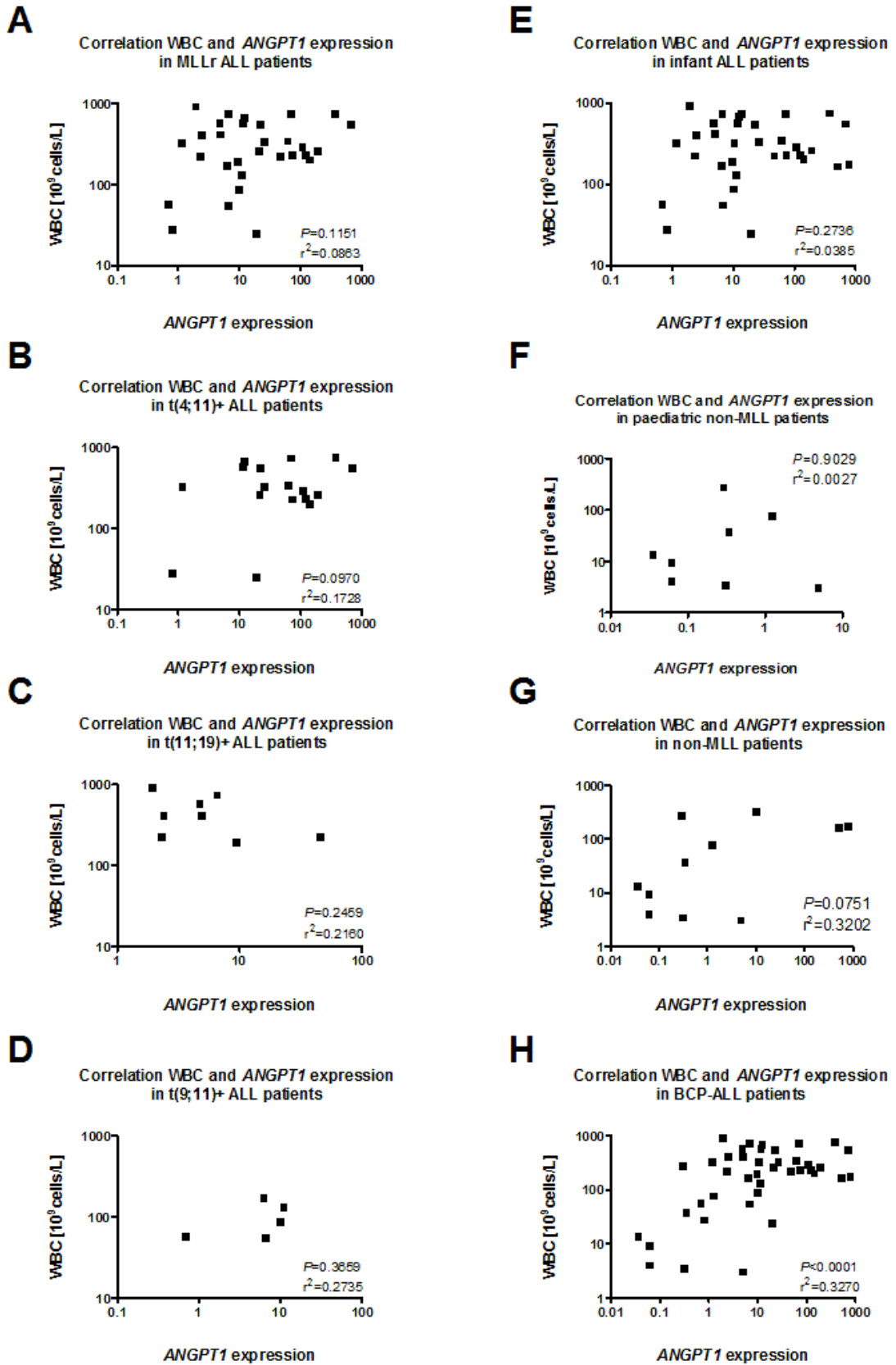
Infant MLLr patients were sorted according to age into presentation, and *ANGPT1* was determined by qRT-PCR using the ΔC_t -method with *TBP* levels as endogenous control. Blasts originating from patients younger than 6 months at diagnosis (n=18) expressed *ANGPT1* to approximately the same levels as blasts from older infants (n=12). Statistical analysis was performed using an unpaired Student's t-test on of-transformed values.

A very important clinical parameter associated with disease progression and outcome is the blast burden at presentation, as measured by the WBC. This information was available from n=42 patients, and correlation analyses of the patient cohort pairing the respective *ANGPT1* levels and the WBC was performed. There was no statistically significant correlation between *ANGPT1* levels and WBC within the MLLr ALL patient cohort ($P=0.1209$, $r^2=0.06377$), as shown in fig. 5-14A. Breaking down the MLLr cohort into the respective cytogenetic subtypes, there was no statistically significant correlation between *ANGPT1* levels and WBC within neither the t(9;11)-positive nor the t(11;19)-positive ALL cohort, (fig.

5-14C, D). Correlation analysis between *ANGPT1* expression and WBC within the t(4;11)-positive patient group showed a trend towards high expression levels correlating with high WBC (fig. 5-14B). This observation was borderline statistically non-significant ($P=0.097$, $r^2=0.1728$). There was no correlation of *ANGPT1* expression and WBC within the infant ALL cohort as a whole, which contained both MLLr and non-MLL patients. Analysing the non-MLL cohort, there was no correlation, although again here a trend could be observed, as the statistical non-significance was borderline ($p=0.0751$, $r^2=0.321$). Finally, analysing all the patient cohort without taking into account age and MLLr status, there was a very high statistical significance between *ANGPT1* expression levels and high WBC ($p<0.0001$, $r^2=0.2977$). This latter result has to be taken with caution, due to the skewedness of the patient cohort composition, with its strong MLLr-ALL bias.

Fig. 5-14: Correlation between *ANGPT1* expression levels and WBC in ALL

The ALL patient cohort (n=43) was subdivided according to MLLr status and age at presentation, and the *ANGPT1* expression levels correlated with WBC at diagnosis. MLLr patients showed no significant correlation between *ANGPT1* and blast burden (A) nor within the MLLr cytogenetic subgroups (B-D), although t(4;11)-positive ALL patients showed a definitive trend with high expression correlating with increased WBC at presentation (B). A similar trend could be observed when analysing the correlation within non-MLLr patients (G). Grouping the patients according to age at presentation showed no significant correlation within infant patients regardless of MLLr status (E), or in nonMLLr paediatric ALL patients (F). Analysing the complete patient panel however revealed a very significant correlation between *ANGPT1* expression and WBC at diagnosis (H), although this result has to be taken with caution due to the high bias of the cohort towards MLLr patients (n=31), which have *per definitionem* a high WBC and high *ANGPT1* expression at diagnosis. Statistical analysis was performed using a Pearson Correlation test on log-transformed data.



5.3.2 Correlation analysis of ANGPT1 expression with biological prognostic factors

In parallel to clinical parameters, there are a number of biological factors that have been associated with disease outcome in MLLr-ALL and especially with t(4;11)-positive ALL, such as specific DNA methylation and gene expression signatures. Part of these specific signatures is the family of the HOXA transcription factors. In a healthy setting, wild-type MLL is important to maintain *HOXA* gene expression during early haematopoiesis, while *HOXA* genes are down-regulated in differentiating haematopoietic cells. Conversely, an aberrant *HOXA* gene expression has been implicated in acute leukaemia, and different leukaemia subtype-specific mechanisms have been suggested. In MLLr acute leukaemia, both MLL/AF4 and other MLL fusion oncogenes have been found to directly bind to promoters of the *HOXA* gene cluster and to regulate their aberrant expression, and until recently, up-regulation of members of the *HOXA* gene had been heralded as one of the hallmarks of MLLr leukaemia. However, latest reports indicate that MLLr infant ALL patients can be subdivided into a *HOXA*-high and a *HOXA*-low expressing group, with low *HOXA* levels having an adverse effect on survival¹⁶⁸.

Not much is known about target genes of HOXA transcription factors; recently, our research group identified the HOXA family member HOXA7 to bind and regulate TERT expression¹⁷⁰. TERT is the catalytic subunit of the ribozyme telomerase, which has been associated with the self-renewal capability of stem cells and implicated in oncogenesis. The fact that ANGPT1, too, had been reported to play a role in haematopoietic stem cells, and now in this work has been shown to be up-regulated in MLLr-ALL, led to the question whether *ANGPT1* was a HOXA target gene. This was investigated *in silico*, using the Transcription Element Search System (TESS) software to analyse the *ANGPT1* promoter. An area 5kb upstream and 1kb downstream of the *ANGPT1* transcription start site (TSS) was screened for transcription factor binding motifs. The *ANGPT1* promoter revealed several putative HOXA transcription factor binding sites as illustrated in fig. 5-15.

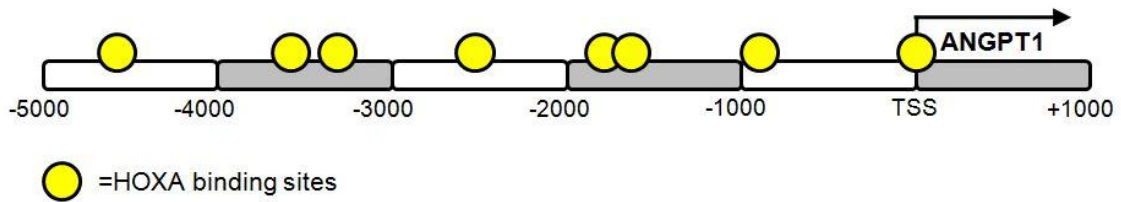


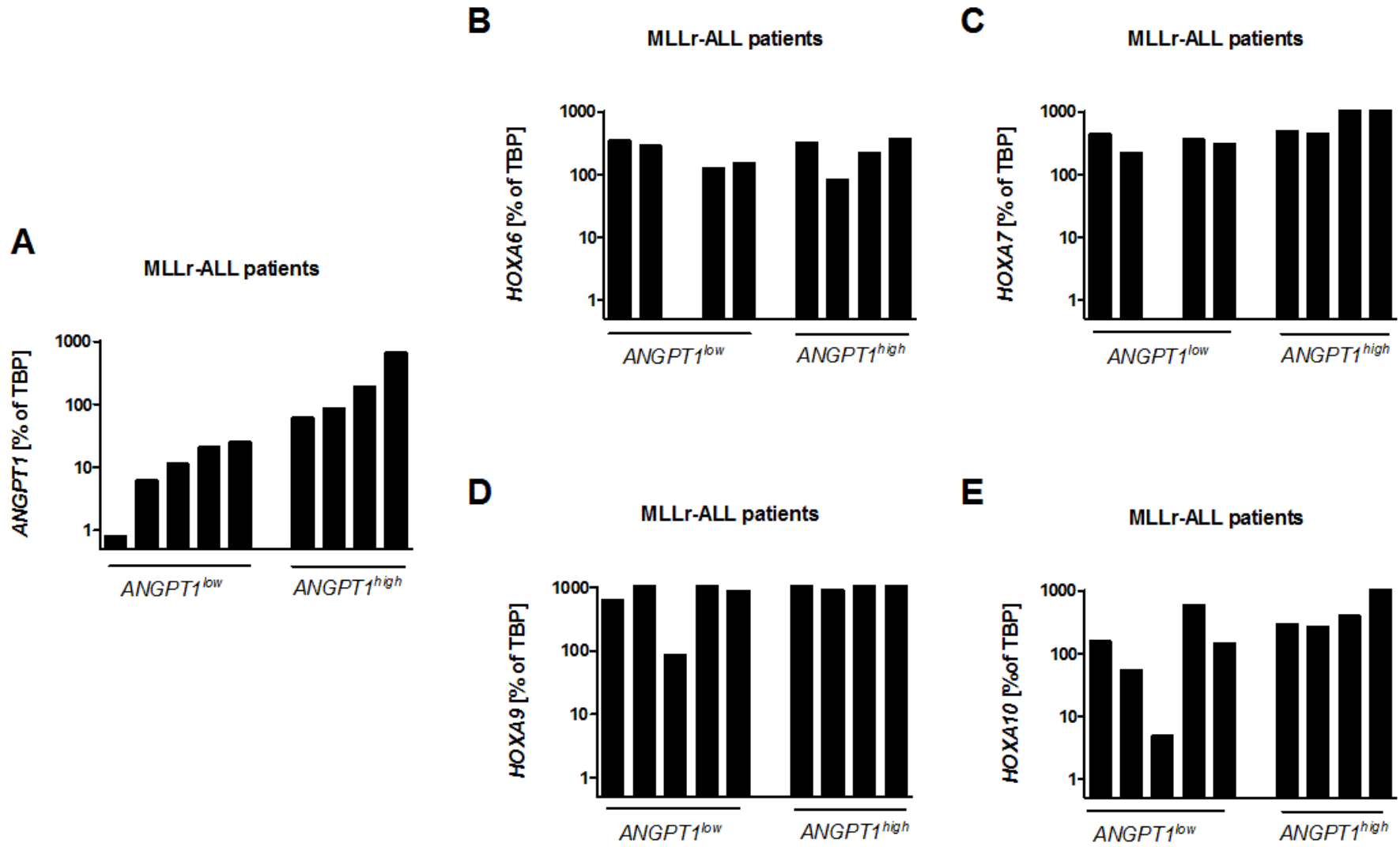
Fig. 5-15: Scheme HOXA gene binding sites within the ANGPT1 promoter

Bioinformatic analysis of transcription factor binding sites within the *ANGPT1* promoter region encompassing 5000bp upstream and 1000bp downstream of the transcription start site (TSS) using Transcription Element Search System (TESS) analysis software platform (<http://www.cbil.upenn.edu/cgi-bin/tess/tess>).

Consequentially, a correlation study between *ANGPT1* and *HOXA* gene expression levels was conducted in a panel of n=9 MLLr-ALL patients. The patients were subdivided into either *ANGPT1*-high or *ANGPT1*-low expressing cells, with the panel-specific median *ANGPT1* expression level as cut-off, and sorted according to increasing levels. Subsequently, the expression of the *HOXA* gene cluster members *HOXA6*, *HOXA7*, *HOXA9* and *HOXA10* was analysed using qRT-PCR. As indicated in fig. 5-16, there was no obvious correlation between *ANGPT1* levels and those of any of the *HOXA* gene cluster members assayed; this was confirmed further by statistical analyses using Pearson correlation tests (tab. 5-8).

Fig. 5-16: Correlation between *ANGPT1* and *HOXA* gene expression levels

A MLLr patient cohort was analysed for *HOXA6*, *HOXA7*, *HOXA9* and *HOXA10.2* expression levels by qRT-PCR, and subsequently sorted according to *ANGPT1* expression. No correlation between the respective expression levels could be detected.



Tab. 5-8 Statistical Correlation of *ANGPT1* and *HOXA* gene expression

Analyses	P-Value	Pearson r ²
MLLr and HOXA6	0.6769	0.0263
MLLr and HOXA7	0.3267	0.1067
MLLr and HOXA9	0.0825	0.3694
MLLr and HOXA10.2	0.1554	0.3055

In concordance with these results, siRNA-mediated depletion of *HOXA7* in the t(4;11)-positive ALL cell line SEM showed no effects on *ANGPT1* expression (fig. 5-17).

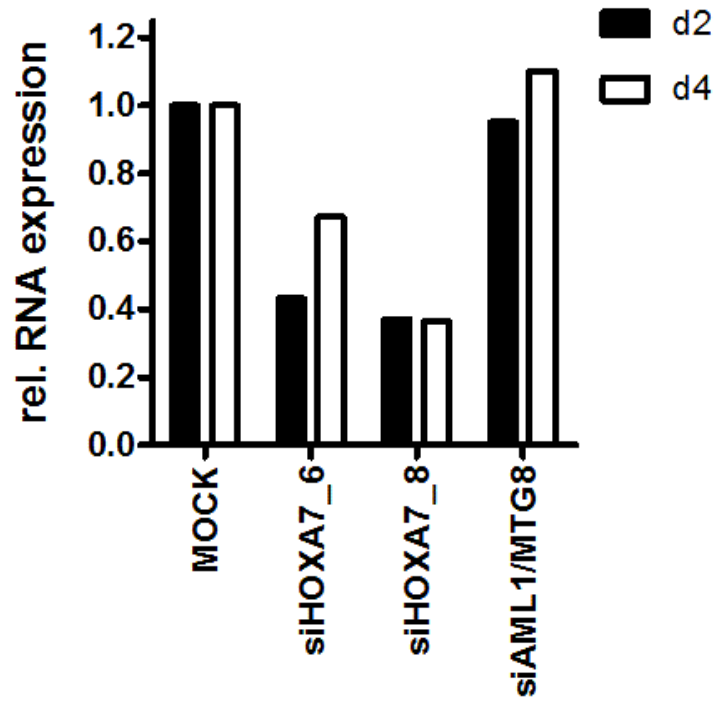
Although the overall rationale of this study indicated a possible connection between *ANGPT1* and *HOXA* gene cluster expression, this could not be confirmed. The promoter analysis revealed other putative binding sites of haematopoietic or oncogenic transcription factors; further work is required to unravel the mechanism by which *ANGPT1* expression is driven in MLLr-ALL.

Fig. 5-17: *HOXA7* and *ANGPT1* expression in siHOXA7 treated SEM cells

SEM cells electroporated were electroporated twice at 2-day intervals with siRNAs against *HOXA7* (siHOXA7_6, siHOXA_8), controls siRNA (siAML1/MTG8) or no siRNA (MOCK). *HOXA7* down-regulation had no effects on *ANGPT1* expression levels when compared to controls. The figure shows one single experiment, each sample was performed in triplicates.

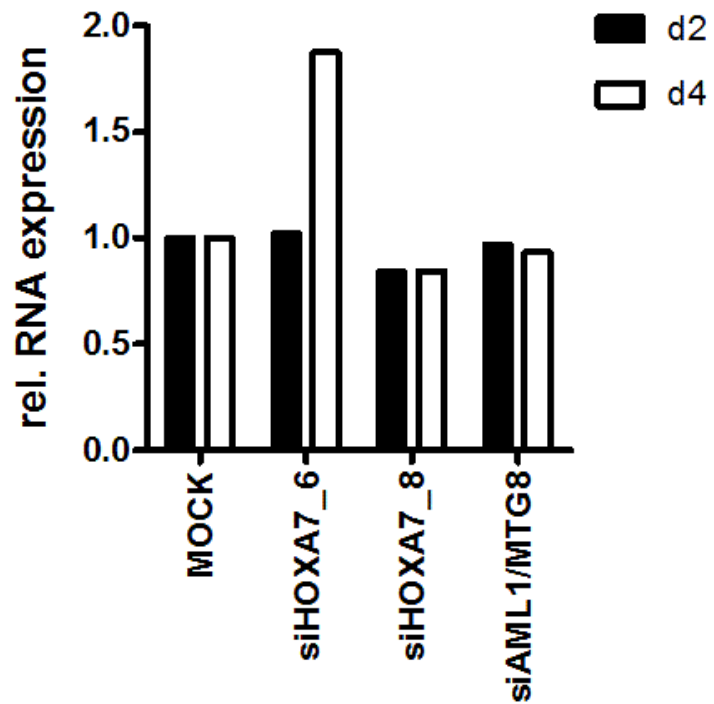
A

HOXA7 qRT-PCR



B

ANGPT1 qRT-PCR



5.3.3 ANGPT1 secretion in t(4;11)-positive ALL patients

The expression of ANGPT1 in patients was not only determined on RNA level, but where material available, also on protein level. Viable t(4;11)-positive patient PB cells were cultured in conditioned medium (CM) for 3 days, and the supernatant harvested and analysed for secreted ANGPT1 by ELISA.

As shown in fig. 5-18, all three patients assessed expressed measurable ANGPT1 levels above the high ANGPT1 background created by the conditioned medium. These secretion levels correlated well with the corresponding *ANGPT1* RNA expression levels detected via qRT-PCR ($r^2=0.5522$).

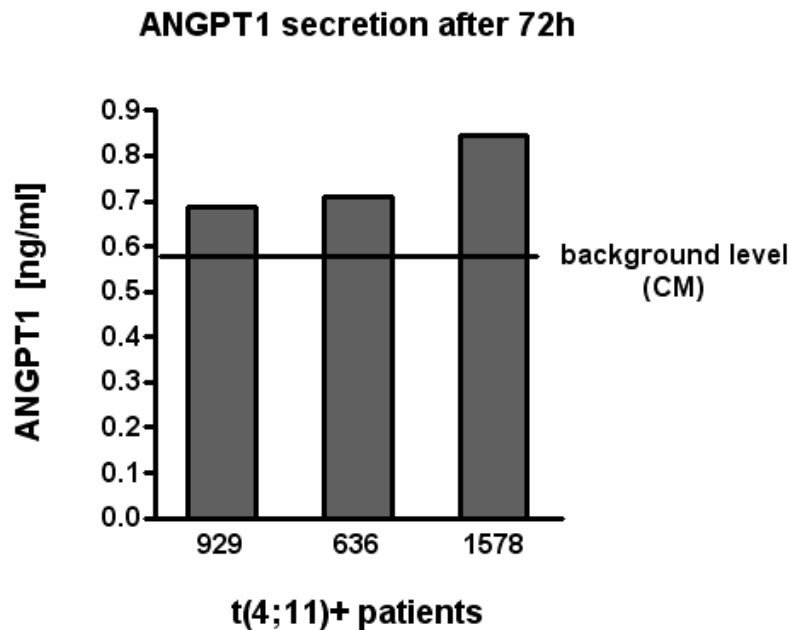


Fig. 5-18: ANGPT1 secretion determined in the supernatant of cultured t(4;11)+ patient blasts

Primary patient material was cultured in conditioned medium (CM) for 72h. ANGPT1 secretion by patient blast was determined in the culture supernatant using an ELISA. The graph represents one single experiment, each sample performed in duplicates.

5.4 FUNCTIONAL ANALYSIS OF ANGPT1 IN t(4;11)-POSITIVE ALL IN VITRO

As shown in previous section ANGPT1 is significantly overexpressed in MLLr-ALL, especially in the t(4;11)-positive subtype; moreover, a functional correlation between MLL/AF4 and ANGPT1 expression levels in both cell line models and patient material could be demonstrated. Hence, I proceeded to assess the functional role of ANGPT1 in t(4;11)-positive ALL; since ANGPT1 is primarily a secreted growth factor, t(4;11)-positive cells were characterised for gene expression of known ANGPT1 receptors, and an autocrine role of ANGPT1 studied analysing the effects of RNAi-mediated ANGPT1 depletion in the model cell line SEM.

5.4.1 Expression Analyses of ANGPT1 Receptors in t(4;11)-positive ALL

The growth factor *ANGPT1* is associated with multiple signalling pathways; canonical *ANGPT1* signalling occurs by binding to the membrane receptor tyrosine kinase (RTK) TIE2, also known as TEK. This ligand-receptor interaction results in autophosphorylation and activation of TIE2, triggering in turn downstream signalling, most notably the PI3K/AKT pathway³²⁸⁻³³⁰. TIE1, an orphan RTK homologous to TIE2, has been implicated to bind ANGPT1, but the effects of this interaction on downstream pathways are not fully understood³³¹. Conversely, non-canonical *ANGPT1* signalling does not require TIE2, but involves specific integrin heterodimers; the concomitant outside-in signalling activates downstream pathways such as the PI3K/AKT or MAPK signalling³³²⁻³³⁴. Additionally, heparin-mediated, integrin- and TIE2-independent ANGPT1 signal-transduction has been reported³³⁵.

In order to study a putative autocrine function of ANGPT1 on t(4;11)-positive ALL cells, the expression of reported ANGPT1 receptors were characterised in t(4,11)-positive cell lines and patients.

A leukaemia cell line panel was screened for expression of the canonical ANGPT1 receptor TIE2. As seen in fig. 5-19A, no *TIE2* could be detected in the BCP-ALL cell

lines, regardless of their MLLr status. Only the t(8;21)-positive AML cell line Kasumi-1 showed *TIE2* expression. Interestingly, *TIE2* RNA was also not present in the t(4;11)-positive AML cell line MV4;11, while the t(9;11)-positive cell line THP-1, expressed *TIE2* strongly. In patients, however, the findings were quite the opposite; the *TIE2* transcript could be detected by RT-PCR in 7 out of 8 screened t(4;11)-positive ALL patients (fig. 5-19B), thus confirming the possibility of an autocrine action by ANGPT1 in t(4;11) cells.

Another membrane receptor associated with ANGPT1 is TIE1, which shares homology with TIE2. Its exact function in ANGPT1 signalling, however, remains to be defined, although there seems to be evidence suggesting it interacts with TIE2, modulating its response to the angiopoietins. Analysis by qRT-PCR of an ALL cell line panel revealed *TIE1* to be ubiquitously expressed, however at different levels and in a MLLr-independent pattern (fig. 5-20).

Apart from the TIE2-mediated signalling, there are also non-canonical pathways described, which involve specific integrins³³⁶. The best-characterised ANGPT1-binding integrins are ITGB1, ITGB3, ITGB5, ITGA4, ITGA5 & ITGAV³³²⁻³³⁴. Expression of these integrins was examined in t(4;11)-positive acute leukaemia cell lines by RT-PCR; as shown in fig. 5-21, both the t(4;11)-positive ALL cell lines SEM and RS4;11, and the t(4;11) cell line MV4;11 express *ITGB1*, *ITGB5*, *ITGA4*, *ITGA5* and *ITGAV*. In contrast, *ITGB3* cannot be detected.

In conclusion, an autocrine function of ANGPT1 on t(4;11)-positive cells might be possible via the canonical signalling pathway in patients, and the non-canonical ANGPT1 signalling axis involving integrins in t(4;11)-positive ALL cell lines.

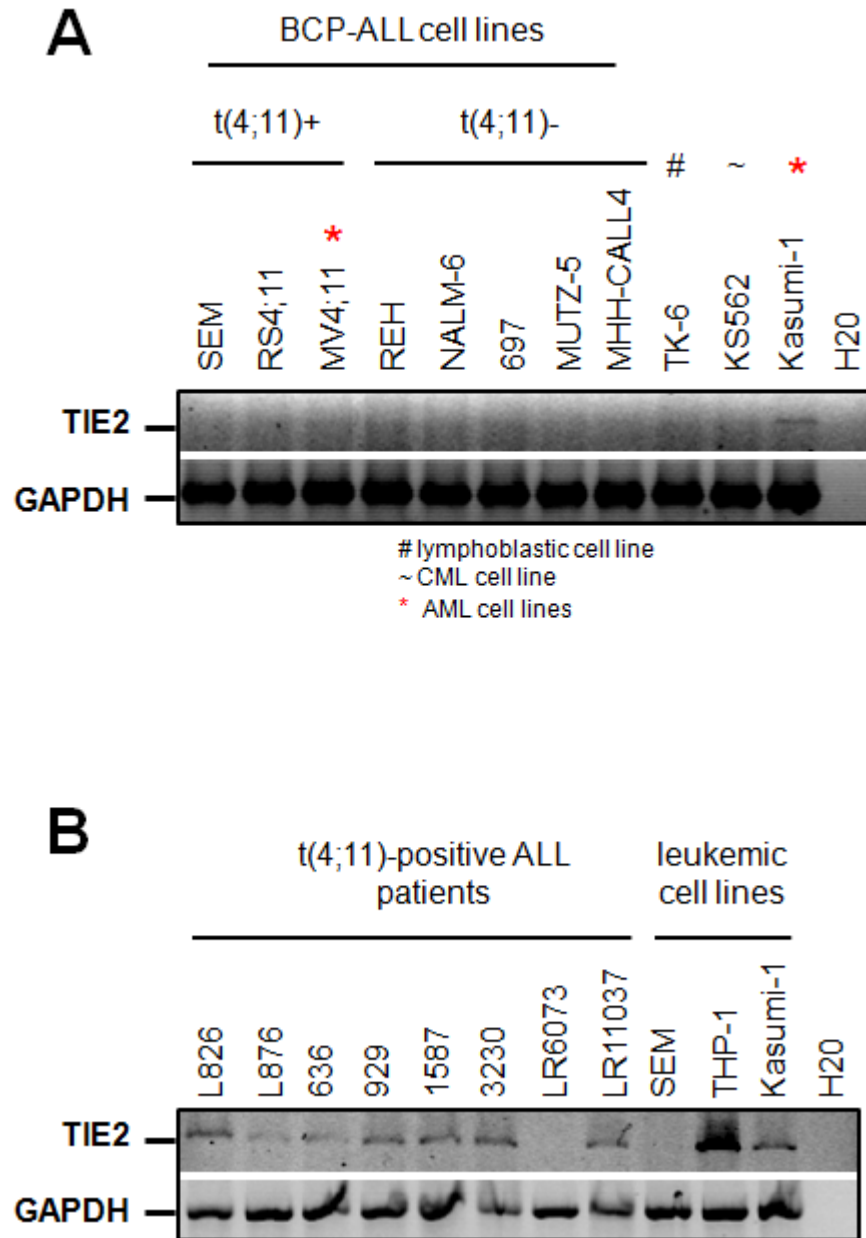


Fig. 5-19 *TIE2* expression analysis in leukaemic cell lines and patients

TIE2 expression was analysed by RT-PCR in a panel of leukaemic cell lines, where it could only be detected in the t(8;21)-positive AML cell line Kasumi-1 (A). In contrast, *TIE2* was present in 7 out of 8 t(4;11)-positive ALL patients assayed (B).

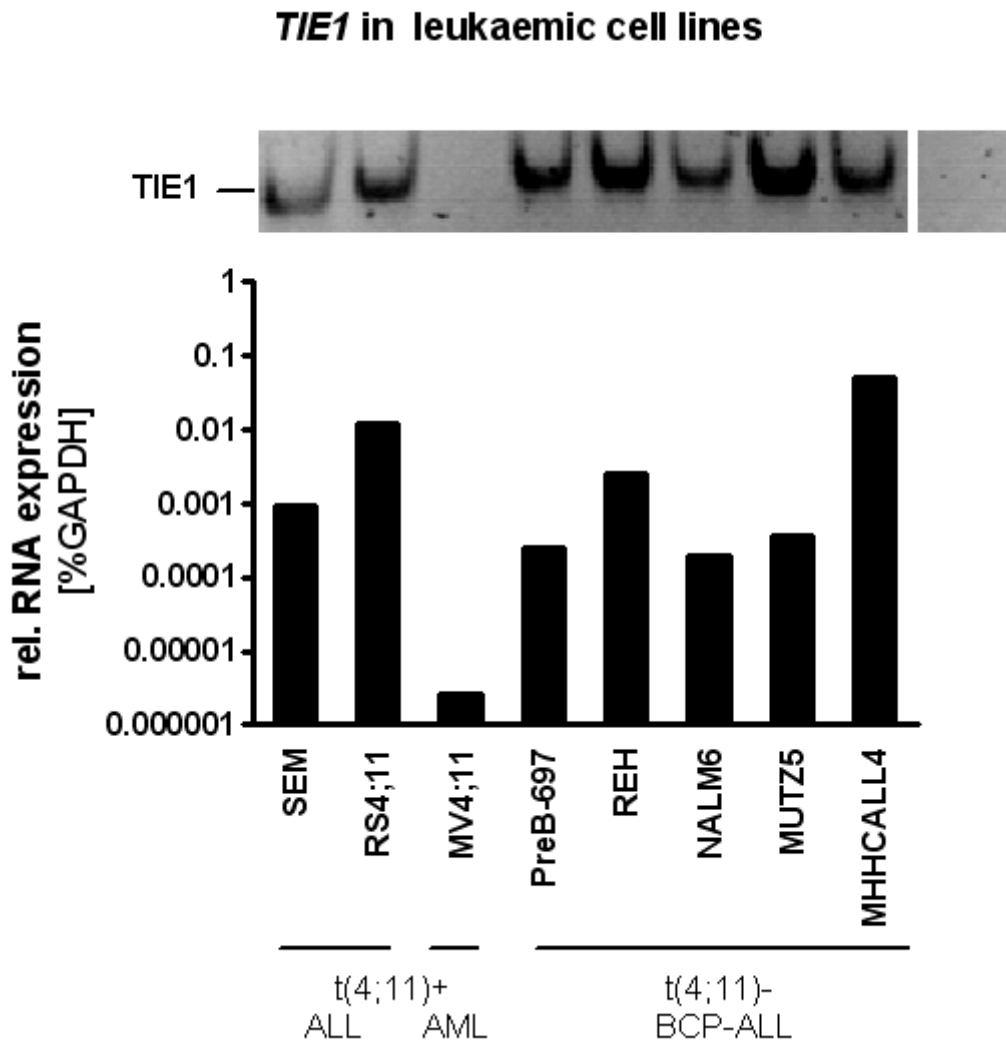


Fig. 5-20: *TIE1* expression analyses in an acute leukaemia cell line panel

TIE1 levels in a leukaemia cell line panel were determined by qRT-PCR using the Δ CT-method with *GAPDH* expression as endogenous reference (lower panel). PCR products were visualised by DNA-polyacrylamide gel electrophoresis (upper panel). *TIE1* is ubiquitously expressed in acute lymphoblastic leukaemia, with the exception of MV4;11, a t(4;11)-positive AML cell line.

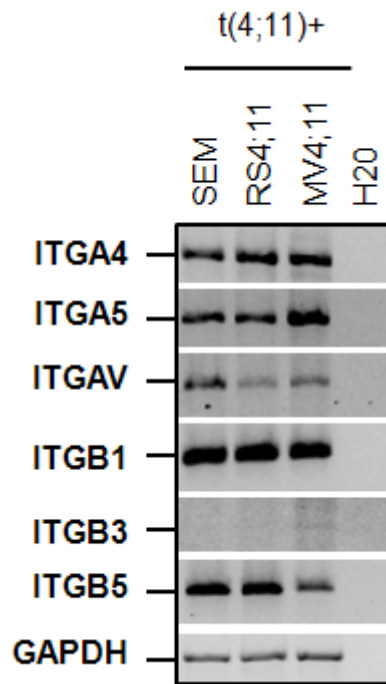


Fig. 5-21: Expression analysis of non-canonical ANGPT1 receptors

Integrin family members associated with ANGPT1 signalling were investigated in MLL/AF4-positive acute leukaemia cell lines by RT-PCR. One representative experiment of two independent ones is shown.

5.4.2 ANGPT1 Depletion in the t(4;11)-positive Cell Line SEM Impinges on Proliferation and Reduces Cell Viability

T(4;11)-positive cells express receptors that bind ANGPT1 and can potentially transduce an autocrine signal. In order to investigate a functional role of ANGPT1 in t(4;11)-positive ALL, RNAi was employed. The SEM cell line was transfected with a panel of four siRNAs directed against the ANGPT1 transcript (fig. 5-22), and knock-down efficiency was determined via qRT-PCR. The two most effective siRNAs were siANGPT1-1 and siANGPT1-3, resulting in an *ANGPT1* reduction by 81% and 89% at 12h post-transfection, respectively; which was maintained for up to 48h. The two remaining siRNAs, siANGPT1-2 and siANGPT1-5, only achieved a 37% and 36%, and were ruled out for further experiments, while both siANGPT1-1 and siANGPT1-3 were selected for further functional studies (fig. 5-23).

ANGPT1 (NM_001146.3/ NM_001199859.1/ ENST00000517746/ ENST00000297450)

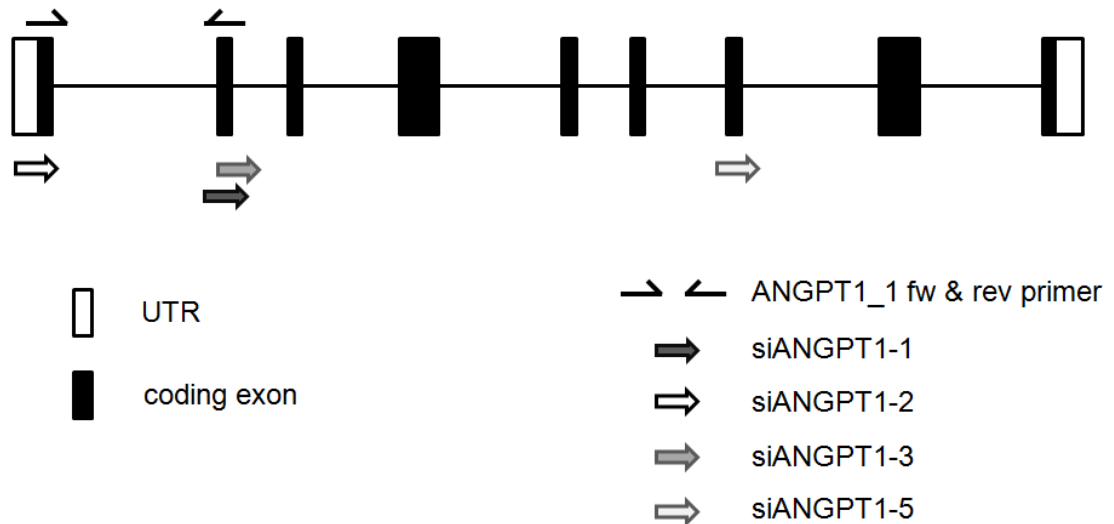


Fig. 5-22: Scheme of the *ANGPT1* exon structure including position of siRNAs and qRT-PCR primers

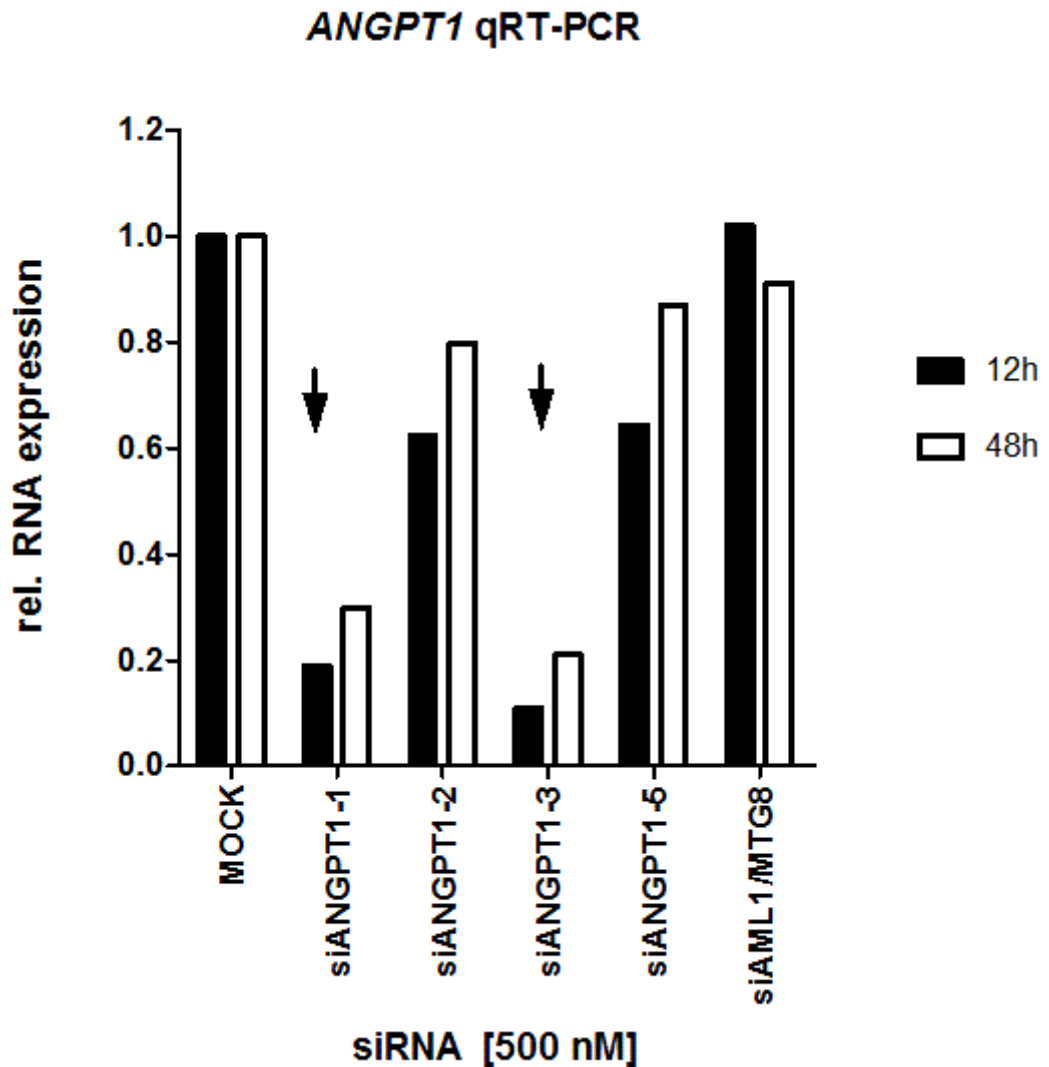


Fig. 5-23: Determination of silencing efficiency of ANGPT1 siRNAs

The SEM cell line was electroporated with four different siRNAs directed against the *ANGPT1* transcript, control siRNA (siAML1/MTG8) or mock-transfected without siRNAs (MOCK). RNA was harvested after 12h and 48h and *ANGPT1* expression by qRT-PCR using the $\Delta\Delta C_t$ -method, normalising against MOCK. One single experiment was performed, each sample assayed in triplicates.

Since the siANGPT1-mediated knockdown lasted for up to 48h (fig. 5-23), a transfection protocol similar to the standard set-up for the MLL/AF4 depletion time course was performed: SEM cells were transfected with siRNA against ANGPT1, control siRNA (siAML1/MTG8), or mock-transfected (MOCK) at two-day intervals for up to 4 times, representing a time course of 8 days of sustained ANGPT1 depletion (fig. 5-24).

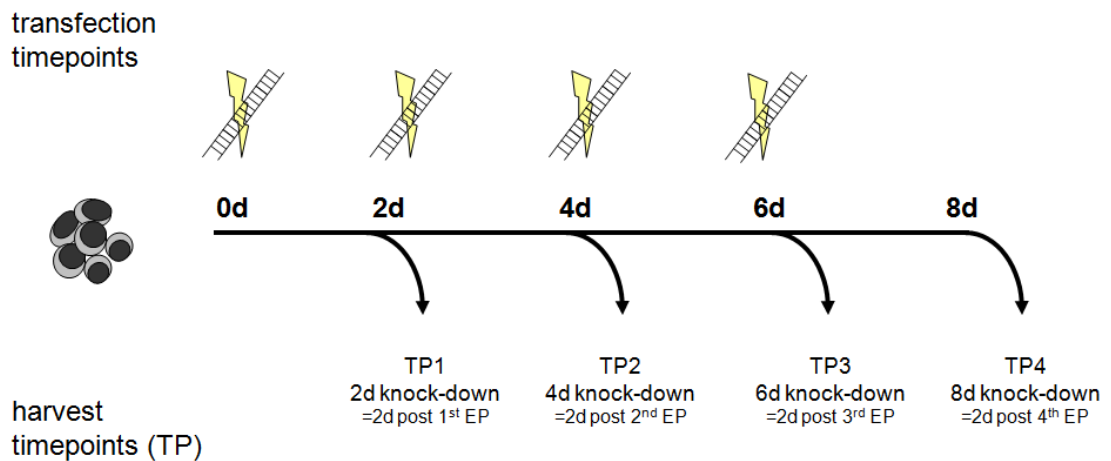


Fig. 5-24: siRNA electroporation time course for ANGPT1 knock-down

SEM cell line was sequentially transfected with either siRNAs against ANGPT1 (siANGPT1-1; siANGPT1-3), control siRNA (siAML1/MTG8), or mock-electroporated (MOCK) at two day intervals for up to 4 times, representing a sustained depletion period of 8 days (8d). Material was harvested for analyses immediately prior to the subsequent electroporation (TP1, TP2, TP3), and at the final timepoint, two days after the 4th electroporation (TP4/8d).

On transcript level, this approach achieved a sustained *ANGPT1* depletion by 63-72% with siANGPT1-1 and 60-77% with siANGPT1-3 compared to corresponding controls, as determined by qRT-PCR (fig. 5-25).

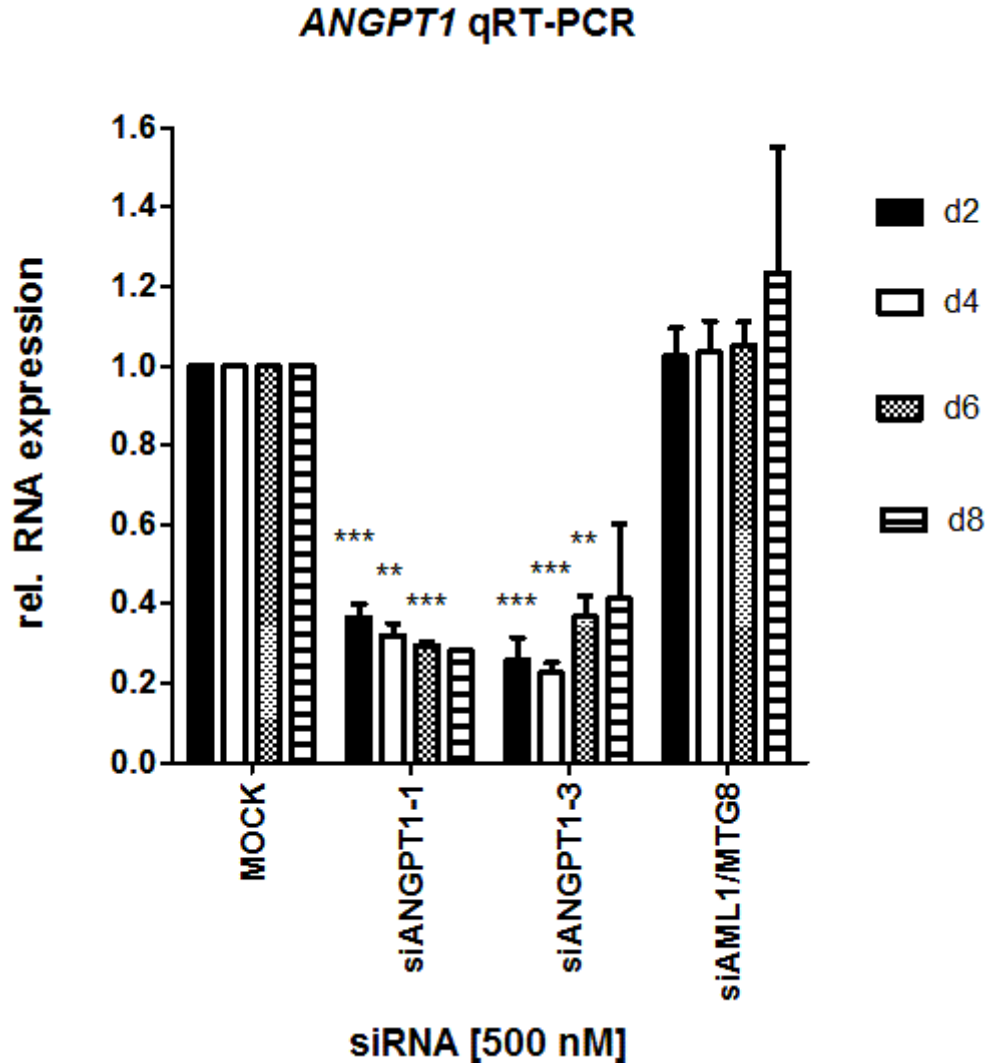


Fig. 5-25: *ANGPT1* levels in SEM cells treated with siANGPT1

SEM cells electroporated with siANGPT1 show a sustained reduction of *ANGPT1* over a time period of 8 days, as measured by qRT-PCR. The Graph represents the mean of n=4 (d2), n=3 (d4), n=3 (d6) and n=2 (d8) individual experiments, error bars indicate standard error of the mean (S.E.M.). Statistic analysis was carried out using an unpaired Student's t-test (** = $p < 0.01$; *** = $p < 0.0001$).

Concomitantly, ANGPT1 secretion was reduced by 72-91% and 86-97% in SEM cells transfected with siANGPT1-1 and siANGPT1-3, respectively, as measured by ELISA (fig. 5-26).

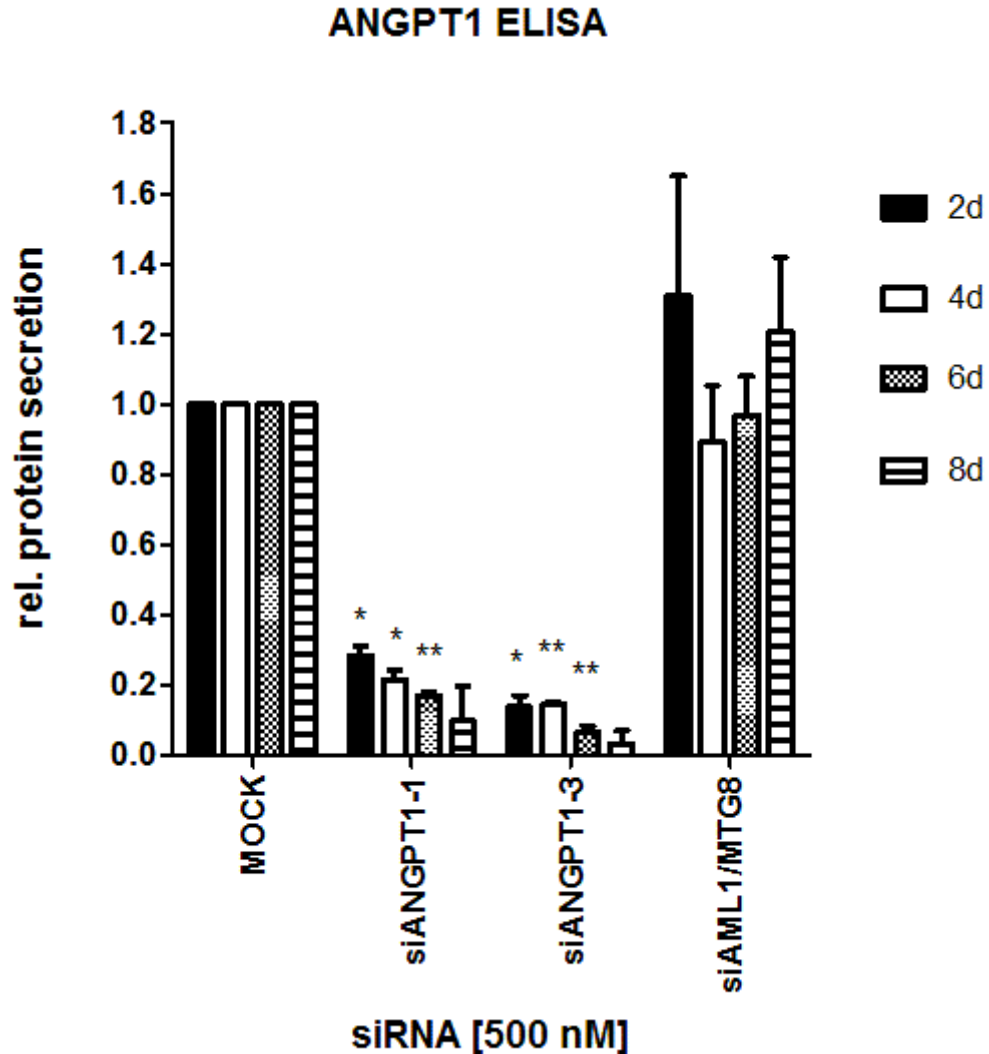


Fig. 5-26 :ANGPT1 secretion levels in SEM cells treated with siANGPT1

Cell culture supernatant of SEM cells electroporated with either siRNA against ANGPT1, control siRNA (siAML1/MTG8) or pulsed without siRNAs (MOCK) was harvested over a time course of 2, 4, 6 and 8 days and soluble ANGPT1 protein levels were quantified using an ELISA. ANGPT1 secretion was significantly decreased in siANGPT1-treated cells, and could be sustained at these reduced levels over the course of the experiment. The graph represents the mean of n=4 (d2), n=3 (d4, d6) and n=2 (d8) individual experiments, error bars indicate S.E.M. Statistic analysis was carried out using an unpaired Student's t-test (*= $p < 0.05$; ** = $p < 0.01$; *** = $p < 0.001$).

The phenotypic consequences of sustained ANGPT1 depletion in the SEM cells were analysed, assessing proliferation and viability. Reduced ANGPT1 levels over a prolonged period of time impinged markedly on cell proliferation of SEM cells (fig. 5-27), increasing the doubling time by 23 % and 47% when normalised to MOCK-treated cells (tab. 5-9).

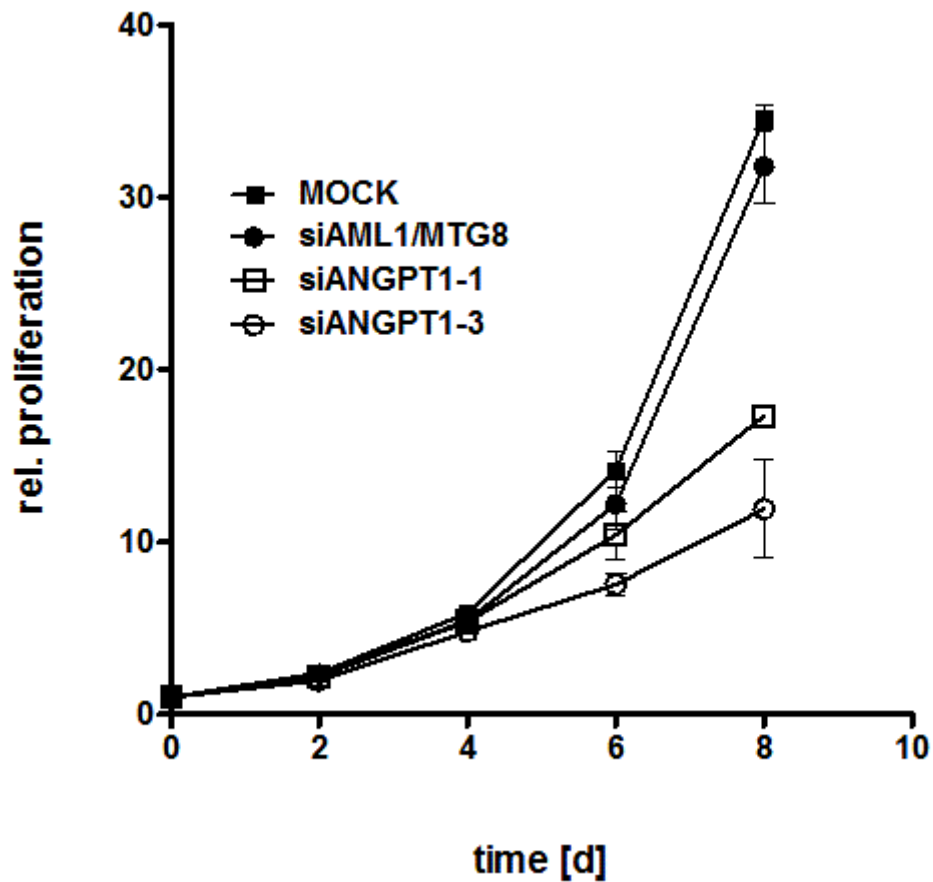


Fig. 5-27: Growth curve of ANGPT1-depleted SEM cells

Sustained knock-down of ANGPT1 over a period of 8 days was achieved by serial transfection of the SEM cell line with siRNAs against ANGPT1 (siANGPT1-1, siANGPT1-3) at two day-intervals; controls were electroporated with either non-targeting siRNA (siAML1/MTG8) or no siRNA (MOCK). SEM cells depleted of ANGPT1 showed a substantially reduced proliferation compared to controls. Cell numbers were determined immediately prior to the siRNA-transfection time points using a haematocytometer; viability was assessed by trypan blue exclusion. The graph represents the mean of n=2 independent experiments, the error bars show the data range.

Tab. 5-9 Changes in proliferation rates of SEM cells depleted of ANGPT1

	doubling time [h]	relative change [%]
MOCK	37.6 (+/- 0.74)	-
siAML1/MTG8	39.1 (+/- 0.25)	4
siANGPT1-1	46.2 (+/- 1.22)	23
siANGPT1-3	55.2 (+/- 6.78)	47

This anti-proliferative effect of ANGPT1 knockdown was also reflected in the cell cycle progression, as RNAi-mediated ANGPT1 depletion in SEM cells for a duration of 8 days resulted in changes of the cell cycle distribution when compared to controls: in concordance with the reduction of the proliferation rate in response to ANGPT1 knock-down, SEM cells treated with siRNA against ANGPT1 showed an increased accumulation of cells in the G1/G0-phase and concomitant depletion of cells cycling in S-phase (fig. 5-28).

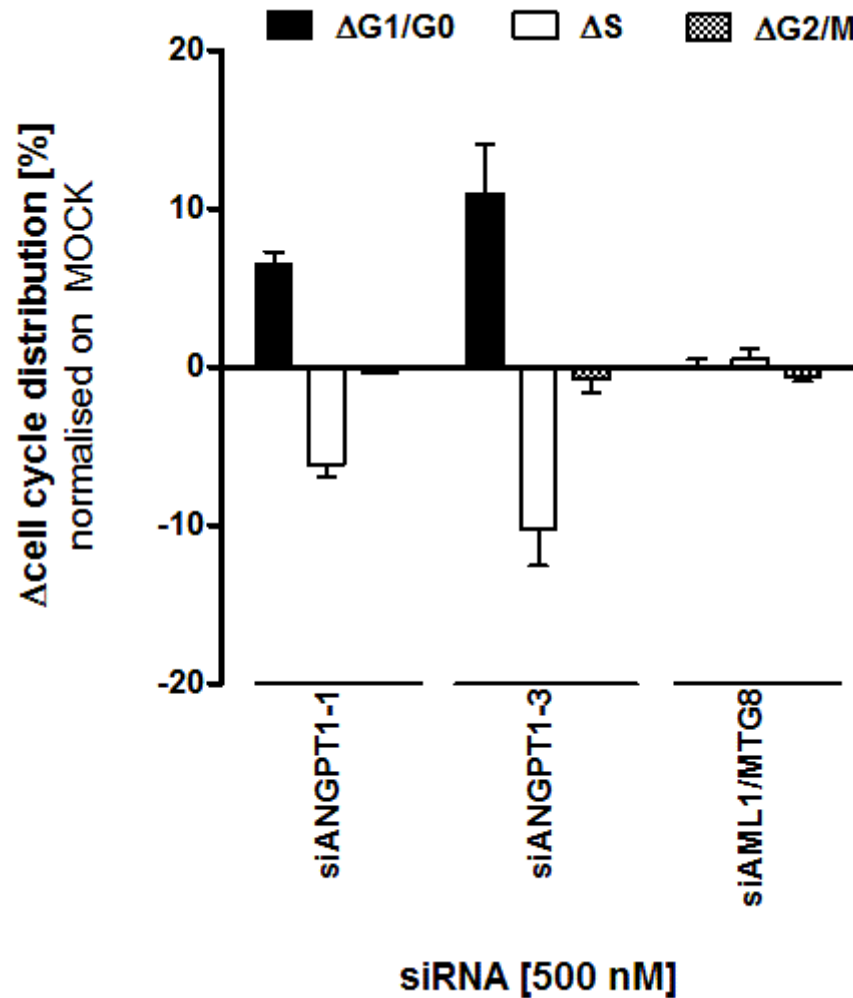


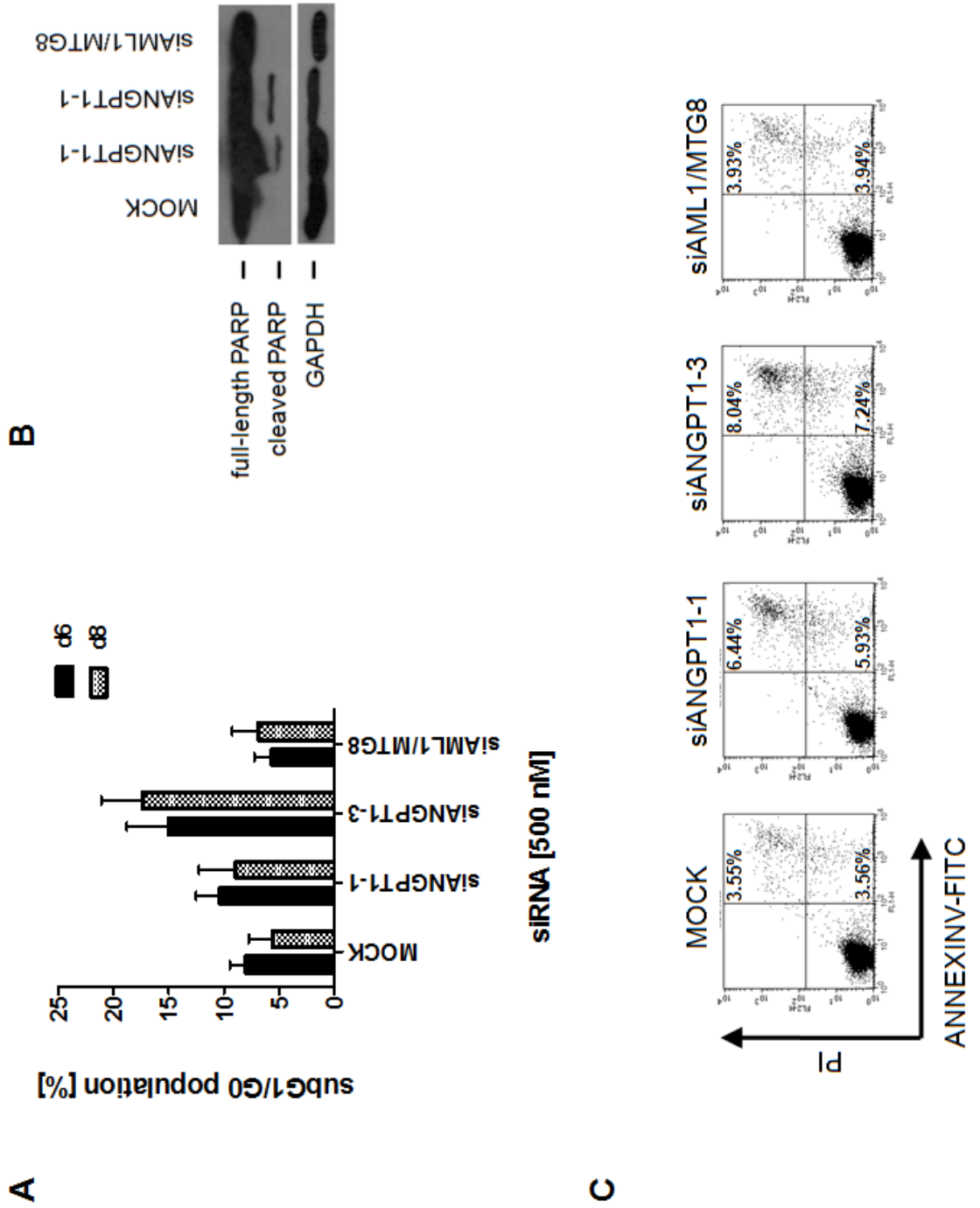
Fig. 5-28: Changes in cell cycle distribution in SEM cells depleted of ANGPT1

Flow cytometric cell cycle analysis of SEM cells treated for 8 days showed that prolonged ANGPT1 knockdown resulted in differences of cell cycle distribution when compared to controls (MOCK, siAML1/MTG8). The fraction of cells in the different cell cycle stages G1/G0, S and G2/M was determined using ModFit LT (Verity Software House) software, and the changes in siRNA-treated cells calculated by normalising on the cell cycle distribution of MOCK-transfected cells. The mean of n=2 independent experiments are shown; error bars represent the data range.

In addition to impinging on proliferation and cell cycle progression, ANGPT1 knock-down also had a negative effect on viability. RNAi-mediated reduction of ANGPT1 levels resulted in a subtle induction of apoptosis, as illustrated by the increased fraction of cells in sub-G1 at 6 and 8 days of siANGPT1 treatment (fig. 5-29A). Indeed, already after 6 days of RNAi-mediated ANGPT1 depletion onset of cell death could be observed. SEM cells transfected with siANGPT1-1 and siANGPT1-3 showed increased phosphatidylserine exposure onto the cell surface and uptake of propidium iodide (PI), both markers associated with cell death, as determined flow cytometrically by AnnexinV-binding and PI-positivity (fig. 5-29C). Immunoblotting also revealed proteolytic cleavage of PARP in cells depleted of ANGPT1 but not in controls (fig. 5-29B). PARP cleavage is mediated by activated effector caspases, and serves as a surrogate marker for apoptosis cell death. These observations point out a dependency of t(4;11)-positive cells on ANGPT1 signalling for survival. In order to understand this on a molecular level, whole-genome profiling of cells depleted of ANGPT-1 was performed.

Fig. 5-29: SEM cell viability and survival are compromised upon sustained ANGPT1 depletion analysis

Flow cytometric cell cycle analysis of SEM cells treated for 6 or 8 days showed that prolonged ANGPT1 knockdown resulted in an increase of the sub-G1/G0 subpopulation when compared to controls (MOCK, siAML1/MTG8). The fraction of cells was determined using ModFit LT software. This graph represent the mean of n=3 independent experiments for time point d6, and n=2 independent experiments at time point d8. Error bars indicate standard error of the mean (A). Concomitantly, after 6 days of siANGPT1 treatment SEM cells showed evidence of caspase-mediated PARP cleavage, while controls (siAML1/MTG8, MOCK) only revealed unprocessed full-length PARP. One representative figure of two independent experiments is shown. (B). This was accompanied by an increased ANNEXINV-single and ANNEXINV/PI-double positivity when compared to controls, indicating activation of the cell death pathways. Graph represents one single experiment. (C)



5.5 WHOLE GENOME EXPRESSION PROFILING OF SEM CELLS DEPLETED OF ANGPT1

In order to elucidate the contribution of ANGPT1 to t(4;11)-positive leukaemogenesis on a molecular level, gene expression profiling (GEP) of SEM cells depleted of ANGPT1 and corresponding controls was carried out. SEM cells were transfected with siANGPT1-3 or control siRNA (siAML1/MTG8). In addition, since the ANGPT1 content in serum-containing growth medium is substantial (fig. 5-30) and might contribute to the delayed effect of the ANGPT1 knockdown, the transfected cells were subsequently starved for 48h before harvesting the RNA. Successful knock-down was confirmed on RNA and protein level by qRT-PCR and ELISA, respectively (fig. 5-31).

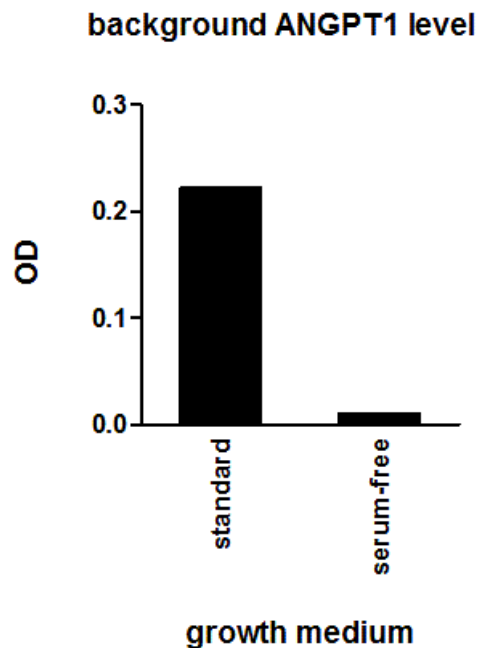


Fig. 5-30: ANGPT1 background level in standard and serum-free growth medium

Standard growth medium supplemented with 10% FCS is an exogenous source of ANGPT1. One representative of several comparable experiments is shown.

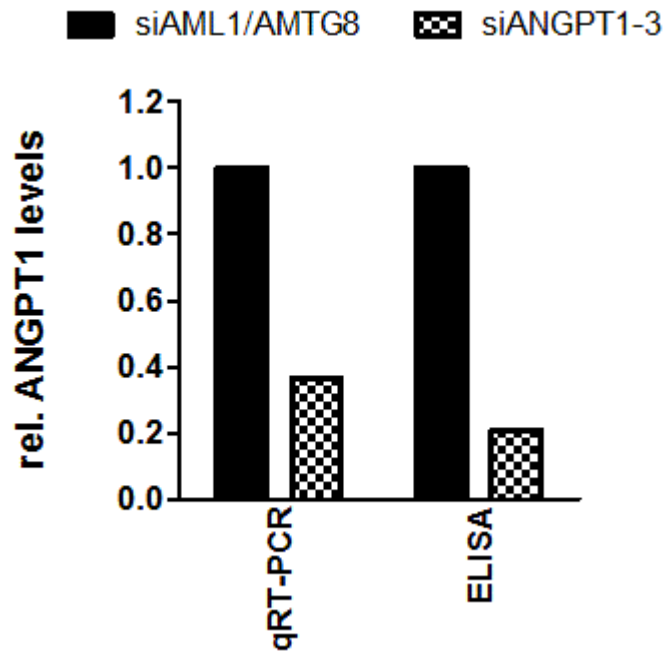


Fig. 5-31: ANGPT1 expression analysis of siRNA-treated SEM cells in serum-free medium

SEM cells were singly electroporated with either siANGPT1-3 or control siRNA (siAML1/MTG8) and cultured in serum-free growth medium in order to remove the exogenous ANGPT1 source that FCS represents. Cells and supernatant were harvested after 2 days, and ANGPT1 RNA and protein expression quantified by qRT-PCR and ELISA, respectively. Graph shows one single experiment, each sample was performed in triplicates (qRT-PCR) or duplicates (ELISA).

Prior to submitting the samples to GEP, the RNA quality was measured by determining the RNA integrity number (RIN) via lab-ob chip technology, using a Bioanalyzer 2100 RNA 6000 Nano Assay (Tab. 5-10).

Tab. 5-10: RIN values of samples submitted to GEP

sample	RIN
siANGPT1-3	9.2
siAML1/MTG8	9.4

The samples were processed at a service provider facility according to manufacturer’s protocols, and assayed using an Illumina HT-12 V.4 bead array (Illumina Inc.). The resulting expression files were processed using Genome Studio.

Tab. 5-11: Array Statistics after processing using GenomeStudio

array statistics	siAML1/MTG8	siANGPT1-3
No. Detected probes		
<i>Detection P-value <0.05</i>	11872	12058
<i>Detection P-value <0.01</i>	9504	9904

Differential expression was analysed using GeneSpring GX11 software (Agilent Technologies, Inc): arrays were processed using a quantile normalisation algorithm, and presence calls determined using the parameters described previously. Differentially expressed probes between siANGPT1-3 and control-treated cells were calculated using two different stringency settings: on the high stringency setting, array probes were filtered on “present” calls only for all samples; a fold-change expression value cut-off of 2.0 applied. Thus determined probe sets were termed gene signature A.

On the low stringency analysis settings, all array probes were retained, regardless of their call status, and a fold-change expression value cut-off of 2.0 was applied. Subsequently, the analysis results were manually curated, filtering out probes which flagged up “absent” and “marginal” in the control sample, putatively correlating to non-expressed or low-abundance genes. In contrast, probes with both “absent”, “marginal” and “present” calls in the siANGPT1 sample were retained. This analysis method allowed identifying genes strongly down-regulated or silenced in response to ANGPT1 depletion; the resulting genes were defined as gene signature B.

Using the high stringency analysis parameters, 918 differentially expressed probes were identified, corresponding to 909 genes, of which 389 were up- and 520 down-regulated. The low-stringent (curated) analysis revealed 3985 differentially expressed probes, equating to 3858 genes, of which 389 were up- and 3469 down-regulated (tab. 5-12).

Tab. 5-12. Number of differentially expressed probe sets and genes for gene signatures A and B

siANGPT1 vs. siCtrl	Signature A	Signature B
No. of differentially expressed probes	918	3985
<i>up-regulated probes</i>	393	393
<i>down-regulated probes</i>	526	3592
No. of differentially expressed genes	909	3858
<i>up-regulated genes</i>	389	389
<i>down-regulated genes</i>	520	3469

Since only changes in the stringency settings were applied for the siANGPT1-treated sample, the list of up-regulated genes was identical in both analysis settings. The top-50 up-regulated genes in response to ANGPT1 are listed in tab. 5-13.

The list of down-regulated genes differed between the two stringency settings. Since gene signature B also contains gene so strongly down-regulated that they fall into the marginally expressed or the absent/unexpressed category, the fold-changes were far greater than in signature A. In addition, signature B contained far more predicted and unannotated loci than signature A. (tab 5-14, tab. 5-15).

Tab. 5-13: Top-50 Up-regulated Genes in SEM cells depleted of ANGPT1

Gene	Fold change ([siANGPT1-3] vs. [siCtrl])	Accession	Probe_Id
FLI44054	4.80	NR_024609.1	ILMN_3236599
ARID5A	4.64	NM_212481.1	ILMN_1689700
SPRYD4	4.49	NM_207344.2	ILMN_1729868
HS.581788	4.16	AI073406	ILMN_1859493
HS.564216	3.99	BM678612	ILMN_1856751
MAPKSP1	3.99	NR_024170.1	ILMN_3225432
CLDN14	3.98	NM_012130.2	ILMN_2328575
WBP11	3.98	NM_016312.2	ILMN_1661051
FKBP1A	3.96	NM_054014.1	ILMN_1702237
ARHGAP5	3.85	NM_001173.2	ILMN_2322747
LOC652330	3.76	XM_001716137.1	ILMN_3205030
HS.538554	3.76	AI699581	ILMN_1875887
PPP2CB	3.74	NM_001009552.1	ILMN_1675693
HS.542027	3.63	BQ448172	ILMN_1832529
LOC54103	3.63	NM_017439.1	ILMN_1772064
SLC22A1	3.62	NM_153187.1	ILMN_1715742
RHOBTB2	3.56	NM_015178.1	ILMN_2195957
LOC100132494	3.55	XM_001722666.1	ILMN_3236752
MARS2	3.47	NM_138395.2	ILMN_2136423
CYP4F3	3.45	NM_000896.1	ILMN_1736190
ATPBD4	3.42	NM_080650.2	ILMN_2140207
CDC2L2	3.39	NM_033531.1	ILMN_2330552
DPH2	3.39	NM_001384.4	ILMN_2276431
DUSP2	3.37	NM_004418.2	ILMN_1712959
ETV5	3.35	NM_004454.1	ILMN_1723260
CHRNA2	3.35	NM_000742.1	ILMN_1698849
PRKAR2A	3.34	NM_004157.2	ILMN_1681888
LOC644373	3.33	XM_932154.1	ILMN_1701857
LOC202134	3.30	XM_932129.1	ILMN_1652689
DDB1	3.27	NM_001923.2	ILMN_1774735
TMTC4	3.22	NM_001079669.1	ILMN_1762095
SDHALP1	3.22	NR_003264.1	ILMN_1734640
SERTAD3	3.21	NM_203344.1	ILMN_1813955
WASF1	3.20	NM_003931.2	ILMN_2342174
PHF12	3.19	NM_001033561.1	ILMN_1808781
HS.489952	3.17	CK905566	ILMN_1873967
ZNF3	3.17	NM_017715.2	ILMN_2390739
LOC654340	3.16	XM_946373.1	ILMN_1722730
HIST1H2BJ	3.14	NM_021058.3	ILMN_1658702
C22ORF33	3.14	NM_178552.2	ILMN_1663417
CTGF	3.13	NM_001901.2	ILMN_2115125
PILRB	3.10	NM_013440.3	ILMN_1807712
LOC100133409	3.09	XM_001714245.1	ILMN_3239121
L3MBTL4	3.07	NM_173464.3	ILMN_3307954
MLL5	3.04	NM_182931.2	ILMN_2344988
LOC648408	3.03	XM_937458.1	ILMN_1734427
LOC644647	3.03	XM_927755.1	ILMN_1659432
PTP4A3	3.01	NM_007079.2	ILMN_2359710
ITGB5	3.00	NM_002213.3	ILMN_1796755
NAT11	2.99	NM_024771.1	ILMN_2178244

Tab 5-14. Top-50 down-regulated genes in SEM cells depleted of ANGPT1 - Signature A

ILMN_Gene	Fold change ([siANGPT1-3] vs. [Ctrl])	Accession	Probe_Id
MPO	-18.69	NM_000250.1	ILMN_1705183
ELANE	-5.33	NM_001972.2	ILMN_1706635
LOC727761	-4.37	XM_001126211.1	ILMN_1732006
SNHG3-RCC1	-4.13	NM_001048198.1	ILMN_2311497
TJP1	-4.00	NM_175610.2	ILMN_2403006
CTSG	-3.97	NM_001911.2	ILMN_1680424
BRCA1	-3.86	NM_007295.2	ILMN_1771065
TRIOBP	-3.79	NM_007032.5	ILMN_2370588
HS.332056	-3.73	BX647714	ILMN_1866460
ERCC6	-3.73	NM_000124.1	ILMN_1786882
OR2A20P	-3.68	NR_002158.1	ILMN_1738976
CD34	-3.66	NM_001773.1	ILMN_1694249
MARCH8	-3.66	NM_001002265.1	ILMN_2341626
C16ORF7	-3.61	NM_004913.2	ILMN_1693630
HS.98960	-3.59	BE894306	ILMN_1858001
LOC100130138	-3.58	XM_001726935.1	ILMN_3181439
SNORA16A	-3.57	NR_003035.1	ILMN_3246465
MED12	-3.54	NM_005120.1	ILMN_1793386
LOC728734	-3.50	XM_001132754.1	ILMN_1687571
LOC550112	-3.41	XR_001037.1	ILMN_1798472
HS.539123	-3.38	AA629336	ILMN_1872049
DDX59	-3.37	NM_001031725.1	ILMN_2357193
C6ORF184	-3.37	XM_168053.6	ILMN_1765438
LOC643950	-3.35	XM_931938.2	ILMN_1677857
LOC442232	-3.34	XR_018484.1	ILMN_3279987
TNKS	-3.33	NM_003747.2	ILMN_1657891
FLJ40330	-3.29	XR_015919.1	ILMN_1746695
RNASE2	-3.27	NM_002934.2	ILMN_1730628
STAT1	-3.27	NM_007315.2	ILMN_1777325
STXBP1	-3.27	NM_003165.1	ILMN_1728747
CTHRC1	-3.23	NM_138455.2	ILMN_2117508
SLC19A2	-3.21	NM_006996.1	ILMN_2201668
C10RF222	-3.21	NM_001003808.1	ILMN_1749317
ISM1	-3.21	NM_080826.1	ILMN_3239288
VPREB3	-3.19	NM_013378.1	ILMN_1700147
PJCG6	-3.18	NM_001040066.1	ILMN_2081344
MAG	-3.16	NM_080600.1	ILMN_2380181
DYNC111	-3.15	NM_004411.3	ILMN_1690397
DHX58	-3.14	NM_024119.2	ILMN_1678422
SBF2	-3.14	NM_030962.2	ILMN_2123665
CSMD1	-3.13	NM_033225.3	ILMN_1746945
LILRB2	-3.11	NM_001080978.1	ILMN_1695744
HS.130260	-3.11	AI263926	ILMN_1888658
KIAA1660	-3.11	XM_929784.1	ILMN_1796029
LOC642993	-3.11	XM_926372.1	ILMN_1702586
LOC642255	-3.09	XM_001127807.1	ILMN_1679371
CCBL2	-3.08	NM_019610.3	ILMN_2130003
LOC642216	-3.08	XM_942785.1	ILMN_1724508
LOC441698	-3.08	XR_019206.1	ILMN_1725455
ZNF574	-3.06	NM_022752.5	ILMN_1790460

Tab. 5-15 Top-50 down-regulated genes in SEM cells depleted of ANGPT1 - Signature B

Gene	Fold change ([siANGPT1-3] vs. [siCtrl])	Accession	Probe_Id
PRTN3	-72.24	NM_002777.3	ILMN_1668460
LOC648585	-50.35	XM_944740.1	ILMN_1763374
C18ORF26	-47.06	NM_173629.1	ILMN_1746670
LOC653127	-47.06	XM_927004.1	ILMN_1732830
LOC644923	-45.35	XM_932518.1	ILMN_1791242
DKFZP586I1420	-39.17	NR_002186.1	ILMN_2216838
SLC6A19	-37.07	NM_001003841.1	ILMN_1724021
LOC441268	-34.76	NM_001013725.1	ILMN_1675258
TACSTD1	-33.14	NM_002354.1	ILMN_2160210
HS.564211	-33.05	AA846343	ILMN_1857425
MEF2A	-30.95	NM_005587.2	ILMN_3251100
ZNF578	-30.30	NM_152472.1	ILMN_1693996
HS.541852	-30.30	BX115082	ILMN_1886969
LOC647210	-29.71	XM_930248.1	ILMN_1727977
ABCB1	-29.28	NM_000927.3	ILMN_1812070
LOC440225	-28.91	XR_017179.1	ILMN_1667052
PCDHA1	-28.81	NM_031411.1	ILMN_2393077
LOC643242	-28.46	XM_927615.1	ILMN_1693966
LOC652377	-28.35	XR_019346.1	ILMN_1808122
LOC651790	-28.26	XM_941017.1	ILMN_1808307
LOC642325	-28.16	XM_925864.2	ILMN_1712886
HIST1H2AB	-27.21	NM_003513.2	ILMN_1753524
HS.43938	-27.12	CD370005	ILMN_1826420
CHKB	-26.93	NM_152253.1	ILMN_1689711
C2ORF86	-26.47	NM_001042692.1	ILMN_1717010
SERPINB7	-26.42	NM_003784.2	ILMN_2395139
HS.577495	-26.42	DA880232	ILMN_1831363
KIAA0427	-26.22	NM_014772.1	ILMN_1655563
LOC100130220	-26.22	XM_001713697.1	ILMN_3244638
MPZL2	-26.22	NM_005797.2	ILMN_1752932
LOC100128096	-25.79	XR_038482.1	ILMN_3179148
UQCRB	-25.67	NM_006294.3	ILMN_3251491
HS.543803	-25.41	BM986885	ILMN_1882543
HS.44984	-25.30	BX101040	ILMN_1890263
C12ORF27	-25.21	NR_024345.1	ILMN_3245684
LOC652354	-25.02	XM_941784.1	ILMN_1808462
CD34	-24.94	NM_001773.2	ILMN_2341229
ANRIL	-24.85	NR_003529.1	ILMN_1887731
LOC644038	-24.76	XM_928871.2	ILMN_1769281
LOC644756	-24.66	XM_927853.2	ILMN_1734679
LOC643509	-24.59	XM_932666.2	ILMN_1665821
LOC126520	-24.50	XR_015464.1	ILMN_1762151
LOC645986	-24.50	XM_933324.1	ILMN_1799826
LOC729786	-24.33	XR_015655.1	ILMN_1791605
FREM2	-24.21	NM_207361.4	ILMN_1703174
MAPK14	-24.10	NM_139013.1	ILMN_1720656
LOC653543	-23.91	XM_928000.2	ILMN_1806813
C4B	-23.80	NM_000592.4	ILMN_1813695
PCDHA11	-23.80	NM_031861.1	ILMN_1740494
SMAD6	-23.78	NM_005585.3	ILMN_1767068

5.5.1 Functional categorisation of gene expression profiling data using Ingenuity Pathway Analysis

In order to identify pathways and functional networks affected by ANGPT1 down-regulation, the gene signatures were analysed using the Ingenuity Pathway Analysis (IPA) software (Ingenuity Systems Inc.).

5.5.1.1 Functional analysis of gene signature A

Gene signature A, consisting of 393 up- and 526 down-regulated probes, showed enrichment of biological functions associated with cancer, cell death, and particularly, haematopoiesis and related haematologic processes and disorders. Additional functions affected were molecular transport, nucleic acid and vitamin metabolism, as well as tumour morphology and tissue development associated physiological processes (tab. 5-16).

Tab. 5-16: Significantly enriched functional categories in gene signature A

Top 5 Biofunctions	P-value
Diseases and Disorders	
<i>Dermatological Diseases and Conditions</i>	1.59E-04 - 3.74E-02
<i>Genetic Disorder</i>	9.51E-04 - 4.46E-02
<i>Nutritional Disease</i>	1.73E-03 - 4.94E-02
<i>Cancer</i>	1.65E-04 - 4.55E-02
<i>Haematological Disease</i>	1.73E-03 - 4.46E-02
Molecular and Cellular Functions	
<i>Cell Death</i>	8.81E-04 - 4.35E-02
<i>Molecular Transport</i>	9.51E-04 - 3.63E-02
<i>Nucleic Acid Metabolism</i>	9.51E-04 - 4.35E-02
<i>Small Molecule Biochemistry</i>	9.51E-04 - 4.35E-02
<i>Vitamin and Mineral Metabolism</i>	9.51E-04 - 3.09E-02
Physiological System Development and Function	
<i>Tumour Morphology</i>	2.80E-03 - 3.09E-02
<i>Tissue Development</i>	3.53E-03 - 4.35E-02
<i>Haematological System Development & Function</i>	1.30E-02 - 4.51E-02
<i>Haematopoiesis</i>	1.31E-02 - 3.09E-02
<i>Lymphoid Tissue Structure and Development</i>	1.31E-02 - 3.09E-02

P-Value range describes the *p*-values of associated subcategories as determined by Fisher's exact test.

The top-5 biological networks affected fit in well with the functional categories described, as they comprise cellular growth and development, haematological disease and development, cell-to-to cell signalling, cell death and cellular movement, amongst others (tab. 5-17)

Tab. 5-17: Top 5 significantly enriched networks in gene signature A.

Name	Score
Cellular Development, Cellular Growth and Proliferation, Embryonic Development	31
Cell-To-Cell Signalling and Interaction, Haematological Disease, Cellular Movement	13
Gene Expression, Digestive System Development and Function, Hepatic System Development and Function	12
Cancer, Reproductive System Disease, Cell Death	10
Inflammatory Response, Cellular Movement, Haematological System Development and Function	10

ANGPT1 depletion resulted in a marked down-regulation of factors associated with cellular growth, proliferation and development (18 out of 34 network-associated genes) as well as up-regulation of cell death mediators, such as CASP7 (fig. 5-32). In addition, networks mediating cellular processes associated with cell-to-cell signalling & interaction, cellular movement and haematological disease showed also predominantly down-regulation in response to decreased ANGPT1 levels (fig. 5-33).

Network: Cellular Development, Cellular Growth and Proliferation, Embryonic Development

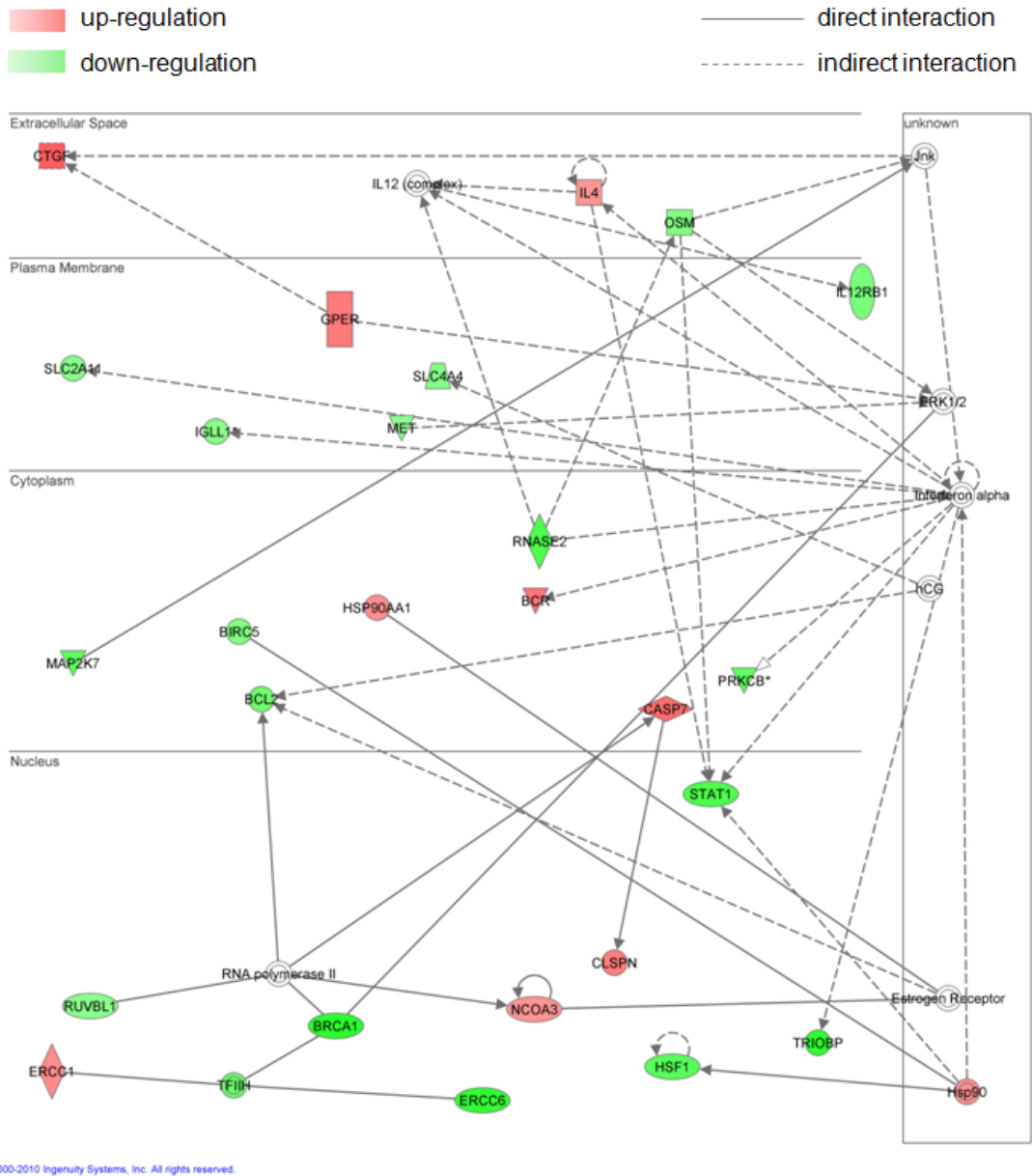


Fig. 5-32. ANGPT1 depletion affects functions associated with cellular growth, proliferation and development

Network: Cell-To-Cell Signalling and Interaction, Haematological Disease, Cellular Movement

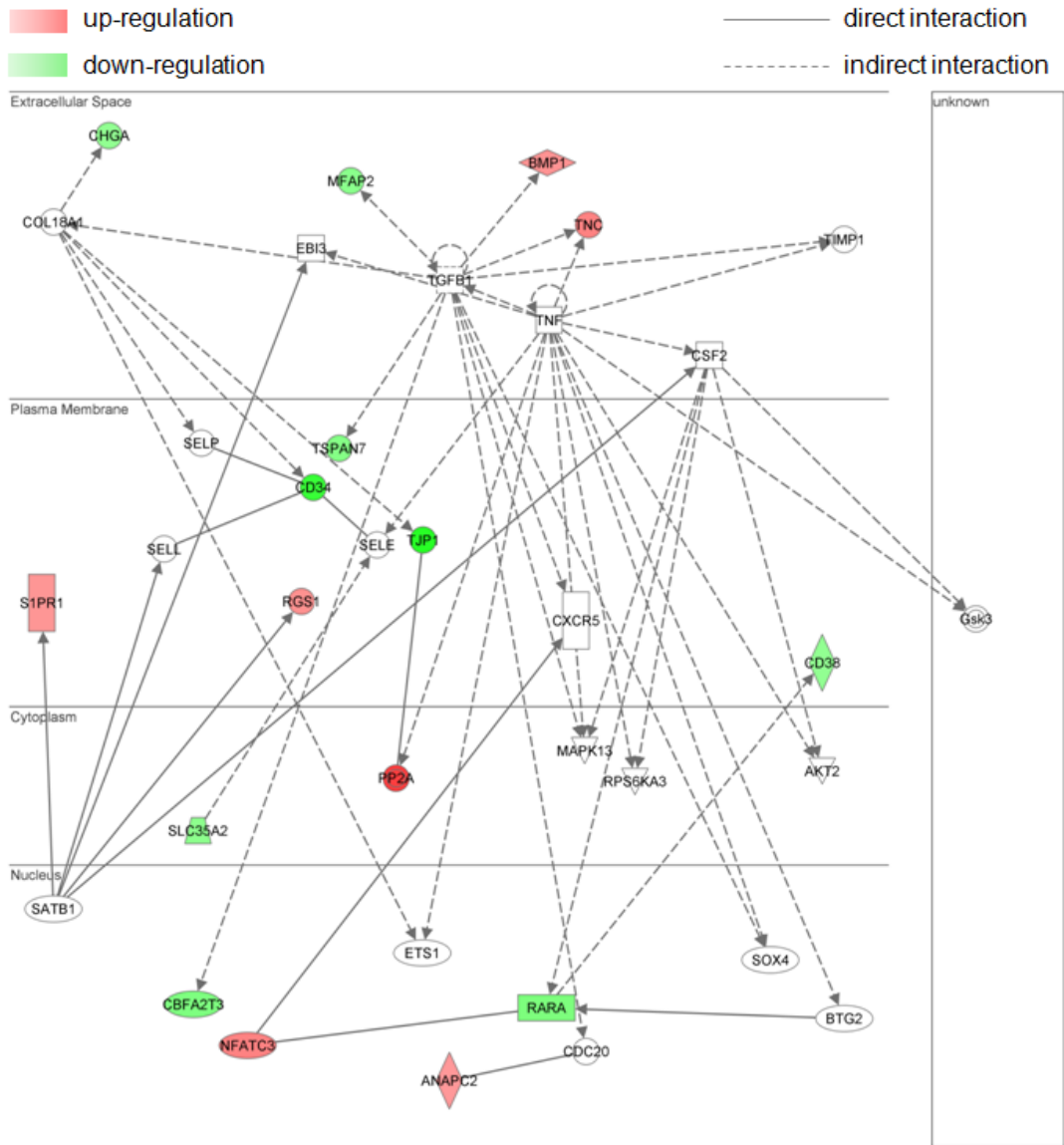


Fig. 5-33: ANGPT1 depletion results in down-regulation of the functions associated with cell-to-cell signalling and interactions, cellular motility and haematological disease.

Pathway analysis of gene signature A showed significant enrichment ($p < 0.05$) of 9 canonical pathways (fig. 5-34A), which could be subsumed into 4 pathway categories: G-protein coupled receptor (GPCR)/cAMP/PKA signalling axis, cytokine/mitogenic signalling, nuclear hormone receptor-associated and cancer-associated signalling (fig. 5-34B). Functionally, these pathways are related to the networks and biological functions associated with gene signature A, as both the GPCR/cAMP/PKA signalling axis as well as cytokine signalling pathways are implicated in cell-to-cell signalling, proliferation, cell death and a range of disorders, including haematological cancer.

The most prominently enriched pathway was the glucocorticoid-receptor (GR) signalling cascade, which showed differential expression of several effectors of this pathway; ANGPT1 depletion resulted in up-regulation of the gene coding for the GR (*NR3C1*) and its coactivator NCOA3, as well as molecular chaperones HSP90 and HSP70 (*HSPA6*) required for GR signalling. Downstream effectors, such as MKK7 (*MAP2K7*), and target genes such as *CREB1* are also affected (tab. 5-18).

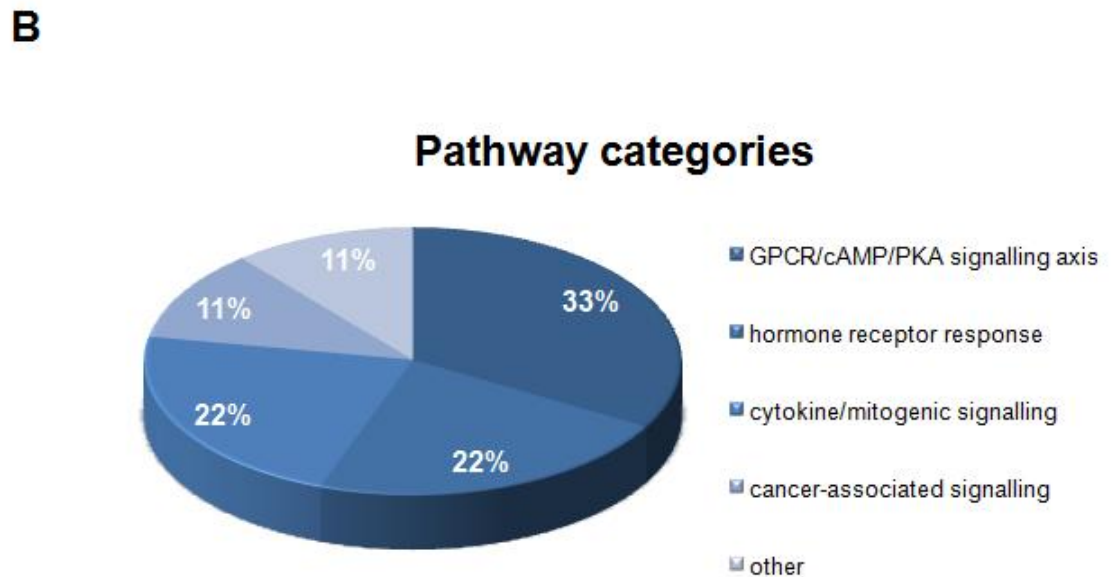
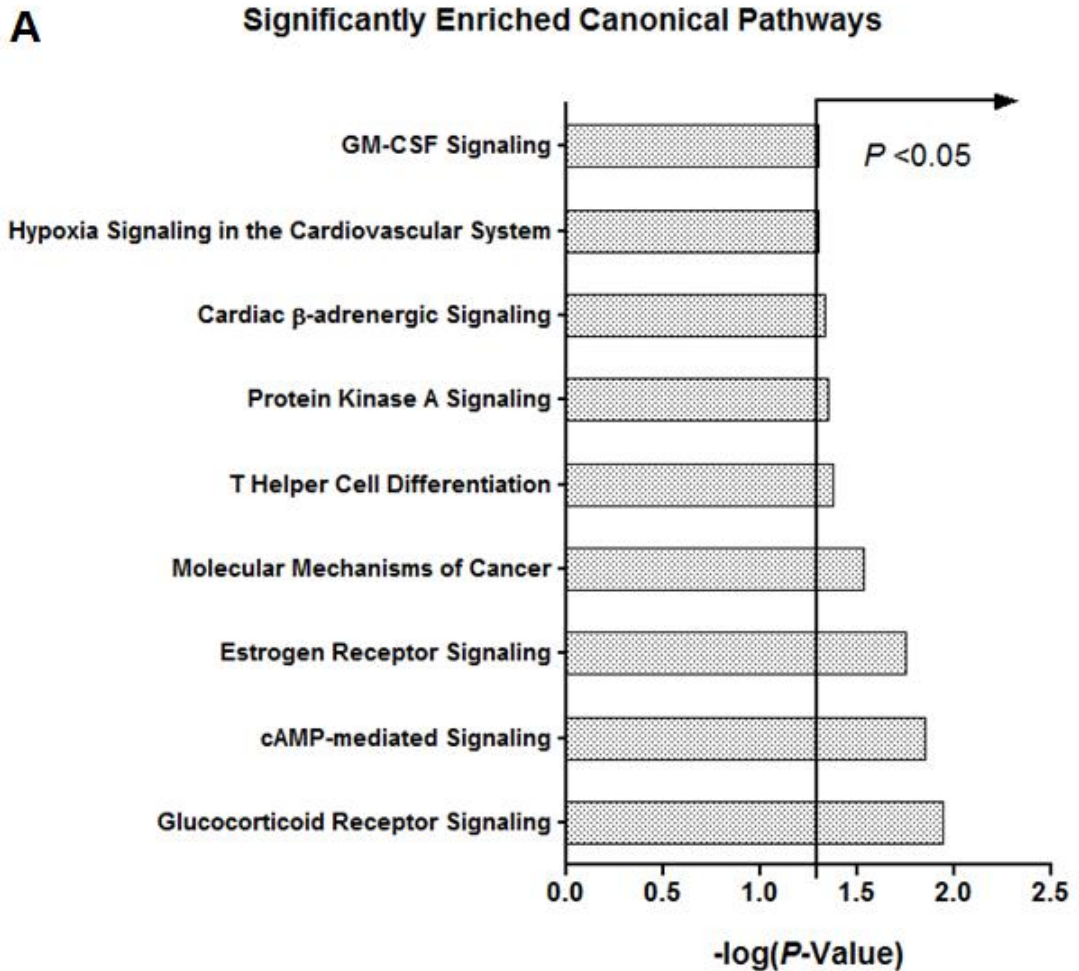


Fig. 5-34: Pathway analysis of gene signature A

Gene signature A was significantly enriched for 9 canonical pathways (A) which could be attributed to 5 functional categories (B). Statistical analysis was performed using a Fisher's Exact test.

Tab. 5-18: Regulation of probes associated with GR signalling in ANGPT1-depleted SEM cells

Gene Symbol	Fold change	Accession	Probe_Id
MAP2K7	2.94	NM_145185.2	ILMN_1781104
NR3C1	2.63	NM_001018076.1	ILMN_1668525
NFATC3	2.43	NM_173163.1	ILMN_1685810
TAF11	2.20	NM_005643.2	ILMN_1690545
HSP90AA1	2.16	NM_001017963.1	ILMN_1687546
NCOA3	2.06	NM_181659.1	ILMN_2347693
IL4	2.04	NM_172348.1	ILMN_1669174
HSPA6	2.03	NM_002155.3	ILMN_1806165
SOS2	-2.05	NM_006939.2	ILMN_1764414
SUMO1	-2.11	NM_003352.4	ILMN_1790105
CREB1	-2.18	NM_134442.2	ILMN_2382758
TAF15	-2.40	NM_003487.2	ILMN_2402131
BCL2	-2.66	NM_000657.2	ILMN_2363250
GTF2H2	-2.71	NM_001515.3	ILMN_1691485
STAT1	-3.27	NM_007315.2	ILMN_1777325

ANGIOPOIETIN-1, a novel factor implicated in t(4;11)-positive ALL

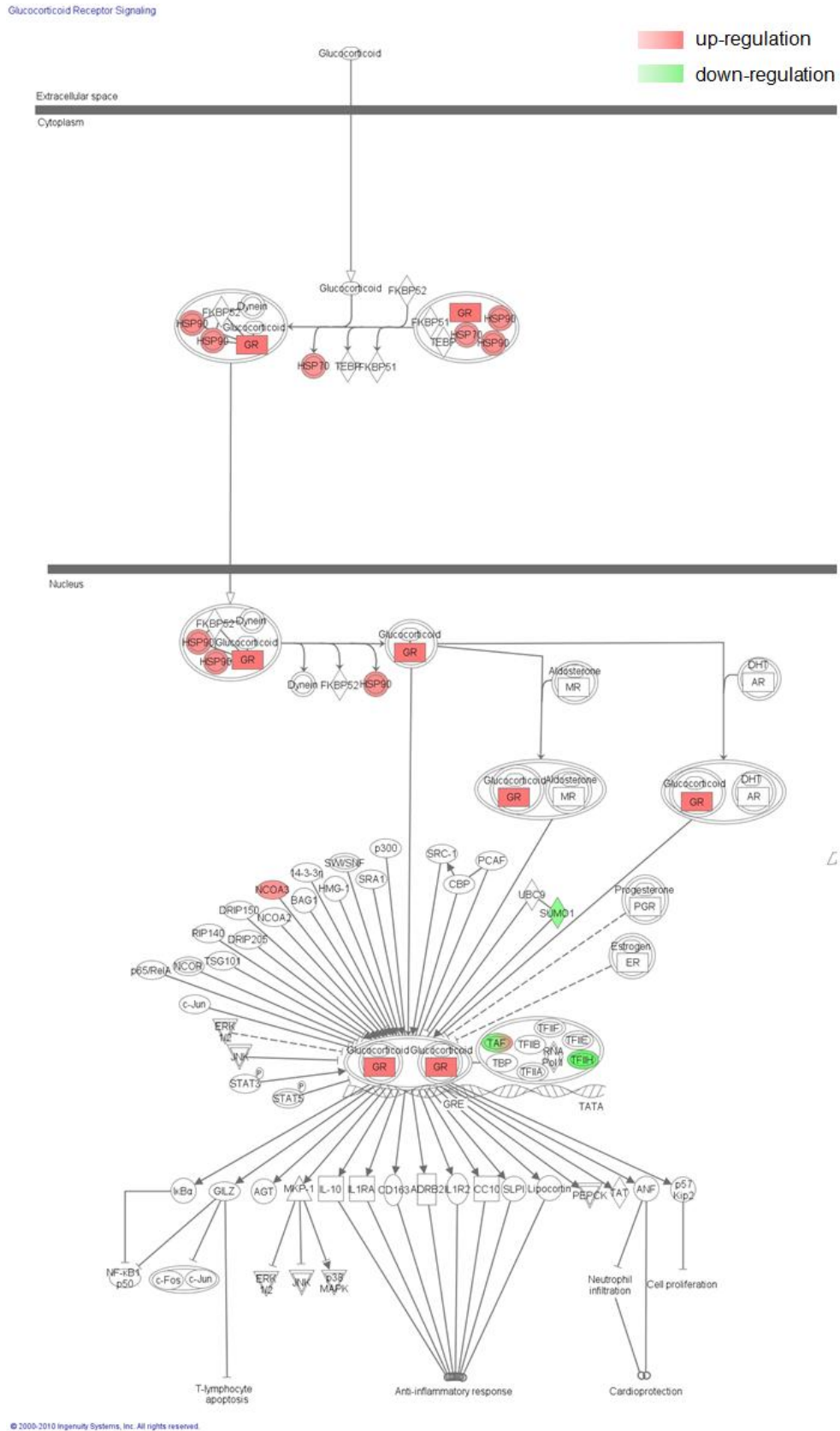


Fig. 5-35: GR signalling pathway machinery is up-regulated in response to *ANGPT1* depletion

5.5.1.2 Functional analysis of gene signature B

Gene signature B, consisting of 393 up- and 3592 down-regulated probes, showed association with cell-to-cell interactions and signalling, development of haematopoiesis and related haematologic processes. Additional molecular and cellular functions affected were molecular transport, carbohydrate and lipid metabolism, as well as tissue and organ-related physiological processes (tab. 5-19).

Tab. 5-19. Significantly enriched functional categories in gene signature B.

Top 5 Biofunctions	P-value
Diseases and Disorders	
<i>Connective Tissue Disorders</i>	1.33E-04 - 1.14E-03
<i>Inflammatory Disease</i>	1.33E-04 - 4.55E-02
<i>Skeletal and Muscular Disorders</i>	1.33E-04 - 4.36E-02
<i>Endocrine System Disorders</i>	1.65E-04 - 4.55E-02
<i>Genetic Disorder</i>	1.65E-04 - 4.77E-02
Molecular and Cellular Functions	
<i>Gene Expression</i>	3.87E-04 - 4.36E-02
<i>Cell-To-Cell Signalling and Interaction</i>	4.93E-04 - 4.03E-02
<i>Cellular Development</i>	9.25E-04 - 4.94E-02
<i>Carbohydrate Metabolism</i>	1.55E-03 - 3.09E-02
<i>Lipid Metabolism</i>	2.06E-03 - 3.40E-02
Physiological System Development and Function	
<i>Haematological System Development and Function</i>	6.78E-04 - 4.55E-02
<i>Digestive System Development and Function</i>	1.17E-03 - 1.17E-03
<i>Organ Development</i>	1.17E-03 - 8.46E-03
<i>Haematopoiesis</i>	2.06E-03 - 4.55E-02
<i>Tissue Morphology</i>	5.41E-03 - 4.27E-02

P-Value range describes the P-values of associated subcategories as determined by Fisher's exact test.

While these differ from the biological functions associated with signature A, they correlated with its linked functional networks, emphasising the implications of ANGPT1 in cell-to-cell interactions. These functions are also reflected in the top 5 molecular networks represented by signature B, which comprise cellular proliferation, cell-to-cell signalling and interactions, as well as haematological processes (tab. 5-20, fig. 5-36). The net effect appears to be a down-regulation of such functions, which is in concordance with the reported physiological functions of ANGPT1 in the BM niche.

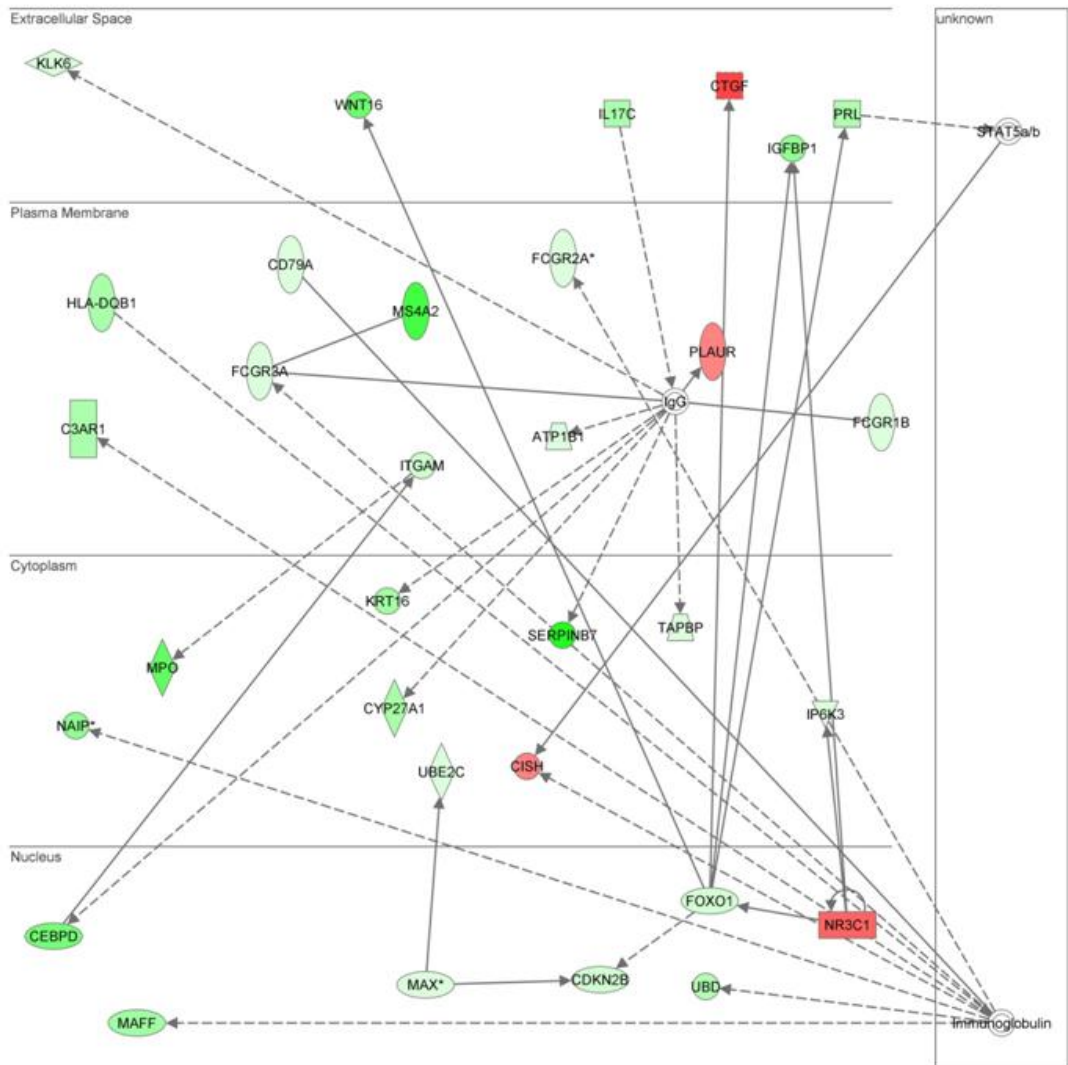
Tab. 5-20: Top 5 significantly enriched networks in gene signature B.

Name	Score
Cellular Growth & Proliferation, Haematological Disease, Immunological Disease	29
DNA Replication, Recombination, and Repair, Cell Cycle, Cellular Development	27
Tissue Morphology, Cardiac Hypertrophy, Cardiovascular Disease	23
Cellular Movement, Cancer, Cellular Development	22
Antigen Presentation, Cell-To-Cell Signalling & Interaction, Haematological System Development and Function	14

Pathway analyses revealed significant enrichment of 18 canonical pathways which could be attributed to 7 subcategories. The most affected pathways were linked to GPCR/cAMP/PKA signalling, in which several effectors were down-regulated (fig. 5-38). Other pathways down-regulated as well were those linked to maintenance of stemness, in particular the WNT/beta-CATENIN and the TGF-beta axis (fig. 5-39), which fits with the role of ANGPT1 in maintaining HSC quiescence in the BM.

Network: Cellular growth & proliferation, haematological and immunological disease

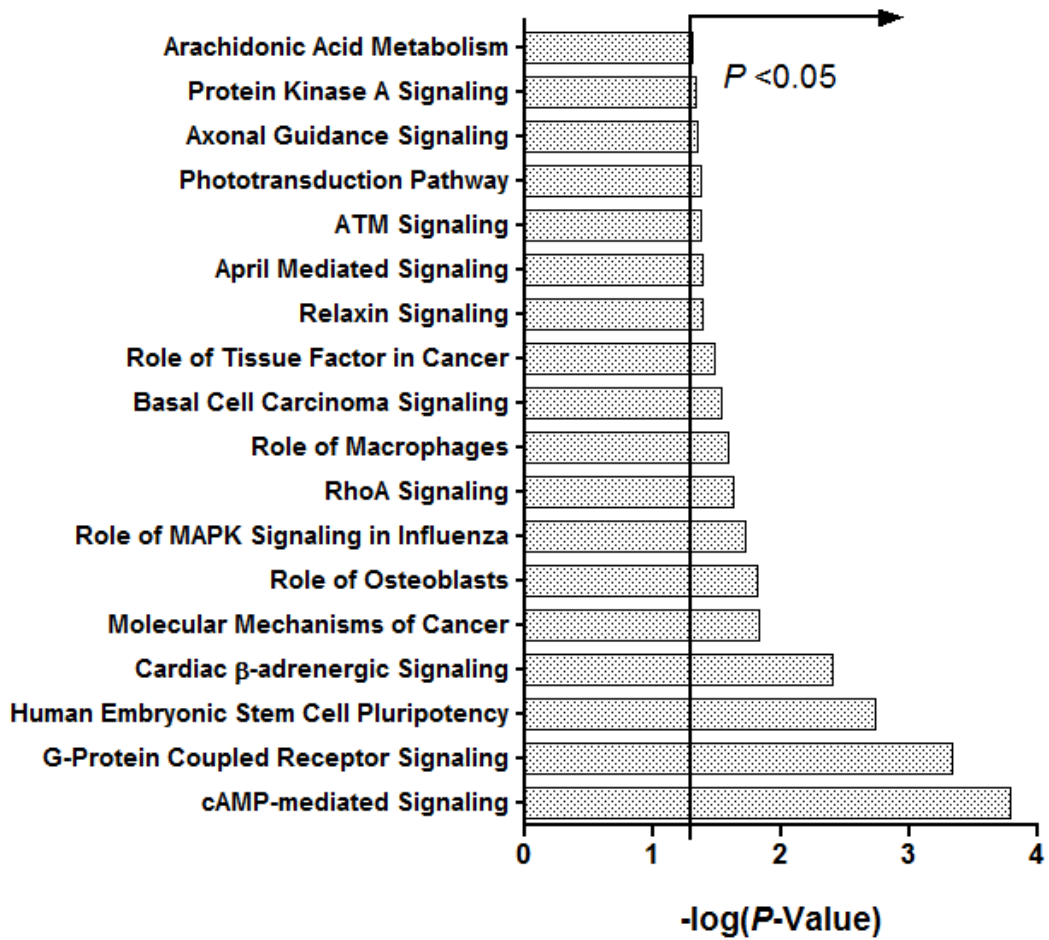
■ up-regulation ——— direct interactions
■ down-regulation - - - indirect interactions



© 2000-2010 Ingenuity Systems, Inc. All rights reserved.

Fig. 5-36: ANGPT1 depletion results in down-regulation of the functions associated with proliferation and haematological processes.

A Significantly Enriched Canonical Pathways



B

Pathway categories

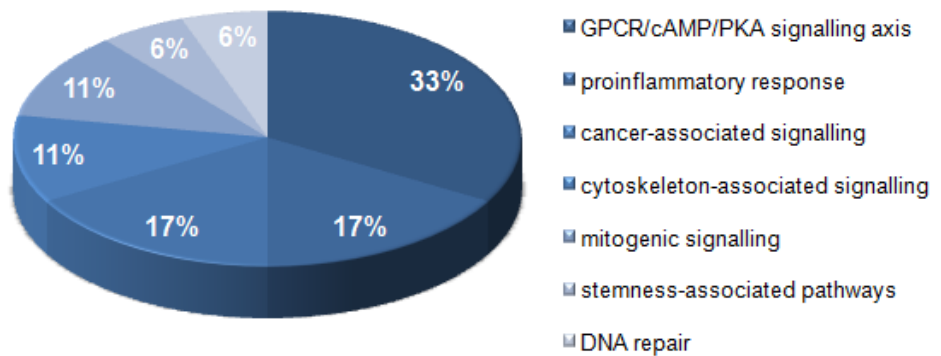


Fig. 5-37: Pathway analysis of gene signature B

Gene signature B was significantly enriched for 18 canonical pathways (A) which could be attributed to 7 functional categories (B). Statistical analysis was performed using a Fisher's Exact test.

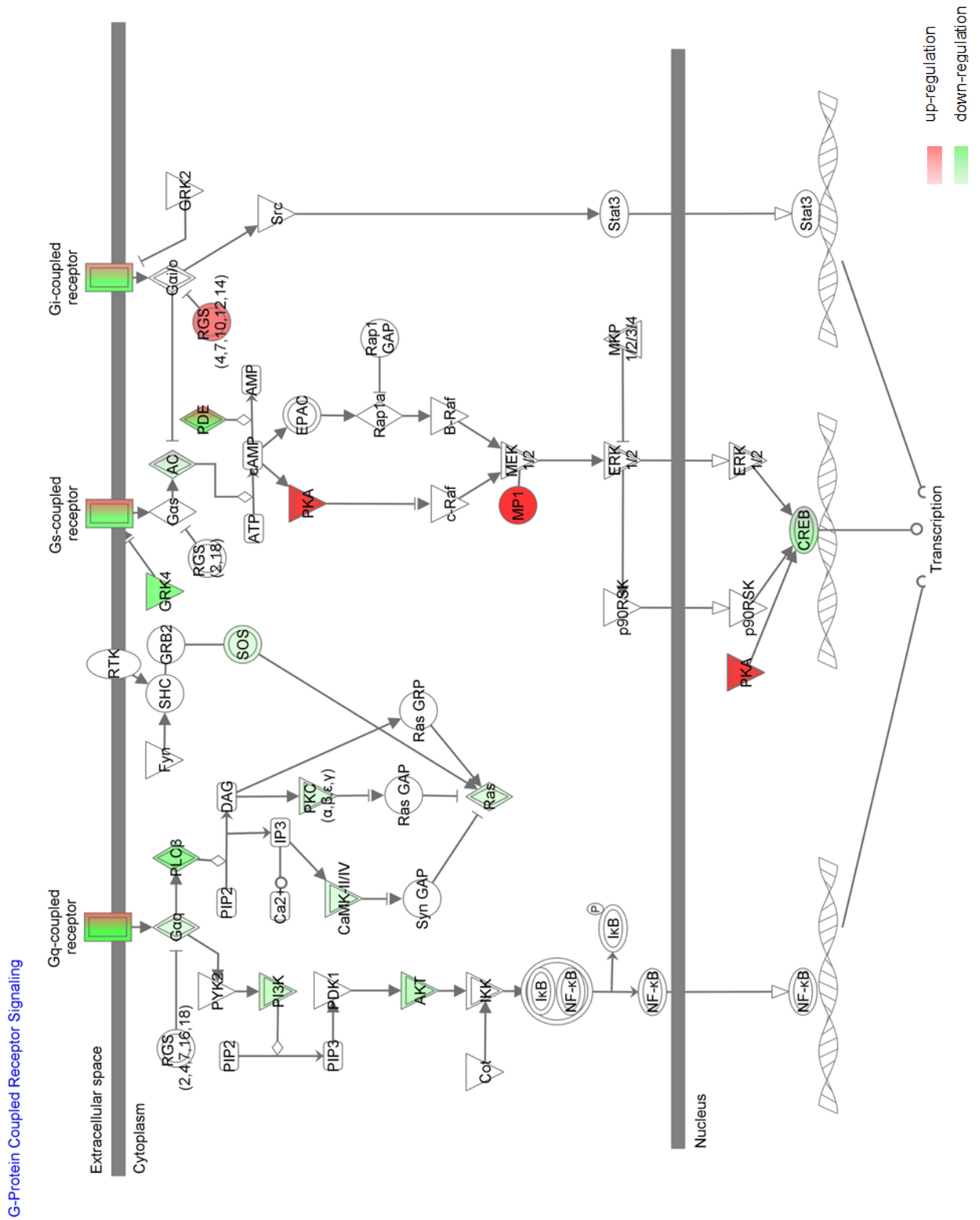


Fig. 5-38: GPCR/cAMP/PKA signalling is down-regulated in response to ANGPT1 depletion.

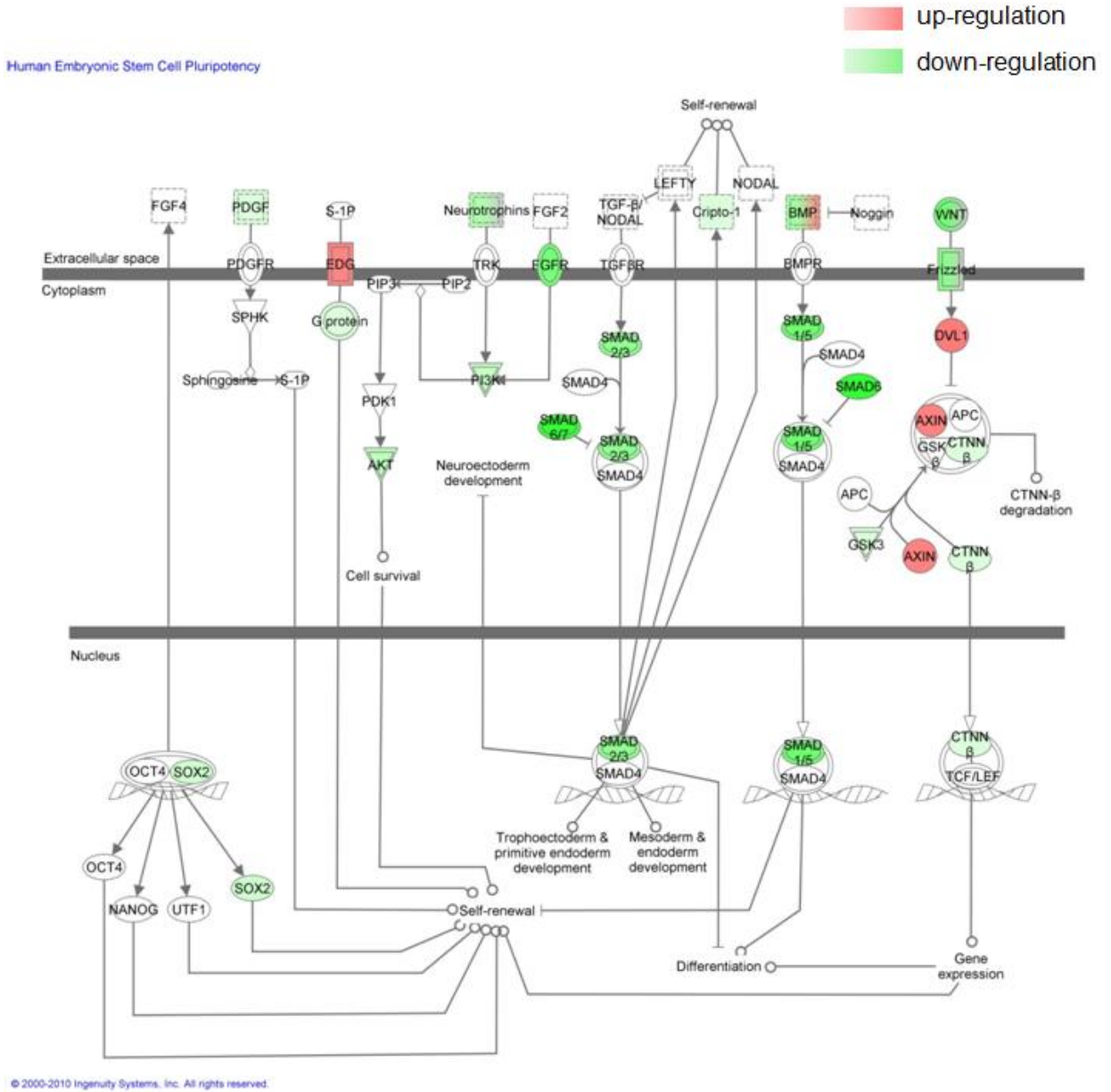


Fig. 5-39: Pathways associated with stemness signalling are down-regulated in response to ANGPT1 depletion.

5.5.2 ANGPT1 Depletion Does Not Sensitise the t(4;11)-positive Cell Line SEM Towards the Glucocorticoid Dexamethasone

One of the most prominently up-regulated pathways in response to ANGPT1 depletion is the glucocorticoid receptor (GR) signalling pathway. Pharmacological glucocorticoids (GC), such as dexamethasone and prednisolone, are used for the first-line treatment in ALL. GCs irreversibly bind the GR and induce leukaemic blast cell death, and poor response to GC is an adverse prognostic factor in ALL. Clinically, there is a high proportion of t(4;11)-positive ALL patients belonging to the poor-responder category. Several different mechanisms for GC resistance have been described so far, including loss of the GR and deregulated GR signalling. In SEM cells, ANGPT1 depletion results in up-regulation of several positive mediators of the GR signalling pathway; thus, a potential role of ANGPT1 in mediating GC resistance was investigated by evaluating whether either RNAi-mediated ANGPT1 knockdown or MLL/AF4 depletion sensitised SEM cells to the glucocorticoid dexamethasone (DEX). SEM cells were electroporated with the corresponding siRNA species or mock-treated and split into two treatment groups, of which one was supplemented with recombinant human ANGPT1 (rhANGPT1, 2 μ g/ml) while the other was left untreated. This approach allowed assessing the reversibility of effects mediated by ANGPT1 depletion. After an 8h post-electroporation equilibration period, electroporated cells were exposed to a DEX-dose range from 0-100 μ M for 96h. Viability was measured at the experimental endpoint using a MTT viability assay. No substantial sensitisation of SEM cells treated with siRNA could be observed in response to DEX exposure, although treatment with siANGPT1-1 and siANGPT1-3 seemed to very subtly decrease viability; this effect could be partially reversed by exogenous ANGPT1 (fig.5-40).

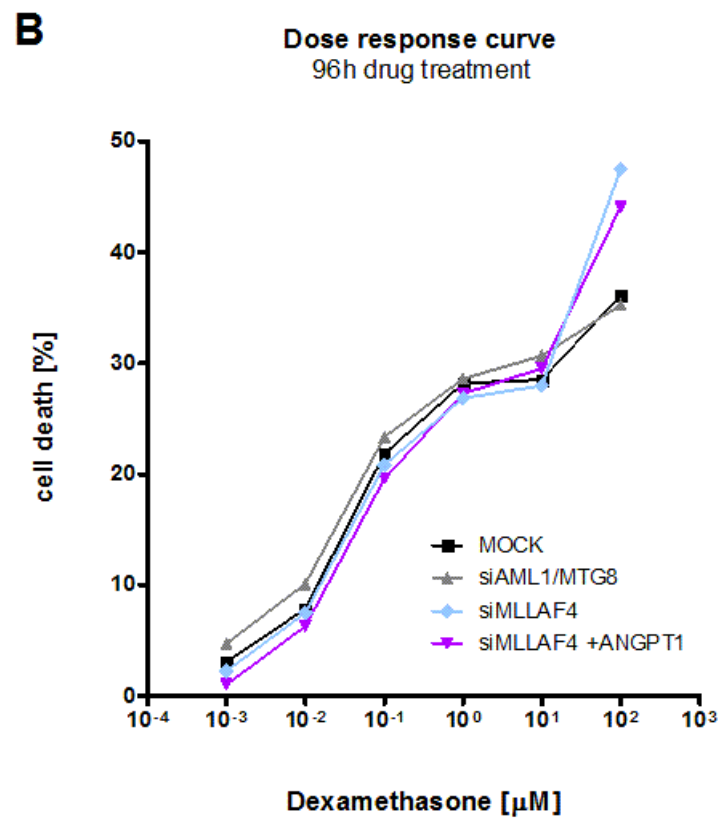
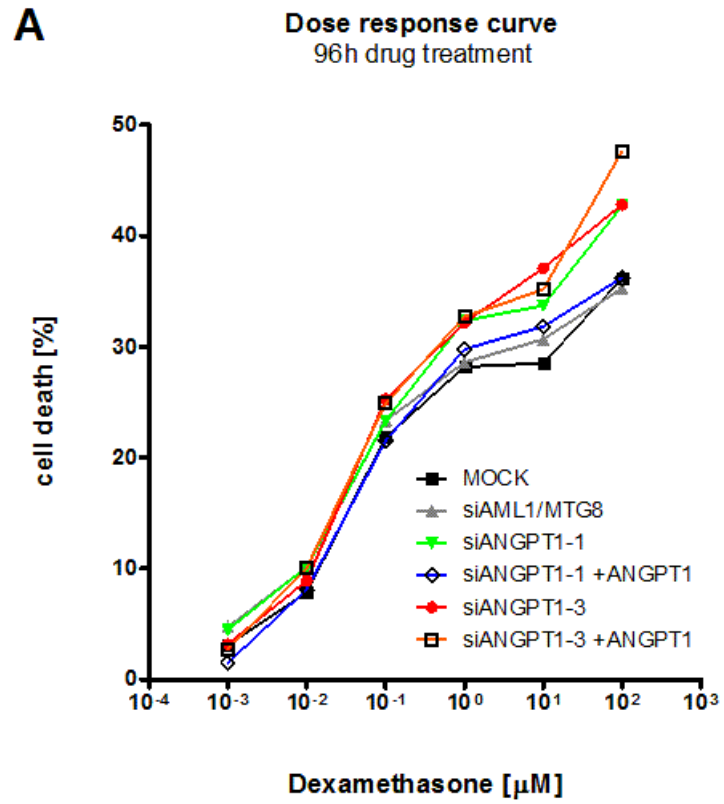


Fig.5-40: Dexamethasone response curve of siRNA-treated SEM cells.

SEM cells electroporated with siMLL/AF4, siANGPT1-1 & siANGPT1-3 were exposed for 96h to a DEX dose range. In order to investigate the role of ANGPT1 in mediation of GC-resistance, an identically treated group was in parallel treated with rhANGPT1 (2µg/ml). Controls (siAML1/MTG8-treated and the pulse control sample MOCK) were incubated with DEX without rhANGPT1. Viability was determined by a MTT assay. Graphs represent the mean of two independent experiments.

5.6 ANGPT1 DEPLETION AFFECTS LEUKAEMOGENESIS IN VIVO

5.6.1 Establishing an inducible shRNA expression system in SEM-SLIEW cells

Assessing the role of ANGPT1 in t(4;11)-positive ALL *in vitro*, it was revealed that sustained knock-down of ANGPT1 impinged on proliferation, cell cycle progression and viability. ANGPT1 has been postulated to be important for regulating HSCs and their interactions with the bone marrow microenvironment, thus implying a potential role of ANGPT1 in the leukaemic blast-niche interactions. This aspect was investigated *in vivo*, using the NOD.Cg-*Prkdc^{scid} Il2rg^{tm1Wjl}/SzJ* (NSG) mouse model. This mouse strain is derived from the NOD/SCID (*non-obese diabetic/severe combined immune deficiency*) background, lacking a functional *Prkcd* gene, which codes for the catalytic subunit of the DNA-PK holoenzyme. Consequently, this transgenic strain is deficient in functional haematopoietic cells of the lymphocytic lineage. The additional knock-out mutation in the *Il2rg* gene, which codes for the Il2 receptor gamma chain, results in loss of functional natural killer (NK) cells. This profoundly immunodeficient mouse model is currently the gold standard for studying leukaemogenesis and disease progression³³⁷⁻³³⁹.

In order to study the effect of ANGPT1 knock-down in t(4;11)-positive ALL development and progression in NSG mice, a stably expressed knock-down system was developed using a commercially available lentiviral shRNA expression vector (pTRIPZ backbone) and the SEM-SLIEW (*gfp⁺luc⁺*) cell line as target cell line. The SEM-SLIEW cell line is a modified SEM cell line transduced to stably and constitutively express the reporter gene *GFP* (*green fluorescent protein*) and *LUC* gene, coding for fire fly luciferase. The use of the SEM-SLIEW cell line allows *in vivo* bioluminescence imaging, a non-invasive technique to track the location of luciferase-expressing cells in the body of living animals. The SEM-SLIEW cell line was generated in our research group by Ms Elda Latif.

Lentivirus particles containing the expression cassette for either a shRNA against ANGPT1, *shANGPT1*, or a *non-target control* shRNA (*shNTC*) were produced by transient cotransfection of the packaging cell line 293T with the

pTRIPZ-shRNA expression vector constructs & the packaging vectors pMD.2g and pCMVdR8.91 using the CaPO₄-method. The lentiviral particles for either construct were harvested, concentrated, and the SEM-SLIEW cells transduced via spinoculation (fig. 5-41). The employed shRNA expression plasmids were inducible vectors regulated by a Tet-On system; transcription of either the shRNA or the reporter gene RFP occurred only under the presence of a tetracycline-derivative. In this study, the cell culture medium was supplemented with the tetracycline family antibiotic doxycycline.

Virus production in the 293T packaging cell line

three-way cotransfection using the CaPO₄-Method

- pTRIPZ-shRNA expression vector
- pMD.2g packaging vector
- pCMVdR8.91 packaging

Virus transduction in target cell line

Harvest and concentration of viral particles

Infection of target cell line by spinoculation

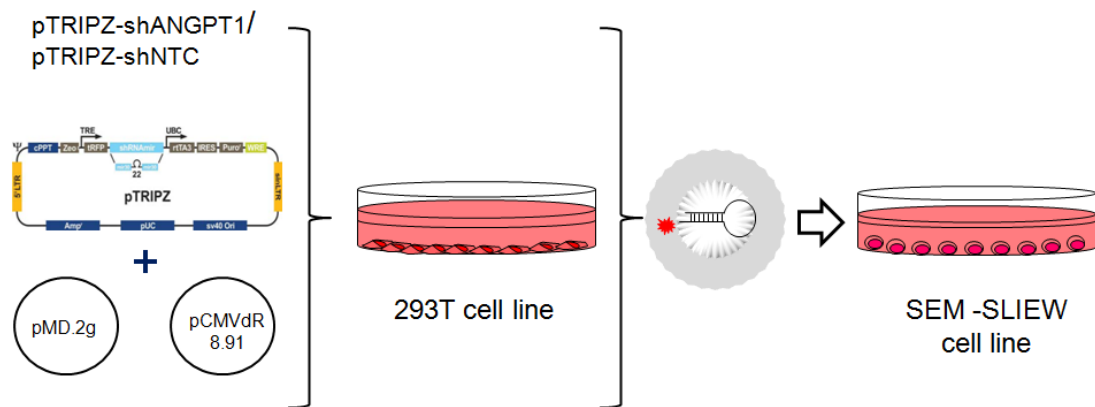


Fig. 5-41: Scheme depicting the workflow for lentiviral particle production and subsequent infection of the target cell line SEM-SLIEW

Post-transduction, the cells were selected with puromycin for at least 4 weeks and then kept growing in growth medium supplemented with 2 µg/ml puromycin. Induction of shRNA-RFP expression with doxycycline revealed RFP-fluorescence positivity of 80-93%. (fig. 5-42), which could not be increased by augmenting puromycin dose and exposure.

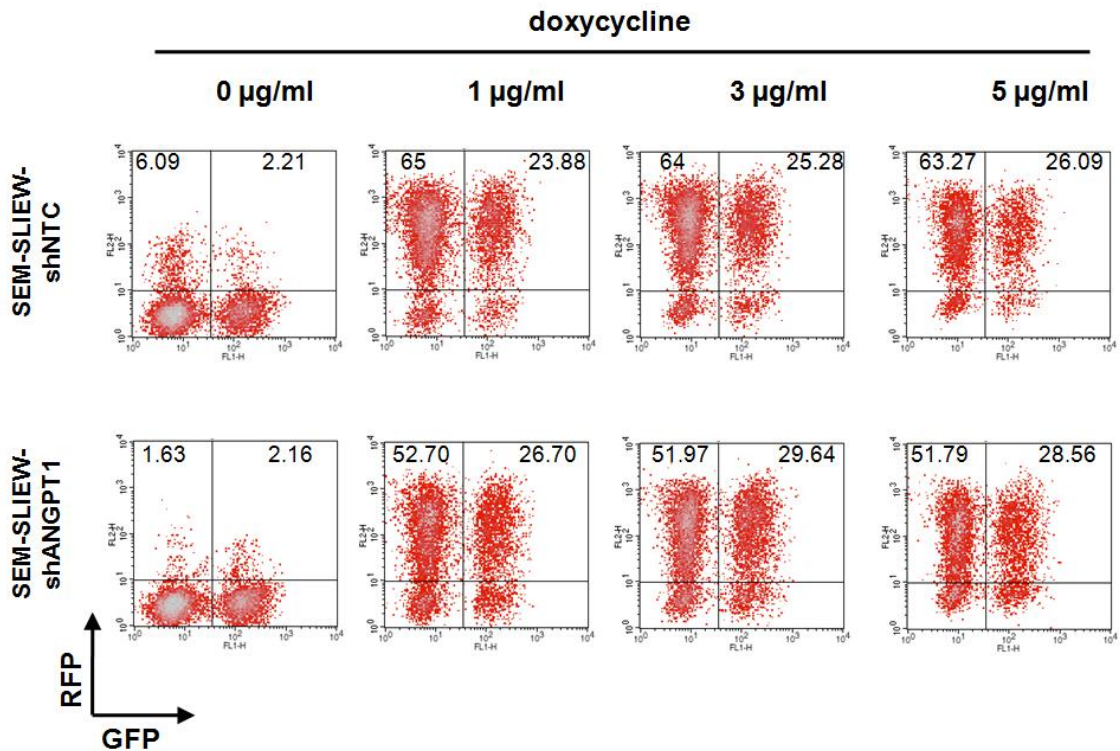


Fig. 5-42: Flow cytometric analysis of shRNA induction

SEM-SLIEW cells transduced with shRNA were cultured for 3 days in growth medium supplemented with doxycycline at different concentrations. Induction of shRNA was measured by the surrogate marker of RFP expression, as determined by flow cytometry. SEM-SLIEW cells were heterogeneous for GFP-expression. Numbers indicate percentage of cells in the corresponding subfraction. One experiment representative of at least n=3 comparable experiments is shown.

Induction of shRNA expression by exposing shRNA-transduced SEM-SLIEW cells to 4 days of a dose range of doxycycline (0-5 $\mu\text{g}/\mu\text{l}$), resulted in a reduction of *ANGPT1* transcript level by 70-75% in shANGPT1 expressing cells when compared to corresponding shNTC controls (fig. 5-43). The extent of knock-down was not dose-dependent within the range assayed, as the lowest concentration of 1 $\mu\text{g}/\text{ml}$ already achieved 70%, and this was not substantially altered at 3 $\mu\text{g}/\text{ml}$ or 5 $\mu\text{g}/\text{ml}$.

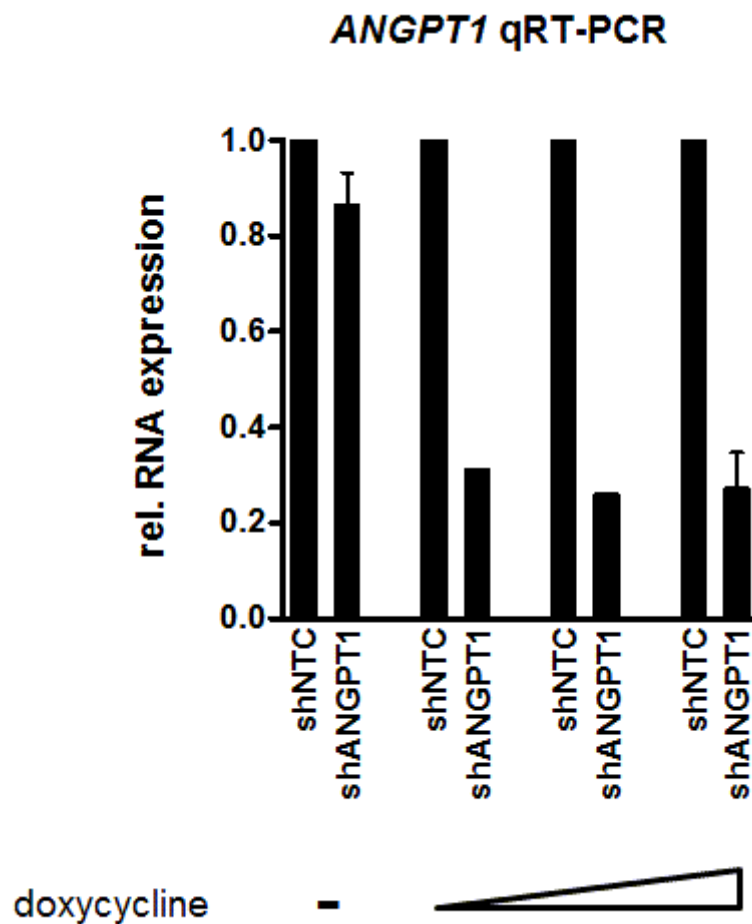


Fig. 5-43: qRT-PCR analysis of ANGPT1 in SEM-SLIEW cells expressing shRNA

SEM-SLIEW-shRNA cells were cultured for 4d with doxycycline-supplemented growth medium at increasing concentrations. *ANGPT1* expression was determined by qRT-PCR. The graph shows the mean of n=2 two independent experiments at dox=0 and dox = max concentration, error bars indicate data range. The intermediate dose range (dox=min, dox= intermediate) represent one single experiment.

5.6.2 Effects of RNAi-mediated ANGPT1 knock-down in vivo

The SEM-SLIEW cell line was heterogeneous for GFP expression. Therefore, prior to the inoculation of NSG mice, shRNA expressing SEM-SLIEW cells were sorted for luciferase expression purity using fluorescence-activated cell sorting on GFP fluorescence, achieving a post-sort enrichment of >89% (fig. 5-44).

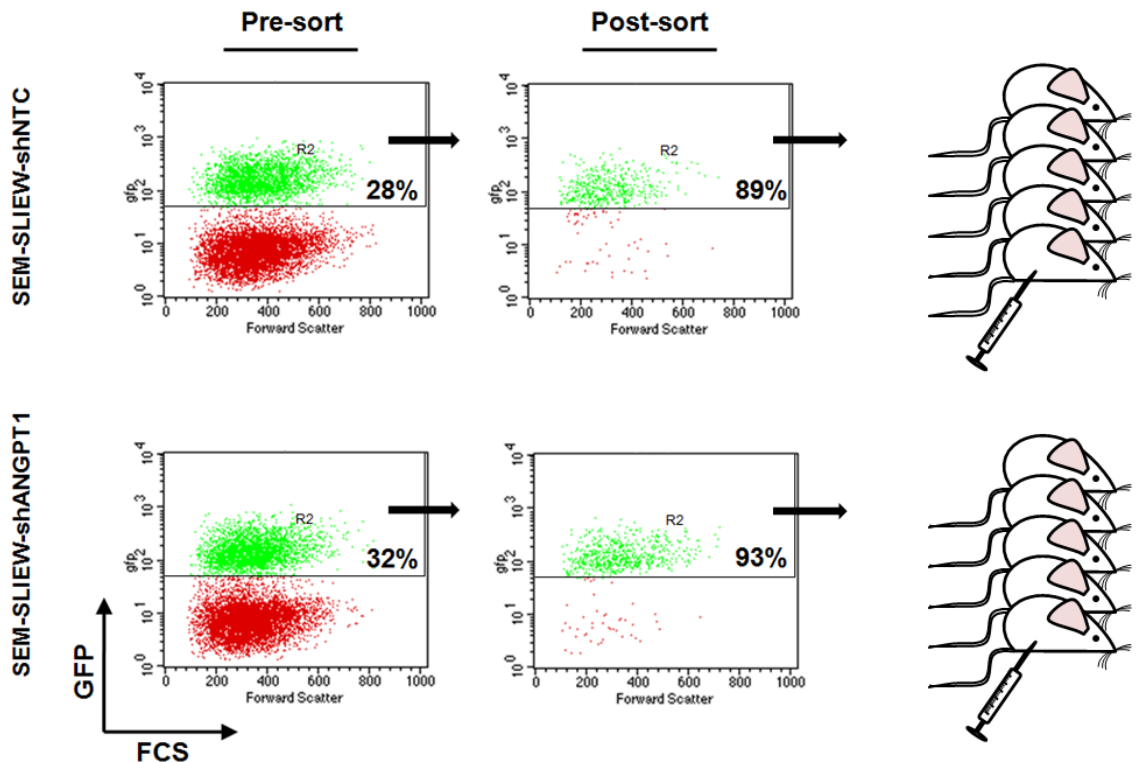


Fig. 5-44: Scheme - Purification of the GFP-expressing shRNA-SEM-SLIEW fraction by fluorescence-activated cell sorting (FACS) and subsequent IF injection into NSG mice

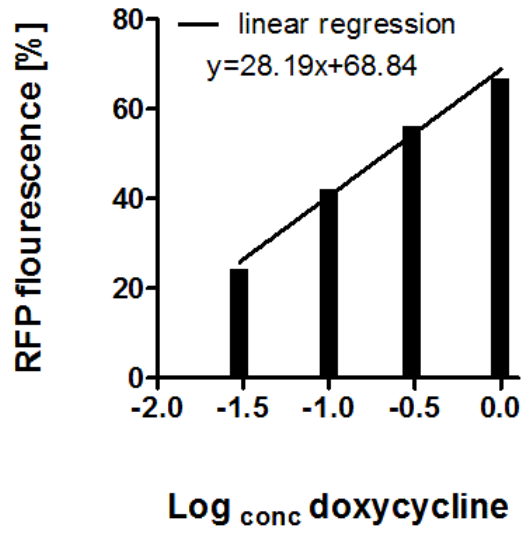
SEM-SLIEW cells transduced with either shNTC or shANGPT1 were sorted on GFP-expression using FACS, enriching the population from 28% to > 89%. The sorted populations were transplanted directly into the BM of NSG mice. Per treatment group n=5 mice were treated with approximately 50,000 cells each.

Two experimental animal groups consisting of n=5 NSG mice each were used for the xenograft study. One group was transplanted intrafemorally (IF) with approximately 50,000 SEM-SLIEW-shANGPT1 cells per mouse, while the control group was inoculated IF with the same number of SEM-SLIEW-shNTC cells. Immediately post-transplantation each mouse was injected intraperitoneally (IP) with 100 μ l 40 μ g/ml doxycycline solution in order to start *in vivo* shRNA expression induction, and this expression was maintained using drinking water supplemented with 1 mg/ml doxycycline.

In order to assess bioavailability of the supplemented or injected doxycycline, an *ex vivo* bioassay using plasma from the transplanted NSG mice was developed. PB was harvested from a mouse both injected IP with doxycycline and fed with supplemented drinking water, and from a mouse only treated with supplemented drinking water. Plasma was collected from PB and diluted 1:5 with cell culture growth medium. This conditioned medium was used to culture SEM-SLIEW shANGPT1 cells for 48h. Both IP injection and the drinking water alone resulted in sufficiently elevated doxycycline plasma levels to induce RFP expression *ex vivo* and *in vitro*, as determined by flow cytometry (fig. 5-45B). In order to quantify the plasma doxycycline levels, a titration experiment was performed in parallel: SEM-SLIEW shANGPT1 cell were cultured for 48h in cell culture growth medium supplemented with a dose range from 0 - 1 μ M doxycycline. The resulting RFP induction augmented linearly with increasing doxycycline expression (fig. 5-45A), and regression analysis provided the equation employed to calculate the plasma doxycycline levels from the measured RFP fluorescence, taking into account the dilution factor. Doxycycline-containing drinking water alone elevated plasma levels to 0.2 μ g/ml, an additional IP injection with doxycycline yielded a doxycycline plasma concentration of 0.53 μ g/ml.

A

Doxycycline titration



B

**Bioassay
plasma doxycycline levels**

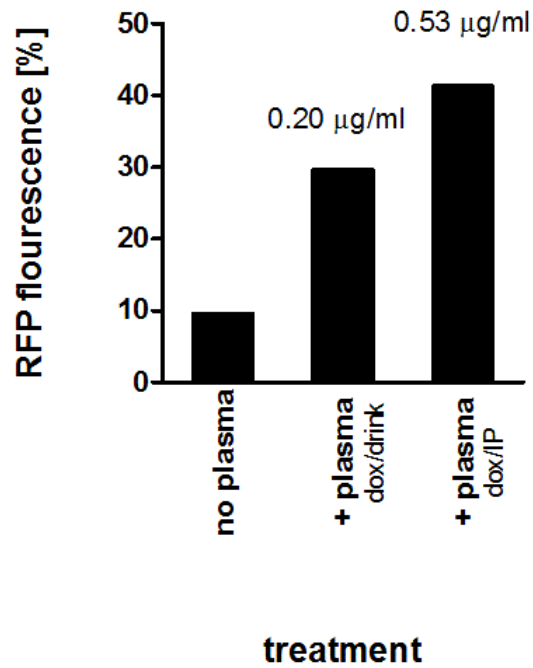


Fig. 5-45: Bioassay to determine doxycycline plasma levels

PB was harvested from a mouse approximately 2-3h after receiving an IP bolus injection of 0.1 ml doxycycline (40ug/ml), and from a control mouse which only had doxycycline administered via drinking water. The plasma was diluted five-fold with growth culture medium, and this conditioned medium was used to culture SEM-SLIEW shANGPT1 cells for 2 days. The resulting RFP induction was measured by flow cytometry (B). In order to correlate the fluorescence to a doxycycline concentration, SEM-SLIEW shANGPT1 cells were cultured with a doxycycline range from 0.1 to 3ug/ml (A).

Disease development was monitored *in vivo* using bioluminescence imaging, and the mice sacrificed humanely when presenting clinically unwell or when disease burden exceeded animal welfare regulations. Disease penetrance was 100% in the mice treated with SEM-SLIEW shNTC cells, while 80% of the mice transplanted with SEM-SLIEW shANGPT1 cells engrafted. The associated survival and disease statistics of both treatment groups are summarised in Tab. 5-21.

Tab. 5-21: Survival and disease burden statistics of both xenograft treatment groups

	SEM-SLIEW shNTC n=5 NSG mice	SEM-SLIEW shANGPT1 n=5 NSG mice
penetrance	5/5 (100%)	4/5 (80%)
median survival [d]	76 (47-76)	64 (56-76)
median BM engraftment [%]	25.1 (4-55.14)	7.45 (0-7.9)
median spleen infiltration [%]	28.15 (22.9-41.6)	16 (0-37.5)

Although the median survival between both experimental groups did not differ significantly (fig. 5-46), both disease phenotype and the disease burden were vastly different.

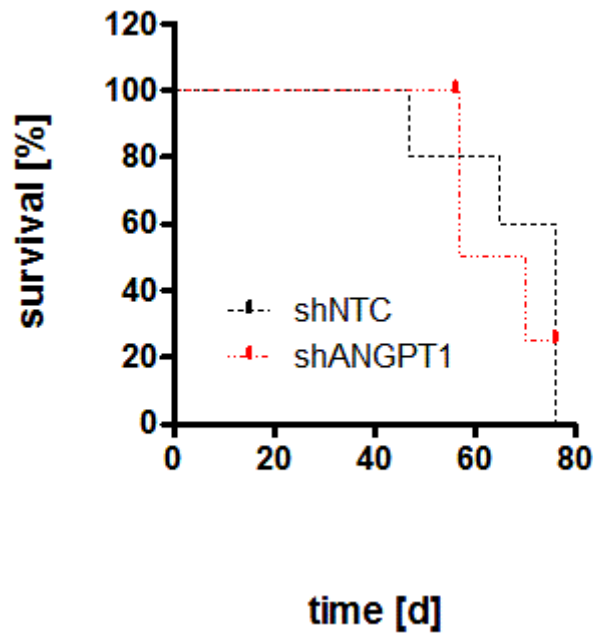


Fig. 5-46: Kaplan-Meier plot depicting survival of the two treatment groups

There was no difference ($P=0.9885$) in survival between mice injected with SEM-SLIEW shNTC cells and the group inoculated with SEM-SLIEW-shANGPT1 expressing cells. Statistical survival analysis was performed using a log-rank test.

The NSG mice injected with SEM-SLIEW shNTC cells developed overt leukaemia and were sacrificed within 47 to 76 days. They presented a median engraftment in the BM of 25.1%, ranging from 4-55.14% (averaged over all hind limb femurs and tibiae per mouse assayed, fig. 5-47). The mice displayed massive splenomegaly as indicated by organ size (fig. 5-48), weight (fig. 5-48) and

infiltration with human cells (median of 28.15%, ranging from 22.9-41.6%, fig. 5-47). In contrast, the shANGPT1 xenograft group showed only slightly enlarged spleen organs and increased spleen weight fig. 5-48A, B), and a reduced engraftment in the BM and the spleen, with a median of 7.45%, ranging from 0-7.9%, and 16% (0-37.50%), respectively (fig. 5-47).

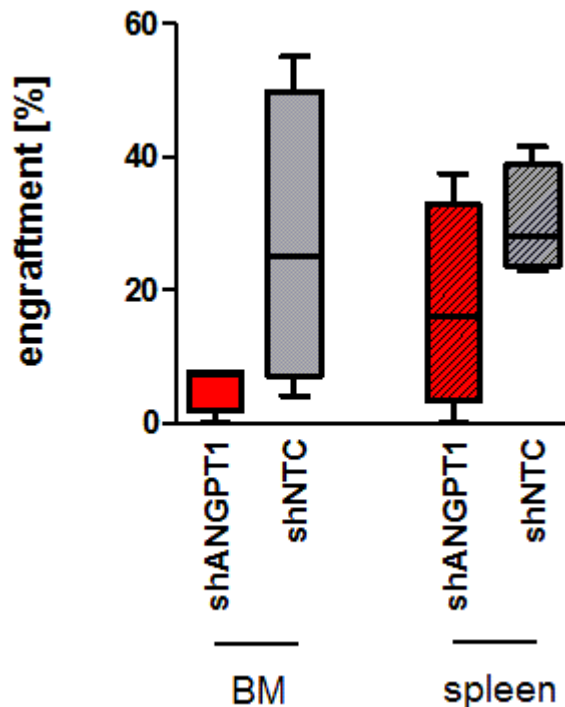


Fig. 5-47 : Engraftment of human ALL cells in the BM and splenic infiltration

Mice transplanted with SEM-SLIEW-shANGPT1 cells show a lower extent of BM engraftment and extramedullary disease, as illustrated by the percentage of human ALL cells in the spleen, than the control group inoculated with SEM-SLIEW-shNTC cells. The BM engraftment was determined averaging the percentage of ALL cells in the femurs and tibiae of the hind limbs of each mouse (number of positive events/number of total events*100). The box and whisker plots represent the interquartile range and the minimal/maximal values, respectively; the horizontal line indicates the median.

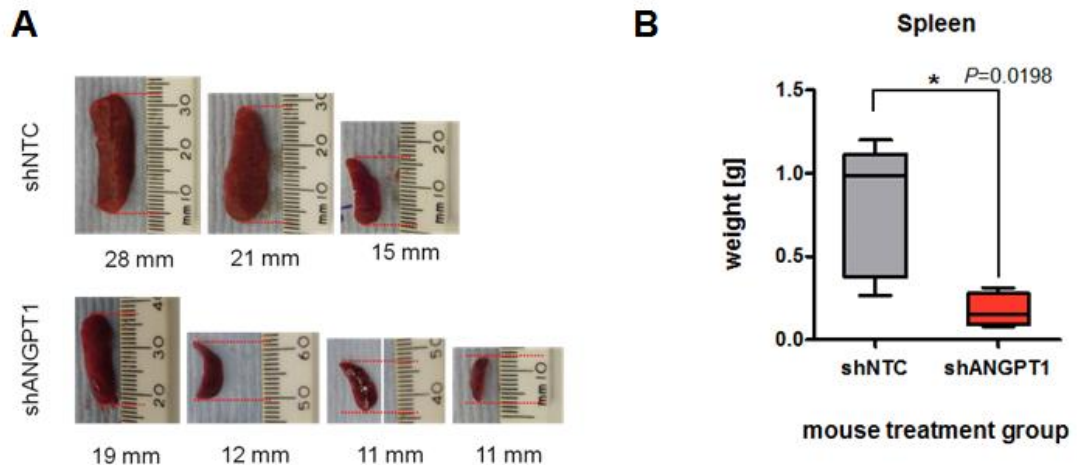


Fig. 5-48: Spleen characteristics in transplanted NSG mice

Mice transplanted with SEM-SLIEW-shANGPT1 cells show less infiltration of the spleen with human ALL cells when compared to the control group inoculated with SEM-SLIEW-shNTC cells, displaying reduced enlargement of the spleen in both size (A) and weight (B). The box and whisker plots represent the interquartile range and the minimal/maximal values, respectively; the horizontal line indicates the mean.

Tracking the disease development *in vivo* via bioluminescence imaging showed a systemic spread of the disease in the shNTC xenograft group, while the disease spread in the group transplanted with SEM-SLIEW shANGPT1 was substantially lower (Fig. 5-49 , upper panel). However, they developed a solid tumour composed of human cells at the injection site, as indicated by their luciferase activity (fig. 5-49, lower panel) and subsequent histological analyses via flow cytometry (fig. 5-50A). The SEM-SLIEW shANGPT1 treated mouse group was eventually terminated due to tumour size according to animal welfare restrictions (fig. 5-50B, C), albeit not due to overt leukaemia or presenting clinically unwell. This was further supported by the significant difference in body weight loss, a surrogate parameter to monitor mouse welfare (fig. 5-51).

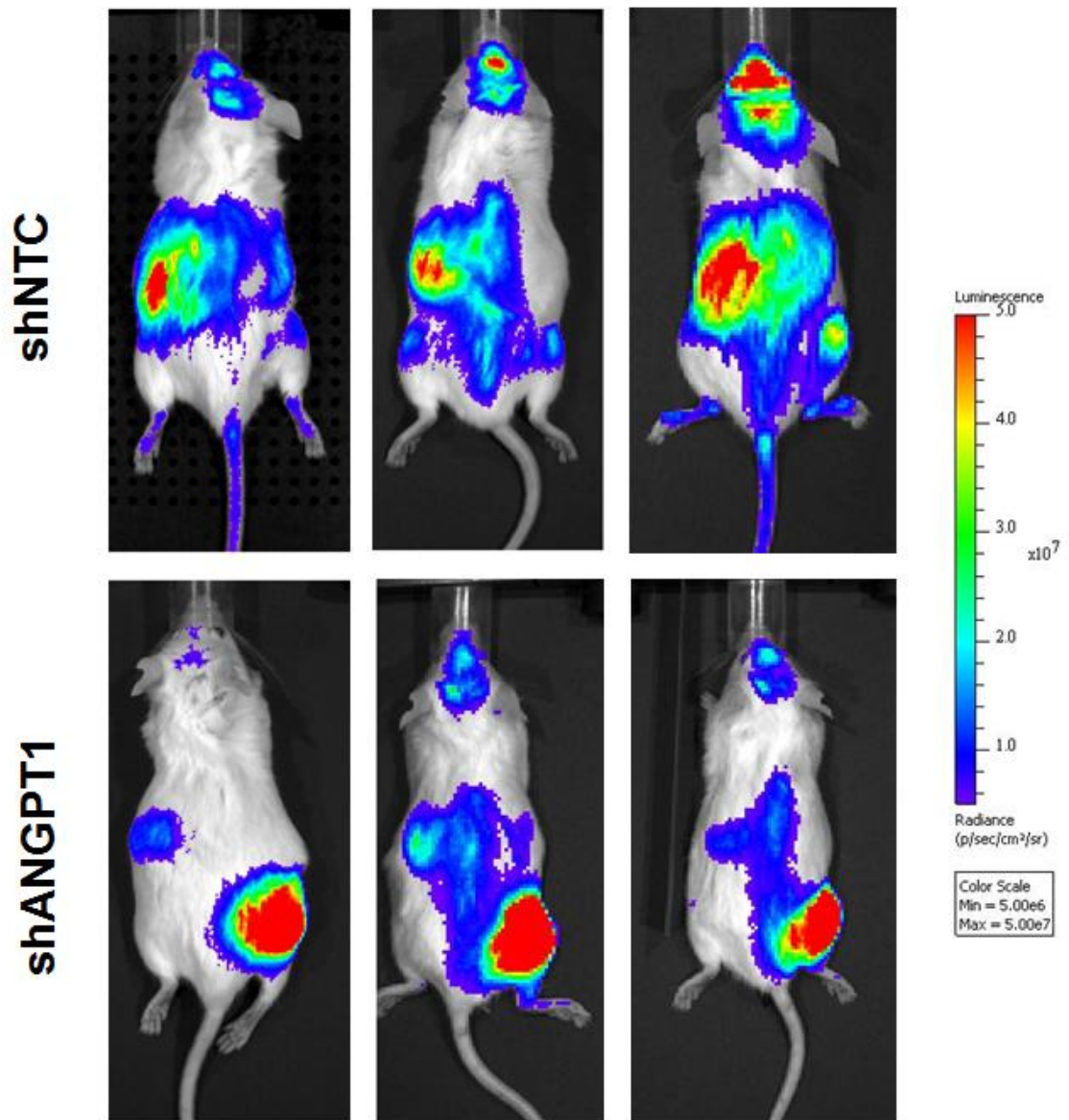


Fig. 5-49: Bioluminescence *in vivo* imaging of leukaemic disease spread in NSG mice

In order to monitor disease progression both xenotransplanted mouse groups were subjected to *in vivo* bioimaging. The mice were injected IP with 0.1 ml luciferin which was metabolised by the luciferase enzyme expressed in the SEM-SLIEW cells, thereby releasing a luminescent signal. Mice transplanted with SEM-SLIEW shANGPT1 cells showed a marked reduction of systemic spread (lower panel) compared to the control group (SEM-SLIEW shNTC, upper panel). Interestingly, the SEM-SLIEW shANGPT1 mice showed a strong signal in the right hind limb, the area surrounding the injection site. This could be attributed to the development of a solid tumour composed of human SEM-SLIEW cells in the adjacent tissue. Three representative mice from each treatment group are shown.

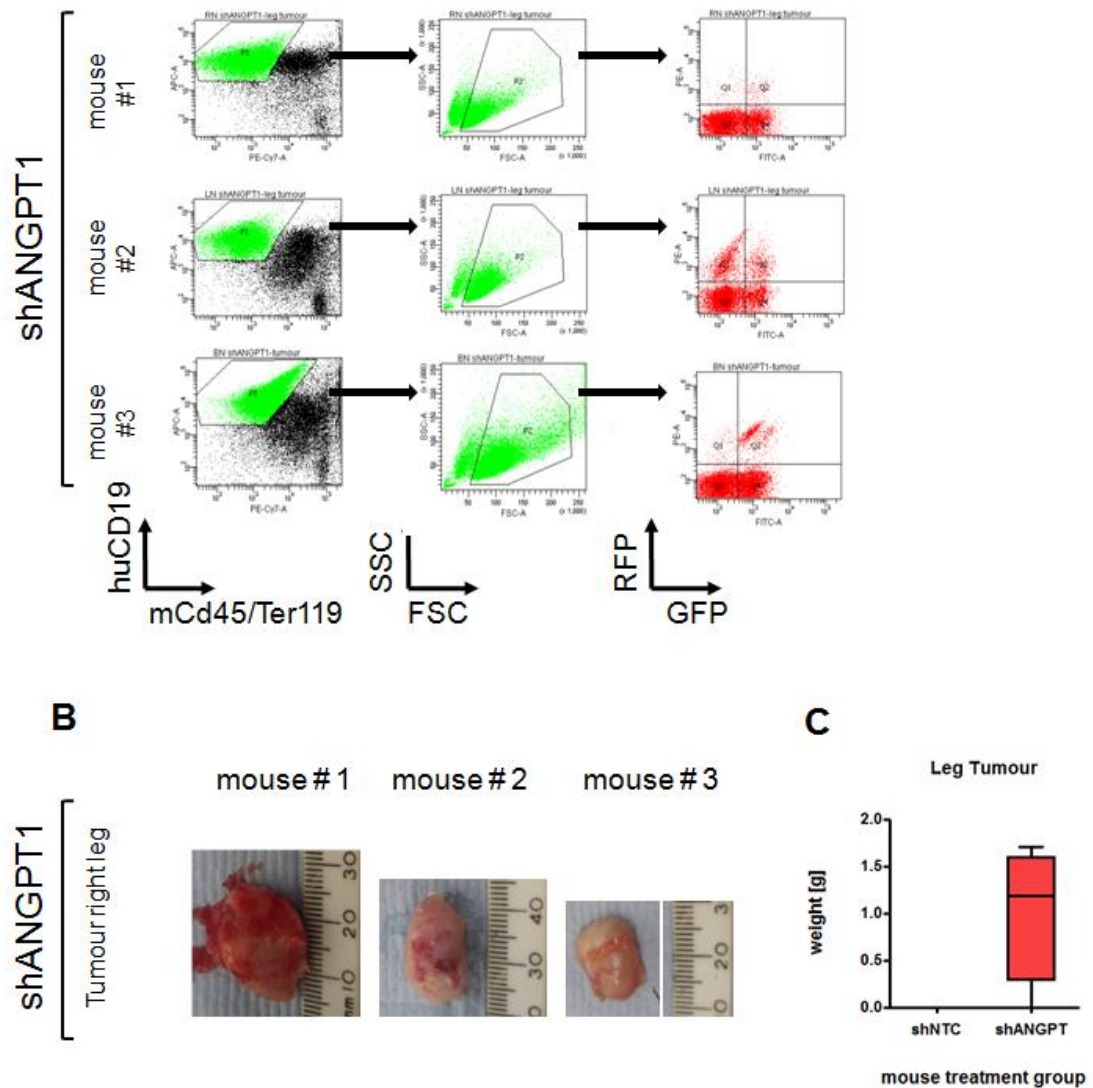


Fig. 5-50: Tumour characteristics of SEM-SLIEW shANGPT1-transplanted mice.

Mice injected with SEM-SLIEW shANGPT1 cells developed a solid tumour adjacent to the injection site composed of human cells (A), which grew to be of substantial size (B) and weight (C); eventually, this hind limb tumour exceeded animal welfare regulations, and the mice were humanely killed.

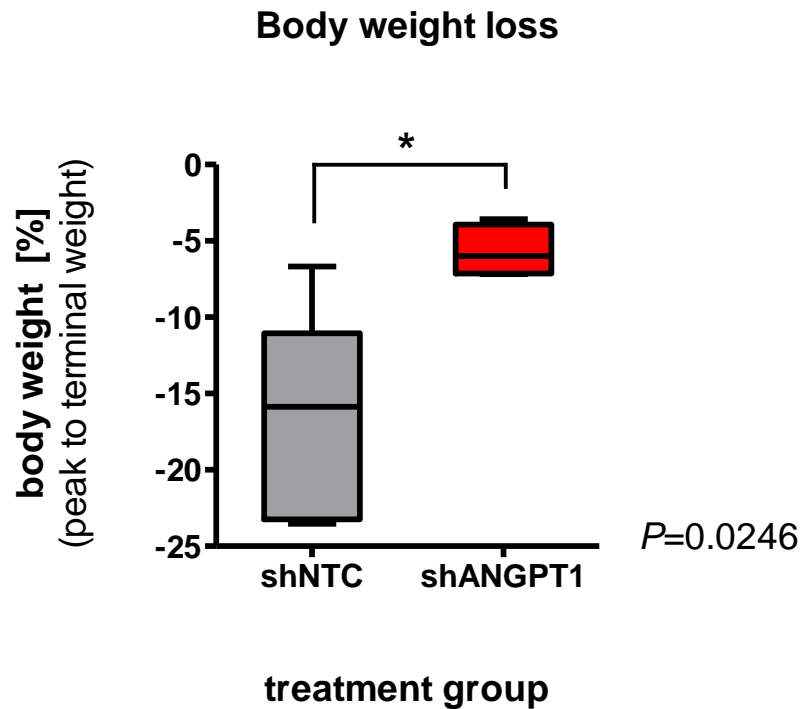


Fig. 5-51: Terminal body weight loss in xenograft treatment groups

Mice were weighed at regular intervals to monitor for body weight loss indicative of overt leukaemia. The changes were calculated on the difference between the peak body weight (set as 100%) of each mouse and respective body weight at the last weighing time point. The treatment group transplanted with SEM-SLIEW shNTC showed a drastic weight loss, while the SEM-SLIEW shANGPT1 injected mice displayed no substantial changes. This difference in body weight loss was statistically significant as determined by an unpaired Student's t-test Welch-corrected for unequal variances.

In conclusion, the results of this pilot study show that ANGPT1 knock-down impinges on leukaemic disease development and spread *in vivo*. Further studies with a constitutively expressing shRNA system as well as bigger treatment groups in order to provide the necessary statistical power are required for validation of these observations.

5.7 EXPRESSION ANALYSIS OF OTHER ANGIOPOIETIN GENE FAMILY MEMBERS AND ANGIOGENIC FACTORS IN T(4;11)-POSITIVE ALL AND THEIR REGULATION BY MLL/AF4

ANGPT1 works in a finely tuned balance with other angiogenic factors, particularly with its endogenous antagonist Angiopoietin-2 (ANGPT2). Thus, this study was expanded to investigate the effect of MLL/AF4 depletion on this system and also on other members of the ANGIOPOIETIN family.

Screening of a BCP-ALL cell line panel for expression of several members of the Angiopoietin family revealed ubiquitous expression of ANGPT2 and ANGPTL2, while ANGPT4 was restricted to the t(4;11)-positive cell lines. ANGPTL4 was widely expressed in BCP-ALL cell lines, albeit not in the model cell line SEM (fig. 5-52).

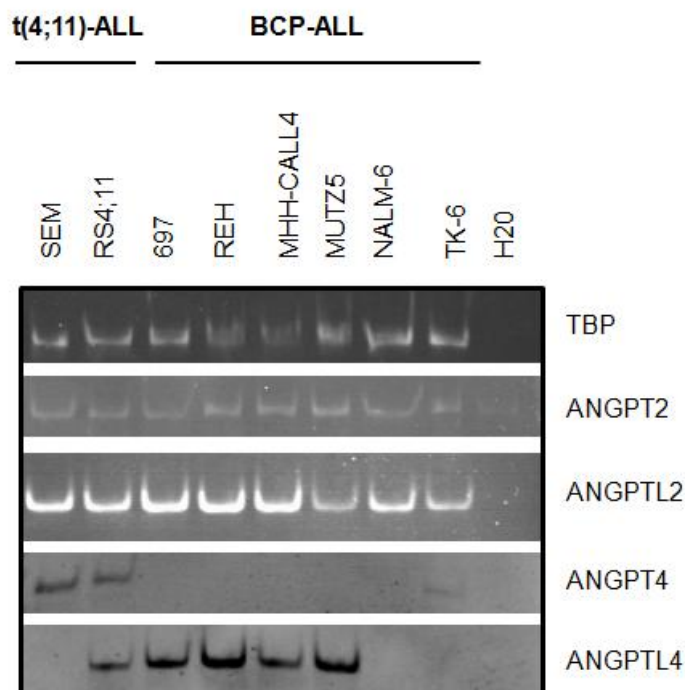


Fig. 5-52: Expression Analysis of ANGIOPOIETIN family members in ALL cell lines

ANGIOPOIETIN family member expression was determined in a BCP-ALL leukaemia cell line panel by qRT-PCR, and amplicons were visualised by DNA-polyacrylamide gel electrophoresis. Results from one single experiment are shown, each sample was performed in triplicates.

Apart from ANGPT1, also another angiopoietins family member, *ANGPTL2*, showed differential expression in the Illumina HT12 BeadChip array in response to siMLL/AF4 treatment.

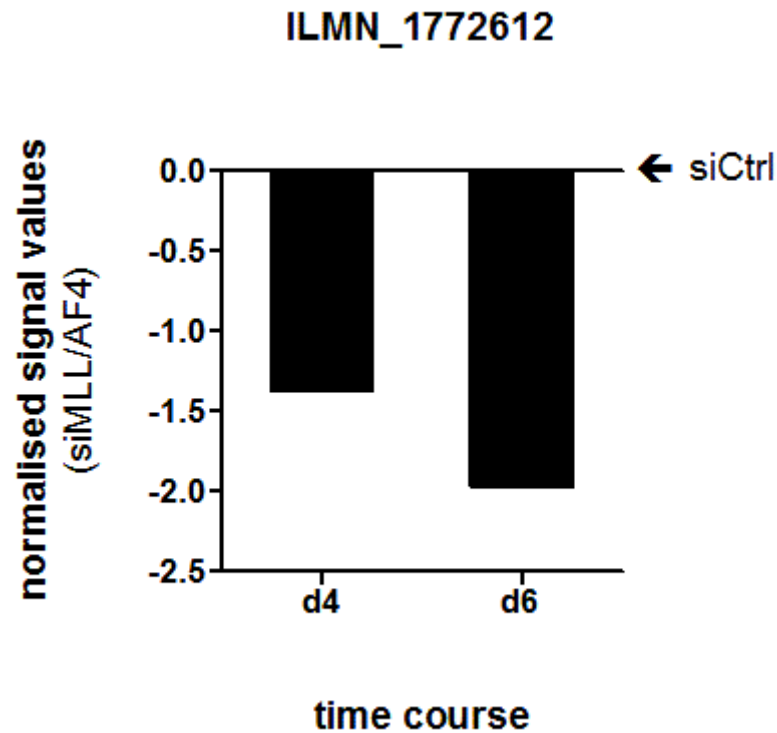


Fig. 5-53: Normalised *ANGPTL2* probe signal values in samples depleted of MLL/AF4

SEM cells had been depleted of MLL/AF4 for 4 & 6 days (d4, d6) using siMLL/AF4, or cells were transfected with control siRNA (siCtrl). Signal intensity values of the Illumina HT12 bead array probes for *ANGPTL2* of the siMLL/AF4 samples at each time point were normalised against corresponding controls samples, and the signal value fold-change \log_2 -transformed.

This result was validated *in vitro* using qRT-PCR (fig. 5-54). Knock-down of MLL/AF4 for 4d resulted in a 52% decrease of *ANGPTL2* mRNA when compared to the corresponding controls ($p < 0.001$).

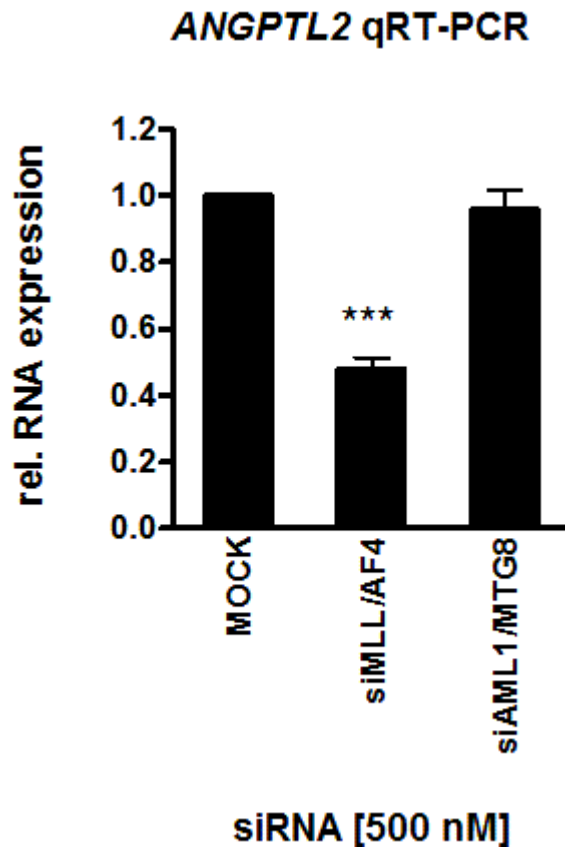


Fig. 5-54: *ANGPTL2* expression analysis by qRT-PCR in MLL/AF4 depleted SEM cells

ANGPTL2 is down-regulated in response to a sustained siMLL/AF4 treatment for 4d in SEM cell, when compared to controls. The graph represents the mean of $n=3$ independent experiments, error bars show S.E.M. Statistical analysis was performed using an unpaired Student's t-test (***) = $p < 0.001$).

The dependency of *ANGPTL2* expression on the MLL/AF4 status of the cell however could not be validated in primary patient material; electroporation of patient cells carrying MLL/AF4 fusion gene (e9-e4 breakpoint) with siMLL/AF4, control siRNA (siAML1/MTG8) or without siRNA (MOCK) did not result in *ANGPTL2* expression changes (fig. 5-55) at the time points queried.

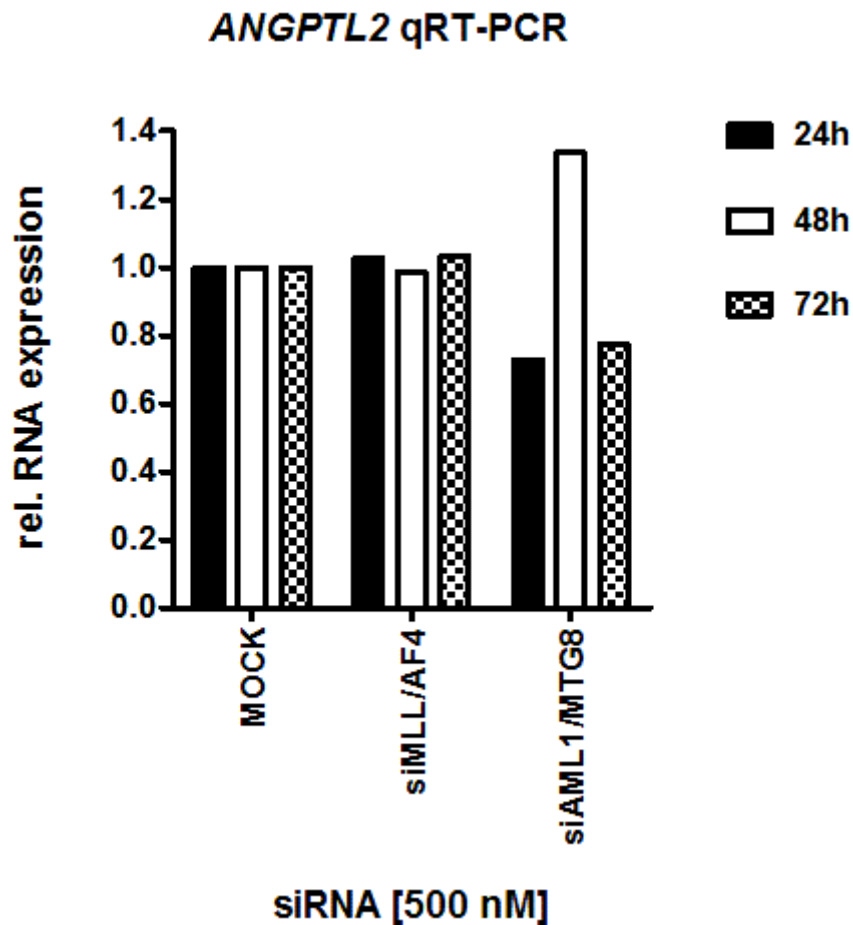


Fig. 5-55: *ANGPTL2* expression analysis by qRT-PCR in MLL/AF4 depleted primary patient blasts.

Primary patient blasts were electroporated with siMLL/AF4, control siRNA (siAML1/MTG8) or without oligonucleotides (MOCK). *ANGPTL2* show no alteration in expression levels in response to a siMLL/AF4 treatment for 24h, 48h and 72h, when compared to controls. The graph represents the mean of one single experiments; each sample performed in triplicate.

Not much is known about the function of ANGPTL2, however it has been reported that it plays a role in HSC expansion *ex vivo*. Other ANGPTL proteins, such as ANGPTL3, ANGPTL7, have also been implicated in HSC proliferation and stemness. Since MLL/AF4-positive ALL has been associated with a stem cell-like signature in literature, which has been supported in this study, not least by the MLL/AF4-dependent expression of the HSC-factor ANGPT1, the *ANGPTL2* expression levels in CD34+ CB cells was investigated. In concordance to its reported function, the median *ANGPTL2* expression was 3.3-fold higher in CD34+ CB cells compared to bulk CB cells. Due to the small sample size and the variable distribution, no statistical significance could be concluded (fig. 5-56).

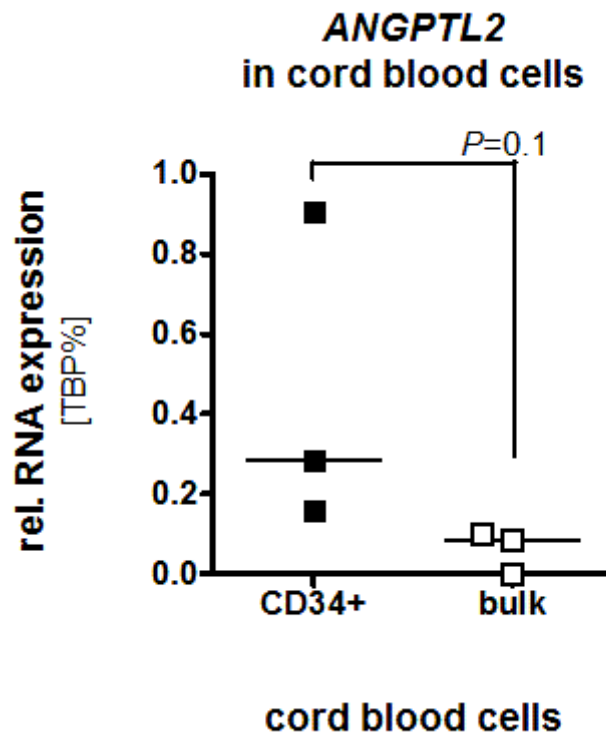


Fig. 5-56: *ANGPTL2* expression analysis in purified and fractioned CB cell populations

Mononuclear CB cells were fractionated using MACS on the cell surface marker CD34. The bulk population was simultaneously purified by negative selection. *ANGPTL2* levels were determined by qRT-PCR. The graph represents n=3 individual CB, statistical analysis was performed using a Mann-Whitney test.

In contrast to ANGPTL2, no differential expression of the ANGPT1 antagonist *ANGPT2* could be observed in the Illumina HT-12 BeadChip arrays. However, *ANGPT2* showed a response to MLL/AF4 down-regulation. Interestingly, while ANGPT1 expression decreased, knock-down of MLL/AF4 had the reverse effect on *ANGPT2* in SEM cells, and resulted in a 4.9-fold up-regulation compared to controls (fig. 5-57).

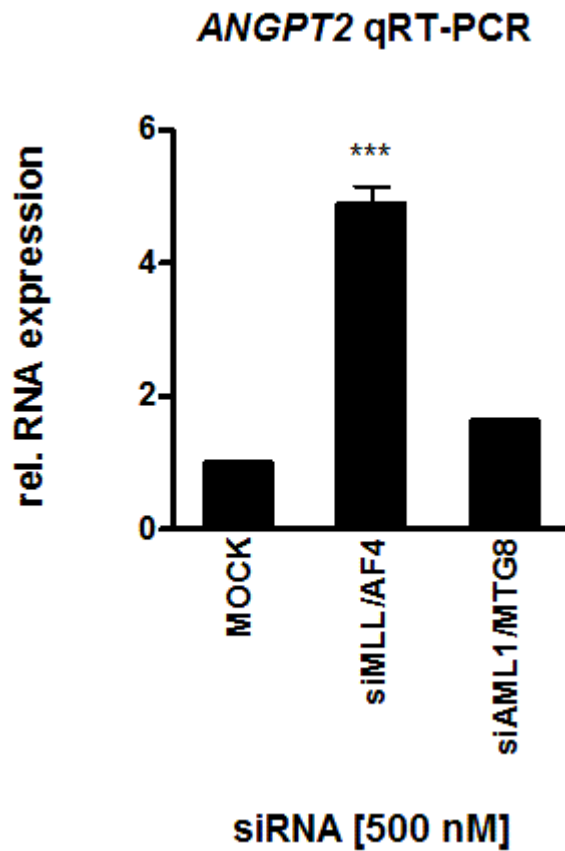


Fig. 5-57: *ANGPT2* expression analysis by qRT-PCR in MLL/AF4 depleted SEM cells

ANGPT2 is up-regulated in response to a sustained siMLL/AF4 treatment for 4d in SEM cells, when compared to controls. The graph represents the mean of n=3 independent experiments, error bars show S.E.M. Statistical analysis was performed using an unpaired parametric Student's t-test (***) = $p < 0.001$).

This result could not be validated in primary patient material; electroporation of patient cells carrying the MLL/AF4 fusion gene (e9-e4 breakpoint) with siMLL/AF4, control siRNA (siAML1/MTG8) or without siRNA (MOCK) did not result in ANGPT2 expression changes (fig. 5-58).

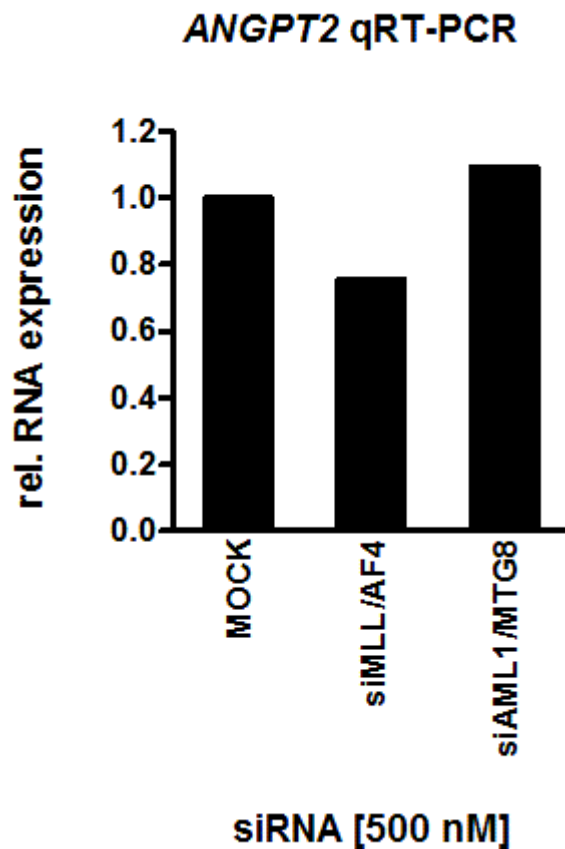


Fig. 5-58: ANGPT2 expression analysis by qRT-PCR in MLL/AF4 depleted primary patient blasts.

ANGPT2 show no alteration in expression levels in response to a siMLL/AF4 treatment for 72h in primary patient blasts, when compared to controls. The graph represents the mean of one single experiment; each sample was performed in triplicate.

There have been no reports about a potential role of ANGPT2 in either haematopoiesis or the microenvironment. Of note is that *ANGPT2* was expressed to a high level in CB, but there was no enrichment in the CD34-positive CB fraction when compared to the bulk CB cells (fig. 5-59).

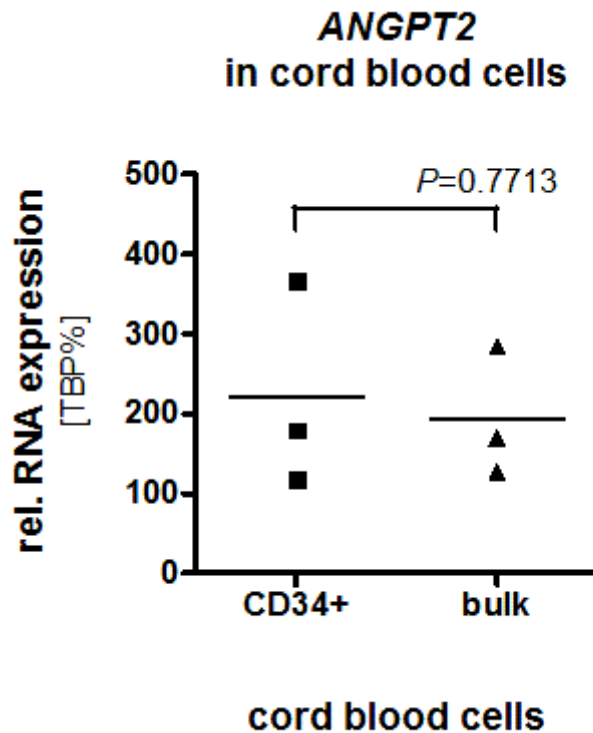


Fig. 5-59: *ANGPT2* expression analysis in purified and fractioned CB cell populations

Mononuclear CB cells were fractionated using MACS on the cell surface marker CD34. The bulk population was simultaneously purified by negative selection. *ANGPT2* levels were determined by qRT-PCR. The graph represents n=3 individual CB, statistical analysis was performed using a parametric unpaired Student's t-test.

5.8 CONCLUSIONS

The body of evidence in this chapter showed that,

- ANGPT1 expression is dependent on MLL/AF4, since fusion gene depletion in t(4;11)-positive ALL cells results in ANGPT1 down-regulation on RNA and protein level.
- ANGPT1 is required for proliferation and viability of the t(4;11)-positive cell line SEM *in vitro*, as well as leukaemic disease propagation *in vivo*.
- ANGPT1 is substantially overexpressed in MLLr-ALL, particularly t(4;11)-positive ALL compared to controls.
- ANGPT1 is highly expressed in haematopoietic stem cells.
- Other Angiopoietins are also regulated in a MLL/AF4-dependent manner.

5.9 DISCUSSION – ANGPT1 IS OVEREXPRESSED IN MLLR-ALL AND REGULATED IN A FUSION GENE-DEPENDENT MANNER

Tumour angiogenesis and the remodelling of the neoplastic microenvironment via tumour-derived angiogenic factors has been regarded as one of the established hallmarks of cancer, providing the rationale for antiangiogenic therapy strategies²⁵⁰⁻²⁵¹. In recent years, the effect of BM neoangiogenesis in haematological malignancies and its importance in therapy-response and disease maintenance has been of increasing interest. Involvement of angiogens such as VEGF-family members, their receptors (VEGFR-1-3), the angiopoietins ANGPT1, ANGPT2 and their cognate receptor TIE2 have been associated with disease outcome in AML, myeloma, lymphoma and chronic lymphocytic leukaemia (CLL)³⁴⁰⁻³⁴⁶; as a consequence, therapies involving anti-angiogenic drugs have been developed and implemented in clinical trials³⁴⁷⁻³⁵¹. In contrast, the role of BM angiogenesis and angiogenic factors in ALL remains as of yet poorly understood. Expression of VEGF family members and other proangiogenic cytokines, such as basic Fibroblast Growth Factor (bFGF), IL-8, and iNOS, as well as increased BM vascularity have been reported in ALL, however the role of these factors and their impact on disease progression and outcome has been discussed controversially^{340,342,352-356}.

One recent study showed that ALL blasts expressing VEGFR-1 had a proliferative advantage upon receptor stimulation *in vitro*, and VEGFR-1+ ALL blasts were associated with increased egress from the BM and onset of systemic organ infiltration in a NOD/SCID xenograft animal model, providing functional evidence for the role of angiogenic factors in ALL disease maintenance and progression.³⁵⁷ Interestingly, there are absolutely no reports on the role of the ANGIOPOIETIN family in ALL. Thus, in this current study, expression of ANGPT1, ANGPT2 and ANGPTL2 in BCP-ALL is reported for the first time, and in particular ANGPT1 is identified as a novel proleukaemic cytokine overexpressed in MLLr-ALL and regulated in a MLL fusion protein-dependent manner.

T(4;11)-positive ALL cell lines and patient blasts express ANGPT1 to high levels, and RNAi-mediated down-regulation of the fusion protein MLL/AF4 results in a

decrease of *ANGPT1* on RNA and protein level (fig. 5-2, fig. 5-3). This is a graded effect, and occurs in a time-dependent manner, with substantial *ANGPT1* reduction being first measured at 48h post MLL/AF4 knock-down; this reduction augments with prolonged siMLL/AF4 treatment. This delayed response argues against *ANGPT1* being a direct target gene of MLL/AF4. Indeed, ChIP-Seq data mapping MLL/AF4 binding sites in the SEM cells corroborate this; while the *ANGPT1* gene locus contains activating histone modification marks it is not occupied by the fusion protein¹³². Hence, *ANGPT1* overexpression and the fusion gene-dependent down-regulation seem to occur downstream of MLL/AF4.

The three investigated MLLr-ALL subtypes, t(4;11), t(11;19) and t(9;11) have a median 10-208 fold higher *ANGPT1* levels when compared to non-MLLr BCP-ALL, albeit each fusion gene to a different extent, arguing for a possible underlying common process (fig. 5-11). Indeed, gain-of-function studies using overexpression of different MLL fusion genes resulted in *ANGPT1* up-regulation: transient transfection of MLL/AF4 in murine embryonic fibroblasts resulted in increased *Angpt1* (personal communication with Prof. R. Marschalek). Concordantly, Chen *et al.* showed that transduction of murine lineage-negative (*lin*⁻) HSCs and common lymphoid progenitors (CLP) with MLL/AF9 resulted in *ANGPT1* up-regulation³⁵⁸. Thus, what are the potential molecular mechanisms of *ANGPT1* overexpression in MLLr-ALL?

First, we investigated involvement of *HOXA* transcription factors in *ANGPT1* regulation. Yassin and colleagues showed that transformation of HSCs with the myeloid fusion oncogenes NUP98-DDX10 or NUP98-HOXA9 resulted in concomitant up-regulation of the *HOXA* gene cluster and *ANGPT1*³⁵⁹. Since one of the hallmarks associated with MLLr acute leukaemia is aberrant 5'-*HOXA* gene cluster expression³⁶⁰⁻³⁶¹, and, most importantly, MLL/AF4 knockdown resulted in down-regulation of *HOXA6*, *HOXA7*, *HOXA9* and *HOXA10* (fig. 3-43, fig. 3-44,¹⁷⁰), this provided a solid rationale for a potential MLL-FP/*HOXA*/*ANGPT1* axis. Indeed, *in silico* analysis of the *ANGPT1* promoter, spanning 5kb upstream and 1 kb downstream of the TSS, revealed several putative *HOXA* gene binding sites (fig. 5-15). However, RNAi-mediated *HOXA7*

depletion had no effect on *ANGPT1* levels, and there was no correlation between *ANGPT1* RNA expression and the transcript levels of the *HOXA* family members, *HOXA6-HOXA10*, disproving a potential role of *HOXA* genes in mediating *ANGPT1* transcription (fig. 5-16 to fig. 5-17).

Recently, *EVI-1* has been identified as a target gene of the MLL-fusions MLL/AF9 and MLL/ENL in transformed murine *lin*⁻ HSCs, as well as being up-regulated in MLLr-AML³⁶². Similarly, the study by Chen and colleagues showed that overexpression of MLL/AF9 in HSCs/CLPs resulted in higher levels of *EVI-1* when compared to the *EVI-1* expression of transduced myeloid progenitors³⁵⁸. *EVI-1* is an important transcription factor in haematopoietic development, and, what is more, it has been shown to mediate *ANGPT1* expression in HSCs³⁶³, providing a tangible link between MLL-FP and *ANGPT1*. Interestingly, while well established in AML, *EVI-1* has so far not been implicated in ALL in general, or MLLr-ALL in particular. Indeed, in the MLL/AF4-positive ALL gene expression profiling (GEP) study performed in this PhD thesis as well as GEPs of MLLr-ALL performed by others^{132,168}, *EVI-1* is associated with absent calls in the arrays, denoting lack of expression. These studies were performed by two different platforms, the Illumina HT-12 bead array in present thesis, in which *EVI-1* is covered by one probe set, as well as the Affymetrix HU-133 plus 2.0 platform, in which 5 probe sets cover a locus described as MECOM (*MDS1* and *EVI-1*). However, a potential limitation in the probe designs cannot be ruled out, and validation of *EVI-1* expression *in laboratorio* should provide an indication whether *EVI-1* is both expressed in MLLr-ALL and involved in *ANGPT1* expression regulation.

Another potential mechanism of *ANGPT1* expression in MLLr-ALL could be explained from the so-called “cell-of-origin” hypothesis, which addresses the aetiology of the leukaemia, indicating at which stage in haematopoietic differentiation the oncogenic hit occurred or the transformed cell was arrested. MLL/AF4-positive ALL is associated with a very immature pro-B immunophenotype¹³⁷, as well as a HSC-like gene signature¹³². In healthy BM, *ANGPT1* is part of the “normal” (*i.e.* healthy) HSC gene signature, being expressed by lineage negative HSCs, as well as by BM endothelial cells, acting in

a paracrine and autocrine manner to promote HSC quiescence^{327,364-365}. Concordantly, in present PhD thesis, significant overexpression of *ANGPT1* in CD34-positive CB cells, a population enriched for HSCs, was shown when compared to the bulk CB cells (fig. 5-6). Thus, conceivably, *ANGPT1* up-regulation in MLLr-ALL might be an epiphenomenon, since it could be part of the normal genetic/transcriptional make-up of the cell of origin/ arrested cell. This is further supported by the fact that MLL germline infant ALL patient cells show strong up-regulation of *ANGPT1*, albeit in a very small patient panel (2/4 cases), and these two cases are associated with a pro-B immunophenotype. Another corroborating fact to take into account is that, although they share the same primary oncogene, MLLr-AML cell lines showed more than a 1,000-fold lower *ANGPT1* expression when compared to the MLLr-ALL cell lines (fig. 5-9). While the two MLL/AF4-positive ALL cell lines SEM and RS4;11 are pro-B-ALL, MV4;11 (MLL/AF4-positive) and THP-1 (MLL/AF9-positive) are classed as M5-AML according to the FAB classification system, indicating a more mature differentiation stage. In keeping with this, a study in infant AML identified elevated *ANGPT1* expression in M0-AML patients, which characterises a very immature AML subtype with dismal prognosis. In contrast, *ANGPT1* expression was shown to be low in MLLr-infant AML patients, which belong to the more mature M4/M5-AML subtypes³⁶⁶. Consequently, a possible explanation for the dependency of *ANGPT1* expression on the MLL/AF4 status of the cells might be that down-regulation of MLL/AF4 depletion results in increased differentiation of the cells, as shown in a reduction of the stem cell marker CD133 (*PROM1*) previously reported by our group¹⁴⁸ and also observed in the GEP studies performed in this project, as well as the decrease of several other genes associated with stemness, such as *TERT*, the *HOXA* gene cluster, *HMGA2*, etc (tab. 3-20).

However, the differentiation status of the leukaemic cell, while most probably an important contributory factor, seems unlikely to explain the *ANGPT1* expression in MLLr-ALL and its dependency on MLL/AF4 on its own, since this concept is contradicted, as discussed before, by the fact that ectopic overexpression of MLL-FP in HPCs results in *ANGPT1* up-regulation. Another argument supporting *ANGPT1* expression to be a MLLr-inherent characteristic

is that t(4;11)-positive cells have been reported to possess an intrinsic angiogenic programme, as evidenced by their ability to recruit blood vessels in a NOD/SCID xenograft model, and the expression of multiple angiogenic factors³⁶⁷. In order to unravel the link between MLL/AF4 and other MLL fusion genes in ALL and ANGPT1, further studies are required.

ANGPT1 expression also plays functional role in t(4;11)-positive ALL, acting in a proleukaemic fashion. Here, we show that RNAi-mediated down-regulation of ANGPT1 impinges on proliferation and viability *in vitro*, and affects leukaemic disease progression in an *in vivo* NSG xenograft model. In previous studies in AML, ANGPT1 has been shown to promote proliferation and survival of blasts *in vitro*³⁶⁸. Furthermore, recently it has been reported that ANGPT1 can promote HSC proliferation in an autocrine manner³⁶⁴. Associated pathways were the PI3K/AKT- & the STAT- signalling cascades, mainly controlled by the TIE2 receptor³⁶⁹⁻³⁷¹. However, the SEM cell line does not express TIE2 (fig. 5-19), but TIE1 (fig. 5-20) and specific integrins (fig. 5-21), which are mediators of the non-canonical ANPGT1 signalling. Integrins have been shown to stimulate proliferation and survival in response to angiopoietins, as well as promoting metastasis. This occurs by outside-in signalling, involving FAK (focal adhesion kinase) and ILK (integrin-linked kinase) signalling and downstream PI3K/AKT- and ERK- pathways^{332-335,372}. ANGPT1 depletion in SEM cells resulted in an anti-proliferative and anti-survival phenotype (fig. 5-27 to fig. 5-29), suggesting presence of an autocrine signalling axis, most likely mediated by integrins; however the downstream pathways are unknown to date and require further investigation.

An indication about possible signalling cascades mediating the effects of ANGPT1 on the leukaemic cells is given by the results of the GEP performed on siANGPT1-treated SEM cells. Pathway analysis revealed differential expression of factors associated with GPCR/cAMP/PKA- and cytoskeleton-associated signalling, with a net inhibitory effect (fig. 5-34, fig. 5-38, fig. 5-37), pathways well characterised in their leukaemia promoting function. Notably, while these factors might well play a role in the SEM cell line, there might be other

mechanisms involved in ANGPT1-mediated proleukaemic functions in t(4;11)-positive ALL patients, as these blasts, contrary to the SEM cell line, widely expressed *TIE2* (fig. 5-19), allowing for a canonical autocrine pathway, reportedly involving PI3K and STAT signalling.

Next to the aforementioned pathways, the most significantly affected signalling cascade entail the glucocorticoid receptor (GR) machinery, which is induced in ANGPT1-depleted SEM cells. Glucocorticoid resistance has long been established as an adverse prognostic factor in ALL, and several mechanisms underlying have been so far proposed, including reduced GR expression³⁷³, overexpression of antiapoptotic mediators like MCL1^{167,374} and XIAP³⁷⁵ as well as mutations in specific miRNA species³⁷⁶. Interestingly, down-regulation of ANGPT1 resulted in up-regulation of genes encoding the GR itself as well as cofactors and downstream mediators (fig. 5-35). Thus, a putative sensitisation in SEM cells towards the chemotherapeutic glucocorticoid dexamethasone (DEX) was assessed in SEM cells transfected with siANGPT1 or depleted of MLL/AF4. ANGPT1 down-regulation only subtly increased the response towards DEX, which could be partially rescued by exogenous rhANGPT1 (fig. 4-40). MLL/AF4 depletion did not affect sensitivity, but although MLL/AF4 regulates ANGPT1, this is a delayed effect, and one could hypothesise that the timepoint queried might have been too early, thus remaining above a putative ANGPT1 dosage threshold. Nevertheless, ANGPT1 seems to play only a very minor role, if at all, in GC-resistance in SEM cells, and is clearly superseded by other molecular mechanisms.

Due to time constraints, no further investigation into the downstream ANGPT1 signalling pathways could be performed in this thesis, and further future studies need to be performed into this aspect.

The observation that ANGPT1 down-regulation has an anti-leukaemic effect in the SEM cell line *in vitro* could also be translated into an *in vivo* setting. Transplantation experiments in the immunodeficient NSG mouse model with SEM cells modified to express shRNA against ANGPT1 revealed a striking phenotype associated with ANGPT1 depletion. In contrast to the control group, mice transplanted with shANGPT1-transduced cells did not develop overt

leukaemia, but grew tumours composed of SEM cells at the injection site (fig. 5-50). In addition, the engraftment and systemic spread of the leukaemic was significantly reduced, as indicated by *in vivo* imaging studies (fig. 5-49) and the observation that both the blast burden in the BM and extramedullary leukaemic infiltration in the spleen was decreased (fig. 5-48). The fact that only one treatment group, the mice inoculated with the shANGPT1-transduced SEM cells, developed extrafemoral tumours argues against this being a technical artefact. On the contrary, it is suggestive that ANGPT1 depletion affects the interactions of the leukemic cells with the BM, impairing lodgement of the cells within the microenvironment. This would be consistent with the reported role of ANGPT1 in the BM, as well as in accordance with the results, albeit not validated as of yet, from the GEP and associated pathway analyses of siANGPT1-treated SEM cells. However, contradictory to the *in vitro* findings on ANGPT1 depletion, where it impinged on proliferation and viability, *in vivo*, SEM cells depleted of ANGPT1 can grow to form a tumoural mass. A possible explanation of this could be found in the shRNA expression system employed and associated pharmacodynamics. The expression vector is an inducible Tet-On system under regulation of doxycycline; while doxycycline was initially administered to the mice via an i.p. bolus and subsequently continuously dispensed in the drinking water, the bioavailability of doxycycline *in situ* might not have been equal in the different tissues where the SEM cells were located. Although plasma levels were sufficient to induce shRNA expression *ex vivo* (fig. 5-45), it has been shown that spleen and skeletal muscle tissue have a lower dox penetration³⁷⁷ than other organ and cell compartments. Thus, one could hypothesise that SEM not lodged in the BM and exiting through the injection injury were then located in haven-like environment, where proliferation was not impaired due to absence of ANGPT1 depletion. The observed limited systemic spread of the leukaemic cells could then be attributed to dissemination from the tumour site, and subsequent extramedullary infiltration. In order to confirm the role of ANGPT1 in leukaemogenesis *in vivo*, similar transplantation experiments using a constitutive expression system would be very informative.

Apart from ANGPT1, MLL/AF4 depletion also affected other ANGIOPOIETIN family members. For instance ANGPT2, the endogenous antagonist of ANGPT1. In contrast to ANGPT1, this gene showed a ubiquitous expression pattern, where the transcript could be detected in both MLLr- and MLL germline BCP-ALL cell lines (fig. 5-52). *ANGPT2* expression levels where, like ANGPT1, affected by MLL/AF4 depletion in SEM cells, but regulated opposingly, as *ANGPT2* was significantly up-regulated in response to MLL/AF4 depletion (fig. 5-57). To date, no reciprocal expression regulation or feedback loops between the two ANGIOPOIETIN proteins have been observed. How can this observation be interpreted? In a normal haematological setting, ANGPT2 does not seem to play a major role: although inhibiting ANGPT1-mediated signalling in TIE2-expressing BM-derived HSCs *in vitro*,³⁷⁸ it is not expressed in the in the BM at a high level³⁷⁹. Furthermore, ANGPT2-deficient mice did not show any haematopoietic defects.³⁸⁰ Concordantly, no significant differences could be detected between the ANGPT2 levels in cord blood-derived HSCs and the bulk cord blood population (fig. 5-59). Of note, however, is that ANGPT2 has been described as a mediator of inflammation³⁸¹ as well as reportedly being up-regulated by inflammatory factors³⁸²⁻³⁸³. Since MLL/AF4 depletion induces pro-inflammatory cytokines and mediators such as *IFI44*, *IFIT3* and *IFIT2* (section 3), this might be a possible explanation for MLL/AF4-mediated ANGPT2 up-regulation. The question however remains about the effect of ANGPT2 induction in this leukaemic setting. In haematologic malignancies the role of ANGPT2 has been shown to be very much context-dependent: in AML, high levels of systemically circulating ANGPT2 are linked with an adverse prognosis³⁸⁴⁻³⁸⁶, and in CLL, elevated ANGPT2 expression in blasts has been linked to poor survival³⁸⁶. Moreover, ANGPT2 is a well-established factor promoting tumour angiogenesis in solid cancers³⁸⁷. Conversely, high secretion by PBMCs in AML patients correlates with increased survival³⁸⁸⁻³⁸⁹, particularly in conjunction with low VEGF-C levels³⁶⁸, and recently, in an *in vivo* RNAi screen for lymphomagenesis, ANGPT2 was identified as a key tumour suppressor gene³⁹⁰. Furthermore, locally produced angiopoietins might be antagonised - or its function influenced- by the interplay of systemic angiopoietins levels and/or the presence of other angiogens. This plethora of contradictory results only

highlights the complex biology surrounding angiopoietins, cancer and tumour angiogenesis. Ultimately, MLL/AF4 depletion disturbs the fine-tuning between ANGPT1 and ANGPT2, which might contribute to the observed phenotypes.

Next to *ANGPT2*, there is another MLL/AF4 responsive Angiopoietin family member, namely *ANGPTL2*. It plays like ANGPT1 a role in HSC biology, as it has been shown to promote *ex vivo* proliferation of HSCs while retaining their self-renewal capacity³⁹¹⁻³⁹². Also similar to ANGPT1, depletion of MLL/AF4 is accompanied by a reduction in *ANGPTL2* levels (fig. 5-53), and although expressed at lower levels than ANGPT1, *ANGPTL2* is up-regulated in CD34+ CB compared to the bulk CB cells (fig. 5-56). Possibly, a reduction of *ANGPTL2* levels in MLL/AF4 depleted cells could be a response to the down-regulation of the HSC-like signature, as described in chapter 3. The role of *ANGPTL2* in malignancy has not been studied to date.

What are the implications of Angiopoietins in infant MLLr-ALL? On the one hand, ANGPT1 is an important regulator of HSC quiescence and stemness, and suppression of ANGPT1 signalling induces HSC cycling and promotes differentiation³⁹³. Furthermore, ANGPT1 mediates tight interactions between the HSCs with the support cells in the BM microenvironment³²⁷. Translating this into a clinical setting, infant MLLr-ALL patients show a slow response to treatment, and although eventually the CR rate is 95%, MRD in the BM is high and a great proportion of the patients relapse on treatment, with BM as primary site of relapse^{54,57}. The ANGPT1/TIE2 axis could contribute to this phenotype, as infant t(4;11)-positive ALL patients not only overexpress ANGPT1, but also its cognate receptor TIE2, providing the mechanism for an autocrine signalling loop which might promote both increased quiescence and interactions with the BM in a subset of the cells, important factors implicated in therapy-resistance and -evasion.

On the other hand, ANGPT1 not only regulates the interactions between HSCs and the BM microenvironment, it has also been shown to act as a potent prosurvival factor in diverse cell types, including AML blasts. Consistent with his

notion, ANGPT1 depletion impinged on the survival of the t(4;11)-positive ALL cell line SEM, and reduced BM engraftment in the an *in vivo* xenograft model. Hence, ANGPT1 might not only contribute to the lodgement of the blasts into the BM and their quiescence, but provide a strong anti-apoptotic signal as well. Last but not least, the BM is a complex compartment, consisting of several different cell types, a range of soluble cytokines and a hypoxic environment. There is increasing evidence that secreted cytokines from leukaemic blasts might activate the BM endothelial cells to produce factors which in turn promote leukaemic survival. Thus ANGPT1 secreted by the MLLr-ALL patient blasts might contribute to the leukaemic remodelling of the BM microenvironment.

Apart from ANGPT1, another factor involved in HSC maintenance and able to exert proangiogenic effects, ANGPTL2, was down-regulated in response to MLL/AF4 knock-down. To date, it has not been investigated in the context of a leukaemic setting, and not much is known about ANGPTL2 signalling; but there seems to be evidence involving integrins³⁹⁴, not unlike the non-canonical ANGPT1 signalling pathway. Further studies are required to elucidate its role in t(4;11)-positive ALL pathobiology.

Currently, there are several drugs targeting angiopoietins and malignant angiogenesis in clinical trials, for instance AMG-386, an angiopoietin inhibitor, is being employed in breast cancer therapy³⁹⁵. Additionally, antiangiogenic drugs like bortezomib are well-established chemotherapeutics in myeloma³⁹⁶; a recent *in vitro* study in AML with bortezomib showed a strong down-regulation of ANGPT1³⁷⁰. The findings in current thesis provide evidence that Angiopoietin signalling might represent a potentially interesting therapeutic target in MLLr-ALL, both via the ANGPT1/TIE2 axis and the non-canonical pathway involving integrins; and infant MLLr patients might benefit from an antiangiogenic therapy.

6. Concluding Remarks

Acute lymphoblastic leukaemia, like all malignancies, is characterised by aberrant self-renewal capacity, apoptosis-evasion and limitless proliferation. Here, in this thesis, it was shown that MLL/AF4 represents a crucial gatekeeper of these oncogenic functions in t(4;11)-positive ALL; RNAi-mediated ablation of this fusion gene in the t(4;11)-positive ALL cell line SEM resulted in an invariable collapse of the cellular processes, impinging on cell cycle progression, proliferation, clonogenicity and eventually leading to cell death.

6.1.1 MLL/AF4 depletion perturbs leukaemic cell survival

This loss of viability was particularly striking, as t(4;11)-positive ALL marks a disease resistant to chemotherapy, and MLL/AF4-positive cells have been shown to be very impervious to metabolic and genotoxic stress signals. To date, the molecular processes mediating this resistance are not fully understood, however, several upstream factors have been implicated, such as up-regulation of the antiapoptotic Bcl2 family members MCL-1 and BCL-2, aberrant expression of the HOXA gene cluster as well as deregulation of specific miRNAs.

In order to identify both down-stream effectors and the time flow of the molecular processes underlying the anti-leukaemic phenotype, the RNAi time course study was combined with global transcriptome analysis. *MLL/AF4*-depleted cells revealed the induction of a programme comprising proapoptotic and anti-proliferative genes, prominently *NOXA* (PMAIP1), *ANXA1*, *GABARAPL1*, *REEP3* but also the interferon-stimulated gene family members *IFI44*, *IFIT2*, *IFIT3*, which all formed part of the MLL/AF4 and zVAD core signatures. This indicated a high dependency of these genes on MLL/AF4, and, assuming a hierarchical molecular process, that these genes might potentially play an instrumental role in apoptosis induction. However, only *REEP3* has been reported as a direct MLL/AF4 target, suggesting an indirect regulatory mechanism for the remainder.

Interestingly, *NOXA*³⁹⁷ and *ANXA1*³⁹⁸ both are p53 target genes, and p53 has been recently implicated in the up-regulation of interferon-stimulated gene family³⁹⁹⁻⁴⁰⁰. Loss-of-function mutations of the tumour suppressor p53 occur in about 50% of cancer cells, but although this method of inactivation rarely occurs in childhood ALL⁴⁰¹, loss of p53 activity can also be mediated by other mechanisms. Particularly in MLLr leukaemias, the MLL fusion proteins MLL/ENL, MLL/ELL, MLL/AF9, MLL/AF10 and MLL/MEN have been shown to directly interact with p53, impairing its transactivation activity in response to genotoxic injury⁴⁰²⁻⁴⁰⁴. This inhibition is based on direct binding via the fusion partner moieties, and as MLL/AF4 has been found to interact with several of these genes as part of the SEC and DOT1L complexes, it is likely that MLL/AF4 might impinge on p53 activity via this mechanism. Thus, loss of MLL/AF4 might derepress p53 transcriptional activity, subsequently promoting the cell cycle arrest and apoptosis observed via specific target genes such as the aforementioned. However, this hypothesis has to be tested, in order to see whether p53 inhibition plays any role in MLL/AF4-mediated apoptosis resistance.

Strikingly, the cell death programme initiated by MLL/AF4 ablation could not be rescued; treatment of MLL/AF4-depleted cells with the broad-spectrum caspase inhibitor zVAD-FMK suppressed apoptosis induction, but subsequently caused a switch of programmed cell death type towards one with a more necroptotic phenotype. Concomitant global transcriptome profiling found in addition to the aforementioned proapoptotic genes also induction of factors recently described as key mediators of the necroptosis pathway²⁹¹; in contrast, these genes were not part of the corresponding MLL/AF4 signature. This differential expression could be validated *in vitro*; where it was found that the key necroptosis mediators TNF, CYLD and RIPK1 were exclusively up-regulated in SEM cells treated with both siMLL/AF4 and zVAD.

The anti-proliferative and proapoptotic programme initiated in response to MLL/AF4 depletion was supported by the concerted down-regulation of pro-survival signalling cascades on a transcriptional level. Interestingly, those pathways had been previously reported to be constitutively active in MLLr ALL,

such as IGFR1, ERK1/2, JAK/STAT and ephrin signalling. These are also widely implicated in ALL and in other malignancies, and there are several different mechanisms underlying their aberrant activation. While an influence of MLL/AF4 on IGFR1 expression could be explained via the MLL/AF4-HOXA9-IGFR1 axis and MLL fusion genes have been reported to directly regulate ephrin receptors and their ligands, the transcriptional link between MLL/AF4 and STAT3 and MLL/AF4 and ERK could not be derived.

6.1.2 MLL/AF4 depletion results in down-regulation of stemness-associated markers

In addition to the loss of viability, MLL/AF4 depletion also resulted in impaired clonogenicity, which represents an *in vitro* assay for self-renewal. This coincides with previous *in vivo* studies from our group, where MLL/AF4 ablation impinged on leukaemia propagation¹⁴⁸. Furthermore, in concordance with the literature, gene expression profiling showed that MLL/AF4 regulated a subset of stemness-associated genes, including the HOXA gene cluster (*HOXA6-HOXA10*), which represents to date the best-characterised target genes of MLL fusion proteins. In addition, MLL/AF4 modulates *TERT* expression, one of the key factors of transformation and aberrant self-renewal in malignancies; our group could now report that this occurs in a HOXA7-dependent manner¹⁷⁰. Furthermore, in this study it was possible to identify novel MLL/AF4-regulated stem cell markers, such as *HMGA2*, *ANGPTL2* and *ANGPT1*; MLL/AF4 depletion correlated with a substantial decrease in their respective expression levels.

Particularly *ANGPT1* was of interest, since it is vital cytokine implicated in HSC homeostasis³²⁷. *ANGPT1* expression regulation was found to be strongly linked to MLL fusion genes; screening of a B-cell precursor ALL patient cohort showed a substantial and significant overexpression of *ANGPT1* in MLLr ALL when compared to ALL with a MLL germline configuration or healthy controls. Moreover, MLL/AF4 ablation in both the SEM cell line and in primary patient blasts resulted in a strong down-regulation in *ANGPT1* expression

Interestingly, although an important regulator in haematopoietic stem-cell quiescence, in present cellular context ANGPT1 plays an important role in proliferation and survival of MLL/AF4-positive ALL cells. Functional analyses revealed ANGPT1 to contribute to the leukaemic phenotype *in vitro*, and to be important for the disease propagation *in vivo*. The latter could indeed be an indication of a certain loss of stemness of the ANGPT1-depleted cells, however this has to be studied more in-depth before such a conclusion can be drawn.

In conclusion, it was found that t(4;11)-positive ALL cells display a high degree of oncogene addiction towards MLL/AF4, since depletion strongly perturbed the leukaemic phenotype, compromising survival and self-renewal, and this process could not be rescued using inhibitors against the identified cell death programmes. Furthermore, ANGPT1 was identified as a novel MLL/AF4-regulated gene, which cooperates with MLL/AF4 in maintaining the leukaemic disease.

7. Future work

In this study, global transcriptome analysis of a MLL/AF4-RNAi time course in t(4;11)-positive ALL cells illustrated transcriptional processes which might contribute towards the fusion gene-driven disease. In addition, novel MLL/AF4-regulated genes were identified and functionally characterised. However, the results, although very informative, raise further questions which will have to be addressed by future work, both to gain more in-depth insight into the MLL/AF4-mediated programmes, but also in order to confirm the conclusions drawn in this thesis:

- In order to explore the relevance of the pro-apoptotic factors identified, the observed induction has to be validated at the protein level. Subsequently, ectopic expression studies of these genes should be carried out to test the extent to which they are able to initiate cell death in t(4;11)-positive cells on its own, or whether they can sensitise these cells towards chemotherapeutic drugs. Concomitantly, rescue-experiments using combined RNAi of both MLL/AF4 and specific pro-apoptotic genes will help to identify any hierarchical processes in the observed cell death induction. Conversely, if cell death suppression addressing a single gene cannot be achieved, this would also illustrate that MLL/AF4 ablation perturbs multiple processes eventually compromise viability.
- MLL/AF4 depletion in a caspase-deficient environment causes switch from apoptosis to a more necroptosis-like cell death. However, inhibitor studies were also not able to suppress this cell death programme. Further work should address this on a post-transcriptional level, using RNAi to deplete key regulators of the necroptotic pathway, such as TNFR1, TNF, CYLD and RIPK1, as well as key regulators of other caspase-independent cell death pathways, such as ATG7, in order to elucidate the exact mechanism of the alternative cell death route. This approach might

result in identification of relevant down-stream mediators which might be therapeutically exploitable.

- Signalling pathways are regulated post-translationally, therefore it would be important to confirm the identified down-regulation of the pathways at the protein level. Moreover, inhibitor studies are needed to validate their relevance for t(4;11)-positive ALL cell survival.
- Although the phenotypical consequences of ANGPT1 ablation in t(4;11)-positive ALL cells have been characterised, it was not possible to pin point the exact regulatory mechanism by which MLL/AF4 mediates ANGPT1 expression. RNAi-mediated *HOXA7* depletion did not show an effect on *ANGPT1*, but regulation by other members of the HOXA gene family, for instance *HOXA10*, cannot be ruled out and requires further investigation. Moreover, as the signalling pathways modulated by ANGPT1 in t(4;11)-ALL are not known, it is of utmost importance to elucidate this aspect, in order to be able to fully understand the role of ANGPT1 in t(4;11)-positive ALL.

8. Bibliography

1. Provan DS, C.R.J; Baglin, T.; Willeyman, J. Oxford Handbook of Clinical Haematology (ed 2nd): Oxford University Press; 2004.
2. Dini G, Banov L, Dini S. Where should adolescents with ALL be treated? Bone Marrow Transplant. 2008;42 Suppl 2:S35-39.
3. Medical Research Council Working Party on Leukaemia in Children - UK National Randomised Trial For Children and Young Adults with Acute Lymphoblastic Leukaemia (ALL) - UKALL 2003 Version 7; 2009.
4. Kaatsch P. Epidemiology of childhood cancer. Cancer Treat Rev. 2010;36:277-285.
5. Szczepanski T, van der Velden VH, van Dongen JJ. Classification systems for acute and chronic leukaemias. Best Pract Res Clin Haematol. 2003;16:561-582.
6. van Lochem EG, van der Velden VH, Wind HK, te Marvelde JG, Westerdal NA, van Dongen JJ. Immunophenotypic differentiation patterns of normal hematopoiesis in human bone marrow: reference patterns for age-related changes and disease-induced shifts. Cytometry B Clin Cytom. 2004;60:1-13.
7. le Viseur C, Hotfilder M, Bomken S, et al. In childhood acute lymphoblastic leukemia, blasts at different stages of immunophenotypic maturation have stem cell properties. Cancer Cell. 2008;14:47-58.
8. Greaves M. Childhood leukaemia. Bmj. 2002;324:283-287.
9. Pui CH, Carroll WL, Meshinchi S, Arceci RJ. Biology, risk stratification, and therapy of pediatric acute leukemias: an update. J Clin Oncol. 2011;29:551-565.
10. Pui CH, Relling MV, Downing JR. Acute lymphoblastic leukemia. N Engl J Med. 2004;350:1535-1548.
11. Harris NL, Jaffe ES, Diebold J, et al. World Health Organization classification of neoplastic diseases of the hematopoietic and lymphoid tissues: report of the Clinical Advisory Committee meeting-Airlie House, Virginia, November 1997. J Clin Oncol. 1999;17:3835-3849.

12. Huret JL.
<http://atlasgeneticsoncology.org/Anomalies/Anomliste.html#B-ALL>.
13. Moorman AV, Ensor HM, Richards SM, et al. Prognostic effect of chromosomal abnormalities in childhood B-cell precursor acute lymphoblastic leukaemia: results from the UK Medical Research Council ALL97/99 randomised trial. *Lancet Oncol.* 2010;11:429-438.
14. Djabali M, Selleri L, Parry P, Bower M, Young B, Evans GA. A trithorax-like gene is interrupted by chromosome 11q23 translocations in acute leukaemias. *Nat Genet.* 1993;4:431.
15. Meyer C, Kowarz E, Hofmann J, et al. New insights to the MLL recombinome of acute leukemias. *Leukemia.* 2009;23:1490-1499.
16. Hunger SP, Galili N, Carroll AJ, Crist WM, Link MP, Cleary ML. The t(1;19)(q23;p13) results in consistent fusion of E2A and PBX1 coding sequences in acute lymphoblastic leukemias. *Blood.* 1991;77:687-693.
17. Rowley JD. Letter: A new consistent chromosomal abnormality in chronic myelogenous leukaemia identified by quinacrine fluorescence and Giemsa staining. *Nature.* 1973;243:290-293.
18. Harewood L, Robinson H, Harris R, et al. Amplification of AML1 on a duplicated chromosome 21 in acute lymphoblastic leukemia: a study of 20 cases. *Leukemia.* 2003;17:547-553.
19. Strefford JC, van Delft FW, Robinson HM, et al. Complex genomic alterations and gene expression in acute lymphoblastic leukemia with intrachromosomal amplification of chromosome 21. *Proc Natl Acad Sci U S A.* 2006;103:8167-8172.
20. Mullighan CG, Collins-Underwood JR, Phillips LA, et al. Rearrangement of CRLF2 in B-progenitor- and Down syndrome-associated acute lymphoblastic leukemia. *Nat Genet.* 2009;41:1243-1246.

21. Russell LJ, Capasso M, Vater I, et al. Deregulated expression of cytokine receptor gene, CRLF2, is involved in lymphoid transformation in B-cell precursor acute lymphoblastic leukemia. *Blood*. 2009;114:2688-2698.
22. Rand V, Parker H, Russell LJ, et al. Genomic characterization implicates iAMP21 as a likely primary genetic event in childhood B-cell precursor acute lymphoblastic leukemia. *Blood*. 2011.
23. Moorman AV, Richards SM, Robinson HM, et al. Prognosis of children with acute lymphoblastic leukemia (ALL) and intrachromosomal amplification of chromosome 21 (iAMP21). *Blood*. 2007;109:2327-2330.
24. Ensor HM, Schwab C, Russell LJ, et al. Demographic, clinical, and outcome features of children with acute lymphoblastic leukemia and CRLF2 deregulation: results from the MRC ALL97 clinical trial. *Blood*. 2011;117:2129-2136.
25. Cario G, Zimmermann M, Romey R, et al. Presence of the P2RY8-CRLF2 rearrangement is associated with a poor prognosis in non-high-risk precursor B-cell acute lymphoblastic leukemia in children treated according to the ALL-BFM 2000 protocol. *Blood*. 2010;115:5393-5397.
26. Den Boer ML, van Slegtenhorst M, De Menezes RX, et al. A subtype of childhood acute lymphoblastic leukaemia with poor treatment outcome: a genome-wide classification study. *Lancet Oncol*. 2009;10:125-134.
27. Mullighan CG, Su X, Zhang J, et al. Deletion of IKZF1 and prognosis in acute lymphoblastic leukemia. *N Engl J Med*. 2009;360:470-480.
28. Hasle H. Pattern of malignant disorders in individuals with Down's syndrome. *Lancet Oncol*. 2001;2:429-436.
29. Hasle H, Clemmensen IH, Mikkelsen M. Risks of leukaemia and solid tumours in individuals with Down's syndrome. *Lancet*. 2000;355:165-169.
30. Podvin D, Kuehn CM, Mueller BA, Williams M. Maternal and birth characteristics in relation to childhood leukaemia. *Paediatr Perinat Epidemiol*. 2006;20:312-322.

31. Kotecha RS, Murch A, Kees U, Cole CH. Pre-natal, clonal origin of t(1;11)(p32;q23) acute lymphoblastic leukemia in monozygotic twins. *Leuk Res.* 2011.
32. Ford AM, Bennett CA, Price CM, Bruin MC, Van Wering ER, Greaves M. Fetal origins of the TEL-AML1 fusion gene in identical twins with leukemia. *Proc Natl Acad Sci U S A.* 1998;95:4584-4588.
33. Bateman CM, Colman SM, Chaplin T, et al. Acquisition of genome-wide copy number alterations in monozygotic twins with acute lymphoblastic leukemia. *Blood.* 2010;115:3553-3558.
34. Maia AT, Tussiwand R, Cazzaniga G, et al. Identification of preleukemic precursors of hyperdiploid acute lymphoblastic leukemia in cord blood. *Genes Chromosomes Cancer.* 2004;40:38-43.
35. Maia AT, van der Velden VH, Harrison CJ, et al. Prenatal origin of hyperdiploid acute lymphoblastic leukemia in identical twins. *Leukemia.* 2003;17:2202-2206.
36. Bayar E, Kurczynski TW, Robinson MG, Tyrkus M, al Saadi A. Monozygotic twins with congenital acute lymphoblastic leukemia (ALL) and t(4;11)(q21;q23). *Cancer Genet Cytogenet.* 1996;89:177-180.
37. Hong D, Gupta R, Ancliff P, et al. Initiating and cancer-propagating cells in TEL-AML1-associated childhood leukemia. *Science.* 2008;319:336-339.
38. Greaves M. In utero origins of childhood leukaemia. *Early Hum Dev.* 2005;81:123-129.
39. Menegaux F, Steffen C, Bellec S, et al. Maternal coffee and alcohol consumption during pregnancy, parental smoking and risk of childhood acute leukaemia. *Cancer Detect Prev.* 2005;29:487-493.
40. Barjesteh van Waalwijk van Doorn-Khosrovani S, Janssen J, Maas LM, Godschalk RW, Nijhuis JG, van Schooten FJ. Dietary flavonoids induce MLL translocations in primary human CD34+ cells. *Carcinogenesis.* 2007;28:1703-1709.

41. Azarova AM, Lin RK, Tsai YC, Liu LF, Lin CP, Lyu YL. Genistein induces topoisomerase II β - and proteasome-mediated DNA sequence rearrangements: Implications in infant leukemia. *Biochem Biophys Res Commun.* 2010;399:66-71.
42. Ross JA, Potter JD, Reaman GH, Pendergrass TW, Robison LL. Maternal exposure to potential inhibitors of DNA topoisomerase II and infant leukemia (United States): a report from the Children's Cancer Group. *Cancer Causes Control.* 1996;7:581-590.
43. Pui CH, Pei D, Campana D, et al. Improved prognosis for older adolescents with acute lymphoblastic leukemia. *J Clin Oncol.* 2011;29:386-391.
44. Mitchell C, Richards S, Harrison CJ, Eden T. Long-term follow-up of the United Kingdom medical research council protocols for childhood acute lymphoblastic leukaemia, 1980-2001. *Leukemia.* 2010;24:406-418.
45. Moricke A, Zimmermann M, Reiter A, et al. Long-term results of five consecutive trials in childhood acute lymphoblastic leukemia performed by the ALL-BFM study group from 1981 to 2000. *Leukemia.* 2010;24:265-284.
46. Kamps WA, van der Pal-de Bruin KM, Veerman AJ, Fiocco M, Bierings M, Pieters R. Long-term results of Dutch Childhood Oncology Group studies for children with acute lymphoblastic leukemia from 1984 to 2004. *Leukemia.* 2010;24:309-319.
47. Bruggemann M, Schrauder A, Raff T, et al. Standardized MRD quantification in European ALL trials: proceedings of the Second International Symposium on MRD assessment in Kiel, Germany, 18-20 September 2008. *Leukemia.* 2010;24:521-535.
48. Conter V, Bartram CR, Valsecchi MG, et al. Molecular response to treatment redefines all prognostic factors in children and adolescents with B-cell precursor acute lymphoblastic leukemia: results in 3184 patients of the AIEOP-BFM ALL 2000 study. *Blood.* 2010;115:3206-3214.

49. Pui CH, Jeha S. New therapeutic strategies for the treatment of acute lymphoblastic leukaemia. *Nat Rev Drug Discov.* 2007;6:149-165.
50. ALL R3: An International Collaborative Trial for Relapsed and Refractory ALL.
http://www.medicinemanchester.ac.uk/images/cancer/PAYAC/documents/pdf/R3Protocolv4_31Aug2007.pdf.
51. UK Clinical Research Network : Portfolio Database EsPhALL.
52.
<http://www.cancer.gov/clinicaltrials/search/view?version=healthprofessional&cdrid=573996>.
53. Bassan R, Hoelzer D. Modern therapy of acute lymphoblastic leukemia. *J Clin Oncol.* 2011;29:532-543.
54. Pieters R, Schrappe M, De Lorenzo P, et al. A treatment protocol for infants younger than 1 year with acute lymphoblastic leukaemia (Interfant-99): an observational study and a multicentre randomised trial. *Lancet.* 2007;370:240-250.
55. Hilden JM, Dinndorf PA, Meerbaum SO, et al. Analysis of prognostic factors of acute lymphoblastic leukemia in infants: report on CCG 1953 from the Children's Oncology Group. *Blood.* 2006;108:441-451.
56. Itoyama K, Eguchi M, Hibi S, et al. Risk-directed treatment of infant acute lymphoblastic leukaemia based on early assessment of MLL gene status: results of the Japan Infant Leukaemia Study (MLL96). *Br J Haematol.* 2002;118:999-1010.
57. Van der Velden VH, Corral L, Valsecchi MG, et al. Prognostic significance of minimal residual disease in infants with acute lymphoblastic leukemia treated within the Interfant-99 protocol. *Leukemia.* 2009;23:1073-1079.
58. Mann G, Attarbaschi A, Schrappe M, et al. Improved outcome with hematopoietic stem cell transplantation in a poor prognostic subgroup of

infants with mixed-lineage-leukemia (MLL)-rearranged acute lymphoblastic leukemia: results from the Interfant-99 Study. *Blood*. 2010;116:2644-2650.

59. Gaynon PS. Childhood acute lymphoblastic leukaemia and relapse. *Br J Haematol*. 2005;131:579-587.

60. Breene RA, Williams RM, Hartle J, Gattens M, Acerini CL, Murray MJ. Auxological changes in UK survivors of childhood acute lymphoblastic leukaemia treated without cranial irradiation. *Br J Cancer*. 2011;104:746-749.

61. Leung W, Hudson M, Zhu Y, et al. Late effects in survivors of infant leukemia. *Leukemia*. 2000;14:1185-1190.

62. Rothdiener M, Muller D, Castro PG, et al. Targeted delivery of SiRNA to CD33-positive tumor cells with liposomal carrier systems. *J Control Release*. 2010;144:251-258.

63. Pui CH, Ribeiro RC, Hancock ML, et al. Acute myeloid leukemia in children treated with epipodophyllotoxins for acute lymphoblastic leukemia. *N Engl J Med*. 1991;325:1682-1687.

64. Shivakumar R, Tan W, Wilding GE, Wang ES, Wetzler M. Biologic features and treatment outcome of secondary acute lymphoblastic leukemia--a review of 101 cases. *Ann Oncol*. 2008;19:1634-1638.

65. Gu Y, Nakamura T, Alder H, et al. The t(4;11) chromosome translocation of human acute leukemias fuses the ALL-1 gene, related to *Drosophila trithorax*, to the AF-4 gene. *Cell*. 1992;71:701-708.

66. Nakamura T, Alder H, Gu Y, et al. Genes on chromosomes 4, 9, and 19 involved in 11q23 abnormalities in acute leukemia share sequence homology and/or common motifs. *Proc Natl Acad Sci U S A*. 1993;90:4631-4635.

67. Downing JR, Head DR, Raimondi SC, et al. The der(11)-encoded MLL/AF-4 fusion transcript is consistently detected in t(4;11)(q21;q23)-containing acute lymphoblastic leukemia. *Blood*. 1994;83:330-335.

68. Kowarz E, Burmeister T, Lo Nigro L, et al. Complex MLL rearrangements in t(4;11) leukemia patients with absent AF4.MLL fusion allele. *Leukemia*. 2007;21:1232-1238.
69. Thirman MJ, Gill HJ, Burnett RC, et al. Rearrangement of the MLL gene in acute lymphoblastic and acute myeloid leukemias with 11q23 chromosomal translocations. *N Engl J Med*. 1993;329:909-914.
70. Strissel PL, Strick R, Rowley JD, Zeleznik-Le NJ. An in vivo topoisomerase II cleavage site and a DNase I hypersensitive site colocalize near exon 9 in the MLL breakpoint cluster region. *Blood*. 1998;92:3793-3803.
71. Broeker PL, Harden A, Rowley JD, Zeleznik-Le N. The mixed lineage leukemia (MLL) protein involved in 11q23 translocations contains a domain that binds cruciform DNA and scaffold attachment region (SAR) DNA. *Curr Top Microbiol Immunol*. 1996;211:259-268.
72. Broeker PL, Super HG, Thirman MJ, et al. Distribution of 11q23 breakpoints within the MLL breakpoint cluster region in de novo acute leukemia and in treatment-related acute myeloid leukemia: correlation with scaffold attachment regions and topoisomerase II consensus binding sites. *Blood*. 1996;87:1912-1922.
73. Scharf S, Zech J, Bursen A, et al. Transcription linked to recombination: a gene-internal promoter coincides with the recombination hot spot II of the human MLL gene. *Oncogene*. 2007;26:1361-1371.
74. Yano T, Nakamura T, Blechman J, et al. Nuclear punctate distribution of ALL-1 is conferred by distinct elements at the N terminus of the protein. *Proc Natl Acad Sci U S A*. 1997;94:7286-7291.
75. Caslini C, Alarcon AS, Hess JL, Tanaka R, Murti KG, Biondi A. The amino terminus targets the mixed lineage leukemia (MLL) protein to the nucleolus, nuclear matrix and mitotic chromosomal scaffolds. *Leukemia*. 2000;14:1898-1908.

76. Cierpicki T, Risner LE, Grembecka J, et al. Structure of the MLL CXXC domain-DNA complex and its functional role in MLL-AF9 leukemia. *Nat Struct Mol Biol.* 2010;17:62-68.
77. Ayton PM, Chen EH, Cleary ML. Binding to nonmethylated CpG DNA is essential for target recognition, transactivation, and myeloid transformation by an MLL oncoprotein. *Mol Cell Biol.* 2004;24:10470-10478.
78. Birke M, Schreiner S, Garcia-Cuellar MP, Mahr K, Titgemeyer F, Slany RK. The MT domain of the proto-oncoprotein MLL binds to CpG-containing DNA and discriminates against methylation. *Nucleic Acids Res.* 2002;30:958-965.
79. Erfurth FE, Popovic R, Grembecka J, et al. MLL protects CpG clusters from methylation within the *Hoxa9* gene, maintaining transcript expression. *Proc Natl Acad Sci U S A.* 2008;105:7517-7522.
80. Chang PY, Hom RA, Musselman CA, et al. Binding of the MLL PHD3 finger to histone H3K4me3 is required for MLL-dependent gene transcription. *J Mol Biol.* 2010;400:137-144.
81. Fair K, Anderson M, Bulanova E, Mi H, Tropschug M, Diaz MO. Protein interactions of the MLL PHD fingers modulate MLL target gene regulation in human cells. *Mol Cell Biol.* 2001;21:3589-3597.
82. Park S, Osmers U, Raman G, Schwantes RH, Diaz MO, Bushweller JH. The PHD3 domain of MLL acts as a CYP33-regulated switch between MLL-mediated activation and repression. *Biochemistry.* 2010;49:6576-6586.
83. Hom RA, Chang PY, Roy S, et al. Molecular mechanism of MLL PHD3 and RNA recognition by the Cyp33 RRM domain. *J Mol Biol.* 2010;400:145-154.
84. Muntean AG, Giannola D, Udager AM, Hess JL. The PHD fingers of MLL block MLL fusion protein-mediated transformation. *Blood.* 2008;112:4690-4693.
85. Chen J, Santillan DA, Koonce M, et al. Loss of MLL PHD finger 3 is necessary for MLL-ENL-induced hematopoietic stem cell immortalization. *Cancer Res.* 2008;68:6199-6207.

86. Nakamura T, Mori T, Tada S, et al. ALL-1 is a histone methyltransferase that assembles a supercomplex of proteins involved in transcriptional regulation. *Mol Cell*. 2002;10:1119-1128.
87. Hsieh JJ, Cheng EH, Korsmeyer SJ. Taspase1: a threonine aspartase required for cleavage of MLL and proper HOX gene expression. *Cell*. 2003;115:293-303.
88. Yokoyama A, Wang Z, Wysocka J, et al. Leukemia proto-oncoprotein MLL forms a SET1-like histone methyltransferase complex with menin to regulate Hox gene expression. *Mol Cell Biol*. 2004;24:5639-5649.
89. Yokoyama A, Kitabayashi I, Ayton PM, Cleary ML, Ohki M. Leukemia proto-oncoprotein MLL is proteolytically processed into 2 fragments with opposite transcriptional properties. *Blood*. 2002;100:3710-3718.
90. Xia ZB, Anderson M, Diaz MO, Zeleznik-Le NJ. MLL repression domain interacts with histone deacetylases, the polycomb group proteins HPC2 and BMI-1, and the corepressor C-terminal-binding protein. *Proc Natl Acad Sci U S A*. 2003;100:8342-8347.
91. Yokoyama A, Cleary ML. Menin critically links MLL proteins with LEDGF on cancer-associated target genes. *Cancer Cell*. 2008;14:36-46.
92. Canaani E, Nakamura T, Rozovskaia T, et al. ALL-1/MLL1, a homologue of *Drosophila* TRITHORAX, modifies chromatin and is directly involved in infant acute leukaemia. *Br J Cancer*. 2004;90:756-760.
93. Dou Y, Milne TA, Tackett AJ, et al. Physical association and coordinate function of the H3 K4 methyltransferase MLL1 and the H4 K16 acetyltransferase MOF. *Cell*. 2005;121:873-885.
94. Milne TA, Briggs SD, Brock HW, et al. MLL targets SET domain methyltransferase activity to Hox gene promoters. *Mol Cell*. 2002;10:1107-1117.

95. Dou Y, Milne TA, Ruthenburg AJ, et al. Regulation of MLL1 H3K4 methyltransferase activity by its core components. *Nat Struct Mol Biol.* 2006;13:713-719.
96. Ayton PM, Cleary ML. Molecular mechanisms of leukemogenesis mediated by MLL fusion proteins. *Oncogene.* 2001;20:5695-5707.
97. Breen TR, Harte PJ. Trithorax regulates multiple homeotic genes in the bithorax and Antennapedia complexes and exerts different tissue-specific, parasegment-specific and promoter-specific effects on each. *Development.* 1993;117:119-134.
98. Breen TR, Harte PJ. Molecular characterization of the trithorax gene, a positive regulator of homeotic gene expression in *Drosophila*. *Mech Dev.* 1991;35:113-127.
99. Yu BD, Hanson RD, Hess JL, Horning SE, Korsmeyer SJ. MLL, a mammalian trithorax-group gene, functions as a transcriptional maintenance factor in morphogenesis. *Proc Natl Acad Sci U S A.* 1998;95:10632-10636.
100. Yu BD, Hess JL, Horning SE, Brown GA, Korsmeyer SJ. Altered Hox expression and segmental identity in *Mll*-mutant mice. *Nature.* 1995;378:505-508.
101. Diehl F, Rossig L, Zeiher AM, Dimmeler S, Urbich C. The histone methyltransferase MLL is an upstream regulator of endothelial-cell sprout formation. *Blood.* 2007;109:1472-1478.
102. Lim DA, Huang YC, Swigut T, et al. Chromatin remodelling factor *Mll1* is essential for neurogenesis from postnatal neural stem cells. *Nature.* 2009;458:529-533.
103. Hess JL, Yu BD, Li B, Hanson R, Korsmeyer SJ. Defects in yolk sac hematopoiesis in *Mll*-null embryos. *Blood.* 1997;90:1799-1806.
104. Gan T, Jude CD, Zaffuto K, Ernst P. Developmentally induced *Mll1* loss reveals defects in postnatal haematopoiesis. *Leukemia.* 2010;24:1732-1741.

105. Ernst P, Fisher JK, Avery W, Wade S, Foy D, Korsmeyer SJ. Definitive hematopoiesis requires the mixed-lineage leukemia gene. *Dev Cell*. 2004;6:437-443.
106. McMahon KA, Hiew SY, Hadjur S, et al. Mll has a critical role in fetal and adult hematopoietic stem cell self-renewal. *Cell Stem Cell*. 2007;1:338-345.
107. Jude CD, Climer L, Xu D, Artinger E, Fisher JK, Ernst P. Unique and independent roles for MLL in adult hematopoietic stem cells and progenitors. *Cell Stem Cell*. 2007;1:324-337.
108. Ernst P, Mabon M, Davidson AJ, Zon LI, Korsmeyer SJ. An Mll-dependent Hox program drives hematopoietic progenitor expansion. *Curr Biol*. 2004;14:2063-2069.
109. Liu H, Cheng EH, Hsieh JJ. Bimodal degradation of MLL by SCFSkp2 and APCCdc20 assures cell cycle execution: a critical regulatory circuit lost in leukemogenic MLL fusions. *Genes Dev*. 2007;21:2385-2398.
110. Liu H, Takeda S, Kumar R, et al. Phosphorylation of MLL by ATR is required for execution of mammalian S-phase checkpoint. *Nature*. 2010;467:343-346.
111. Beesley AH, Rampellini JL, Palmer ML, et al. Influence of wild-type MLL on glucocorticoid sensitivity and response to DNA-damage in pediatric acute lymphoblastic leukemia. *Mol Cancer*. 2010;9:284.
112. Blobel GA, Kadauke S, Wang E, et al. A reconfigured pattern of MLL occupancy within mitotic chromatin promotes rapid transcriptional reactivation following mitotic exit. *Mol Cell*. 2009;36:970-983.
113. Tyagi S, Chabes AL, Wysocka J, Herr W. E2F activation of S phase promoters via association with HCF-1 and the MLL family of histone H3K4 methyltransferases. *Mol Cell*. 2007;27:107-119.
114. Kotake Y, Zeng Y, Xiong Y. DDB1-CUL4 and MLL1 mediate oncogene-induced p16INK4a activation. *Cancer Res*. 2009;69:1809-1814.

115. Milne TA, Hughes CM, Lloyd R, et al. Menin and MLL cooperatively regulate expression of cyclin-dependent kinase inhibitors. *Proc Natl Acad Sci U S A.* 2005;102:749-754.
116. Guenther MG, Jenner RG, Chevalier B, et al. Global and Hox-specific roles for the MLL1 methyltransferase. *Proc Natl Acad Sci U S A.* 2005;102:8603-8608.
117. Taki T, Kano H, Taniwaki M, Sako M, Yanagisawa M, Hayashi Y. AF5q31, a newly identified AF4-related gene, is fused to MLL in infant acute lymphoblastic leukemia with ins(5;11)(q31;q13q23). *Proc Natl Acad Sci U S A.* 1999;96:14535-14540.
118. von Bergh AR, Beverloo HB, Rombout P, et al. LAF4, an AF4-related gene, is fused to MLL in infant acute lymphoblastic leukemia. *Genes Chromosomes Cancer.* 2002;35:92-96.
119. Isnard P, Core N, Naquet P, Djabali M. Altered lymphoid development in mice deficient for the mAF4 proto-oncogene. *Blood.* 2000;96:705-710.
120. Bitoun E, Davies KE. The robotic mouse: unravelling the function of AF4 in the cerebellum. *Cerebellum.* 2005;4:250-260.
121. Oliver PL, Bitoun E, Clark J, Jones EL, Davies KE. Mediation of Af4 protein function in the cerebellum by Siah proteins. *Proc Natl Acad Sci U S A.* 2004;101:14901-14906.
122. Isaacs AM, Oliver PL, Jones EL, et al. A mutation in Af4 is predicted to cause cerebellar ataxia and cataracts in the robotic mouse. *J Neurosci.* 2003;23:1631-1637.
123. Erfurth F, Hemenway CS, de Erkenez AC, Domer PH. MLL fusion partners AF4 and AF9 interact at subnuclear foci. *Leukemia.* 2004;18:92-102.
124. Jo SY, Granowicz EM, Maillard I, Thomas D, Hess JL. Requirement for Dot1l in murine postnatal hematopoiesis and leukemogenesis by MLL translocation. *Blood.* 2011;117:4759-4768.

125. Steger DJ, Lefterova MI, Ying L, et al. DOT1L/KMT4 recruitment and H3K79 methylation are ubiquitously coupled with gene transcription in mammalian cells. *Mol Cell Biol.* 2008;28:2825-2839.
126. Mohan M, Herz HM, Takahashi YH, et al. Linking H3K79 trimethylation to Wnt signaling through a novel Dot1-containing complex (DotCom). *Genes Dev.* 2010;24:574-589.
127. Feng Q, Wang H, Ng HH, et al. Methylation of H3-lysine 79 is mediated by a new family of HMTases without a SET domain. *Curr Biol.* 2002;12:1052-1058.
128. Zhang W, Xia X, Reisenauer MR, Hemenway CS, Kone BC. Dot1a-AF9 complex mediates histone H3 Lys-79 hypermethylation and repression of ENaC α in an aldosterone-sensitive manner. *J Biol Chem.* 2006;281:18059-18068.
129. Bitoun E, Oliver PL, Davies KE. The mixed-lineage leukemia fusion partner AF4 stimulates RNA polymerase II transcriptional elongation and mediates coordinated chromatin remodeling. *Hum Mol Genet.* 2007;16:92-106.
130. Lin C, Smith ER, Takahashi H, et al. AFF4, a component of the ELL/P-TEFb elongation complex and a shared subunit of MLL chimeras, can link transcription elongation to leukemia. *Mol Cell.* 2010;37:429-437.
131. Okada Y, Feng Q, Lin Y, et al. hDOT1L links histone methylation to leukemogenesis. *Cell.* 2005;121:167-178.
132. Guenther MG, Lawton LN, Rozovskaia T, et al. Aberrant chromatin at genes encoding stem cell regulators in human mixed-lineage leukemia. *Genes Dev.* 2008;22:3403-3408.
133. Krivtsov AV, Feng Z, Lemieux ME, et al. H3K79 methylation profiles define murine and human MLL-AF4 leukemias. *Cancer Cell.* 2008;14:355-368.
134. Smith E, Lin C, Shilatifard A. The super elongation complex (SEC) and MLL in development and disease. *Genes Dev.* 2011;25:661-672.

135. Bursen A, Moritz S, Gaussmann A, Dingermann T, Marschalek R. Interaction of AF4 wild-type and AF4.MLL fusion protein with SIAH proteins: indication for t(4;11) pathobiology? *Oncogene*. 2004;23:6237-6249.
136. Ikawa Y, Sugimoto N, Koizumi S, Yachie A, Saikawa Y. Dense methylation of types 1 and 2 regulatory regions of the CD10 gene promoter in infant acute lymphoblastic leukemia with MLL/AF4 fusion gene. *J Pediatr Hematol Oncol*. 2010;32:4-10.
137. Gleissner B, Goekbuget N, Rieder H, et al. CD10- pre-B acute lymphoblastic leukemia (ALL) is a distinct high-risk subgroup of adult ALL associated with a high frequency of MLL aberrations: results of the German Multicenter Trials for Adult ALL (GMALL). *Blood*. 2005;106:4054-4056.
138. Bertrand FE, Vogtenhuber C, Shah N, LeBien TW. Pro-B-cell to pre-B-cell development in B-lineage acute lymphoblastic leukemia expressing the MLL/AF4 fusion protein. *Blood*. 2001;98:3398-3405.
139. Pui CH, Kane JR, Crist WM. Biology and treatment of infant leukemias. *Leukemia*. 1995;9:762-769.
140. Slany RK, Lavau C, Cleary ML. The oncogenic capacity of HRX-ENL requires the transcriptional transactivation activity of ENL and the DNA binding motifs of HRX. *Mol Cell Biol*. 1998;18:122-129.
141. So CW, Karsunky H, Wong P, Weissman IL, Cleary ML. Leukemic transformation of hematopoietic progenitors by MLL-GAS7 in the absence of Hoxa7 or Hoxa9. *Blood*. 2004;103:3192-3199.
142. So CW, Lin M, Ayton PM, Chen EH, Cleary ML. Dimerization contributes to oncogenic activation of MLL chimeras in acute leukemias. *Cancer Cell*. 2003;4:99-110.
143. So CW, Karsunky H, Passegue E, Cozzio A, Weissman IL, Cleary ML. MLL-GAS7 transforms multipotent hematopoietic progenitors and induces mixed lineage leukemias in mice. *Cancer Cell*. 2003;3:161-171.

144. So CW, Cleary ML. MLL-AFX requires the transcriptional effector domains of AFX to transform myeloid progenitors and transdominantly interfere with forkhead protein function. *Mol Cell Biol.* 2002;22:6542-6552.
145. Montes R, Ayllon V, Gutierrez-Aranda I, et al. Enforced expression of MLL-AF4 fusion in cord blood CD34+ cells enhances the hematopoietic repopulating cell function and clonogenic potential but is not sufficient to initiate leukemia. *Blood.* 2011.
146. Gaussmann A, Wenger T, Eberle I, et al. Combined effects of the two reciprocal t(4;11) fusion proteins MLLAF4 and AF4.MLL confer resistance to apoptosis, cell cycling capacity and growth transformation. *Oncogene.* 2006.
147. Kumar AR, Yao Q, Li Q, Sam TA, Kersey JH. t(4;11) leukemias display addiction to MLL-AF4 but not to AF4-MLL. *Leuk Res.* 2011;35:305-309.
148. Thomas M, Gessner A, Vornlocher HP, Hadwiger P, Greil J, Heidenreich O. Targeting MLL-AF4 with short interfering RNAs inhibits clonogenicity and engraftment of t(4;11)-positive human leukemic cells. *Blood.* 2005;106:3559-3566.
149. Chen W, Li Q, Hudson WA, Kumar A, Kirchhof N, Kersey JH. A murine Mll-AF4 knock-in model results in lymphoid and myeloid deregulation and hematologic malignancy. *Blood.* 2006;108:669-677.
150. Metzler M, Forster A, Pannell R, et al. A conditional model of MLL-AF4 B-cell tumorigenesis using invertor technology. *Oncogene.* 2006;25:3093-3103.
151. Liang DC, Shih LY, Fu JF, et al. K-Ras mutations and N-Ras mutations in childhood acute leukemias with or without mixed-lineage leukemia gene rearrangements. *Cancer.* 2006;106:950-956.
152. Tamai H, Miyake K, Takatori M, et al. Activated K-Ras protein accelerates human MLL/AF4-induced leukemo-lymphomogenicity in a transgenic mouse model. *Leukemia.* 2011;25:888-891.
153. Montes R, Ayllon V, Gutierrez-Aranda I, et al. Enforced expression of MLL-AF4 fusion in cord blood CD34+ cells enhances the hematopoietic

repopulating cell function and clonogenic potential but is not sufficient to initiate leukemia. *Blood*. 2011;117:4746-4758.

154. Bursen A, Schwabe K, Ruster B, et al. The AF4.MLL fusion protein is capable of inducing ALL in mice without requirement of MLL.AF4. *Blood*. 2010;115:3570-3579.

155. Nguyen AT, Taranova O, He J, Zhang Y. DOT1L, the H3K79 methyltransferase, is required for MLL-AF9-mediated leukemogenesis. *Blood*. 2011.

156. Chang MJ, Wu H, Achille NJ, et al. Histone H3 lysine 79 methyltransferase Dot1 is required for immortalization by MLL oncogenes. *Cancer Res*. 2010;70:10234-10242.

157. Bennett CA, Winters AC, Barretto NN, Hemenway CS. Molecular targeting of MLL-rearranged leukemia cell lines with the synthetic peptide PFWT synergistically enhances the cytotoxic effect of established chemotherapeutic agents. *Leuk Res*. 2009;33:937-947.

158. Palermo CM, Bennett CA, Winters AC, Hemenway CS. The AF4-mimetic peptide, PFWT, induces necrotic cell death in MV4-11 leukemia cells. *Leuk Res*. 2008;32:633-642.

159. Hiatt WR, Hirsch AT, Cooke JP, Olin JW, Brater DC, Creager MA. Randomized trial of AT-1015 for treatment of intermittent claudication. A novel 5-hydroxytryptamine antagonist with no evidence of efficacy. *Vasc Med*. 2004;9:18-25.

160. Milne TA, Kim J, Wang GG, et al. Multiple interactions recruit MLL1 and MLL1 fusion proteins to the HOXA9 locus in leukemogenesis. *Mol Cell*. 2010;38:853-863.

161. Benedikt A, Baltruschat S, Scholz B, et al. The leukemogenic AF4-MLL fusion protein causes P-TEFb kinase activation and altered epigenetic signatures. *Leukemia*. 2011;25:135-144.

162. Pless B, Oehm C, Knauer S, Stauber RH, Dingermann T, Marschalek R. The heterodimerization domains of MLL-FYRN and FYRC--are potential target structures in t(4;11) leukemia. *Leukemia*. 2011;25:663-670.
163. Stumpel DJ, Schneider P, van Roon EHJ, et al. Specific Promoter CpG Island Methylation Patterns Identify Different Subgroups of MLL - Rearranged Infant Acute Lymphoblastic Leukemia, and Define Clinical Outcome. *ASH Annual Meeting Abstracts*. 2008;112:596-.
164. Stumpel DJ, Schotte D, Lange-Turenhout EA, et al. Hypermethylation of specific microRNA genes in MLL-rearranged infant acute lymphoblastic leukemia: major matters at a micro scale. *Leukemia*. 2011;25:429-439.
165. Stam RW, den Boer ML, Passier MM, et al. Silencing of the tumor suppressor gene FHIT is highly characteristic for MLL gene rearranged infant acute lymphoblastic leukemia. *Leukemia*. 2006;20:264-271.
166. Robinson BW, Behling KC, Gupta M, et al. Abundant anti-apoptotic BCL-2 is a molecular target in leukaemias with t(4;11) translocation. *Br J Haematol*. 2008;141:827-839.
167. Stam RW, Den Boer ML, Schneider P, et al. Association of high-level MCL-1 expression with in vitro and in vivo prednisone resistance in MLL-rearranged infant acute lymphoblastic leukemia. *Blood*. 2010;115:1018-1025.
168. Stam RW, Schneider P, Hagelstein JA, et al. Gene expression profiling-based dissection of MLL translocated and MLL germline acute lymphoblastic leukemia in infants. *Blood*. 2010;115:2835-2844.
169. Trentin L, Giordan M, Dingermann T, Basso G, Te Kronnie G, Marschalek R. Two independent gene signatures in pediatric t(4;11) acute lymphoblastic leukemia patients. *Eur J Haematol*. 2009;83:406-419.
170. Gessner A, Thomas M, Castro PG, et al. Leukemic fusion genes MLL/AF4 and AML1/MTG8 support leukemic self-renewal by controlling expression of the telomerase subunit TERT. *Leukemia*. 2010;24:1751-1759.

171. Kuiper RP, Schoenmakers EF, van Reijmersdal SV, et al. High-resolution genomic profiling of childhood ALL reveals novel recurrent genetic lesions affecting pathways involved in lymphocyte differentiation and cell cycle progression. *Leukemia*. 2007;21:1258-1266.
172. Bardini M, Galbiati M, Lettieri A, et al. Implementation of array based whole-genome high-resolution technologies confirms the absence of secondary copy-number alterations in MLL-AF4-positive infant ALL patients. *Leukemia*. 2011;25:175-178.
173. Bardini M, Spinelli R, Bungaro S, et al. DNA copy-number abnormalities do not occur in infant ALL with t(4;11)/MLL-AF4. *Leukemia*. 2010;24:169-176.
174. Sun L, Heerema N, Crotty L, et al. Expression of dominant-negative and mutant isoforms of the antileukemic transcription factor Ikaros in infant acute lymphoblastic leukemia. *Proc Natl Acad Sci U S A*. 1999;96:680-685.
175. Muyrers-Chen I, Rozovskaia T, Lee N, et al. Expression of leukemic MLL fusion proteins in *Drosophila* affects cell cycle control and chromosome morphology. *Oncogene*. 2004;23:8639-8648.
176. Xia ZB, Popovic R, Chen J, et al. The MLL fusion gene, MLL-AF4, regulates cyclin-dependent kinase inhibitor CDKN1B (p27kip1) expression. *Proc Natl Acad Sci U S A*. 2005;102:14028-14033.
177. Zhang Q, Wu J, Nguyen A, et al. Molecular mechanism underlying differential apoptosis between human melanoma cell lines UACC903 and UACC903(+6) revealed by mitochondria-focused cDNA microarrays. *Apoptosis*. 2008;13:993-1004.
178. Trapasso F, Pichiorri F, Gaspari M, et al. Fhit interaction with ferredoxin reductase triggers generation of reactive oxygen species and apoptosis of cancer cells. *J Biol Chem*. 2008;283:13736-13744.
179. Wang JS, Wang FB, Zhang QG, Shen ZZ, Shao ZM. Enhanced expression of Rab27A gene by breast cancer cells promoting invasiveness and the metastasis

potential by secretion of insulin-like growth factor-II. *Mol Cancer Res.* 2008;6:372-382.

180. Fukuda M, Itoh T. Direct link between Atg protein and small GTPase Rab: Atg16L functions as a potential Rab33 effector in mammals. *Autophagy.* 2008;4:824-826.

181. Itoh T, Fujita N, Kanno E, Yamamoto A, Yoshimori T, Fukuda M. Golgi-resident small GTPase Rab33B interacts with Atg16L and modulates autophagosome formation. *Mol Biol Cell.* 2008;19:2916-2925.

182. Nadiminty N, Chun JY, Hu Y, Dutt S, Lin X, Gao AC. LIGHT, a member of the TNF superfamily, activates Stat3 mediated by NIK pathway. *Biochem Biophys Res Commun.* 2007;359:379-384.

183. Pierer M, Brentano F, Rethage J, et al. The TNF superfamily member LIGHT contributes to survival and activation of synovial fibroblasts in rheumatoid arthritis. *Rheumatology (Oxford).* 2007;46:1063-1070.

184. Yant LJ, Ran Q, Rao L, et al. The selenoprotein GPX4 is essential for mouse development and protects from radiation and oxidative damage insults. *Free Radic Biol Med.* 2003;34:496-502.

185. Ran Q, Liang H, Gu M, et al. Transgenic mice overexpressing glutathione peroxidase 4 are protected against oxidative stress-induced apoptosis. *J Biol Chem.* 2004;279:55137-55146.

186. Keller JN, Kindy MS, Holtsberg FW, et al. Mitochondrial manganese superoxide dismutase prevents neural apoptosis and reduces ischemic brain injury: suppression of peroxynitrite production, lipid peroxidation, and mitochondrial dysfunction. *J Neurosci.* 1998;18:687-697.

187. Nakanishi H, Nakamura T, Canaani E, Croce CM. ALL1 fusion proteins induce deregulation of EphA7 and ERK phosphorylation in human acute leukemias. *Proc Natl Acad Sci U S A.* 2007;104:14442-14447.

188. Cooper CL, Brady G, Bilia F, Iscove NN, Quesenberry PJ. Expression of the Id family helix-loop-helix regulators during growth and development in the hematopoietic system. *Blood*. 1997;89:3155-3165.
189. Ling MT, Wang X, Zhang X, Wong YC. The multiple roles of Id-1 in cancer progression. *Differentiation*. 2006;74:481-487.
190. Whelan JT, Ludwig DL, Bertrand FE. HoxA9 induces insulin-like growth factor-1 receptor expression in B-lineage acute lymphoblastic leukemia. *Leukemia*. 2008;22:1161-1169.
191. Zhang B, Zheng Y. Regulation of RhoA GTP hydrolysis by the GTPase-activating proteins p190, p50RhoGAP, Bcr, and 3BP-1. *Biochemistry*. 1998;37:5249-5257.
192. Tarricone C, Xiao B, Justin N, et al. The structural basis of Arfapatin-mediated cross-talk between Rac and Arf signalling pathways. *Nature*. 2001;411:215-219.
193. Wang W, Reeves WB, Ramesh G. Netrin-1 increases proliferation and migration of renal proximal tubular epithelial cells via the UNC5B receptor. *Am J Physiol Renal Physiol*. 2009;296:F723-729.
194. Veillat V, Carli C, Metz CN, Al-Abed Y, Naccache PH, Akoum A. Macrophage migration inhibitory factor elicits an angiogenic phenotype in human ectopic endometrial cells and triggers the production of major angiogenic factors via CD44, CD74, and MAPK signaling pathways. *J Clin Endocrinol Metab*. 2010;95:E403-412.
195. Epting D, Wendik B, Bennewitz K, Dietz CT, Driever W, Kroll J. The Rac1 regulator ELM01 controls vascular morphogenesis in zebrafish. *Circ Res*. 2010;107:45-55.
196. Karaulanov E, Bottcher RT, Stannek P, et al. Unc5B interacts with FLRT3 and Rnd1 to modulate cell adhesion in *Xenopus* embryos. *PLoS One*. 2009;4:e5742.

197. Fan H, Hall P, Santos LL, et al. Macrophage migration inhibitory factor and CD74 regulate macrophage chemotactic responses via MAPK and Rho GTPase. *J Immunol.* 2011;186:4915-4924.
198. Ohtsubo M, Yasunaga S, Ohno Y, et al. Polycomb-group complex 1 acts as an E3 ubiquitin ligase for Geminin to sustain hematopoietic stem cell activity. *Proc Natl Acad Sci U S A.* 2008;105:10396-10401.
199. Banziger C, Soldini D, Schutt C, Zipperlen P, Hausmann G, Basler K. Wntless, a conserved membrane protein dedicated to the secretion of Wnt proteins from signaling cells. *Cell.* 2006;125:509-522.
200. Bartscherer K, Pelte N, Ingelfinger D, Boutros M. Secretion of Wnt ligands requires Evi, a conserved transmembrane protein. *Cell.* 2006;125:523-533.
201. Biechele S, Cox BJ, Rossant J. Porcupine homolog is required for canonical Wnt signaling and gastrulation in mouse embryos. *Dev Biol.* 2011.
202. Fu J, Ivy Yu HM, Maruyama T, Mirando AJ, Hsu W. Gpr177/mouse Wntless is essential for Wnt-mediated craniofacial and brain development. *Dev Dyn.* 2011;240:365-371.
203. Corcoran AE, Smart FM, Cowling RJ, Crompton T, Owen MJ, Venkitaraman AR. The interleukin-7 receptor alpha chain transmits distinct signals for proliferation and differentiation during B lymphopoiesis. *EMBO J.* 1996;15:1924-1932.
204. Zha J, Zhou Q, Xu LG, et al. RIP5 is a RIP-homologous inducer of cell death. *Biochem Biophys Res Commun.* 2004;319:298-303.
205. Takeda Y, Fu J, Suzuki K, et al. Expression of GPI-80, a beta2-integrin-associated glycosylphosphatidylinositol-anchored protein, requires neutrophil differentiation with dimethyl sulfoxide in HL-60 cells. *Exp Cell Res.* 2003;286:199-208.
206. Bahubeshi A, Bal N, Frio TR, et al. Germline DICER1 mutations and familial cystic nephroma. *J Med Genet.* 2010;47:863-866.

207. Lambertz I, Nittner D, Mestdagh P, et al. Monoallelic but not biallelic loss of Dicer1 promotes tumorigenesis in vivo. *Cell Death Differ.* 2010;17:633-641.
208. Raaijmakers MH, Mukherjee S, Guo S, et al. Bone progenitor dysfunction induces myelodysplasia and secondary leukaemia. *Nature.* 2010;464:852-857.
209. Zigelboim I, Reinhart AJ, Gao F, et al. DICER1 expression and outcomes in endometrioid endometrial adenocarcinoma. *Cancer.* 2011;117:1446-1453.
210. Huang da W, Sherman BT, Lempicki RA. Systematic and integrative analysis of large gene lists using DAVID bioinformatics resources. *Nat Protoc.* 2009;4:44-57.
211. Huang da W, Sherman BT, Lempicki RA. Bioinformatics enrichment tools: paths toward the comprehensive functional analysis of large gene lists. *Nucleic Acids Res.* 2009;37:1-13.
212. Huang da W, Sherman BT, Stephens R, Baseler MW, Lane HC, Lempicki RA. DAVID gene ID conversion tool. *Bioinformatics.* 2008;2:428-430.
213. Arribas J, Baselga J, Pedersen K, Parra-Palau JL. p95HER2 and breast cancer. *Cancer Res.* 2011;71:1515-1519.
214. Messina S, Frati L, Leonetti C, et al. Dual-specificity phosphatase DUSP6 has tumor-promoting properties in human glioblastomas. *Oncogene.* 2011.
215. Gu B, Sun P, Yuan Y, et al. Pygo2 expands mammary progenitor cells by facilitating histone H3 K4 methylation. *J Cell Biol.* 2009;185:811-826.
216. Kramps T, Peter O, Brunner E, et al. Wnt/wingless signaling requires BCL9/legless-mediated recruitment of pygopus to the nuclear beta-catenin-TCF complex. *Cell.* 2002;109:47-60.
217. Thompson B, Townsley F, Rosin-Arbesfeld R, Musisi H, Bienz M. A new nuclear component of the Wnt signalling pathway. *Nat Cell Biol.* 2002;4:367-373.

218. Miller TC, Rutherford TJ, Johnson CM, Fiedler M, Bienz M. Allosteric remodelling of the histone H3 binding pocket in the Pygo2 PHD finger triggered by its binding to the B9L/BCL9 co-factor. *J Mol Biol.* 2010;401:969-984.
219. Nair M, Nagamori I, Sun P, et al. Nuclear regulator Pygo2 controls spermiogenesis and histone H3 acetylation. *Dev Biol.* 2008;320:446-455.
220. Schwab KR, Patterson LT, Hartman HA, et al. Pygo1 and Pygo2 roles in Wnt signaling in mammalian kidney development. *BMC Biol.* 2007;5:15.
221. Wang ZX, Chen YY, Li BA, et al. Decreased pygopus 2 expression suppresses glioblastoma U251 cell growth. *J Neurooncol.* 2010;100:31-41.
222. Andrews PG, Lake BB, Popadiuk C, Kao KR. Requirement of Pygopus 2 in breast cancer. *Int J Oncol.* 2007;30:357-363.
223. Moens CB, Selleri L. Hox cofactors in vertebrate development. *Dev Biol.* 2006;291:193-206.
224. Abramovich C, Humphries RK. Hox regulation of normal and leukemic hematopoietic stem cells. *Curr Opin Hematol.* 2005;12:210-216.
225. Kersey JH, Wang D, Oberto M. Resistance of t(4;11) (MLL-AF4 fusion gene) leukemias to stress-induced cell death: possible mechanism for extensive extramedullary accumulation of cells and poor prognosis. *Leukemia.* 1998;12:1561-1564.
226. Caslini C, Serna A, Rossi V, Introna M, Biondi A. Modulation of cell cycle by graded expression of MLL-AF4 fusion oncoprotein. *Leukemia.* 2004;18:1064-1071.
227. Ploner C, Kofler R, Villunger A. Noxa: at the tip of the balance between life and death. *Oncogene.* 2008;27 Suppl 1:S84-92.
228. Wensveen FM, Alves NL, Derks IA, Reedquist KA, Eldering E. Apoptosis induced by overall metabolic stress converges on the Bcl-2 family proteins Noxa and Mcl-1. *Apoptosis.* 2011;16:708-721.

229. Tonino SH, van Laar J, van Oers MH, Wang JY, Eldering E, Kater AP. ROS-mediated upregulation of Noxa overcomes chemoresistance in chronic lymphocytic leukemia. *Oncogene*. 2011;30:701-713.
230. Green SR, Choudhary AK, Fleming IN. Combination of sapacitabine and HDAC inhibitors stimulates cell death in AML and other tumour types. *Br J Cancer*. 2010;103:1391-1399.
231. Ohshima-Hosoyama S, Davare MA, Hosoyama T, Nelon LD, Keller C. Bortezomib stabilizes NOXA and triggers ROS-associated apoptosis in medulloblastoma. *J Neurooncol*. 2011.
232. Chiaverini N, De Ley M. Protective effect of metallothionein on oxidative stress-induced DNA damage. *Free Radic Res*. 2010;44:605-613.
233. Wang LD, Yang YH, Liu Y, Song HT, Zhang LY, Li PL. Decreased expression of annexin A1 during the progression of cervical neoplasia. *J Int Med Res*. 2008;36:665-672.
234. Vishwanatha JK, Salazar E, Gopalakrishnan VK. Absence of annexin I expression in B-cell non-Hodgkin's lymphomas and cell lines. *BMC Cancer*. 2004;4:8.
235. Maschler S, Gebeshuber CA, Wiedemann EM, et al. Annexin A1 attenuates EMT and metastatic potential in breast cancer. *EMBO Mol Med*. 2010;2:401-414.
236. Cao Y, Li Y, Edelweiss M, et al. Loss of annexin A1 expression in breast cancer progression. *Appl Immunohistochem Mol Morphol*. 2008;16:530-534.
237. Luthra R, Singh RR, Luthra MG, et al. MicroRNA-196a targets annexin A1: a microRNA-mediated mechanism of annexin A1 downregulation in cancers. *Oncogene*. 2008;27:6667-6678.
238. Ang EZ, Nguyen HT, Sim HL, Putti TC, Lim LH. Annexin-1 regulates growth arrest induced by high levels of estrogen in MCF-7 breast cancer cells. *Mol Cancer Res*. 2009;7:266-274.

239. Zhu F, Wang Y, Zeng S, Fu X, Wang L, Cao J. Involvement of annexin A1 in multidrug resistance of K562/ADR cells identified by the proteomic study. *OMICS*. 2009;13:467-476.
240. Tabe Y, Jin L, Contractor R, et al. Novel role of HDAC inhibitors in AML1/ETO AML cells: activation of apoptosis and phagocytosis through induction of annexin A1. *Cell Death Differ*. 2007;14:1443-1456.
241. Zhang Z, Huang L, Zhao W, Rigas B. Annexin 1 induced by anti-inflammatory drugs binds to NF-kappaB and inhibits its activation: anticancer effects in vitro and in vivo. *Cancer Res*. 2010;70:2379-2388.
242. Cabrera S, Marino G, Fernandez AF, Lopez-Otin C. Autophagy, proteases and the sense of balance. *Autophagy*. 2010;6:961-963.
243. Mansuy V, Boireau W, Fraichard A, Schlick JL, Jouvenot M, Delage-Mourroux R. GEC1, a protein related to GABARAP, interacts with tubulin and GABA(A) receptor. *Biochem Biophys Res Commun*. 2004;325:639-648.
244. Chen Y, Chen C, Kotsikorou E, Lynch DL, Reggio PH, Liu-Chen LY. GEC1-kappa opioid receptor binding involves hydrophobic interactions: GEC1 has chaperone-like effect. *J Biol Chem*. 2009;284:1673-1685.
245. Chen C, Li JG, Chen Y, Huang P, Wang Y, Liu-Chen LY. GEC1 interacts with the kappa opioid receptor and enhances expression of the receptor. *J Biol Chem*. 2006;281:7983-7993.
246. Chakrama FZ, Seguin-Py S, Le Grand JN, et al. GABARAPL1 (GEC1) associates with autophagic vesicles. *Autophagy*. 2010;6.
247. Betin VM, Lane JD. Caspase cleavage of Atg4D stimulates GABARAP-L1 processing and triggers mitochondrial targeting and apoptosis. *J Cell Sci*. 2009;122:2554-2566.
248. Tanida I, Sou YS, Minematsu-Ikeguchi N, Ueno T, Kominami E. Atg8L/Apg8L is the fourth mammalian modifier of mammalian Atg8 conjugation mediated by human Atg4B, Atg7 and Atg3. *FEBS J*. 2006;273:2553-2562.

249. Berthier A, Seguin S, Sasco AJ, et al. High expression of gabarapl1 is associated with a better outcome for patients with lymph node-positive breast cancer. *Br J Cancer*. 2010;102:1024-1031.
250. Hanahan D, Weinberg RA. The hallmarks of cancer. *Cell*. 2000;100:57-70.
251. Hanahan D, Weinberg RA. Hallmarks of cancer: the next generation. *Cell*. 2011;144:646-674.
252. Ng MH, Ng RK, Kong CT, Jin DY, Chan LC. Activation of Ras-dependent Elk-1 activity by MLL-AF4 family fusion oncoproteins. *Exp Hematol*. 2010;38:481-488.
253. Qazi S, Uckun FM. Gene expression profiles of infant acute lymphoblastic leukaemia and its prognostically distinct subsets. *Br J Haematol*. 2010;149:865-873.
254. Copland JA, Pardini AW, Wood TG, et al. IGF-1 controls GLUT3 expression in muscle via the transcriptional factor Sp1. *Biochim Biophys Acta*. 2007;1769:631-640.
255. Wang M, Bao YL, Wu Y, et al. Basic FGF downregulates TSP50 expression via the ERK/Sp1 pathway. *J Cell Biochem*. 2010;111:75-81.
256. Bomken S, Fiser K, Heidenreich O, Vormoor J. Understanding the cancer stem cell. *Br J Cancer*. 2010;103:439-445.
257. Heidenreich O, Vormoor J. Malignant stem cells in childhood ALL: the debate continues! *Blood*. 2009;113:4476-4477; author reply 4477.
258. Tada J, Omine M, Suda T, Yamaguchi N. A common signaling pathway via Syk and Lyn tyrosine kinases generated from capping of the sialomucins CD34 and CD43 in immature hematopoietic cells. *Blood*. 1999;93:3723-3735.
259. Vodyanik MA, Thomson JA, Slukvin, II. Leukosialin (CD43) defines hematopoietic progenitors in human embryonic stem cell differentiation cultures. *Blood*. 2006;108:2095-2105.

260. Merchant MS, Garvy BA, Riley RL. Autoantibodies inhibit interleukin-7-mediated proliferation and are associated with the age-dependent loss of pre-B cells in autoimmune New Zealand Black Mice. *Blood*. 1996;87:3289-3296.
261. Rawat VP, Thoene S, Naidu VM, et al. Overexpression of CDX2 perturbs HOX gene expression in murine progenitors depending on its N-terminal domain and is closely correlated with deregulated HOX gene expression in human acute myeloid leukemia. *Blood*. 2008;111:309-319.
262. Rice KL, Licht JD. HOX deregulation in acute myeloid leukemia. *J Clin Invest*. 2007;117:865-868.
263. Scholl C, Bansal D, Dohner K, et al. The homeobox gene CDX2 is aberrantly expressed in most cases of acute myeloid leukemia and promotes leukemogenesis. *J Clin Invest*. 2007;117:1037-1048.
264. Bansal D, Scholl C, Frohling S, et al. Cdx4 dysregulates Hox gene expression and generates acute myeloid leukemia alone and in cooperation with Meis1a in a murine model. *Proc Natl Acad Sci U S A*. 2006;103:16924-16929.
265. Dik WA, Brahim W, Braun C, et al. CALM-AF10+ T-ALL expression profiles are characterized by overexpression of HOXA and BMI1 oncogenes. *Leukemia*. 2005;19:1948-1957.
266. Magnusson M, Brun AC, Miyake N, et al. HOXA10 is a critical regulator for hematopoietic stem cells and erythroid/megakaryocyte development. *Blood*. 2007;109:3687-3696.
267. Faber J, Krivtsov AV, Stubbs MC, et al. HOXA9 is required for survival in human MLL-rearranged acute leukemias. *Blood*. 2009;113:2375-2385.
268. Belgiovine C, Chiodi I, Mondello C. Telomerase: cellular immortalization and neoplastic transformation. Multiple functions of a multifaceted complex. *Cytogenet Genome Res*. 2008;122:255-262.
269. Chen C, Grennan K, Badner J, et al. Removing batch effects in analysis of expression microarray data: an evaluation of six batch adjustment methods. *PLoS One*. 2011;6:e17238.

270. Wang QF, Wu G, Mi S, et al. MLL fusion proteins preferentially regulate a subset of wild type MLL target genes in the leukemic genome. *Blood*. 2011.
271. Luty AA, Kwok JB, Dobson-Stone C, et al. Sigma nonopioid intracellular receptor 1 mutations cause frontotemporal lobar degeneration-motor neuron disease. *Ann Neurol*. 2010;68:639-649.
272. Maruszak A, Safranow K, Gacia M, et al. Sigma receptor type 1 gene variation in a group of Polish patients with Alzheimer's disease and mild cognitive impairment. *Dement Geriatr Cogn Disord*. 2007;23:432-438.
273. Uchida N, Ujike H, Tanaka Y, et al. A variant of the sigma receptor type-1 gene is a protective factor for Alzheimer disease. *Am J Geriatr Psychiatry*. 2005;13:1062-1066.
274. Banerjee A, Gugasyan R, McMahon M, Gerondakis S. Diverse Toll-like receptors utilize Tpl2 to activate extracellular signal-regulated kinase (ERK) in hemopoietic cells. *Proc Natl Acad Sci U S A*. 2006;103:3274-3279.
275. Loniewski KJ, Patial S, Parameswaran N. Sensitivity of TLR4- and -7-induced NF kappa B1 p105-TPL2-ERK pathway to TNF-receptor-associated-factor-6 revealed by RNAi in mouse macrophages. *Mol Immunol*. 2007;44:3715-3723.
276. Jager J, Gremeaux T, Gonzalez T, et al. Tpl2 kinase is upregulated in adipose tissue in obesity and may mediate interleukin-1beta and tumor necrosis factor- α effects on extracellular signal-regulated kinase activation and lipolysis. *Diabetes*. 2010;59:61-70.
277. Yaomura T, Tsuboi N, Urahama Y, et al. Serine/threonine kinase, Cot/Tpl2, regulates renal cell apoptosis in ischaemia/reperfusion injury. *Nephrology (Carlton)*. 2008;13:397-404.
278. Rousseau S, Papoutsopoulou M, Symons A, et al. TPL2-mediated activation of ERK1 and ERK2 regulates the processing of pre-TNF alpha in LPS-stimulated macrophages. *J Cell Sci*. 2008;121:149-154.

279. Lu SC. Regulation of glutathione synthesis. *Mol Aspects Med.* 2009;30:42-59.
280. Tan X, Jin G, Tian M, et al. The co-transduction of Nurr1 and Brn4 genes induces the differentiation of neural stem cells into dopaminergic neurons. *Cell Biol Int.* 2011.
281. Hart GT, Wang X, Hogquist KA, Jameson SC. Kruppel-like factor 2 (KLF2) regulates B-cell reactivity, subset differentiation, and trafficking molecule expression. *Proc Natl Acad Sci U S A.* 2011;108:716-721.
282. Ralph JA, Ahmed AU, Santos LL, et al. Identification of NURR1 as a mediator of MIF signaling during chronic arthritis: effects on glucocorticoid-induced MKP1. *Am J Pathol.* 2010;177:2366-2378.
283. Zahlten J, Steinicke R, Opitz B, et al. TLR2- and nucleotide-binding oligomerization domain 2-dependent Kruppel-like factor 2 expression downregulates NF-kappa B-related gene expression. *J Immunol.* 2010;185:597-604.
284. Saijo K, Winner B, Carson CT, et al. A Nurr1/CoREST pathway in microglia and astrocytes protects dopaminergic neurons from inflammation-induced death. *Cell.* 2009;137:47-59.
285. Wang F, Zhu Y, Huang Y, et al. Transcriptional repression of WEE1 by Kruppel-like factor 2 is involved in DNA damage-induced apoptosis. *Oncogene.* 2005;24:3875-3885.
286. Komiya T, Coxon A, Park Y, et al. Enhanced activity of the CREB co-activator Crtc1 in LKB1 null lung cancer. *Oncogene.* 2010;29:1672-1680.
287. Cotterman R, Knoepfler PS. N-Myc regulates expression of pluripotency genes in neuroblastoma including *lif*, *klf2*, *klf4*, and *lin28b*. *PLoS One.* 2009;4:e5799.
288. Xie P, Tang Y, Shen S, et al. Smurf1 ubiquitin ligase targets Kruppel-like factor KLF2 for ubiquitination and degradation in human lung cancer H1299 cells. *Biochem Biophys Res Commun.* 2011;407:254-259.

289. Cogoi S, Paramasivam M, Membrino A, Yokoyama KK, Xodo LE. The KRAS promoter responds to Myc-associated zinc finger and poly(ADP-ribose) polymerase 1 proteins, which recognize a critical quadruplex-forming GA-element. *J Biol Chem.* 2010;285:22003-22016.
290. Castermans D, Vermeesch JR, Fryns JP, et al. Identification and characterization of the TRIP8 and REEP3 genes on chromosome 10q21.3 as novel candidate genes for autism. *Eur J Hum Genet.* 2007;15:422-431.
291. Hitomi J, Christofferson DE, Ng A, et al. Identification of a molecular signaling network that regulates a cellular necrotic cell death pathway. *Cell.* 2008;135:1311-1323.
292. Fischer R, Maier O, Naumer M, Krippner-Heidenreich A, Scheurich P, Pfizenmaier K. Ligand-induced internalization of TNF receptor 2 mediated by a di-leucine motif is dispensable for activation of the NFkappaB pathway. *Cell Signal.* 2011;23:161-170.
293. Vandenabeele P, Vanden Berghe T, Festjens N. Caspase inhibitors promote alternative cell death pathways. *Sci STKE.* 2006;2006:pe44.
294. Tanida I, Ueno T, Kominami E. LC3 and Autophagy. *Methods Mol Biol.* 2008;445:77-88.
295. Kroemer G, Galluzzi L, Vandenabeele P, et al. Classification of cell death: recommendations of the Nomenclature Committee on Cell Death 2009. *Cell Death Differ.* 2009;16:3-11.
296. Thompson MR, Xu D, Williams BR. ATF3 transcription factor and its emerging roles in immunity and cancer. *J Mol Med.* 2009;87:1053-1060.
297. Scheller C, Riederer P, Gerlach M, Koutsilieri E. Apoptosis inhibition in T cells triggers the expression of proinflammatory cytokines--implications for the CNS. *J Neural Transm Suppl.* 2006:45-51.
298. Scheller C, Sopper S, Ehrhardt C, et al. Caspase inhibitors induce a switch from apoptotic to proinflammatory signaling in CD95-stimulated T lymphocytes. *Eur J Immunol.* 2002;32:2471-2480.

299. Ameri K, Harris AL. Activating transcription factor 4. *Int J Biochem Cell Biol.* 2008;40:14-21.
300. Albershardt TC, Salerni BL, Soderquist RS, et al. Multiple BH3 mimetics antagonize anti-apoptotic MCL1 by inducing the endoplasmic reticulum stress response and up-regulating BH3-only protein NOXA. *J Biol Chem.* 2011.
301. Galehdar Z, Swan P, Fuerth B, Callaghan SM, Park DS, Cregan SP. Neuronal apoptosis induced by endoplasmic reticulum stress is regulated by ATF4-CHOP-mediated induction of the Bcl-2 homology 3-only member PUMA. *J Neurosci.* 2010;30:16938-16948.
302. Li H, Gade P, Xiao W, Kalvakolanu DV. The interferon signaling network and transcription factor C/EBP-beta. *Cell Mol Immunol.* 2007;4:407-418.
303. Colonna M. TLR pathways and IFN-regulatory factors: to each its own. *Eur J Immunol.* 2007;37:306-309.
304. Gao J, Senthil M, Ren B, et al. IRF-1 transcriptionally upregulates PUMA, which mediates the mitochondrial apoptotic pathway in IRF-1-induced apoptosis in cancer cells. *Cell Death Differ.* 2010;17:699-709.
305. Wu YT, Tan HL, Huang Q, Sun XJ, Zhu X, Shen HM. zVAD-induced necroptosis in L929 cells depends on autocrine production of TNFalpha mediated by the PKC-MAPKs-AP-1 pathway. *Cell Death Differ.* 2011;18:26-37.
306. Abedin MJ, Wang D, McDonnell MA, Lehmann U, Kelekar A. Autophagy delays apoptotic death in breast cancer cells following DNA damage. *Cell Death Differ.* 2007;14:500-510.
307. Yu L, Alva A, Su H, et al. Regulation of an ATG7-beclin 1 program of autophagic cell death by caspase-8. *Science.* 2004;304:1500-1502.
308. Mahoney DJ, Cheung HH, Mrad RL, et al. Both cIAP1 and cIAP2 regulate TNFalpha-mediated NF-kappaB activation. *Proc Natl Acad Sci U S A.* 2008;105:11778-11783.

309. Wu CJ, Conze DB, Li T, Srinivasula SM, Ashwell JD. Sensing of Lys 63-linked polyubiquitination by NEMO is a key event in NF-kappaB activation [corrected]. *Nat Cell Biol.* 2006;8:398-406.
310. Vandenabeele P, Galluzzi L, Vanden Berghe T, Kroemer G. Molecular mechanisms of necroptosis: an ordered cellular explosion. *Nat Rev Mol Cell Biol.* 2010;11:700-714.
311. Lin Y, Devin A, Rodriguez Y, Liu ZG. Cleavage of the death domain kinase RIP by caspase-8 prompts TNF-induced apoptosis. *Genes Dev.* 1999;13:2514-2526.
312. Bonapace L, Bornhauser BC, Schmitz M, et al. Induction of autophagy-dependent necroptosis is required for childhood acute lymphoblastic leukemia cells to overcome glucocorticoid resistance. *J Clin Invest.* 2010;120:1310-1323.
313. Degterev A, Hitomi J, Gemscheid M, et al. Identification of RIP1 kinase as a specific cellular target of necrostatins. *Nat Chem Biol.* 2008;4:313-321.
314. Zhang DW, Shao J, Lin J, et al. RIP3, an energy metabolism regulator that switches TNF-induced cell death from apoptosis to necrosis. *Science.* 2009;325:332-336.
315. Vandenabeele P, Declercq W, Van Herreweghe F, Vanden Berghe T. The role of the kinases RIP1 and RIP3 in TNF-induced necrosis. *Sci Signal.* 2010;3:re4.
316. Zhang DW, Zheng M, Zhao J, et al. Multiple death pathways in TNF-treated fibroblasts: RIP3- and RIP1-dependent and independent routes. *Cell Res.* 2011;21:368-371.
317. Zheng W, Degterev A, Hsu E, Yuan J, Yuan C. Structure-activity relationship study of a novel necroptosis inhibitor, necrostatin-7. *Bioorg Med Chem Lett.* 2008;18:4932-4935.
318. Ling YH, Aracil M, Zou Y, et al. PM02734 Induces Caspase-Independent Cell Death Associated with Features of Autophagy, Inhibition of the Akt/mTOR Signaling Pathway, and Activation of DAP Kinase. *Clin Cancer Res.* 2011.

319. Okada M, Adachi S, Imai T, et al. A novel mechanism for imatinib mesylate-induced cell death of BCR-ABL-positive human leukemic cells: caspase-independent, necrosis-like programmed cell death mediated by serine protease activity. *Blood*. 2004;103:2299-2307.
320. Menendez D, Shatz M, Azzam K, Garantziotis S, Fessler MB, Resnick MA. The Toll-like receptor gene family is integrated into human DNA damage and p53 networks. *PLoS Genet*. 2011;7:e1001360.
321. Stawowczyk M, Van Scoy S, Kumar KP, Reich NC. The interferon stimulated gene 54 promotes apoptosis. *J Biol Chem*. 2011;286:7257-7266.
322. Hallen LC, Burki Y, Ebeling M, et al. Antiproliferative activity of the human IFN-alpha-inducible protein IFI44. *J Interferon Cytokine Res*. 2007;27:675-680.
323. Tania M, Khan A, Zhang H, Li J, Song Y. Autotaxin: a protein with two faces. *Biochem Biophys Res Commun*. 2010;401:493-497.
324. Calero M, Whittaker GR, Collins RN. Yop1p, the yeast homolog of the polyposis locus protein 1, interacts with Yip1p and negatively regulates cell growth. *J Biol Chem*. 2001;276:12100-12112.
325. Wu Z, Lee ST, Qiao Y, et al. Polycomb protein EZH2 regulates cancer cell fate decision in response to DNA damage. *Cell Death Differ*. 2011;18:1771-1779.
326. Chou JL, Su HY, Chen LY, et al. Promoter hypermethylation of FBX032, a novel TGF-beta/SMAD4 target gene and tumor suppressor, is associated with poor prognosis in human ovarian cancer. *Lab Invest*. 2010;90:414-425.
327. Arai F, Hirao A, Ohmura M, et al. Tie2/angiopoietin-1 signaling regulates hematopoietic stem cell quiescence in the bone marrow niche. *Cell*. 2004;118:149-161.
328. Davis S, Aldrich TH, Jones PF, et al. Isolation of angiopoietin-1, a ligand for the TIE2 receptor, by secretion-trap expression cloning. *Cell*. 1996;87:1161-1169.

329. Davis S, Papadopoulos N, Aldrich TH, et al. Angiopoietins have distinct modular domains essential for receptor binding, dimerization and superclustering. *Nat Struct Biol.* 2003;10:38-44.
330. Kontos CD, Stauffer TP, Yang WP, et al. Tyrosine 1101 of Tie2 is the major site of association of p85 and is required for activation of phosphatidylinositol 3-kinase and Akt. *Mol Cell Biol.* 1998;18:4131-4140.
331. Seegar TC, Eller B, Tzvetkova-Robev D, et al. Tie1-Tie2 interactions mediate functional differences between angiopoietin ligands. *Mol Cell.* 2010;37:643-655.
332. Carlson TR, Feng Y, Maisonpierre PC, Mrksich M, Morla AO. Direct cell adhesion to the angiopoietins mediated by integrins. *J Biol Chem.* 2001;276:26516-26525.
333. Dallabrida SM, Ismail N, Oberle JR, Himes BE, Rupnick MA. Angiopoietin-1 promotes cardiac and skeletal myocyte survival through integrins. *Circ Res.* 2005;96:e8-24.
334. Dallabrida SM, Ismail NS, Pravda EA, et al. Integrin binding angiopoietin-1 monomers reduce cardiac hypertrophy. *FASEB J.* 2008;22:3010-3023.
335. Ismail NS, Pravda EA, Li D, Shih SC, Dallabrida SM. Angiopoietin-1 reduces H₂O₂-induced increases in reactive oxygen species and oxidative damage to skin cells. *J Invest Dermatol.* 2010;130:1307-1317.
336. Chen X, Fu W, Tung CE, Ward NL. Angiopoietin-1 induces neurite outgrowth of PC12 cells in a Tie2-independent, beta1-integrin-dependent manner. *Neurosci Res.* 2009;64:348-354.
337. Agliano A, Martin-Padura I, Mancuso P, et al. Human acute leukemia cells injected in NOD/LtSz-scid/IL-2Rgamma null mice generate a faster and more efficient disease compared to other NOD/scid-related strains. *Int J Cancer.* 2008;123:2222-2227.

338. Shultz LD, Lyons BL, Burzenski LM, et al. Human lymphoid and myeloid cell development in NOD/LtSz-scid IL2R gamma null mice engrafted with mobilized human hemopoietic stem cells. *J Immunol.* 2005;174:6477-6489.
339. Shultz LD, Saito Y, Najima Y, et al. Generation of functional human T-cell subsets with HLA-restricted immune responses in HLA class I expressing NOD/SCID/IL2r gamma(null) humanized mice. *Proc Natl Acad Sci U S A.* 2010;107:13022-13027.
340. Noren-Nystrom U, Heyman M, Frisk P, et al. Vascular density in childhood acute lymphoblastic leukaemia correlates to biological factors and outcome. *Br J Haematol.* 2009;146:521-530.
341. Negaard HF, Iversen N, Bowitz-Lothe IM, et al. Increased bone marrow microvascular density in haematological malignancies is associated with differential regulation of angiogenic factors. *Leukemia.* 2009;23:162-169.
342. Perez-Atayde AR, Sallan SE, Tedrow U, Connors S, Allred E, Folkman J. Spectrum of tumor angiogenesis in the bone marrow of children with acute lymphoblastic leukemia. *Am J Pathol.* 1997;150:815-821.
343. Shanafelt TD, Byrd JC, La PB, et al. Pretreatment angiogenic cytokines predict response to chemoimmunotherapy in patients with chronic lymphocytic leukaemia. *Br J Haematol.* 2009;146:660-664.
344. Loges S, Heil G, Bruweleit M, et al. Analysis of concerted expression of angiogenic growth factors in acute myeloid leukemia: expression of angiopoietin-2 represents an independent prognostic factor for overall survival. *J Clin Oncol.* 2005;23:1109-1117.
345. Joshi S, Khan R, Sharma M, Kumar L, Sharma A. Angiopoietin-2: A potential novel diagnostic marker in multiple myeloma. *Clin Biochem.* 2011.
346. Koenecke C, Kumpers P, Lukasz A, et al. Shedding of the endothelial receptor tyrosine kinase Tie2 correlates with leukemic blast burden and outcome after allogeneic hematopoietic stem cell transplantation for AML. *Ann Hematol.* 2010;89:459-467.

347. Fenchel M, Konaktchieva M, Weisel K, et al. Early response assessment in patients with multiple myeloma during anti-angiogenic therapy using arterial spin labelling: first clinical results. *Eur Radiol.* 2010;20:2899-2906.
348. Jia D, Koonce NA, Halakatti R, et al. Repression of multiple myeloma growth and preservation of bone with combined radiotherapy and anti-angiogenic agent. *Radiat Res.* 2010;173:809-817.
349. Shanafelt T, Zent C, Byrd J, et al. Phase II trials of single-agent anti-VEGF therapy for patients with chronic lymphocytic leukemia. *Leuk Lymphoma.* 2010;51:2222-2229.
350. Fiedler W, Mesters R, Tinnefeld H, et al. A phase 2 clinical study of SU5416 in patients with refractory acute myeloid leukemia. *Blood.* 2003;102:2763-2767.
351. Anargyrou K, Terpos E, Vassilakopoulos TP, et al. Normalization of the serum angiopoietin-1 to angiopoietin-2 ratio reflects response in refractory/resistant multiple myeloma patients treated with bortezomib. *Haematologica.* 2008;93:451-454.
352. Schneider P, Vasse M, Sbaa-Ketata E, et al. The growth of highly proliferative acute lymphoblastic leukemia may be independent of stroma and/or angiogenesis. *Leukemia.* 2001;15:1143-1145.
353. Stachel D, Albert M, Meilbeck R, Paulides M, Schmid I. Expression of angiogenic factors in childhood B-cell precursor acute lymphoblastic leukemia. *Oncol Rep.* 2007;17:147-152.
354. Noren-Nystrom U, Roos G, Bergh A, Forestier E. Prognostic impact of vascular density and fibrosis in the bone marrow of children with high-risk acute lymphoblastic leukemia. *Leukemia.* 2005;19:1998-2001.
355. Pule MA, Gullmann C, Dennis D, McMahon C, Jeffers M, Smith OP. Increased angiogenesis in bone marrow of children with acute lymphoblastic leukaemia has no prognostic significance. *Br J Haematol.* 2002;118:991-998.

356. Veiga JP, Costa LF, Sallan SE, Nadler LM, Cardoso AA. Leukemia-stimulated bone marrow endothelium promotes leukemia cell survival. *Exp Hematol.* 2006;34:610-621.
357. Fragoso R, Pereira T, Wu Y, Zhu Z, Cabecadas J, Dias S. VEGFR-1 (FLT-1) activation modulates acute lymphoblastic leukemia localization and survival within the bone marrow, determining the onset of extramedullary disease. *Blood.* 2006;107:1608-1616.
358. Chen W, Kumar AR, Hudson WA, et al. Malignant transformation initiated by Mll-AF9: gene dosage and critical target cells. *Cancer Cell.* 2008;13:432-440.
359. Yassin ER, Abdul-Nabi AM, Takeda A, Yaseen NR. Effects of the NUP98-DDX10 oncogene on primary human CD34+ cells: role of a conserved helicase motif. *Leukemia.* 2010;24:1001-1011.
360. Armstrong SA, Staunton JE, Silverman LB, et al. MLL translocations specify a distinct gene expression profile that distinguishes a unique leukemia. *Nat Genet.* 2002;30:41-47.
361. Yeoh EJ, Ross ME, Shurtleff SA, et al. Classification, subtype discovery, and prediction of outcome in pediatric acute lymphoblastic leukemia by gene expression profiling. *Cancer Cell.* 2002;1:133-143.
362. Arai S, Yoshimi A, Shimabe M, et al. Evi-1 is a transcriptional target of MLL oncoproteins in hematopoietic stem cells. *Blood.* 2010.
363. Yuasa H, Oike Y, Iwama A, et al. Oncogenic transcription factor Evi1 regulates hematopoietic stem cell proliferation through GATA-2 expression. *EMBO J.* 2005;24:1976-1987.
364. Momose Haruka TK, Kuramitsu Madoka, Mizukami Takuo, Masumi Atsuko, Yamaguchi Kazunari, Hamaguchi Isao. Ang1 Functions as An Autocrine Activating Factor of Tie2 Signaling In Hematopoietic Stem Cells. *ASH Annual Meeting Abstracts.* 2010;116:1548.
365. Arai F, Hirao A, Suda T. Regulation of hematopoietic stem cells by the niche. *Trends Cardiovasc Med.* 2005;15:75-79.

366. Wildenhain S, Ruckert C, Rottgers S, et al. Expression of cell-cell interacting genes distinguishes HLXB9/TEL from MLL-positive childhood acute myeloid leukemia. *Leukemia*. 2010;24:1657-1660.
367. Hu Z, Li XM, Jorgensen ML, Slayton WB. MLL/AF-4 leukemic cells recruit new blood vessels but do not incorporate into capillaries in culture or in a NOD/SCID xenograft model. *Leukemia*. 2009;23:990-993.
368. Hatfield KJ, Hovland R, Oyan AM, et al. Release of angiopoietin-1 by primary human acute myelogenous leukemia cells is associated with mutations of nucleophosmin, increased by bone marrow stromal cells and possibly antagonized by high systemic angiopoietin-2 levels. *Leukemia*. 2008;22:287-293.
369. Hatfield K, Oyan AM, Ersvaer E, et al. Primary human acute myeloid leukaemia cells increase the proliferation of microvascular endothelial cells through the release of soluble mediators. *Br J Haematol*. 2009;144:53-68.
370. Reikvam H, Hatfield KJ, Lassalle P, Kittang AO, Ersvaer E, Bruserud O. Targeting the angiopoietin (Ang)/Tie-2 pathway in the crosstalk between acute myeloid leukaemia and endothelial cells: studies of Tie-2 blocking antibodies, exogenous Ang-2 and inhibition of constitutive agonistic Ang-1 release. *Expert Opin Investig Drugs*. 2010;19:169-183.
371. Reikvam H, Hatfield KJ, Oyan AM, Kalland KH, Kittang AO, Bruserud O. Primary human acute myelogenous leukemia cells release matrix metalloproteases and their inhibitors: release profile and pharmacological modulation. *Eur J Haematol*;84:239-251.
372. Imanishi Y, Hu B, Jarzynka MJ, et al. Angiopoietin-2 stimulates breast cancer metastasis through the alpha(5)beta(1) integrin-mediated pathway. *Cancer Res*. 2007;67:4254-4263.
373. Tissing WJ, Lauten M, Meijerink JP, et al. Expression of the glucocorticoid receptor and its isoforms in relation to glucocorticoid resistance in childhood acute lymphocytic leukemia. *Haematologica*. 2005;90:1279-1281.

374. Wei G, Twomey D, Lamb J, et al. Gene expression-based chemical genomics identifies rapamycin as a modulator of MCL1 and glucocorticoid resistance. *Cancer Cell*. 2006;10:331-342.
375. Hundsdoerfer P, Dietrich I, Schmelz K, Eckert C, Henze G. XIAP expression is post-transcriptionally upregulated in childhood ALL and is associated with glucocorticoid response in T-cell ALL. *Pediatr Blood Cancer*. 2010;55:260-266.
376. Kotani A, Ha D, Schotte D, den Boer ML, Armstrong SA, Lodish HF. A novel mutation in the miR-128b gene reduces miRNA processing and leads to glucocorticoid resistance of MLL-AF4 acute lymphocytic leukemia cells. *Cell Cycle*. 2010;9.
377. Kistner A, Gossen M, Zimmermann F, et al. Doxycycline-mediated quantitative and tissue-specific control of gene expression in transgenic mice. *Proc Natl Acad Sci U S A*. 1996;93:10933-10938.
378. Gomei Y, Nakamura Y, Yoshihara H, et al. Functional differences between two Tie2 ligands, angiopoietin-1 and -2, in regulation of adult bone marrow hematopoietic stem cells. *Exp Hematol*. 2010;38:82-89.
379. Sato A, Iwama A, Takakura N, Nishio H, Yancopoulos GD, Suda T. Characterization of TEK receptor tyrosine kinase and its ligands, Angiopoietins, in human hematopoietic progenitor cells. *Int Immunol*. 1998;10:1217-1227.
380. Gale NW, Thurston G, Hackett SF, et al. Angiopoietin-2 is required for postnatal angiogenesis and lymphatic patterning, and only the latter role is rescued by Angiopoietin-1. *Dev Cell*. 2002;3:411-423.
381. Fiedler U, Reiss Y, Scharpfenecker M, et al. Angiopoietin-2 sensitizes endothelial cells to TNF-alpha and has a crucial role in the induction of inflammation. *Nat Med*. 2006;12:235-239.
382. Kim I, Kim JH, Ryu YS, Liu M, Koh GY. Tumor necrosis factor-alpha upregulates angiopoietin-2 in human umbilical vein endothelial cells. *Biochem Biophys Res Commun*. 2000;269:361-365.

383. Tressel SL, Kim H, Ni CW, et al. Angiopoietin-2 stimulates blood flow recovery after femoral artery occlusion by inducing inflammation and arteriogenesis. *Arterioscler Thromb Vasc Biol.* 2008;28:1989-1995.
384. Schliemann C, Bieker R, Thoennissen N, et al. Circulating angiopoietin-2 is a strong prognostic factor in acute myeloid leukemia. *Leukemia.* 2007;21:1901-1906.
385. Kumpers P, Koenecke C, Hecker H, et al. Angiopoietin-2 predicts disease-free survival after allogeneic stem cell transplantation in patients with high-risk myeloid malignancies. *Blood.* 2008;112:2139-2148.
386. Martinelli S, Maffei R, Castelli I, et al. Increased expression of angiopoietin-2 characterizes early B-cell chronic lymphocytic leukemia with poor prognosis. *Leuk Res.* 2008;32:593-597.
387. Huang H, Bhat A, Woodnutt G, Lappe R. Targeting the ANGPT-TIE2 pathway in malignancy. *Nat Rev Cancer.* 2010;10:575-585.
388. Lee CY, Tien HF, Hu CY, Chou WC, Lin LI. Marrow angiogenesis-associated factors as prognostic biomarkers in patients with acute myelogenous leukaemia. *Br J Cancer.* 2007;97:877-882.
389. Schliemann C, Bieker R, Padro T, et al. Expression of angiopoietins and their receptor Tie2 in the bone marrow of patients with acute myeloid leukemia. *Haematologica.* 2006;91:1203-1211.
390. Bric A, Miething C, Bialucha CU, et al. Functional identification of tumor-suppressor genes through an in vivo RNA interference screen in a mouse lymphoma model. *Cancer Cell.* 2009;16:324-335.
391. Zhang CC, Kaba M, Ge G, et al. Angiopoietin-like proteins stimulate ex vivo expansion of hematopoietic stem cells. *Nat Med.* 2006;12:240-245.
392. Zhang CC, Kaba M, Iizuka S, Huynh H, Lodish HF. Angiopoietin-like 5 and IGFBP2 stimulate ex vivo expansion of human cord blood hematopoietic stem cells as assayed by NOD/SCID transplantation. *Blood.* 2008;111:3415-3423.

393. Nakajima H, Ito M, Smookler DS, et al. TIMP-3 recruits quiescent hematopoietic stem cells into active cell cycle and expands multipotent progenitor pool. *Blood*;116:4474-4482.
394. Tabata M, Kadomatsu T, Fukuhara S, et al. Angiopoietin-like protein 2 promotes chronic adipose tissue inflammation and obesity-related systemic insulin resistance. *Cell Metab.* 2009;10:178-188.
395. Mita AC, Takimoto CH, Mita M, et al. Phase 1 study of AMG 386, a selective angiopoietin 1/2-neutralizing peptibody, in combination with chemotherapy in adults with advanced solid tumors. *Clin Cancer Res*;16:3044-3056.
396. Roccaro AM, Hideshima T, Raje N, et al. Bortezomib mediates antiangiogenesis in multiple myeloma via direct and indirect effects on endothelial cells. *Cancer Res.* 2006;66:184-191.
397. Oda E, Ohki R, Murasawa H, et al. Noxa, a BH3-only member of the Bcl-2 family and candidate mediator of p53-induced apoptosis. *Science.* 2000;288:1053-1058.
398. Lecona E, Barrasa JI, Olmo N, Llorente B, Turnay J, Lizarbe MA. Upregulation of annexin A1 expression by butyrate in human colon adenocarcinoma cells: role of p53, NF- κ B, and p38 mitogen-activated protein kinase. *Mol Cell Biol.* 2008;28:4665-4674.
399. Rathi AV, Cantalupo PG, Sarkar SN, Pipas JM. Induction of interferon-stimulated genes by Simian virus 40 T antigens. *Virology.* 2010;406:202-211.
400. Munoz-Fontela C, Macip S, Martinez-Sobrido L, et al. Transcriptional role of p53 in interferon-mediated antiviral immunity. *J Exp Med.* 2008;205:1929-1938.
401. Hendy OM, Elghannam DM, El-Sharnouby JA, Goda EF, El-Ashry R, Al-Tonbary Y. Frequency and prognostic significance of murine double minute protein-2 overexpression and p53 gene mutations in childhood acute lymphoblastic leukemia. *Hematology.* 2009;14:335-340.

402. Wiederschain D, Kawai H, Shilatifard A, Yuan ZM. Multiple mixed lineage leukemia (MLL) fusion proteins suppress p53-mediated response to DNA damage. *J Biol Chem.* 2005;280:24315-24321.
403. Maki K, Mitani K, Yamagata T, et al. Transcriptional inhibition of p53 by the MLL/MEN chimeric protein found in myeloid leukemia. *Blood.* 1999;93:3216-3224.
404. Wiederschain D, Kawai H, Gu J, Shilatifard A, Yuan ZM. Molecular basis of p53 functional inactivation by the leukemic protein MLL-ELL. *Mol Cell Biol.* 2003;23:4230-4246.

9. Appendix I

9.1 SUPPLEMENTARY DATA

9.1.1 Vector maps

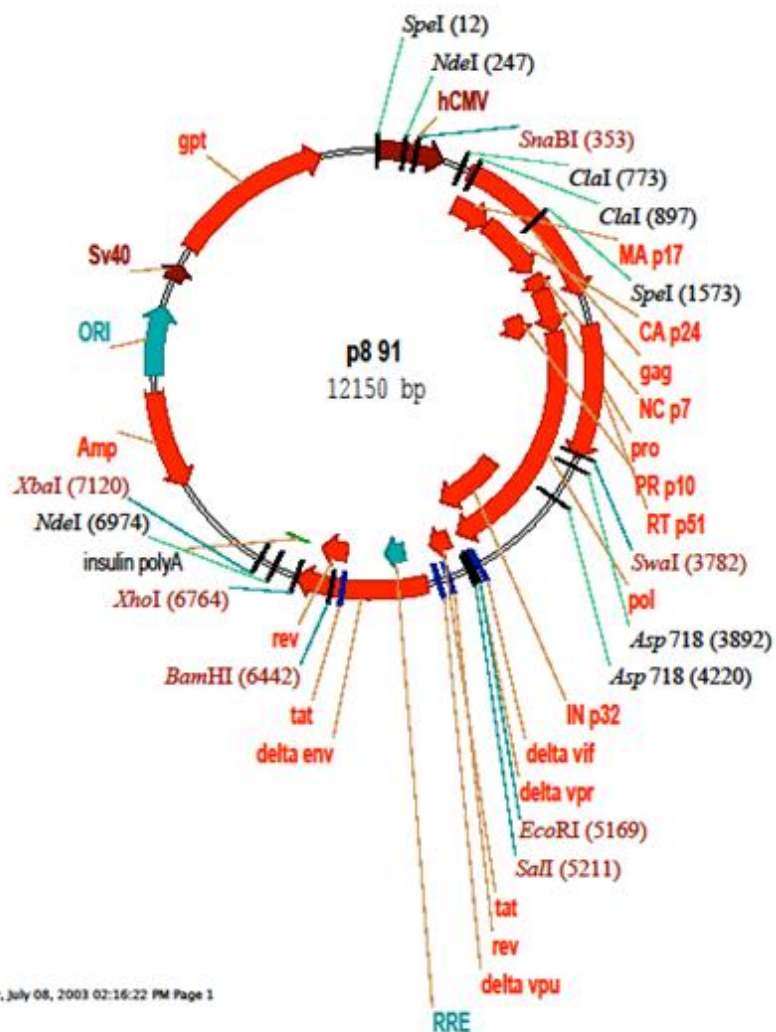


Fig. 9-1: Vector map of the lentiviral pCMVdeltaR8.91 packaging plasmid (<http://tronolab.epfl.ch/>)

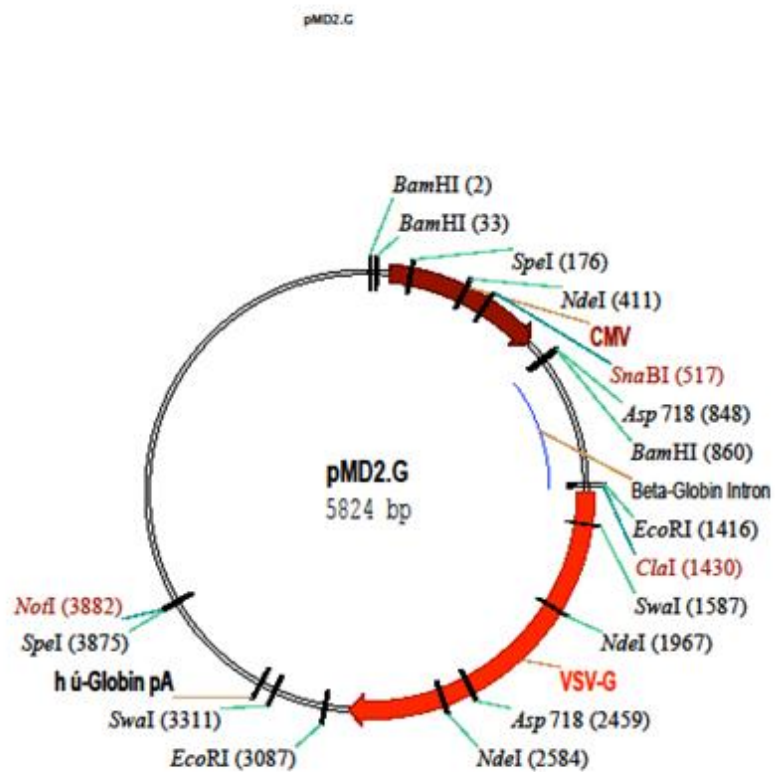


Fig. 9-2: Vector map of the lentiviral envelope plasmid pMD2.G (<http://tronolab.epfl.ch/>)

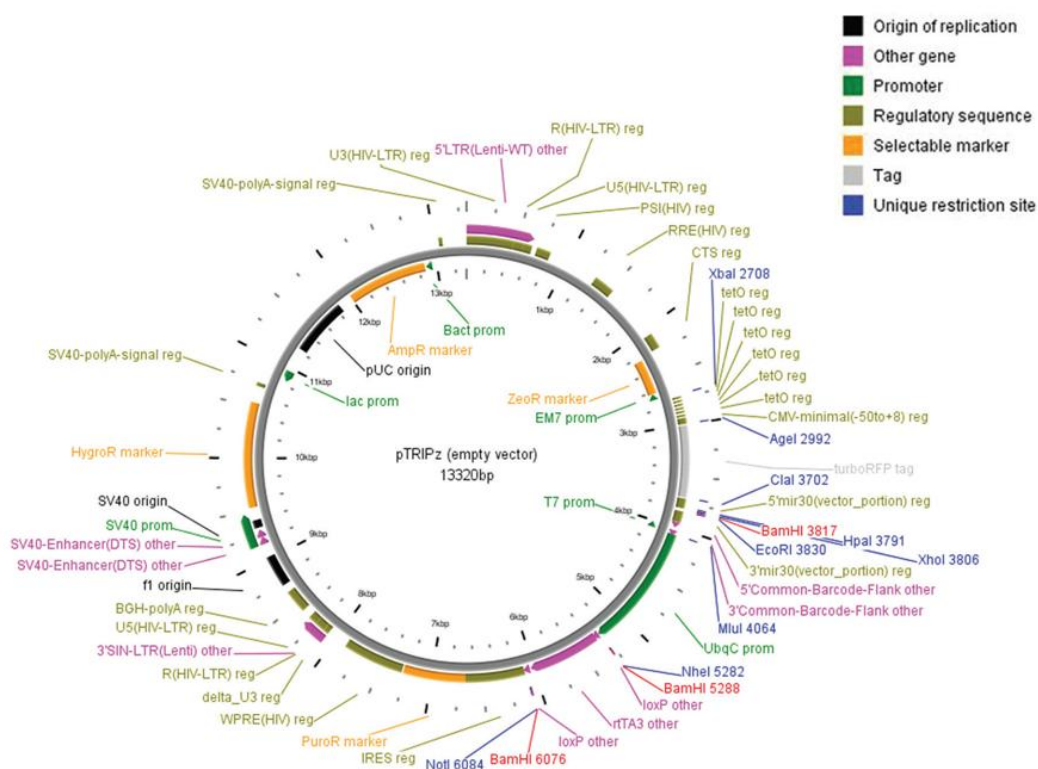


Fig. 9-3: Vector map of the lentiviral expression vector pTRIPZ-shRNA (www.openbiosystems.com)

9.2 R-SCRIPTS

9.2.1 *Venn*-Script for intersection analysis of data sets

```
library(limma)

setwd("/Users/directory of choice")

table.1 = read.table("table of choice A_.txt", sep="\t", header=TRUE)
table.2 = read.table("table of choice B_.txt", sep="\t", header=TRUE)

probes.table.1 = levels(table.1$header of table A)
probes.table.2 = levels(table.2$header of table B)

probes.combined = c(probes.table.1,probes.table.2)

probes.unique = unique(probes.combined)

col.1 = probes.unique %in% probes.table.1
col.2 = probes.unique %in% probes.table.2

venn_list = as.data.frame(matrix(c(col.1,col.2), ncol=2))
row.names(venn_list) = probes.unique
colnames(venn_list) = c("list A","list B")

write.table(venn_list, file="output table.txt")
```

9.2.2 *Extraction* Script in order to extract expression data of a specific entity set from a parental file

```
setwd("/Users/directory of choice")  
expr = read.table("parental file.txt", header=TRUE, sep="\t", row.names=1)  
  
#probe selection  
probes = read.table("probe of interest.txt", header=TRUE, sep="\t", row.names=1)  
expr.probes = expr[rownames(expr) %in% rownames(probes),]  
write.table(expr.probes, file="output expression data.txt", sep="\t")
```

9.2.3 DVD with array metrics and IPA results

10. Appendix II

10.1 CURRICULUM VITAE

Curriculum Vitae

Patricia Garrido Castro
Jeruzalemstraat 103
3061 GM Rotterdam, The Netherlands
+31 10 3418660
 p.garridocastro@erasmusmc.nl

Personal Details

Name: Patricia
 Surname: Garrido Castro
 Date of Birth: 22nd July 1982
 Place of Birth: Stuttgart, Germany
 Nationality: Spanish

Education

1988-1992: Elementary School (Heusteigschule, Stuttgart, Germany)

1992-2001: Grammar School (Ev. Moerike-Gymnasium, Stuttgart, Germany)

June 2001: **Abitur** (grammar school graduation exam):
1.0 (Sehr Gut = Excellent)

2001- 2007: **Masters Degree in Biochemistry (Diplom-Biochemie):**
1.2 (Sehr Gut = Excellent)
 Eberhard-Karls Universitaet Tuebingen, Tuebingen, Germany

2004-2005: Academic exchange (Erasmus) at the University of Sussex, Brighton, UK

2006- 2007: **Master Thesis** (laboratory-based research):
1.0 (Sehr Gut = Excellent)

Expression Analysis of the Putative Tumour Suppressor ARTS in t(4;11)-positive Acute Lymphoblastic Leukaemia

Dept. for Cell Biology, Eberhard-Karls Universitaet Tuebingen, Tuebingen, Germany,

Supervisors: Prof A. Nordheim and Dr. O. Heidenreich

May 2007-31.12.2010: **PhD Molecular Biology of Leukaemia**
Role of MLL/AF4 in t(4;11)-positive Leukaemogenesis and Leukaemic Maintenance

Supervisors: Dr. Olaf Heidenreich and Prof. Josef Vormoor

Northern Institute for Cancer Research, Newcastle University, Newcastle upon Tyne, UK

14.01.2011-ongoing: **Postdoctoral research associate** at the Erasmus MC, (Rotterdam, The Netherlands), Department of Paediatric Haematology/Oncology, Infant ALL research group

Supervisor: Dr. Ronald Stam

21.09.2011: ***Viva voce PhD thesis***
“Role of MLL/AF4 in t(4;11)-positive Leukaemogenesis and Leukaemic Maintenance”

10.2 PUBLICATIONS

Targeted Delivery of SiRNA to CD33-positive Tumor Cells with Liposomal Carrier Systems

M Rothdiener, D Müller, **P Garrido Castro**, A Scholz, M Schwemmlein, G Fey, O Heidenreich, RE Kontermann

Journal of Controlled Release, Vol.144 (2), 2010, pp 251-258

Leukemic Fusion Genes MLL/AF4 and AML1/MTG8 Support Leukemic Self-renewal by Controlling Expression of the Telomerase Subunit TERT

A Gessner, M Thomas, **P Garrido Gastro**, L Büchler, T Brümmendorf, N Martinez Soria, J Vormoor, J Greil, O Heidenreich

Leukemia, Vol.24, 2010, pp 1751-1759

Conference Presentations

ARTS - a Mediator of Apoptosis Suppressed in t(4;11)-positive ALL?

(oral presentation)

XX. Annual Meeting of the Kind-Phillip-Stiftung for Leukaemia Research 2007, Wilsede, Germany

Caspase Inhibition Blocks Apoptosis Caused By MLL/AF4 Depletion In t(4;11)-positive ALL Cell Lines, But Cannot Abrogate Subsequent Necroptosis-Like Cell Death

(poster presentation)

14th EHA Congress 2009, Berlin, Germany

Caspase Inhibition Blocks Apoptosis Caused By MLL/AF4 Depletion In t(4;11)-positive ALL Cell Lines, But Cannot Abrogate Subsequent Necroptosis-Like Cell Death

(oral presentation)

XXII. Annual Meeting of the Kind-Phillip-Stiftung for Leukaemia Research 2009, Wilsede, Germany

Oncogene addiction in t(4;11)-positive ALL: MLL/AF4 depletion results in multi-phenotypical cell death

(oral presentation)

North East Post Graduate Conference 2009, Newcastle upon Tyne, UK

The Prosurvival Cytokine ANGIOPOIETIN-1 is Overexpressed in t(4;11)-positive ALL and Regulated in a MLL/AF4-dependent manner

(poster presentation)

15th EHA Congress 2010, Barcelona, Spain

ANGIOPOIETIN-1 Expression is Modulated by Leukaemic Fusion Genes

(oral presentation)

XXIII. Annual Meeting of the Kind-Phillip-Stiftung for Leukaemia Research 2010, Wilsede, Germany

ANGIOPOIETIN1 - a Novel Factor Implicated in MLL-rearranged Acute Lymphoblastic Leukaemia and Regulated in a Fusion Gene-dependent Manner.

(oral presentation)

ASH, 52nd Annual Meeting, 2010, Orlando, FL